IAEA-SMR-93

NUCLEAR THEORY FOR APPLICATIONS—1982

PROCEEDINGS OF THE COURSE ON ADVANCES IN NUCLEAR THEORY
AND NUCLEAR DATA FOR REACTOR APPLICATIONS
HELD AT TRIESTE, 25 JANUARY–19 FEBRUARY 1982
DURING THE WINTER COLLEGE ON NUCLEAR PHYSICS AND REACTORS
JOINTLY ORGANIZED BY THE
INTERNATIONAL ATOMIC ENERGY AGENCY
AND THE
INTERNATIONAL CENTRE FOR THEORETICAL PHYSICS
AND HELD AT THE
INTERNATIONAL CENTRE FOR THEORETICAL PHYSICS, TRIESTE
25 JANUARY–26 MARCH 1982

INTERNATIONAL CENTRE FOR THEORETICAL PHYSICS, TRIESTE, 1984

NUCLEAR THEORY FOR APPLICATIONS – 1982

THE INTERNATIONAL CENTRE FOR THEORETICAL PHYSICS (ICTP) in Trieste was established by the International Atomic Energy Agency (IAEA) in 1964 under an agreement with the Italian Government and with the assistance of the City and University of Trieste.

The IAEA and the United Nations Educational, Scientific and Cultural Organization (UNESCO) subsequently agreed to operate the Centre jointly from 1 January 1970.

Member States of both organizations participate in the work of the Centre, the main purpose of which is to foster, through training and research, the advancement of theoretical physics with special regard to the needs of developing countries.

NUCLEAR THEORY FOR APPLICATIONS – 1982

PROCEEDINGS OF THE COURSE ON ADVANCES IN NUCLEAR THEORY
AND NUCLEAR DATA FOR REACTOR APPLICATIONS
HELD AT TRIESTE, 25 JANUARY–19 FEBRUARY 1982
DURING THE WINTER COLLEGE ON NUCLEAR PHYSICS AND REACTORS
JOINTLY ORGANIZED BY THE
INTERNATIONAL ATOMIC ENERGY AGENCY
AND THE
INTERNATIONAL CENTRE FOR THEORETICAL PHYSICS
AND HELD AT THE
INTERNATIONAL CENTRE FOR THEORETICAL PHYSICS, TRIESTE
25 JANUARY–26 MARCH 1982

INTERNATIONAL CENTRE FOR THEORETICAL PHYSICS, TRIESTE, 1984

NUCLEAR THEORY FOR APPLICATIONS–1982, IAEA, VIENNA, 1984

Printed by the IAEA in Austria
April 1984

FOREWORD

The International Centre for Theoretical Physics has maintained an interdisciplinary character in its research and training programmes in different branches of theoretical physics. In pursuance of this objective, the Centre has organized extended research courses and workshops, including topical conferences, with a comprehensive and synoptic coverage in varying disciplines. The first of these – on Plasma Physics – was held in 1964 and then repeated in 1977; the second in 1965 was concerned with the Physics of Particles. Between then and now, the following courses were organized: four on Nuclear Physics (1966, 1969, 1971, 1973), two on Nuclear Theory for Applications and Power Reactors (1978, 1980), seven on the Physics of Condensed Matter (1967, 1970, 1972, 1974, 1976, 1978, 1980), four on Atomic Physics (1973, 1977, 1979, 1981), three on Geophysics (1975, 1977, 1980), one on Control Theory and Functional Analysis (1974), two on Complex Analysis (1975, 1980), one on Applications of Analysis to Mechanics (1976), one on Mathematical Economics (1975), one on Systems Analysis (1978), two on Teaching of Physics at Tertiary Level (in English in 1976, in French in 1977), and four on Solar Energy (1977, 1978, 1979, 1981). Most of the Proceedings of these courses have been published by the International Atomic Energy Agency (Vienna, Austria).

The present volume contains the Proceedings of the Winter College on Advances in Nuclear Theory and Nuclear Data for Reactor Applications conducted from 25 January to 9 February 1982. The Course was held in response to the growing need of developing countries which plan to establish a nuclear power programme to familiarize themselves with the nuclear physics foundations of nuclear energy and their applications in the design of nuclear reactors.

The programme of lectures and working sessions was organized by J.J. Schmidt (International Atomic Energy Agency, Vienna, Austria) and M.K. Mehta (Bhabha Atomic Research Centre, Bombay, India).

Abdus Salam

PREFACE

This volume contains the text of invited lectures presented during the Course on Advances in Nuclear Theory and Nuclear Data for Reactor Applications held at the International Centre for Theoretical Physics (ICTP) in Trieste, Italy, from 25 January to 19 February 1982, within the framework of the nuclear physics activities of the ICTP during the winter of 1982. The Course was jointly organized by the IAEA Nuclear Data Section and ICTP, and was attended by 70 participants from 23 developing countries, 2 from 2 developed countries and 1 from an international organization.

The purpose of the Course was, pursuant to similar courses held in 1978 and 1980, to offer nuclear scientists from developing countries who are implementing a nuclear science and technology programme a review of recent progress in the theory of low-energy neutron nuclear reactions, to introduce new advanced nuclear model computer codes and to review the nuclear physics and data-bases needed for thermal reactor physics design and safety analysis.

The Course comprised lectures, special seminars and extended topical discussion sessions primarily covering:

1. Advances in the theory of basic fast neutron/nuclear interaction mechanisms and its applications;
2. Advances in the understanding of nuclear fission dynamics;
3. Nuclear data for nuclear power reactor core and safety analysis.

Discussions were held during the Course for follow-up action based on the findings of the special workshop held during the second Course in 1980 regarding the new IAEA Technical Co-operation Interregional Project on Nuclear Data Techniques and Instrumentation (TC/INT/1/018).

The lectures given during the Course built upon those given at the two earlier Courses on Nuclear Theory for Applications held at the ICTP in Trieste in 1978 and 1980 and published as reports IAEA-SMR-43 and IAEA-SMR-68/1, respectively. They are expected to be of interest to nuclear scientists both from developing countries where the interest in nuclear data and reactor physics research is steadily growing and from developed countries where such research is in an advanced stage. To keep the size of the Proceedings within reasonable limits and to avoid duplication of published material, only an outline of the lecture content with references to the published literature is given for those cases where the lecturer felt that full text was not necessary. It is expected that the Proceedings will serve as reference in the field and as an advanced textbook for post-graduate studies.

The organizers wish to express their deep appreciation to the lecturers, speakers at the special seminars and participants at the extended discussions for their very active engagement and co-operation in achieving the objectives of the Course. The excellent of the staff of the ICTP was indispensable for the successful organization and conduct of this Course and is most gratefully acknowledged.

CONTENTS

III. NUCLEAR DATA BASE FOR REACTOR DESIGN AND SAFETY

RECENT ADVANCES IN UNDERSTANDING LOW-ENERGY REACTIONS

S.E. KOONIN
W.K. Kellogg Radiation Laboratory,
California Institute of Technology,
Pasadena, California,
United States of America

These lectures were a pedagogic review of some recent theoretical work in low-energy nuclear reaction theory, with particular emphasis on the multi-step compound and multi-step direct reaction mechanisms. The goals were to impart a basic understanding of the physics involved, to review some of the formalism developed to treat such processes, and to describe some schematic models which implement this formalism.

The first lecture began with a review of the basic classification of low-energy reactions and of the various physical characteristics associated with each type. These ranged from the statistical compound to the dynamical direct, with the multi-step pre-equilibrium falling between these two extremes. The simple exciton model of equilibration through a sequence of increasingly complex nuclear configurations was then introduced and was used to estimate the time-scales involved, as well as the spectral characteristics of each reaction mechanism. Simple Fermi-gas expressions for the total nuclear level density and for the density of levels at each stage in the equilibration process were derived, and the basic physical features governing evaporation and pre-equilibrium spectra (e.g., damping widths relative to escape widths) were discussed.

The second lecture started with a review of single-particle scattering theory. The Lippmann-Schwinger equation, the Green's function, the S-matrix, and the T-matrix were introduced and were related to observable cross sections. The elaboration of this mathematical apparatus to treat many-body reactions was then discussed, with emphasis on the partition of the Hilbert space into "relevant" and "irrelevant" sectors using projection operators. The resulting expressions for the S-matrix in the case of a single resonance were related to the familiar Breit-Wigner form. The concepts of energy-averaging and fluctuation cross-sections were then introduced to handle the many-resonance case and expressions were derived for the fluctuation cross section in terms of the average resonance parameters and, ultimately, in terms of the energy-averaged S-matrix. Connection was also made with the naive Hauser-Feshbach expressions.

The third lecture was concerned with the extension of the many-body reaction formalism to multi-step processes. The notion of a chained-partition of Hilbert space was introduced and, using several key algebraic identities, the many-body T-matrix was expressed as a sum of contributions from different regions of the chain, beginning with the simple direct reactions and ending with compoud-nucleus processes. Upon invoking extreme statistical assumptions, including "self-averaging" and the presence of incoherent "exit modes", the cross section was shown to be composed of both multi-step compound and multi-step direct contributions. The former involves only quasi-bound processes and corresponds to decay following propagation along the bound portion of the chain; it results in an angular distribution symmetric about 90°. The multi-step direct contribution is a set of convolutions of single-step direct cross sections; its angular distribution is forward peaked and, in certain limits, it can be described by a diffusion equation.

The final lecture was devoted to an explicit schematic model of multi-step compound processes. States along the chained partition were modelled by increasing numbers of particle-hole excitations coupled to a fixed total angular momentum. Simple but plausible estimates were made of the matrix elements of the residual interaction; these resulted in explicit expressions for the double-differential (energy-angle) cross section. Particular physical features of the model were discussed and a sucessful application to the experimental data on ^{181}Ta(p,n)^{181}W was described.

BIBLIOGRAPHY

Formalism:

H. Feshbach, A. Kerman, and S. Koonin, Ann. Phys. 125, 429 (1980)

D. Agassi, H. Weidenmuller, and G. Mantzouranis, Phys. Rep. C22, 145 (1975)

K. McVoy, W. Friedman, M. Hussein, and P. Mello, Phys. Rep. C77, 48 (1981)

Models:

M. Blann, Ann. Rev. Nuc. Sci. 25, 123 (1975)
E. Gadioli and L. Milazzo-Colli, Lecture Notes in Physics No. 22, Springer-Verlag (1973)
R. Bonetti et. al., Phys. Rev. 21C, 816 (1980)

CONTINUUM SPECTRA IN PROTON- AND NEUTRON-INDUCED REACTIONS

T. TAMURA
Department of Physics,
University of Texas,
Austin, Texas,
United States of America

It does not seem necessary to publish the notes of the lectures, given at the Winter College, 1982, with the title shown above. It is beeause the lecture was given based on a paper entitled as "Multi-Step Direct Reaction Analysis of Continuum Spectra in Reactions Induced by Light Ions" by T. Tamura, T. Udagawa and H. Lenske, and this paper is published in the Physical Review C 26 (1982) 379. There is, however, a remark to make.

During the Winter College, I detected a significant interest among the participants in getting access to the computer program, which our Austin group had been using. I thus decided to publish the program in the Computer Physics Communications, and it will be submitted for publication in a few weeks. The paper will be coauthored by T. Udagawa and M. Benmahou, and the program will be called ORION/TRISTAR. The version we are publishing this time handles the direct reaction as one-step only, but may be used well to analyze continuum data induced by nucleons whose energy does not exceed 40 MeV, say. (Multi-step version will be published later.) It calculates, not only the angular distribution of various reactions as a function of E_x, the excitation energy of the residual nucleus, but also gives the cross sections in the form of $\sigma(E_x;IM)$, where I is the spin of the residual nucleus and M is its projection. One may use this information as an input to the usual Hauser-Feshbach program, and thus calculate the contribution to the evaporation component, which is additional to the usual Hauser-Feshbach contribution. I hope the reader will find the program ORION/TRISTAR useful for his/her research.

RECENT ADVANCES IN NUCLEAR MODEL CODE DEVELOPMENTS

M. UHL
Institut für Radiumforschung und Kernphysik,
University of Vienna,
Vienna, Austria

Abstract

Model calculations can be used to provide nuclear data for applications. Computer codes for the calculation of average cross sections are reviewed. The codes are discussed together with the models - the spherical and deformed optical model, the statistical compound nucleus model and phenomenological precompound models - and the required parameters.

1. Introduction

Nuclear cross section data are needed for many applications in science and technology. A comprehensive review on this topic has been presented by Schmidt at the 1978 Trieste Winter Course /1/. In general these cross section data are supplied by experiment. There are, however, many situations where model calculations can supplement experimental cross sections. Some examples are:

i) Gaps in excitation functions can be filled by model calculations as illustrated in fig. 1. Many excitation functions of threshold reactions of importance for reactor neutron dosimetry are based on calculations in some energy regions.

ii) The development d+Li neutron sources for fusion materials irradiation test facilities requires the knowledge of neutron cross sections for energies up to 40-50 MeV. As the experimental data are very scarce in this energy region most of the requirements have to be met by model calculations which reproduce experimental data at lower energies. Similar "extrapolations" of experimental cross sections are employed for biomedical applications, too.

iii) There exist many cross sections of interest with no experimental data at all and for which no measurements will likely exist as the target nuclei are instable. Great efforts to calculate such cross sections for astrophysical applications are reported by Woosley et al. /2/. Cross sections for instable target nuclei are also important in energy related technology as for instance for the assessment of the build-up of fission products and actinides.

These examples show how nuclear model calculations can be used to provide lacking cross section data. However, they cannot replace experiment at all. On the contrary, the various reaction models rely on auxiliary information in terms of model parameters which for the time being cannot be derived from pure nuclear theory with sufficient accuracy and hence have to be adjusted to carefully selected experimental data; examples are optical model parameters, fission barrier parameters and level density parameters. These parameters are as important as the computer codes used to perform the model calculations. To obtain reliable results each calculation of an unknown cross section should be based on parameters which simultaneously reproduce available experimental data in the mass region of interest.

These lectures concern computer codes for average cross sections which are based on the optical model (spherical and deformed), the statistical compound nucleus model and on various phenomenological precompound models. By means of these models nearly all cross sections of interest for applications can be calculated as illustrated in Dr.Strohmaiers lectures at this course.

I will mainly concentrate on representative codes which are internationally avaiable and hence can immedeately be applied by each participant of this course. In this connection I would like to direct your attention to the N.E.A. Nuclear Data Bank Program Library, Saclay, 91191 Gif-Sur-Yvette CEDEX, France, whic distributes free of charge a large number of computer codes. A program package consists of the source program, a sample input and output and a reference manual. Further I would like to encourage authors of new codes to make them available to this institution.

At the 1978 Trieste course lectures on the same topic were presented by Prince /3/. Most of the codes discussed then are still in use; some of them were substantially extended in the meantime. A few new codes, mainly referring to preequilibrium decay were developed since.

I will discuss the codes in connection with the employed models and the required model parameters. The above mentioned models are not independent. The relations between them show up when calculating the average cross section in terms of the scattering matrix.

2. Average cross sections

In general the energy dependence of nuclear reaction cross sections is very complicated and therefore is best described in terms of statistics. For practical applications in the region of overlapping resonances one is mainly concerned with averages of cross sections $\sigma(E)$ with respect to energy E

$$\langle\sigma\rangle = \frac{1}{\Delta E} \int dE\sigma(E),$$

where ΔE is a suitably chosen energy interval.

In nuclear reaction theory cross sections are expressed in bilinear terms of the scattering matrix S. The scattering matrix element S_{ab} is the ratio of the amplitude of the outgoing wave in channel b to that of the incoming wave in entrance channel a. Due to this definition the integrated cross sections for a binary reaction from channel a to channel b is essentially (except for trivial factors) given by

$$\sigma_{ab}(E) = |\delta_{ab} - S_{ab}(E)|^2 \quad . \qquad (2.1.)$$

Time reversal invariance and flux conservation require the S-matrix to be symmetric $S_{ab} = S_{ba}$ and unitary

$$\sum_c S_{ac}(E) S^*_{bc}(E) = \delta_{ab} . \qquad (2.2.)$$

The complicated energy dependence of the S-matrix which is responsible for the statistical behaviour of the cross sections becomes apparent in form of a resonance pole expansion /4/

$$S_{ab}(E) = S^{(o)}_{ab} - i \sum_\mu \frac{g_{\mu a} g_{\mu b}}{E - \varepsilon_\mu + \frac{i}{2}\Gamma_\mu} \quad . \qquad (2.3.)$$

The first term is approximately constant in the energy range of interest. In the isolated resonance situation each pole term represents a resonance at $E = \varepsilon_\mu$ with width Γ_μ. The statistical properties of the resonance parameters $\{\varepsilon_\mu, g_{\mu c}\}$ are known and well understood in the frame of the statistical theory of spectra /5/. As soon as the average width $\langle\Gamma\rangle$ of the resonances exceeds their average spacing D ($\langle\Gamma\rangle/D > 1$, overlapping resonances) the pole parameters have not such a clear physical meaning and their statistical properties are much more complicated /6/.

In the statistical theory of cross sections the S matrix is decomposed into its average $\langle S_{ab}\rangle$ and a fluctuating part $S^{fl}_{ab}(E)$

$$S_{ab}(E) = \langle S_{ab}\rangle + S^{fl}_{ab}(E) \quad .$$

The average $\langle S_{ab}\rangle$ is related to direct reactions and can be calculated by means of models involving relatively few degrees of freedom: the single channel optical model in case that $\langle S_{ab}\rangle$ is diagonal and the multi-channel optical model otherwise (see section 3). The fluctuating part S^{fl}_{ab} reflects the excitation of complicated degrees of freedom and thus describes compound nucleu reactions.

The resulting average cross section

$$\langle\sigma_{ab}\rangle = |\delta_{ab} - \langle S_{ab}\rangle|^2 + \langle|S^{fl}_{ab}|^2\rangle = \sigma^{DR}_{ab} + \langle\sigma^{fl}_{ab}\rangle \qquad (2.4.)$$

consists of two contributions: the direct reaction cross section $\sigma^{DR}_{ab} = |\delta_{ab} - \langle S_{ab}\rangle|^2$ and the average of the fluctuating cross section $\langle\sigma^{fl}_{ab}\rangle = \langle|S^{fl}_{ab}|^2\rangle$ which represents the compound nucleus cross section $\langle\sigma^{CN}_{ab}\rangle$.

The average of the unitarity relation (2.2.)

$$\sum_c \langle S_{ac}\rangle\langle S_{bc}\rangle^* + \sum_c \langle S^{fl}_{ac} S^{fl*}_{bc}\rangle = \delta_{ab} \qquad (2.5.)$$

shows that the average of the scattering matrix $\langle S_{ab}\rangle$ is not unitary.

Its unitary deficit is the penetration matrix P /7/.

$$P_{ab} = \delta_{ab} - \sum_c \langle S_{ac}\rangle\langle S_{bc}\rangle^* \quad . \qquad (2.6.)$$

In absence of direct reactions the diagonal elements of P_{ab} are just the (single channel) optical model transmission coefficients $T_a = 1 - |\langle S_{aa}\rangle|^2$

$$P_{ab} = \delta_{ab}\,(1 - |\langle S_{aa}\rangle|^2) = \delta_{ab}\, T_a \quad . \qquad (2.7.)$$

The statistical theory of nuclear reactions aims at expressing the average fluctuating cross section $\langle\sigma^{fl}_{ab}\rangle = \langle|S^{fl}_{ab}|^2\rangle$ or more generally averages of the type $\langle S_{ab} S^*_{cd}\rangle$ in terms of the average S-matrix. Analytic formulae were derived for isolated resonances $\langle\Gamma\rangle/D \ll 1$ or for strongly overlapping resonances $\langle\Gamma\rangle/D \gg 1$. For intermediate values of $\langle\Gamma\rangle/D$ convenient formulas were found which accurately reproduce the results of computer experiments (see section 4). Excellent reviews exist on this topic by Moldauer /6/, Mahaux and Weidenmüller /8/ and Brody et al. /5/.

The above mentioned formulae are based on the statistical properties of the S-matrix characterizing an equilibrated compound nucleus. Thus they do not account for preequilibrium decay and their applicability is restricted to low incident energies, say below 10 MeV. Recently several fundamental approaches /9/ - /12/ to describe preequilibrium decay in the frame of general reaction theory were proposed. They are discussed in other lectures at this course. For practical applications, however, preequilibrium

decay is treated in the frame of simple phenomenological models (see section 5). The average of the fluctuating cross section is decomposed into an equilibrium and an equilibrium portion

$$\langle\sigma_{ab}^{fl}\rangle = \langle\sigma_{ab}^{fl,eq}\rangle + \langle\sigma_{ab}^{fl,pre}\rangle . \qquad (2.8.)$$

Finally it should be pointed out that the formulae for actual cross sections are more complicated than equ. (2.1.). In particular, differential cross sections $\frac{\partial\sigma_{ab}}{\partial\Omega}$ require the consideration of angular momentum coupling. The formulae for various coupling schemes can be found in a review article by Robsen /13/.

3. Elastic scattering and direct reactions (optical model)

At the 1978 Trieste Winter course the theoretical background of the optical model was reviewed by Mahaux /14/ and its practical aspects by Prince /3/. The next section presents a short description of some of the concepts required for the characterization of the pertinent codes.

3.1. Models and parameters

The single channel or spherical optical model describes the scattering of a particle by a complex (absorptive) spherical potential U(r). The Schrödinger equation for the radial wave function $u_a(r)$ in channel a reads

$$[-\frac{h^2}{2\mu}(\frac{d^2}{dr^2} - \frac{l(l+1)}{r^2}) + U(r) - E]\, u_a(r) = 0 . \qquad (3.1.)$$

Each channel can be treated separately. The average of the scattering matrix $\langle S_{aa}\rangle$ is obtained by numerically integrating this equation from the origin to a point where the potential U(r) can b neglected and by matching the asymptotic solution.

In addition to the transmission coefficients $T_a = 1-|\langle S_{aa}\rangle|^2$ the following quantities are obtained in terms of $\langle S_{aa}\rangle$ by well known formulas (see e.g. ref. /15/): total, elastic and absorption cross section, polarisations, scattering radius and the s and p-wave strength functions.

The phenomenological optical model potentials used in most investigations are of the following form:

$$U(r) = -V f(r,R,a) + i[4a_s W_s \frac{d}{dr} f(r,R_s,a_s) - W_v f(r,R_v,a_v)] +$$
$$+ V_c(r,R_c) + 2 V_{so} \frac{1}{r}\frac{d}{dr} f(r,R_{so},a_{so}) . \qquad (3.2.)$$

Thus the potential consists of a real part with depth V, an absorptive surface and an absorptive volume component with depths W_s and W_v respectively, a Coulomb potential and a spin orbit term with strength V_{so}. The depth V, W_s and W_v depend on energy E. The radial form factors commonly used are of Woods-Saxon type

$$f(r,R,a) = [1 + \exp(\frac{r-R}{a})]^{-1} , \qquad (3.3.)$$

where R and a represent the radius and the diffuseness, respectively. The Coulomb potential is assumed to result from a uniformly charged sphere.

The phenomenological optical potentials depend on many parameters which have to be determined by comparison with experimental data. Automatic search procedures to find an optimum set of parameters have been developed; they are usual based on the least square fit method.

Theoretical considerations require the optical potential to be non-local. For a non-local potential equ. (3.1.) has to be replaced by an integro-differential equation with a kernel $k_a(r,r')$

$$[-\frac{h^2}{2\mu}(\frac{d^2}{dr^2} - \frac{l(l+1)}{r^2}) - E]\, u_a(r) + \int dr' K_a(r,r') u_a(r') = 0 . \qquad (3.1'.)$$

Perey and Buck /16/ demonstrated that an energy independent non-local potential reproduced experimental data over an extended ener range. They found also a recipe how to construct an energy dependent local equivalent of an energy independent non-local potential. In this sense the phenomenological energy dependent potentials of equ. (3.2.) can be regarded as local equivalents of a non-local potential.

While the single channel optical model for $\langle S_{aa}\rangle$ treats each (elastic) channel separately the coupled channels optical model considers coupling between different channels.Such calculations ar more involved - in particular if rearrangement channels are accoun ted for. Therefore in practical applications the only direct reaction usually considered is excitation of low lying collective levels by inelastic scattering. Compared to other direct reactions these processes have large cross sections. The theory of direct inelastic scattering was reviewed by Tamura /17/, Madsen /18/ and Delaroche et al. /19/.

A model which describes elastic and collective inelastic scattering on a macroscopic basis assumes that the phenomenological optical potential of equ. (3.1.) is deformed ("deformed optica potential").

For permanently deformed nuclei the radii R_i entering in the various radial form factors of equ. (3.2.) are expressed in terms of deformation parameters β_λ

$$R_i(\Theta') = R_{oi}(1 + \sum_\lambda \beta_\lambda Y_{\lambda o}(\Theta')) \ , \qquad (3.4.)$$

where Θ' refers to a body fixed system. For spherical (vibrational nuclei the corresponding equation reads

$$R_i(\Omega) = R_{oi}(1 + \sum_\lambda \alpha_{\lambda\mu} Y_{\lambda\mu}(\Omega)), \qquad (3.4'.)$$

where Ω refers to an arbitrary space fixed system and the $\alpha_{\lambda\mu}$ are operators describing the vibrational motion; deformation parameters β_λ can be defined in terms of expectation values of these operators:

$$\beta_\lambda^2 = \langle | \sum_\mu |\alpha_{\lambda\mu}|^2 | \rangle .$$

The wave function Ψ of the considered system is expanded in terms of channel surface functions ϕ_c which are defined by Lane and Thomas /20/: $\Psi = \sum_c \Phi_c u_c(r)/r$. These quantities Φ_c consist of the wave functions of the projectile, the target nucleus in its different states and the angle dependent part of the wave function of relative motion and include the angular momentum coupling. The set of coupled equations for the radial wave function results from the Schrödinger equation $(H - E)\Psi = 0$ and the orthogonality of the surface functions and reads

$$[-\frac{h^2}{2\mu}(\frac{d^2}{dr^2} - \frac{l(l+1)}{r^2}) + \langle \Phi_a | U | \Phi_a \rangle - E_a] u_a(r) =$$

$$= -\sum_{b \neq a} \langle \Phi_a | U | \Phi_b \rangle \, u_b(r), \qquad (3.5.)$$

where U is the deformed (local) potential and E_a represents the channel energy. The coupling between different channels is caused by the matrix elements $\langle \Phi_a | U | \Phi_b \rangle$ which depends on the deformation parameters β_λ and the structure of the target states. Analytic expressions were derived by Tamura /17/ in the frame of a vibrational and/or a rotational model for the target nucleus.

The average S-matrix $\langle S_{ab} \rangle$ is found by numerically integratin the coupled equations (3.5.) and matching the appropriate asymptot solution. In addition to all the quantities which result from the spherical optical model the coupled channels optical model also provides the (direct) inelastic cross sections for the considered levels of the target nucleus and the penetration matrix

$P_{ab} = \delta_{ab} - \sum_c \langle S_{ac} \rangle \langle S_{bc} \rangle^*$.

Unfortunately coupled channels calculations are rather time consuming. In case of vibrational nuclei with small deformation parameters inelastic scattering cross sections can be calculate by means of the much faster DWBA method /15/ which only considers the coupling between the entrance and one exit channel in first approximation. Fu /21/ and Arthur et al. /22/ recently applied the DWBA method for the evluation of neutron induced cross section for ^{40}Ca and $^{54,56}Fe$, respectively. For strong coupling between channels, however, the use of the coupled channels models is indispensable; this applies in particular to strongly deformed nuclei.

With regard to applications the most important problem is the parameterization of the optical potentials. In the past years several global potentials were proposed which are valid in a wide mass and energy region /15/. Global neutron potentials were reviewed by Wilmore et al. /23/ and by Delaroche et al. /19/. Such global potentials do a reasonable good job in predicting the overa trends but when applied to a particular nucleus it often turns out that the experimental data are not adequately reproduced. Therefore for accurate evaluations one has to optimize the parameters i a more restricted mass region. For this purpose the Bruère-le-Châtel-group developed for neutrons the very efficient "SPRT-method" /19/, /24/. The parameters are found by an analysis of low energy data in the keV region namely the s- and p-wave strengt functions and the potential scattering radius R' and by reproducin the total cross section from a few keV to 20 MeV. An additional restriction is the reproduction of differential elastic and inelastic cross sections. Due to the wide energy range covered by the SPRT-method the resulting potentials are particularly useful for deriving the transmission coefficients for statistical model calculations.

Of special theoretical and practical interest are nucleon opt cal potentials which in the frame of the Lane-model /25/ simultaneously reproduce (p,p), (n,n) and quasi-elastic (p,n) data. Successful applications of this approach to light /26/ and intermediate nuclei /27/, /28/ were reported. Extensive experimental and theoretical investigations of Lane-model consistent potentials for actinides are being performed by Hansen et al. /29/ at Livermore.

A comprehensive review on the determination of nuclear deformation parameters from fast nucleon scattering was presented by Haouat at the 1979 Smolenice Symposium /30/. In general the deformation parameters derived from inelastic scattering and from electromagnetic excitations are very similar. For vibrational nuclei systematics trends of the small difference of deformation parameters for different "probes" can be explained in the frame of a theory proposed by Madsen et al. /31/ and Brown et al. /32/. A recent comparison of β_2 for vibrational nuclei obtained with different probes was published by Bernstein et al. /33/.

3.2. Computer codes

A first I present some characteristic examples of computer codes based on the spherical or the deformed optical model which in addition have the advantage of being generally available at the N.E.A. Data Bank Program Library. For an easier comparison these codes are compiled in table 1. Column 1 contains information on the documentation and in most cases on the size of th code. Special features of each program are listed in column 2. Many optical model codes also perform compound nucleus model calcu lations. These are characterized in column 3 and discussed later c

Among the codes equipped with an automatic parameter search procedure (CRAPONE, ELIESE, PELINSCA) I would like to mention in particular CRAPONE which was developed by the Bologna group. This code has an efficient search routine which in case that a non-local potential is used fits simultaneously data sets at up to 10 different energies.

The DWBA code DWUCK-4 allows for various direct reaction mechanisms. The calculation of inelastic scattering cross sections with macroscopic form factors corresponding to a deformed optical potential is only one of the options of this code.

Due to its flexibility JUPITOR-1 is certainly the most popula coupled channels code. Many different versions exist all over the world. In fact, a recent international intercomparison of coupled channels codes which was organized by E. Sartori /34/ from the N.E.A. Nuclear Data Bank actually turned out to become ar intercomparison of different versions of JUPITOR.

Naturally there are many other codes with features similar to those compiled in table 1. At first I would like to mention F. Perey's famous unpublished GENOA code. This code is equipped with a very flexible and efficient search procedure which permits to fit simultaneously several sets of data by one average potential. These data sets may refer to different nuclei and different energies. Hence GENOA can search for a global potential.

J. Raynal developed a powerful method to solve coupled differential or coupled integro-differential equations by sequential iteration. This ECIS method (Equations Couplées en Itérations Séqentielle) is described in ref. /35/. This method, though requiring more storage, is much faster than the conventional integration methods. It is incorporated in Raynal's ECIS code. From an informal Karlsruhe (KFK)-report I learned that in particular at higher energies the ECIS code is at least three times faster than conventional coupled channels codes. In view of the large amount of computation time spent for coupled channels calculations this is an important achievement.

Finally I want to mention two recent spherical optical model codes. The first one - SCAT2 (Fortran-IV, 27 k words) was develope by Bersillon /36/ at Bruère-le-Châtel. Besides a local potential also the local equivalent of a non-local potential may be used. In addition to the usual optical model cross sections the code calculates polarisations, strength functions and scattering radius and transmission coefficients. By an advanced programming techniq the running times are very short. SCAT2 is extensively used at Bruère-le-Châtel and at Los Alamos.

P.A. Moldauer /37/ developed a new version ABAREX (Fortran, 250 k bytes) of Auerbach's ABACUS code /38/. ABAREX uses a spherical optical model and calculates the total, differential elastic and inelastic cross sections as well as the fission and the capture cross section. The compound nucleus model calculations are based on the "M-cancellation" principle to be discussed in the next section. A search procedure is available. Fits to the total, differential elastic and differential inelastic (up to seven groups of levels) cross sections may be performed simultanec ly at up to 14 different energies. At present the code is devised for neutrons; inclusion of charged particle channels is planned. The code ABAREX will be made available for general distribution.

4. Statistical compound nucleus reactions

4.1. Models and parameters

Processes involving an equilibrated compound nucleus are described by generalisations of the celebrated Hauser-Feshbach formula /39/, which gives the cross section in terms of the (spherical) optical model transmission coefficients $T_c = 1 - |\langle S_{cc}\rangle|^2$

$$\langle\sigma_{ab}^{fl}\rangle = \langle\sigma_{ab}\rangle = \langle|S_{ab}^{fl}|^2\rangle = \frac{T_a T_b}{\Sigma\, T_c} \quad . \qquad (4.1.)$$

At first we neglect direct reactions and hence assume a diagonal average S-matrix: $\langle S_{ab}\rangle = \delta_{ab}\langle S_{aa}\rangle$. For that case Moldauer /40/ porposed in 1975 the following formula for the average of the fluctuating cross section

$$\langle\sigma_{ab}^{fl}\rangle = W_{ab}\,\frac{T_a T_b}{\Sigma_c\, T_c} \quad ,$$

$$W_{ab} = (1 + \frac{2}{\nu_a}\,\delta_{ab}) \int_0^\infty dt \prod_c (1+\frac{2t}{\nu_c}\,\frac{T_c}{\Sigma T_{c'}})^{-(\frac{1}{2}\nu_c+\delta_{ac}+\delta_{bc})} \quad , \qquad (4.2.)$$

where the sums and the product are over all open channels. The quantities ν_c (the "channel degree of freedom parameters") depend on the transmission coeffciients; recently Moldauer /41/ found the following representation:

$$\nu_c(T_c, \Sigma T_c) = 1.78 + (T_c^{1.212} - \phi.78)e^{-\Sigma T_c} \quad . \qquad (4.3.)$$

The two preceeding formulae are based on Moldauer's "M-cancellatic principle" which is discussed in detail in refs. /6/, /40/. For weak absorption ($T_c << 1$) equs. (4.2.) and (4.3.) reduce to the "width-fluctuation-corrected Hauser-Feshbach formula"/42/ which ca be derived for isolated resonances ($<\Gamma>/D << 1$) from equ. (2.3.) unde the assumption of uncorrelated partial width distributed according to the law of Porter and Thomas /43/ (i.e. $\nu_c = 1$!). In the gener case equs. (4.2.) and (4.3.) are verified by computer experiments based on unitary S-matrices constructed according to the statistic theory of spectra; no analytic derivation exists.

Various properties of the width fluctuation correction factor W_{ab} in equ. (4.2.) are discussed by Gruppelaar et al. /44/ and Reffo et al. /45/.

The M-cancellation principle can also be used to evaluate averages of the follwing type

$$<S^{fl}_{aa}\, S^{fl*}_{bb}> = \sqrt{\left(\frac{2}{\nu_a} - 1\right)\left(\frac{2}{\nu_b} - 1\right)}\; <|S_{ab}|^2> \qquad (4.4.)$$

$$<S^{fl}_{ab}\, S^{*fl}_{cd}> = 0 \text{ unless to pairs of indices coincide.} \qquad (4.5.)$$

These expressions are e.g. required for the calculation of average differential cross sections. Note that due to equ. (4.5.) average differential cross sections for compound nucleus reactions are symmetric about 90^o.

A different method to calculate average cross sections was developed by Hofmann, Tepel, Richert and Weidenmüller. This HRTW-approach is described in detail in refs. /46/ and /47/. Under the assumption of a diagonal average S-matrix the results of computer experiments are fitted by the following expression:

$$<\sigma^{fl}_{ab}> = \frac{V_a V_b}{\Sigma V_c}\,(1 + \delta_{ab}\,(W_{aa} - 1)) \qquad (4.6.)$$

which accounts for factorisation and elastic enhancement. The unitary condition (2.2.) relates the V_c to the channel transmissic coefficient by

$$T_a = V_a + \frac{V_a^2}{\Sigma V_c}\,(W_{aa} - 1)\,. \qquad (4.7.)$$

This relation can be solved for the V_c by iteration. A convenient formula for the enhancement factor W_{aa} in terms of the channel transmission coefficients was found as well as for $<S^{fl}_{aa}\, S^{*fl}_{bb}>$ (see ref. /47/).

Numerical studies have shown that in general the agreement between the HRTW-approach and the M-cancellation scheme is very goo Some exceptions were discussed by Moldauer /48/. In the limit of strong absorption both methods give essentially the Hauser-Feshbach formula with a compound elastic enhancement by a factor of 2:

$$<\sigma^{fl}_{ab}> \sim (1 + \delta_{ab})\,\frac{T_a T_b}{\Sigma T_c}\,. \qquad (4.8.)$$

Experimental evidence of compound elastic enhancement of this magni tude has been given by Kretschmer et al. /49/.

Both methods hold for the case of diagonal average S-matrix. Engelbrecht and Weidenmüller /50/ found a way to transform a proble with direct reactions to the previously considered case. The Engelbrecht-Weidenmüller transformation is the unitary transformation U that diagonalizes the penetration matrix P_{ab} defined in equ. (2.6.)

$$(U\,P\,U^+)_{ab} = T_a'\,\delta_{ab} \qquad , \; 0 \le T_a' \le 1. \qquad (4.9.)$$

By means of U and its transposed U^T one constructs a transformed scattering matrix $S' = U\,S\,U^T$ with diagonal average. Further, S' ha the same statistical properties as the S-matrix in absence of direc reactions. Hence the average of bilinear expressions in S' can be evaluated in terms of the eigenvalues T_a' of the matrix P by means of the M-cancellation scheme or the HRTW-approach.

As discussed by Moldauer /51/ direct reactions between channel a and b cause an enhancement of the fluctuating cross section. This effect may be of the same order as the elastic enhancement if there are just two channels strongly coupled by direct reactions. For three or more coupled channels the enhancement is in general not very significant.

The theory described so far is restricted to binary reactions. It is extended to multiple particle emission by assuming that the particles are emitted sequentially and that for any intermediate nucleus the branching ratio for decay in channel d is given in term of the transmission coefficients by $T_d/\Sigma T_c$ as suggested by the simp lest version of the Hauser-Feshbach formula equ. (4.1.). In a very schematic way one may represent cross sections for reactions with two or three emitted particles as

$$<\sigma^{CN}_{abc}> = <\sigma^{CN}_{ab}>\frac{T_c}{\Sigma T_c}\,, \quad <\sigma_{abcd}> = <\sigma^{CN}_{abc}>\frac{T_d}{\Sigma T_c}\,. \qquad (4.10.)$$

Similar expressions are used for the treatment of gamma-ray cascade /52/. Calculations based on equ. (4.10.) under consideration of angular momentum and parity conservation are referred to as multi-step Hauser-Feshbach calculations (m.s. HF). To save time one may use instead multi-step Weisskopf-Ewing calculations (m.s. WE) /53/ which neglect angular momentum and parity.

This section is concluded with some remarks on the most important model parameters and auxiliary quantities.

The level density which describes the excited states of the residual nuclei at higher excitation energies is of crucial importance. Most codes employ phenomenological models the most popula being the Gilbert-Cameron model /54/ and the back-shifted Fermi gas model /55/. Both models use parameters which are adjusted to reproduce information on resonances and low lying levels and assume the same density for both parities. Reffo /56/ improved the Gilbert-Cameron model in the low energy region by deriving the parity dependence and a more realistic spin cut-off factor from level data; these improvements are incorporated into the codes CERBERO and ERINNI listed in table 1.

The above mentioned phenomenological models do not account for the effects of shell structure and pairing on the energy dependence of the level density. These deficiencies may be overcome by a "microscopic" calculation of the level density based on the BCS model and on realistic single particle states /57/. A recent comparison of such calculations with experimental s-wave resonance spacings was reported by Benzi et al. /58/. So far microscopic level density calculations are not used for routine calculations of cross section.

In the past few years new semi-empirical level density formulae were proposed by Kataria and Ramamurthy /59/, Jensen /60/ and by Ignatyuk et al. /61/. These formulae parametrize shell effects in terms of the shell correction to the nuclear ground state mass. The latter two approaches also account for pairing. I believe that due to its simplicity this type of parametrization is extremely useful for applications. Furthermore it provides a better basis for extrapolations to higher energies and to nuclei with no resonance data than the two phenomenological models mentioned before.

While the transmission coefficients for particles are provided by the optical model additional assumptions are required for those of other decay modes.

Gamma-ray transmission coefficients $T_{XL}(\varepsilon_\gamma)$ of multipole type and for energy ε_γ are related to the gamma-ray strength function $f_{\gamma XL}(\varepsilon_\gamma)$ by $T_{XL}(\varepsilon_\gamma) = 2\pi\, \varepsilon_\gamma^{2L+1} f_{\gamma XL}(\varepsilon_\gamma)$. Two models for the strength functions are generally used. The Weisskopf model /62/ assumes the strength function to be energy independent while the Brink-Axel model relates it to the gamma-ray absorption cross section. Often the transmission coefficients are normalized so as to reproduce $\langle\Gamma_\gamma\rangle/D$, the ratio of the average radiation width $\langle\Gamma_\gamma\rangle$ and average spacing D of s-wave neutron resonances. If information on $\langle\Gamma_\gamma\rangle/D$ is lacking the use of systematics for this quantity may lead to considerable errors in particular near closed shells. Gardner et al. /64/ reduced these difficulties by developing systematics for E1 and M1 strength functions (the most important ones) in a limited Z-A range. The E1-strength function is related to the giant dipole resonance while for $f_{\gamma M1}(\varepsilon_\gamma)$ the Weisskopf model is used. As the normalization of the strength functions varies slowly between neighbouring nuclei it can be found by fitting low energy capture cross sections. The resulting strength functions can be used in this Z,A range to calculate $T_{E1}(\varepsilon_\gamma)$ and $T_{M1}(\varepsilon_\gamma)$ for nuclei with no capture data. Fig. 2 illustrates that the capture cross sections of ^{85}Rb and ^{87}Rb though differing by a factor of 10 can be reproduced with the same E1-strength function.

The transmission coefficients for fission are related to the transition states at saddle point deformation /65/. For a single humped fission barrier of parabolic shape with height E_f and curvature $\hbar\omega$ the penetrability P(E) is given by the Hill-Wheeler formula /66/

$$P(E) = \{1 + \exp[\tfrac{2\pi}{\hbar\omega}(E_f - E)]\}^{-1}. \qquad (4.11.)$$

The total fission transmission coefficient $T(E,J,\Pi)$ for compound nucleus states with excitation energy E, spin J and parity Π is the sum of the contributions of all transition states with quantum number $J\Pi$.

$$T_f(E,J,\Pi) = \int_0^\infty dE'\ \rho_f(E',J,\Pi)\ \{1 + \exp[\tfrac{2\pi}{\hbar\omega}(E'-E)]\}^{-1}, \qquad (4.12.)$$

where $\rho_f(E',J,\Pi)$ is the density of transition states.

For a double humped fission barrier the follwoing consequences of the secondary minimum have to be considered:

i) Damping in the second well: Interaction of the fission mode with internal degrees of freedom excites compound nucleus states in the second well. Fission decay of these states provide an "indirect" contribution to fission in addition to the "direct" contribution.

ii) Intermediate class II structure: Coupling of compound nucleus states in the first well (class I-states) and those in the second well (class II-states) enhances the indirect fission contribution for energies near a class-II state. This intermedia structure in fission cross sections is of importance mainly for sub-barrier fission.

Back et al. /67/ formulated a model which allows for all these effects. Of special interest is the limit of complete damping (no direct fission contribution) and smeared out class-II structure which is realized at higher incident energies. In that case the total fission transmission coefficient is given by

$$T_f(E,J,\Pi) = \frac{T_f^A(U,J,\Pi)\,T_f^B(U,J,\Pi)}{T_f^A(U,J,\Pi) + T_f^B(U,J,\Pi)}, \qquad (4.13.)$$

where T_f^A and T_f^B refer to the inner and the outer barrier respectively and are calculated as in equ. (4.12.). As described in ref. /52/, the model of Back et al. /67/ is incorporated into the code STAPRE (see section 5.2.).

The parametrization of fission is by no means simple nor unique. Recent reviews of interest for the calculation of fission cross sections are quoted in refs. /68/ - /73/. Furthermore fission is treated in detail in three lectures in this course.

4.2. Computer Codes

Some of the codes listed in table 1 compute also cross sections for statistical compound nucleus reactions.

ERINNI which is designed for higher incident energies uses the original Hauser-Feshbach formula equ. (4.1.). All other codes of table 1 correct for width fluctuation and elastic enhancement under the assumption of no direct reactions $\langle S_{ab} \rangle = \delta_{ab} \langle S_{aa} \rangle$. While PELINSCA employs the HRTW-approach the others rely on Moldauer's formalism. Some of them (ELIESE-3 and COMNUC) use a somewhat older formulation which was proposed in 1964 /74/. The most recent version of the M-cancellation principle is incorporated in Moldauer's ABAREX code mentioned in section 3.2.

As far as I know there exists only one code which calculates the average fluctuating cross section under consideration of direct reactions. This is Moldauer's program JUSTSO /37/ which incorporates the JUPITOR code to generate the penetration matrix. However, JUSTSO is not yet available for general distribution.

While most codes of table 1 are restricted to binary reactions ERINNI and COMNUC are multi-step Hauser-Feshbach codes. At the Lawrence Livermore Laboratory an extended version of COMNUC is used which includes charged particle emission. The Los Alamos version of COMNUC was recently improved by Arthur /75/ by incorporating a double humped fission barrier in the frame of the model of Back et al. /67/ and by updating the calculation of the width fluctuation correction.

All the codes mentioned so far do not account for preequilibriu emission. Thus their results are not very reliable at higher incident energies when this mechanism becomes important. This also applies to the m.s. HF codes ERINNI and COMNUC which in principle could be used for higher incident energies. All considerations of section 4.1., however, are also relevant to those m.s. HF codes which in addition to compound nucleus reaction consider preequilibri decay (see section 5.2.).

5. Preequilibrium reactions

This section is devoted to the description of computer codes which account for preequilibrium and equilibrium reactions. As the more sophisticated theories of preequilibrium decay and the associated codes are subject of other lectures of this course I will restrict the discussion to programs which employ relatively simple phenomenological models. So far, these are the models commonly used in nuclear data evaluation. A list of representative codes of this type which are extensively used for the evaluation of neutron induced reaction data is presented in table 2. Some features of the underlying models which are required to characterize these codes are reviewed in the next section.

Due to shortage of time these lectures do not deal with codes based on the intranuclear cascade model which in general are used at rather high energies of at least several tens of MeV. However, it should at least be mentioned that Alsmiller et al /76/ recently applied this model to the calculation of (n,n') double differential cross sections between 14.9 and 60 MeV and that Alsmiller et al. /77 included the fission process into the intranuclear cascade model code developed at the ORNL.

5.1. Phenomenological preequilibrium models

All cross sections considered in the following are average cross sections. Hence the symbol < > is omitted. The codes referred to are listed in table 2 and further described in section (5.2.).

5.1.1. The exciton model

The exciton model was suggested by Griffin /78/ in 1966. In this model the states of the system are characterized by the excitation energy E and the numbers p of excited particles and h of excited holes. Particles and holes are defined with respect to a closed shell reference state and are called excitons. The exciton number is given by $n = p + h$.

Starting from a simple particle hole configuration the composit system is assumed to equilibrate through a series of two body interactions and to emit particles from all intermediate states. Two body interactions may change the exciton number by an amount of +2, 0 or -2; the respective average rates are: $\lambda_+(n,E)$, $\lambda_0(n,E)$ and $\lambda_-(n,E)$. The equilibration of the system is described by a version of the Pauli master equation of quantum statistics for the dependenc on time t of the population probabilities q(n,t) of configurations with n excitons and excitation energy E /79/, /80/:

$$\frac{dq(n,t)}{dt} = \lambda_+(n-2)q(n-2,t)+\lambda_-(n+2)q(n+2,t)-q(n,t)(\lambda_+(n)+\lambda_-(n)+L(n)). \qquad (5.1.)$$

The quantity L(n) in the loss term accounts for particle emission an is given in terms of the average rates $W_\beta(p,h,E,\varepsilon_\beta)$ for emission of particle β with channel energy ε_β from states with p particles and h holes

$$L(n) = L(p,h,E) = \sum_\beta \int_0^{\varepsilon_{\beta max}} d\varepsilon_\beta W_\beta(p,h,E,\varepsilon_\beta).$$

This master equation was justified by Agassi et al. /9/ in the frame of the statistical theory of nuclear reactions in connection with a random matrix model for the nuclear Hamiltonian.

The initial conditions for the master equation $q(n,t=0) = \delta_{nn_0}$ depends on the projectile type. For nucleon induced reaction the commonly used inital condition is $n_0 = 3$ corresponding to $p_0 = 2$ and $h_0 = 1$.

In matrix form equ. (5.1.) reads

$$\frac{d}{dt}\, q(t) = A.\vec{q}(t)\,, \qquad (5.1'.)$$

where $\vec{q}(t)$ is the vector with the components $q(n,t)$ and A is a tri-diagonal matrix.

The master equation represents a system of coupled linear differential equations which can be solved either numerically by a finite difference method /79/, /80/ or more elegantly in terms of the eigenvalues and eigenvectors of the matrix A /81/, /82/.

The angle integrated spectrum of particle β is obtained in terms of the absorption cross section of the projectile σ_α^c and the particle emission rates $W_\beta(n,E,\varepsilon_\beta)$

$$\frac{d\sigma_{\alpha\beta}}{d\varepsilon_\beta}(\varepsilon_\beta) = \sigma_\alpha^c \sum_n \int_o^\infty dtq(n,t)W_\beta(n,E,\varepsilon_\beta) = \sigma_\alpha^c \sum_n (-\vec{Aq}(0))_n W_\beta(n,E,\varepsilon_\beta), \qquad (5.2.)$$

where the relation $q(n,\infty) = 0$ has been used. The master equation is supposed to describe the equilibrated system, too. Hence the spectrum given by equ. (5.2.) contains the preequilibrium and the equilibrium contributions as well. The codes AMALTEE and PREANG employ equ. (5.2 to calculate the total emission spectrum.

The preequilibrium contribution to the spectrum is given by

$$\frac{d\sigma_{\alpha\beta}}{d\varepsilon_\beta}(\varepsilon_\beta) = \sigma_\alpha^c \sum_n \int_o^{t_{eq}} dtq(n,t)W_\beta(n,E,\varepsilon_\beta), \qquad (5.3.)$$

where t_{eq} is the time at which the system has reached a (partial) equilibrium. The codes GNASH, HAUSER-5, PRECO-A/B and STAPRE use the master equation to derive the preequilirbium contribution according to equ. (5.3.) and add an equilibrium contribution $\frac{d\sigma_{\alpha\beta}^{eq}}{d\varepsilon_\beta}$ which is corrected for depletion by preequilibrium decay:

$$\frac{d\sigma_{\alpha\beta}}{d\varepsilon_\beta} = \frac{d\sigma_{\alpha\beta}^{pre}}{d\varepsilon_\beta} + \frac{d\sigma_{\alpha\beta}^{eq}}{d\varepsilon_\beta}\,. \qquad (5.4.)$$

Most of these codes account for conservation of angular momentum J and parity Π and assume for the preequilibrium portion the same JΠ-distribution in the residual nuclei as given by the compound nucleus model. So, the equilibrium contribution has to be calculated in any case.

The master equation (5.2.) depends on time as a continuous variable. The equilibration process can be described also by means of a discrete variable M which represents the number of internal transitions after the formation of the composite system. The corresponding master equation for the population probability reads

$$q(n,M) = \frac{\lambda_+(n-2)}{\lambda(n-2)}\, q(n-2,M-1) + \frac{\lambda_o(n)}{\lambda(n)}\, q(n,M-1) + \frac{\lambda_-(n+2)}{\lambda(n+2)}\, q(n+2,M-1)\,,$$

$$\lambda(n) = \lambda_+(n) + \lambda_o(n) + \lambda_-(n) + L(n). \qquad (5.5.)$$

The spectrum of emitted particles is given by

$$\frac{d\sigma_{\alpha\beta}}{d\varepsilon_\beta} = \sigma_\alpha^c \sum_n \Big[\sum_{M=0}^{\infty} q(n,M)\lambda^{-1}(n)\Big]\, W_\beta(n,E,\varepsilon_\beta)\,. \qquad (5.6.)$$

These equations are used in the code STAPRE /52/ to calculate the preequilibrium contribution of the spectrum $\frac{d\sigma_{\alpha\beta}}{d\varepsilon_\beta}$ (the M-sum in equ. (5.6.) extends up to a suitably chosen value M_{eq}).

Recently Ackermans et al. /83/ studied the properties of equs. (5.5.) and (5.6.) in great detail and extended them to the calculations of angular distributions by applying the model of Mantzouranis et al. /84/ and to the treatment of multiparticle preequilibrium emission. The authors of ref. /83/ pointed out that equs. (5.5.) and (5.6.) describe the equilibration process as "random walk" in particle hole space and showed that the resulting particle emission spectra agree with those from equs. (5.1.) and (5.2.) Another stochastic preequilibrium model was proposed by Gudima et al. /85/.

Closed form expressions for the preequilibrium emission spectra result from the "random walk equations" (5.5.) and (5.6.) by neglecting the rates $\lambda_-(n)$ and $\lambda_o(n)$:

$$\frac{d\sigma_{\alpha\beta}^{pre}}{d\varepsilon_\beta} = \sigma_\alpha^c \sum_n^{\bar{n}} D_n \frac{W_\beta(n,E,\varepsilon_\beta)}{\lambda_+(n)+L(n)}, \qquad (5.7.)$$

where the "depletion factors" D_n are given by

$$D_n = \prod_{r=n_o+2}^{n} \frac{\lambda_+(\nu)}{\lambda_+(\nu)+L(\nu)}\,, \quad D_{n_o} = 1, \qquad (5.8.)$$

and $\bar{n} \sim \sqrt{2gE}$ represents the most probable exciton number at equilibrium which depends on the single particle state density g of the composite system.

Before applying the model the rates $\lambda_{\Delta n}(n) \equiv (\lambda_+(n),\lambda_o(n),\lambda_-(n))$ for internal transitions and the particle emission rates $W_\beta(n,E,\varepsilon_\beta)$ have to be specified.

Two different approaches are used for the calculations of the internal transition rates. The first one relies on first order perturbation theory (Fermi's golden rule):

$$\lambda_{\Delta n}(p,h,E) = \frac{2\pi}{\hbar}\,|M|^2 \omega_{\Delta n}(p,h,E), \qquad (5.9.)$$

where $|M|^2$ is an average squared matrix element for residual interactions and $\omega_{\Delta n}(p,h,E)$ is the number of final states accessible by a two body interaction. The first formulae for $\omega_{\Delta n}(p,h,E)$ were derived by Williams /86/. The problem was reinvestigated by Obložinský et al /87/. An error in Willams' derivation was corrected and the Pauli principle was accounted for.
Most of the codes in table 2 employ for $\omega_{\Delta n}(p,h,E)$ the formulas of Obložinský et al. /87/ or the somewhat simpler expressions by Cline /88/. Both results assume equidistant single particle states. A very elegant method to calculate the density of final states accessible by a two body interaction for arbitrary single particle states was proposed by Dobeš et al. /89/, /90/.

By analysis of appropriate experimental data Kalbach /91/ found the following relation for the dependence of the average squared matrix element on mass number A and excitation energy E of the composite system

$$|M|^2(E) = K\, A^{-3}\, E^{-1} \quad , \qquad (5.10.)$$

where K is a constant which depends on the expression used for the particle emission rates; for $g = A/13$ and the particle emission rates proposed in ref. /92/: $K = 400\ MeV^3$.

A quite different approach to calculate the internal transition rates has been used by Gadioli et al. /93/. As the Milano group employs the closed form expressions (5.7.) and (5.8.) for the pre-equilibrium cross sections only the rates $\lambda_+(p,h,E)$ are considered. Gadioli et al. relate these rates to the average particle and hole collision probabilities $v\rho\sigma$ in nuclear matter, where v is the nucleon velocity, ρ the nuclear density and σ the average nucleon-nucleon cross section in nuclear environment. The resulting rates (see fig. 3a) are independent of the mass number. They are tabulated in ref. /94/. Their absolute values were adjusted to fit appropriate experimental data. Nowadays the Milano group particle hole creation rates are supported by the reproduction of a large amount of experimental data (see refs. /95/, /96/ and further references therein). However, the nucleon mean free path $\lambda^f = 1/\rho\sigma$ corresponding to these rates is considerably larger (by a factor of about four) than that deduced from the Fermi gas model and the free nucleon cross section. This problem is discussed in refs. /97/, /98/.

In order to reproduce Gadioli's /94/ particle hole creation rates Kalbach /99/ proposed a new energy and exciton number dependence for the average squared matrix element $|M|^2$ to be used in the golden rule expressions equ. (5.9.) instead of equ. (5.10.). Her new rate expression are used in the codes PRECO-B/D, GNASH and HAUSER-5. Fig. 3a shows a comparison of Gadioli's rates /94/ with the result of equ. (5.10.) and those of ref. /99/. Though the difference between the two rates used in connection with the golden rule expression is considerable for larger exciton numbers the effect on the cross sections is relatively small (see fig. 3b).

The simplest way to calculate the particle emission rates is to use detailed balance /80/. For the emission rates of particle ß consisting of π_β protons and ν_β neutrons with channel energy ε_β one obtains

$$W_\beta(p,h,E,\varepsilon_\beta) = \frac{2S_\beta + 1}{\pi^2\hbar^3}\,\mu_\beta\varepsilon_\beta\sigma_\beta^{inv}(\varepsilon_\beta)R_\beta(p)\frac{\omega(p-p_\beta,h,U)}{\omega(p,h,E)} \quad , \qquad (5.11.)$$

where S_β, μ_β, p_β and σ_β^{inv} are spin, reduced mass, nucleon number ($p_\beta = \pi_\beta + \nu_\beta$) and inverse cross section respectively. The quantities $\omega(p,h,E)$ and $\omega(p-p_\beta,h,U)$ are state densities for specified numbers of particles and holes; they refer to the composite system at excitation energy E and to the residual nucleus at excitation energy U. The inverse cross section $\sigma_\beta^{inv}(\varepsilon_\beta)$ is replaced by the optical model absorption cross section though there is no sound theoretical basis for doing so.

The factor $R_\beta(p)$ represents the probability that p_β emitted nucleons have the right combination of protons and neutrons. In principle the equilibration process should be treated under consideration of proton-neutron distinguishability. Though two component master equations were proposed /85/, /100/ the commonly used approximation is to apply one component equations as (5.1.) or (5.5.) and to calculate separately the quantity $R_\beta(p)$ which depends on the projectile. The method proposed by Kalbach-Cline /80/, /92/ is used by the codes PRECO-A/B/D, GNASH, HAUSER-5 and AMALTHEE while the correction developed by the Milano group /101/ is employed in their unnamed code described in ref. /94/ and in STAPRE. For nucleons in entrance and exit channel both methods give similar results. A special treatment of the neutron proton distinguishability is incorparated in Fu's code TNG1.

Most codes listed in table 2 use for the particle hole state density the formula of Williams /102/ which is based on equidistant single particle states with density g, or formulas of smilar structure which are, however, corrected for finite well depth /103/, /90/ and for long range deviations from the equidistant spacing model ($g(\varepsilon)\sim\sqrt{\varepsilon}$) /104/, /105/. The Milano group calculates the particle hole state densities for single particle states of a Fermi gas (with Fermi-energy $\varepsilon_F = 20$ MeV) by means of recursion formulas /93/ which account for finite well depth but not for the Pauli principle. Calculations of particle hole state densities for realistic shell model single particle levels have been reported by Williams et al /106/, Albrecht et al. /107/ and Grimes et al. /108/ but their results are, so far I know, not used in routine calculations. Applications of the exciton model often face the problem, how to correct the particle hole state densities for pairing /109/, /92/, /110/, /111/. Theoretical investigations on the calculation pf particle hole state densities in the frame of the BCS formalism have been reported by Ignatyuk et al. /112/ and by Moretto /113/.

Application of detailed balance for the calculation of the particle emission rates requires that all states of a given particle hole configuration are populated with equal probability. As the origin of such a quasi-equilibrium is not evident /114/ the following more general expression for the emission rates should be used /96/:

$$W_\beta(p,h,E,\varepsilon_\beta) = P_{ph}(E,\varepsilon_\beta + B_\beta)\ \lambda_\beta^c\ (\varepsilon_\beta)\ . \qquad (5.12.)$$

For a given particle hole configuration $P_{ph}(E,\varepsilon_\beta + B_\beta)$ represents the number of particles of type β times the probability density to find such a particle at energy $\varepsilon_\beta + B_\beta$ within the nucleus , where ε_β and B are the channel energy and the separation energy respectively. The second factor $\lambda^c(\varepsilon_\beta)$ is the rate for the escape into continuum of those particles and is calculated in terms of the inverse cross section $\sigma_\beta^{inv}(\varepsilon_\beta)$ as proposed by Harp et al. /115/:

$$\lambda_\beta^c(\varepsilon_\beta) = \frac{\sigma^{inv}(\varepsilon_\beta)v_\beta\omega_c(\varepsilon_\beta)}{g(\varepsilon_\beta + B_\beta)V} = \frac{1}{g(\varepsilon_\beta + B_\beta)}\ \frac{2\ S_\beta + 1}{\pi^2\hbar^3}\ \mu_\beta\varepsilon_\beta\sigma_\beta^{inv}(\varepsilon_\beta)\ . \qquad (5.13.)$$

Here v_β is the velocity in the continuum and $g(\varepsilon_\beta + B_\beta)$ and $\omega_c(\varepsilon_\beta)$ respectively represent the density of states of particle β inside the nucleus and in the normalisation volume V which represents the continuum.

By calculating the quantity $P_{ph}(E,\varepsilon_\beta + B_\beta)$ for nucleons on the basis of the nucleon-nucleon scattering Blann et al. /116/ showed that the rates resulting from equs. (5.12.) and (5.13.) esentially agree with those from equ. (5.11.). Thus the application of detailed balance for the nucleon emission rates is supported by the properties of the nucleon-nucleon cross section. This, however, is not true for the emission rates of composite particles. In fact while equ. (5.11.) reproduces quite well experimental data concerning nucleons the detailed balance rates considerably underpredict the emission spectra of clusters /92/ (see fig. 4).

Several methods to treat preequilibrium emission of clusters have been proposed. A substantial improvement of the description of (p,α) and (n,α) reactions was achieved by the model of preformed alpha particles by Milazzo-Colli et al. /117/. This model assumes that the projectile by interaction with preformed alpha particles excites [1 pN 1pα,1hα]-states in addition to [2pN,1hN]-states, where N stands for nucleon. Emission rates for nucleons and alpha-particles are calculated under the assumptions of equal population of all the states of the configurations [(m+1)pN, mhN] and [mpN 1pα, (m-1)hN 1hα]. These rates additionally depend on the probability to excite a [1pN 1pα, 1hα]state which is a free parameter. This model is incorporated in the codes STAPRE and TNG1. Recently the model of preformed alpha-particles has been refined by Ferrero et al. /118/ by including into the exciton model the ideas of the quasi-free scattering model of Blann and coworkers /119/, /120/. The free alpha-nucleon cross section was used to derive the quantity $P_{ph}(E,\varepsilon_\alpha + B_\alpha)$ in equ. (5.12.). By this improvement (p,α) spectra in a wide mass region and for incident energies much higher than with the original model could be described with few unique parameters; see also refs. /95/ and /96/ for further information. This improved model was also successfully applied to the calculation of angular distributions /96/ and to proton induced activation cross sections for ^{48,50}Ti for incident energies up to 85 MeV /121/.

A different approach to deal with cluster emission has been proposed by Kalbach /92/. In addition to a preequilibrium component calculated by means of the detailed balance emission rates equ. (5.11.) she considers contributions from direct reaction processes as pickup, stripping and in case of alpha-particles also knock out. These direct reaction contributions are not calculated in detail but by means of a simple statistical semi-empirical approach which is mainly based on phase space arguments and on consideration of the Coulomb barrier. Fig. 4 shows a comparison of the calculation with experimental data for ^{54}Fe+p at 29 and 62 MeV. The main contribution to the spectra of d, t, ^{3}He and alphas is provided by the pickup process. These semi-empirical direct reaction contributions are incorporated into the codes PRECO-B/D as well as into GNASH and HAUSER-5. The formulae for the direct reaction contributions given in the original paper have been improved in the mean time /122/.

Several efforts in the last years were devoted to the calculation of angular distributions. Mantzouranis et al. /84/ proposed the following generalization of the exciton model. The states of the equilibrating system are characterized in addition to the number of excited particles and holes by the direction Ω of the "fast particle" with respect to the incident direction. The fast particle is the carrier of the memory of the incident direction which is gradually lost by intranuclear collisions. The generalized master equation for the population probability q(n,Ω,t) reads

$$\frac{dq(n,\Omega,t)}{dt} = \sum_{\substack{m=n-2\\ \Delta m=2}}^{n+2} \int d\Omega' \lambda_{mn}(m;\Omega'\to\Omega)q(m,\Omega',t) - q(n,\Omega,t)\Big(\sum_{\substack{m=n-2\\ \Delta m=2}}^{n+2} \lambda_{nm}(n) - L(n,E)\Big), \qquad (5.14.)$$

In order to simplify the solution of these equations it is assumed that the rates $\lambda_{mn}(m,\Omega'\to\Omega)$ can be factorized into the usual internal transition rates $\lambda_{mn}(m)$ and an angle dependent part which is proportional to the free nucleon-nucleon cross section $\frac{\partial\sigma^f}{\partial\Omega'}(\Omega\to\Omega')$

$$\lambda_{mn}(m;\Omega'\to\Omega) = \lambda_{mn}(m)\Big[\int d\Omega \frac{\partial\sigma^f}{\partial\Omega'}\Big]^{-1}\frac{\partial\sigma^f}{\partial\Omega'}\ (\Omega'\to\Omega\ ). \qquad (5.15.)$$

The direction of the emitted particle is supposed to coincide with the direction of the fast particle. The double differential cross section is given by

$$\frac{\partial^2 \sigma_{\alpha\beta}}{\partial \varepsilon_\beta \partial \Omega_\beta} = \sigma_\alpha^c \int_0^\infty dt\, q(n,\Omega_\beta,t) w_\beta(n,E,\varepsilon_\beta). \qquad (5.16.)$$

The calculation of angular distributions in the code PREANG is based on this model. Algebraic solutions of equ. (5.14.) were discussed by Akkermans /123/. A closed form expression for the coefficients of a Legendre polynomial expansion of the double differential cross section was derived by Akkermans et al. /124/. This paper also contains a comparison with (n,n') data at 14.6 MeV and is discussed further in Dr. Strohmaiers lectures.

There exist several other theoretical approaches to deal with angular distributions. Besides the multistep direct reaction models discussed in other lectures of this course I should mention the work of Mädler et al. /125/ who introduced the total linear momentum as additional variable into the exciton model.

A phenomenological way to calculate angular distributions has been developed by Kalbach and Mann /126/. This work uses the concept of statistical multi-step direct (MSD) and statistical multi-step compound (MSC) reactions proposed by Feshbach et al. /11/, which is extensively discussed in Dr. Koonins lectures. Kalbach and Mann represent the double differential cross section in terms of Legendre polynomials and assume that to the odd order coefficients only MSD processes contribute. By analysis of experimental data surprisingly simple relations for the reduced Legendre coefficients were found. The code PRECO-D utilizes these results for the calculation of angular distributions. The extensions of the exciton model required to distinguish between MSD and MSC processes are described by Kalbach in ref. /127/.

5.1.2. The hybrid model

This model which was proposed in 1971 by M. Blann was the first simple preequilibrium model able to predict absolute cross sections.

The hybrid model is mainly concerned with nucleon emission and only this case will be considered in the following. The angle integrated emission spectra are given by the following expression

$$\frac{d\sigma_{\alpha\beta}}{d\varepsilon_\beta} = \sigma_\alpha^c \sum_{n=n_o}^{n} D_n P_{ph}(E,\varepsilon_\beta + B_\beta) \frac{\lambda^c(\varepsilon_\beta)}{\lambda^+(\varepsilon_\beta)+\lambda^c(\varepsilon_\beta)} =$$

$$= \sigma_\alpha^c \sum_{n=n_o}^{n} D_n \frac{p_\beta}{p} \frac{g(\varepsilon_\beta + B_\beta)\omega(p-1,h,U)}{\omega(p,h,E)} \cdot \frac{\lambda^c(\varepsilon_\beta)}{\lambda^+(\varepsilon_\beta)+\lambda^c(\varepsilon_\beta)} \cdot \qquad (5.17.)$$

Here, D_n is the depletion factor defined in equ. (5.8.). In the second step the quantity $P_{ph}(E,\varepsilon_\beta + B_\beta)$ defined below equ. (5.12.) is evaluated under the assumption of equal population probability; with p_β being the number of nucleons of type β the ratio p_β/p just accounts for proton-neutron distinguishability. While $\lambda^c(\varepsilon_\beta)$ is the emission rate for a nucleon of energy $\varepsilon_\beta + B_\beta$ inside the nucleus (see equ. (5.13.)) the quantity $\lambda^+(\varepsilon_\beta)$ represents for such a nucleon the rate to create a further particle hole pair. This rate was related to the mean nucleon free path λ^f in nuclear matter by $\lambda^+(\varepsilon_\beta) = v/\lambda^f(\varepsilon_\beta)$, where v is the velocity, or in later refinements of the model /129/ to the imaginary part of the optical potential W by $\lambda^+(\varepsilon_\beta) = 2W/\hbar$.

Though equ. (5.17.) superficially looks like the corresponding expression (5.7.) of the exciton model there is a substantial and much debated difference in bookkeeping between the two models as in the hybrid model the rates $\lambda^+(\varepsilon_\beta)$ refer to a nucleon at energy $\varepsilon_\beta + B_\beta$ inside the nucleus and not to the average decay rate of the states of a given exciton configuration /97/, /98/, /130/. Successful reproductions of (α,p) spectra were reported by Blann et al. /131/ and Chevarier et al. /132/. In order to improve the description of the high energy portion of (p,p') and (p,n) spectra the geometry-dependent hybrid model was developed by Blann /133/, /129/. This model accounts for nuclear geometry in a local density approximation. For each partial wave of the projectile the mean free path or the imaginary part of the optical model as well as the Fermi energy are averaged over the trajectory. Many applications of this model regarding (p,p') and (p,n) spectra /114/, /134/ as well as (n,n') spectra /135/ were reported.

Mantzouranis /136/ adapted the hybrid model for the calculation of angular distributions using the above described concept of the fast particle /84/.

The hybrid model and its geometry-dependent version are incorporated in Blann's widely used code ALICE.

A generalization of the hybrid model represents the quasi-free scattering model which was developed by Blann and coworkers and applied to (α,α'), (nucleon,α) and (α,nucleon) reactions /119/, /120/. In this model the quantity $P_{ph}(\varepsilon_\beta + B_\beta)$ in equ. (5.12.) for alphas and nucleons is evaluated on basis of the free nucleon-alpha and nucleon-nucleon elastic scattering cross section corrected for the Pauli principle.

Pertinent codes are MIEØØI, NALFA and QFS /137/.

5.1.3. Further developments

Recently Chiang and Hüfner proposed a new treatment of preequilibrium decay. Their "One, two, infinity approach" /138/ claims

that for nucleon induced reactions with nucleons in the exit channels the cross can be written as a sum of three terms

$$\frac{\partial^2\sigma}{\partial\varepsilon\,\partial\Omega} = \frac{\partial^2\sigma(1)}{\partial\varepsilon\,\partial\Omega} + \frac{\partial^2\sigma(2)}{\partial\varepsilon\,\partial\Omega} + \frac{\partial^2\sigma CN}{\partial\varepsilon\,\partial\Omega}\,, \qquad (5.18.)$$

where the first two correspond to single and double scattering, respectively, while the third represents the compound nucleus contribution. The single and double scattering cross sections are expressed in terms of the nucleon mean free path and the kinematics of projectile Fermi gas scattering by attractively simple formulas. Good overall reproduction of experimental data covering a wide range in mass numbers and excitation energies was achieved by use of a nucleon mean free path of the order of 3 to 5 fm, a value consistent with estimates based on the free nucleon-nucleon cross section. An extension of this model to the case of deuterons in the exit channel is reported in ref. /139/.

Most studies of preequilibrium decay refer to reactions with particles in the exit channels. Extensions of the precompound model to gamma-ray emission were reported by Plyuko et al. /140/ and by Běták et al. /141/. A successful application of the model of Běták et al. was recently reported by Basarragtscha et al. /142/.

These two improvements of the description of preequilibrium decay certainly should be considered in future developments of nuclear model codes for evaluation work.

5.2. Computer codes

Table 2 represents a compilation of widely used and generally available computer codes which account for preequilibrium and equilibrium decay as well.

Column 1 contains a superficial specification of the code and the information how to get the program. Most of these codes are distributed by the N.E.A. Data Bank Program Library. Others may be obtained by sending a blank tape to the author.

A short description of the underlying model assumptions in terms of the considerations of sections 4.1. and 5.1. is given in column 2. Codes which perform m.s. HF calculations require much more computation time than those relying on the m.s.W.E. approach. On the other hand angular momentum and parity conservation are essential for the calculation of cross sections near threshold where only a few levels with specific spin and parity contribute. Quantities as isomeric state populations or gamma-ray production spectra can be predicted only if a gamma-ray cascade model is used in connection with the m.s. HF formalism. Apart from Fu's TNG1 all programs employ a preequilibrium model which does not consider angular momentum and parity. The HF codes among them assume for the preequilibrium contribution the same spin parity distribution in the residual nucleus as for the equilibrium portion; this certainly is not an undisputed approximation. All codes which consider fission assume that preequilibrium decay preceeds fission without competition. Some codes accept direct reaction contributions as input and use them for the calculation of particle and gamma-ray production spectra.

Column 3 informs on the considered decay modes and on the complexity of the decay sequences which can be handled in one run. A further entry indicates whether the code has a built-in optical model part or whether externally calculated transmission coefficients are required as input.

The various types of cross sections which can be calculated are listed in the remaining columns.

Table 2 allows an easy comparison of the discussed codes. Some further information on each of them is presented in the following.

ALICE 80 is the most recent version of the ALICE codes and supersedes OVERLAID ALICE. This code is designed for incident energies up to 200 MeV and allows for very complicated decay sequences. Though the m.s. WE formalism is used an approximate treatment of angular momentum effects is provided for by means of the "s-wave approximation" /143/ which assumes the spin distribution of the compound nucleus to hold for all residual nuclei, too. The rotational energies at equilibrium and at saddle point deformation may be calculated from the rotating liquid drop model of Cohen et al. /144/.

In addition I would like to mention Blann's m.s. HF code MB-II /145/ which does similar calculations as ALICE-80 but without consideration of preequilibrium decay. A new version of this code /146/ is dubbed SUPERALERT and is designed mainly for heavy ion induced reactions; it includes many features specially important for high angular momenta.

AMALTHEE, in contrast to most of the other codes, considers second chance preequilibrium emission in the frame of the exciton model with master equations integrated from t=0 to t=∞. It is, however, assumed that the particle hole states of the residual nucleus do not undergo internal transitions but promptly decay by particle emission under consideration of gamma-ray competition. AMALTHEE allows a variety of different choices for particle-hole state densities and the various decay rates.

GNASH is the m.s. HF code developed by the Los Alamos group. In a single run this code handles decay sequences involving up to ten different nuclei each of which decays by emission of gamma rays, up to five different particles and eventually by fission. An example of such a decay sequence used for the calculation of neutron cross sections for energies up to 50 MeV is shown in fig. 5. A great flexibility in choosing the decay sequences is provided for. Among the m.s. HF codes discussed here GNASH handles the most complicated problems in one single calculation. Therefore the memory requirements of this code are considerable. The need of large core memory (LCM) depends on the considered case and can be reduced to 80 k words for a problem of reasonable size. Being designed mainly for high incident energies GNASH does not include the width fluctuation correction.

For lower incident energies the LASL group employs the COMNUC code mentioned in section 4. The treatment of fission in GNASH is based on a single humped barrier. E. Arthur plans to include a double humped barrier and to use the complete damping limit /75/.

HAUSER-5 is extensively used at the Hanford Engineering Development Laboratory. The first approximation of the HTRW-approach is employed for the equilibrium contribution. For the calculation of cross sections of tertiary reactions the branching ratios for the formation of the final nucleus by decay of the respective first residual nucleus have to be supplied as input. Up to 7 final nuclei may be populated by tertiary reactions.

PREANG is based on the codes PREQ by Běták /147/ and PREQ-ECN by Luider /81/ and is mainly used at the ECN, Petten. Recently Akkermans and Guppelaar /83/ reported on a code system PRANG which incorporates PREANG (actually a slightly modified version PREANG2). PRANG is designed to calculate multiple preequilibrium emission on the basis of the master equations without the approximation used in Bersillion's code AMALTHEE. The new code system requires a field length of 57 k words on a CDC-CYBER 175.

PRECO-D is the most recent version of the PRECO codes developed by C. Kalbach. Many experimental data were analysed by use of these codes. PRECO-B is incorporated into the m.s. HF codes GNASH and HAUSER-5. PRECO-D, in particular, has the capability to distinguish between MSD- and MSC contributions and to calculate angular distributions /126/. This code employs a closed from expression to describe equilibration while the two predecessors PRECO-A and PRECO.B rely on the master equation.

STAPRE is mainly used at the IRK, Vienna and at the Lawrence Livermore Laboratory. This code provides a flexible treatment of fission and allows for sequential emission of up to six particles and for gamma-ray cascades. However, in a single calculation STAPRE follows only one reaction path specified by a given sequence of emitted particles.So, for higher incident energies, when many paths contribute to production spectra and activation cross section computation time is wasted. Therefore we are developing in colaboration with D.G. Gardner from the Lawrence Livermore Laboratory a new code MAURINA which overcomes these deficiencies. For the considered end-products arbitrary regions in the Z,N plane can be selected. All paths which populate those nuclei are accounted for in a single run. Provision is made for a convenient combination of statistical equilibrium and preequilibrium contributions with the results of direct reaction codes. MAURINA can be operated under consideration of isospin. Though isospin effects are important only for projectiles with a proton excess analysis of such reactions often provides valuable information on model parameters for neutron reactions on instable target nuclei.

TNG1 is the most recent version of Fu's TNG code and was discussed in great detail at the 1980 Trieste Winter Course by the author /148/. The treatment of preequilibrium decay differs in several respects from that employed in the other codes discussed so far.

i) The master equation and proton neutron distinguishability are formulated in such a way that the compound nucleus evaporation formula results after equilibrium has been reached. C.Y. Fu plans to calculate in future the particle hole state densities on basis of BCS-formalism /149/.

ii) Conservation of angular momentum is introduced in a similar way as proposed by Obložinský et al. /150/ and by Plyuko /151/. The decomposition of detailed balance based emission rates into orbital angular momentum dependent contributions and the assumption that all spin states of the composite system are populated with equal probability lead to a cross section formula which represents a generalization of the Hauser-Feshbach formula.

iii) This analogy is used to calculate the angular distributions in terms of Legendre polynomials. Odd order coefficients which give rise to forward peaking result from averages of bilinear S-matrix terms of the type of equ. (4.5.) which are zero for the equilibrated system. Non vanishing averages are supposed to result from correlations in simple particle hole configurations and are evaluated in terms of an empirically determined weight factor which decreases with increasing hole number. A similar approach was proposed by Plyuko /146/.

Note that this description refers to the most recent version of the TNG-code which, as far as I know, is not yet available at the N.E.A. Program Library.

Table 2 does not represent a complete list of codes dealing with preequilibrium and equilibrium reactions. An important (unnamed) code which has been applied in numerous works of the Milano group is described in a paper by Gadioli et al. /94/. For the evaporation stage the m.s. WE formalism is applied by means of a Monte Carlo technique developed by Dostrovsky et al. /152/. For the preequilibrium contribution a closed form exciton model expression with consideration of 2nd chance emission is used.

Recently a very sophisticated m.s. HF code named PENELOPE has been developed at the C.N.E.N., Bologna by Reffo et al. /111/, /153/. The calculation of the preequilibrium contribution considers the conservation of angular momentum and the effect of pairing on the particle hole state densities.

6. Code intercomparisons

A powerful tool to test the proper working of codes consists in comparing the results of different programs /154/. As an example fig. 6 shows an intercomparison between the results of COMNUC (the Livermore version) and of STAPRE which was reported by Gardner at the 1980 Brookhaven Symposium /155/. The calculations do not include preequilibrium decay. As both codes use distinct integration tech- and treat cascades differently the agreement is gratifying; however it took some time until such an agreement was achieved.

An intercomparison of several mainly U.S. based m.s. HF codes was organized by A. Prince (BNL) and carried out by the Nuclear Model Codes Subcommitee of the Cross Section Evaluation Group (USA). These efforts proved to be very useful for the participating codes.

At present an international intercomparison of nuclear reaction model codes is being organized by E. Sartori from the N.E.A. Data Bank Program Library. After exercises referring to the optical and the statistical compound nucleus model a test case for preequilibrium model calculations is being worked out. I would like to recommend the participation at such code intercomparisons because in

this way the confidence in nuclear model calculations can be increased substantially.

I thank Dr. E.D. Arthur, Dr. O. Bersillon, Prof. M. Blann, Dr. C.Y. Fu and Prof. P.A. Moldauer for providing me with the most recent information on their codes and results. Further I would like to acknowledge Dr. E. Sartori for all his help regarding the codes available at the N.E.A. Data Bank Program Library.

References

/1/ J.J. Schmidt, Proc. Trieste Course on Nulcear Theory for Applications (1978), IAEA-SMR-43, p.1
/2/ S.E. Woosley, W.A. Fowler, J.A. Holmes and B.A. Zimmermann, Atomic and Nucl. Data Tables 22, 5 (1978) 371
/3/ A. Prince, Proc. Trieste Course on Nucl. Theory for Applications (1978), IAEA-SMR-43, p. 149, p. 231 and p. 305
/4/ J. Humblet and L. Rosenfeld, Nucl. Phys. 26 (1961) 529
/5/ T.A. Broody, J. Flores, J.B. French, P.A. Mello, A. Pendey and S.M. Wong, Revs. Mod. Phys. 53 (1981) 385
/6/ P.A. Moldauer, Proc. Trieste Course on Nuclear Theory for Applications (1978), IAEA-SMR-43, p. 165
/7/ G.R. Satchler, Phys. Lett. 7 (1963) 55
/8/ C. Mahaux and H.A. Weidenmüller, Ann. Rev. Nucl. Part. Sci. 29 (1979) 1
/9/ D. Agassi, H.A. Weidenmüller and G. Mantzouranis, Phys. Lett. C22 (1975) 145
/10/ V.E. Bunakov, Proc. Trieste Course on Nuclear Theory for Applications (1978), IAEA-SMR-43, p. 255
/11/ H. Feshbach, A.K. Kerman and S.E. Koonin, Ann. Phys. (N.Y.) 125 (1980) 429
/12/ W.A. Friedmann, M.S. Hussein, K.W. McVoy and P.A. Mello, Phys. Reports (Rev. Section of Physics Letters) 77 (1981) 47
/13/ D. Robson, Nuclear Spectroscopy and Reactions, ed. J. Cerny, part D (Academic Press, N.Y. and London, 1975) 179
/14/ C. Mahaux, Proc. Trieste Course on Nuclear Theory for Applications (1978), IAEA-SMR-43, p. 97
/15/ P.E. Hodgson, Nuclear Reactions and Nuclear Structure, Clarendon Press, Oxford 1971
/16/ F. Perey and B. Buck, Nucl. Phys. 32 (1962) 353
/17/ T. Tamura, Revs. Mod. Phys. 37 (1965) 679
/18/ V.A. Madsen, Nuclear Spectroscopy and Reactions, ed. J. Cerny, part D, Academic Press, N.Y. and London 1975, p. 249
/19/ J.P. Delaroche, Ch. Lagrange and J. Salvy, IAEA-190 (1976) Vol. I, p. 251
/20/ A.M. Lane and R.G. Thomas, Revs. Mod. Phys. 30 (1958) 257
/21/ C.Y. Fu, Atomic Data and Nuclear Data Tables 17 (1976) 127
/22/ E.D. Arthur and P.E. Young, Rept. LA-8626-MS (ENDF-304) (1980)
/23/ D. Wilmore and P.E. Hodgson, IAEA-190 (1976) Vol. II, p. 131
/24/ Ch. Lagrange, Proc. of the Specialists' Meeting on Neutron Cross Sections of Fission Product Nuclei, held at "E. Clementel" CNEN Centre Bologna, Italy, Dec. 12-14, 1979
/25/ A.M. Lane, Phys. Rev. Lett. 8 (1962) 8 and Nucl Phys. 35 (1962) 676
/26/ J.D. Anderson and H. Lutz, Rept. UCRL-14955 (1966)
/27/ J.D. Carlson, D.A. Lind and C.D. Zafiratos, Phys. Rev. Lett. 30 (1973) 99
/28/ D.M. Patterson, R.R. Doering and Aaron Galonsky, Nucl. Phys. A263 (1976) 261
/29/ L.F. Hansen, S.M. Grimes, B.A. Pohl, C.H. Poppe and C. Wong, Proc. of Symposium on Neutron Cross Sections from 10 to 50 MeV, held at BNL, Upton, N.Y., USA, May 12-14, 1980, Vol. II, p.781
/30/ G. Haouat, Proc. of the Second Int. Symp. on Neutron Induced Reactions, June 25-29, Smolenice, VEDA, Bratislava 1980, p. 333
/31/ V.A. Madsen, V.R. Brown and J.D. Anderson, Phys. Rev. Lett. 34 (1975) 1388, Phys. Rev. C12 (1975) 1209
/32/ V.R. Brown and V.R. Madsen, Phys. Rev. C11 (1975) 1298
/33/ A.M. Bernstein, V.R. Brown and V.A. Madsen , Phys. Lett. 103B (1981) 255
/34/ E. Sartori, Rept. NEANDC-A-136, 1981
/35/ J. Raynal, "Computing as a Language of Physics", IAEA-SMR-9/8 (1972)
/36/ O. Bersillon, Rept. CEA-N-227, NEANDC(FR)220 L , INDC(E) 49/L
/37/ P.A. Moldauer, priv. communication
/38/ H.A. Auerbach, Rept. BNL-6592 (1964)
/39/ W. Hauser and H. Feshbach, Phys. Rev. 87 (1952) 366
/40/ P.A. Moldauer, Phys. Rev. C11 (1975) 426
/41/ P.A. Moldauer, Nucl. Phys. A344 (1980) 185
/42/ A.M. Lane and J.E. Lynn, Proc. Phys. Soc. London LXX8-A (1957) 557
/43/ C.E. Porter and R.G. Thomas, Phys. Rev. 104 (1956) 483
/44/ H. Gruppelaar and G. Reffo, Nucl. Sci. Eng. 62 (1977) 756
/45/ G. Reffo and F. Fabbri, Nucl. Sci. Eng. 66 (1978) 251
/46/ J.W. Tepel, H.M. Hofmann and H.A. Weidenmüller, Phys. Lett. B49 (1974) 1
/47/ H.M. Hofmann, J. Richert, J.W. Tepel and H.A. Weidenmüller, Ann. Phys. N.Y. 90 (1975) 403
/48/ P.A. Moldauer, Phys. Rev. C14 (1976) 764
/49/ W. Kretschmer and M. Wangler, Phys. Rev. Lett. 41 (1978) 1224
/50/ C.A. Engelbrecht and H.A. Weidenmüller, Phys. Rev. C8 (1973) 859
/51/ P.A. Moldauer, Phys. Rev. C12 (1975) 744
/52/ B. Strohmaier and M. Uhl, Proc. Trieste Course on Nuclear Theory for Applications (1978), IAEA-SM-43, p. 313
/53/ V.F. Weisskopf and D.H. Ewing, Phys. Rev. 57 (1940) 472
/54/ A. Gilbert and A.G.W. Cameron, Can. J. Phys. 43 (1965) 1446
/55/ W. Dilg, W. Schantl, H. Vonach and M. Uhl, Nucl. Phys. A217 (1973) 269
/56/ G. Reffo, Proc. Trieste Course on Nuclear Theory for Applications (1978), IAEA-SM-43, p. 205 and Theory and Application of Moment Methods in Many Fermion Systems, ed. by B.J. Dalton, S.M. Grimes, J.P. Vary and S.A. Williams, Plenum, New York 1980, p. 167
/57/ L.G. Moretto, Nucl. Phys. A182 16972) 641 and Nucl. Phys. A185 (1972) 145
/58/ V. Benzi, G. Maino, E. Menapace and A. Ventura, Proc. of the Specialists' Meeting on Neutron Cross Sections of Fission Product Nuclei, Bologna, Italy, Dec. 12-14, 1979, ed. by C. Coceva and G.C. Panini, p. 215

/59/ S.K. Kataria, V.S. Ramamurthy and S.S. Kapoor, Phys. Rev. C18 (1978) 549
/60/ A.S. Jensen, Physica Scripta 17 (1978) 107
/61/ A.V. Ignatyuk, K.K. Istekov, and G.N. Smirenkin, Sov. J. Nucl. Phys. 29 (1979) 450
/62/ J.M. Blatt and V.F. Weisskopf, Theoretical Nuclear Physics, Wiley and Sons, New York, 1952
/63/ P. Axel, Phys. Rev. 126 (1962) 671
/64/ D.G. Gardner and M.A. Gardner, Proc. Int. Symposium on Neutron Capture Gamma-Ray Spectroscopy and Related Topics, Plenum Press, New York, 1979, p. 617
/65/ A. Bohr, Proc. Int. Conf. Peaceful Uses Atom. Energy, Geneva 1955, United Nations, New York, Vol. 2, p. 220
/66/ D.L. Hill and J.A. Wheeler, Phys. Rev. 89 (1953) 1102
/67/ B.B. Back, O. Hansen, H.C. Britt and J.D. Garrett, Phys. Rev. C9 (1974) 1924
/68/ J.E. Lynn, Proc. Trieste Course on Nuclear Theory for Applications (1978), IAEA-SMR-43, p. 353
/69/ H. Weigmann, Proc. Trieste Course on Nuclear Theory for Applications (1980), IAEA-SMR-68/1, p. 91
/70/ V.A. Konshin, Proc. Trieste Course on Nuclear Theory for Applications (1980), IAEA-SMR-68/1, p. 139
/71/ H.C. Britt, Proc. Symp. on Physics and Chemistry of Fission 1979, IAEA 1979, Vol. I, p. 3
/72/ S. Bjornholm and J.E. Lynn, Revs. Mod. Phys.52 (1980) 725
/73/ E.D. Arthur, Proc. of OECD/NEA-NDC Specialists' Meeting on Fast Neutron Scattering on Actihide Nuclei, Paris, France, 23-25 Nov. 1981
/74/ P.A. Moldauer, Phys. Rev. B135 (1964) 642
/75/ E.D. Arthur, private communication
/76/ R.G. Alsmiller, jr. and J. Barish, Nucl. Sci. Eng. 69 (1979) 378
/77/ F.S. Alsmiller, R.G. Alsmiller, jr., T.A. Gabriel, R.A. Lillie, and G. Barish, Nucl. Sci. Eng. 79 (1981) 147
/78/ J.J. Griffin, Phys. Lett. 17 (1966) 478 and 24B (1967) 5
/79/ C. Cline and M. Blann, Nucl. Phys. A172 (1971) 225
/80/ C.K. Cline, Nucl. Phys. A193 (1972) 417
/81/ F.L. Luider, Rept. ECN-17 (1977)
/82/ L. Faugere and O. Bersillon, Rept. NEANDC(E)184"L" (1977)
/83/ J.M. Akkermans and H. Gruppelaar, Z. Phys. A300 (1981) 345
/84/ G. Mantzouranis, D. Agassi and H.A. Weidenmüller, Phys. Lett. 57B (1975) 220 and Z. Phys. A276 (1976) 145
/85/ K.K. Gudima, G.A. Ososkov and G.A. Toneev, Sov. J. Nucl. Phys. 21 (1975) 138
/86/ F.C. Williams, jr., Phys. Lett. 31B (1970) 184
/87/ P. Obložinský, I. Ribanský and E. Beták, Nucl. Phys. A226 (1974) 347
/88/ C.K. Cline, Nucl. Phys. A195 (1972) 353
/89/ J. Dobeš and E. Beták, Nucl. Phys. A272 (1976) 353
/90/ E. Beták and J. Dobeš, Z. Phys. A279 (1976) 319
/91/ C. Kalbach-Cline, Nucl. Phys. A210 (1973) 590
/92/ C. Kalbach, Z. Phys. A283 (1977) 401
/93/ E. Gadioli, E. Gadioli Erba and P.G. Sona, Nucl. Phys. A217 (1973) 589
/94/ E. Gadioli, E. Gadioli Erba and J.J. Hogan, Phys. Rev. C16 (1977) 1404
/95/ E. Gadioli, E. Gadioli Erba and G. Tagliaferri, Proc. of the Second Int. Symp. on Neutron Induced Reactions, June 25-29, Smolenice, VEDA, Bratislava 1980, p. 165
/96/ E. Gadioli and E. Gadioli Erba, Proc. Trieste Course on Nuclear Theory for Applications (1980), IAEA-SMR-68/1, p. 3
/97/ M. Blann, Phys. Rev. C17 (1978) 1871
/98/ E. Gadioli, E. Gadioli Erba and G. Tagliaferri, Phys. Rev. C17 (1978) 2238
/99/ C. Kalbach, Z. Phys. A287 (1978)319
/100/ E. Beták and J. Dobeš, Acta Phys. Slov. 29 (1979) 76
/101/ C. Birattari, E. Gadioli, E. Gadioli Erba, A.M. Grassi Strini, G. Strini and G. Tagliaferri, Nucl. Phys. A201 (1973) 579
/102/ F.C. Williams, jr., Nucl. Phys. A166 (1971) 231
/103/ M. Blann, Phys. Rev. Lett. 28 (1972) 757
/104/ C. Kalbach, Phys. Rev. C23 (1981) 124
/105/ C. Kalbach, Phys. Rev. C24 (1981) 819
/106/ F.C. Williams, jr., A. Mignery and M. Blann, Nucl. Phys. A207 (1973) 619
/107/ K. Albrecht and M. Blann, Phys. Rev. C8 (1973) 1481
/108/ S.M. Grimes, J.D. Anderson, J.C. Davis and C. Wong, Phys. Rev. C8 (1973) 1770
/109/ S.M. Grimes, J.D. Anderson and C. Wong, Phys. Rev. C13 (1976) 2224
/110/ C.Y. Fu, Rept. ORNL/TM-7042 (1980)
/111/ J.M. Akkermans, H. Gruppelaar and G. Reffo, Phys. Rev. C22 (1980) 73
/112/ A.V. Ignatyuk and Yu.V. Sokolov, Sov. J. Nucl. Phys. 19 (1974) 628
/113/ L.G. Moretto, Nucl. Phys. A243 (1975) 77
/114/ M. Blann, R.R. Doering, Aaron Galonsky, D.M. Patterson and F.F. Serr, Nucl. Phys. A257 (1976) 15
/115/ G.D. Harp, J.M. Miller and B.J. Berne, Phys. Rev. 165 (1968)1166 and G.D. Harp and J.M. Miller, Phys. Rev. C3 (1971) 1847
/116/ M. Blann, A. Mignerey and W. Scobel, Nukleonika 21 (1976) 335
/117/ L. Milazzo Colli and G.M. Braga Marcazzan, Phys. Lett. B38 (1972) 155 and Nucl. Phys. A210 (1973) 297
/118/ A. Ferrero, E. Gadioli Erba, I. Iori, N. Molho and L. Zetta, Z. Phys. A293 (1979) 123
/119/ A. Mignerey, M. Blann and W. Scobel, Nucl. Phys. A273 (1976)125
/120/ W. Scobel, M. Blann and A. Mignerey, Nucl. Phys. A287 (1977)301
/121/ E. Gadioli, E. Gadioli Erba, J.J. Hogan and K.I. Burns, Z. Phys. A301 (1981) 289
/122/ C. Kalbach, informal report (PRECO-D) available from author
/123/ J.M. Akkermans, Phys. Lett. 82B (1979) 20
/124/ J.M. Akkermans, H. Gruppelaar and G. Reffo, Phys. Rev. C22 (1979) 73
/125/ P. Mädler and R. Reif, Nucl. Phys. A337 (1980) 445
/126/ C. Kalbach and F.M. Mann, Phys. Rev. C23 (1981) 112
/127/ C. Kalbach, Phys. Rev. C23 (1981) 124 and Phys. Rev. C24 (1981) 819
/128/ M. Blann, Phys. Rev. Lett. 27 (1971) 337; E1550

/129/ M. Blann, Nucl. Phys. A213 (1973) 570
/130/ J. Ernst and J. Rama Rao, Z. Phys. A281 (1977) 129
/131/ M. Blann and A. Mignerey, Nucl. Phys. A186 (1972) 245
/132/ A. Chevarier, N. Chevarier, A. Demeyer, A. Hollinger and Tran Minh Duc, Phys. Rev. C8 (1973) 2155
/133/ M. Blann, Phys. Rev. Lett. 28 (1972) 757
/134/ M. Blann, Ann. Rev. Nucl. Sci. 25 (1975) 123
/135/ H. Jahn, Proc. Trieste Course on Nuclear Theory for Applications (1978), IAEA-SMR-43, p. 293
/136/ G. Mantzouranis, Phys. Lett. 63B (1976) 25
/137/ M. Blann, A. Mignerey and W. Scobel, Universität Hamburg, Internal report, January 1978
/138/ H.C. Chiang and J. Hüfner, Nucl. Phys. A349 (1980) 466
/139/ F. Hackenberg, H.C. Chiang and J. Hüfner, Phys. Lett. 97B (1978) 253
/140/ V.A. Plyuko and G.A. Prokopets, Phys. Lett. 76B (1978) 253
/141/ E. Běták and D. Dobeš, Phys. Lett. 84B (1979) 368
/142/ B. Basarragtscha, D. Hermsdorf and E. Paffrath, J. Phys. G8 (1982) 275
/143/ M. Blann and G. Merkel, Phys. Rev. B137 (1965) 367
/144/ S. Cohen, F. Plasil and W.J. Swiatecki, Ann. Phys. (N.Y.) 82 (1974) 557
/145/ M. Blann, Phys. Rev. 157 (1967) 860
/146/ M. Blann, priv. communication
/147/ E. Běták, Comp. Phys. Comm. 9 (1975) 92 and 10 (1975) 71
/148/ C.Y. Fu, Proc. Trieste Course on Nuclear Theory for Applications (1980), IAEA-SMR-68/1, p. 35
/149/ C.Y. Fu, priv. communication
/150/ P. Obložinský and I. Ribanský, Nucl. Phys. A195 (1972) 269
/151/ V.A. Plyuko, Sov. J. Nucl. Phys. 27 (1978) 623
/152/ I. Dostrovsky, Z. Fraenkel and G. Friedlaender, Phys. Rev. 116 (1959) 683
/153/ G. Reffo and F. Fabbri in "Progress Report on Nuclear Data Activities in Italy for the period from January to December 1980", RIT/FIS/LDN (81) 10, NEANDC(E) 222
/154/ A. Prince, IAEA-190 (1976) Vol. I, p. 31
/155/ D.G. Gardner, Symp. on Neutron Cross sections from 10 to 50 MeV, held at BNL, Upton N.Y. USA, May 12-14 (1980), Vol. II, p. 641

Table 1: Some nuclear model codes based on the optical model and the equilibrium compound nucleus model (All these codes are available at the N.E.A. Nuclear Data Bank program library)

Code Author Specifications	Optical model	Equilibrium compound-nucleus model
CERBERO F.Fabbri et al. [1] Fortran IV, 240k bytes	spherical OP; local, non-local and local equivalent of non-local potential.	binary reactions; emission of n,p,α,γ; width fluctuation correction for continuum channels. improvments of Gilbert-Cameron level density at low excitation energies.
COMNUC/CASCADE C. Dunford [2] Fortran IV	spherical OP.	calculates cross sections for: (n,γ), (n,n'), (n,γn), (n,2n), (n,f) and (n,n'f). gamma-ray cascades. single humped fission barrier.
CRAPONE F.Fabbri et al. [3] Fortran IV	spherical OP; local, non-local and local equivalent of non-local potential. automatic search on total, differential elastic- and absorption cross sections as well as on s- and p-wave strength functions and scattering radius.	
DWUCK-4 P.D.Kunz (unpubl.) Fortran IV, 15k words	DWBA-method. transfer reactions and inelastic scattering, optionally deformed OP for inelastic scattering.	
ELIESE-3 S.Igarasi [4] Fortran IV, 332k bytes	spherical OP; local and non local potential, calculates polarisations for spin = 1/2 and 1 particles automatic search on differential elastic cross sections and polarisations.	binary reactions; all type of cross sections involving absorption and emission of n,p,d and α.
ERINNI F.Fabbri et al. [5] Fortran IV, 240 k bytes	spherical OP; local, non-local and local equivalent of non-local potential.	binary and tertiary reactions: (x,a), (x,ab) and (x,abc), where x can be n,p or α; (a,b) can be n,p,α or γ. and c can be n or γ.
JUPITOR-1 T.Tamura [6] Fortran IV, < 32k words	deformed OP; coupled channels method a variety of different coupling schemes for vibrational and rotational nuclei is provided fo..	
PELINSCA C.A. Engelbrecht et al. [7] Fortran IV, 208k bytes	spherical OP; calculates polarisations for spin 1/2 particles, automatic search on total-, differential elastic- and reaction cross section as well as on polarisation.	reactions of the type (a,b) and (a,bγ), differential and integrated cross sections for up to 33 levels of each residual nucleus, decay gamma angular correlations.

References for Table 1

[1] F.Fabbri, G.Fratamico and G.Reffo, Rept. RT/FI(74) 36 (1974) and Rept. RT/RI(77) 6 (1977)
[2] C.L.Dunford, Rept. AI-AEC-12931 (1970)
[3] F.Fabbri, G.Fratamico and G.Reffo, Rept. RT/FI(77) 3 (1977)
[4] S.Igarasi, Rept. JAERI 1224 (1972)
[5] F.Fabbri and G.Reffo, Rept. RT/FI(77) 4 (1977)
[6] T.Tamura, Rept. ORNL-4152 (1967)
[7] C.A.Engelbrecht, H.Fiedeldey and J.W.Tepel, Rept. PEL-202 (Oct. 1974)

Table 2: Nuclear model codes for preequilibrium and equilibrium emission.

Code Author Specifications Distribution	Models [1]	Restrictions decay modes successive decays optical model	Calculated quantities					
			$\frac{\partial\sigma^{2)}}{\partial\varepsilon}$	$\left(\frac{\partial\sigma}{\partial\varepsilon}\right)_\gamma$ [3]	$\frac{\partial^2\sigma}{\partial\varepsilon\partial\Omega}$ [4]	σ [5]	σ^m [6]	σ_f [7]
ALICE 80 M. Blann [1] Fortran, 180 k bytes distr.by Author [2]	HM and GDHM for 1st chance nucleon emiss.. m.s. WE, approx. treatment of ang. mom.. single humped ang. mom. dependent fission barrier.	n,p,d,α,f. Evaporation residues: Grid of 11 mass units wide and by 9 atomic numbers deep.	×			×		×
AMALTHEE O. Bersillon et al. [3] Fortran IV, 55k words distr. by N.E.A. Data Bank	EM, time integrated master equs. give preequ. - and equ. contr. approx. treatment of 2nd chance preequ. decay. no angular momentum effects.	n,p,d,t,^{3}He,α,(γ). binary and tertiary reactions. inv.cross.sections are input.	×					
GNASH P.G. Young et al. [4] Fortran IV, CDC-7600, 49k words SCM and 260k words LCM. distr. by N.E.A. Data Bank	EM for 1st chance particle emission + s.emp. DR, same ang. mom. distribution as equ. contr.. m.s. HF, no WFC, γ-ray cascades. single humped fission barrier. accepts DR input.	n,p,d,t,^{3}He,α,γ,f. 10 decaying nuclei (see text). transm. coeff. are input.	×	×		×	×	×
HAUSER-5 F.M. Mann [5] Fortran IV, 336k bytes. distr. by N.E.A. Data Bank	EM for 1st chance particle emission + s. emp. DR, same ang. mom. distribution as equ. contr.. m.s. HF. double humped fission barrier, complete damping. accepts DR input.	6 reaction pairs, γ and f included. binary and tertiary reactions.	×		×	×		×
PREANG J.M. Akkermans et al. [6] Fortran distr. by N.E.A. Data Bank.	EM generalized for ang. distributions by Mantzouranis et al.[7], time integrated master equations give preequ.- and equ. contribution. no angular momentum effects.	n,p,d,t,^{3}He,α. binary reactions only. (see text for recent extensions) inverse cross sections are input.	×		×			
PRECO-D C. Kalbach [8] Fortran	EM + s.emp. DR, MSC and MSD contribution. WE. single humped fission barrier. phenomon. angular distributions [11]. no angular momentum effects.	n,p,α,f + one arbitrary particle. binary reactions only. inverse cross sections are input.	×		×			×
STAPRE M. Uhl et al. [9] Fortran IV, 45k words distr. by N.E.A. Data Bank	EM for 1st chance particle emiss., same ang. mom. distr. as equ. contr.. m.s. HF, γ-ray cascades. double humped fission barrier, partial or complete damping.	n,p,d,α,γ,f. up to 6 emitted particles but one reaction path only. transm. coeff. are input.	×	×		×	×	×
TNG † C.Y. Fu [10] Fortran IV, 300k bytes distr. by N.E.A. Data Bank	EM for 1st chance particle emiss., considers ang. mom. conservation and accounts for angul. distrib. (see text). m.s. HF, γ-ray cascades. accepts DR input.	n,p,α,γ. up to 3 emitted particles.	×	×	×	×	×	

1) abbreviations:
HM ... hybrid model, GDHM ... geometry dependent hybrid model, EM ... exciton model.
WE ... Weisskopf-Ewing calculation, m.s.WE ... multi-step WE.
m.s. HF ... multi-step Hauser Feshbach calculation, WFC ... width fluctuation correction.
DR ... direct reaction, s. emp. DR ... semi-empirical DR contributions (C. Kalbach, Z.Phys. A283 (1977) 401).
2) particle production spectra, 3) gamma-ray spectra, 4) double differential cross section for particles,
5) activation or production cross section, 6) isomeric state production cross section, 7) fission cross section.

References for table 2

[1] M.Blann, Rept.COO-3494-29 (1975), Rept.UR-NSRL-181 (1978) and private communication
[2] M.Blann, L405, Lawrence Livermore National Laboratory, P.O.Box 808, Livermore, Ca. 94550
[3] O.Bersillon and L.Fangere, Rept. NEANDC(E) 191 "L" (1977)
[4] P.G. Young and E.D. Arthur, Rept. LA-6947 (1977)
[5] F.M.Mann, Rept. HEDL-TME 78-83 (1978)
[6] J.M.Akkermans and H.Gruppelaar, Rept. ECN-60 (1979)
[7] G.Mantzouranis, H.A.Weidenmüller and D.Agassi, Z.Phys. A276 (1976) 145
[8] C.Kalbach, "Preco-D" informal TUNL report available from author; Triangle Universities Nucl. Laboratory, Duke Station, Durham, North Carolina 27706, U.S.A.
[9] M.Uhl and B.Strohmaier, Rept. IRK-76/01 and addenda
[10] C.Y.Fu, Rept. ORNL/TM-7042.
[11] C.Kalbach and F.Mann, Phys.Rev. C23 (1981) 112

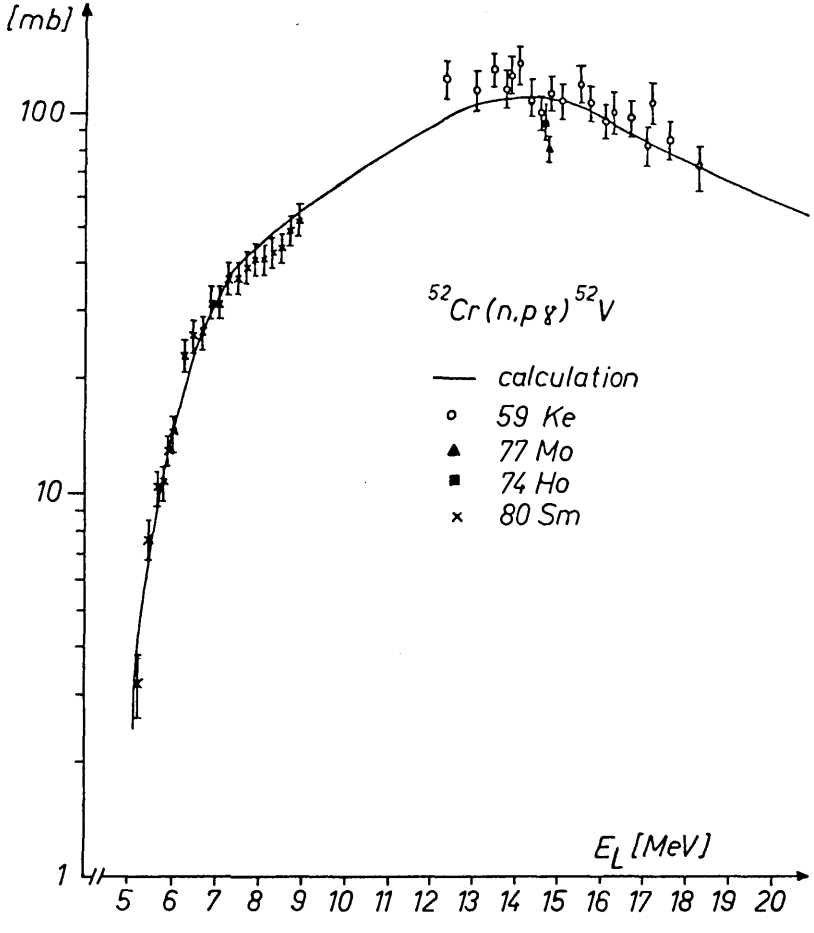

Fig. 1.
Calculated $^{52}Cr(n,p)$ cross sections and experimental data. The calculations can be used to fill the gap between 9 and 12 MeV in this excitation function.

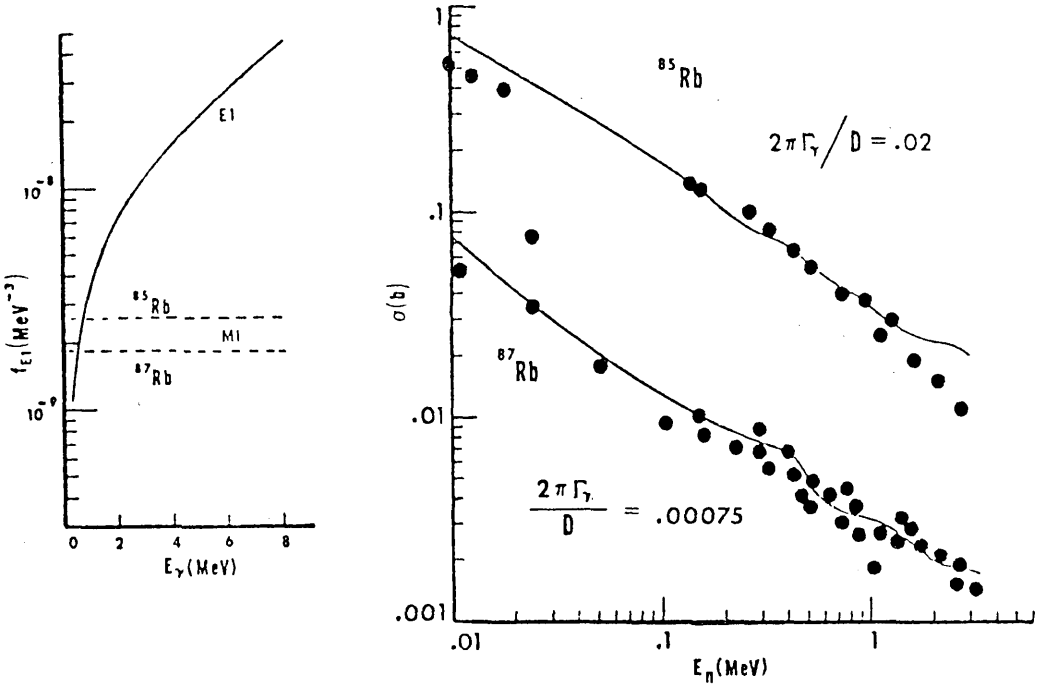

Fig. 2. from D.G. Gardner et al., UCID-18759 (1980)
Calculated $^{87,89}Rb(n,\gamma)$ cross sections (solid curves) and experimental data (points). Both cross sections are reproduced with the same E1-strength function (left hand insert).

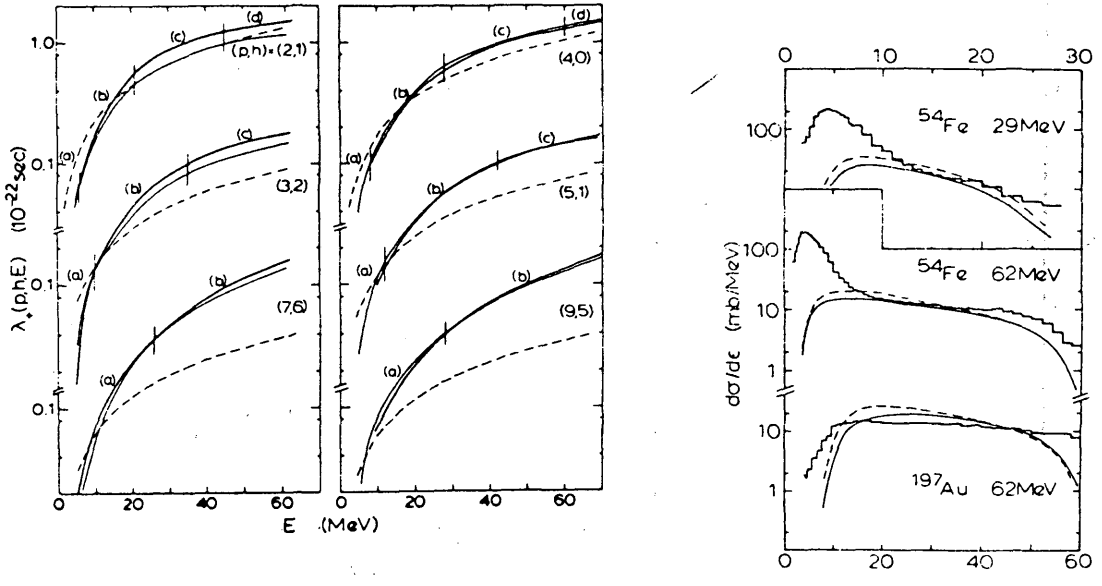

Fig. 3. (from ref. /99/)

a) Comparison of the Milano group particle hole creation rates /94/ (heavy solid curves) with predictions of the golden rule approach equ. (5.9.). The dashed lines result from equ. (5.10.) while for the thin solid curves Kalbach's /94/ exciton number dependent presciption for $|M|^2$ was used.

b) Cross sections resulting from the two presriptions for $|M|^2$. For the dashed curves equ. (5.10.) was used while the thin solid curves were obtained with Kalbach's new prescriptions. The bar graphs represent experimental data.

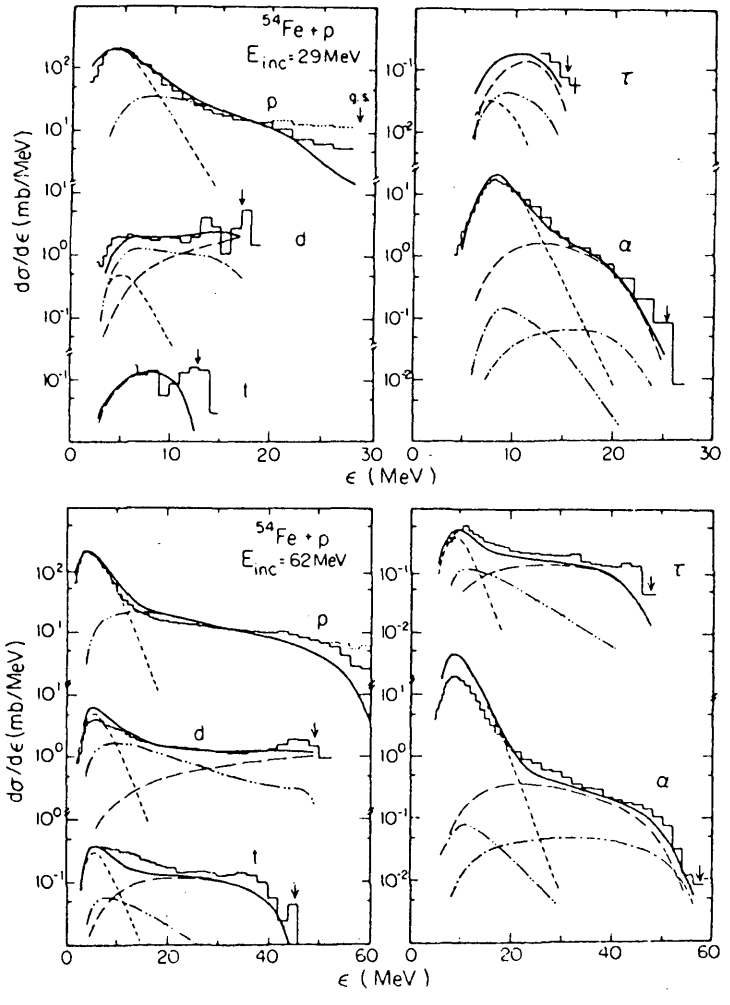

Fig. 4. (from ref. /92/

Comparison between calculated (solid curves) and experimental energy spectra (bar graphs) for the ^{54}Fe+p system. The calculations comprise the folowing contributions: equilibrium (short dash curves), preequilibrium (dash-double dot curves), pickup (long dash curves) and alpha knockout (dot-dash curves).

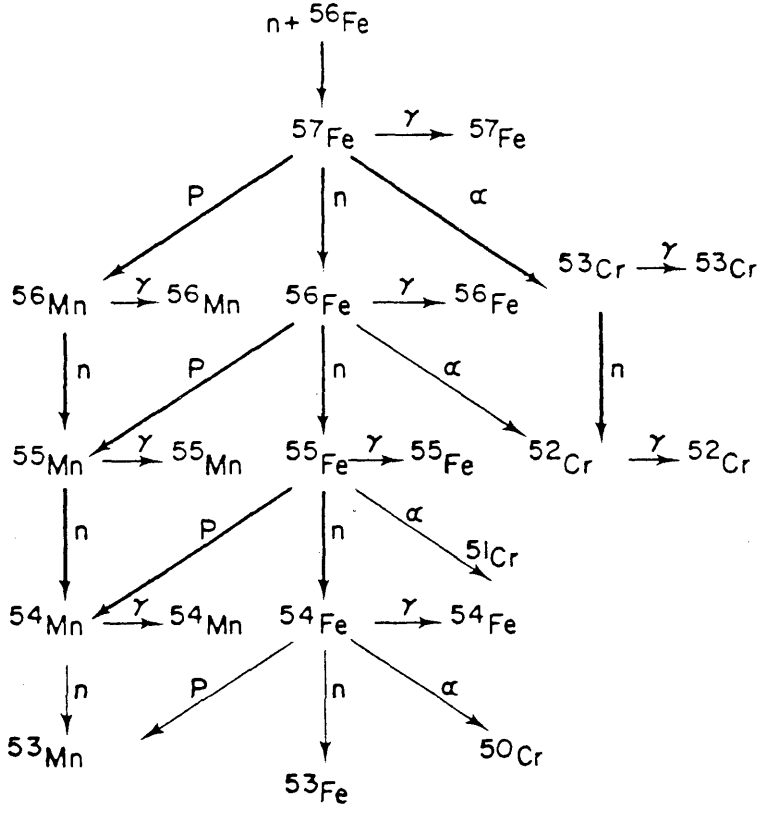

Fig. 5. (from ref. /22/)
An example for a reaction chain which the GNASH code handles in one run. The heavy arrows represent the considered reaction paths.

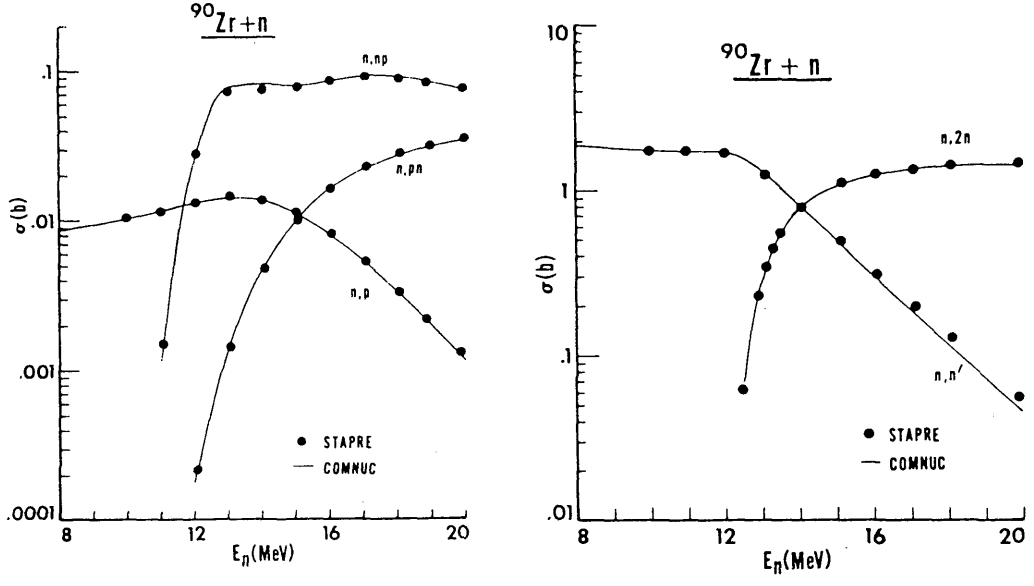

Fig. 6. (from ref. /155/)
Intercomparison of cross sections calculated with the codes COMNUC and STAPRE.

APPLICATION OF NUCLEAR MODEL COMPUTER CODES TO NUCLEAR DATA CALCULATIONS

B. STROHMAIER
Institut für Radiumforschung und Kernphysik,
University of Vienna,
Vienna, Austria

Abstract

This paper has been prepared in close correlation with the preceding one (M. Uhl: Recent advances in nuclear model computer code developments) and is intended to describe more practical aspects of nuclear model calculations, namely the dependence of their results on the choice of the input parameters as well as on the way of treating certain physical aspects. The topics are restricted mostly to the precompound and compound model description of nucleon or light complex particle induced reactions at incident energies of a few to tens of MeV. The work is based on recent publications in the field and, as far as existing, own experience. In particular, it treats attempts of including angular momentum conservation to preequilibrium calculations and describes various models for calculating preequilibrium angular distributions. The influence of optical potentials and of level densities on statistical model calculations is discussed. Further, the applicability of approximations, particularly in connection with width fluctuation and angular momentum conservation, is investigated. Finally, some more general examples of neutron nuclear data evaluation are presented.

Application of nuclear model computer codes to nuclear data calculations

B. Strohmaier
Institut für Radiumforschung und Kernphysik, Vienna, Austria

I. Introduction

Contents: practical aspects of nuclear model calculations:
- . dependence on input parameters
- . dependence on treatment of certain physical aspects

Reactions: nucleon or light complex particle induced, incident energy to tens of MeV

Models: preequilibrium (PE) and compound nucleus model (cf. ref. 1)

II. Angular momentum dependence of PE calculations

Relevance: spin distribution of the population of a nucleus by PE particle emission is important
- . itself, e.g. for isomeric cross section ratios
- . as starting condition for particle emission from this nucleus

Ways of treating angular momentum in PE calculations:

a) if PE formalism does not consider angular momentum: additional assumptions necessary, e.g.:
   - . same spin distribution of PE component as of Hauser-Feshbach (HF) component (used in STAPRE /2/)
   - . orbital angular momentum vectors of incident and outgoing particle parallel, impact parameter equal in incoming and outgoing channel (used by Scobel /3/).

   Example: fig. 1

b) spin dependent PE formalism:
   use of transmission coefficients and level densities under full consideration of angular momentum instead of orbital angular momentum independent inverse cross sections and spin independent state densities (Fu /4/).
   Example: fig. 2 of ref. 4.

III. Calculation of PE angular distributions

a) Generalized master equation for the time dependence of the occupation of excited states (Mantzouranis /5,6/).
   - . "concept of the fast particle"
   - . factorization of internal transition rates in angle and exciton number dependent part

   Matrix method for solution of generalized master equation (Akkermans, Gruppelaar, Luider /7-12/). Comparison to experimental data and parameter studies. Examples: figs. 5, 6 and 7 of ref. 9.

b) Consideration of forward peaking in PE stage by admitting odd Legendre coefficients with a weighting function that decreases with increasing number of collisions and thus describes the loss of correlation to the incident direction (Fu /4, 13/).
   Examples: fig. 2 of ref. 13.

c) Calculation of full dynamics (Gadioli /14/). Only emission from first configuration. Examples: figs. 8 and 9 of ref. 14.

d) Empirical formulae for coefficients of Legendre expansion of angular distributions (Kalbach, Mann /15, 16/). Examples: figs. 7, 8 and 9 of ref. 16 (part 1). Use of this approach and comparison to measurements:
   - ^{89}Y, ^{90}Zr, $^{92,94,95,96}Mo(n,\alpha)$, (n,p), at 15 MeV /17/ } bad agreement
   - $^{93}Nb(n,\alpha)$ at 14.1 MeV /18/, fig. 2

IV. Dependence of statistical model results on optical potentials and level densities

Parameter compilations contain individually determined values as well as prescriptions how to obtain the values from mass number globally. Individually adjusted parameters preferable, especially in the case of optical potentials in some mass regions, particularly when strength function maxima occur.

Examples:

- Calculation of neutron cross sections for ^{52}Cr, ^{55}Mn, ^{56}Fe, $^{58,60}Ni$ (Strohmaier, Uhl /19/). Use of α-particle optical potential by Huizenga /20/ required for reproduction of experimental (n,α) cross sections level density parameters which are inconsistent with resonance data. McFadden potential /21/ reproduces experimental (n,α) data (fig. 3) with level densities which are compatible with the resonance data. Also fair reproduction of α-spectra and (α,n) cross sections (figs. 4,5).
- Huizenga potential /20/ superior to the one by Bock /22/ in reproducing $^{64,66,68}Zn(p,\alpha)$ data at 15 MeV /23/ (fig. 3 of ref. 23). On the other hand, Bock potential /22/ had been obtained and verified by analysis of elastic α-particle scattering data beyond 16 MeV only.
- Importance of strength function maxima:

  Strength function: $\beta_l = \lim_{\varepsilon \to 0} S_l(\varepsilon) = \lim_{\varepsilon \to 0} \frac{T_l(\varepsilon)}{P_l(\varepsilon)}$

  (ε...energy, T_l...transmission coefficient, P_l...penetration factor)
  shows maxima for certain l-values in certain mass regions. Correspondingly, $S_l(\varepsilon)$ strongly varies with ε in such mass regions.

a) Transmission coefficients have to be generated by optical model calculations to sufficiently low energies, whereas they may be obtained by extrapolation in mass regions off strength function extrema. (Such an extrapolation is provided for in STAPRE /2/.)
   Example: $^{31}P(n,p)$ activation cross section (Strohmaier /24/) calculated with two sets of neutron T_l: generated by the optical model for all energies, and extrapolated according to $T_l(\varepsilon) = P_l(\varepsilon) * S_l$ (ε = 1 MeV) (fig. 6). With the latter set, the T_l are too small, not considering the p-wave strength function maximum at A = 30, and therefore the (n,p) cross section is overpredicted by underestimating the low-energy neutron competition.

b) Population cross sections for excited states may not be described properly if population occurs mainly by a partial wave whose strength function maximum is not accounted for by the used optical potential.
   Examples:
   . Vladuca et al. /25/ failed to reproduce experimental neutron inelastic scattering cross section in the A ∿ 90 region with global potentials which did not consider the peaking in the p-wave strength function but succeeded with a potential (Finckh /26/) which reproduced experimentally determined T_l
   . Total and nonelastic cross sections for ^{93}Nb+n are reproduced worse by global potentials than by such fitted to experimental cross section and resonance data in the A = 90 region (figs. 1 and 2 of ref. 27) and therefore such an individual potential (Delaroche, Lagrange /28/) was used for a cross section calculation for the $^{93}Nb(n,n')^{93m}Nb$ reaction (Strohmaier et al. /29/).

c) For neutron cross section calculations individually adjusted potentials are preferred to global ones.
   Examples:
   . Cross section calculations for Y and Zr isotopes /30/: excellent reproduction of experimental data (figs. 7 and 9 of ref. 30) by means of Lagrange potential /28, 40/.
   . Cross section calculations for ^{93}Nb+n /27/: successful application (figs. 3 and 8 of ref. 27) of the same potential /28/.

- Influence of level densities
  Example:
  Effect of a variation of the level density parameters "a" entering into statistical model calculations /31/ of $^{62}Cu(n,2n)^{62}Cu$ (table 1). The variation was done for each nuclide separately and amounted to $\Delta a = +0.5\ MeV^{-1}$ (6-8%).

V. Applicability of approximations

Approximations are often desirable for the sake of computational time

V.1. Width fluctuation correction (WFC)

WFC accounts for statistical distribution of partial widths

Full consideration of WFC: Moldauer

- M-cancellation approach /32/, see ref. 1
- superseded approach /33/ with channel independent degree of freedom parameters even for overlapping resonances

Approximative consideration of WFC: 2 versions by Tepel et al /34/, see ref. 1

Comparison of the various WFC formalisms by Vladuca et al. /25/ showed that the treatment of the WFC due to Tepel et al. /34/ is well suited for the description of neutron inelastic scattering cross sections (figs. 1 and 3 of ref. 25).

V.2. Angular momentum conservation

Complete consideration of angular momentum and parity in statistical model calculations: Hauser-Feshbach (HF) formula

Neglect of angular momentum and parity: Weisskopf-Ewing (WE) formula

Example: Cross section evaluation for several constituents of stainless steel /19/: use of the WE formalism for preliminary calculations (in order to find out which contributions to particle emission spectra and to production

cross sections of transmutation products are small, as well as for studying the dependence of the calculated cross sections on the model parameters) and for final calculation of small contributions. Comparison of HF and WE results in fig. 7 ; discrepancies mostly near thresholds.

V.3. Multiple charged particle emission

Helium and hydrogen production cross sections can approximately be calculated under neglect of multiple charged particle emission. Applicability of this approximation depends on target nucleus and incident energy.

Example: Cross sections for H and He production from ^{58}Ni+n and ^{56}Fe+n /19/, obtained under consideration of particle sequences with only one and up to two charged particles are compared in fig. 8 .

VI. General examples for recent neutron nuclear data calculations

a) neutron induced cross section (XS) evaluation on ^{54,56}Fe to 40 MeV: Arthur, Young /35/

Optical potentials
. Neutrons
search for optical potential on the basis of the following data:
total XS , 2-40 MeV
s- and p-wave strength functions
differential elastic XS , 6-14 MeV
reaction XS , 5-30 MeV
. Protons: Perey /36/, adjusted
. α-particles: Lemos /37/, adjusted

Level densities
conventional shifted Fermi gas (Gilbert & Cameron) parameters Cook /38/

PE model parameters
Kalbach, k = 160 MeV (k... constant determining the two-body interaction matrix element)

γ-ray strength functions
E1... Brink-Axel, normalized

Codes
COMNUC at low incident neutron energies (WFC)
GNASH at higher incident neutron energies (PE)
DWUCK (DWBA for (n,n'))

Examples: figs. 5, 7 and 8 of ref. 35.

b) neutron induced XS evaluation on ^{59}Co to 50 MeV: Arthur, Young, Matthes /39/

Optical potentials
. Neutrons
optical potential determiend so as to reproduce:
s- and p-wave strength function
potential scattering radius
total XS , 0.5 - 30 MeV, supplemented at higher energies by estimates based on Fe total xs to 50 MeV
differential elastic xs: 8., 11., 14., 15. MeV
reaction XS (estimate around 40 MeV based on data from ^{56}Fe+n)
. Protons: Perey /36/, modified
. α-particles: Lemos /37/, modified

Other parameters and codes
as for Fe evaluation

Examples: fig. 5 of ref. 39.

c) neutron induced XS evaluation on Y and Zr isotopes to 20 MeV: Arthur /30/

Optical potentials
. Neutrons
^{89}Y
^{90}Zr } Lagrange et al. /40/, modified
. Protons: Johnson /41/, modified
. α-particles: Park et al. /42/

PE model parameters
k = 135 MeV

other parameters and codes
as above

d) neutron induced XS evaluation on ^{182,183,184,186}W to 20 MeV: Arthur, Young, Smith, Philis /43/
calculations combined with experimental data

Neutron optical potential
Delaroche /28/,modified

Examples: figs. 9 - 11

e) model calculations of compound nucleus contributions to inelastic scattering on actinide nuclei: Arthur /44/

f) model calculations of the ^{237}Np(n,xnf) cross section to 20 MeV: Bak, Uhl, Strohmaier /45/

Example: fig. 12

References

/1/ M. Uhl, Proc. Winter Course on Nuclear Theory for Applications, Trieste, 25 Jan - 19 Feb. 1982, preceding paper
/2/ B. Strohmaier and M. Uhl, Proc. Winter Course on Nuclear Theory for Applications, Trieste, 17 Jan - 10 Feb 1978, IAEA-SMR-43, p. 313 (1980)
/3/ W. Scobel, priv. comm., March 1980
/4/ C.Y. Fu, Rept. ORNL/TM-7042, 1980
/5/ G. Mantzouranis, D. Agassi and H.A. Weidenmüller, Phys. Lett. 57B (1975) 220
/6/ G. Mantzouranis, H.A. Weidenmüller and D. Agassi, Z. Physik A276 (1976) 145

/7/ J.M. Akkermans, Phys. Lett. 82B (1979) 20
/8/ J.M. Akkermans, Z. Physik A292 (1979) 57
/9/ J.M. Akkermans, H. Gruppelaar and G. Reffo, Phys. Rev. C22 (1980) 73
/10/ H. Gruppelaar and J.M. Akkermans, Proc. Int. Symp. Neutron Cross Sections from 10-50 MeV, Upton, N.Y., May 12-14, 1980, BNL-NCS-51245, vol. II, p. 711
/11/ H. Gruppelaar and J.M. Akkermans, Rept. ECN-84, 1980
/12/ F.J. Luider, Z. Physik A284 (1978) 187
/13/ C.Y. Fu, Proc. Int. Symp. Neutron Cross Sections from 10-50 MeV, Upton, N.Y., May 12-14, 1980, BNL-NCS-51245, Vol. II, p. 675
/14/ E. Gadioli and E. Gadioli-Erba, Proc. Winter Course on Nuclear Theory for Applications, Trieste, 22 Jan - 28 Feb 1980, IAEA-SMR-68/I, p. 3
/15/ C. Kalbach and F.M. Mann, Proc. Int. Symp. Neutron Cross Sections from 10-50 MeV, Upton, N.Y., May 12-14, 1980, BNL-NCS-51245, vol. II, p. 689
/16/ C. Kalbach and F.M. Mann, Phys. Rev. C23 (1981) 112 and C. Kalbach, Phys. Rev. C23 (1981) 124
/17/ R.C. Haight, S.M. Grimes, R.G. Johnson, H.H. Barschall, Phys. Rev. C23 (1981) 700
/18/ R. Fischer, C. Derndorfer, B. Strohmaier, H. Vonach, to be published in Annals of Nuclear Energy
/19/ B. Strohmaier, M. Uhl and W. Reiter, Proc. IAEA Advisory Group Meeting on Nuclear Data For Radiation Damage Assessment and Reactor Safety Aspects, Vienna, 12-16 Oct. 1981
/20/ J.R. Huizenga and G.I. Igo, Rept. ANL-6373 (1961)
/21/ L. McFadden and G.R. Satchler, Nucl. Phys. 84 (1966) 177
/22/ R. Bock, P. David, H.H. Duhm, H. Hefele, U. Lynen and R. Stock, Nucl. Phys. A92 (1967) 539
/23/ B. Strohmaier, M. Uhl, G. Staudt and H.G. König, Nucl. Phys. A349 (1980) 141
/24/ B. Strohmaier, unpublished
/25/ G. Vladuca, C. Stan-Sion, A. Berinde and V. Zoran, Z. Physik A295 (1980) 235
/26/ E. Finckh, U. Jahnke, P. Pietrzyk, B. Schreiber and A. Weidinger, Phys. Rev. C1 (1970) 700
/27/ B. Strohmaier, to be published in Annals of Nuclear Energy
/28/ J.P. Delaroche, Ch. Lagrange and J. Salvy, IAEA Consultants Meeting Use Nucl. Theory in Neutron Nucl. Data Evaluation, Trieste, 8-15 Dec. 1975, IAEA-190, vol. I, p. 251
/29/ B. Strohmaier, S. Tagesen, H. Vonach, Phys. Data 13-2 (1980)
/30/ E.D. Arthur, Nucl. Sci. Eng. 76 (1980) 137
/31/ S. Tagesen, H. Vonach and B. Strohmaier, Phys. Data 13-1 (1979), ISSN 0344-8401
/32/ P.A. Moldauer, Phys. Rev. C14 (1975) 426
/33/ P.A. Moldauer, Phys. Rev. 135 (1964) B642
/34/ J.W. Tepel et al., Phys. Lett. 49B (1974) 1 and H. Hofmann, H.M. Richert, J.W. Tepel and H.A. Weidenmüller, Ann. Phys. 90 (1975) 403
/35/ E.D. Arthur and P.G. Young, Proc. Int. Symp. Neutron Cross Sections from 10 -50 MeV, Upton, N.Y., May 12-14, 1980, BNL-NCS-51245, vol. II, p. 731
/36/ F.G. Perey, Phys. Rev. 131 (1962) 745
/37/ O.F. Lemos, Orsay Rept., Series A. No. 136 (1972)
/38/ J.L. Cook, H. Ferguson and A.R.L. Musgrove, Aust. J. Phys. 20 (1967) 477
/39/ E.D. Arthur, P.G. Young and W.K. Matthes, Proc. Int. Symp. Neutron Cross Sections from 10-50 MeV, Upton, N.Y., May 12-14, 1980, BNL-NCS-51245, vol. II, p. 751
/40/ Ch. Lagrange, Proc. 3rd National Soviet Conf. Neutron Physics, Kiev, June 9, 1975, CONF-75061154 Atomizdat (1976)
/41/ C.H. Johnson, Phys. Rev. Lett. 39 (1977) 1604
/42/ Y.S. Park, H.D. Jones, D.E. Bainum, Phys. Rev. C4 (1971) 788
/43/ E.D. Arthur, P.G. Young, A.B. Smith, C.A. Philis, Rept. LA-8757-PR (1980) and E.D. Arthur, priv. comm. to M. Uhl, Dec. 1981
/44/ E.D. Arthur, Proc. OECD/NEA-NDC Specialists' Meeting on Fast Neutron Scattering on Actinide Nuclei, Paris, France, 23-25 Nov 1981
/45/ H.I. Bak, B. Strohmaier and M. Uhl, J. Korean Nucl. Society 13 (1981) 207

Table I. Relative variation (%) of calculated ^{63}Cu(n,2n) activation cross section due to variation of level density parameter "a" of various nuclides ($\Delta a = + 0.5$ MeV^{-1})

Incident energy (MeV) / Nuclide with varied a-param.	11.8	12.8	13.8	14.8	15.8
^{63}Cu	+ 11.4	+ 11.7	+ 12.4	+ 13.3	+ 14.3
^{63}Ni	- 6.3	- 7.6	- 8.9	- 10.3	- 11.5
^{60}Co	- 4.6	- 5.4	- 6.1	- 6.7	- 7.3
^{62}Cu	0	+ 0.2	+ 0.7	+ 1.2	+ 1.5
^{62}Ni	- 0.2	- 0.6	- 0.8	- 1.0	- 1.3
^{59}Co	0	0	0	0	0

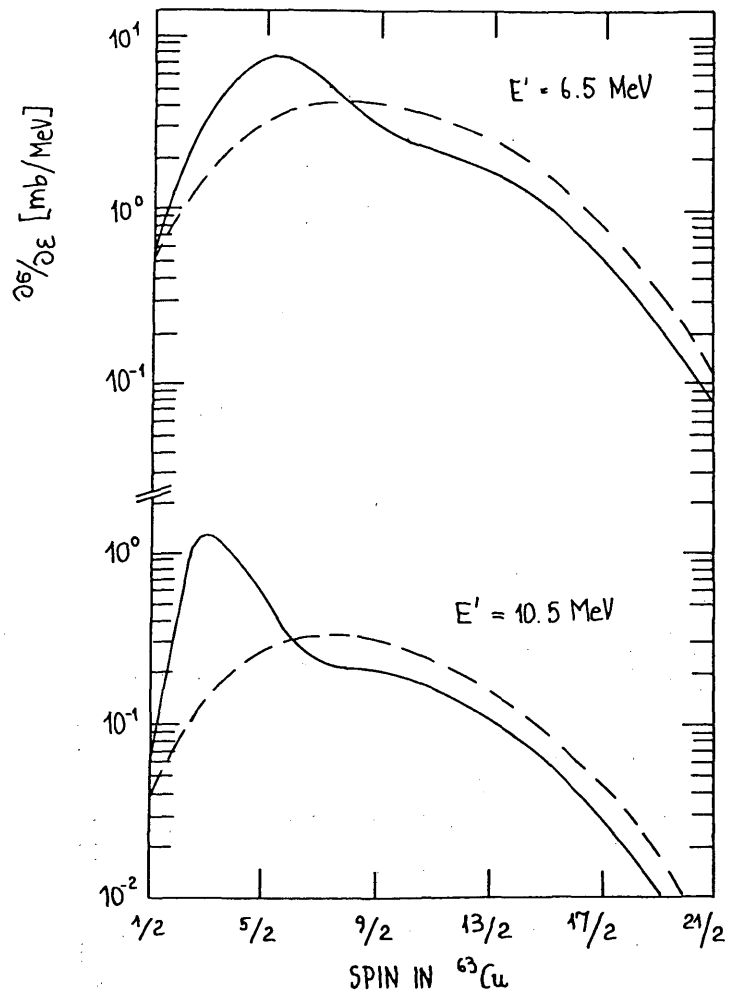

Fig. 1. Spin populations in ^{63}Cu following 14.8 MeV (n,n') reaction for two outgoing energies, E'=6.5 MeV and E'=10.5 MeV. Solid curve: Hauser-Feshbach component plus PE component with spin distribution according to Scobel /3/, dashed curve: pure Hauser-Feshbach calculation.

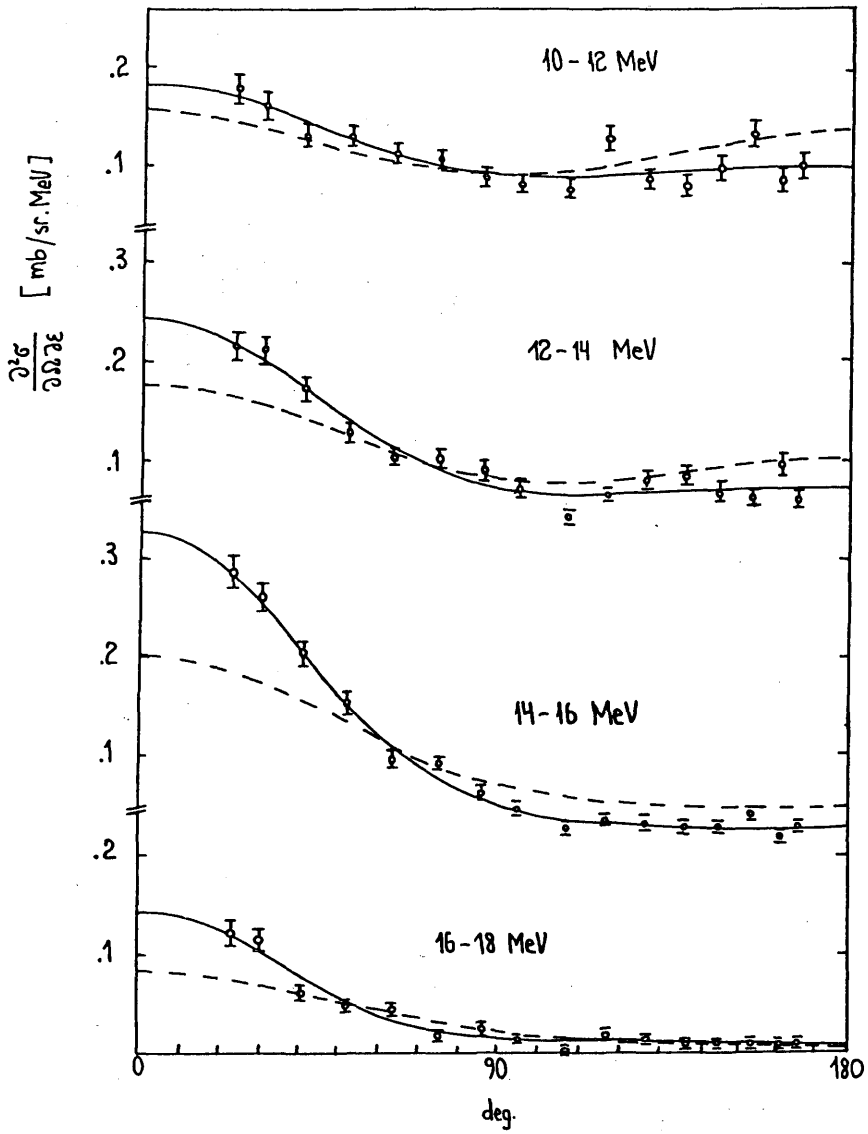

Fig. 2. Angular distributions of α-particles emitted from ^{93}Nb + n at 14.1 MeV. Full circles: experimental data /18/, solid lines: 4th order Legendre fit to the experimental data, dashed lines: calculation according to systematics of refs.15,16.

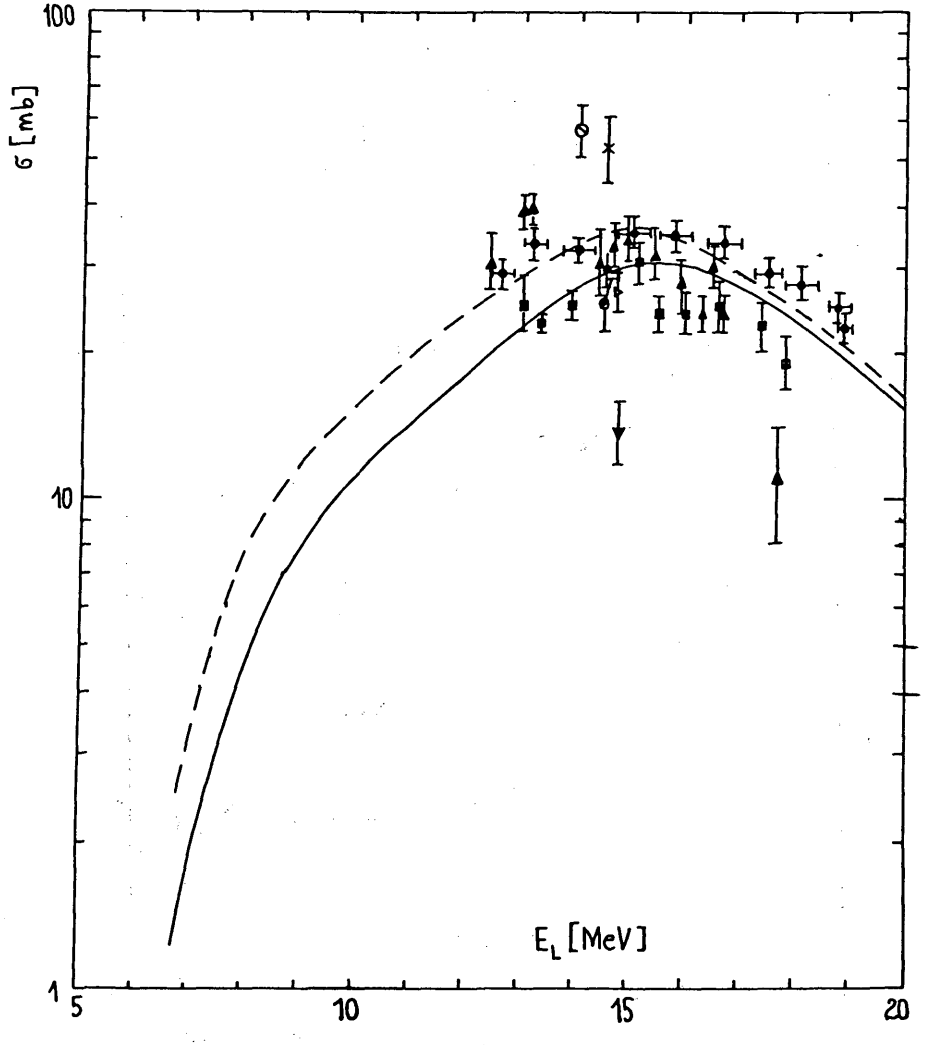

Fig. 3 . Experimental $^{55}Mn(n,\alpha)$ activation cross sections compared to two calcuations which differ in the α-paritcle optical potentialas well as in the level density parameters of ^{52}V which were taken according to the "best fit parameter set" determined for each of the two potentials. Thin solid line: McFadden and Satchler type potential /21/, for ^{52}V: a=6.10 MeV^{-1}, Δ=-1.40 MeV, dashed line: Huizenga and Igo potential /20/, for ^{52}V: a=6.16 MeV^{-1}, Δ=-1.46 MeV.

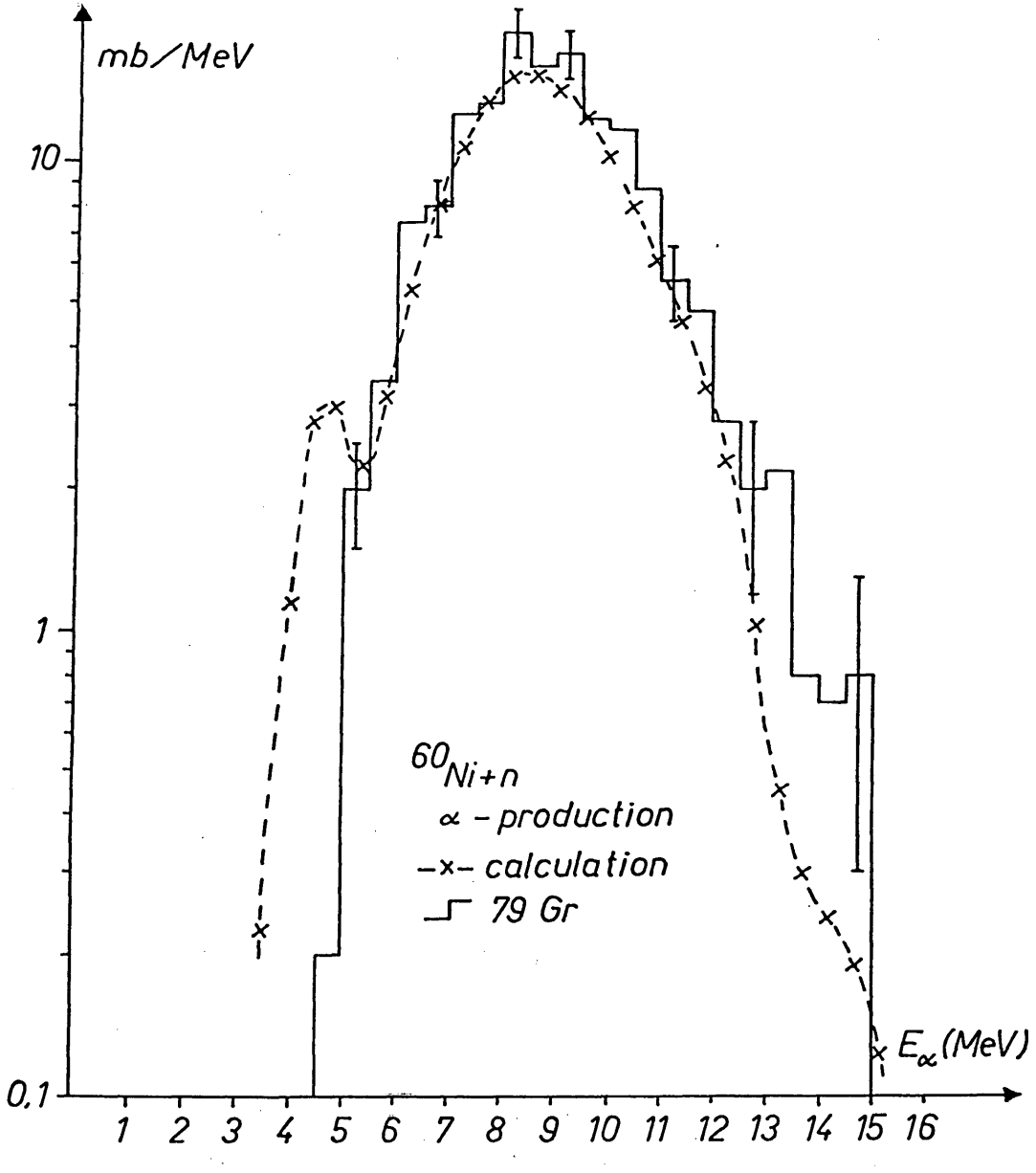

Fig. 4. Experimental and calculated α-particle production spectra at 15 MeV incident neutron energy.

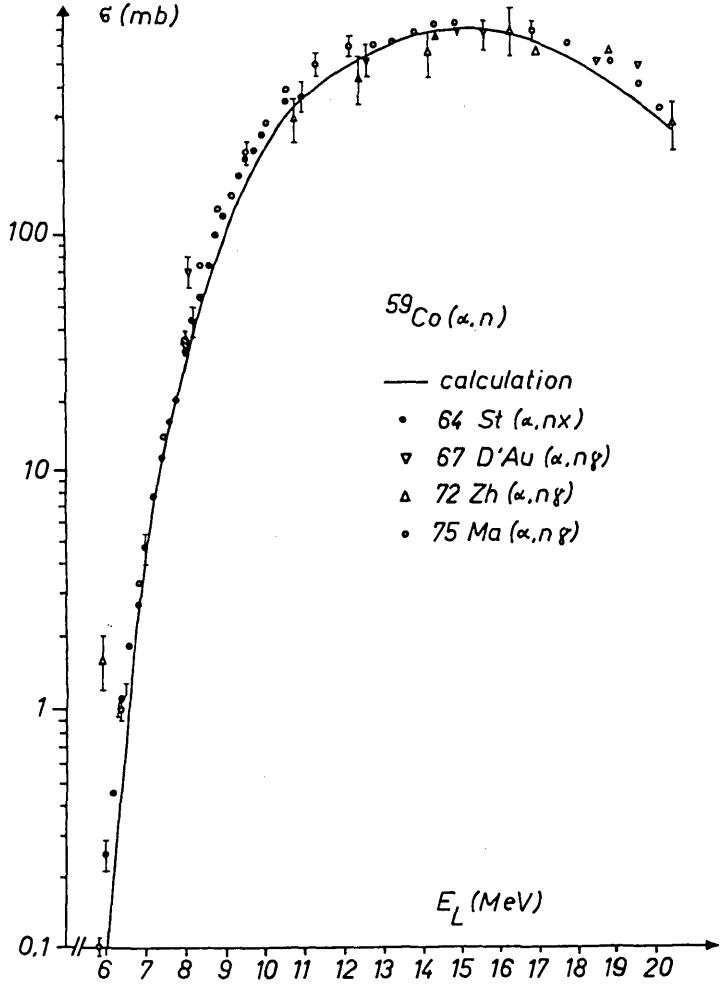

Fig. 5. Experimental and calculated ^{59}Co(α,n) cross sections.

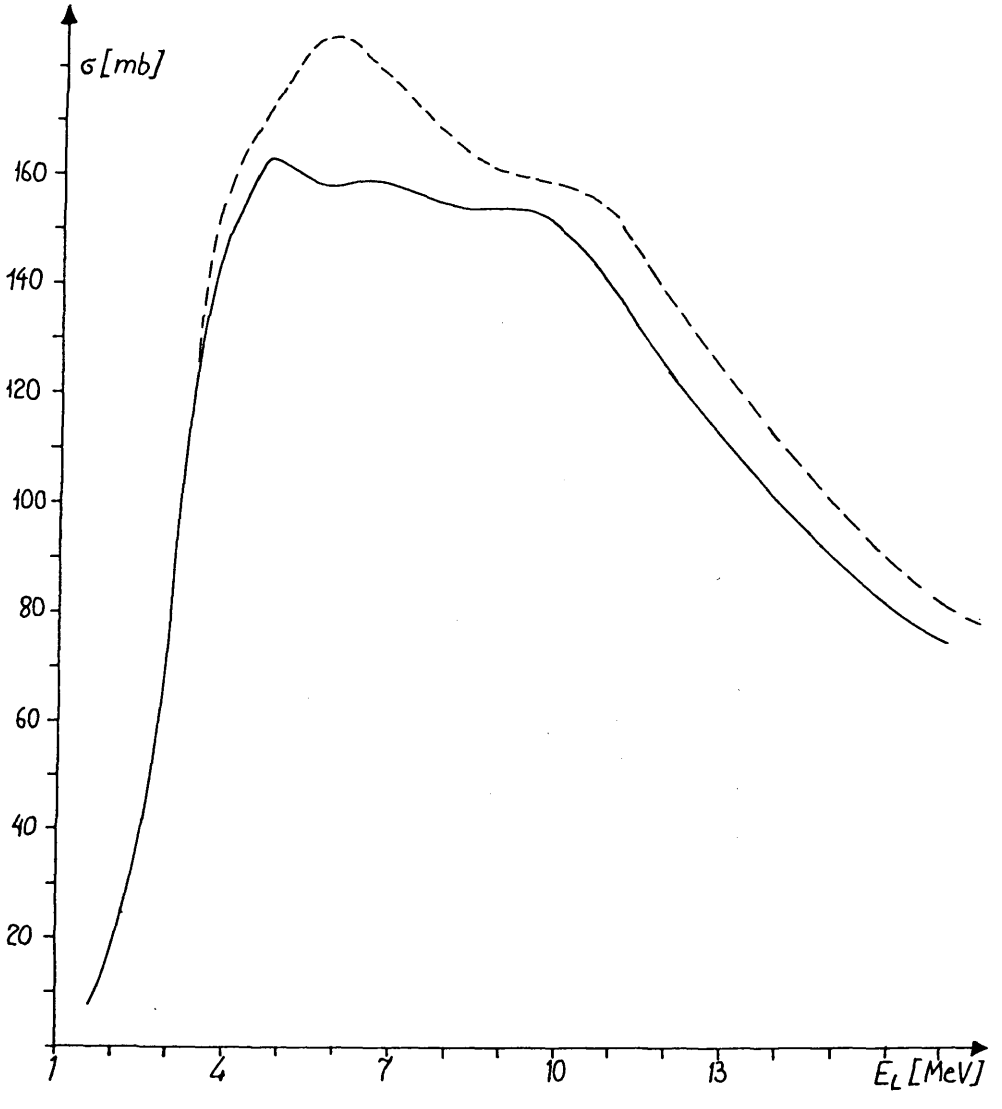

Fig. 6. Two calculations of the 31 P(n,p) activation cross section. Solid line: neutron transmission coefficients created from optical model calculations at all neutron energies, dashed line: neutron transmission coefficients obtained by extrapolation for neutron energies below 1 MeV.

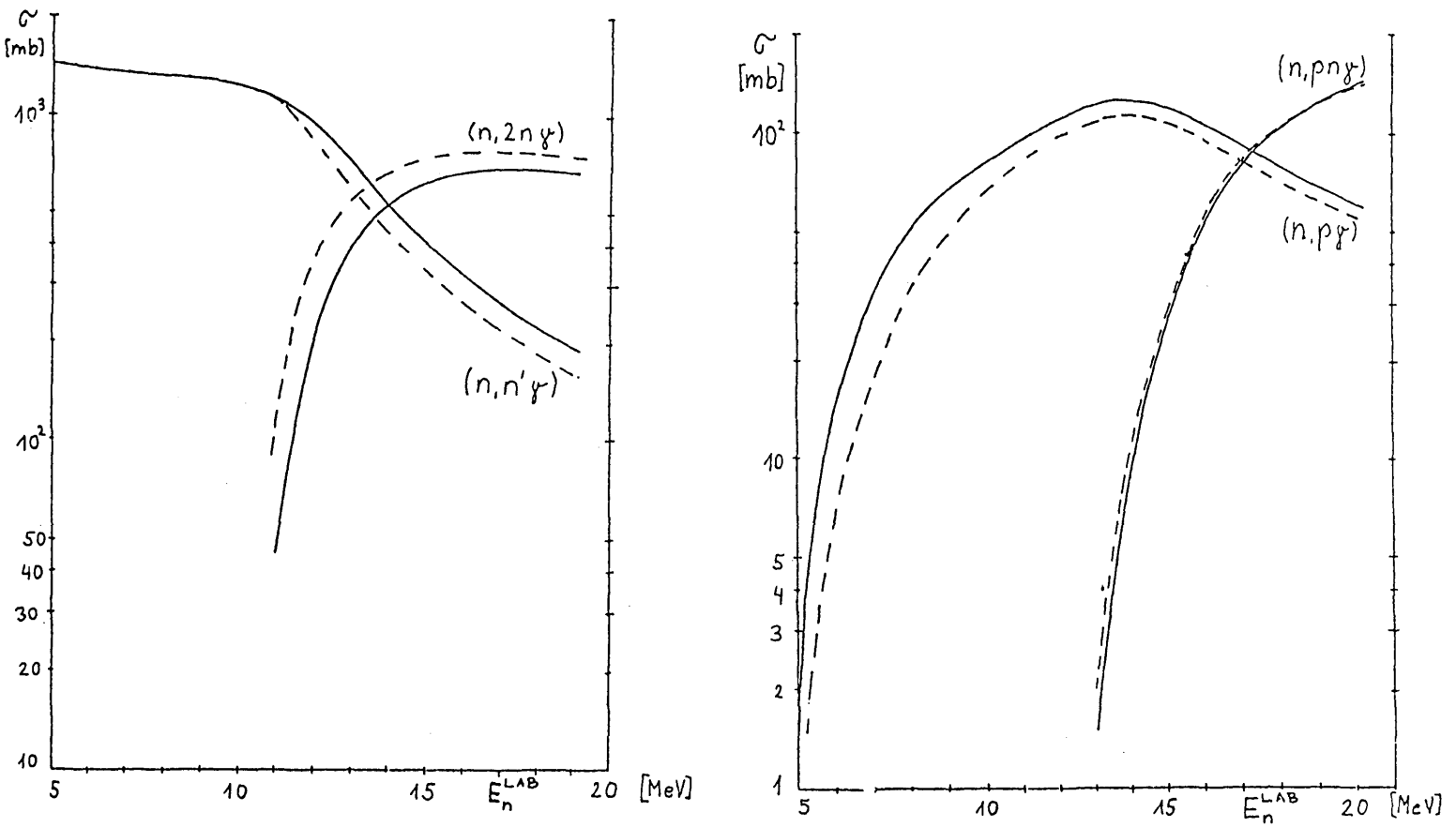

Fig. 7. Calculated activation cross sections for the (n,n'), (n,2n), (n,p) and (n,pn) reaction on 56 Fe. Solid lines: complete consideration of angular momentum and parity, dashed lines: Weisskopf-Ewing calculations.

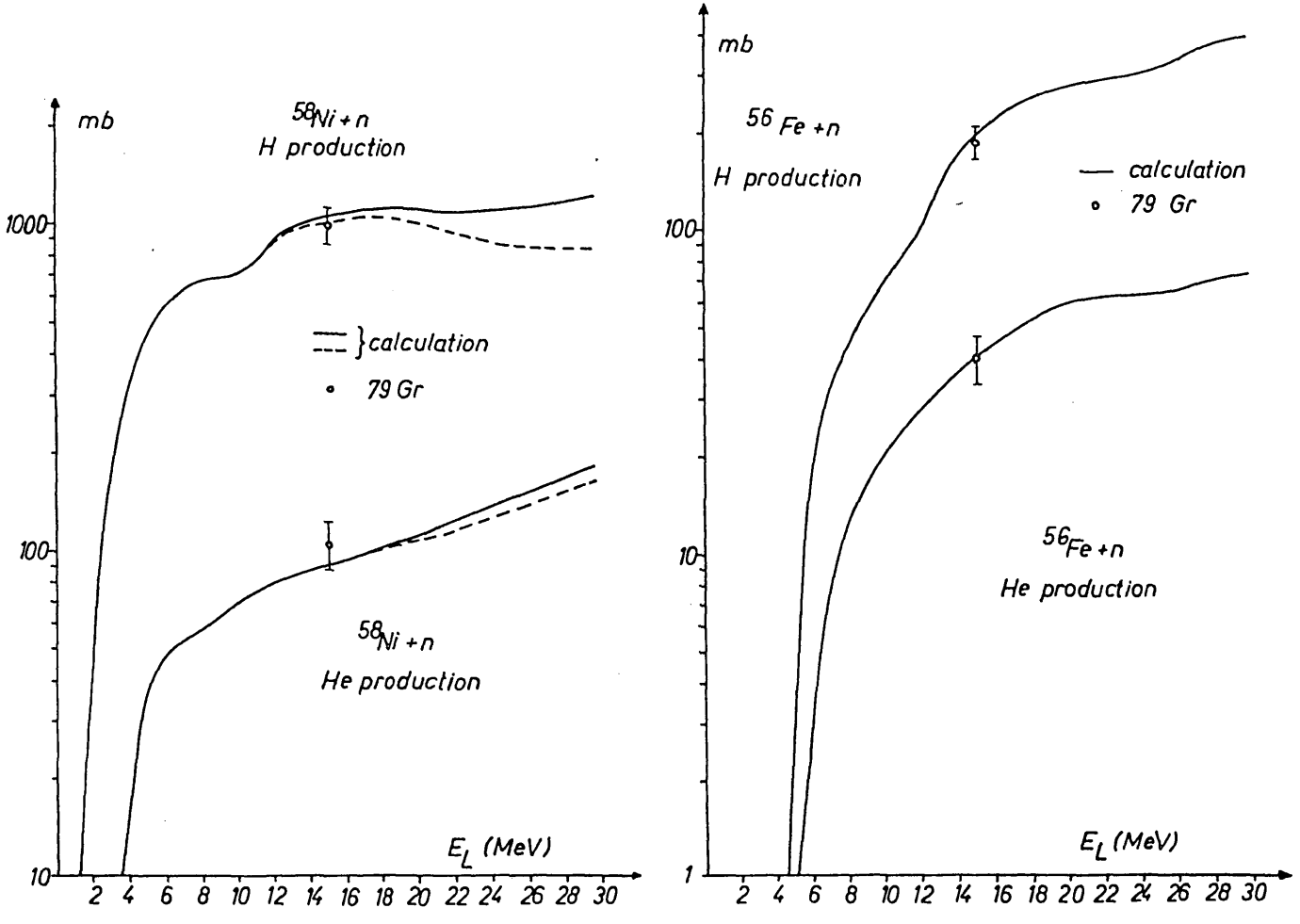

Fig. 8. Gas production from ^{58}Ni + n and ^{56}Fe + n. Calculations: solid lines: up to 2 charged particles considered, dashed lines: only one charged particle considered. For Fe the two curves coincide.

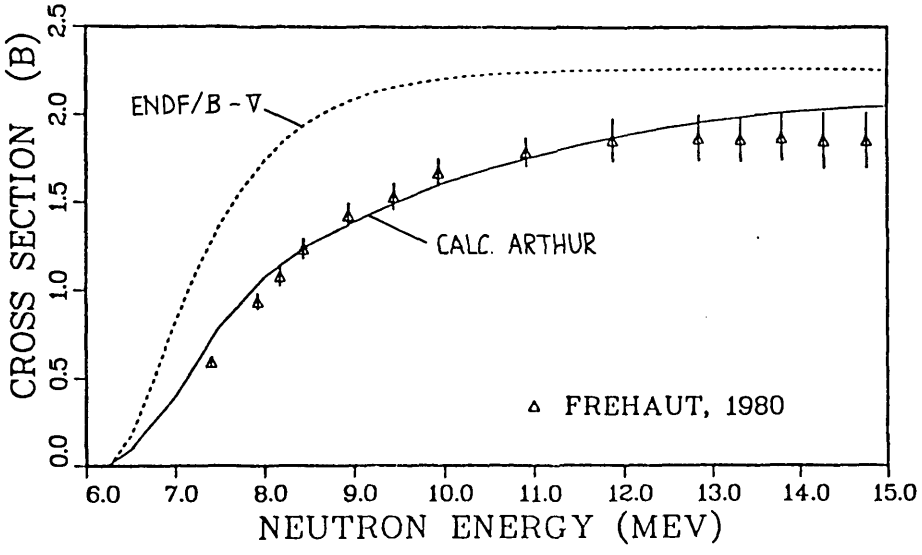

FIG. 9. W−183(N,2N) CROSS SECTION

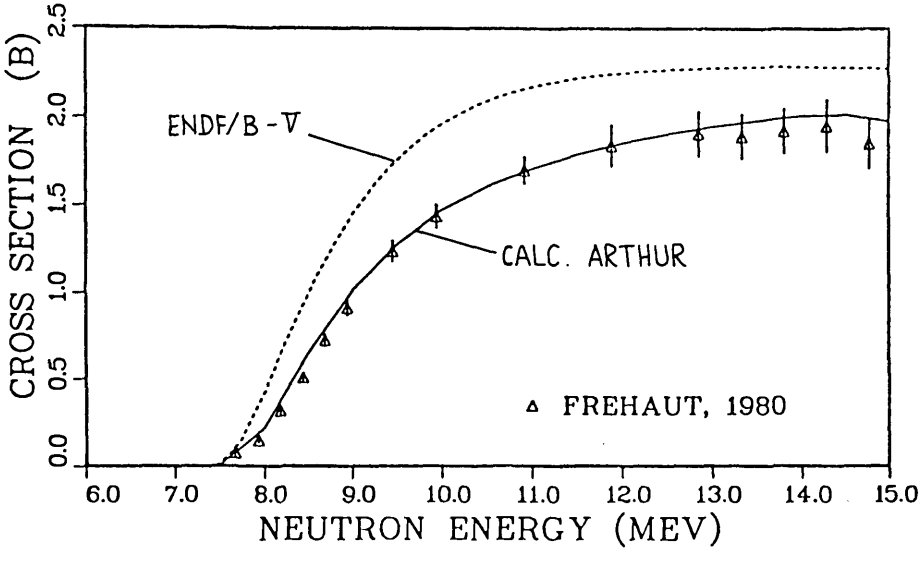

FIG. 10. W−184(N,2N) CROSS SECTION

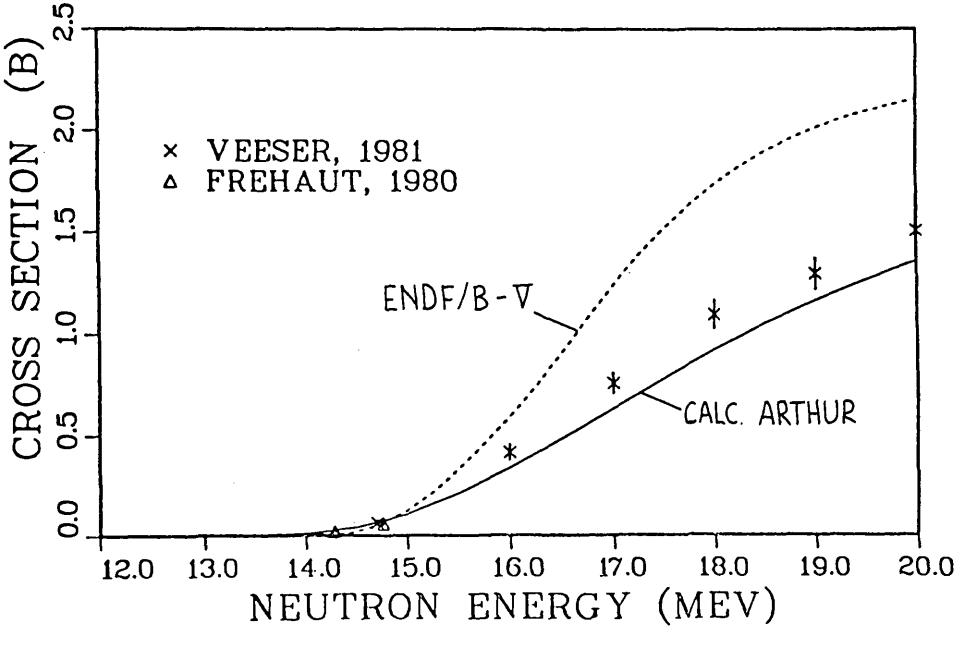

FIG. 11. W−NAT(N,3N) CROSS SECTION

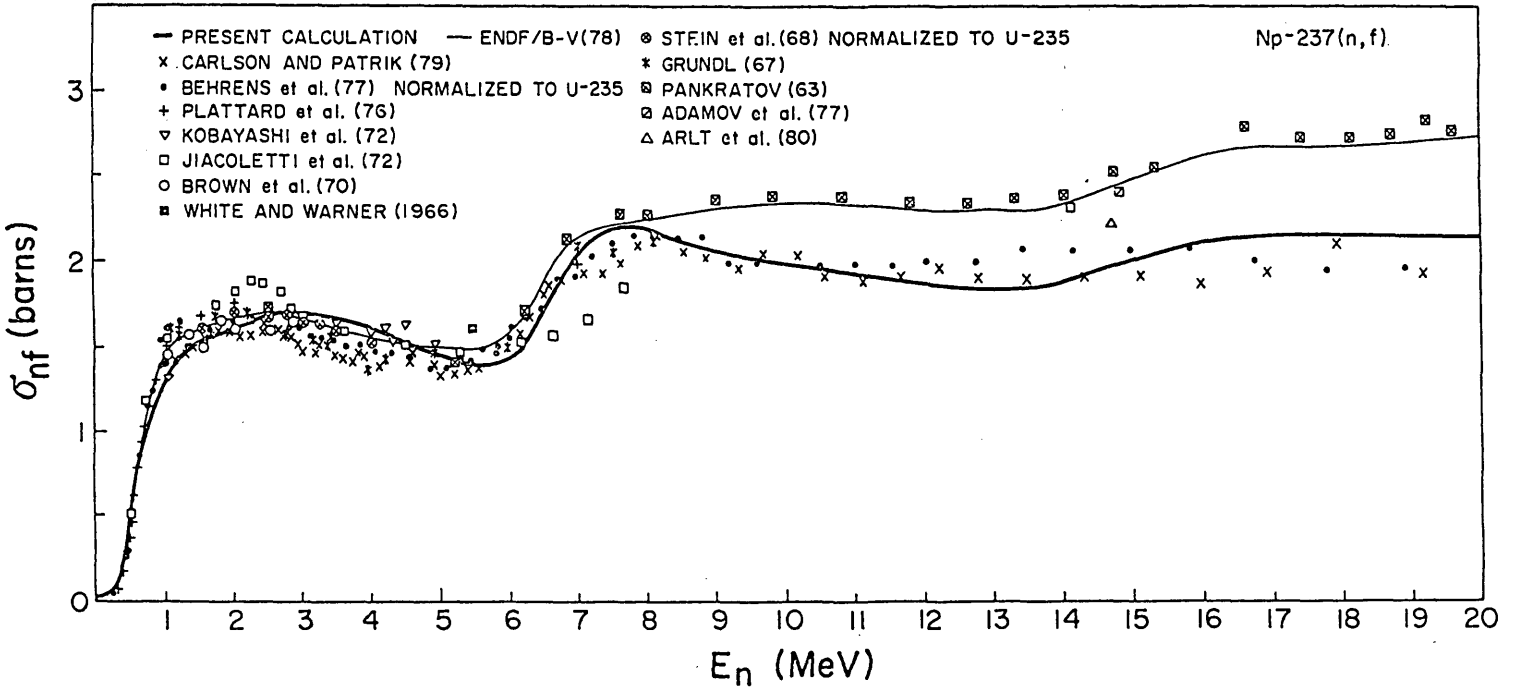

Fig. 12. Comparison of the present calculation of the Np-237 fission cross-section with experiments.

CRITICAL REVIEW OF PRECOMPOUND MODELS

H. JAHN
Institut für Neutronenphysik und Reaktortechnik,
Kernforschungszentrum Karlsruhe,
Karlsruhe, Federal Republic of Germany

Abstract

It is shown that the desired predictive capability most of the commonly used precompound formalism to calculate nuclear reaction cross-sections is seriously reduced by too much arbitrariness of the choice of parameters. The origin of this arbitrariness is analysed in detail and improvements or alternatives are discussed.

Introduction

In recent years many measured data for secondary energy and angular dependent nuclear reaction cross-sections could be understood as representing events which occur during the equilibration process on the way until the compound nuclear states are reached. The formal developments presenting this understanding seemed also to provide the necessary tools to calculate the considered cross-sections. But apparently it is overlooked quite often that there are important quantities occuring in most of the considered formalism which have to be treated as parameters because they are too difficult to calculate and what is obtained is more a fit rather than a genuine predictive calculation. It is the purpose of this paper to show this in details in order to obtain a help for a step on the way towards a more complete theory.

Sketch of the formalism

It is usually assumed that the nuclear reaction cross-sections split into a pre-equilibrium and an equilibrium component according to

$$(1)\quad \frac{d\sigma(\varepsilon_i,\varepsilon_j)}{d\varepsilon_j} = \left(\frac{d\sigma(\varepsilon_i,\varepsilon_j)}{d\varepsilon_j}\right)_{preq.} + \left(\frac{d\sigma(\varepsilon_i,\varepsilon_j)}{d\varepsilon_j}\right)_{eq.}$$

where ε_i is the energy of the incident and ε_j the energy of the emitted particle. This additive splitting according to eq.(1) uses to be verified by means of the solutions of the following set of the so called master equations

$$(2)\quad \frac{dP(n,t)}{dt} = P(n-2,t)\lambda_+^{n-2,n} + P(n+2,t)\lambda_-^{n+2,n} - P(n,t)(\lambda_+^{n,n+2} + \lambda_-^{n,n-2} + L(n,E))$$

describing the evolution in time t of the probability P(n,t) that a certain total number n of particles and holes

$$(3)\quad n = p + h$$

of the nuclear Fermi sea is excited. Cline and Blann /1/ have constructed this set of master equations as a set of genuine balance equations describing the balance between the gains and the losses of probability for excitation of the n so called excitons. These gains and losses are caused by transition probabilities per unit time $\lambda_\pm^{n,n\pm2}(E)$ for creation or destruction of one particle-hole pair and by the total emission probability per unit time L(n,E) of a particle from an n-exciton state. Both $\lambda_+(E)$ and L(n,E) depend on the excitation energy E.

If we now consider t=0 as the time at which the reaction has started then the time T(n,E) spent by the composite nucleus in the n-exciton state obviously is

$$(4)\quad T(n,E) = \int_0^\infty P(n,t)\,dt$$

Moreover we write as $W_j(n,E,\varepsilon_j)$ the probability per unit time for a particle of type j to be emitted with energy ε_j from an n-exciton state of excitation energy E. Thus

$$L(n,E) = \sum_j \int_0^{E-B_j} W_j(n,E,\varepsilon_j)\,d\varepsilon_j \tag{5}$$

where B_j is the binding energy of the particle of type j. With the quantities $T(n,E)$ and $W_j(n,E,\varepsilon_j)$ of (4) and (5) we obtain as the total cross section for emission of a particle of type j with energy between ε_j and $\varepsilon_j + d\varepsilon_j$ by an impact of a particle of type i of energy ε_i

$$\frac{d\sigma(\varepsilon_i,\varepsilon_j)}{d\varepsilon_j} = \sigma_{ci}(\varepsilon_i) \sum_{n=n_o} W_j(n,E,\varepsilon_j)\; T(n,E). \tag{6}$$

$\sigma_{ci}(\varepsilon_i)$ in (6) is the cross section for the formation of the composite system by the incoming particle i of energy ε_i. The summation is taken over all exciton states until the equilibrium is reached where n_o is the initial exciton number corresponding to the initial condition

$$P(n,o) = \delta_{nn_o} \tag{7}$$

According to Cline and Blann/1/, Ribanský, Obložinský and Běták /2/, Wu and Chang /3/ and Dobeš and Běták /4/ the solution of (2) can very well be approximated by an analytic closed-form expression. A corresponding approximate closed-form expression can consequently also be obtained for $T(n,E)$ of eq.(4) which according to Dobeš and Běták /4/ can be written:

$$T(n,E) = T^{o}(n,E) + \alpha\omega_n \tag{8}$$

where

$$T^{c}(n,E) = \tau(n,E)\left[\prod_{\substack{i=n_o \\ \Delta n=2}}^{n-2} \lambda_+^{n,n+2}(E)\;\tau(i,E) + \delta_{nn_o}\right] \tag{8a}$$

with

$$\tau(n,E) = \left[\lambda_+^{n,n+2}(E) + \lambda_-^{n,n-2}(E) + L(n,E)\right]^{-1}. \tag{8b}$$

and

$$\alpha = \frac{(1 - \sum_n T^{o}(n,E)L(n,E))}{\sum_n L(n,E)\,\omega_n} \tag{8c}$$

The quantities $\lambda_\pm^{n,n\pm2}$ and $L(n,E)$ in (8)-(8c) are those of (2) and (5). $T^{o}(n,E)$ in (8) is that part of the time integral (4) which goes from 0 until the equilibrium distribution of the exciton states at the equilibrium time t_{eq} is reached. For $t > t_{eq}$ this equilibrium distribution of the exciton states of course does not change anymore. It has to be taken proportional to the exciton state densities ω_n according to the postulate of equal a priori probability as has been pointed out by Cline and Blann/1/, Ribanský, Obložinský and Běták /2/ and Dobeš and Běták /4/. This has been used in the second term of (8).

In all of the recent work ω_n is expressed by the Ericson formula corrected by Williams /10/ to account for the Pauli principle. Thus

$$\omega_n = g\frac{(gE - A_{p,n})^{n-1}}{p!h!(n-1)!} \tag{9}$$

with the correction term $A_{p,n}$ due to the Pauli principle. $A_{p,n}$ was correctly presented by Williams /10/ only for the case p=h. To get an entirely correct expression for $A_{p,h}$ several papers have been published (/5/, /6/, /7/ and /8/). But none of them has presented the correct expression also for p≠h. The Williams-expression is /5/:

$$A_{p,h} = \tfrac{1}{4}(p^2 + h^2 + p - 3h) \tag{9a}$$

The correct expression has recently been found by Anzaldo / 9 / as:

(9b) $$A_{p,h} = ph - \frac{1}{4}\left[p(p+1) + h(h+1)\right]$$

On the other hand it could be shown / 6/ that neglect of $A_{p,n}$ would not matter very much especially for the case where only one nucleon is incident or emitted and provided the excitation energy is not too small according to

(10) $$E >> \frac{A_{p,n}}{g}$$

But for more than one incident or emitted nucleon such as also for the case of α-particles or heavy ions the contribution of $A_{p,n}$ could become important. Note that (9) is based on the constant single-particle level density g taken at Fermi energy.

The exciton state density ω_n of (9) is of course also a factor in the expression $W_j(n,E,\varepsilon_j)$ of (5) and (6) for the particle emission probability per unit time. From the principle of detailed balance Cline and Blann /1/, /10/ have obtained the expression

(11) $$W_j(n,E,\varepsilon_j) = \frac{2s_j+1}{\pi^2\hbar^3}\mu_j\varepsilon_j\sigma_{cj}Q_j(p)\frac{\omega_{n-1}(U)}{\omega_n(E)}$$

where s_j and μ_j are spin and mass of the emitted particle, U the excitation energy of the residual nucleus which for nucleons incident and emitted is

(12) $$U = \varepsilon_i - \varepsilon_j$$

and $Q_j(p)$ is a combinatorial factor by which the proton-neutron distinguishability and more general the emitted particle type weighting is taken into account to make it possible to use the one-Fermion type density of exciton states. By inserting (8),(9) and (11) into eq.(6) we obtain the additive splitting of eq.(1) where in the equilibrium term the denominator of (11) is cancelled by the ω_n of the second term of (8) and the remaining level density factor of the equilibrium term becomes

(13) $$\omega(U) = \sum_n \omega_{n-1}(U) = \frac{\exp\{2\sqrt{\pi^2 gU/6}\}}{\sqrt{48U}}$$

The last expression of (13) has been obtaines by Williams /5/ showing that the contributions from the Pauli principle correction term $A_{p,h}$ in (9) cancel in the summation of (13). Thus with (13) the one-Fermion type level density expression of Bethe for the free Fermi gas has been obtained in the equilibrium term of (1).

Transition rate problem

The most crucial quantities of the above sketched formalism are the transition rates $\lambda_{\pm}^{n,n+2}$ introduced with the master equation (2). After the first rough estimates of Griffin /1a/ and Blann /1b/ the following Golden Rule expression was stated by Williams /11/

(14) $$\lambda_{\pm}^{n,n+2} = \frac{2\pi}{\hbar}\overline{|M|^2}\omega_{\pm}^{n,n\pm2}$$

where the square of the matrix element M is averaged over the indicated transitions. Correspondingly $\omega_{\pm}^{n,n\pm2}$ are exciton state densities taken for these transitions. The $\omega_{\pm}^{n,n\pm2}$ have first been calculated by Williams /11/ from the Ericson formula without and by Cline /6 / and by Obložinský, Ribanský and Běták /12/ from the Ericson formula with the Pauli correction term of Williams / 5/ (see. eq. (9) and the following text). In addition the proton-neutron distinguishability has been taken into account by the above mentioned authors /12/. It amounts to a factor $\frac{1}{2}$ with whioh the expressions of the previous authors

/11/,/ 6/ have to be multiplied. The expressions thus obtained are /10/,/13/:

$$\omega_{+}^{n,n+2} = g_c \frac{g_c\left[E - E_{Pauli}(p+1,h+1)\right]^2}{2(n+1)} \qquad (15a)$$

$$\omega_{-}^{n,n-2} = g_c \frac{ph(n-2)}{2} \times \left[1 - \frac{(n-1)(p-1)(p-2) + (h-1)(h-2)}{(n-2)8g_c\left[E-E_{Pauli}(p,h)\right]}\right] \qquad (15b)$$

In (15a,b) the single-particle level density of the compound system is denoted by g_c.

But by the way of the same considerations which have been applied in connection with equations (9) and (10) we can find that the Pauli correction terms in (15a,b) can be neglected as in eq.(9) for excitation energies and particle-hole numbers for which the above formalism is mostly discussed here. Thus we do not present here E_{Pauli} of (15 a,b) in detail and refer to the papers /10/ and /13/ which present wrong results corresponding to the differences between (9a) and (9b).

Now in order to obtain a complete theory it would be necessary to calculate $\overline{|M|^2}$. But up to now nobody ever has calculated $\overline{|M|^2}$ in a direct way from a microscopic nuclear model. As an alternative Kalbach /14/ has attempted to find an empirical law for $\overline{|M^2|}$. As such a law Kalbach /14/ made the following proposal

$$\overline{|M|^2} = K \cdot A^{-3} \cdot E^{-1} \qquad (16)$$

hoping that only one universal constant K would be necessary to reproduce the particle emission cross-sections for a wide range of nuclei and excitation energies E.

The above mentioned formalism with relation (16) has been used by the following groups:
Kalbach /10/, Holub, Počanič, Čaplar and Cindro /13/, Fu /15/, Akkermans, Gruppelaar and Reffo /16/ and Gruppelaar, Costa, Nierop and Akkermans /17/. The STAPRE-code formalism of Strohmaier and Uhl /18/ works with a precompound- and compound description separated from the beginning which is not explicitely derived from a common master equation as shown by equations (2)-(9). But the relation (16) is explicitly used in the pre-compound description. Unfortunately no K-values have been reported by Strohmaier and Uhl. But they do report that K has been used by them as an adjustable parameter.

The intercomparison between /10/, /13/ and /15/-/17/ is quite problematic because either pairing energy corrections or emitted particle type weighting or both have been taken into account in very different ways. Unfortunately these ways are not always characterized very thoroughly and clearly in the quoted papers so that important details are difficult to recognize. On the other hand Fu /15/ has demonstrated the enormous influence of the way to take into account the level-density pairing-energy correction. This influence can be so strong that one should conclude that this is another source of arbitrariness in addition to the K-problem of (16). Thus we only can intercompare the results respective within each of the papers /10/, /13/ and /15/ - /17/.

In the papers /13/ and /15/-/17/ the theory is compared with measured cross-sections for 14,6 MeV incident neutrons. Only in the paper /10/ measured charged-particle cross-sections are discussed for incident proton and α-particle energies from 14,6 - 62 MeV within a certain range of the periodic table. As a result of these papers the relation (16) has been roughly confirmed for incident energies from 14,6 - 62 MeV over a range from A = 75 - 200. But because of the different handling of the incorporation of pairing-energy correction and emitted particle type weighting we obtain different K-values for the

different papers, namely:

Table 1

paper	K (MeV^3)	g $(MeV)^{-1}$	$Q_j(p)$ of eq. (11)
/10/	400	$\frac{A}{13}$	see /10/,/13/
/13/	700	$(\frac{6}{\pi^2})a_{GC}$	see /10/,/13/
/15/	700	$(\frac{6}{\pi^2})a_{GC}$	in initial cond.
/16/	190	$g_c = \frac{A}{13}$; $g_r = (\frac{6}{\pi^2})a_{BS}^{GC}$	1
/17/	500	$(\frac{6}{\pi^2})a_{BS}$	see /10/,/13/
/36/	400	$\frac{A}{13}$	1

GC = Gilbert + Cameron /19/, BS = Back-Shifted Fermi-gas
r = residual Nucleus, c = compound nucleus

Thus from the above considerations we can conclude that the relation (16) is confirmed for incident energies from 14,6 up to 62 MeV but with the different values of K which are written above. The preceding formulations with (6)-(16) have been incorporated by F.M. Mann into his computer code HAUSER*5 /20/ where the level density treatment is most similar to /13/. The same is true for the multireaction code GNASH of Young and Arthur /21/.

Ambiguities from unsolved level density problems

The differences of the values of K, as shown in Tab.1 for the different publications /10/,/13/ and /15/-/17/ are as already mentioned partly related to a different handling of the pairing-energy corrections of the compound as well as precompound level densities (exciton state level densities). Thus in the publication /10/ the level density expression (13) was used by C.Kalbach but with U replaced by $U' = U - \delta$ where δ is the pairing energy correction taken from Gilbert and Cameron /19/. A corresponding pairing energy correction was introduced in the exciton state densities (see (6),(8), (8a)-(8c),(9) and (11)). But the way this has been done is not shown very explicitely in publication /10/. In /10/ $g = \frac{A}{13}$ was chosen as in /16/, (see Tab.1).

Contrary to /10/ the Gilbert-Cameron formula /19/ was used instead of (13) in the work of Holub, Počanic, Čaplar and Cindro /13/. In this work /13/ no pairing-energy corrections were introduced into the exciton state densities of the precompound part because odd-odd compound nuclei or compound nuclei with odd number of the incident nucleon type were investigated. Moreover $g = \frac{6}{\pi^2} a$ was used througout in /13/ for values taken from Gilbert and Cameron /19/ (see Tab.1) with the corresponding shell effects. But shell effects were also found in /13/ for the K-values of nuclei near closed shells. Here K very much exceeds the average value K = 700 MeV^3 (see Tab.1) such as K = 7000 MeV^3 for ^{209}Bi and K = 1400 MeV^3 for ^{89}Y. But for other nuclei discussed in /13/ such as ^{197}Au with K = 3500 MeV^3 and ^{103}Rh with K = 175 MeV^3 these K-departures from K = 700 MeV^3 cannot so easily be explained as shell effects.

Now Fu /15/ very much stressed that a certain amount of pairing energy always must be expended if a particle-hole pair excitation is accompanied by a pair breaking. Thus pairing-energy corrections must always be taken into account in the exciton state density expressions. But no rigorous derivation of this influence was given by Fu /15/ and consequently no unique results could be obtained. Yet by way of an estimate Fu /15/ could show the strength of this influence. Thus by taking into account this estimate of Fu /15/ the K-value had to be changed from K = 400 $(MeV)^3$ to K = 700 $(MeV)^3$. This shows that a rigorous treatment of pairing in the level density

expressions of the precompound and compound part with unique results is badly needed in order to give the above formalism a predictive capability with K being not only a fit parameter but a universal constant. This consideration of Fu shows the importance of considering the level densities not only isolated but also in the framework of a consistent nuclear equilibration formalism connected with certain nuclear reaction processes.

In all previous-mentioned work equidistant one-particle levels were assumed. The influence of non-equidistance was investigated by Blann and Albrecht /20/ and by Kalbach /21/.

Transition rates from nucleon-nucleon scattering in nuclear matter

Blann /24/ and Braga-Marcazzan, Gadioli-Erba, Milazzo-Colli and Sona /25/ went ahead to remove the adjustable parameter K in (14) and (16) by calculating the transition rates $\lambda_{\pm}^{n\pm2}$ in eq.(2) from nucleon-nucleon scattering in nuclear matter according to

(17) $$\lambda_{+}^{1,3} = v\rho\langle\sigma\rangle$$

where v is the particle velocity in nuclear matter

(18) $$v = \sqrt{\frac{2(E+E_F)}{m}} \quad ,$$

ρ is the nuclear matter density and $\langle\sigma\rangle$ the effective cross-section for an excited nucleon to interact with nucleons having a Fermi gas momentum distribution. The average $\langle\ \rangle$ is taken over the free nucleon-nucleon scattering cross section with a method due to Goldberger/26/and Hayakawa, Kawai and Kikuchi /27/ with the Pauli principle taken into account. The general transition rates $\lambda_{\pm}^{n,n\pm2}$ then were calculated by Gadioli, Gadioli-Erba, and Sona, /28/ using a recursion procedure derived from the expressions(14) and (9). The transition rates thus calculated were then used by Gadioli, Gadioli-Erba, Sona, Sajo-Bohus, Tagliaferri and Hogan /29/ and /30/ in an extended effort to reproduce absolute values of excitation cross-sections for a wide range of mass numbers ($89 \leq A \leq 169$) and excitation energies ($10\ \text{MeV} < E < 100\ \text{MeV}$). But the mentioned authors found they had to multiply the calculated transition rates by factors of the order of 0.1 to 0.25 in order to obtain satisfactory agreement between the calculated and measured cross-sections. Nevertheless C. Kalbach /33/ has attempted to integrate the more detailed physical knowledge resulting from /29/ and /30/ into an empirical formulation of type (14)-(16) with the result

(19) $$\overline{|M|^2} = \frac{K'}{A^3 e}\left(\frac{e}{7\ \text{MeV}}\right)^{1/2}\left(\frac{e}{2\ \text{MeV}}\right)^{1/2} \qquad e<2\ \text{MeV}$$

$$= \frac{K'}{A^3 e}\left(\frac{e}{7\ \text{MeV}}\right)^{1/2} \qquad 2\ \text{MeV} \leq e < 7\ \text{MeV}$$

$$= \frac{K'}{A^3 e} \qquad 7\ \text{MeV} \leq e \leq 15\ \text{MeV}$$

$$= \frac{K'}{A^3 e}\left(\frac{15\ \text{MeV}}{e}\right)^{1/2} \qquad 15\ \text{MeV} < e;\ e = \frac{E}{n}$$

With (19) and the choice K' = 135 C.Kalbach /31/ was able to reproduce the measured secondary-energy-dependent (p,p') cross-sections of Bertrand and Peelle /32/ for ^{54}Fe and ^{197}Au with incident energies of 29 and 62 MeV in the intermediate secondary energy range. But the high secondary-energy tail came out much too low compared to the measured results of /32/. Nevertheless (14),(15) and (19) have been incorporated by C.Kalbach into her code PRECO-B /33/. Quite good reproductions of experimental results by means of calculations on the basis of (14),(15) and (19) have on the other hand been obtained for (n,2n) and (n,3n) excitation cross-sections by Jhingan, Anand, Gupta and Mehta /34/

for incident energies up to 28MeV in the mass range 89 to 238. But these cross-sections are not very sensitive to $\overline{|M^2|}$. Gudima, Osokov and Tonev /35/ did not need to reduce λ_+. These authors replaced $E+E_F$ in $\langle\sigma\rangle$ and v by the relative kinetic energy

(20) $$T_n = \frac{8}{5} E_F + \frac{E}{n}$$

of the colliding particles in nuclear matter with n excitons and excitation energy E. Eq.(20) results from the so-called right-angle approximation. T_n is the sum of the mean kinetic energy of an excited particle (p)

(20a) $$T_n^{(p)} = E_F + \frac{E}{n}$$

and the kinetic energy of an intranuclear nucleon (N) averaged over the Fermi spectrum,

(20b) $$T_n^{(N)} = \frac{3}{5} E_F.$$

Gudima, Osokov and Tonev /35/ achieved a good reproduction of the absolute values of the secondary-energy-dependent cross sections for the reactions Ta(n,n') at 14.6 MeV, Cu(α,p)Zn at 43 MeV and Ta(p,n) at 18 MeV incident energy. Absolute pre-equilibrium (n,n') cross sections at 14 MeV were calculated in the same way by Hermsdorf, Meister, Seeliger, Sassonov and Seidel/36/ in good agreement with experimental results in the mass range $30 \leq A \leq 200$.
The absorption cross section σ in Eqs.(6)-(8) was obtained from the optical model. No additional fit parameters were needed but a λ_o-term was added to the master equation with

(20c) $$\lambda_o^{n,n} = \frac{2\pi}{\hbar}\overline{|M|^2} g^2 E \frac{3n-2}{2}.$$

and treated as λ_+ in (17), (18), (20) - (20b).
Tests for more incident energies below as well as above 14 MeV and additional secondary-energy-dependent cross sections for a wide range of mass numbers should be performed before the predictive power of the method can be judged conclusively. This seems necessary in particular because the approximations (17)-(20b) were originally derived for kinetic energies of the colliding particles above about 100 MeV, which means for incident neutron energies above about 55 MeV if we consider $E+E_F$ as a measure for the relative energy of the colliding particles. The applications just mentioned, on the other hand, were made for incident neutron energies well below 55 MeV.

Hybrid and geometrie-dependent hybrid model

Blann /21/,/37/,/38/ found out that no fit parameters other than those from the optical model were needed if the excitation energy E in (17) and (18) was replaced by the energy ε of the emitted nucleon, and the Fermi energy E_F by the optical potential depth V. The λ_+ produced this way is then taken the same for each n and is thus independent of n. According to Kikuchi and Kawai/27/,/38/ λ_+ can be expressed as:

(21) $$\lambda_{j+}(\varepsilon_j) = \frac{2W_j(\varepsilon_j)}{\hbar}$$

where W_j is taken from the imaginary part of the optical potential fitted in the elastic channel of the emitted nucleon. The hybrid model was then obtained by Blann /24/ by inserting (21) into the closed form expression which arises by combining (6)-(8c') after replacing $\lambda_+^{n,n+2}$ by (21) and L(n,E) by the factor before $Q_j(p)$ in the expression (11) for $W_j(n,E,\varepsilon_j)$ divided by the one nucleon level density g_j of a nucleon of type j. This factor is called $\lambda_j(\varepsilon_j)$ according to

(22) $$\lambda_j(\varepsilon_j) = \frac{2s_j+1}{\pi^2\hbar^3} \cdot \frac{\mu_j \varepsilon_j \sigma_j}{g_j}$$

where g_j has to be taken as

(22a) $$g_n = (A-Z)/14; \quad g_p = Z/14 \qquad (\mathrm{MeV})^{-1}$$

Moreover $\lambda_-^{n,n-2}$ is omitted and L(n,E) in all the expressions of (6)-(8c) is replaced by $\lambda_j(\varepsilon_j)$ of eq.(22).

Finally $Q_j(p)$ in (11) is replaced by

$$f_{ij} = \frac{p_{ij}}{p} \tag{23}$$

where p is the total number of particles, p_{ij} the number of particles of type j and f_{ij} the corresponding fraction, given an incident particle of type i. Following Blann /37/ p_{ij} should be calculated according to

$$p_{ij} = \delta_{ij} + \frac{(p-1)\sigma_{ij}}{\sum_{j'} \sigma_{ij'}} \tag{24}$$

where σ_{ij} are the free nucleon-nucleon scattering cross-sections used in a representation which is given in /38/. After the changes introduced with (21)-(24) into (6)-(8c) the question arises whether (6)-(8c) then still can be considered as an approximation of the master equation (2). Blann outlined /37/,/38/ that these changes were suggested to him by considering the formalism of Harp, Miller and Berne /39/, /40/. Because of this composition from two different formalisms Blann calls the resulting formulation the "hybrid model". The resulting expression of the hybrid model for precompound reactions thus becomes after introducing (21)-(24) into (6)-(8c)

$$\frac{d\sigma(\varepsilon_i,\varepsilon_j)}{d\varepsilon_j} = \sigma_{ci}(\varepsilon_i) \sum_{n=n_o}^{\bar{n}} \Delta n=2 \; f_{ij} \frac{\omega_{n-1}(U) g_j}{\omega_n(E)} \frac{\lambda_j(\varepsilon_j)}{\lambda_j(\varepsilon_j)+\lambda_{j+}(\varepsilon_j)} D_n \tag{25}$$

$$= \sigma_{ci}(\varepsilon_j) \sum_{n=n_o}^{\bar{n}} \Delta n=2 \; P_{n'ij}(\varepsilon_j)$$

with

$$D_n = \prod_{n_o+2<n'<n}^{n} \left(1 - \sum_{i,j} \left(\int_o^{E-B_j} P_{n'ij}(\varepsilon_j) d\varepsilon_j\right)\right) \tag{26}$$

where $P_{n'ij}(\varepsilon_j)$ is the expression behind the summation sign of (25) and where $\bar{n}$ is the average exciton number at equilibrium obtained from

$$\lambda_+^{\bar{n},\bar{n}+2} = \lambda_-^{\bar{n},\bar{n}-2} \tag{27}$$

according to (15a,b). The result without Pauli correction is

$$\bar{n} = \sqrt{2gE} \tag{28}$$

From (25)-(28) quite satisfactory results were obtained /41/ for parameter free prediction of secondary energy dependent (α,p) cross-sections for nuclides from ^{51} to ^{197}Au at 55 MeV incident energy. Only the optical-model parameters from the elastic α- and p-channel fits were used and no $|M|^2$-type parameter such as that occuring in (14) and (16) was needed.

Much less successful, on the other hand, were attempts to reproduce the measured angle-integrated secondary-energy-dependent ^{197}Au(p,p') cross-section by means of hybrid calculations /42/. In particular the very flat secondary energy dependence of the measured ^{197}Au(p,p') cross-section could not be reproduced by results obtained from calculations on the basis of (25)-(28). These calculated results show a much too steep descent with increasing secondary energy if $n_o = 3$ is chosen. Improvements could be obtained by choosing $n_o = 2$ instead of $n_o = 3$ as the smallest exciton number n_o. But the choice $n_o = 2$ appears quite unphysical unless we assume that at the nuclear surface one of the three initial excitons (a hole) is suppressed. Such an assumption can be understood in the framework of the Thomas-Fermi model, if the Fermi energy, as in the atomic case, is taken as decreasing with the nuclear density d(r) towards the surface according to

$$E_F(r) = \frac{\hbar^2}{2m} \left(\frac{3}{2} \pi^2 d(r)\right)^{2/3} \tag{29}$$

where the density follows the Fermi (or Woods-Saxon) distribution

$$d(r) = d_s \left(e^{(r-c)/z} + 1 \right)^{-1} \tag{30}$$

with the nuclear half-density radius

$$c = c_o A^{1/3} , \qquad c_o = 1.07 \text{ fm} , \tag{30a}$$

the surface thickness

$$z = 0.55 \text{ fm} \tag{30b}$$

and the saturation density

$$d_s = \left(\frac{4\pi}{3} c_o^3 \right)^{-1} . \tag{30c}$$

A reasonable way to account for the influence of the nuclear surface diffuseness can be obtained according to Blann /37/ by averaging along the particle trajectory taking the impact parameter

$$R_\ell = \ell \lambda\!\!\!^{-} \tag{31}$$

as the lower limit and the upper limit as

$$R_s = c + 5z \tag{32}$$

outside the nucleus where the density is practically zero. The quantities ℓ and $\lambda\!\!\!^{-}$ in (31) are the orbital angular momentum quantum number and the de Broglie wave length,

$$\lambda\!\!\!^{-} = \frac{\hbar}{\sqrt{2m\varepsilon_o}} . \tag{33}$$

The averaged density is then defined by

$$\bar{d}(R_\ell) = \frac{1}{R_s - R_\ell} \int_{R_\ell}^{R_s} d(r)dr . \tag{34}$$

Inserting this into the Fermi energy expression (29) one gets the geometry-dependent Fermi energy or potential depth

$$E_F(R_\ell) = E_F \cdot \left(\frac{\bar{d}(R_\ell)}{d_s} \right)^{2/3} \tag{35}$$

where

$$E_F = \frac{\hbar^2}{2m} \left(\frac{3\pi^2}{2} d_s \right)^{2/3} \tag{36}$$

is the usual Fermi energy.

From the good results obtained without surface diffuseness for (α,p) reactions by Mignerey and Blann /38/ and Chevarier et al. /41/ with $n_o = 4$ or 5 and from the failure with $n_o = 3$ in the case of $^{197}Au(p,p')$ Blann /43/ concluded that only for $n_o = 3$ (incident nucleons) must the surface diffuseness be taken into account because only then can an exciton acquire enough energy to sense the bottom of the potential well. In this way Blann /43/ found

$$\omega_{1p1h} = gE_F(R_\ell), \qquad U > E_F(R_\ell); \tag{37}$$

$$\omega_{2p1h} = \frac{1}{4} g^2 E_F(R_\ell)\{2E - E_F(R_\ell)\}, \qquad E > E_F(R_\ell).$$

The Ericson or Williams formula (9) is used in all other cases.

In addition there is an influence of the surface diffuseness on the third factor in each sum term of Eq. (25): g in the expression (22) for $\lambda_j(\varepsilon_j)$ has to be taken as

$$g_j(R_\ell) = \left(\frac{\varepsilon + B + E_F(R_\ell)}{E_F} \right)^{1/2} g_j \tag{38}$$

instead of (22a). Finally also the absorption and excitation rate $\lambda_{j+}(\varepsilon)$ in the third factor of Eq. (25) can be affected by the surface diffuseness. This is the case if $\lambda_{j+}(\varepsilon_j)$ is calculated from

the imaginary part $W_j(r)$ of the optical potential for nucleon scattering according to

$$(39) \qquad \lambda_{j+}^{(\ell)}(\varepsilon) = \frac{2\overline{W}_j(R_\ell)}{\hbar} \quad \text{with} \quad \overline{W}_j(R_\ell) = \frac{1}{R_s - R_\ell} \int_{R_\ell}^{R_s} W_j(r)\,dr \ .$$

In (39) R_s is given by $R_s = r_o A^{1/3} + 5a$ with $r_o = 1.32$fm and $a = 0.51 + 0.7(N-Z)/A$ which is somewhat different from (32).

One can now calculate the pre-equilibrium component of the inelastic-scattering neutron cross section, integrated over emission angles but dependent on the secondary energy, by means of the Eq.(22) - (39). These equations represent the hydrid model with surface diffuseness which was called by Blann the geometry-dependent hybrid model. Apart from general nuclear parameters such as nucleon numbers (N, Z, A), nuclear radius and surface thickness the model contains only the optical-model quantities W and $\sigma(\varepsilon)$. In particular there are no additional fit parameters. Moreover, the geometry-dependent hybrid model is the only existing model that takes the diffuseness of the nuclear surface into account.

On this basis 14.6 MeV (n,n') cross-sections for ^{52}Cr, ^{55}Mn, ^{56}Fe, ^{58}Ni and ^{93}Nb were calculated by Broeders, Broeders and Jahn /44/ (secondary-energy-dependent and angle integrated) which are in rather good agreement with the measured results of the groups in Dresden/45/ and Livermore /46/. Also 62 and 39 MeV (p,p') cross-sections of the same kind on ^{56}Fe and ^{209}Bi were calculated in the same way by Blann /38/ who could obtain satisfactory agreement with the measured results of Bertrand and Peelle /32/, and Scobel, Bissem, Friese, Krause, Langanke, Langkau, Plischke, Scherwinski and Wien /47/ compared their identically calculated 27 MeV-(p,p')-results with their own measured results on $^{58, 60,61,62,64}$Ni and ^{63,65}Cu where also good agreement was obtained.
A computer code was developed by Blann /48/ on the basis of this model the first version of which was called ALICE /48/.

In this code, as in Refs. /37/ and /43/, the expression

$$(40) \qquad g(R_\ell) = \frac{3A}{2E_F(R_\ell)}$$

was used instead of (38). This led to unrealistic results as described in Ref. /49/. The calculations of Hansen, Grimes, Howerton and Anderson (see Ref. /50/) were apparently based on Eq.(40) and therefore give too small pre-equilibrium components of the secondary-energy-dependent inelastic neutron-scattering cross section. Also our own first (n,n') calculations on ^{56}Fe and ^{238}U with the hybrid-model code /48/were only successful after re-introduction of a fit parameter /51/.

This deficiency of ALICE was corrected in the version OVERLAID ALICE /52/ which was successfully applied to (p,p') reactions by Blann (see Ref. /39/)and to d-, He- and ^{4}He-induced reactions by Bisplinghoff, Ernst, Machner, Mayer-Kuckuk and Jahn, Probst, Djaloeis, Davidson and Mayer-Böricke (see Ref. /38/).

Critical summary of the exciton-master equation-approach

Two groups of precompound descriptions and their applications are reviewed in this report. The first group is based on the master-equation (2) with its two different ways of determining the internal transition rates $\lambda_{\pm}^{n,n\pm2}$. One way consists of reducing $\lambda_{\pm}^{n,n\pm2}$ to a universal empirical law with a universal constant K by using the Golden Rule expressions (14)-(16). But the still too small range and number of examples of incident energies as well as the lack of mathematical transparency of the different versions of calculations does not allow a unique conclusion about the universal law and its constant (see Tab.1 and equations (14)-(16)). One source for this nonuniqueness is the nonexistence of a unique prescription or at least convention for the incorporation of pairing-energy corrections into the exciton state densities (see the explanations around Tab. 1 and in the following paragraph).

For reasons of consistency ambiguities are introduced in this way also into the equilibrium state densities. Moreover all the work based on the attempt of the universal $\lambda_{\pm}$ -law (14)-(16) is based on equidistant single-nucleon levels. Thus because of all the nonuniquenèss mentioned above we have the situation that the question of a univeral λ_{+}-law is still in a stage of being explored by fitting measured cross-sections rather than of being used to predict them.

The adherents of the master-equation exciton model approach appear to be very much attracted by its quality of being based on the unique master-equation system, eq.(2), which can be derived directly from the microscopic statistical random matrix model of the nuclear Hamiltonian according to Agassi, Weidenmüller and Mantzouranis /53/. To maintain therefore this exciton master-equation approach the second of the two above-mentioned ways of determining $\lambda_{\pm}^{n,n\pm2}$ was taken by Gadioli et al. /29/, /30/ who went ahead to fully, calculate the $\lambda_{\pm}^{n,n\pm2}$-transition rates from nucleon-nucleon-scattering in nuclear matter. But the transition rates resulting from these calculations had to be reduced by 0,1 to 0,25 in order to get full reproduction of the measured (p,x,n)-excitation cross-sections for mass numbers $89 \leq A \leq 169$ and excitation energies $10 \text{ MeV} \leq E \leq 100 \text{ MeV}$. In other words: The calculated cross-sections are too small by factors of 0,1 to 0,5.

As a way out C.Kalbach proposed the still more complicated universal law of eq.(19) trying to reproduce the numerical results of Gadioli et al. /29/, /30/ with the new universal fit-constant K'. But until now this more complicated universal law could be tested with only few examples and not even very successfully as remarked after eq.(19).

We therefore are inclined to take the result serious that the cross-sections calculated as mentioned above come out too small by 0,1 to 0,5. We think this should be interpreted as an indication that the exciton-master-equation approach does not take into account the full reaction processes. It only takes into account those reactions which are related to the equilibration process. But there should be the direct reaction processes in addition which are not taken fully into account by the exciton-master-equation approach. This is shown very clearly by the formalism of Agassi, Weidenmüller and Mantzouranis /53/ and is also pointed out by Bunakov /54/.

As another strong evidence for the importance of these extra direct reaction contributions it should be considered that the A^{-3}-dependence of $|M^2|$ according to equation (16) appears to be empirically rather well established. ω_{+} in (14) is predominatly A^3-dependent as shown if the g~ A behaviour of Tab. 1 is introduced into (15a). This means approximate A-independence of λ_{+} if the validity of the A^{-3}-dependence of $\overline{|M^2|}$ is assumed according to (16). In other words: The A^3-dependence introduced by (15a) is cancelled by the A^{-3}-dependence of (16). This rises doubts about the Golden Rule treatment of λ_{+} as well as about the predominance of the exciton-master-equation contribution at any range of the secondary-energy dependency of the angle-integrated cross-sections. An A-independence of λ_{+} gives the results of a slow A-dependence of the angle-integrated secondary energy dependent cross-section according to (6), (8a) and (8b) as about $A^{1/3}$ if integrated over the secondary energy. But just this type of behaviour is shown by the cross-sections of the direct processes as pointed out by Cohen in the panel of the Albany Conference on Statistical Properties of Nuclei, August 23 - 27, 1971 /73/ who used the following figure:

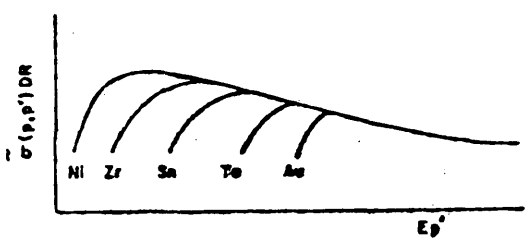

B. Cohen, Pittsburg

Fig.1:

This figure shows how the very strong exponential A-dependent behaviour of the compound-contributions of the (p,p')-emission cross-section at low emission energies goes over to the weakly A-dependent behaviour of the direct contributions at the high-energy tail. Thus this slow A-dependence can be obtained from the direct contributions without the artificial introduction and recancellation of the A^3-behaviour shown by the Golden Rule-method to calculate λ_+ of the exciton-master-equation approach.

Angular distributions of the exciton-master-equation approach

Further strong indications that no direct reaction processes contribute to the results of the pure exciton-master-equation approach can also be read off from the angular distributions resulting from the angular dependent exciton-master-equation approach developed by Mantzouranis, Weidenmüller and Agassi /55/. These angular distributions show at the high secondary energy tail too small contributions to the forward and backward directions as compared to the measured values /56/, /57/ and /16/. This can be seen from the results of Mantzouranis /56/ for 45 MeV-(p,p')-reactions on ^{48}Ca, ^{90}Zr, ^{120}Sn and ^{208}Pb, of the author /57/ for 14,6 MeV-(n,n')-reactions on ^{56}Fe and of Akkermans, Gruppelaar and Reffo /16/ for 14,6 MeV-(n,n')-reactions on 33 isotopes form Be til Bi.

The last mentioned results are presented as averaged over secondary energy intervals 2-11 MeV and 6-11 MeV which rises the question whether this means much information in view of the much better resolved secondary-energy spectra measured by the Dresden group /45/ with secondary-energy- bins ranging from 0,5 MeV to 0,05 MeV. Moreover the wide energy-averaging intervals of Akkermans et al. /16/ prevent the pretended possibility of applying their results in the field of fusion reactor design calculations where at least about seven secondary energy groups are needed.

We thus consider the foregoing stated deviations between the calculated and the measured angular distributions as a further limitation indicating that the direct reaction processes are not taken into account by the exciton-master-equation approach.

Model with explicit account of the direct reaction processes

As a way out it therefore seems to be adequate at first sight to resort to those approaches which take into account the direct processes explicitely in addition to the precompound or compound contributions.

There are several approaches of this type which can be grouped according to the names of the following authors:

1. Austern with his book on direct reaction theories /58/.
2. Blokhin, Ignatyuk, Lunev and Pronaev /59/.
3. Tamura, Udagawa and Lenske /60/.
4. Feshbach, Kerman and Koonin /61/.

Approach 1 was developed to treat those direct reaction processes by which single low lying resolved levels of nuclei can be reached. For our context it was used to calculate the high energy tail of the secondary-energy-dependent (p,p')- and (n,n')-cross-sections respectively.
This was done by Fu /62/ for ^{56}Fe on the basis of two DWBA-(p,p') analyses of Peterson /63/ and Mani /64/ of measured cross-sections for 17,5 and 45,35 MeV incident energies. From these (p,p')-analyses in particular of the angular distributions the DWBA-parameter of the first 30 levels were obtained and used by Fu /62/ to calculate the corresponding 14,6 MeV-(n,n')-cross-sections by means of the computer program SALLY/63/. In this way a secondary-energy-distributed 14,6 MeV-(n,n')-cross-section was obtained by Fu /62/ with rather sharp lines around each of the first 25 levels of ^{56}Fe. This DWBA cross-section-distribution obtained for the first 25 discrete levels of ^{56}Fe was then averaged by the author /66/ over the

intervals 10-11, 11-12 MeV etc. of the secondary neutron energy and a step-curve was obtained /66/ which agreed quite well with the experimental step-curves of the Livermore /46/ and Dresden /45/ groups.

On the other hand we already mentioned that the smooth curve calculated from the geometry-dependent hybrid model as explained after eq.(38) and presented in /44/ agreed also quite well with the measured Dresden /45/ and Livermore /46/ results. This is in accord with Blanns repeated statements that he considers the n_0 = 3-component of the geometry-dependent hybrid model as the direct component /37/ as demonstrated also by its surface dependence shown by eqs.(29)-(39). This is the only surface dependence shown by any precompound model.

Finally there is the close relationship of the geometry-dependent hybrid model to the Harp-Miller-Berne equations as pointed out by Blann (see the remarks concerning eq.(24)). Now Bunakov /54/ gave a derivation of improved Harp-Miller-Berne equations and showed that the direct contributions are included in them in contrast to the exciton-master-equation approach. The residual interactions of Bunakovs new HMB-equations were completely expressed by the parameters of the optical model /54/. Thus Bunakov's new equations depend of no fit parameters other than those of the optical model although they even include the direct contributions. These properties are the same as shown by the hybrid and geometry-dependent hybrid models. Therefore it should be possible to derive those or similar models rigorously from Bunakov's new equations. In case of success we would consider the obtained approach as most preferable against all the other models discussed in this report because the direct contributions would be included and no fit-parameters other than those from the optical model would be needed. But, as already mentioned, this approach 1. till now was only tested for the case of low lying resolved levels.

We therefore have to discuss approaches 2.-4.developed to calculate the excitation of the unresolved region of levels, the so called continuum part of the spectrum. This was carried out by approach 2. in the random-phase approximation of a phonon model with a self-consistent choice of the effective residual interaction. Two phonon excitations were taken into account. Satisfactory reproductions of the measured results were presented for the angular distribution of 20 MeV protons emitted following the impact of 62 MeV protons on ^{54}Fe as well as for the secondary energy dependent cross-section of 39 MeV protons incident on ^{54}Fe. Only rough agreement with the measured results was achieved for the secondary energy dependent cross-sections of 62 MeV protons on ^{54}Fe and on ^{208}Pb.

Approach 3. has much similarity with approach 2. The only difference is that particle-hole excitations are introduced instead of phonon excitations. Measured angular distributions of 62 MeV incident protons on ^{27}Al and ^{209}Bi are rather well reproduced for secondary proton-energy intervals of 42-52, 32-42 and 22-32 MeV. But Tsai and Bertsch /67/ noted that the energy-weighted sum rule comes out too large with the ph-approximated deformation parameters. Thus Tamura et al. switched to RPA-states and finally to microscopic ph-states and two-step-ph-contributions had to be added /60/. Also Arndt and Reif attempted a similar approach /68/.

Tamura et al. have shown /60/ that approach 4. can be obtained from approach 3. if some simplifications are introduced into the multi-step (predominantly two-step) contributions. So far the one-step contribution of 4. is the same as that of 3. with the difference that the excited level densities are given by RPA response functions in 2. and 3. but by the Ericson ph-function in 4. The latter rises the same level density problems as in the forementioned precompound oontributions of the exciton master-equation approach which will become important in particular below 20 MeV excitation energy. Pairing energy corrections are taken into account only in approach 2. The effective interaction of approach 4. has to be adjusted. Good agreement between cal-

culated and measured angular distributions could be obtained by Bonetti et al. /69/ with the same effective interaction force constant V_0 = (27,9 ± 3,5)MeV for angular distributions of 20-40 MeV neutrons emitted from 25-45 MeV protons incident on ^{40}Ca, ^{90}Zr, ^{120}Sn and ^{208}Pb. For the lower incident energies as 25 MeV the statistical multi-step compound contributions of approach 4. become significant, see Bonetti et al. /70/.
The appearence of the so called statistical multistep compound contributions in addition to the statistical multi-step direct contributions is a typical aspect of approach 4. which was derived from Feshbachs general framework of nuclear reaction theories /71/ with its P and Q projection-operators onto the open and closed channel spaces leading to both, statistical multi-step direct and statistical multi-step compound contributions. The latter have some similarity with the precompound- and compound contributions of the exciton master-equation approach. Contributions of this type have not been taken into account by approach 3. for the high-energy examples considered there. A Hauser-Feshbach-contribution has been successfully added only for the examples of low-energy α-emission cross-sections (< 25 MeV) from 62 MeV protons incident on ^{54}Fe. A similar evaporation contribution has also been taken into account by approach 2.

Whereas in approaches 2. and 3. the effective residual interactions are fixed by self-consistency requirements or sum rules, free fit-parameters are left in approach 4. for the residual interactions. Even <u>two strengths of residual interactions were needed in approach 4.:</u> one for the multistep-direct contributions with V_0 = (27 ± 3,5) MeV according to Bonetti et al. /69/ and one for the multi-step-compound contributions with V_0 = 0,70 MeV /70/. But different functions were chosen for the two cases: A Yukawa function for the multi-step direct residual interaction, and a δ-function for the multi-step compound residual interaction. This must be taken into account in comparison of both interaction strengths. But nevertheless they appear to be extremely different, and the question must remain open whether and how this difference can be explained. Moreover this independent adjustability of <u>the two residual interactions of approach 4. can be another source of ambiguity.</u> This has been pointed out by Tamura et al. /60/ by means of the fact that reproductions of measured (p,α)-angular-distributions could be achieved with <u>the same success by a one- step direct plus Hauser-Feshbach approach (see Dragun et al. /72/). as well as by a two-step direct approach (see Tamura et al. /60/)</u> In spite of different incident proton energies in these two cases (44,3 and 34,6 MeV in case of Dragun et al. and 62 MeV in case of Tamura et al.) we consider these two successes with the two different approaches as a hint at the above-mentioned ambiguity which should be investigated somewhat more but which eventually could perhaps be removed by self-consistency requirements or sum rules as in the cases of the approaches 2. and 3.
In any case approaches 1. - 4. demonstrate the occurence of the direct reaction processes and by selecting the advantages it might be possible to obtain a unified and simpler procedure.

Conclusions

The approaches 1. - 3. to take into account the direct reaction processes are substantially able to predict cross-sections whereas approach 4. is a fitting procedure with possible ambiguities. But until now they have been tested only by a few examples. This might have to do with the necessary extensive numerical expense. Simpler is the exciton-master-equation approach. But apparently it does not take into account the direct reaction processes and thus cannot fully describe the forward peaked angular distributions. Moreover it is more a fitting procedure rather than a predictive theory which latter is badly needed to test measured results and to close gaps where measuring is too

difficult or even impossible. But as a unique fitting procedure the exciton master-equation approach could still be useful. Right now it cannot be obtained this way because of the unnecessary different writing versions of the same solution of the exciton master-equation approach which is one reason for the different values of the K-constant in Tab.1. Another reason is the lack of a unique procedure to take into account the pairing-energy and shell corrections into the analytic exciton-state and nuclear level density expressions. Also the Pauli-correction term used until now is partially wrong. The same nuclear level density problems occur also if the hybrid or the geometry-dependent hybrid model are used. However, these models have more predictive capability than the exiton master equation approach, specially for the cases of (n,n') and (p,p') reactions, but for the two nucleon and composite particle emission hybrid and geometry-dependent hybrid versions have not yet been developed. Thus more consolidation and unification of the very many hitherto existing approaches seem to be necessary rather than still more diversification and blowing up.

References

/1/ Cline,C.K, Blann, M., Nucl. Phys. A172, 225 (1971)

/1a/ Griffin, J.J., Phys. Rev. Lett. 17, 478, Phys.Lett. 24B,5(1967)

/1b/ Blann, M., Phys. Rev. Lett 21, 1357 (1968)

/2/ Ribanský, I., Obložinský, P. and Betak, E., Nucl. Phys. A205, 545 (1973)

/3/ Wu, R.J., Chang, C.C., Phys. Lett. 60b, 423 (1976)

/4/ Dobeš, J., Betak, E., Z. Phys. A288, 175 (1978)

/5/ Williams, F.C., Nucl. Phys. A166, 231 (1971)

/6/ Cline, C.K., Nucl. Phys. A195, 353 (1972)

/7/ Kalbach, C., Nuov. Cim. 29A,283 (1975)

/8/ Kalbach, C., Phys. Rev. C24, 819 (1981)

/9/ Anzaldo Meneses, A.M., privat communication, Karlsruhe, Fed . Rep. of. Germany, (1982); see also Proceedings of the IAEA Advisory Group Meeting on Basic and Applied Problems of Nuclear Level Densities, Brookhaven, USA, April 1983

/10/ Kalbach, C., Z.Phys. A283, 401 (1977)

/11/ Williams, F.C., Phys. Lett. B31, 183 (1970)

/12/ Obložinsky, P., Ribanský, I. and Běták, E., Nucl.Phys. A226, 347 (1974)

/13/ Holub,E., Počanič, D., Čaplar, R. and Cindro, N., Z.Physics. A296, 341 (1980)

/14/ Kalbach-Cline, C.Nucl. Phys. A210, 590 (1973)

/15/ Fu, C.F., ORNL/TM-7042, Proceedings of the Knoxville Conference on Nuclear Data (1979); see also Proceedings of the IAEA Advisory Group Meeting on Basic and Applied Problems of Nuclear Level Densities, Brookhaven, USA, April 1983

/16/ Akkermans, J.M., Gruppelaar, H and Reffo, G., Phys. Rev. C22 73, (1980)

/17/ Gruppelaar, H., Costa, C., Nierop, D. and Akkermans, J.M., ECN-82-114 Petten, August 1982, Antwerp Conference on Nuclear Data, 6-10.Sept. 1982.

/18/ Strohmaier, B. and Uhl. M., Antwerp Conf. on Nucl. Data, 6-10.Sept. 1982

/19/ Gilbert, A. and Cameron, A.G.W., Can. Journ. Phys. 43,1446 (1965)

/20/ Mann, F.M. HAUSER-5: A Computer Code to Calculate Nuclear Cross-Sections, Hanford Report HEDL-TME-78-83

/21/ Young, P.G. and Arthur, E.D, : GNASH: A Preequilibrium Statistical Nuclear Model Code for Calculations of Cross Sections and Emission Spectra, Los Alamos report, LA-6947 (1977)

/22/ Albrecht, K., and Blann, M., Phys. Rev. C8,1481 (1973)

/23/ Kalbach, C., Nuov. Cim. 29,284 (1975)

/24/ Blann, M., Phys.Rev. Lett. 27, 337(1971)700E, 1550E

/25/ Braga-Marcazzan, G.M., Gadioli-Erba, E., Milazzo-Colli,L., and Sona, P.G., Phys. Rev. C6,1398 (1972)

/26/ Goldberger, M., Phys.Rev. 74, 1269 (1948)
/27/ Kikuchi, K. and Kawai, M., Nucl. Matter and Nucl. Interactions, North-Holland Publishing Comp., Amsterdam, 1968, p.33-40.
/28/ Gadioli, E., Gadioli-Erba, E. and Sona, P.G., Nucl. Phys. A217 589 (1973)
/29/ Gadioli, E., Gadioli-Erba, E., Sajo-Bohus, L. Tagliaferri, G., Riv, Nuov. Cim. 6,(1976)
/30/ Gadioli, E., Gadioli-Erba, E., Tagliaferri, G., Hogan, J.I. Phys. Rev. Lett. 65B. 311 (1976)
/31/ Kalbach, C., Z. Physik A287, 319 (1978)
/32/ Bertrand, F.E., Peelle, R.W., Phys. Rev. C8, 1045(1973)
/33/ Kalbach, C.,: PRECO-B: Programme for Calculating Pre-equilibrium Particle Energy Spectra, informal TUNL report available on request.
/34/ Jhingan, M.L., Anand, R.P., Gupta, S.K. and Mehta, M.K., Antwerp Conference on Nuclear Data, 6. - 10.Sept. 1982.
/35/ Gudima, K.K., Osokov, G.A., Toneev, V.D., Sov. J. Nucl. Phys. 21 138 (1975)
/36/ Hermsdorf, D., Meister, A., Sassonov, S., Seeliger, D., Seidel, K. in Nuclear Theory in Neutron Nuclear Data Evaluation 1975/76, IAEA-190,I,p.663,270,272,274,283; ATOMKIc Kozlemenyek 18,229(1976)
/37/ Blann, M., Nucl. Phys. A213,570 (1973)
/38/ Blann, M., Ann. Rev. Nucl. Sci. 25, 123 (1975)
/39/ Harp, G.D., Miller, J.M., Berne, B.J., Phys. Rev. 165,1166(1968)
/40/ Harp, G.D. and Miller, J.M., Phys. Rev. C3,1847 (1971)
/41/ Chevarier, A., Chevarier, N., Demeyer, A., Hollinger, G., and Tran Minh Duc, Phys. Rev. C8,2155(1973)
/42/ Blann, M., Mignerey, A., Nucl. Phys. A 186, 245 (1972)
/43/ Blann, M., Phys. Rev. Lett. 28, 757; see also the comments in Phys. Rev. C 17, 187 and 2238 (1978)
/44/ Jahn, H., Broeders C, Broeders I., ICTP, Trieste, Jan/Feb. 1978, IAEA-SMR-43
/45/ Hermsdorf, D., Meister, A., Sassonov, S., Seeliger, D., Seidel, V. and Shahin, F., Kernenergie 17, 259 (1974) ZfK-277
/46/ Hansen, I.F., Anderson, I.D., Brown, P.S., Howerton, R.I., Kamerdiener, I.L., Logan, C.M., Plechaty, E.F. and Wong, C., Nucl. Sci. Eng. 51, 278 (1973)
/47/ Scobel, W., Bissem, H.H., Friese, J., Krause, H., Langanke, H.J., Langkau, R., Plischke, P., Scherwinski, R. and Wien, R., in Proceedings of the International Workshop on Radiation Models for Continuum Spectra of Light Particles edited by J. Ernst (University of Bonn, Bonn Germany, 1978) p.65 and Internal Report, Univ. of Hamburg, 1 Inst. für Experimentalphysik, Luruper Chaussee 149, D-2000 Hamburg 50, September, 1979, HH 79-01.
/48/ Blann, M., Hybrid Code, US-AEC Report No. COO-3494-9 (1973), Blann, M. and Plasil, F., ALICE a Nuclear Evaporation Code, US-AEC Report No. COO-3494-10 (1973)
/49/ Jahn, H., in Nuclear Theory in Neutron Nuclear Evaluation, Trieste, 1975/76, IAEA-190, Vol. II p.315
/50/ Hansen, L.F., Grims, S.M., Howerton, R.J. and Anderson J.D., Nucl. Sci. Eng. 1, 201, (1961)
/51/ Broeders, C., Broeders, I., Jahn, H., and Lalovic, M., AERE-R-8636, NEANDC(UK)-170L, NEACRP-176 (1977), Proc. Spec. Meeting on Inelastic Scattering and Fission Neutron Spectra, held at AERE, Harwell, April 14-16,1975.
/52/ Blann, M., OVERLAID ALICE, USERDA Report No. COO-3494-29; ADDITIONS and Corrections to OVERLAID ALICE, USERDA Report No. COO-3494-32 (1976)
/53/ Agassi, D., Weidenmüller, H.A. and Mantzouranis, G., Physics Reports 22C, 147 (1975)
/54/ Bunakov, V., Proceedings of the Trieste Course on Nuclear Theory for Applications, ICTP, Trieste, Jan/Feb. 1978, IAEA-SMR-43, Vienna 1980.
/55/ Mantzouranis, G., Weidenmüller, H.A. and Agassi, D., Z. Physics A276, 145 (1976)
/56/ Mantzouranis, G., Phys. Rev. C14, 2018 (1976)

/57/ Jahn, H., in Proceedings of the 3rd International Symposium on NEUTRON INDUCED REACTIONS, June 21-25, 1982, Smolenice, Czechoslovakia.

/58/ Austern, N., Direct Nuclear Reaction Theories (Wiley New York, 1970)

/59/ Blokhin, A.I., Ignatyuk, A.V., Lunev, V.P., Pronyaev, V.G., in Materials of the Fourth Kiev Conf. on Neutron Physics Part II, p.131, 1977
Blokhin , A.I., Pronyaev, V.G., Yad. Fiz. 30,1258-1269 (November 1979) Sov. J. Nucl. Phys. 30 (5)655, Nov. 1979

/60/ Tamura, T., Udagawa, T., and Lenske, H., Phys. Rev. C26, 379,(1982)

/61/ Feshbach, H., Kerman, A.K. and Koonin, An. Phy. (NY) 125, 429 (1980)

/62/ Fu , C.F., Proceedings of the Conference on Nuclear Cross Sections and Technology, Washington, D.C., March 3-7, 1975, 328

/63/ Peterson, R.J., An.of Phys. 53, 40 (1969)

/64/ Mani, G.S., Nucl. Phys. A165, 225 (1971)

/65/ SALLY: Bassel, R.H., Drisko, R.M. and Satchler, ORNL-3240 (1962)

/66/ Jahn, H., in Proceedings of an International Conference on Neutron Physics and Nuclear Data for Reactors, Harwell, United Kingdom, Sept. 1978, p.502-507.

/67/ Tsai, S.F., and Bertsch, G.F., Phys. Lett. 73B, 247, (1978)

/68/ Arndt, E. and Reif. R. in Nuclear Theory in Neutron Nuclear Data Evaluation, Trieste, 1975/76, IAEA-190, Vol. II p.353

/69/ Bonetti, R., Cammasio, M., Colli Milazzo, L., and Hodgson. P.E., Phys. Rev. C24, 71 (1981)

/70/ Bonetti, R., Commasio, M., Colli Milazzo, L. and de Rosa Phys. Rev. C21, 816 (1980)

/71/ Feshbach, H., Kerman, A.K., Lemmer, R.H., Ann. Phys. (NY), 41 230 (1967)

/72/ Dragun, O., Ferrero, A.M., and Pacheco, A., Nucl. Phys. A369 149, (1981)

/73/ Proceedings of the International Conference on Statistical Properties of Nuclei, held at Albany, New York, August 23-27,1971

A NEW LEVEL DENSITY FORMULA FOR ARBITRARY SINGLE PARTICLE LEVEL DENSITY BY NUMBER THEORETICAL METHODS

A.M. ANZALDO MENESES*
Kernforschungszentrum Karlsruhe GmbH,
Institut für Neutronenphysik und Reaktortechnik,
Karlsruhe, Federal Republic of Germany

Abstract

The nuclear level density problem has been treated using modern methods of analytical number theory. In particular the asymptotical calculation of the partition function leads to more rigorous and more general results than the usual Bethe-formula. The partition function is expressed with the help of a Dirichlet series. The parameters of this series determine the obtained level density. For the case of constant single particle level density the resulting parameters yield the usual Bethe-formula. In general the parameters lead to another energy and nucleon number dependence of the level densities. They correspond to more general single particle level densities which include the shell structure. Also the BCS type of pairing has been taken into account.

Introduction

As it is well known[1),2),3)], the relations actually in use to compute nuclear level densities are not able to reproduce quantitatively the experimental results over a wide energy range. Moreover the mathematical methods normally used make very restrictive physical assumptions in order to obtain simple analytical expressions.

*DAAD-Stipendiat. On leave from the UNAM (Universidad Nacional Autónoma de México)

At the very beginning of the investigations on nuclear level densities[4)5a)] it was clear that for large excitation energies, there was a strong relation between the methods of number theory (computation of the so called "partitions of integer numbers") and those needed to calculate the level densities. Thus for example, for the simple case of a constant single particle level density it was found that the number of partitions $p(N,E)$ of an integer number E (i.e. the excitation energy given in units of the spacing between particle levels) in parts not exceeding N(the number of particles) is equal to the level density $\rho(N,E)$ of a one component fermi gas with N particles and total energy $\varepsilon = E + \frac{1}{2}N(N+1)$. Moreover, for an infinitely degenerated system we have an exact representation given by the convergent asymptotic expansion:

$$p(E) = \frac{1}{\Pi\sqrt{2}} \sum_{k=1}^{\infty} A_k(E)\sqrt{k} \left[\frac{d}{dx} \frac{\sin\left\{\frac{\pi}{k}\left(\frac{2}{3}(x-\frac{1}{24})\right)^{1/2}\right\}}{(x-1/24)^{1/2}} \right]_{x=E}$$

where $A_k(E)$ are certain functions, the first being $A_1(E)=1$. The first term of this asymptotic expansion gives the well known result of Bethe, whereas the other terms correct this first estimation to lead to the exact result.
After these very early investigations till now there has been little progress in this sense, although the mathematical methods of number theory have experienced several important advances[6)].

In this paper the recent methods of modern number theory will be applied to obtain an asymptotical expression for the partition function which leads to a more rigorous and more general result than the usual level density formulae.

Derivation of the new level density formula

We start from the usual relation for the nuclear level density including pairing effects and obtained with help of the saddle

point method[7]. The nuclear level density reads:

$$\rho(N_n,N_p,\varepsilon) = \frac{\exp S}{(2\pi)^{3/2}\sqrt{\det|\partial^2\mu_i\mu_j S|}} \tag{1}$$

where ε is the total energy, $N_{n,p}$ is the number of neutrons (protons), $\mu_{n,p}$ are the Lagrange parameters for neutrons (protons), to be determined, S is the entropy and $\det|\partial^2\mu_i\mu_j S|$ is a certain determinant.
The entropy is given by:

$$S = \ln Z(\mu_n,\mu_p,\beta) + \beta\varepsilon - \mu_n N_n - \mu_p N_p \tag{2}$$

where $Z(\mu_n,\mu_p,\beta)$ is the partition function given by:

$$\ln Z = -\beta\sum_k(\varepsilon_k-\lambda-E_k)-\beta\frac{\Delta^2}{G}+2\sum_k\ln\left[1+\exp(-\beta E_k)\right] \tag{3}$$

The quasiparticle energies E_k are given in terms of the single particle energies, ε_k, the chemical potential λ and the energy gap Δ by:

$$E_k = \sqrt{(\varepsilon_k-\lambda)^2+\Delta^2} \tag{4}$$

G is the related to Δ by the equation:

$$\frac{2}{G} = \sum_k \frac{1}{E_k}\,\mathrm{tgh}\left(\frac{1}{2}\beta E_k\right) \tag{5}$$

The saddle point equations are:

$$\partial_{\mu_n}\ln Z_n = N_n,\ \partial_{\mu_p}\ln Z_p = N_p,\ -\partial_\beta \ln Z = \varepsilon \tag{6}$$

if $\ln Z = \ln Z_n + \ln Z_p$, from which is possible to obtain:

$$S_{n,p} = 2\left[1-\beta\partial_\beta\sum_k\ln\left(1+\exp(-\beta E_k)\right)\right]_{n,p} \tag{7a}$$

$$\varepsilon_{n,p} = \sum_k \varepsilon_k\left[1-\frac{\varepsilon_k-\lambda}{E_k}\mathrm{tgh}\left(\frac{1}{2}\beta E_k\right)\right]_{n,p} - \frac{\Delta^2_{n,p}}{G_{n,p}} \tag{7b}$$

$$N_{n,p} = \sum_k\left[1-\frac{\varepsilon_k-\lambda}{E_k}\tanh\left(\frac{1}{2}\beta E_k\right)\right]_{n,p} \tag{7c}$$

where the subscripts n,p denote neutrons and protons respectively and $S = S_n + S_p, \varepsilon = \varepsilon_n + \varepsilon_p$.

To compute these expressions asymptotically it is useful to define the "quasiparticle partition function" $\hat{Z}(\beta)$:

$$\hat{Z}(\beta) = \prod_k(1+\exp(-\beta E_k)) \tag{8}$$

and rewrite:

$$S = 2\left[1-\beta\partial_\beta\right]\ln\hat{Z}(\beta) \tag{9}$$

The estimation of $\hat{Z}(\beta)$ goes as follows:
First $|\varepsilon_k-\lambda| = \hat{\varepsilon}_k$ are substituted by integral multiples of some energy unit 1/g:

$$\hat{\varepsilon}_k = e_k/g, \text{ for } e_k \text{ positive integers} \tag{10}$$

thus:

$$\ln\hat{Z} = \sum_n a_n \ln\left[1+\exp\left(-\beta\sqrt{(n/g)^2+\Delta^2}\right)\right] \tag{11}$$

where

a_n = degeneracy of $\hat{\varepsilon}_k$, if $n=e_k$ for some e_k

and

a_n = 0 otherwise

We apply now the Mellin transformation[8]:

$$\exp\left\{-\beta m\sqrt{(n/g)^2+\Delta^2}\right\} = \frac{1}{2\pi i}\int_{c-i\infty}^{c+i\infty} dz\left(\frac{n}{g}\right)^{-z}\frac{\Delta}{\sqrt{\pi}}\left(\frac{2\Delta}{\beta m}\right)^{\frac{1}{2}z-\frac{1}{2}} \tag{12}$$

$$x\Gamma\left(\frac{z}{2}\right)K_{\frac{1}{2}z+\frac{1}{2}}(\Delta\beta m)$$

where $K_\nu(t)$ is a modified Bessel function of the second kind.

We define the Dirichlet series:

$$D(t) = \sum_n \frac{a_n}{n^t} \tag{13}$$

which will be assumed to be analytic except for simple poles at the points $\alpha > \alpha_1 > \ldots\ldots > \alpha_N > 0$ with the residues A_o, A_1, etc. Thus $Z(\beta)$ will be given by:

$$\ln Z = \frac{1}{2\pi i}\int_{c-i\infty}^{c+i\infty} dz g^z D(z)\, \frac{\Delta}{\sqrt{\pi}}\Gamma\left(\frac{z}{2}\right)\sum_m \left(\frac{2\Delta}{\beta m}\right)^{\frac{1}{2}z-\frac{1}{2}}$$

$$\frac{(-)^{m+1}}{m} K_{\frac{1}{2}z+\frac{1}{2}}(\Delta\beta m) \tag{14}$$

Using the representation:

$$t^\nu K_\nu(t) = 2^\nu \Gamma(\nu+1) e^{-t} \sum_{m=0}^{\infty} \frac{(\frac{1}{2}-\nu)_m}{(\frac{1}{2}+\nu)_{m+1}} L_m(2t) \tag{15}$$

where L_m denotes the Laguerre polynomials,

$$\ln\hat{Z} = \frac{1}{2\pi i}\int_{c-i\infty}^{c+i\infty} dz g^z D(z)\{\beta^{-z}\Gamma(z)\ (1-2^{-z})\zeta(1+z)+O(\beta^{-z+1})\}$$

$$= \sum_i A_i (1-2^{-\alpha_i})\zeta(\alpha_i+1)\Gamma(\alpha_i)(\beta/g)^{-\alpha_i} + D(0)\ln Z + O(\beta^{-\alpha_{N+1}}) \tag{16}$$

where $\zeta(x)$ denotes the Riemann ζ-function.

And for the entropy at the saddle-point:

$$S = 2D(0)\ln 2 + \sum_i (1-2^{-\alpha_i})\Gamma(\alpha_i+1)\zeta(1+\alpha_i)2A_i(\beta/g)^{-\alpha_i}(1+\frac{1}{\alpha_i}) + O(\beta^{-\alpha_{N+1}}) \tag{17}$$

which leads after some algebra to:

$$S = \sum_j M_j(\alpha_i, A_i) E^{m_j(\alpha_i)}, \quad m_j > m_{j+1} \tag{18}$$

This is a descending series of the excitation energy $E = \varepsilon - \varepsilon_o - \delta P$ (ε_o is the ground state energy and δP is a correction for pairing and shell effects). The coefficients $M_j(\alpha_i, A_i)$ and the exponents $m_j(\alpha_i)$ are given by Lagrange equations for ε and N. The leading term is of the form:

$$2^{\frac{1}{1+\alpha_o}}(1+\frac{1}{\alpha_o})\{(1-2^{-\alpha_o})\zeta(1+\alpha_o)\Gamma(1+\alpha_o)A_o\}^{\frac{1}{1+\alpha_o}} E^{\frac{\alpha_o}{1+\alpha_o}} \tag{19}$$

With equation (18) we have thus arrived at an explicit analytic expression for the entropy which shows how the relevant characteristics of the discrete single particle spectrum determines the nuclear level density for large excitation energies.
For the simple case of a constant single particle level density without pairing forces, it is easy to see that:

$$D(s) = \frac{1}{2}\{\zeta(s,x) + \zeta(s,1-x)\},\ 0<x\leq 1/2 \tag{20}$$

(where $\zeta(s,x)$ denotes the generalized Riemann ζ-function) and to find $D(0) = 0$, $A = 1$, $\alpha = 1$ which leads to:

$$\rho(E) = g\left(\frac{g^2}{g_n g_p}\right)^{1/2} \frac{6^{1/4}}{12} \frac{e^{\pi\sqrt{\frac{2}{3}gE}}}{(gE)^{5/4}} \tag{21}$$

which is the well known[1] Bethe-formula for the nuclear level density with $g = g_n + g_p$. In this case $m(\alpha)$ should be 1/2 and $M(\alpha,A)$ should be $\pi\sqrt{\frac{2}{3}g}$. It is also of interest to note that the

shell structure effects obtained for periodic single particle schemes in reference[5b] can be easily reproduced. The single particle energies are given by:

$$\varepsilon_{kl} = k + \eta(l),\ k=0,1.....;\ l=1,2.....,g$$

with

$$\sum_{l=1}^{g} \eta(l) = 0$$

where g is the number of the levels in each shell and $\eta(l)$ represent the derivation of the l-th level from the "center of gravity" of the shell. For this case the Dirichlet series has again only one pole at $\alpha = 1$ and the level density is given by the usual formula:

$$\rho(E) = \frac{1}{\sqrt{48}\,E} \exp\{\pi \sqrt{\frac{2}{3} gE}\}$$

and for the effective excitation energy we obtain

$$E = \varepsilon - \varepsilon_0 + \frac{1}{12}g - \frac{1}{2g}(n-\frac{1}{2}g)^2 + \sum_{l=1}^{n}\eta(l) + \frac{1}{2}\sum_{l=1}^{g}\eta^2(l)$$

where n is the number of particles in the last shell. This relations are in agreement with those of reference[5b].
It is also possible to compute analytic expressions for other single particle spectra. For example for an harmonic oscillator with energies $\varepsilon_k = (k+3/2)\hbar\omega$ we obtain:

$$D_{osc.}(S) = \frac{2}{(\hbar\omega)^s}\{\zeta(s-2,1/2)+(\frac{\lambda^2}{(\hbar\omega)^2} - \frac{1}{4})\ \zeta(s,\ 1/2)\} \qquad (22)$$

and for the partition function $\hat{Z}$:

$$\ln\hat{Z}_{osc.} = \frac{\pi^2}{6\hbar\omega\beta}\left|\frac{\lambda^2}{(\hbar\omega)^2} - \frac{1}{4}\right| + \frac{7\pi^2}{180(\hbar\omega\beta)^3} + O(\beta) \qquad (23)$$

The shell correction method

The mathematical treatment applied in the preceding section provides also a method to study the closely related Strutinsky calculations for ground state shell corrections[9].
The effect of the shell structure on the potential energy surface is expressed usually in the form

$$\delta U = U - \tilde{U} \qquad (24)$$

where U is the total single particle energy sum given by:

$$U = \int_{-\infty}^{\lambda} d\varepsilon\varepsilon g(\varepsilon),\ N = \int_{-\infty}^{\lambda} d\varepsilon\ g(\varepsilon) \qquad (25)$$

with

$$g(\varepsilon) = \frac{1}{2\pi i}\int_{-i\infty}^{i\infty} d\beta\ e^{\beta\varepsilon}\ Z_0(\beta) \qquad (26)$$

using the partition function:

$$Z_0(\beta) = \sum_k e^{-\beta\varepsilon_k} \qquad (27)$$

The smoothed energy $\tilde{U}$ is given by the system:

$$\tilde{U} = \int_{-\infty}^{\tilde{\lambda}} d\varepsilon\varepsilon\tilde{g}(\varepsilon),\ N = \int_{-\infty}^{\tilde{\lambda}} d\varepsilon\tilde{g}(\varepsilon) \qquad (28)$$

where $\tilde{g}(\varepsilon)$ is the smoothed level density function[10]:

$$\tilde{g}(\varepsilon) = \frac{1}{\gamma}\sum_k \zeta_M\left[\frac{1}{\gamma}(\varepsilon-\varepsilon_k)\right] \qquad (29)$$

defined by the energy-smoothing parameter γ and by the smearing functions $\zeta_M(x)$:

$$\zeta_M(x) = P_M(x)\omega(x) \qquad (30)$$

where $P_M(x)$ is a so-called curvature correction polynomial of Mth degree and $\omega(x)$ is a weight function.

To compute $\tilde{g}(\varepsilon)$ we proceed first with an asymptotical computation of $Z_o(\beta)$ using the Mellin transformation

$$e^{-\beta\varepsilon} = \frac{1}{2\pi i}\int_{c-i\infty}^{c+i\infty} ds\,(\beta\varepsilon)^{-s}\Gamma(s),\ \mathrm{Re}\beta\varepsilon > 0,\ c > 0 \qquad (31)$$

to find

$$Z_o(\beta) = \sum_{j=1}^{n} B_j\Gamma(\lambda_j)B^{-\lambda_j} + D_o(0)+O(\beta^{-\lambda n+1}) \qquad (32)$$

where

$$D_o(s) = \sum_k \frac{b_k}{\varepsilon_k^s},\ \varepsilon_k \neq \varepsilon_m \text{ for } k \neq m \qquad (33)$$

b_k is the degeneracy of the level ε_k and we assume that $D_o(s)$ has only simple poles at $s = \lambda_j > \lambda_{j+1} > 0$ with residues B_j.
We obtain in this way:

$$\tilde{g}(\varepsilon) = \sum_j B_j\varepsilon^{\lambda_j-1} + D_o(0)\delta(\varepsilon) \qquad (34)$$

without the introduction of any parameters in addition to those defining the single particle spectrum.
As a simple example it is easy to find for the single particle level density of a cubic box potential of side L, the smoothed expression:

$$\tilde{g}(\varepsilon) = \frac{1}{4\pi^2}\left(\frac{2mL^2}{\hbar^2}\right)^{3/2}\sqrt{\varepsilon} - \frac{3}{8\pi}\left(\frac{2mL}{\hbar^2}\right)^{1/2}\frac{1}{\sqrt{\varepsilon}} - \frac{1}{8}\delta(\varepsilon) \qquad (35)$$

which agrees with the result of reference [11] obtained using a semiclassical procedure.
Another example very easy to compute is the isotropic harmonic oscillator with a constant spin-orbit interaction with hamiltonian:

$$H = \frac{-\hbar^2}{2M}\nabla^2 + \frac{1}{2}M\omega^2r^2 - k\hbar\omega\mathbf{l}\cdot\sigma \qquad (36)$$

leading to

$$\tilde{g}(\varepsilon) = \frac{(1-k^2)\varepsilon^2}{3(\hbar\omega)^3(1-k^2)^2} - \frac{k^3\varepsilon}{(\hbar\omega)^2(1-k^2)^2} + \frac{10k^4-9k^2-3}{12\hbar\omega(1-k^2)^2} + \frac{5k^3-2k^5\delta(\varepsilon)}{12(1-k^2)^2} \qquad (37)$$

which is also in agreement with the semiclassical calculation of the same quantity [12].

Conclusions

It is easy to see that the obtained asymptotic expression for the entropy (eq.(18)) will lead to more general relations than for the case of only one pole. But even for only one pole we obtain a more general expression than the usual Bethe-formula.
It must be stressed that the analytic properties of the Dirichlet series D(t) depend only on the structure of the quasiparticle spectra and that the knowledge of this would determine entirely the nuclear level density through the parameters appearing in eq.(18).
The usual assumptions of a continuous single particle level density were not required, representing thus another advantage of this method. Of special interest is the possibility to study through the analytic behaviour of D(t) very important contributions like those arising from the shell structure of the spectra and their expected disappearance for very high excitation energies.

The so-called a-parameter defined by

$$a = S^2/4E \qquad (38)$$

can also be calculated in term of the general characteristics of the single particle spectrum. Preliminary calculations using deformed single particle potentials of the Nilsson type reproduce qualitatively the energy dependence of the a-parameter reported in reference [13),14)] and [15)]. Figure 1 shows the results

of reference[13] computed numerically for a single-component system having particle numbers 40 and 50 with a Nilsson spectrum. Figure 2 shows the parametrized energy dependence of the a-parameter of reference[14] for ^{210}Po and ^{232}U. Figure 3 shows the energy dependence of the a-parameter of the neutron channel (a_n) derived from an analysis of cross-section for the reaction ^{206}Pb (α,f) from ref.[15]. It is clear that the observed energy dependence can be well reproduced by the expansion given by equation (19). Additional calculations as well as a study of the effect of deformation on the level densities are actually in progress.

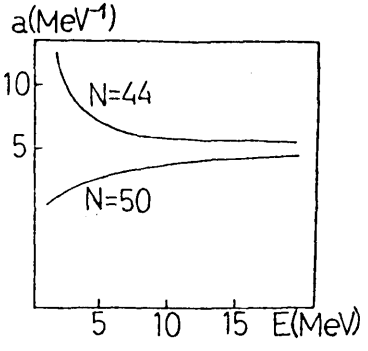

FIG. 1

Energy dependence of the a-parameter for a single component system.

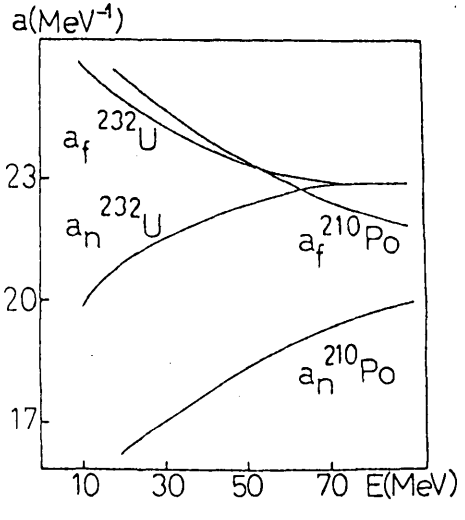

FIG. 2

In this figure a_f is the a-parameter at the fission saddle point deformation and a_n is the a-parameter at equilibrium.

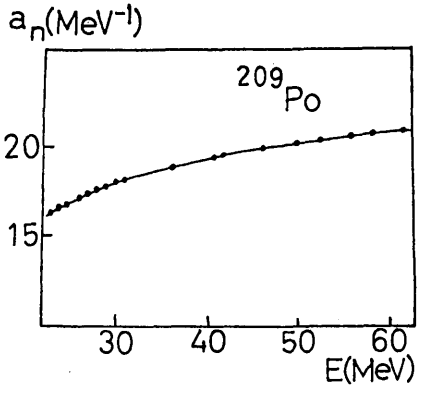

FIG. 3

Energy dependence of the a-parameter of the neutron chanel (a_n) derived from an analysis of cross-sections for the reaction $^{206}Pb(\alpha,f)$ from ref[15].

References

1. T.Ericson, Adv.Physics 9(1960) 425.
2. V.S.Stavinskii, Sov.J.Part.Nucl.3,(1973) 417.
3. V.S.Rammamurthy, Nuclear Theory of Applications IAEA-SMR-43, Vienna; 1980, p.187.
4. H.A.Bethe, Phys. Rev.50,(1936) 332.
5a. C. van Lier, G.E. Uhlenbeck, Physica 4, (1937) 531.
5b. P.B.Kahn+N.Rosenzweig, Phys. Rev. 187(1969) 1193
6. C.E.Andrews, The Theory of Partitions, Addison Wesley Publishing Co., Reading, Massachussetts (1976).
7. M.Sano and S.Yamasaki, Progr. Theor. Phys.29, (1963) 397.
8. F.Oberhettinger, Tables of Mellin Transforms, Springer-Verlag Berlin, (1974)
9. P.A.Gottschalk, T.Lederberger, Nucl.Phys. A278, (1977) 16
   G.G. Bunatyan, Yad. Fiz. 29,(1979) 38
   W.Z.Reisdorf, Z.Phys. A300, (1981) 227
10. V.M.Strutinsky, F.A.Ivan juk, Nucl. Phys. A255,(1975) 405
11. R.K.Bhaduri, C.K.Ross, Phys. Rev. Lett. 27,(1971) 606
12. B.K.Jennigs, R.K.Bhaduri, M.Brack, Nucl.Phys. A253,(1975) 29
13. A.V.Ignatyuk, Y.N.Shubin, Sob. J. Phys. 8,(1969) 660
14. M.Ploszajcak and M.E.Faber, Phy. Rev.C25, (1982) 1538
15. M.G.Itkis et al., Yad.Fiz. 16,(1972) 1150

DEUTERON EXCHANGE MECHANISM FOR ^{6}Li(n, α)

H. WEIGMANN
Central Bureau for Nuclear Measurements,
Joint Research Centre,
Commission of the European Communities,
Geel, Belgium

Abstract:

In this lecture the analysis of the low energy ^{6}Li(n,α) cross section in a model which combines resonance amplitudes with a direct deuteron exchange mechanism, is presented. Advantages and shortcomings of the present analysis are discussed, and directions of a future improvement of the model are indicated.

The model.

The ^{6}Li(n,α) reaction is of great practical importance: Its cross section is one of the most frequently used standards for neutron cross section measurements, and the reaction plays an essential role for tritium breeding in fusion reactors.

A complete multi-channel R-matrix analysis of the ^{7}Li system has been given by Hale /1/. Although this analysis describes the neutron cross sections of ^{6}Li very well, it has the disadvantage of needing an ad hoc assumption: One of the characteristic features of the ^{6}Li(n,α) reaction is its large 1/v cross section with a thermal value of 945 barn. This large 1/v cross section is usually interpreted as being due to a positive parity bound state or a far away resonance of positive parity. However, no such state has ever been positively identified.

Mahaux and Robaye /2/ have analysed the ^{6}Li(n,α) cross section and its angular distribution within S-matrix theory, including the large 250 keV 5/2- resonance and a constant s-wave background amplitude which, however, is purely phenomenological in nature.

It has been proposed by Weigmann and Manakos /3/ that the major part of the 1/v cross section of ^{6}Li may be explained as being due to a direct deuteron exchange mechanism. This proposal is based on the observation that the ^{6}Li ground state has pronounced α+d cluster properties. In ref./3/ the deuteron exchange contribution to the ^{6}Li(n,α) reaction amplitude is described by a simple pole graph, using the method of Shapiro /4/. It is shown to reproduce the channel spin 1/2 component of the thermal cross section which according to the experimental data of Glättli et.al./5/ constitutes 80% of the total thermal cross section. The channel spin 3/2 component remains unexplained at this stage.

The ^{6}Li(n,α) cross section and angular distribution at higher energies (up to 400 keV) are described within the frame of S-matrix theory. The description of the resonance amplitude follows closely the formulation of Mahaux and Robaye /2/, with two resonances (5/2- at 250 keV neutron energy and 3/2+ at 3.5 MeV) being considered. The constant background amplitude of ref./2/ is replaced by the deuteron exchange amplitude which exhibits a characteristic contribution to the angular distribution. For the details the reader is referred to ref./3/.

In fig.1 experimental and calculated values for the ratio B_1/B_0 of Legendre polynomial coefficients are shown. The experimental points are from a recent measurement of Knitter et.al./6/. For comparison, fig.2 shows the same experimental data together with calculated B_1/B_0 values which result when the deuteron exchange amplitude is replaced by a constant background amplitude. In both cases, the parameters of the model, i.e. the parameters of the two resonances taken into account and the ratio of the channel spin 3/2 and channel spin 1/2 components of the 1/v cross section, have been adjusted to reproduce the experimental data as closely as possible. The channel spin 3/2 contribution to the thermal cross section required in both cases, is indicated in the figures; it is to be compared to the experimental value

$$\sigma(s=3/2)/\sigma_{tot} = 0.20 \pm 0.023$$

from the polarization experiment of Glattli et.al./5/.

Discussion.

According to the discussion in ref./3/ the following observations can be made :

At low neutron energies (E_n < 0.5 MeV) the angular distribution is mainly determined by the interference of the 5/2- resonance with the 3/2+ background amplitude. A minor contribution to the angular distribution originates from the channel spin 1/2 deuteron exchange amplitude. Thus, the presence of a 3/2+ background is required not only by the polarisation experiment of Glättli et.al./5/, but also in order to reproduce the ^{6}Li(n,α) angular distribution at low neutron energies. Its magnitude has to be in agreement with the data of ref./5/.

At higher neutron energies the deuteron exchange mechanism will have a stronger influence on the angular distribution. The analysis is hampered, however, by the lack of accurate experimental angular distribution data, and due to the fact that the parameters of the higher energy resonances are not well known.

More in general, it can be stated that the R-matrix fit of Hale /1/ reproduces the ^{6}Li(n,α) cross sections slightly better than the present model. This is not surprising, however, since the R-matrix fit of ref./1/ is much more complete with respect to the resonance contributions to the cross sections. The present model is justified by the fact that the proposed deuteron exchange mechanism is physically realistic and that it avoids the artificial introduction of a strong 1/2+ state which experimentally is not observed, rather than by the quality of the fit obtained with the present version of the model.

Future improvement of the model.

A number of shortcomings of the analysis in its present state can be identified, and suggestions for future improvements can be made :

The treatment of the resonance contribution is incomplete. As an obvious extension, more higher energy resonances should be included in the analysis. In order to determine their parameters, also more experimental work, especially on the ^{6}Li(n,α) angular distribution at higher energies, is necessary.

The simple deuteron exchange graph is a rather crude approximation equivalent to a PWBA. The effect of higher order graphs corresponding to distorted waves should be investigated.

The origin of the channel spin 3/2 background amplitude, which constitutes 20% of the thermal cross section and predominantly determines the angular distribution at low neutron energies, should be investigated. A deuteron exchange with spin flip or, more probably, the sequential exchange of a proton and a neutron one after the other, are candidate processes.

Other reaction channels than the (n,α) channel have not been considered in the present analysis, and it is not clear how the additional direct deuteron exchange amplitude influences these other channels. This is an expression of the fact that the model in its present version which simply uses the sum of the deuteron exchange and a resonance amplitude, is not in line with the requirement of a unitary S-matrix. Thus the model should be improved in the sense that both, the resonance and direct exchange processes should be incorporated in a complete unitary S-matrix theory, and other channels besides the (n,α) channel should be included in the analysis.

Finally, the same kind of analysis can be applied to other reactions between light nuclei. The most important candidate reactions are D(d,n)^{3}He and T(d,n)^{4}He. In the latter case two exchange processes may contribute significantly: The transfer of a proton from the incoming deuteron to the triton, and the transfer of a deuteron from the triton to the incoming deuteron.

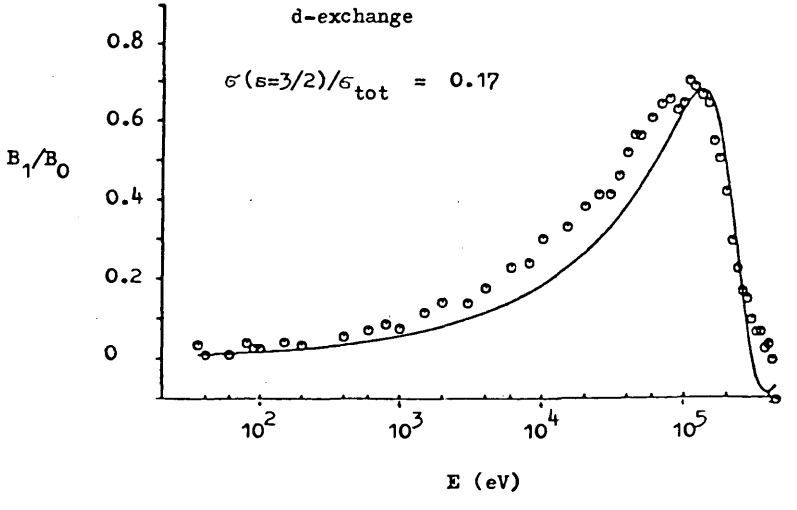

Fig.1: Experimental /6/ and calculated ratios of Legendre polynomial coefficients. Calculation with deuteron exchange model.

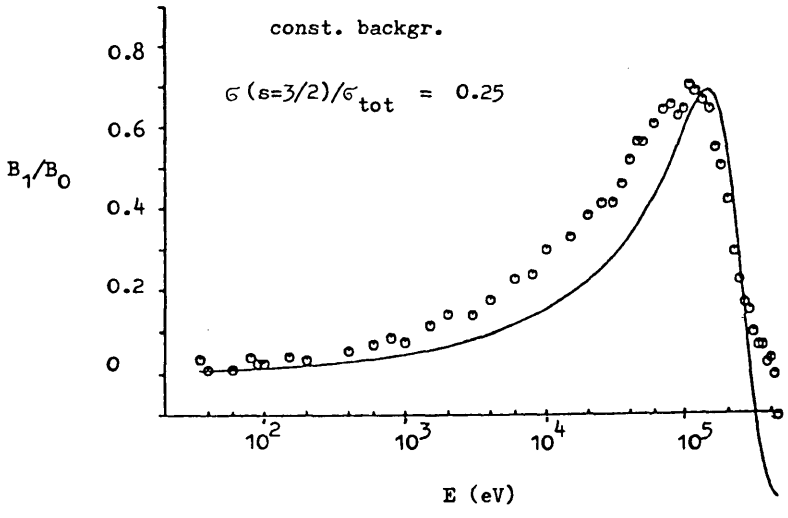

Fig.2: Experimental /6/ and calculated ratios of Legendre polynomial coefficients. Calculation with constant background.

References

1. G.M. Hale, NBS Special Publication 493 (1977) 30.

2. C. Mahaux and G. Robaye, Nucl. Phys. 74 (1965) 161.

3. H. Weigmann and P. Manakos, Z. Physik A289 (1979) 383.

4. J. Shapiro, Nucl. Phys. 28 (1961) 244 ; and "Selected Topics in Nuclear Theory", IAEA, Vienna 1963.

5. H. Glattli, A. Abragam, G.L. Bacchella, M. Fourmond, P. Meriel, J. Piesvaux and M. Pinot, Phys. Rev. Lett. 40 (1978) 748.

6. H.-H. Knitter, C. Budtz-Jorgensen, D.L. Smith and D. Marletta, accepted for publication in Nucl. Sci. Eng.

DYNAMICAL THEORIES OF NUCLEAR FISSION, VISCOSITY AND DISSIPATIVE EFFECTS

A.S. JENSEN, A. MIRANDA
Institute of Physics,
University of Aarhus,
Aarhus, Denmark

Abstract

A number of dynamical theories of nuclear fission are described. Their state of development, scope and complexity are very different. Special attention is devoted to viscosity and dissipation. One of the theories, the collective transport theory for nuclei also called the linear response theory, is of special interest. It is a general theory containing all necessary ingredients and the numerical results compare favorably with available experimental data.

Introduction

The dynamical theories claimed applicable to nuclear fission are numerous. They differ both in their potentialities for describing various aspects of the fission process and in the complexity of their structure and practical applications. As a consequence many of them have never been applied to fission. Some have been used only in single test cases, in rather schematic situations or the first stage of a full calculation. Only one theory has been extensively applied to fission. Unfortunately, it is not solidly related to any microscopic theory of the nucleus and it is only able to describe average quantities and not their fluctuations. On the other hand some of the theories have shown very encouraging preliminary results both numerically and in capability.

We want to focus especially on viscosity and dissipation. It is therefore essential from the beginning to make clear what we mean by these words. The system we study is the nucleus. It is an isolated system. Thus viscosity has nothing to do with the nucleus moving in a medium. The many interacting nucleons moving around in the nucleus, constituting the nucleus, can be viewed as a liquid of a certain viscosity. This perhaps quite natural definition is again not what is meant by viscosity in the present context.

The nucleus has many degrees of freedom. Let us chose a particular one viz. one of the so-called collective coordinates f.ex. the quadrupole deformation parameter. Let us follow its time development, resulting from a given set of initial conditions, over a time period. If it shows a decaying behaviour towards an equilibrium value, the motion is damped, energy is irreversibly dissipated into the other degrees of freedom and the coordinate behaves like a particle in one dimension under the influence of a friction force. This behaviour is not something unavoidable. It depends on the intrinsic structure of the nucleus, and the time interval we follow the motion. Thus a necessary, but not sufficient, condition for irreversible dissipation and viscosity is that we consider only a part of the total number of degrees of freedom. The interaction with the remaining part may then act as a friction force.

In most of the theories, it is necessary to chose a priori a set of collective coordinates q, perhaps given as operators. To do so we must have sufficient knowledge of the process under investigation in order to make an educated guess about the most important degrees of freedom in the dynamical description of the process. This choice is very essential for the outcome. On the other hand, the physical interpretation is simpler, and the practical work required often considerably reduced. As soon as the collective parameters are selected, we have specified a subset of the complete set of degrees of freedom and viscosity and dissipation are possible features of the behaviour of collective coordinates.

The theories can be divided into three groups (i) time dependent Hartree Fock and its approximations and extensions, (ii) influence functionals and (iii) collective transport theory for nuclei. There are, of course, relationships and links between these groups, but they are not necessarily well understood, perhaps because too little effort has been devoted to clarify such connections. The collective transport theory uses the technique of linear response theory. It is in our opinion the most promising theory on the market. It has a much broader application range than just fission. It contains all the necessary ingredients, it can be applied in practical calculations and the results compare very favourably with available experimental evidence.

These lecture notes have been written for the occasion. They are therefore only notes and not a thoroughly digested, corrected and tested piece of a textbook. The material covered is enormous. Almost each theory would need several hours for a reasonable description. It is then clear that the notes must pass quickly over many points. The selection is presumably not always logically founded but rather a result of coincidence and the authors previous interests. Thus the notes appear perhaps rather inhomogenous, but they do on the other hand reflect the situation they pretend to review, i.e. the dynamical theories of nuclear fission.

The notes are divided into three main sections according to the division of the theories. The equations are numbered consecutively within each main section and only in case of cross referencing is the section number used.

I. THE TIME-DEPENDENT HARTREE-FOCK, ITS APPROXIMATIONS AND EXTENSIONS

The discussion falls in two parts, where the first contains a description of the methods and their formal relations and the second describes the results obtained in actual applications to nuclear fission.

1. Formal development and connections

A. Time dependent Hartree Fock (TDHF)

We are interested in studying a system consisting of Z protons and N neutrons (N+Z=A nucleons) in mutual interaction. We assume that the assembly can be described by the Hamiltonian

$$H = T + V$$
$$T = \sum_i \frac{p_i^2}{2m_i} \qquad (1)$$
$$V = \frac{1}{2} \sum_{j \neq k} V_{jk}$$

The "bare" nucleons masses are represented by m_i and the "bare" interaction between two nucleons j and k by the potential V_{jk}. These parameters are to be taken from measurements on the "free" nucleon systems[1]. The potential V_{jk} shows a complicated dependence on everything that characterizes the nucleons and their relative motions, i.e. their relative separation $\underset{\sim}{r}_{jk}=\underset{\sim}{r}_j-\underset{\sim}{r}_k$ their relative momentum $\underset{\sim}{p}_{jk}=\underset{\sim}{p}_j-\underset{\sim}{p}_k$, their spins $\underset{\sim}{\sigma}_j$ and $\underset{\sim}{\sigma}_k$ as well as their charge quantum numbers q_j and q_k.

One can take nowadays this "bare" potential between two nucleons from the meson theory of nuclear forces[1]. The potential is mostly due to exchange of pions (the lightest of hadrons), though dominated by various pion resonances. A very schematic summary of the present understanding is shown in fig.1.

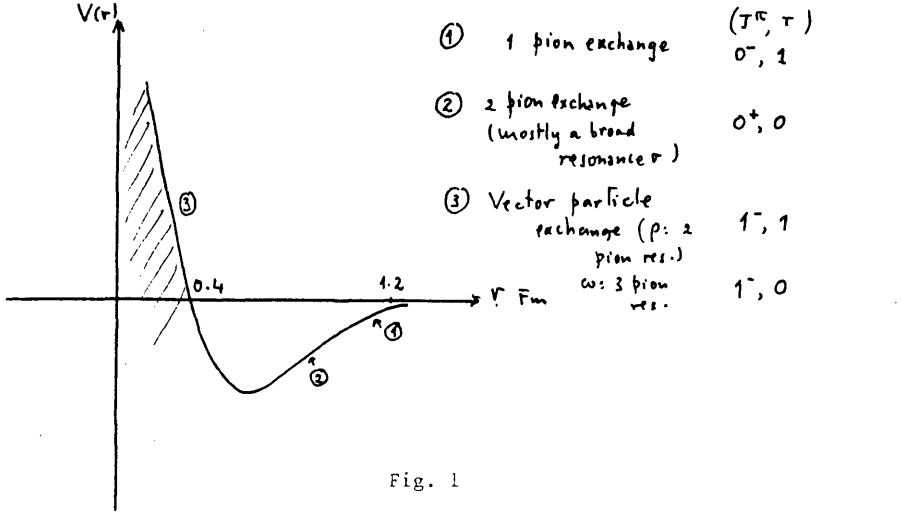

Fig. 1

The figure pretends to reproduce the main features of the interaction in a low relative angular momentum state of the two nucleons. The spin J,

parity π and isospin T of the resonances are indicated. The upshot of all this is that these potentials in the decisive NN-channels are rather singular, with a strong short-range repulsive core at about r= 0.4 Fm, and an attractive medium range potential due to two pion exchange, fairly well represented by a σ -resonance. The single pion exchange provides the tail of the potential at about 2 Fm, and is also responsible for most of the very important tensor force in the effective potential. The existence of the repulsive core is essential for the stability of nuclear matter and for its saturation properties. As a consequence of this, it is fairly obvious that there must be short range correlations between two nucleons inside the nucleus: as they approach each other, strong repulsions become operative which prevents them coming closer to each other than about 0.4 Fm. It is this very essential fact about short range correlations that has been in the past one of the main sources of our troubles. When attempting to use Hartree-Fock methods (so successful in atomic and molecular physics) to nuclei, one finds immediately that these methods cannot handle the situation referred to above. The remedy was found many years ago by Brueckner, and later perfectioned by Bethe and his collaborators[2]. The Brueckner-Bethe theory shows how to reduce this violent, instantaneous interaction to a pseudopotential that is well-behaved, soft and non-singular. Unfortunately it is also energy-dependent, that is, it contains a built-in time-delay. This again is a source of much trouble in applications of the Brueckner-Bethe theory.[2]

Let us return to (1). Choose a (hermitean) potential

$$U = \sum_i U(i)$$

and write

$$H = (T+U) + (V-U)$$

$$= H_0 + W \qquad (2a)$$

$$H_0 = \sum_i \frac{p_i^2}{2m_i} + U(i)$$

$$W = \frac{1}{2}\sum_{j\neq k} V_{jk} - \sum_j U(j) \qquad (2b)$$

The auxiliary potential U is to be chosen so that it helps improving the convergence of the many-body perturbation theory based upon H_o. Brueckners theory gives a definite prescription about how best to pick up H_o and W in order to completely and efficiently solve the hard-core problem mentioned previously[2]. However, as also mentioned, the practical problems for nuclear applications are considerable.

We shall not follow the Brueckner theory here, but go to work in a much more phenomenological way. That is, we consider H_o to be the kinetic energy, and W as some suitably chosen interaction (not necessarily two-body). We now believe that a good candidate for this is the Skyrme interaction[3]. To a fair extent, it seems to reproduce some of the main features of the Brueckner-Bethes effective interaction. But with the Skyrme interaction we can again use Hartree-Fock methods[3]. The price to be paid is of course that the relationship to the bare nuclear forces is at best very remote.

Let us now recapitulate the main ideas behind the Hartree-Fock method (or the self-consistent field method)[4].

It is one of a rather large family of variational methods.

Suppose we are looking for the equilibrium states of our N-nucleon system. Choose a suitably parametrized many-body wavefunction $\Psi(1,2,\ldots,N)$ and compute

$$E = \frac{\int \bar{\Psi}^*(1,2,\ldots,N)\, H\, \Psi(1,2,\ldots N)\, d(1)\ldots d(N)}{\int \bar{\Psi}^*(1,2,\ldots N)\, \Psi(1,2,\ldots N)\, d(1)\ldots d(N)} \qquad (3)$$

Determine now the parameters of Ψ in such a way that small variations

$$\Psi \to \Psi + \delta\Psi\,(1,2,\ldots,N)$$

$$\Psi^* \to \Psi^* + \delta\Psi^*\,(1,2,\ldots,N)$$

imply

$$\delta E = 0$$

to the first order of small quantitites $\delta\Psi$ and $\delta\Psi^*$.

Alternatively, the normalization condition on the wave-function may be considered as a constraint. Then consider

$$E = \langle \underline{\Psi} | H | \underline{\Psi} \rangle$$

and extremize it subject to the constraint

$$\langle \underline{\Psi} | \underline{\Psi} \rangle = 1$$

To achieve this, use the method of Lagrange multipliers. Define

$$E' = E - \lambda \langle \underline{\Psi} | \underline{\Psi} \rangle \qquad (4a)$$

where λ is a Lagrange multiplier. Carry now the unconstrained variation on E'

$$\delta E' = 0 \qquad (4b)$$

If there are no further á priori conditions on $\underline{\Psi}$ and its variations then one gets simply the Schrödinger equation

$$H \underline{\Psi}(1,2,\dots N) = \lambda \underline{\Psi}(1,2,\dots N) \qquad (5)$$

where λ appears now as the energy eigenvalue. The Hartree-Fock approximation consists in picking up a particular trial wavefunction $\underline{\Psi}$, á priori restricted to be in the class of Slater determinants (or a product of Slater determinants, if the protons and neutrons are treated as distinguishable)

$$\underline{\Psi}(1,2,\dots,A) = \frac{1}{\sqrt{N!}} \begin{vmatrix} \varphi_{\nu_1}(1) & \varphi_{\nu_2}(1) & \dots & \varphi_{\nu_N}(1) \\ \varphi_{\nu_1}(2) & \dots & \dots & \varphi_{\nu_N}(2) \\ \vdots & & & \vdots \\ \varphi_{\nu_1}(N) & \dots & \dots & \varphi_{\nu_N}(N) \end{vmatrix} \qquad (6)$$

This wavefunction is automatically normalized if

$$\int \varphi_\nu^+(1)\, \varphi_\nu(1)\, d(1) = 1 \qquad (7)$$

The φ's are single-particle wavefunctions, to be determined. They are in fact 2-spinors

$$\varphi_\nu(1) = \begin{pmatrix} \varphi_{\nu_1}(1) \\ \varphi_{\nu_2}(1) \end{pmatrix} \qquad \varphi_\nu^+(1) = \left(\varphi_{\nu_1}^*(1)\ \varphi_{\nu_2}^*(1) \right)$$

with complex components $\varphi_{\nu\sigma}(1)$ $(\sigma = 1, 2)$. We are going to choose them in such a way that

$$E = \langle \underline{\Psi} | H | \underline{\Psi} \rangle$$

is extremized, subject to the conditions (7). We insist then that

$$\delta E' = \delta \left(E - \sum_{\nu=1}^{N} \lambda_\nu \int \varphi_\nu^+(1)\, \varphi_\nu(1)\, d(1) \right) = 0 \qquad (8)$$

The E' is thus a functional of the φ_ν and φ_ν^+. We have

$$E'\{\varphi_\nu, \varphi_\nu^+\} = \sum_{\nu \text{ occ.}} \int \varphi_\nu^+(1) (h_\sigma(1) - \lambda_\nu) \varphi_\nu(1)\, d(1) + \qquad (9)$$

$$+ \frac{1}{2} \sum_{\nu_a \nu_b} \int d(1) \int d(2)\, \varphi_{\nu_a}^+(1)\, \varphi_{\nu_b}^+(2)\, v(1,2) \left[\varphi_{\nu_a}(1)\, \varphi_{\nu_b}(2) - \varphi_{\nu_a}(2)\, \varphi_{\nu_b}(1) \right]$$

From (8) and (9) we get the equations

$$\frac{\delta E'\{\varphi, \varphi^+\}}{\delta \varphi_\nu^+(1)} = 0 \qquad (10a)$$

$$\frac{\delta E'\{\varphi, \varphi^+\}}{\delta \varphi_\nu(1)} = 0 \qquad (10b)$$

This leads to the Hartree-Fock equations

$$h_0(1)\varphi_\nu(1) + \sum_{\mu\ occ.} \int d(2)\, \varphi_\mu^+(2)\, v(1,2) \left[\varphi_\nu(1)\,\varphi_\mu(2) - \varphi_\nu(2)\,\varphi_\mu(1) \right] = \lambda_\nu \varphi_\nu(1) \qquad (11)$$

In all of these equations, the notation $\sum_{\nu occ}$ means that the sum must be carried out over the single particle states represented in the Slater determinant (6).

The system of highly non-linear equations (11) must now be solved.

Note that the trial wavefunction (6) contains no build-in dynamical correlations. It does contain, however, and exactly, the statistical correlations demanded by the Pauli principle for Fermions.

The idealized result of completely solving (eq.11) is schematized in fig. 2.

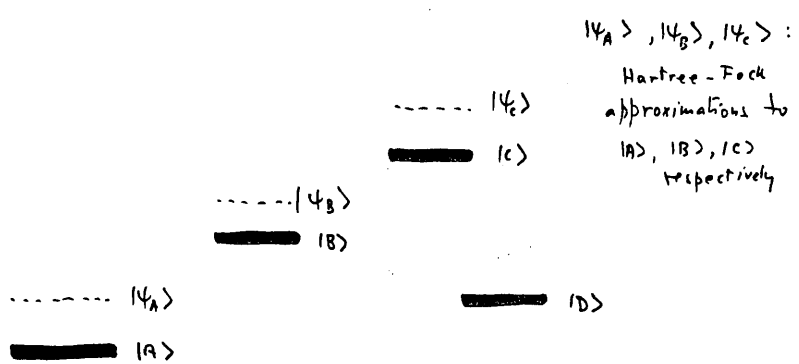

Fig. 2

In this figure $|A\rangle$, $|B\rangle$, $|C\rangle$ ..., are true physical states of our nuclear system, all having definite symmetries. Ideally, we should get approximations to at least some of these states, if H_o and W were correctly chosen, and if we could solve (11) and find all the solutions. Notice that the Hartree-Fock approximation, being based on a variational principle, approaches the lowest state of a given symmetry from above.

In practice, unfortunately, we are far from achieving anything like this. There are considerable problems (even if we knew how to pick up H_o and W correctly) connected with the non-linearity of (11). Some iterative methods must be used. Convergence is not guaranteed. As a consequence, unless some further assumptions are made, we cannot be sure of reaching the stationary state that we want to approximate.

The above method provides only static solutions, of course. It is in particular well-suited for studying ground states. In fission problems (and problems connected with deep inelastic nuclear scattering) we are also interested in time-dependent (non-stationary) states, ideally solutions of the time-dependent Schrödinger equation

$$i\hbar \frac{\partial \Psi}{\partial t} = H\Psi \qquad (12)$$

It can be shown that this equation (like (5)), results from a variational principle that generalizes (8). Consider the action

$$S_{t_1,t_2} = \int_{t_1}^{t_2} dt\ L(t) \qquad (13)$$

$$L(t) = \langle \Psi(t) \left| H - i\frac{\partial}{\partial t} \right| \Psi(t) \rangle \qquad (14)$$

The solutions Ψ (and Ψ^*) of eq.(12) are the functions that extremize the action (13), i.e. they make

$$\delta S_{t_1,t_2} = 0 \qquad (15)$$

for small (arbitrary) variations around $\Psi(t)$ and $\Psi^*(t)$.

Our approximation consists in assuming that $\Psi(t)$ (and its conjugate) are a priori restricted to the class of (time-dependent) Slater determinants. The time-dependence is carried by the single-particle wavefunctions

$$\varphi_\nu(1,t)$$

Thus the variation principle results in the time-dependent Hartree-Fock equations[4]

$$i\hbar \frac{\partial}{\partial t} \varphi_\nu(1,t) = h_0(1)\, \varphi_\nu(1,t) + \qquad (16)$$

$$+ \sum_{\mu \text{ occ.}} \int d(2)\, \varphi_\mu^+(2,t)\, v(1,2) \left[\varphi_\nu(1,t)\, \varphi_\mu(2,t) - \varphi_\nu(2,t)\, \varphi_\mu(1,t) \right]$$

These equations must now be solved subject to appropriate initial conditions.

B. The Time-Dependent Hartree-Fock-Bogoliubov Approximation (TDHFBA).

Let us consider again the H.F. approximation to the ground-state, i.e. the solution of the system of equations (11) that corresponds to the absolute minimum of the energy. This leads to the approximate ground state energy

$$E_0 = \sum_{\nu \text{ occ}} \int \varphi_\nu^+(1)\, h_0\, \varphi_\nu(1)\, d(1) + \frac{1}{2} \sum_{\substack{\nu \mu \\ \text{occ.}}} \int d(1) \int d(2)\, \varphi_\nu^+(1) \cdot \qquad (17)$$

$$\cdot \varphi_\mu^+(2)\, v_{12} \left[\varphi_\nu(1)\, \varphi_\mu(2) - \varphi_\nu(2)\, \varphi_\mu(1) \right]$$

where now the $\varphi_\nu, \varphi_\nu^+$ are supposed to be solutions of the system (11) corresponding to the absolute minimum of the energy. However, whether this is in fact a minimum depends on the dynamics: it may happen that the actual residual forces in nuclei are such that a solution that is supposed to be the absolute minimum not only is not the absolute minimum, but is not stable at all. This is in fact the case for nuclei, as is well known.[5] The so-called pairing residual forces tend to destabilize the Hartree-Fock solution. We shall define here a "pairing force" to be any attractive residual force between two identical nucleons occupying two orbitals that are time-reversed of each other. As a result of such forces, bound states of two identical nucleons are formed. These time-reversed orbitals are assumed of course to be degenerate (Coriolis forces in rotating deformed nuclei do tend to lift this degeneracy, and thereby they oppose the effects of the pairing forces). The energies of the orbitals involved in this phenomenon lie rather close to the Fermi energy of the nucleus. In practice, this means that pairing forces act mostly among the orbitals of the last major shell that is being filled up. Therefore the energy spread of the contributing orbitals is significantly less than say the spacing between two consecutive major shells. Typical orders of magnitude of these parameters are[5]

$$\text{Pairing force} \rightarrow \quad \Delta \sim \frac{12}{\sqrt{A}} \ \text{MeV} \qquad (18)$$

$$\text{Major shell spacing} \rightarrow \quad \hbar\omega_0 \sim \frac{41}{A^{1/3}} \ \text{MeV}$$

This means that this pairing effect is in fact only a perturbation upon the basal shell structure of nuclei. That it nevertheless takes such an enermous importance in the physics of nuclei is a reflection of the circumstance that it is operative (as we mentioned) in a narrow energy band around the Fermi energy, which is precisely the area that controls most of the low energy nuclear phenomenology. We could mention here that the Skyrme force referred to above is not really designed to account for pairing forces - it therefore is usually supplemented by further components that do have the specific pairing character mentioned above[6].

The formal treatment of pairing in nuclei is most conveniently carried out in the second quantized formalism.[5] Let us therefore begin by reformulating the above in this formalism.

Consider the Hamiltonian

$$H = \sum_i h_0(i) + \frac{1}{2} \sum_{i \neq k} W_{ik} \qquad (19)$$

consisting for simplicity of at most two-body terms - there is no real reduction of generality. Furthermore, we continue considering only one kind of fermions, again with no loss of generality. We can express H in a second quantized form[5]:

$$H = \sum_{\mu\nu} \langle \mu | h_0 | \nu \rangle\, a_\mu^+ a_\nu + \frac{1}{4} \sum\sum_{\mu\nu\alpha\beta} V_{\mu\nu\alpha\beta}\, a_\mu^+ a_\nu^+ a_\beta a_\alpha \qquad (20)$$

where a^+_μ (a_ν) are single-fermion creation (and annihilation) operators, that respectively creates (destroys) a fermion in the (for the moment unspecified) single particle state $|\mu\rangle$ ($|\nu\rangle$). The amplitudes $V_{\mu\nu\alpha\beta}$ are the antisymmetrized matrix elements of the two-body part of H:

$$V_{\mu\nu\alpha\beta} \equiv \langle \mu\nu | v_{12} | \alpha\beta \rangle = \langle \mu\nu | v_{12} | \alpha\beta \rangle - \langle \mu\nu | v_{12} | \beta\alpha \rangle$$

$$\equiv \int d(1) \int d(2)\, \varphi^+_\mu(1)\, \varphi^+_\nu(2)\, v_{12}\, \varphi_\alpha(1)\, \varphi_\beta(2) - \int d(1) \int d(2)\, \varphi^+_\mu(1)\, \varphi^+_\nu(2)\, v_{12}\, \varphi_\alpha(2)\, \varphi_\beta(1) \qquad (21)$$

Let us go over to the Heisenberg picture:

$$a^+_\mu(t) = e^{iHt}\, a^+_\mu\, e^{-iHt} \qquad (22)$$

The stationary states of H are denoted by $|n\rangle$:

$$H|n\rangle = E_n |n\rangle$$

The ground state in particular is $|0\rangle$ with energy E_0.

The Heisenberg equations of motion for these quasiparticle operators are obtaiend from (22):

$$i \frac{d}{dt} a^+_i(t) = -[H, a^+_i(t)] \qquad (23a)$$

$$\begin{cases} i \dot{a}^+_k(t) = -\sum_\mu h_{\mu k} a^+_\mu(t) - \frac{1}{2} \sum_{\mu\nu} \sum_{\alpha\beta} V_{\mu\nu k\beta}\, a^+_\mu(t)\, a^+_\nu(t)\, a_\beta(t) \\ i \dot{a}_j(t) = \sum_\mu h^*_{\mu j}\, a_\mu(t) + \frac{1}{2} \sum_{\mu\nu} \sum_{\alpha\beta} V^*_{\mu\nu j\beta}\, a^+_\beta(t)\, a_\nu(t)\, a_\mu(t) \end{cases} \qquad (23b)$$

Consider now the so-called density matrix:

$$\rho_{jk}(t) = \langle 0 | a^+_k(t)\, a_j(t) | 0 \rangle \qquad (24)$$

By using (23a) and £23b) we get the equation of motion for $\rho_{jk}(t)$:

$$i \frac{d}{dt} \rho_{jk}(t) = \sum_\nu h_{j\nu}\, \rho_{\nu k}(t) - \sum_\nu h_{\nu k}\, \rho_{j\nu}(t) + \qquad (25)$$

$$+ \frac{1}{2} \sum_{\nu_i} V_{\nu_1\nu_2\nu_3 k} \langle 0 | a^+_{\nu_1}(t)\, a^+_{\nu_2}(t)\, a_{\nu_3}(t)\, a_j(t) | 0 \rangle - \frac{1}{2} \sum_{\nu_i} V_{j\nu_2\nu_3\nu_4} \langle 0 | a^+_k(t)\, a^+_{\nu_2}(t)\, a_{\nu_3}(t)\, a_{\nu_4}(t) | 0 \rangle$$

These equations are of course exact. They constitute the first link of a a rather long chain of coupled equations. The remaining links can be obtained by considering next the equation of motion of the higher density matrices

$$\langle 0 | a^+_k a^+_j a_\ell a_m | 0 \rangle \qquad (26)$$

Solving this huge chain of equations is of course tantamount to solving the Schrödinger equation (12) itself.

Here we can begin our series of approximations. The leading approximation boils down to the TDHF. We assume that we can approximate $|0\rangle$ by a Slater determinant, symbolized in the following figure

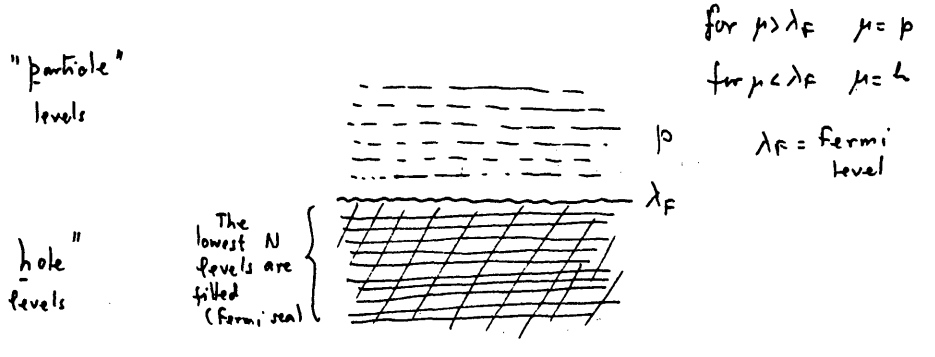

Fig. 3

The Hartree-Fock ground state $|0\rangle$ satisfies the condition

$$a_p |0\rangle = 0$$
$$a^+_h |0\rangle = 0 \qquad (27)$$

Next assume the following:

$$a_\mu^+ = \sum_p \langle p|\mu\rangle a_p^+ + \sum_h \langle h|\mu\rangle a_h^+ \qquad (28)$$

or

$$a_\mu = \sum_p a_p \langle \mu|p\rangle + \sum_h a_h \langle \mu|h\rangle$$

where $\langle p|\mu\rangle$, $\langle h|\mu\rangle$ are (for the moment) unknown amplitudes. With these assumptions, it is an easy matter to verify that

$$\langle 0|a_1^+ a_2^+ a_4 a_3|0\rangle = \langle 0|a_1^+ a_3|0\rangle \langle 0|a_2^+ a_4|0\rangle - \langle 0|a_1^+ a_4|0\rangle \langle 0|a_2^+ a_3|0\rangle \qquad (29)$$

This is the approximation: it allows us to break the chain at an early stage. Inserting (29) into the equations (25) we get

$$i\dot\rho_{12} = \sum_3 h_{13}\rho_{32} - \sum_3 \rho_{13} h_{32} + \sum_3\sum_4\sum_5 v_{1345}\rho_{42}\rho_{53} - \sum_3\sum_4\sum_5 v_{4523}\rho_{14}\rho_{35}$$

Defining

$$w_{14}\{\rho\} \equiv \sum_3\sum_5 v_{1345}\rho_{53} \qquad (30)$$

we get

$$i\dot\rho_{12} = \sum_3 h_{13}\rho_{32} - \sum_3 \rho_{13}h_{32} + \sum_4 w_{14}\rho_{42} - \sum_4 \rho_{14} w_{42} = [(h_0+w)\rho]_{12} - [\rho(h_0+w)]_{12} \qquad (31a)$$

or in matrix form

$$i\dot\rho = [h\{\rho\}, \rho(t)] \qquad (31b)$$

where

$$h\{\rho\} = h_0 + w\{\rho\} \qquad (32)$$

is the Hartree-Fock Hamiltonian. The reader can easily verify that within our approximation the matrix ρ behaves like a projection operator

$$\rho^2 = \rho \qquad (33)$$

(eq(31b) is the time-dependent Hartree-Fock equation. Result (31b) is easily shown to be equivalent to our previous results.

Let us now examine what we have done. We have chosen a "vacuum state" (i.e. the ground state) to have the following properties:

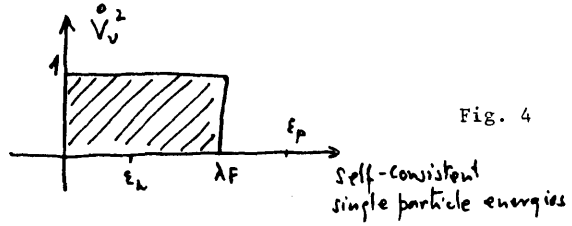

Fig. 4

The Fermi level λ_F is determined by the conditions

$$\langle 0|\hat N|0\rangle = \sum_k \langle 0|a_k^+ a_k|0\rangle = N$$

The first N states under λ_F are occupied with probability 1, and the levels above λ_F are empty with probability 1. Define these probabilities respectively as $\mathring{V}_k^2$ and $\mathring{U}_k^2$:

$$\mathring{U}_k^2 + \mathring{V}_k^2 = 1$$

$$\mathring{V}_k^2 = \begin{cases} 1 & k = h < \lambda_F \\ 0 & k = p > \lambda_F \end{cases} \qquad (34)$$

$$a_p|0\rangle = 0$$
$$a_h^+|0\rangle = 0$$

Define the amplitudes

$$v_k^0 = + \sqrt{v_k^{0\,2}} \qquad (35)$$

$$u_k^0 = + \sqrt{u_k^{0\,2}}$$

to be real. Then conditions (34) can be summarized thus:

$$\alpha_k |0\rangle = 0 \qquad \text{all } k \qquad (36)$$

if

$$\alpha_k = u_k^0 a_k + v_k^0 a_{\bar{k}}^+ \qquad (37)$$

The notation $\bar{k}$ means "the time-reversed state of k":

$$|\bar{k}\rangle = T|k\rangle \qquad (38)$$

where T is the time-reversal operator as defined in ref. 5. In the context of the present Hartree-Fock theory, there is no motivation for introducing these conventions. We do it for future convenience.

The Hartree-Fock approximation is thus characterized by these sharp probability distributions for occupancies of the self-consistent set of single-particle states (at least for the case of zero temperature that we are considering now). The existence of pairing forces among time-reversed single-particle states leads to the conclusion that the above cannot be a description of the ground state of our system. The correct approximation, as is well-known, consists in choosing a new trial state for $|0\rangle$ (the BCS-state), and new quasiparticles satisfying the property

$$\alpha_k |0\rangle = 0 \qquad \text{all } k \qquad (39a)$$

with

$$\alpha_k = u_k a_k + v_k a_{\bar{k}}^+ \qquad (39b)$$

The amplitudes u_k and v_k can be chosen to be real, and such that

$$u_k = u_{\bar{k}} \quad , v_k = v_{\bar{k}} \quad , u_k^2 + v_k^2 = 1 \qquad (40)$$

However, in contrast to u_k^0 and v_k^0 the new probabilities are no longer step-like distributions over the quasiparticle states. They turn out to have in general the form sketched in the following figure

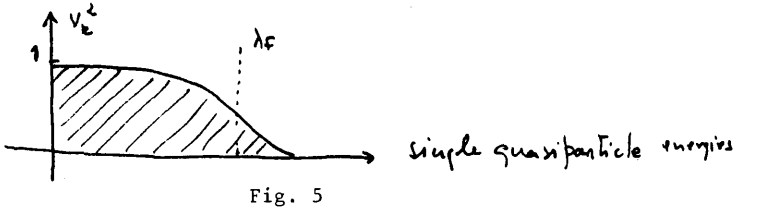

Fig. 5

The essential point is, there is no longer any Fermi surface, and hence no natural distinction between p-type and h-type quasiparticle states, as is the case with the Hartree-Fock approximation. The exact form of v_k can be determined from the variation principle - the result is that they are found by solving the Hartree-Fock-Bogoliubov equations, to which we now turn[7].

Consider again the linear transformation (28), and write

$$a_\mu^+ = \sum_\nu \langle \nu | \mu \rangle \alpha_\nu^+$$

We shall now allow a more general linear transformation, the so-called generalized Bogoliubov-Valatin canonical transformation, designed to take into account the basic features of the pairing correlations

$$a_\mu^+ = \sum_\nu \left[\langle \nu | \mu \rangle \alpha_\nu^+ + \langle \bar{\nu} | \mu \rangle \alpha_{\bar{\nu}} \right] \qquad (41)$$

With this more general transformation, the result (29) must be corrected. We now get, as the reader can verify

$$\langle 0 | a_1^+ a_2^+ a_4 a_3 | 0 \rangle = \langle 0 | a_1^+ a_3 | 0 \rangle \langle 0 | a_2^+ a_4 | 0 \rangle - \langle 0 | a_1^+ a_4 | 0 \rangle \langle 0 | a_2^+ a_3 | 0 \rangle + \langle 0 | a_1^+ a_2^+ | 0 \rangle \langle 0 | a_4 a_3 | 0 \rangle \qquad (42)$$

With these assumptions, it should be clear that we no longer are describing a system with fixed number of fermions, as hitherto we have been doing. This is the price we must pay for the simplest possible extension of the self-consistent field method that allows for pairing. We can thus restore particle number conservation only in the mean. We introduce therefore a constraint, that on the average the particle number is to be fixed at N, i.e.

$$\langle 0|\hat{N}|0\rangle = N \tag{43}$$

This constraint must be taken into account in the usual way through Lagrange multipliers, before we proceed to the variational calculations. Then define

$$H' = H - \lambda \hat{N} = \sum_{\nu_1\nu_2} \langle \nu_1|h_0 - \lambda\delta_{\nu_1\nu_2}|\nu_2\rangle a_{\nu_1}^+ a_{\nu_2} + \frac{1}{4}\sum_{\nu_1\cdots} V_{\nu_1\nu_2\nu_3\nu_4} a_{\nu_1}^+ a_{\nu_2}^+ a_{\nu_4} a_{\nu_3} \tag{44}$$

$$H' = \sum_{\nu_1\nu_2} h'_{\nu_1\nu_2} a_{\nu_1}^+ a_{\nu_2} + \frac{1}{4}\sum_{\nu_1\cdots} V_{\nu_1\nu_2\nu_3\nu_4} a_{\nu_1}^+ a_{\nu_2}^+ a_{\nu_4} a_{\nu_3} \tag{45}$$

with

$$h'_{\nu_1\nu_2} = \langle \nu_1|h_0 - \lambda\delta_{\nu_1\nu_2}|\nu_2\rangle \tag{46}$$

The approximation (42) shows that we must now consider other types of densities, besides the Hartree-Fock density (24) - the pair densities:

$$\tilde{\rho}_{12} = \langle 0|a_2 a_1|0\rangle \tag{47a}$$

$$\tilde{\rho}_{12}^* = \langle 0|a_1^+ a_2^+|0\rangle \tag{47b}$$

Equations of motion for all these densities (generalizing 31b) can be easily found by considering the so-called Nambu representation

$$N_\nu = \begin{pmatrix} a_\nu \\ a_{\bar{\nu}}^+ \end{pmatrix} \tag{48}$$

Consider then the generalized density matrix (including pair densities)

$$\hat{\rho}_{\nu\mu} = \langle 0|N_\nu N_\mu^+|0\rangle \equiv \langle N_\nu N_\mu^+\rangle = \begin{pmatrix} \langle a_\nu a_\mu^+\rangle & \langle a_\nu a_{\bar{\mu}}\rangle \\ \langle a_{\bar{\nu}}^+ a_\mu^+\rangle & \langle a_{\bar{\nu}}^+ a_{\bar{\mu}}\rangle \end{pmatrix} \tag{49}$$

The equations of motion for its elements, now using the approximation (42), are

$$i\frac{d}{dt}\langle a_2^+ a_1\rangle = \sum_\nu h'_{1\nu}\langle a_2^+ a_\nu\rangle - \sum_\nu h'_{\nu_2}\langle a_\nu^+ a_1\rangle + \sum_\nu W_{1\nu}\langle a_2^+ a_\nu\rangle - \sum_\nu W_{\nu_2}\langle a_\nu^+ a_1\rangle + \sum_\nu \Delta_{1\nu}\langle a_2^+ a_\nu^+\rangle + \sum_\nu \Delta_{\nu_2}^*\langle a_\nu a_1\rangle \tag{50a}$$

and

$$i\frac{d}{dt}\langle a_2^+ a_1^+\rangle = \sum_\nu h'_{\nu 1}\langle a_\nu^+ a_2^+\rangle - \sum_\nu h'_{\nu_2}\langle a_\nu^+ a_1^+\rangle - \sum_\nu W_{\nu_2}\langle a_\nu^+ a_1^+\rangle + \sum_\nu W_{\nu_1}\langle a_\nu^+ a_2^+\rangle - \sum_\nu \Delta_{\nu_2}^*\langle a_1^+ a_\nu\rangle - \sum_\nu \Delta_\nu^*\langle a_2^+ a_\nu\rangle + \Delta_{12}^* \tag{50b}$$

and its complex conjugate. We have defined

$$W_{\alpha\beta} = \sum_{\nu_1\nu_2} V_{\alpha\nu_1\beta\nu_2}\langle a_{\nu_1}^+ a_{\nu_2}\rangle \tag{51}$$

$$\Delta_{\alpha\beta} = \frac{1}{2}\sum_{\nu_1\nu_2} V_{\alpha\beta\nu_1\nu_2}\langle a_{\nu_2} a_{\nu_1}\rangle \tag{52}$$

By means of def.(49) , eqs. (50a) and (50b), we can neatly summarize all these equations:

$$i\frac{d}{dt}\hat{\rho} = [H_{HFB}, \hat{\rho}] \qquad (53)$$

as the self-consistent equation extending the Hartree-Fock equation (31). The matrix

$$H_{HFB} = \begin{pmatrix} \mathcal{H} & \Delta \\ -\Delta^{+} & -\bar{\mathcal{H}}^{+} \end{pmatrix} \qquad (54)$$

is the Hartree-Fock-Bogoliubov matrix. The sub-matrices Δ have matrix elements given by (52). The submatrix H is the single-particle energy matrix, already encountered in the Hartree-Fock approximation (cf.(32))

$$\mathcal{H}_{\mu\nu} = (h' + w)_{\mu\nu} \qquad (55)$$

These equations are still too complicated for the extensive numerical work demanded by fission theory. People proceed therefore to further approximations, that might be good enough for a first orientation. As an example of an useful approximation, that actually has been applied in studies of nuclear fission, consider the following case, discussed by Blocki and Flocard.[8] Assume:

a) That the canonical transformation (41) is of the simple type

$$\begin{aligned} a_{\mu}^{+} &= u_{\mu}\,\alpha_{\mu}^{+} - v_{\mu}\,\alpha_{\bar{\mu}} \\ a_{\bar{\mu}}^{+} &= u_{\mu}\,\alpha_{\bar{\mu}}^{+} + v_{\mu}\,\alpha_{\mu} \end{aligned} \qquad (56)$$

with

$$u_{\mu} = u_{\bar{\mu}} \quad , v_{\mu} = v_{\bar{\mu}}$$

b) That the pairing matrix elements contributing to the "gap equation" (52b) are of the type

$$V_{\alpha\beta\nu\mu} = -\delta_{\beta\bar{\alpha}}\,\delta_{\mu\bar{\nu}}\,G \qquad (57)$$

where G is a constant. This is the case that has been very popular in studies of static pairing (nuclear spectroscopy).

The amplitudes u_{μ} and v_{μ} in (56) need not be real; however, all that matters is their relative phase. We shall therefore assume that u_{μ} is real, but that v_{μ} may be complex.

With these assumptions, we get from (52)

$$\begin{aligned} \Delta_{\bar{\alpha}\beta} &= \frac{1}{2}\sum_{\nu_1\nu_2} V_{\bar{\alpha}\beta\bar{\nu}_1\nu_2}\,\langle a_{\nu_2}\, a_{\bar{\nu}_1}\rangle \\ &= -\delta_{\alpha\beta}\,\Delta^{*} \end{aligned} \qquad (58a)$$

with

$$\Delta = G\sum_{\nu>0} K_{\nu} \qquad (58b)$$

and

$$K_{\nu} = u_{\nu}v_{\nu} \qquad (58c)$$

The notation $\sum_{\nu>0}(\cdots)$ means that the time-reversed state of ν must not be included in the summation, as it has already been accounted for.

Eq(50b) gives

$$i\dot{K}_{\nu} = \left(\mathcal{H}_{\nu\nu} + \mathcal{H}_{\bar{\nu}\bar{\nu}}\right)^{*}K_{\nu} + \Delta\,(2\rho_{\nu} - 1) \qquad (59a)$$

where we have defined

$$\rho_{\nu} = |v_{\nu}|^{2} = \rho_{\bar{\nu}} \qquad (59b)$$

From (46), 51a) and (55) we have

$$\mathcal{H}_{\nu\nu} = \langle\nu|\, h_0 - \lambda + w\,|\nu\rangle = \epsilon_{0\nu} - \lambda + w_{\nu\nu} \qquad (60a)$$

with

$$\epsilon_{0\nu} = \langle \nu | t_0 | \nu \rangle$$

$$W_{\nu\nu} = \sum_{\nu_1\nu_2} V_{\nu\nu_1\nu\nu_2} \langle a^+_{\nu_1} a_{\nu_2} \rangle \qquad (60b)$$

$$= \sum_{\alpha} \rho_{\alpha} V_{\nu\alpha\nu\alpha}$$

Hence

$$H_{\nu\nu} = H_{\bar{\nu}\bar{\nu}} = H_{\nu\nu}^* = H_{\bar{\nu}\bar{\nu}}^* = \qquad (60c)$$

$$= e_\nu - \lambda$$

with

$$e_\nu = \epsilon_{0\nu} + \sum_{\alpha} \rho_{\alpha} V_{\nu\alpha\nu\alpha} \qquad (60d)$$

Inserting these results into (59a) we get

$$i\dot{K}_\nu = 2(e_\nu - \lambda) K_\nu + \Delta (2\rho_\nu - 1) \qquad (61)$$

Eq.(50a) gives

$$i\dot{\rho}_\nu = \Delta^* K_\nu - \Delta K_\nu^* \qquad (62)$$

Eq.(61) and (62) are the so-called dynamical pairing equations. They must be solved self-consistently, together with (43) and (58b). A simple two-pairing levels model has been thoroughly discussed by Blocki and Flocard[7], as an illustration.

At this point, these authors introduce further assumptions designed to facilitate the actual determination of the "single particle energies" e_ν. They show for example that one can determine e_ν by defining them to be

$$e_\nu = \int d^3\underline{r}\ \varphi_\nu^+(\underline{r},t)\, \hat{H}(\rho)\, \varphi_\nu(\underline{r},t) \qquad (63)$$

where $\varphi_\nu(r,t)$ are single particle wavefunctions satisfying the TDHF-equations

$$i\frac{\partial \varphi_\nu}{\partial t} = \left(\hat{H}(\rho) - e_\nu\right)\varphi_\nu \qquad (64)$$

$\hat{H}(\rho)$ is a one-particle Hartree-Fock Hamiltonian. It could be derived for instance from a Skyrme-type effective interaction.[3] ρ is the single particle density.

Further discussions of this model, as well as other examples of plausible approximations, inspired by studies of static pairing (nuclear spectroscopy), can be found in the paper by Blocki and Flocard.

C. The Adiabatic Time-Dependent Hartree-Fock Theory (ATDHF).

The self-consistent theories outlined in the previous sections are the starting point of much contemporary theoretical work relevant to the fission problem. Much of this work attempts to simplify, or to extend, the above-formulation[9,10,11,38,39]. All the basic problems one encounters in this connection appear already at the level of the TDHF theory. We shall therefore in this section restrict ourselves to this theory in order to avoid unnecessary complications. The following discussion could, however, with little effort, be extended to the TDHFB theory.

The selection of the approximation method is to a large extent guided by physical considerations, i.e. by the understanding one has achieved of the physics of the problems that have to be solved. In the case of nuclear fission, understanding of some of the basic features of this process has been achieved through the intelligent use of the nuclear collective model, the earliest version of which came to be known as the Liquid Drop Model. It provided the first successful theory of fission. The collective model has furthermore had tremendous success in the field of nuclear spectroscopy, as is well-known.[5] Nonetheless, its relationships to the basic effective forces among nucleons in nuclei are very obscure.

Practitioners of the TDHF theory claim that this theory can provide a microscopic basis for the collective model.[7] This connection is the object of study of much of the above-mentioned work. If established, it would obviously reduce much of the apparent arbitrariness that characterizes the collective model, thus enhancing its predictive power.

The adiabatic approximations to the TDHF theory is one of the main approach roads to this desirable goal. Recall that adiabacity is also one of the basic assumptions of the collective model. Adiabacity means here essentially that the collective motion has velocities that are in some sense small compared to intrinsic particle velocities in nuclei. As a consequence, the nucleonic motion adjusts itself practically instantaneously to the changes in the collective coordinates with time.

Consider a single coordinate q = q(t), say the β-deformation parameter of a fissioning nucleus. In the context of the collective model, as applied to the quadrupole mode, this corresponds to ignoring the γ-coordinate and the 3 Euler angles defining the orientation in space of the deformed nucleus. Within the adiabatic approximation, the Hamiltonian for this coordinate can be put in the form

$$H = \frac{1}{2} M(q) \dot{q}^2 + V(q) \qquad (65)$$

where M(q) is a mass parameter characterixing the q-motion, and V(q) a given potential energy. Recall that the Bohr Hamiltonian for the quadrupole mode[5], for example, is determined partly by adiabacity requirements (which allow one to retain no more than quadratic terms in the collective velocity, linear terms being ruled out by time-reversal invariance), and partly by general symmetry requirements. This alone does not of course fix the form of the functions M and V in the Hamiltonian. Notice also that the Hamiltonian (65) is entirely classical. Quantization can of course be carried out in a straightforward manner, even if somewhat complicated by the fact that in general the collective coordinates are curvilinear.

One of the main goals of the ATDHF theory is to obtain the Hamiltonian in the form (65). If this is achieved, then that would be progress, as both the mass parameter of the motion and the potential energy surface V should then in principle be determined by the effective nuclear forces.

The ATDHF theory uses two basic features of the TDHF:

a) If the density matrix $\rho(t)$ obeys the property

$$\rho^2 = \rho \qquad \mathrm{Tr}\,\rho = N \qquad (66)$$

at time t, and also obeys the TDHF equation, then the property (66) is preserved for all times.

That is, if at time $t = t_0$, the solution of the TDHF equation is a Slater determinant, then the TDHF equation can only transform it into another Slater determinant.

b) The function

$$E = \langle \Psi(t) | H | \Psi(t) \rangle$$

where $\Psi(t)$ is a Slater determinant obeying the HF equation, is independent of time :

$$\frac{dE}{dt} = 0 \qquad (67)$$

E can therefore be interpreted as the total energy of the system, E_0 (see eq.(17))- it is conserved. Recall that

$$E_0 = \sum_{\nu \in \mathrm{occ}} \int \varphi_\nu^\dagger(1)\, h_0\, \varphi_\nu(1)\, d(1) + \frac{1}{2} \sum_{\substack{\nu_1 \nu_2 \\ \mathrm{occ.}}} \int d(1) \int d(2) \Big[\cdot \varphi_{\nu_1}^\dagger(1)\, \varphi_{\nu_2}^\dagger(2)\, v_{12} \left(\varphi_{\nu_1}(1)\, \varphi_{\nu_2}(2) - \varphi_{\nu_1}(2)\, \varphi_{\nu_2}(1) \right) \Big]$$

$$\therefore E_0 = \sum_{\mu\nu} h_{\mu\nu}\, \rho_{\mu\nu} + \frac{1}{2} \sum_{\mu\nu} \sum_{\alpha\beta} \rho_{\beta\alpha}\, v_{\alpha\beta\mu\nu}\, \rho_{\nu\beta} \qquad (68)$$

$$\therefore E_0 = \mathrm{Tr}\, h\rho + \frac{1}{2}\, \mathrm{Tr}(1)\, \mathrm{Tr}(2)\, \rho(1)\, v(1,2)\, \rho(2)$$

The Hartree-Fock Hamiltonian (32) is in this notation

$$h(1) = h_0(1) + \mathrm{Tr}\, V(1,2)\, \rho(2) \qquad (69)$$

Properties a) and b) can easily be proved: both are vital for the following approximations[9].

We now search for a way (hopefully unique!) to put (68) in the "phenomenological" form (65).

One of our tasks will then be to identify what q(t) and $\dot{q}(t)$ are. Expressions (68) and (69) contain only microscopically defined coordinates (the nucleonic positions, spins and charge quantum numbers). There is no obvious prescription as how to define something like q or $\dot{q}$. It is true that in the so-called RPA-approximation to the TDHF equation (31b), these collective coordinates and velocities (or rather, momenta) arise naturally as a consequence of the equations themselves[5], but the RPA is a small amplitude approximation, i.e. valid only for small deviations from the (stable) equilibrium solution ρ_{eq}, i.e. the solution satisfying

$$i\frac{\partial \rho_{eq}}{\partial t} = 0 = \left[h\{\rho_{eq}\}, \rho_{eq} \right]$$

We are however not interested in this small amplitude approximation, as it is a meaningless approximation in the context of fission.

Whichever way we choose to define q and $\dot{q}$, we shall have to satisfy a basic property that distingushes one from the other in the classical formulation: q(t) is even under time-reversal (at least in the absence of external magnetic forces), whereas $\dot{q}(t)$ is odd. With this in mind, we shall restrict ourselves here to even-N systems; for odd-N, the properties under time-reversal will be more complicated.

One of the possible ways of introducing these collective coordinates in the theory would be through a constrained Hartree-Fock approximation. For example, choose a set of time-even one-particle opearators $\hat{q}_i$ (i=1,2,...K), such as the zero components of even multipole operators

$$\hat{q}^{\lambda}_{0} = \sum_{p=1}^{N} r_p^{\lambda} Y^{\lambda}_{0}(p)$$

Then insist that the Hartree-Fock state $|\Psi(t)\rangle$ satifies the constraints

$$\langle \Psi(t) | \hat{q}_i | \Psi(t) \rangle = q_i(t) \qquad (70)$$

This can be achieved through the usual Lagrange multipliers. The Hamiltonian H is to be modified to

$$H' = H - \sum_{i=1}^{K} \lambda_i \hat{q}_i \qquad (71)$$

The λ's are to be determined by the conditions (70). Thus the Hartree-Fock determinants

$$\Psi(\xi_1, \xi_2 \ldots \xi_N; q_1, q_2 \cdots q_K)$$

become parametrized by these K time-dependent parameters. We have

$$\hat{q} = \sum_{\nu_1\nu_2} \langle \nu_1 | \hat{q} | \nu_2 \rangle a^{+}_{\nu_1} a_{\nu_2} = \sum_{\nu_1\nu_2} q_{\nu_1\nu_2} a^{+}_{\nu_1} a_{\nu_2}$$
$$\langle \Psi(t) | \hat{q} | \Psi(t) \rangle = q(t) = \mathrm{Tr}(\rho(t)\hat{q}) \qquad (72)$$

The constraint operator $\hat{q}$ is usually time-even; if q(t) is to be time-even, then $\rho(t)$ must be time-even. That is to say, if T is the time-reversal operator then

$$\rho_T = T \rho T^{-1} \qquad (73)$$

is required to be equal to ρ. It can be shown that, except for static Hartree-Fock solutions, this is not in general the case[9].

The solution to this problem proposed by Baranger and Veneroni[9] is the following:

Introduce two new hermitean, time-even matrices χ and ρ_0, and the similarity transformation

$$\rho(t) = e^{i\chi(t)} \rho_0(t) e^{-i\chi(t)} \qquad (74)$$

As a consequence of (66), one can immediately see that

$$\rho_0^2 = \rho_0$$
$$\mathrm{Tr}\,\rho_0 = N \qquad (75)$$

That is, ρ_0 is also a Slater determinant, now time-even by definition. How can such a time-even Slater determinant be obtained in practice? That is easy. Take, for example, a time-even potential such as a Nilsson potential[5] and fill up the first N levels (recall that N is even) at a given deformation. The resulting Slater determinant would be an example of a ρ_0.

Let us now **make use** of the idea of adiabacity. If the collective motion is assumed to be slow, then $\Psi(t)$ is almost in static equilibrium at t. Hence, the matrix

$$\rho_T = e^{-i\chi(t)} \rho_0(t) e^{i\chi(t)} \tag{76}$$

that represents the time-reversed motion, must be almost the same as ρ. This implies that the (dimensionless) $\chi(t)$ must be small relative to unity: it is our adiabacity parameter. We expand everything in powers of χ and retain only the leading powers - at least as many as are required to produce an Hamiltonian of the form (65).

Before doing that, however, let us note that transformation (74) by itself does not define uniquely the matrices χ and ρ_0, of course. Baranger and Veneroni have shown that it is possible to impose further conditions on χ and ρ_0 so that they become uniquely defined.

Consider

$$\sigma_0 = 1 - \rho_0 \tag{77}$$

The additional conditions could be

$$\rho_0 \chi \rho_0 = \sigma_0 \chi \sigma_0 = 0 \tag{78}$$

$$-\frac{\pi}{4} < \text{eigenvalues of } \chi < \frac{\pi}{4}$$

The first condition states that χ has no particle-particle and no hole-hole matrix elements in a representation that diagonalizes ρ_0. In this case, we can write

$$\chi = \chi_{ph} + \chi_{hp}$$

These conditions makes the restricted χ, after the adiabacity assumption is applied, to behave like a canonical momentum conjugate to the generalized coordinate ρ_0, and hence a natural adiabacity paramter.

Write then

$$\rho(t) = \rho_0(t) + \rho_1(t) + \rho_2(t) + \cdots$$
$$h(t) = h^{(0)}(t) + h^{(1)}(t) + h^{(2)}(t) + \cdots \tag{79}$$

with

$$\rho_1 = i[\chi, \rho_0]$$
$$\rho_2 = -\frac{1}{2}[\chi, [\chi, \rho_0]] \tag{80}$$

and the Hartree-Fock potential

$$h_0^{(0)} = h_0 + \mathrm{Tr}\, V \rho_0$$
$$h^{(1)} = \mathrm{Tr}\, V \rho_1 \tag{81}$$
$$h^{(2)} = \mathrm{Tr}\, V \rho_2$$

The even terms in these expansions correspond to time-even parts and the odd terms to time-odd parts.

Inserting these expressions in the Hartree-Fock equation one gets, separating time-even from the time-odd parts

$$i\dot{\rho}_0 = [h^{(0)}, \rho_1] + [h^{(1)}, \rho_0] \tag{82}$$
$$i\dot{\rho}_1 = [h^{(0)}, \rho_0] + [h^{(0)}, \rho_2] + [h^{(1)}, \rho_1] + [h^{(2)}, \rho_0]$$

The result is that the energy E_0 can be expressed in the form

$$E_0 = T + V \tag{83a}$$

where T is the kinetic energy of the collective motion

$$T = T(\rho_0, \dot{\rho}_0) = \mathrm{Tr}\, h^{(0)} (\sigma_0 \rho_1^2 \sigma_0 - \rho_0 \rho_1^2 \rho_0) + \frac{1}{2} \mathrm{Tr}\, h^{(1)} \rho_1 \qquad (83b)$$

and the potential energy

$$V = V(\rho_0) = \mathrm{Tr}\, h_0 \rho_0 + \frac{1}{2} \mathrm{Tr}(1)\, \mathrm{Tr}(2)\, \rho_0(1)\, V(1,2)\, \rho_0(2) \qquad (83c)$$

is just the expectation value of the many-body Hamiltonian H for the Slater determinant ρ_0. It represents that which in the collective model parlance would be called the "energy surface", or "deformation energy".

If we choose to parametrize ρ_0 in terms of generalized coordinates $q_i(t)$ as mentioned above, then the potential energy V would become simply a function of the q's:

$$V = V(q_1, q_2, \cdots, q_K) \qquad (84)$$

Using now the formula

$$\dot{\rho}_0 = \sum_{i=1}^{K} \frac{\partial \rho_0}{\partial q_i} \dot{q}_i \qquad (85)$$

the kinetic energy (83b) can be put in the form

$$T = \frac{1}{2} \sum_{ij} m_{ij}(q)\, \dot{q}_i \dot{q}_j \qquad (86)$$

Explicit expressions for the mass tensor $m_{ij}(q)$ are discussed by Baranger and Veneroni[9].

Note that adiabacity is a vital ingredient of the theory sketeched above. Terms in the Hamiltonian corresponding to viscous forces, and traceable to the splitting of coordinates into collective and internal coupled together, do not arize. Thus the theory outlined above cannot be applied to fission, without introducing some modifications or further refinements and extensions. In view of the successful solution that it provides for the problem of how to establish contact between the microscopic self-consistent field methods and the phenomenology of the collective model, the task of improving the ATDHF theory outlined above appears to be well worth-while.

D. Restricted TDHF

The time dependent Hartree-Fock method has the defect that an enormous number of (mostly) unphysical dynamical variables are needed to describe a large system, since all orbitals in the determinantal wave function are treated similarly. A method[11] to avoid this difficulty is available. A large part of the TDHF determinant, the "core" is described by a few collective parameters. The basic assumption is that this core is inert, apart from changes associated with the motion of the collective parameters. The remainder of the determinant, the "particles", is treated microscopically in the standard way. This separation results in a dynamics in which the core is polarized by the particles which in turn evolve in the core's one-body potential. The usual self-consistent particle-particle interactions and the collective and potential energies of the core are also included. In addition to offering the possibility of significant computational advantage, our particles-core separation is the natural dynamical generalization of the microscopic-macroscopic methods used for calculating potential energy surfaces.

We employ a variational formulation of the many-body Schrödinger equation[12]. The result is a coupled set of time dependent equations of motion for the expansion coefficients describing the core particles and the collective coordinates describing the core.

In the extreme limit where the system is allowed to vary only through the core, i.e. the collective coordinates, the equations of motion are much simpler[13]. For one coordinate q they can be reduced to one second order differential equation

$$\frac{B^2}{2K} \ddot{q} + \frac{\partial E}{\partial q} = \dot{q}^2 \frac{B}{2K} \left(\frac{B}{2K} \frac{\partial K}{\partial q} - \frac{\partial B}{\partial q} \right) \qquad (87)$$

where E is the energy of the system and B and K are given in terms of the nuclear density ρ and a function Q by

$$B = \hbar \int Q \frac{\partial \rho}{\partial q} d\tau \tag{88}$$

$$K = \frac{\hbar^2}{2m} \int |\vec{\nabla} Q|^2 \rho \, d\tau \tag{89}$$

Here Q is related to the velocity potential describing the current arising from variations of q. It satisfies the continuity equation

$$\frac{\hbar}{m} \rho \, \mathrm{div}(\rho \vec{\nabla} Q) + \dot{q} \frac{\partial \rho}{\partial q} = 0 \tag{90}$$

where p (the collective momentum or velocity) is proportional to $\dot{q}$ with an arbitrary proportionality constant.

These expression can easily be generalized to more than one-collective coordinate. The equations of motion contain only quantities expressed by the nuclear density and the velocity functions Q. Thus although the starting point was Hartree-Fock, i.e. one Slater determinant, the result appears to be more general, since the parametrization of the nuclear density now can be made directly.

When the process is understood well enough to allow an educated guess of the essential degrees of freedom (parametrization) the method gives fast and accurate average quantities, which are simple approximations to those obtained by the enormously more complicated time-dependent Hartree-Fock procedure. For such processes the method is well suited for exploratory calculations of average properties. The results, i.e. the collective coordinates as function of time, are easily interpreted in simple physical terms.

The variations of the system is only through the collective coordinates and consequently it is impossible to transfer energy to the intrinsic degrees of freedom. As it stands, this formulation therefore excludes the description of dissipative phenomena. An extension in this direction would be very interesting and useful.

E. Generator coordinate method

The limitation in TDHF to a single Slater determinant can be removed by allowing linear combinations of Slater determinants. Let us assume a continous one-parameter family of Slater determinants Ψ labeled by an index α. We can think of the set arising in a constrained Hartree-Fock calculation. The wave function $\Phi(x_i)$ depending on the particle coordinates can then be written

$$\Phi(x_i) = \int d\alpha \; C(\alpha) \; \Psi(x_i, \alpha) \tag{91}$$

where $c(\alpha)$ is a function of α to be determined later.

The integral in eq.(91) is now approximated by a discrete sum of N contributions. They have to be selected carefully, close enough that no information is lost and far enough apart to avoid degenerate Slater determinants (basis states). One state Φ, labeled by an index k is then given by

$$\Phi_k(x_i) = \sum_{n=1}^{N} C_n^{(k)} \; \Psi(x_i, \alpha_n) \tag{92}$$

The given Hamiltonian H, which should be given in terms of two, three or higher-body interactions, is now diagonalized in the non-orthogonal basis set $\Psi(x_i, x_n)$.

$$H \Phi_k = E_k \Phi_k \qquad (k = 1,2,\ldots,N) \tag{93}$$

The result is N set of energies and coefficients E_k, $(c_1^k, c_2^k, \ldots c_N^k)$. The time dependence of these solutions Φ_k is then trivially given by $\Phi_k \exp(-iE_k t/\hbar)$. Thus any linear combination Φ of the Φ_k develop in time as

$$\Phi = \sum a_k \Phi_k e^{-iE_k t/\hbar} \tag{94}$$

where the expansion coefficients a_L define the state Φ at time t = 0.

Let us now imagine that the collective coordinate α is a one-dimensional path leading from the nuclear ground state over the fission barrier to two completely separated fragments. The N solutions ϕ_k described by c_i^k, i = 1,...,N then contain at least one solution where the non-vanishing c-coefficients are concentrated around the α-value corresponding to the nuclear ground state. The lowest of these is the new and improved ground state. There would also be at least one solution where all non-vanishing c-coefficients corresponds to completely separated fragments.

We want to study the time evolution of the fission process. The expansion coefficients a_k in eq.(94) are chosen such that ϕ for t = 0 reproduces $\psi(x_i, \alpha_{nB})$ where α_{nB} means the collective coordinate slightly beyond the barrier. The time dependence of ϕ, trivially given by eq.(94), is then readily obtained. The information gained is thereby limited to the time evolution along the preselected path described by α.

By choosing two degrees of freedom α and β, which could be a symmetric and a particular asymmetric division of the nucleus, we can learn several things. The procedure is in principle the same as for the one parameter case, since the elements of a finite two-dimensional matrix can be ordered into a vector. If the initial condition again is chosen to be slightly outside the barrier, we obtain besides the time evolution also the probability for symmetric and asymmetric fission.

The obvious most general countinuation of this line of thought is to choose as many degrees of freedom as we have possible mass and charge divisions of the nucleus. In principle we can then obtain the dynamic evolution of the fission process ending up with definite probabilities for each mass and charge division. This is of course absurd, since the number of collective coordinates in this type of approach must be very small, i.e. at the most about 5. Thus only a few points on the mass distribution curve can reasonably be expected to be calculated this way.

Does this procedure include any damping mechanism? To investigate this we consider again the initial condition of $\phi = \psi(x_i, \alpha_{nB})$ and study its time evolution. At a given time $t>0$ we have a distribution of α-values around the most probable α_m of them. Instead of viewing the wave function this way we may expand the individual $\psi(x_i, \alpha_n)$ in the distribution on the complete set of wave functions for α_m of non-vanishing intrinsic excitation energy. Thus the distribution of α-values is equivalent to an intrinsic excitation energy distribution for given $\alpha = \alpha_m$. In other words energy has been transferred from the collective motion to the intrinsic degrees of freedom. Therefore damping is included and can be recognized as a broadening of the distribution in the collective coordinates space.

F. TDHF with collision terms

We shall now consider yet another line of development that tries to push the TDHF theory in a direction that seems most needed in studies of low energy, large amplitude, nuclear dynamics (specially fission and deep inelastic nuclear scattering).

Recall that the time-dependent Hartree-Fock wavefunction (a Slater determinant) does not contain any dynamical correlations among quasiparticles, but does describe exactly the statistical correlations resulting from the exclusion principle. Thus the HF-quasiparticles are sharply defined states, with infinite lifetimes, a situation that clearly is unphysical. The optical model of the nucleus indeed implies that a quasiparticle in a nucleus does have a finite lifetime. These finite lifetimes may, in certain contexts (fission, deep inelastic scattering) play a vital role in the development of the actual dynamics, and therefore they must somehow be included in the formalism. We shall return to this question in the last chapter (linear response theory) of these notes.

The simplest way to do this seems to be the following[10].

We return once again to our starting point, the TDHF-equation (11). Let $\varphi_\nu(r,t)$ be a single particle time-dependent wavefunction, solution of the TDHF equation

$$i\hbar \frac{\partial}{\partial t}\varphi_\nu(1) = [h_0(1) + U_{HF}(1)]\varphi_\nu(1) \qquad (95)$$

where

$$U_{HF}(1)\varphi_\nu(1) = \int d(2)\Big[\sum_{\mu}^{occ}\varphi_\mu^+(2)v_{12}\varphi_\mu(2)\Big]\varphi_\nu(1) - \int d(2)\Big[\sum_{\mu}^{occ}\varphi_\mu^+(2)v_{12}\varphi_\mu(1)\Big]\varphi_\nu(2) \qquad (96)$$

The HF quasiparticle energies are

$$\varepsilon_\nu = \int d(1)\, \varphi_\nu^+(1)\, h(1)\, \varphi_\nu(1) \qquad (97)$$

with

$$h(1) = h_0(1) + U_{HF}(1) \qquad (98)$$

By using the known Hartree-Fock occupation probabilities $n_\nu = \overset{\circ}{V}{}_\nu^2$ (fig.4), we can drop the restriction on the summations in (96). Thus

$$U_{HF}(1)\,\varphi_\nu(1) = \int d(2)\left[\sum_\mu n_\mu\, \varphi_\mu^+(2)\, v_{12}\, \varphi_\mu(2)\right]\varphi_\nu(1) -$$

$$- \int d(2)\left[\sum_\mu n_\mu\, \varphi_\mu^+(2)\, v_{12}\, \varphi_\mu(1)\right]\varphi_\nu(2) \qquad (99)$$

The point with which we are concerned now is that these occupation probabilities n_ν must be stationary in the Hartree-Fock approximation

$$\frac{dn_\nu}{dt} = 0 \qquad (100)$$

For zero temperature, they have the step-like form shown in fig.4; for higher temperatures, they would become the Fermi-like distributions characterizing an ideal Fermi-gas.

One can perhaps in a qualitative way see how an improvement upon this situation could be achieved.

Assume that there are residual interactions among the Hartree-Fock quasiparticles (for the moment, we shall ignore pairing forces). For the sake of argumentation, let us imagine the residual forces to be two-body forces. This is no real restriction. These interactions would then introduce dynamical correlations that would invalidate (100). This means that the total rate of change of the population in quasiparticle state 1 would be

$$\frac{dn_1}{dt} = \text{Rate of creation of 1} - \text{Rate of annihilation of 1} \qquad (101)$$

For two free fermions in the initial states (with energy E_i) a and b, the rate of the transition to the final states c and d with the energy $E_f = E_i$

$$a + b \to c + d$$

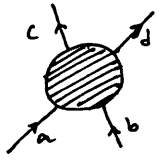

$E_i = E_f = E$

Fig. 6

is

$$W_{free}(cd;ab) = \frac{2\pi}{\hbar}\,\left|\langle cd|\,\hat{T}_{free}(E)\,|ab\rangle\right|^2 \qquad (102)$$

The matrix element on the right hand side is the antisymmetrized matrix element of the collision operator T defined by

$$S = 1 - 2\pi i\,\delta(E_i - E_f)\,\hat{T} \qquad (103)$$

S being the S-matrix. The collision is of course assumed to be energy conserving.

If the particles are quasiparticles in a medium, then the probability of collision should depend on the probabilities of occupancy of the relevant quasiparticle states, according to the Pauli Principle. Thus, the amplitude for creation of quasiparticle in state 1 is given by the sum (indicated by the blob) of all possible amplitudes of the type

A:

$E = \epsilon_3 + \epsilon_4 = \epsilon_1 + \epsilon_2$

Fig. 7

There the ϵ's are HF quasiparticle energies. It is zero, unless the states 3 and 4 have some probability of being occupied, and of course, unless states 1 and 2 have some probability of being vacant. Thus

$$\text{Rate of creation of } 1 = \frac{2\pi}{\hbar} \sum_{2} \sum_{3<4} |\langle 12|T(\epsilon)|34\rangle|^2 \delta(\epsilon_1+\epsilon_2-\epsilon_3-\epsilon_4) \cdot n_3 n_4 (1-n_1)(1-n_2) \quad (104)$$

T(E) is the collision operator in the medium, at collision energy $E = \epsilon_1 + \epsilon_2 = \epsilon_3 + \epsilon_4$. The symbol $3<4$ means that these should be no double counting of the contributions from states 3 and 4. The quasiparticle energies are given by (97). By the same token, the amplitude for annihilation of a quasiparticle in state 1 is

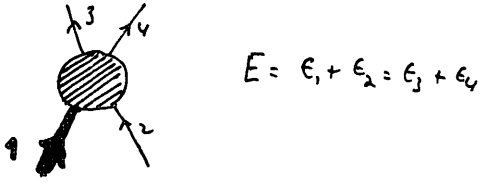

Fig. 8

with the rate

$$\text{Rate of destruction of } 1 = \frac{2\pi}{\hbar} \sum_{2} \sum_{3<4} |\langle 34|T(\epsilon)|12\rangle|^2 \delta(\epsilon_3+\epsilon_4-\epsilon_1-\epsilon_2) \cdot n_2 n_1 (1-n_3)(1-n_4) \quad (105)$$

If

$$|\langle 34|T(\epsilon)|12\rangle|^2 = |\langle 12|T(\epsilon)|34\rangle|^2$$

Then

$$\frac{dn_1}{dt} = \sum_{2} \sum_{3<4} W(12;34)\, \delta(\epsilon_1+\epsilon_2-\epsilon_3-\epsilon_4) \left[n_3 n_4 (1-n_1)(1-n_2) - n_1 n_2 (1-n_3)(1-n_4) \right] \quad (106)$$

with

$$W(12;34) = \frac{2\pi}{\hbar} |\langle 12|T(\epsilon)|34\rangle|^2 \quad (107)$$

The idea is the following: we shall assume that eq.(95) still holds, but with a modified Hartree-Fock mean field given by

$$U_{HHF}(1)\psi_\nu(1) = \int d(2) \left[\sum_\mu n_\mu(t)\, \varphi_\mu^+(2)\, v_{12}\, \varphi_\mu(2) \right] \varphi_\nu(1) - \int d(2) \left[\sum_\mu n_\mu(t)\, \varphi_\mu^+(2)\, v_{12}\, \varphi_\mu(1) \right] \varphi_\nu(2) \quad (108)$$

and

$$i\hbar \frac{\partial}{\partial t} \psi_\nu(1) = \left[h_0(1) + U_{HHF}(1) \right] \psi_\nu(1) \quad (109)$$

The probabilities $n_\nu(t)$ are now solutions of the equation (106). Thus, the Hartree-Fock equation (109) accounts for the effects of the time-varying mean field, whereas the effects of collisions are given by (106). Eq.(106) and (109) must of course be solved self-consistently. As an output, we expect among other things that this extension of the HF-thoery will show that the quasiparticles have finite lifetimes and at the same time, we will get the desired widths for the quasiparticles. Needless to say that the exact solution of (106) and (109) is quite beyond our capabilities.

Further approximations must then be made. The next main approximation consists in a simplification of the full collision matrix T(E). If the residual interactions among quasiparticles are in some sense "perturbative", then we could say that it should be sufficient to restrict ourselves to the leading approximation to T(E), i.e. to an energy-independent potential V

$$T(\epsilon) \approx V + \cdots \quad (110)$$

Then we get

$$W(12;34) = \frac{2\pi}{\hbar} |\langle 12|V|34\rangle|^2 \quad (111)$$

which is none other than the Fermi Golden Rule. The rate equation (106) simplifies

$$\frac{dn_1}{dt} = \frac{2\pi}{\hbar} \sum_{2} \sum_{34} |\langle 12|v|34\rangle|^2 \delta(\epsilon_1 + \epsilon_2 - \epsilon_3 - \epsilon_4) \cdot \left[n_3 n_4 (1-n_1)(1-n_2) - n_1 n_2 (1-n_3)(1-n_4) \right] \quad (112)$$

The system (109) and (112) is still formidable. An attempt to solve this system under various simplifying assumptions have been made by C.Y.Wong and his collaborators.[10] They have shown that the leading approximation to the n_ν's indeed has an exponential form

$$n_\nu(t) = n_\nu(0)\, e^{-\frac{\Gamma_\nu}{\hbar} t} \quad (113)$$

where the width Γ_ν is related to the quasiparticle liftetime

$$\Gamma_\nu = \frac{\hbar}{\tau_\nu} \quad (114)$$

When evaluating the collision matrix, the single particle energies (97) must then be replaced by the complex energies

$$\epsilon_\nu - i\frac{\Gamma_\nu}{2} \quad (115)$$

whereas the time-dependent probabilities $n_\nu(t)$ are "frozen" to their Hartree-Fock values. Wong et al.[10] have shown that when this is done the delta function in (112) must be smeared out to a Lorenzian form factor

$$\delta(\epsilon_1 + \epsilon_2 - \epsilon_3 - \epsilon_4) \to D(\epsilon_1 + \epsilon_2 - \epsilon_3 - \epsilon_4) = \frac{1}{2\pi} \frac{\Gamma_{1234}}{(\epsilon_1 + \epsilon_2 - \epsilon_3 - \epsilon_4)^2 + \left(\frac{\Gamma_{1234}}{2}\right)^2} \quad (116)$$

with the definition

$$\Gamma_{1234} = \Gamma_1 + \Gamma_2 + \Gamma_3 + \Gamma_4 \quad (117)$$

Other approximations are also discussed by Wong et al.[10] but which is both the best approximation scheme and the most practical one, is still an open subject. Other ways of finding practical methods of going beyond TDHF with explicit inclusion of collision terms have recently been attempted by Weidenmüller et al.[38].

G. Macroscopic nuclear dynamics

The theory is completely classical although individual quantities may be calculated using models that are partially quantal. It gives a prescription to calculate average quantities. Dissipation is included from the beginning but the corresponding diffusion can not be treated in this framework. This is a serious drawback, since fission is believed to be a diffusion process.

G1. Equations of motion

The first step is to choose a set $\{q_k\}$, $q = q_1, \ldots q_N$ of N generalized coordinates that specify those degrees of freedom of the system we want to study. They shall be called collective coordinates. The remaining coordinates needed for a complete specification of the state of the system shall be called internal coordinates. In case of fission the natural collective coordinates are the shape parameters of the nucleus.

In terms of these time dependent collective coordinates and their first derivatives we then calculate the kinetic energy T, the potential energy V and the rate of dissipation of collective energy 2F into internal excitation energy. The equations of motion are the generalized Lagrange equations[14]

$$\frac{d}{dt}\left(\frac{\partial L}{\partial \dot{q}_k}\right) - \frac{\partial L}{\partial q_k} = -\frac{\partial F}{\partial \dot{q}_k} \qquad (k = 1, 2, \ldots, N) \quad (118)$$

where the Lagrange function L for the system is given by

$$L(q, \dot{q}) = T(q, \dot{q}) - V(q) \quad (119)$$

Thus when T, V and F are known functions of q and $\dot{q}$, the equations of notion are well defined, and the time evolution of q can be found for a given set of initial conditions.

As discussed in the following subsections T and V may in principle be obtained in the framework of Hartree-Fock theory. This has usually not been the case in practice where the purely macroscopic concepts are much simpler to apply. This only reflects the present state of the theory which obviously must have a microscopic origin in order to be fully understood. The function F is more difficult to interpret in the framework of Hartree-Fock theory, although there clearly must be a connection.

G2. The potential energy.

If the degree of freedom described by each of the collective coordinate corresponds to a known operator, the potential energy surface can in principle be calculated from an effective nuclear interaction by means of the constrained Hartree-Fock method[15]. This results in a selfconsistently determined potential energy as a function of the expectation values of the operators corresponding to the collective coordinates.

One proceeds assuming that the lowest single configurations are occupied. Thus the intrinsic excitation energy is then zero, contrary to the realistic case where transfer of energy to the intrinsic degrees of freedom takes place. In order to overcome this problem one can perform temperature dependent constrained Hartree-Fock calculations[16]. The average intrinsic excitation energy is then uniquely determined from the temperature, which therefore must change according to the amount of transferred energy.

An evaluation of the potential energy as outlined above has never been carried out for a sufficient number of degrees of freedom to be usable in the present context. We have in any case the pairing force, which in principle requires Hartree-Fock-Bogoliubov calculations[15]. Such investigations are of interest in themselves, but on account of the fact that other parts of the Lagrangian are treated in a very crude fashion they are for the time being much too sophisticated for macroscopic nuclear dynamical studies.

Instead, the liquid drop[17] (or droplet) energy expression is used as the first approximation. If required it can then be improved by adding shell and pairing corrections calculated by the Strutinsky method[18]. The potential energy can thereby be shown to approximate the constrained Hartree-Fock-Bogoliubov energy. Both liquid drop parameters[19] and Strutinsky shell corrections[20] may be obtained as functions of temperature.

G3. The kinetic energy.

The kinetic energy could presumably most accurately, but also at the expense of an enormous amount of work, be obtained from the mass parameters of adiabatic time-dependent Hartree-Fock calculations[11]. In the present context this has so far not been attempted. Simpler expressions for the kinetic energy are available, viz. one due to the cranking model (an approximation to adiabatic time-dependent Hartree-Fock) and another corresponding to irrotational flow of an incompressible fluid.

G3a. Cranking mass.

The cranking model assumes that the lowest lying state of the Hamiltonian H for each q is occupied with probability unity. Since q is a function of time the energy of this state changes in time and the total energy conservation is assured through a compensating change of kinetic energy. Such a calculation[26] leads to

$$T = \frac{1}{2} \sum_{i,k} B_{ik}(q)\, \dot{q}_i \dot{q}_k \qquad (120)$$

where the inertia tensor is given by

$$B_{ik}(q) = 2\hbar^2 \sum_{n>0} \frac{\langle 0 | \frac{\partial}{\partial q_i} | n \rangle \langle n | \frac{\partial}{\partial q_k} | 0 \rangle}{E_n - E_0} \qquad (121)$$

where $|n\rangle$ is the many-body state of energy E_n corresponding to H and $|n = 0\rangle$ is the ground state. The only crucial assumption made is that of adiabaticity (i.e. only the lowest state is occupied) which is equivalent to assuming a small collective velocity ($\dot{q}$).

It is easy to generalize eq.(121) to finite temperature ($1/\beta$). The result[24] which is intuitively obvious is

$$B_{ij}(q) = 2\hbar^2 \sum_{m \neq n} w_m \frac{\langle m | \frac{\partial}{\partial q_j} | n \rangle \langle n | \frac{\partial}{\partial q_i} | m \rangle}{E_n - E_m} \qquad (122)$$

where w_m is the occupation probability of the state $|m\rangle$ given in terms of the partition function Z by

$$w_m = e^{-\beta E_m} / Z \qquad (123)$$

The zero temperature cranking mass is a rapidly varying function of deformation[15]. At finite temperature the fluctuations are expected to be even more pronounced due to the smallness (or vanishing) of many more possible energy denominators. Such a behaviour is in contradiction to the basic assumption of adiabaticity. The problem can be traced back to crossing of single

particle levels and the equivalent degeneracy of the many-body state. We should perhaps mention at this point that expression (122) does not diverge at these level crossing, althoug a superficial inspection seems to show this.

G3b Irrotational, incompressible mass

The cranking mass is rather good for nuclei at zero temperature (excitation energy) at their ground state deformation. It has been argued[22] that the irrotational value should be better at larger deformation (collective coordinate) and for higher internal excitation of the nucleus. The arguments are based on the cranking model formula eq.(121) which in itself is a very dubious expression at high temperature. Furthermore for finite viscosity the hydrodynamical flow deviates from irrotational flow due to the non-conservative friction force. As the kinetic energy for irrotational flow is a minimum[23], the inertia calculated under this assumption is bound to be too small. At the moment the only good reason for using the irrotational mass therefore seems to be that it is the easiest to calculate in practice. For this reason, and because it is this inertia tensor the one actually used in numerical applications to the fission process, we shall consider the resulting kinetic energy.

For irrotational flow of a fluid in a container, the velocity field $\underset{\sim}{v}(\underset{\sim}{r})$ can be found from a potential $\Phi(\underset{\sim}{r})$ by

$$\underset{\sim}{v}(\underset{\sim}{r}) = -\underset{\sim}{\nabla}\Phi(\underset{\sim}{r}) \tag{124}$$

If the fluid furthermore is incompressible, the continuity equation is

$$\underset{\sim}{\nabla}\cdot\underset{\sim}{v} = 0 \tag{125}$$

and therefore the Laplacian operator acting on Φ vanishes, i.e.

$$\Delta\Phi = 0 \tag{126}$$

This equation and the boundary condition that the fluid and the container must have identical velocities perpendicular to the surface of the container determines the velocity potential uniquely. Since the container surface velocity is a linear combination of q_i also V comes out as linear in q_i. The total kinetic energy is

$$T = \frac{1}{2}\rho\int \underset{\sim}{v}^2 dz \tag{127}$$

where

$$\rho = M/\left(\tfrac{4}{3}\pi R^3\right) \tag{128}$$

is the nuclear mass density and the integration is over the container. T can be written in the form of eq.(120).

Eq.(126) is difficult to solve in general and approximations often have to be made. A popular, but not a particularly accurate method, is that of Werner and Wheeler described in ref. 21. The inertia tensor obtained by this method for axially symmetric shapes around the z-axis is

$$B_{ij} = \pi\rho_0\int_{z_{min}}^{z_{max}}\left(A_i A_j + \frac{1}{8}P^2 A_i' A_j'\right)P^2 dz \tag{129}$$

where $P = p(z,q)$ is the value of $\rho=\sqrt{x^2+y^2}$ on the surface of the container, z_{min} and z_{max} are respectively the smallest and largest z-values, A_i is the derivative of A with respect to z and A_i is given by

$$A_i(z,q) = \frac{1}{P^2(z,q)}\frac{\partial}{\partial q_i}\int_z^{z_{max}} P^2(z',q)\,dz' \tag{130}$$

for z to the right of the container's midplane and for z to the left of this midplane

$$A_i(z,q) = -\frac{1}{P^2(z,q)}\frac{\partial}{\partial q_i}\int_{z_{min}}^{z} P^2(z',q)\,dz' \tag{131}$$

An exact result may be obtained when the usual multipole expansion coefficients are used as collective coordinates, i.e.

$$R = R_0\left(1+\sum_{n=1}^{\infty}\alpha_n P_n(\cos\theta)\right) \tag{132}$$

where P_n are Legendre polynomials and R_0 the radius of the spherical shape. The diagonal mass parameter for irrotational incompressible flow then is[21]

$$B_n^{irr} = \frac{3}{n(2n+1)} M \cdot R_0^3 \qquad (133)$$

This can be compared with the approximation in eq.(129) which gives[21]

$$B_n = \frac{n^2+n+6}{4(n+1)} \cdot B_n^{irr} \qquad (134)$$

Numerically the approximation is then within about 30% for the lowest multipoles and with increasing deviations for larger n.

G4. The dissipated energy

The mechanism for transfering energy from the collective degrees of freedom into internal excitation energy depends strongly on the mean free path λ of the particles (nucleons) making the system (nucleus). If λ is small compared to the spatial dimension R, the dissipation is expected to proceed via two-body collisions. Due to the Pauli exclusion principle this condition is not satisfied[27]. The extreme of $\lambda \gg R$ is expected to lead to the one-body dissipation mechanism of nucleons colliding with the wall of the moving average potential. Since the motion of the nucleons themselves is the ultimate source of the time dependence of the mean field there is a connection between nucleon-wall collisions and nucleon-nucleon collisions. Thus the main mechanism would be one-body dissipation which in turn is related to two-body collisions.

The rate of dissipated energy (2F) is expressed by the Rayleigh dissipation function[23] F, which consequently should be calculated for the type of dissipation under investigation.

G4a. Two body dissipation

For an incompressible fluid with a constant two-body viscosity, coefficient μ, the Rayleigh dissipation function is given by[21, 23]

$$F = \frac{1}{2}\mu \int \phi(\underset{\sim}{r})\, d^3\underset{\sim}{r} \qquad (135)$$

where

$$\phi(\underset{\sim}{r}) = \Delta \underset{\sim}{v}^2 + \omega^2 - 2\,\underset{\sim}{\nabla}\cdot(\underset{\sim}{v}\times\underset{\sim}{\omega}) \qquad (136)$$

$$\underset{\sim}{\omega} = \underset{\sim}{\nabla}\times\underset{\sim}{v} \qquad (137)$$

and $\underset{\sim}{V}$ is the velocity field for the fluid. Since $\underset{\sim}{V}$ is linear in $\dot{q}_i$ (see sect. G3b) we obtain F in the form

$$F = \frac{1}{2}\sum_{i,k} \eta_{ik}\dot{q}_i\dot{q}_k \qquad (138)$$

where η_{ik} is called the viscosity tensor.

For the shape parametrization, eq.(132), and the collective parameters α_n we get the exact result of the diagonal viscosity tensor

$$\eta_n^{irr} = 8\pi \frac{n-1}{n} R_0^3 \cdot \mu \qquad (139)$$

Usually one has to make approximations to calculate F. The method used to obtain the inertia tensor, i.e. the Werner-Wheeler method[21], leads to the general expression for the viscosity tensor in terms of the quantities defined in sect.G3b

$$\eta_{ij} = \pi\mu \int_{z_{min}}^{z_{max}} \rho^2 \left(3A_i'A_j' + \frac{1}{8}\rho^2 A_i''A_j''\right) dz \qquad (140)$$

where double primes denote second derivatives with respect to z. Using the parametrization of eq.(132) this leads to

$$\eta_n^{ww} = \frac{(n+2)(n^2+n+30)}{48\cdot(n+1)}\,\eta_n^{irr} \qquad (141)$$

Numerically the approximation, eq.(141), is within 25% and increasing with n.

G4b. One body dissipation

The collisions of the nucleons with the moving walls of the nuclear potential results under certain conditions in an irreversible flow of energy from collective to internal degrees of freedom. When the shape of the potential has no neck the so-called wall-formula for the dissipated energy arises, and for two potential pockets connected by a fairly narrow neck (the window) the window-formula arises for the dissipated energy.

The wall-formula is derived in ref.30. The essential assumption is that (i) The mean free parth of the nucleons is large compared to nuclear dimensions. (ii) at each instant of time the surface elements are bombarded by

nucleons as if these originated from the bulk of a gas with no macroscopic motion. (The randomization hypothesis).

The rate of dissipation for a surface element $d\sigma$ is $\rho \bar{v} \dot{n}^2 d\sigma$ where ρ is the nuclear density, $\bar{v} = \frac{3}{4} v_F$ is the mean velocity of the nucleons expressed by the Fermi velocity and n is the normal velocity of the surface element. The total dissipated energy then is

$$\frac{dE_{dis}}{dt} = \rho \bar{v} \oint \dot{n}^2 d\sigma \qquad (142)$$

If the nuclear surface is very regular, e.g. spherical, the second assumption is not fulfilled, since the nucleons then can remember where they came from. Their motion when hitting the surface is not random.

The window-formula is derived in ref. 30 and contains the same basic assumptions as that of the wall-formula. The rate of dissipation is

$$\frac{dE_{dis}}{dt} = \frac{1}{4} \rho \bar{v} \cdot \Delta\sigma \cdot \left(u_t^2 + 2 u_r^2 \right) \qquad (143)$$

where $\Delta\sigma$ is the area of the window and u_r and u_t are the relative radial and tangential velocity components of the two potential pockets.

For the set of collective coordinates specifying the shape in eq.(132) the diagonal terms of the viscosity tensor resulting from the wall formula eq.(142) is[28]

$$\eta_n^{1\text{-body}} = R_0^4 \cdot \rho \cdot v_F \cdot \frac{3\pi}{2n+1} \qquad (144)$$

where V_F is the Fermi velocity of the nucleons. If the viscosity tensor is assumed proportional to a viscosity coefficient as in the case of two-body dissipation we obtain from eqs.(139) and (144)

$$\mu_n^{1\text{-body}} = \frac{\eta_n^{1\text{-body}}}{\eta_n} \cdot \mu = R_0 \rho \cdot v_F \cdot \frac{3n}{8(n-1)(2n+1)} \qquad (145)$$

$$\approx \frac{n}{12(n-1)(2n+1)} \cdot A^{1/3} \cdot \frac{\hbar}{f_m^3} \approx \frac{A^{1/3}}{30} \frac{\hbar}{f_m^3} \quad \text{for } n=2$$

The one-body dissipation expression for the change of dissipated energy per time unit, i.e. the wall formula, results in dissipation for translational motion. This is clearly incorrect. In an attempt to improve the expression, the authors of ref.28 argue that the normal velocity should be replaced by the relative normal velocity v_n between wall and nuclear matter, which is expanded in a Taylor series. This leads to

$$\frac{dE_{dis}}{dt} = \frac{3}{4} \rho_m v_F \lambda^2 \oint \left(\hat{n} \cdot \frac{\partial \underset{\sim}{v}}{\partial n} \right)^2 dS \qquad (146)$$

where λ is a length parameter of the same order as the range of the internucleon force. This expression has properties very different from that of the original wall-formula, f.ex. the viscosity tensor (diagonal terms) for the coordinates in eq. (132) (see ref.28)

$$\eta_n^{1\text{-body mod}} = \frac{3\pi}{2n+1} \rho v_F R_0^4 \cdot \left(\frac{\lambda}{R_0} \right)^2 (n-1)^2 = \eta_n^{1\text{body}} \left[\frac{(n-1)\lambda}{R_0} \right]^2 \qquad (147)$$

Thus it increases with n contrary to $\eta_n^{1\text{body}}$ which decreases. In ref.29 some very harsh comments are made about this modified expression. The proper corrections when the gas of nucleons has a macroscopic motion is in ref30 derived (argued) to be

$$\frac{dE_{dis}}{dt} = \frac{3}{4} \rho \theta_F \int (\dot{n} - D)^2 \, dS \qquad (148)$$

$$D = (\underset{\sim}{V} + \underset{\sim}{\Omega} \times \underset{\sim}{R}) \cdot \underset{\sim}{n} \qquad (149)$$

where $\underset{\sim}{V}$ is the translational velcity, $\underset{\sim}{\Omega}$ the angular velocity, $\underset{\sim}{R}$ radius vector from origin to the surface element. The vectors $\underset{\sim}{V}$ and $\underset{\sim}{R}$ satisfy the equations.

$$\oint (\dot{n} - D) \underset{\sim}{n} \cdot d\underset{\sim}{S} = 0 \qquad (150a)$$

$$\oint (\underset{\sim}{R} \times \underset{\sim}{n}) (\dot{\underset{\sim}{R}} - \underset{\sim}{D}) \, dS = 0 \qquad (150b)$$

It is now possible to give a generalization of the wall and window formulae, i.e.

$$\frac{dE_{dis}}{dt} = \frac{1}{4} \rho \bar{v} \Delta\sigma \left(u_t^2 + 2u_r^2\right) + \rho \bar{v} \left[\int_1 (\dot{n} - D_1) dS + \int_2 (\dot{n} - D_2) dS \right] \qquad (151)$$

where the drifts D_1 and D_2 given by eq.(169) belong to the motion of the two pockets.

The wall and window formulae were derived under the complete randomization hypothesis. If this is not fulfilled the wall formula should be generalized to include a non-local part [31]

$$= \frac{3}{4} \rho v_F \int d^2a \int d^2b \; n(a) \gamma(a,b) n(b) \qquad (152)$$

where the symmetric dissipation kernel can be written

$$\gamma(a,b) = \delta^2(a-b) + \gamma_{non\text{-}local} \qquad (153)$$

The physics behind eq.(152) is that the long mean free path of the nucleons may connect the event at one surface point to that at another point. If the surface is very regular, e.g. spherical or ellipsoidal, the nucleons can remember their origin. The way they hit the surface is related to the way they hit the surface at another point.

The expression in eq.(152) also results from [32] a classical limit of the linear response theory discussed in sect.III.

H. Time dependent Thomas-Fermi approximation, Fluid dynamics, Hydrodynamics

The basic quantities are the time and space dependent density and current of nuclear matter. This approach has by chance (see the introduction) not been reviewed. We can therefore only give the reader a few key references [40-46].

2. Fission Applications and Numerical Results

Only the time dependent Hartree-Fock method and the method we have here called macroscopic nuclear dynamics, or a mixture of these (microscopic non-selfconsistent calculations) have been applied to the fission process.

A. Time dependent Hartree-Fock

TDHF calculations for finite nuclei applied to the fission process have only been published in one case [33]. The results are adequately described in the review of Flocard [34]. We shall therefore here only draw attention to the main points. In the first column of fig. 9 (taken from ref.33) is shown the time evolution of the nuclear density of the ^{236}U nucleus. The starting point of the calculation is 1 MeV below the top of the barrier. The time to reach scission is 3.5×10^{-21} sec. The translational kinetic energy at scission is 12 MeV and the resulting fragment kinetic energy is 142 MeV (the corresponding experimental number is 168 MeV for an excitation energy of about 60 MeV). There are several problems in this calculation, but the most serious is related to the choice of the pairing gap Δ in the BCS wave function.

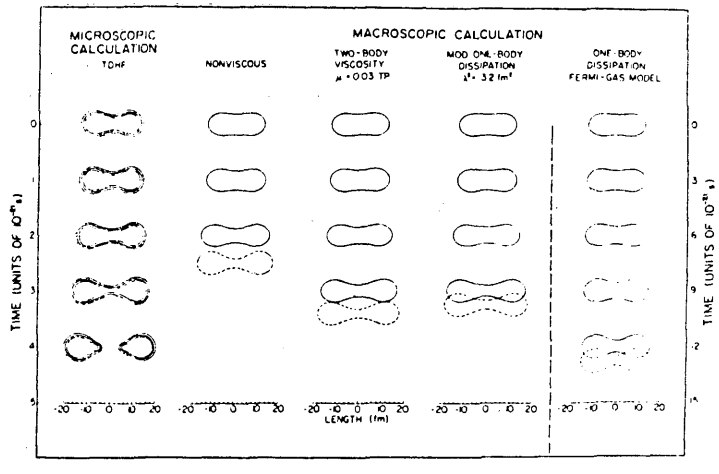

FIG. 9. Comparison of time evolution of densities calculated in a self-consistent model with those of several classical calculations.

For $\Delta = 0$, the system can not fission at all, due to the strictly mathematical crossings of the single particle levels. For $\Delta = 2$ MeV the already quoted numbers are obtained. For $\Delta = 6$ MeV the scission time is 5.0×10^{-21} sec. and the fragment kinetic energy is 166 MeV. Thus $\Delta = 6$ MeV seems to be the experimentally preferred value in contradiction to the original interpretation of Δ as a pairing gap. Instead Δ could represent an effective coupling between single particle levels, but then why should it result in the BCS type of wave fucntions used in the calculation?

Recently there appeared a one-dimensional time dependent Hartree-Fock study of the fission process. The system is infinite in (xy)-direction and finite in the z-direction. The time evolution of this slab of charged nuclear matter is investigated under various initial conditions. Fission occurs at high excitation energies after typical times of $(1\text{-}3) \times 10^{-21}$ sec. The snatching of the neck is characterized by a rapid rise ($\approx 0.3 \times 10^{-21}$ sec.) of a potential barrier between the two fragments.

B. Macroscopic nuclear dynamics

B1. Two body viscosity

Two body viscosity is used in the calculation[8] of the most probable fission-fragment kinetic energies for nuclei from ^{80}Sr to ^{278}110. The results are shown in fig.10 (taken from ref.8) and compared with experimental values obtained at moderately high excitation energies where symmetric fission is most probable. Then single particle effects on the nuclear potential should be small. The liquid drop model energy is used for the potential and the irrotational flow value of an incompressible fluid for the kinetic energy tensor.

Two-body viscosity slows down the dynamical descent from saddle to scission and hinders the formation of a neck, which leads to a more elongated scission configuration. For both reasons the calculated kinetic energy decreases with increasing two-body viscosity. The best agreement with experiments is obtained for $\mu = 0.015$ MeV/fm^3 . If the neck rupture is fast and scission actually takes palce at a finite neck of 2 fm, a viscosity coefficent of $\mu = 0.03$ MeV/fm^3 is in better agreement with experiments. The dissipated energy for ^{236}U appearing as excitation energy in the two fragments is then about 12 MeV and the time to reach scission around 3×10^{-21} sec. The nuclear shape evolution can be seen in the third column of fig. 9.

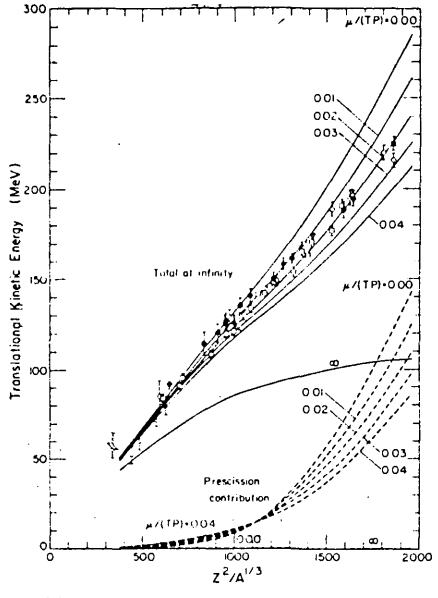

FIG.10. Comparison of experimental most probable fission-fragment kinetic energies with results calculated for different values of the viscosity coefficient μ (solid curves). The calculations include the effect of the finite range of the nuclear force on the nuclear macroscopic energy. The experimental data are for the fission of nuclei at high excitation energies, where the most probable mass division is into two equal fragments. The open symbols represent values for equal mass divisions only, and the solid symbols represent values averaged over all mass divisions. Open circles are used for data obtained in Ref. 60, and open squares are used for data obtained in Refs. 61–64 and reported in Ref. 60. Open downward-pointing triangles refer to Ref. 65, open upward-pointing triangles to Ref. 66, open diamonds to Ref. 67, and open hexagons to Ref. 68. Solid circles are used for data obtained in Ref. 69 and corrected in Ref. 70. The solid square refers to Ref. 71 and the solid downward-pointing triangle to Ref. 72. The dashed curves give the calculated translational kinetic energies acquired prior to scission (see references from paper [8]).

Since we now have an estimate of the two-body viscosity coefficient, it is possible to compare with the corresponding value for one-body viscosity where the size is given by the theory and not by a fit to experiments. From eq.(145) for n = 2 we obtain

$$\mu^{1\text{-body}} \simeq 5 \cdot \mu^{2\text{-body}}$$

for a medium heavy nucleus. For n = 4 they are of the same order and for larger n the two-body viscosity coefficient is larger.

B2. One body viscosity

One-body viscosity, described by the wall formula, is used[35] to calculate the most probable fission-fragment kinetic energies for the same nuclei as in fig.10. The potential and kinetic energies are also the same as those used in the calculation of fig.10. The results are shown in fig.11 taken from ref.35. They are in remarkable agreement with experiments, considering the fact that no parameter to adjust the size of the damping has been used.

It is clear that the wall formula should be replaced by the wall-plus-window formula at some point after the necked in shapes have appeared. Calculations where such a switch is made have also been performed[36]. The results are shown in fig.12 taken from ref.36. Clearly the slight discrepancy in fig.11 can on average be removed by chosing an appropriate switching point.

The dissipated energy for ^{236}U is about 18 MeV and the time to reach scission is around $13 \cdot 10^{-21}$ sec. The nuclear shape evolution can be seen in the last column of fig.9. The fission time is large compared to the two-body viscosity calculation. The motion is very slow due to the fairly large viscosity. This behaviour can also be reproduced with a large two-body viscosity but then the fragment kinetic energies come out systematically larger than the experimental values (see fig.11).

C. Microscopic non-selfconsistent calculation

The Hamiltonian is of the form [37]

$$H = \sum_i \epsilon_i(t)\, a_i^\dagger a_i - G(t) \sum_{i,j} a_i^\dagger a_{\bar{i}}^\dagger a_{\bar{j}} a_j$$

The time dependent equations of motion for $\rho_{ij} = \langle a_i^\dagger a_j \rangle$ and $\kappa_{ij} = \langle a_i a_j \rangle$ are derived. The excitation energy is approximated by the total energy minus the usual (now time dependent) BCS energy expression. The steps in the calculation are described by the authors of ref.37 as:

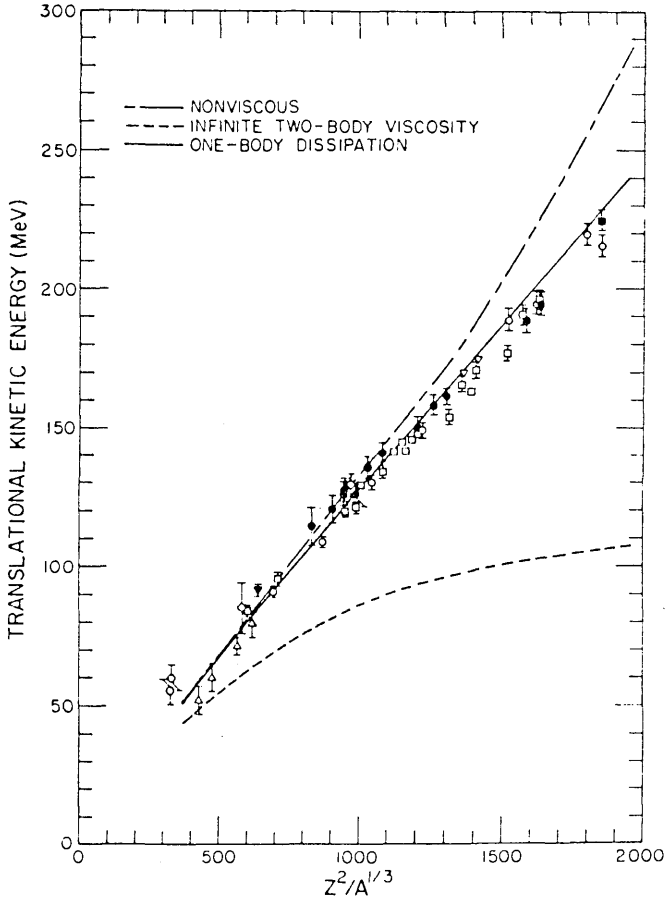

Figure 11. Comparison of calculated and experimental most probable fission fragment kinetic energies as a function of $Z^2/A^{1/3}$. The kinetic energies calculated for nonviscous flow are given by the dot-dashed curve. The dashed curve shows the results for very large two-body viscosity, and the solid curve shows the results for the one-body dissipation considered here. The experimental data are for cases in which the most probable mass division is into two equal fragments; the open symbols represent values for equal mass divisions only and the solid symbols represent values averaged over all mass divisions.

" We consider the fission of a ^{236}U nucleus that initially is set in motion from its macroscopic saddle point with 1 MeV of kinetic energy in the fission mode. The reflection-symmetric and axially symmetric system is studied during its descent to the scission configuration. The total calculation is divided into five steps: (1) We first perform a classical macroscopic hydrodynamical calculation with a given value of the nuclear viscosity coefficient in order to determine a sequence of shapes for the fissioning system. (2) From the shapes as a function of time we determine the instantaneous single-particle potential $U(t)$ and the single-particle eigenvalues $\epsilon_i(t)$. (3) We obtain the pairing strength $G(t)$ that is required to yield a constant average pairing gap $\bar{\Delta}$. (4) We integrate the time-dependent pairing Eqs. (8) for initial conditions at the saddle point corresponding to the BCS ground state. Then from Eq. (16) we find the energy $E^*(t)$ dissipated microscopically along the fission path. (5) We compare $E^*(t)$ with the energy $E_d(t)$ dissipated in the macroscopic hydrodynamical calculation. By varying the viscosity coefficient in the macroscopic hydrodynamical calculations until the two energies are equal we hope to determine the viscosity coefficient. "

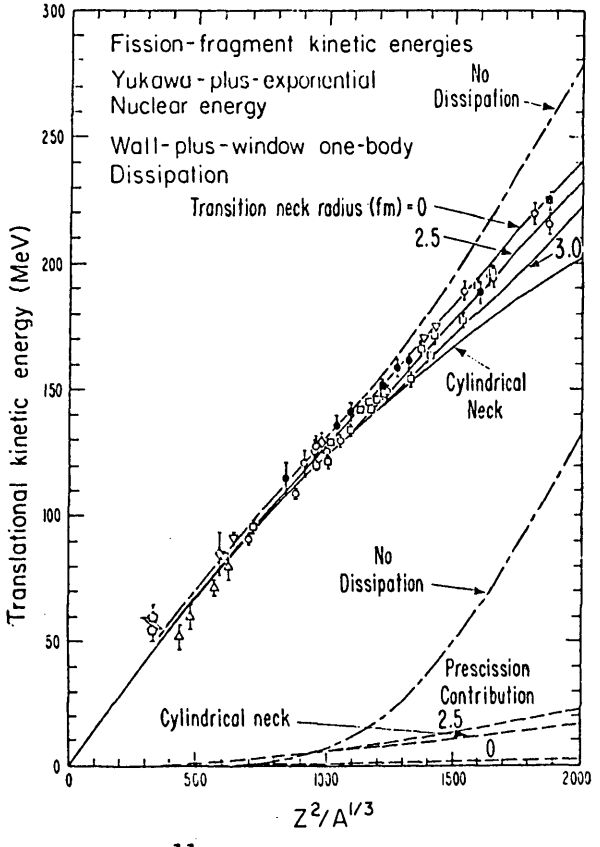

Fig.12. This is like Fig. 11 but in the dynamical calculations a switch was made from the Wall Formula to the Wall-Plus-Window formula when the neck radius had reached the value indicated by the labels on the solid curves. "Cylindrical Neck" means the switch was made at the instant of first appearance of a constriction. The lower part of the figure shows the kinetic energy of the fragments at the instant of scission. Note the very large kinetic energies at scission when there is no dissipation, the very small values when the Wall Formula is used all the way to scission, and the moderate values when the switch is made before scission.

For ^{236}U this leads to a dissipated energy of 34 MeV in contrast to the 18 MeV from the macroscopic calculation. The viscosity coefficient then is μ = (0.04-0.08) $\hbar$/fm^3 which is substantially larger than that of the macroscopic calculation.

The most likely reasons (in my opinion) for this significant discrepancy are (i) The excitation energy calculated as described here deviates appreciably from the dissipated energy. (ii) The nuclear inertia is significantly larger than the nearly irrotational value used in the macroscopic calculation (iii) the viscosity tensor is of one-body nature and not two-body as used in the macroscopic calculation.

D. Summary

The time it takes to move from saddle to scission for a fissioning ^{236}U-nucleus is of the order 10^{-21} sec.- 10^{-20}sec. The dissipated energy appearing as excitation energy in the two fragments is around 15 MeV. (The 34 MeV obtained in the non-selfconsistent microscopic calculation is presumably not reliable). The fragment kinetic energies can on average be reprocuded for nuclei between ^{80}Sr and $^{278}110$ with both one and two-body viscosity. Contrary to one-body viscosity there is a free adjustable parameter in the two-body viscosity formulation.

The macroscopic calculations employ the irrotational and incompresible fluid value for the kinetic energy. This is small compared to the value obtained in the cranking model. The experimental results used in the comparison are all taken at moderately high excitation energies. It is conceivable that quite different results would be obtained if a low excitation energy comparison could be made.

The viscosity coefficient seems to lie in the range between 0.02 and 0.25 $\hbar$/fm^3. This is presumable true for fairly high excitation energies perhaps with the upper bound extended by a factor of about two. For smaller excitation energies a better mass tensor could probably influence the necessary size of the viscosity tensor.

REFERENCES TO CHAPTER I

1) G.E.Brown and A.D.Jackson, The nucleon-nucleon interaction (North-Holland, 1976)
2) H.Bethe, Ann.Rev.Nucl.Sc., Vol.21, 1971, 95-243
3) J.P.Blaizot, Phys.Rep.64, (1980) 171-248
4) S.E.Koonin, Progress in Particle and Nuclear Physics, Vol.4 (1980), 283
5) A.Bohr and B.Mottelson, Nuclear Structure, Vol.I and Vol.II , W.A.Benjamin Inc. 1975
6) P.Quentin and H.Flocard, Ann.Rev.Nucl.Sc.28 (1978)
7) H.J.Mang, Phys.Rep.18 (1975) 325-368
8) J.Blocki and H.Flocard, Nucl.Phys.A273 (1976) 45
9) M.Baranger and M.Veneroni, Ann.of Phys.114 (1978) 123
10) C.Y.Wong and H.K.Tang, Phys.Rev.C20 (1979) 1419
11) A.S.Jensen and S.E.Koonin, Phys.Lett.73B (1978) 243
12) A.K.Kerman and S.E.Koonin, Ann.Phys.100 (1976) 332
13) A.S.Jensen and S.M.Larsen, Phys.Lett.94B (1980) 280
14) H.Goldstein, Classical Mechanics, Add.-Wesley, 1959
15) H.Flocard et al., Nucl.Phys.A203 (1973) 433
16) M.Brack and P.Quentin, in Nuclear Self-Consistant Fields, ed.G.Ripka and M.Porneuf (North Holland, Amsterdam 1975) 399
17) W.Meyers and W.Swiatecki, Ann.of Phys.55 (1969) 395
18) M.Brack et al., Rev.Mod.Phys.44 (1972) 320
19) R.W.Hasse and W.Stocker, Phys.Lett.44B (1973) 26
20) M.Brack and P.Quentin, Nucl.Phys.A361 (1981) 35-82
21) P.Davies, A.J.Sierk and J.R.Nix, Phys.Rev.C13 (1979) 2385
22) J.R.Nix and A.J.Sierk, Phys.Ser.C0A (1974) 94
23) H.Lamb, Hydrodynamics (Dover, New York, 1945)
24) T.Grin, Soviet Phys.JETP 16, (1963) 1327
25) T.Ledergerber and H.C.Pauli, Nucl.Phys.A207 (1973) 1
26) D.R.Inglis, Phys.Rev.96 (1954) 1059
27) G.Wegmann, Phys.Lett.50B (1974) 327
28) A.J.Sierk, S.E.Koonin and J.R.Nix, Phys.Rev.C17 (1978) 646
29) J.Randrup and W.Swiatecki, Ann.Phys.125 (1980) 193
30) J.Blocki et al., Ann.Phys.113 (1978) 330
31) S.E.Koonin and J.Randrup, Nucl.Phys.A289 (1977) 475
32) S.E.Koonin, R.L.Hatch and J.Randrup, Nucl.Phys.A283 (1977) 87-107
33) J.Negele et al., Phys.Rev.C17 (1978) 1098
34) H.Flocard, Proc.Int.Symp. on Chemistry and Physics of Fission, Jülich 1979, Vol.II
35) W.J.Swiatecki, Progress in Particle and Nuclear Physics, 4 (1980) 383 ff.
36) S.E.Koonin and J.R.Nix, Phys.Rev.C13 (1976) 209
37) K.Dietrich and J.Nemeth, Zeit.Phys.A300 (1981) 183
38) P.Grangé, H.A.Weidenmüller and G.Wolschin, Ann.Phys.136 (1981) 190
39) R.Balian and M.Véneroni, Ann.Phys.135 (1981) 270
40) D.M.Brink and M.Di Toro, Nucl.Phys. A372 (1981) 151
41) C.Y.Wong, J.A.Maruhn and T.A.Welton, Nucl.Phys. A253 (1975) 469
42) C.Y.Wong, T.A.Welton and J.A.Maruhn, Phys.Rev.C15 (1977) 1558
43) C.Y.Wong and J.A.McDonald, Phys.Rev.C16 (1977) 1196
44) C.Y.Wong, C17 (1978) 1832
45) G.Holzward and G.Eckart, Nucl.Phys. A325 (1979) 1
46) V.M.Kolomietz and Henry H.K.Tang, Physica Scripta 24 (1981) 915

II. INFLUENCE FUNCTIONALS

1. The Feynman Influence Functional: definition and general properties

The problem we shall be dealing with in this section can be stated as follows. Assume that we have a system that can be described in terms of two sets of generalized time-dependent coordinates (in the Lagrangian sense)

$$\{ q_a(t),\ q_b(t),\ q_c(t),\ \dots \}$$

and

$$\{ \xi_\alpha(t),\ \xi_\beta(t),\ \xi_\gamma(t),\ \dots \}$$

we shall call them for short $\{q(t)\}$ and $\{\xi(t)\}$, respectively. We assume that all these coordinates are dynamically coupled together. One is often interested in measuring observables that can be more or less directly expressed in terms of one

set of coordinates alone, say $\{q(t)\}$. No attempt is made to predict, or to measure, anything related to the other set. We shall refer to the set selected for analysis as "the system", whereas the other set is defined as "the medium". The roles of system and medium can of course be interchanged. Our problem is to formulate our theory so that it deals exclusively with the coordinates and velocities describing the system, after suitably averaging over the medium. Let us exemplify this with the case we have in mind - nuclear fission. As shown in previous sections, we have a good starting point for the analysis of nuclear dynamics (including fission processes) if we begin by splitting the enormous number of coupled degrees of freedom of a nucleus into two sets: a set consisting of a few, suitably selected "collective" coordinates - such as for instance the geometrical shape parameters characterizing the equipotentials of the binding field, or the gap parameters connected with the superfluidity of the nucleus or yet the isoscalar and isovector nuclear densities - and another set of coordinates, which sometimes are referred to as "internal" coordinates, that describes say the positions, spins and isospins of the constituent quasiparticles confined by the mean field. We would like to concentrate on the dynamics of "the system" (= collective coordinates) and consider the internal quasiparticle coordinates as the (essentially unanalysed) medium, in which the system "moves".

Let us begin then by following the dynamical evolution of the entire assembly (system + medium), between an initial instant t_1 and a final instant t_2.

We assume that there is a mechanical action S_{t_1,t_2} associated with the assembly, given by the sum of actions associated respectively with the system alone $S^{(1)}_{t_1,t_2}\{q\}$, with the medium alone $S^{(2)}_{t_1,t_2}\{\xi\}$ and with both $S^{(3)}_{t_1,t_2}\{q,\xi\}$:

$$S_{t_1,t_2} = S^{(1)}_{t_1,t_2}\{q\} + S^{(2)}_{t_1,t_2}\{\xi\} + S^{(3)}_{t_1,t_2}\{q,\xi\} \qquad (1)$$

The various pieces of action are supposed to be functionals of the generalized coordinates $\{q(t)\}$ and $\{\xi(t)\}$.

In problems of common interest, actions can be defined as being localized in time. They can then be expressed as time integrals of Lagrangians (actions per unit time):

$$S^{(i)}_{t_1,t_2} = \int_{t_1}^{t_2} L_i\,(q_i, \dot{q}_i, t)\,dt \qquad (2)$$

Suppose now that our assembly develops from an initial state at time t_1

$$|\xi(t_1)\, q(t_1)\rangle \equiv |\xi_1, q_1\rangle$$

to a final state at time t_2

$$|\xi(t_2)\, q(t_2)\rangle \equiv |\xi_2, q_2\rangle$$

in obvious notation.

For a large class of actions, the transition amplitude

$$K_{S_{t_1,t_2}}(\xi_2 q_2; \xi_1, q_1) \equiv \langle \xi_2 q_2 | \xi_1, q_1 \rangle_{S_{t_1,t_2}} \qquad (3)$$

can be expressed as the Feynman path integral

$$K_{S_{t_1,t_2}}(\xi_2 q_2; \xi_1 q_1) = \int\int \mathcal{D}\xi\, \mathcal{D}q \quad e^{\frac{i}{\hbar} S_{t_1,t_2}} \qquad (4)$$

where we assume

$$S_{t_1,t_2} = \int_{t_1}^{t_2} L(\xi, q, \dot{\xi}, \dot{q}, t)\,dt \qquad (5)$$

The subscripts S_{t_1,t_2} in (3) and (4) are to remind the reader that the transition is assumed to occur under some specific action S .

The sums (or rather, functional integrals) in def.(4) are integrations over all paths or histories connecting the initial configuration $\{\xi_1, q_1\}$ at time t_1 to the final configuration $\{\xi_2, q_2\}$ at time t_2, each path being weighed with the amplitude

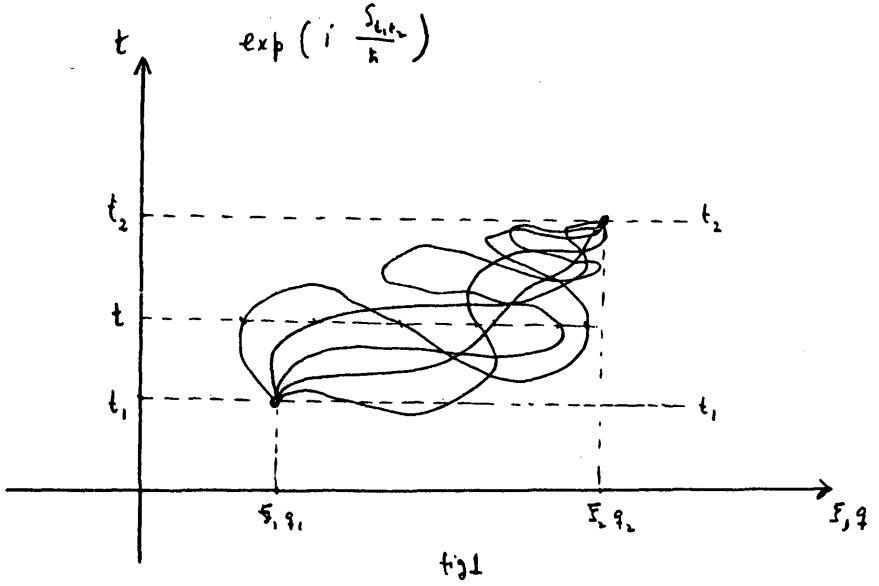

fig.1

The symbol $\mathcal{D}\xi\mathcal{D}q$ in def.(4) denotes the appropriate integration measure in path space (fig.1). The probability for this particular transition to occur is then

$$P(\xi_2 q_2 ; \xi_1 q_1) = \left| K_{S_{t_1 t_2}}(\xi_2 q_2 ; \xi_1 q_1) \right|^2 \qquad (6)$$

Suppose now that we cannot, or wish not, measure anything about the medium. We must then, as usual,

a) sum over all values of the coordinates ξ_1 in the initial state $|i\rangle$ of the medium at time t_1, and average over all initial states $|i\rangle$;

b) sum over all possible values of the final coordinates ξ_2, and sum over all possible final states $|f\rangle$.

Thus we are asking for the <u>inclusive probability</u> for the transition

$$\{q_1\} \longrightarrow \{q_2\} + \text{anything} \qquad (7)$$

Define the inital wavefunction

$$\varphi_i(\xi_1) = \langle \xi_1 | i \rangle$$

and the final wavefunction

$$\varphi_f(\xi_2) = \langle \xi_2 | f \rangle$$

associated respectively with the stationary states $|i\rangle$ and $|f\rangle$ of the medium. Thus the probability amplitude for going from a definite $|i\rangle$ to a definite $\langle f|$ for all values of ξ_1 and ξ_2 is

$$A_{i\to f} = \int d\xi_2 \int d\xi_1 \, \varphi_f^*(\xi_2) \left[\iint \mathcal{D}\xi \, \mathcal{D}q \, e^{\frac{i}{\hbar} S_{t_1 t_2}} \right] \varphi_i(\xi_1)$$

and therefore the desired inclusive probability is

$$P(\{q_1\} \to \{q_2\} + \text{anything}) = \sum_f \sum_i p_i |A_{i\to f}|^2 =$$

$$= \sum_f \sum_i p_i \int d\xi_2 \int d\xi_1 \int d\xi_2' \int d\xi_1' \varphi_f(\xi_2) \left[\iint e^{\frac{i}{\hbar}(S_{t_1 t_2}\{q\} - S_{t_1 t_2}\{q'\})} \mathcal{D}\xi' \mathcal{D}q' \mathcal{D}\xi \mathcal{D}q \right] \cdot \varphi_i(\xi_1) \varphi_i^*(\xi_1') \qquad (8a)$$

where $q = q(t)$, etc. The probability that the medium is in the initial state $|i\rangle$ is denoted by p_i. It is supposed to be normalized, so that

$$\sum_i p_i = 1$$

Imagine, for example, that the fissioning nucleus is gone past the saddle-point, starting its descent towards scission. Initially, the quasiparticles ("the medium") may exist in very many states with some definite probability p_i that they actually are in state $|i\rangle$. This probability could conceivably be a factor proportional to the Boltzmann factor

$$\exp(-\beta E_i)$$

where E_i is the energy of the state $|i\rangle$ and β is inversely proportional to the nuclear temperature. From (8a) we thus get the result

$$P(\{q_1\} \to \{q_2\} + \text{anything}) = \iint \mathcal{D}q \, \mathcal{D}q' \, e^{\frac{i}{\hbar}\left[S^{(1)}_{t_1 t_2}\{q\} - S^{(1)}_{t_1 t_2}\{q'\}\right]} \cdot F(\{q\}, \{q'\}) \qquad (8b)$$

We have defined

$$F(\{q_f\},\{q'_f\}) \equiv \sum_f \sum_i p_i \int dx_1 \int dx_2 \int dx'_1 \int dx'_2 \; \varphi_f^*(x_2)\, \varphi_f(x'_2) \cdot$$

$$\cdot \left[\int\int \mathcal{D}x\, \mathcal{D}x' \exp\left[\frac{i}{\hbar} \left(S^{(2)}_{t_1,t_2}\{x\} - S^{(2)}_{t_1,t_2}\{x'\} + S^{(3)}_{t_1,t_2}\{x,q_f\} - S^{(3)}_{t_1,t_2}\{x',q'_f\} \right) \right] \right] \cdot$$

$$\cdot \varphi_i(x_1)\, \varphi_i^*(x'_1)$$

This can be put into a more lucid form

$$F(\{q_f\},\{q'_f\}) = \sum_f \sum_i p_i\, M^*_{fi}\{q'(t)\}\, M_{fi}\{q(t)\}$$

$$= \sum_i p_i\, F_i(\{q_f\},\{q'_f\}) \qquad (9b)$$

where

$$M_{fi}\{q(t)\} = \int dx_1 \int dx_2\, \varphi_f^*(x_2) \left[\int \mathcal{D}x\, e^{\frac{i}{\hbar}\left[S^{(2)}_{t_1,t_2}\{x\} + S^{(3)}_{t_1,t_2}\{x,q\} \right]} \right] \cdot \varphi_i(x_1)$$

$$\equiv \int dx_1 \int dx_2\, \varphi_f^*(x_2) \langle x_2 | x_1 \rangle_{q(t)}\, \varphi_i(x_1) \qquad (9c)$$

with the definition

$$\langle x_2 | x_1 \rangle_{q(t)} \equiv \int \mathcal{D}x\; e^{\frac{i}{\hbar} S_{eff}\{x,q\}_{t_1,t_2}} \qquad (9d)$$

and

$$S_{eff}\{x,q\}_{t_1,t_2} \equiv S^{(2)}_{t_1,t_2}\{x\} + S^{(3)}_{t_1,t_2}\{x,q\} \qquad (9e)$$

$F(\{q_f\},\{q'_f\})$ defined by (9), is called the influence functional (IF). It clearly summarizes in a compact form all the influences that the unobserved medium has on the quantum transition (7). These influences depend of course on the couplings between the medium and the system.

The meaning of (9c) is obvious: it is just the total amplitude that the medium, starting off with the initial wavefunction $\varphi_i(x_1)$ at time t_1, propagates to the final wavefunctions $\varphi_f^*(x_2)$ at time t_2 under an effective action given by (9e). This effective action consists of two parts: the "free" action, described by the first term in (9e) giving the "free" propagation between t_1 and t_2, and a "driving" action, described by the second term of (9e) giving the influence of a "source" q(t) - i.e. our "system" - on the propagation of the medium. By using now the assumed completeness and orthonormality of the medium wavefunctions φ_i and φ_f it is easy to show that if $q(t) = q'(t)$ then

$$F(\{q(t)\},\{q'(t) \equiv q(t)\}) = \sum_i p_i\, M^*_{fi}(\{q(t)\})\, M_{fi}(\{q(t)\}) = 1 \qquad (10)$$

a result that shall be useful later.

An important aspect of (9) should be noted at this point. The (microscopic) details of the medium do not enter into the picture. When computing the IF (9b) the coordinates q(t) (or q'(t)) must be given functions of time. Thus, insofar the set {q} is the relevant set, two different media that somehow produce the same IF are fully equivalent media. For instance, a set of harmonic oscillators in computing IF. We may then consider the medium just as a set of harmonic oscillators suitable coupled to the system, even if the real medium has nothing to do with harmonic oscillators. Specific examples are given in ref.[1].

The IF can be cast in the following form:

$$F(\{q_f\},\{q'_f\}) = \sum_k p_k\, e^{\frac{i}{\hbar} W_{t_1,t_2,k}\{q,q'\}} \qquad (11)$$

For the time being, the reader may regard this just as a definition of a generally complex functional $W_{t_1,t_2,k}\{q_1 q'\}$. Inserting (11) into (9) we get

$$P(\{q_1\} \to \{q_2\} + \text{anything}) = \sum_i p_i\, P(i + \{q_1\} \to \{q_2\} + \text{anything}) \qquad (12a)$$

where

$$P(k + \{q_1\} \to \{q_2\} + \text{anything}) = \int\int \mathcal{D}q\, \mathcal{D}q'\, e^{\frac{i}{\hbar} \tilde{S}_{eff}\{q,q'\}_{t_1,t_2,k}} \qquad (12b)$$

We have introduced the effective action

$$\tilde{S}_{eff}\{q,q'\}_{t_1,t_2,k} \equiv S^{(1)}_{t_1,t_2}\{q\} - S^{(1)}_{t_1,t_2}\{q'\} + W_{t_1,t_2,k}\{q,q'\} \qquad (13)$$

The main job is to compute the functional (11) as well as one can, or at least extract as much information as possible out of it.

The functional F $(\{q\},\{q'\})$ has some general properties that are not only useful in practical work but also must be satisfied if we are to identify any proposed F as an influence functional. These properties have been spelled out by Feynman and his collaborators[1,2]. We reproduce some relevant ones here for completeness sake: the reader could try to prove them for himself using the above definitions.

Some rules for the IF:

Rule 1. The complex conjugate of $F(\{q_+\},\{q_-\})$ must obey the following condidition:

$$F^*(\{q_+\},\{q'_-\}) = F(\{q'_+\},\{q_-\}) \tag{14}$$

Rule 2. If for times $t > a$ one has

$$q(t) = q'(t) \tag{15}$$

then F is independent of q(t) for $t > a$.

Rule 3. Let the medium interacting with the system be composed of two parts, A and B, which not only do not interact directly with each other but also have no correlations in the initial state. Let F_A and F_B be the influence functionals associated respectively with A alone and B alone. Then

$$F = F_A \cdot F_B \tag{16}$$

2. The saddle-point approximation to the IF

The main problem for the present approach is the evaluation of the functional (11). When this is done, we can insert the result into (12) and obtain the desired inclusive probability. In practice this can be done only through more or less drastic approximations that depend of course on the nature of the problem at hand. We shall consider here a semiclassical approximation that may have interest in a nuclear context.[4]

The main point of the approximation is the following: assume that the integral (12) is strongly dominated by the stationary points of the effective action (13). In this case, we may try the usual saddle-point approximation[1] to P. The leading term will then give the classical probability for the transition, whereas the higher order terms will lead to various quantum corrections. This approximation method will therefore be of use if the quantum corrections to the "classical" result are small.

We consider then a pair $q = q_o(t)$ and $q' = q'_o(t)$ that makes the $\tilde{S}_{eff}\{q,q'\}$ stationary, i.e.

$$\tilde{S}_{eff}\{q,q'\} - \tilde{S}_{eff}\{q_o,q'_o\} = \delta\tilde{S}_{eff} + \delta^2\tilde{S}_{eff} + \cdots$$

with the condition

$$\delta\tilde{S}_{eff} \equiv \int\left[\frac{\delta\tilde{S}_{eff}}{\delta q(t)}\,\delta q(t) + \frac{\delta\tilde{S}_{eff}}{\delta q'(t)}\,\delta q'(t)\right]dt \equiv 0 \tag{17}$$

for arbitrary (small) δq and $\delta q'$. This leads to the equations of motion

$$\frac{\delta\tilde{S}_{eff}}{\delta q(t)} = 0 \tag{18a}$$

$$\frac{\delta\tilde{S}_{eff}}{\delta q'(t)} = 0 \tag{18b}$$

We have dropped for ease the subscript $(t_1 t_2 R)$ in the above expressions for the action. Write

$$W\{q,q'\} = R\{q,q'\} + i\,I\{q,q'\} \tag{19}$$

where R and I are <u>real</u> functionals of q, and q'. Then eqs.(18), and defs.(13), (19) give

$$\frac{\delta S^{(1)}\{q\}}{\delta q(t)} + \frac{\delta R\{q,q'\}}{\delta q(t)} = 0 \tag{20a}$$

$$\frac{\delta S^{(1)}\{q'\}}{\delta q'(t)} + \frac{\delta R\{q',q\}}{\delta q'(t)} = 0 \tag{20b}$$

$$\frac{\delta I\{q,q'\}}{\delta q(t)} = 0 \tag{20c}$$

$$\frac{\delta I\{q,q'\}}{\delta q'(t)} = 0 \tag{20d}$$

These equations must be solved subject to the boundary conditions

$$q(t_1) = q'(t_1) = q_1 \qquad q(t_2) = q'(t_2) = q_2 \tag{20e}$$

In writing eq.(20b) we have used a property of these functionals that can easily be derived. Using rule 1 (sect.1) we get

$$R\{q,q'\} = -R\{q',q\} \tag{21a}$$

$$I\{q,q'\} = I\{q',q\} \tag{21b}$$

Define

$$\eta(t) = q(t) - q'(t) \tag{22a}$$

$$Q(t) = \frac{1}{2}\left(q(t) + q'(t)\right) \tag{22b}$$

and express q(t) and q'(t) as functions of the antisymmetric (symmetric) functions $\eta(t)$ (Q(t)). Then results (21) mean that

The real part of $W\{q,q'\}$ must be an odd function of $\eta(t)$ (23)

The imaginary part of $W\{q,q'\}$ must be an even function of $\eta(t)$ (24)

Using the def.

$$S^{(1)}_{t,t_2}\{q\} = \int_{t_1}^{t_2} L(q,\dot{q},t)\,dt$$

we have from (20a)

$$\frac{\partial L}{\partial q(t)} - \frac{d}{dt}\frac{\partial L}{\partial \dot{q}(t)} + \frac{\delta R\{q,q'\}}{\delta q(t)} = 0 \tag{25}$$

and similarly from (20b). The special case corresponding to the solution of eqs.(20) satisfying

$$q_0(t) = q_0'(t) \tag{26}$$

merits some attention. If (26) is satisfied, then condition (10) leads to the conclusion that

$$R\{q_0,q_0'\} = I\{q_0,q_0'\} = 0 \tag{27}$$

which implies $S_{eff}\{q_0,q_0\} = 0$. On the other hand, we may conclude from the condition (26) that the equations of motion (20c, d) are identically satisfied for solutions of the type (26). Eq.(20a) and (20b) are then completely equivalent to the equation

$$\frac{\partial L}{\partial q(t)} - \frac{d}{dt}\frac{\partial L}{\partial \dot{q}(t)} + \left[\frac{\delta R\{q,q'\}}{\delta q(t)}\right]_{\eta=0} = 0 \tag{28}$$

Again, eqs.(25) (or (28)) must satisfy the boundary conditions (20e), and not initial conditions, in contrast to what normally would be the case for classical equations of motion. This reflects the quantal origin of eqs.(25) and (28). The importance of this remark in the context of the theory of deep inelastic nuclear reactions is emphasized in ref. 4.

Eqs. like (25) (or (28)) are reminiscent of classical equations of motion, with the term $\frac{\delta R}{\delta q(t)}$ playing the role of dissipative forces. Instead of embarking upon a general analysis of these equations (which could be done on the basis of the above-mentioned rules)[4], we will rather examine special cases where the connections may be easier to see.

Let us restrict ourselves to a single generalized coordinate q(t) specifying our system:

$$\{q(t)\} \longrightarrow q(t)$$

This entails of course no real loss of generality. Next, we shall assume that the functional $W\{q,q'\}$ is at most quadratic in q(t) and q'(t). Specifically, we shall be considering solutions of the type q(t) = q'(t), corresponding to $\eta = 0$. The rest of this section boils down to a discussion of an expansion in η around $\eta = 0$, keeping the leading terms only. It turns out that in many interesting applications of the IF method, we are led precisely to an IF of the type we are going to consider in general terms.

We have then, using (23) and (24)

$$W\{q,q'\} = R\{q,q'\} + i\, I\{q,q'\}$$

$$R\{q,q'\} = \int_{t_1}^{t_2} d\tau\, a(\tau)\eta(\tau) + \int_{t_1}^{t_2} d\tau_1 \int_{t_1}^{t_2} d\tau_2\, b(\tau_1,\tau_2)\eta(\tau_1) q(\tau_2) + \cdots \tag{29}$$

$$I\{q,q'\} = \frac{1}{2}\int_{t_1}^{t_2} d\tau_1 \int_{t_1}^{t_2} d\tau_2\, c(\tau_1,\tau_2)\eta(\tau_1)\eta(\tau_2) + \int_{t_1}^{t_2} d\tau_1 \int_{t_1}^{t_2} d\tau_2\, d(\tau_1,\tau_2) q(\tau_1) q(\tau_2) + \cdots$$

as the most general expression obeying our conditions. The functions a, b, c, d, are of course assumed to be real functions of their arguments. Does this lead to an IF? As we mentioned earlier, certain conditions must be fulfilled first. We have already used rule 1. We will now use rule 2 in order to see whether there are further restrictions on the coefficients in (29). To that purpose, it is convenient to rewrite these integrals using the identity,

$$\int_{t_1}^{t_2} d\tau_1 \int_{t_1}^{\tau_1} d\tau_2\, H(\tau_1,\tau_2) = \frac{1}{2}\int_{t_1}^{t_2} d\tau_1 \int_{t_1}^{t_2} d\tau_2 \left[\theta(\tau_1-\tau_2) H(\tau_1,\tau_2) + \theta(\tau_2-\tau_1) H(\tau_2,\tau_1)\right] \tag{30}$$

where $\theta(x)$ is the usual step function

$$\theta(x) = \begin{cases} 1 & x > 0 \\ 0 & x < 0 \end{cases} \tag{31}$$

Let us consider the quadratic part of W:

$$W^{quad}\{q,q'\} = \int_{t_1}^{t_2} d\tau_1 \int_{t_1}^{t_2} d\tau_2 \left[A(\tau_1,\tau_2) q(\tau_1) q(\tau_2) + B(\tau_1,\tau_2) q'(\tau_1) q(\tau_2) + C(\tau_1,\tau_2) q(\tau_1) q'(\tau_2) + D(\tau_1,\tau_2) q'(\tau_1) q'(\tau_2)\right] \tag{32}$$

where A,..., can be expressed in terms of b, c, d, using def.(22). Expression (32) can be rewritten thus, by using (30)

$$W^{quad}\{q,q'\} = \int_{t_1}^{t_2} d\tau_1 \int_{t_1}^{\tau_1} d\tau_2 \left[A'(\tau_1,\tau_2) q(\tau_1) q(\tau_2) + B'(\tau_1,\tau_2) q'(\tau_1) q(\tau_2) + C'(\tau_1,\tau_2) q(\tau_1) q'(\tau_2) + D'(\tau_1,\tau_2) q'(\tau_1) q'(\tau_2)\right] \tag{33}$$

Now consider the first two integrals of (33) together: take an arbitrary time a between t_1 and t_2 (clearly $\tau_1 > a$ and $\tau_2 < a$) and consider a piece of these integrals viz.

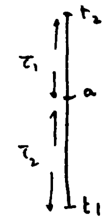

$$\int_a^{t_2} d\tau_1 \int_{t_1}^{a} d\tau_2 \left[A'(\tau_1,\tau_2) q(\tau_1) q(\tau_2) + B'(\tau_1,\tau_2) q'(\tau_1) q(\tau_2)\right] \tag{34}$$

Put

$$q'(\tau_1) = q(\tau_1) \qquad (\tau_1 > a)$$

Then, rule 2 tells us that the integral (34) must be independent of $q(\tau_1)$. Therefore

$$A'(\tau_1,\tau_2) = -B'(\tau_1,\tau_2) \qquad (\tau_1 > \tau_2,\ \tau_1 > a)$$

But a is arbitrary. Therefore

$$A'(\tau_1,\tau_2) = -B'(\tau_1,\tau_2) \qquad (\tau_1 > \tau_2) \tag{35}$$

The same argument applied to the last two terms of (33) leads to the conclusion that

$$C'(\tau_1,\tau_2) = -D'(\tau_1,\tau_2) \qquad (\tau_1>\tau_2) \tag{36}$$

From the above, we may conclude that

$$d(\tau_1,\tau_2) = 0 \qquad (\tau_1>\tau_2) \tag{37}$$

Putting these results together we deduce that rule 1 and rule 2 demand that

$$W\{q,q'\} = \int_{t_1}^{t_2} d\tau\, a(\tau)\,(q(\tau)-q'(\tau)) + \int_{t_1}^{t_2} d\tau_1 \int_{t_1}^{\tau_1} d\tau_2\,(q(\tau_1)-q'(\tau_1))\,(A'(\tau_1,\tau_2)\,q(\tau_2) + A'^{*}(\tau_1,\tau_2)\,q'(\tau_2)) + \dots$$

where

$$A'(\tau_1,\tau_2) = \frac{1}{2}\alpha(\tau_1,\tau_2) + \frac{i}{2}\beta(\tau_1,\tau_2) \qquad (\tau_1>\tau_2)$$

$$\therefore\quad W\{q,q'\} = \int_{t_1}^{t_2} d\tau_1\, \eta(\tau_1)\left[a(\tau_1) + \int_{t_1}^{\tau_1} d\tau_2\,\alpha(\tau_1,\tau_2)\,q(\tau_2)\right] + \tag{38}$$

$$+ \frac{i}{2}\int_{t_1}^{t_2} d\tau_1 \int_{t_1}^{\tau_1} d\tau_2\ \beta(\tau_1,\tau_2)\,\eta(\tau_1)\eta(\tau_2) \qquad (\alpha,\beta \text{ real})$$

Therefore

$$\left[\frac{\delta R\{q,q'\}}{\delta\eta(t)}\right]_{\eta=0} = a(t) + \int_{t_1}^{t} d\tau\,\alpha(t,\tau)\,q(\tau) \tag{39}$$

The equation of motion determining the path is then using (28):

$$\frac{\partial L}{\partial q} - \frac{d}{dt}\frac{\partial L}{\partial \dot q} + a(t) + \int_{t_1}^{t} d\tau\,\alpha(t,\tau)\,q(\tau) = 0 \tag{40}$$

The equation is of the type of generalized Langevin equation[3,4].

Recall that the Langevin equation is often introduced in connection with the theory of Brownian motion, a subject to which we shall return presently.

Note, that the last two terms of eq.(40) are a kind of generalized force acting on the degree of freedom q(t) from the medium. The last term of eq.(40) depends on the entire <u>past</u> history of q(t), in accordance with the classical ideas of causality. This same last term contains dissipative effects. This can easily be seen by extracting from it any conservative parts by a partial integration: we get

$$\int_{t_1}^{t_2} d\tau\,\alpha(t,\tau)\,q(\tau) = r(t)\,q(t) - \int_{t_1}^{t_2} d\tau\, s(t,\tau)\,\dot q(\tau) \tag{41}$$

apart from an unimportant integration constant. The functions r(t) and s(t,τ) are of course related to $\alpha(t,\tau)$.

This gives then

$$\frac{d}{dt}\frac{\partial L}{\partial \dot q} = F(q,t) - \int_{t_1}^{t} d\tau\, s(t,\tau)\,\dot q(\tau) \tag{42}$$

In this equation, the first term on the r.h.s. represents the conservative part of the generalized force acting on the degree of freedom q(t), resulting from its interaction with the medium, together eventually with external forces:

$$F(q,t) = \frac{\partial L}{\partial q} + r(t)\,q(t) + a(t) \tag{43}$$

The last term of (42) suggests that the medium is also influencing the motion of the system through viscous forces, which tend <u>to damp</u> its motion. Again, eq.(42) shows that this force is in general dependent on the past history of the system - it "remembers" its entire past.

It turns out that in particular applications of the IF method the damping function represented by s(t,τ) in (42) depends only on the difference between its arguments, i.e.

$$s(t,\tau) = s(t-\tau) \tag{44}$$

suggesting that the average properties of the medium do not depend on the absolute time.

Let us now assume that the systems "memory" is represented by a time τ_m and that s has the general form shown in fig. 2, say an exponential

$$s = \frac{\alpha_0}{\tau_m} \exp\left(-\frac{t-\tau}{\tau_m}\right)$$

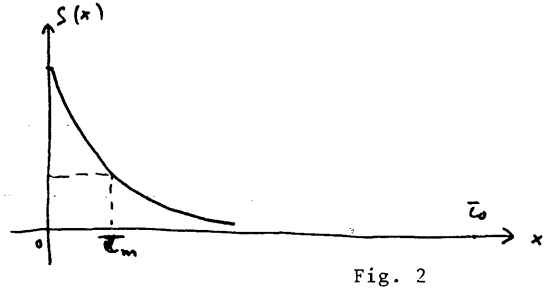

Fig. 2

This fucntion acts then as a damping factor on the velocity $\dot{q}$ of the system, causing it to decay, say within a typical time τ_0 - the relaxation time. If the memory time τ_m is much less than the relaxation time τ_0, we can make the following approximation to the integral on the r.h.s. of (42):

$$-\int_{t_1}^{t} d\tau\, s(t-\tau)\,\dot{q}(\tau) \approx -\alpha_0\,\dot{q}(t)$$

and then eq.(42) becomes

$$\frac{d}{dt}\frac{\partial L}{\partial \dot{q}} = F(q,t) - \alpha_0\,\dot{q}(t) \qquad (46)$$

This is an example of a so-called Markovian approximation: all "memory" effects have been suppressed in approximating the non-Markovian eq.(42) with the Markovian eq.(46).

3. Applications to special models

The above considerations are rather formal, therefore independent of detailed assumptions and models. The basic assumption however was that the functional $W\{q,q'\}$ could be expanded around the "point" $\eta(t) = 0$, and that at most quadratic terms in η were to be retained. This we may call the Gaussian approximation. We saw how this led to a generalized Langevin equation. Upon certain conditions, this non-Markovian equation could be approximated by a Markovian one.

We shall now illustrate the above discussion with a couple of examples, which may perhaps give some feeling about possible structures that may lie behind the characteristic features of Gaussian approximation. More detailed discussions can be found in ref. 1 and 2.

We shall continue assuming that our system is represented by a single generalized coordinate.

Let us return to our original definition of the IF (9) and consider the matrix element

$$M_{fi}\{q(t)\} = \int d\xi_1 \int d\xi_2\, \varphi_f^*(\xi_2)\langle \xi_2 | \xi_1 \rangle_{q(t)}\, \varphi_i(\xi_1)$$

where

$$\langle \xi_2 | \xi_1 \rangle_{q(t)} \equiv \int \mathcal{D}\xi\; e^{\frac{i}{\hbar} S_{eff}\{\xi, q\}_{t_1,t_2}}$$

and

$$S_{eff}\{\xi,q\}_{t_1,t_2} = S^{(2)}_{t_1,t_2}\{\xi\} + S^{(3)}_{t_1,t_2}\{\xi, q\}$$

Assume now that

$$S^{(2)}_{t_1,t_2}\{\xi\} = \int_{t_1}^{t_2} L_0(\xi, \dot{\xi}, t)\, dt$$

and

$$S^{(3)}_{t_1,t_2}\{\xi, q\} = \int_{t_1}^{t_2} V(\xi, q)\, dt \qquad (47b)$$

L_0 represents the Lagrangian of the medium and V is the interaction between the medium and the system, moving along a given path q(t). We assume of course that both L_0 and V are hermitean.

An important special case occurs when this interaction is linear in the system coordinate q(t), i.e.

$$V(\xi, q) = q\, F(\xi) \tag{48}$$

Associated with the Lagrangian

$$L = L_0(\xi, \dot{\xi}, t) + V(\xi, q)$$

there is an Hamiltonian H, obtained the usual way through a Legendre transformation,

$$H = H_0(\xi) - V(\xi, q) \tag{49}$$

The states $|i\rangle$, $|f\rangle$ are assumed to be **eigenstates** of H_0:

$$H_0|n\rangle = \epsilon_n |n\rangle$$
$$\sum_n |n\rangle\langle n| = 1$$
$$\langle m|n\rangle = \delta_{mn} \qquad |n\rangle_t = e^{-i\frac{\epsilon_n}{\hbar}t}|n\rangle$$
$$\langle \xi|n\rangle_t = \varphi_n(\xi_t) = e^{-i\frac{\epsilon_n}{\hbar}t}\varphi_n(\xi) \tag{50}$$

We shall consider two cases first, where perturbation theory will be used. In one case, we shall assume that the coupling term V is small compared to L_0 (weak coupling); in the next case, we drop this assumption, but instead assume that q(t) changes slowly with time in comparison with an intrinsic time scale that characterizes the motions of the medium (the adiabatic approximation). In both cases, we shall eventually be led to Gaussian functionals of the type discussed in the previous section.

A) The weak coupling approximation

Assume that V is small relative to L_0; expand in powers of V, then retain the leading terms only. Consider then

$$M_{fi}\{q\} = \int d\xi_1 \int d\xi_2\, \varphi_f^*(\xi_2) \int \mathcal{D}\xi\, e^{\frac{i}{\hbar}S^{(1)}_{t_1t_2}\{\xi\}} \cdot \left[1 + \frac{i}{\hbar}S^{(3)}_{t_1t_2}\{\xi, q\xi\} + \frac{1}{2!}\left(\frac{i}{\hbar}S^{(3)}_{t_1t_2}\{\xi, q\xi\}\right)^2 + \cdots\right]\varphi_i(\xi_1)$$
$$\equiv \sum_{n=0}^{\infty} M_{fi}^{(n)}\{q\} \tag{51}$$

The leading contributions are:

$$M_{fi}^{(0)} = \int d\xi_1 \int d\xi_2\, \varphi_f^*(\xi_2) \int \mathcal{D}\xi\, e^{i\frac{S^{(1)}_{t_1t_2}\{\xi\}}{\hbar}}\varphi_i(\xi_1)$$

$$M_{fi}^{(1)} = \frac{i}{\hbar}\int d\xi_1 \int d\xi_2\, \varphi_f^*(\xi_2)\left[\int \mathcal{D}\xi\, e^{i\frac{S^{(2)}_{t_1t_2}\{\xi\}}{\hbar}} S^{(3)}_{t_1t_2}\{\xi, q\xi\}\right]\varphi_i(\xi_1)$$

$$M_{fi}^{(2)} = \frac{1}{2}\left(\frac{i}{\hbar}\right)^2 \int d\xi_1 \int d\xi_2\, \varphi_f^*(\xi_2)\left[\int \mathcal{D}\xi\, e^{i\frac{S^{(2)}_{t_1t_2}\{\xi\}}{\hbar}} S^{(3)}_{t_1t_2}\{\xi, q\xi\} S^{(3)}_{t_1t_2}\{\xi, q\xi\}\right]\varphi_i(\xi_1)$$

etc

Therefore:

$$M_{fi}^{(0)} = \int d\xi_1 \int d\xi_2\, \varphi_f^*(\xi_2)\langle \xi_2|\xi_1\rangle \varphi_i(\xi_1) = \delta_{fi} \tag{52}$$

Then

$$M_{fi}^{(1)} = \frac{i}{\hbar}\int_{t_1}^{t_2} dt \int d\xi_1 \int d\xi_2\, \varphi_f^*(\xi_2)\left[\int \mathcal{D}\xi\, e^{i\frac{S^{(2)}_{t_1t_2}\{\xi\}}{\hbar}} V(\xi, q(t))\right]\varphi_i(\xi_1)$$
$$= \frac{i}{\hbar}\int_{t_1}^{t_2} dt \int d\xi_1 \int d\xi_2\, \langle f|\xi_2\rangle\langle \xi_2|\xi_1\rangle\langle \xi_1|i\rangle\, V(\xi, q(t)) \tag{53}$$

$$\therefore\ M_{fi}^{(1)}\{q\} = \frac{i}{\hbar}\int_{t_1}^{t_2} dt\, \langle f|V(\xi, q(t))|i\rangle\, e^{i\frac{\epsilon_f - \epsilon_i}{\hbar}t}$$

and finally

$$H_{fi}^{(2)}\{q,q'\} = \frac{1}{\hbar}\left(\frac{i}{\hbar}\right)^2 \int d\xi_1 \int d\xi_2\, \varphi_f^*(\xi_2) \int \mathcal{D}\xi\, e^{\frac{i}{\hbar}S_{fi}^{(2)}\{q,q'\}} \cdot \int_{t_1}^{t_2} d\tau_1 V(\xi(\tau_1), q(\tau_1)) \int_{t_1}^{t_2} d\tau_2 V(\xi(\tau_2), q(\tau_2))\, \varphi_i(\xi_1)$$

$$\therefore H_{fi}^{(2)}\{q,q'\} = \left(\frac{i}{\hbar}\right)^2 \int_{t_1}^{t_2} d\tau_1 \int_{t_1}^{\tau_1} d\tau_2 \int d\xi_1 \int d\xi_2\, \varphi_f^*(\xi_2) \langle \xi_2 | \xi_{\tau_1} \rangle \cdot V(\xi(\tau_1), q(\tau_1)) \langle \xi_{\tau_1} | \xi_{\tau_2} \rangle V(\xi(\tau_2), q(\tau_2)) \cdot \langle \xi_{\tau_2} | \xi_1 \rangle \varphi_i(\xi_1) \qquad (54)$$

$$= \left(\frac{i}{\hbar}\right)^2 \sum_n \int_{t_1}^{t_2} d\tau_1 \int_{t_1}^{\tau_1} d\tau_2\, e^{\frac{i}{\hbar}\frac{\epsilon_f - \epsilon_n}{\hbar}\tau_1} \langle f | V(\xi, q(\tau_1)) | n \rangle \cdot e^{\frac{i}{\hbar}\frac{\epsilon_n - \epsilon_i}{\hbar}\tau_2} \langle n | V(\xi, q(\tau_2)) | i \rangle$$

We now have

$$F_{fi}\{q,q'\} = \sum_f H_{fi}^{(0)*}\{q,q'\} H_{fi}^{(0)}\{q,q'\} + \sum_f \left(H_{fi}^{(0)*}\{q,q'\} H_{fi}^{(1)}\{q,q'\} + H_{fi}^{(1)*}\{q,q'\} H_{fi}^{(0)}\{q,q'\} \right) + \sum_f \left(H_{fi}^{(2)*}\{q,q'\} H_{fi}^{(0)}\{q,q'\} + H_{fi}^{(0)*}\{q,q'\} H_{fi}^{(2)}\{q,q'\} + H_{fi}^{(1)*}\{q,q'\} H_{fi}^{(1)}\{q,q'\} \right) + \cdots \qquad (55)$$

and of course

$$F\{q,q'\} = \sum_i p_i\, F_i\{q,q'\} \qquad (56)$$

Inserting the results (52), (53), (54) in (55) we get to zeroth order

$$F_i^{(0)}\{q,q'\} = 1 \qquad (57a)$$

$$f^{(0)}\{q,q'\} = 1 \qquad (57b)$$

To first order:

$$F_i^{(1)}\{q,q'\} = \frac{i}{\hbar}\int_{t_1}^{t_2} dt \left[V_{ii}(q(t)) - V_{ii}(q'(t)) \right] \qquad (58a)$$

$$F^{(1)}\{q,q'\} = \frac{i}{\hbar}\int_{t_1}^{t_2} dt \sum_i p_i \left[V_{ii}(q(t)) - V_{ii}(q'(t)) \right] \qquad (58b)$$

and to second order

$$F_i^{(2)}\{q,q'\} = \left(\frac{i}{\hbar}\right)^2 \sum_n \int_{t_1}^{t_2} d\tau_1 \int_{t_1}^{\tau_1} d\tau_2 \left[V_{ni}(q(\tau_1)) - V_{ni}(q'(\tau_1)) \right] \cdot \left[e^{-i\omega_{ni}(\tau_1-\tau_2)} V_{ni}(q(\tau_2)) - e^{i\omega_{ni}(\tau_1-\tau_2)} V_{ni}(q'(\tau_2)) \right] \qquad (59a)$$

and

$$F^{(2)}\{q,q'\} = \left(\frac{i}{\hbar}\right)^2 \sum_n \sum_i \int_{t_1}^{t_2} d\tau_1 \int_{t_1}^{\tau_1} d\tau_2\, p_i \left[V_{ni}(q(\tau_1)) - V_{ni}(q'(\tau_1)) \right] \cdot \left[e^{-i\omega_{ni}(\tau_1-\tau_2)} V_{ni}(q(\tau_2)) - e^{i\omega_{ni}(\tau_1-\tau_2)} V_{ni}(q'(\tau_2)) \right] \qquad (59b)$$

We have defined

$$\langle n | V(\xi, q(\tau)) | i \rangle e^{i\frac{\epsilon_n - \epsilon_i}{\hbar}\tau} \equiv V_{ni}(q(\tau)) e^{i\omega_{ni}\tau} \qquad (60)$$

with

$$\omega_{ni} = (\epsilon_n - \epsilon_i)/\hbar$$

We have also assumed that the phasing of the states $|i\rangle$, $|n\rangle$ etc. is chosen in such a way that the matrix elements are real.

Collecting results we have then

$$F_i\{q,q'\} = 1 + f_i^{(1)}\{q,q'\} + f_i^{(2)}\{q,q'\} + \cdots \qquad (61a)$$

with of course

$$F\{q,q'\} = \sum_i p_i f_i\{q,q'\} \qquad (61b)$$

We can put this in the form

$$F_i\{q,q'\} = e^{i\frac{W_i}{\hbar}\{q,q'\}} \qquad (62a)$$

and

$$F\{q,q'\} = e^{i\frac{W}{\hbar}\{q,q'\}} \qquad (62b)$$

These forms must be equivalent of course to (61a) (or (61b)) to the order to which the perturbation expansion has been carried out. With this in mind we get the result

$$W_i\{q,q'\} = \int_{t_1}^{t_2} dt \left[V_{ii}(q(t)) - V_{ii}(q'(t)) \right] + \tag{63a}$$

$$+ \frac{i}{\hbar} \sum_{n \neq i} \int_{t_1}^{t_2} d\tau_1 \int_{t_1}^{\tau_1} d\tau_2 \left[V_{ni}(q(\tau_1)) - V_{ni}(q'(\tau_1)) \right] \cdot$$

and of course

$$\cdot \left[e^{-i\omega_{ni}(\tau_1-\tau_2)} V_{ni}(q(\tau_2)) - e^{i\omega_{ni}(\tau_1-\tau_2)} V_{ni}(q'(\tau_2)) \right]$$

$$W\{q,q'\} = \sum_i p_i W_i\{q,q'\}$$

If we are interested in looking at solutions in the neighbourhood of $\eta(t) = 0$, we can proceed by Taylor-expanding these expressions. We have, using the definitions (22)

$$V(\xi, q(\tau)) = V(\xi, Q(\tau)) + \frac{1}{2}\eta(\tau) \frac{\partial V}{\partial Q(\tau)} + \cdots \tag{64}$$

$$V(\xi, q'(\tau)) = V(\xi, Q(\tau)) - \frac{1}{2}\eta(\tau) \frac{\partial V}{\partial Q(\tau)} + \cdots$$

neglecting second (and higher) order derivatives of V. Inserting these expansions in (63a) we get

$$W_i\{q,q'\} = \int_{t_1}^{t_2} dt\, f(t)\eta(t) + \frac{i}{\hbar} \int_{t_1}^{t_2} d\tau_1 \int_{t_1}^{\tau_1} d\tau_2\, C(\tau_1,\tau_2)\eta(\tau_1)\eta(\tau_2) \tag{65}$$

with the definitions

$$f(t) = \langle i | \frac{\partial V}{\partial Q(t)} | i \rangle - \frac{2}{\hbar^2} \sum_n \int_{t_1}^{t} d\tau \langle n | \frac{\partial V(\xi,Q)}{\partial Q(t)} | i \rangle \cdot \tag{66a}$$

$$\cdot \langle n | V(\xi, Q(\tau)) | i \rangle \cdot \sin\omega_{ni}(t-\tau)$$

and

$$C(\tau_1,\tau_2) = \sum_{n \neq i} \langle n | \frac{\partial V}{\partial Q(\tau_1)} | i \rangle \langle n | \frac{\partial V}{\partial Q(\tau_2)} | i \rangle \cos\omega_{ni}(\tau_1-\tau_2) \tag{66b}$$

The expression (65) has been put in the form arrived at the last section (def.38). Note the two different types of constributions to f(t). The first term is just the average force (in a medium in state $|i\rangle$) between the system and the medium.

The second term arises partly from the contributions from virtual (or real) transitions occurring among the medium states, caused by the coupling between medium and system: it contains the origin of frictional forces.

The equation of motion according to (28) is

$$\frac{d}{dt}\frac{\partial L}{\partial \dot{q}} = \frac{\partial L}{\partial q} + f(t)$$

By doing an integration by part on f(t) we get

$$\frac{1}{dt}\frac{\partial L}{\partial \dot{q}} = \frac{\partial L}{\partial q} + \alpha(t) + \int_{t_1}^{t} \gamma(q(t),q(\tau),t-\tau)\dot{Q}(\tau)\,d\tau \tag{66c}$$

where the "coefficient of friction" is defined by

$$\gamma(q(t),q(\tau),t-\tau) = \frac{2}{\hbar^2} \sum_{n \neq i} \langle n | \frac{\partial V(\xi,q(t))}{\partial q(t)} | i \rangle \frac{1}{\omega_{ni}} \langle n | \frac{\partial V(\xi,q(\tau))}{\partial q(\tau)} | i \rangle \cdot$$

$$\cdot \cos\omega_{ni}(t-\tau) \tag{66d}$$

There is no singularity coming from terms $n \equiv i$, as these terms do not contribute anayway to f(t) (see 66a). Notice the connection between γ and C. We shall return to it presently.

B) The adiabatic approximation

There is a vast class of problems in nuclear physics where the weak coupling approximation discussed above is just not good enough. The fission problem certainly falls into this class. Fortunately, it is possible to use an alternative approximation scheme based on the so-called adiabacity of the

collective motion. This boils down to assuming that our systems generalized velocity $\dot{q}(t)$ in some sense (to be specified below) is small relative to the characteristic speeds of the constituents of the medium. In the theory of collective nuclear motion this is expressed by stating that the collective frequencies of interest are much smaller than typical single particle frequencies. We shall now use this assumed adiabacity to find an alternative solution to the IF.

We want to compute the amplitude $M_{fi}\{q(t)\}$:

$$M_{fi}\{q(t)\} = \int d\xi_1 \int d\xi_2\, \varphi_f^*(\xi_2)\langle \xi_2 | \xi_1 \rangle_{q(t)} \varphi_i(\xi_1)$$
$$= \int d\xi_2\, \varphi_f^*(\xi_2)\, \Psi_i(\xi_2, q(t))$$
$$\therefore M_{fi}\{q(t)\} = \langle f | \Psi_i(q(t)) \rangle \qquad (67)$$

The Hamiltonian corresponding to (49) is represented by

$$H(\xi, q(t)) = H_0(\xi) + W(\xi, q(t)) \qquad (68)$$

where W is the coupling between the system q and the medium $\{\xi\}$. There is an implicit time dependence of this coupling through the time dependence of q. For a fixed t, that is to say, for a fixed q(t), we diagonalize this Hamiltonian:

$$H(\xi; q(t))\, \varphi_n(\xi; q(t)) = E_n(q(t))\, \varphi_n(\xi; q(t)) \qquad (69)$$

obtaining the orthonormal set of stationary states $\varphi_n(\xi; q(t))$:

$$\int \varphi_m^*(\xi; q(t))\, \varphi_n(\xi; q(t))\, d\xi = \delta_{mn} \qquad (70)$$

with the energies $E_n(q(t)) = E_n(t)$.

This procedure defines the moving basis φ_n. A general (non-stationary) wavefunction obeys the Schrödinger equation

$$i\hbar \frac{\partial}{\partial t} \Psi(\xi; q(t)) = H\, \Psi(\xi; q(t)) \qquad (71)$$

Put

$$\Psi_i(\xi; q(t)) = \sum_n C_{ni}(t)\, e^{-\frac{i}{\hbar}\int_{t_1}^{t} E_n(\tau)\, d\tau}\, \varphi_n(\xi; q(t)) \qquad (72)$$

The subscript i means that we are going to use the initial conditions

$$C_{ni}(t = t_1) = \delta_{ni} \longleftarrow \Psi_i(\xi; q(t_1)) = \varphi_i(\xi; q(t_1)) \qquad (73)$$

The desired amplitude $M_{fi}\{q\}$ is then

$$M_{fi}\{q\} = C_{fi}(q = q(t)) \qquad (74)$$

Inserting (72) into (71), and using (69) and (73) we get

$$C_{mi}(t) = \delta_{mi} - \sum_n \int_{t_1}^{t} d\tau\, W_{mn}(\tau)\, C_{ni}(\tau) \qquad (75)$$

where

$$W_{mn}(t) = W_{mn}(q(t)) = \begin{cases} 0 & (m = n) \\ \dfrac{\dot{q}(t)}{\hbar\, \Omega_{mn}(q(t))}\, e^{i\int_{t_1}^{t} \Omega_{mn}(q(\tau))\, d\tau} \cdot \langle m; q(t) | \dfrac{\partial V}{\partial q(\tau)} | n; q(\tau) \rangle & (m \neq n) \end{cases} \qquad (76)$$

with

$$\hbar\, \Omega_{mn}(q) = \left[E_m(q(t)) - E_n(q(t)) \right]$$

These results can be simply obtained from (69). At the same time we get

$$\frac{dE_n(q(t))}{dt} = \int \varphi_n(\xi; q(t)) \frac{\partial V(\xi, q)}{\partial q(t)} \varphi_n(\xi; q(t))\, d\xi \equiv \langle n; q(t) | \frac{\partial V}{\partial q(t)} | n; q(t) \rangle \qquad (77)$$

We have assumed that the eigenfunctions φ_n are real. We can then separate the real and the complex parts of w_{mn}: define

$$W_{mn}(q(t)) = V_{mn}(q(t))\, e^{i\int_{t_1}^{t} \Omega_{mn}(q(\tau))\, d\tau} \qquad (78)$$

with the real matrix elements

$$V_{mn}(q(t)) = \begin{cases} 0 & m = n \\ \dfrac{\dot{q}(t)}{\hbar\,\Omega_{mn}(q(t))} \langle m\,q(t)| \dfrac{\partial V}{\partial q(t)} |n\,q(t)\rangle & m \neq n \end{cases} \tag{79}$$

Note that

$$W^{*}_{mn}(q(t)) = -W_{nm}(q(t)) \tag{80}$$

We shall now state what is it that we consider to be the "small parameter" in the present approximation. Let τ_{int} be some typical time scale characterizing the internal motion of the medium: then we assume

$$\tau_{int}\,|V_{mn}| \ll 1 \tag{81}$$

We claim then that the approximation (using (75))

$$W_{fi}(q(t)) = \delta_{fi} - \int_{t_1}^{t} d\tau\, W^{*}_{fi}(q(\tau)) + \tag{82}$$
$$+ \sum_{n} \int_{t_1}^{t} d\tau_1\, W_{fn}(q(\tau_1)) \int_{t_1}^{\tau_1} d\tau_2\, W_{ni}(q(\tau_2)) + \dots$$

should be good enough.

We can now proceed as in the last subsection, and deduce that to the order to which we carried out the expansion the result is equivalent to

$$F_i\{q,q'\} = e^{\frac{i}{\hbar} W_i\{q,q'\}} \tag{83}$$

with

$$W_i\{q,q'\} = -i\hbar \sum_f \int_{t_1}^{t} d\tau_1 \int_{t_1}^{\tau_1} d\tau_2 \Big\{ \Big[W_{fi}(q(\tau_1)) -$$
$$- W_{fi}(q'(\tau_1)) \Big] W^{*}_{fi}(q'(\tau_2)) -$$
$$- \Big[W_{fi}(q(\tau_1)) - W_{fi}(q'(\tau_1)) \Big]^{*} W_{fi}(q(\tau_2)) \Big\} \tag{84}$$

This can again be put into the standard form (def. 38) by making a further approximation on (78) compatible with our adiabacity hypothesis[4]. We shall leave this as an exercise to the reader; give also an expression for the coefficient of friction in this approximation.

4. The Weidenmüller model

The above formulation of dynamical and statistical laws plays an important role in a theory due to H.Weidenmüller, D.Brink et al.,[3] a theory that hitherto has been applied chiefly to deep inelastic nuclear scattering processes. It could though equally well be applied to nuclear fission. We shall give here a short account of the basic ideas of this theory, following a simplified version due to D.Brink.[3]

In previous sections we were led to consider non-Markovian equations of motion for our system (still represented by a single generalized coordinate q(t)) of form

$$\frac{d}{dt}\frac{\partial L}{\partial \dot{q}} - \frac{\partial L}{\partial q} = a(t) - \int_{t_1}^{t} d\tau\, s(t-\tau)\,\dot{q}(\tau) \tag{85}$$

Possible linear terms in q have been absorbed into $\frac{\partial L}{\partial q}$. We derived this from an IF of form

$$F\{q,q'\} = e^{\frac{i}{\hbar} W\{q,q'\}} \tag{86a}$$

where

$$W\{q,q'\} = \int_{t_1}^{t_2} d\tau\, \eta(\tau) f(\tau) + \frac{i}{\hbar} \int_{t_1}^{t_2} d\tau_1 \int_{t_1}^{\tau_1} d\tau_2\, C(\tau_1,\tau_2)\,\eta(\tau_1)\eta(\tau_2) \tag{86b}$$

and

$$f(t) = a(t) + \int_{t_1}^{t} d\tau\, \alpha(t,\tau)\, Q(\tau) \tag{86c}$$

Both f(t) and $C(\tau_1,\tau_2)$ are assumed to be real functions of their arguments. The weak coupling approximation suggests that f(t) - i.e., the function appearing in the real part of $W\{q,q'\}$ - is the average force exerted by the

medium on the system. It includes viscosous forces. The function $C(\tau_1, \tau_2)$ that appears in the pure imaginary part of $W\{q,q'\}$ will be referred to as the "correlation function" for reasons that will be clear soon - although the very form of the double integral in (86b) suggests the appropriateness of this designation. In the case of weak coupling, it is given by formula (66b). A comparison with the coefficient of friction (66d) suggests a relationship. We shall return to this presently.

As already mentioned, eq.(85) happens to be of the type of a generalized Langevin equation. The original Langevin equation is quoted in connection with the theory of Brownian motion. Consider a particle of mass m_o suspended in a fluid. Assume that the whole assembly is in thermal equillibrium.

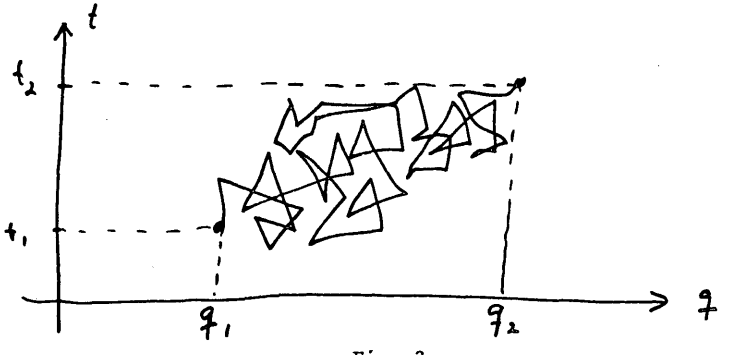

Fig. 3

Let q be the projection of the particle path onto some fixed axis, and consider its motion between t_1 and t_2 (Fig. 3). Let $\dot{q} = \frac{dq}{dt}$ be the component along this axis of the particle velocity. The Langevin equation tells us that

$$m_o \frac{d\dot{q}}{dt} = -\alpha_o \dot{q} + F_L(t) \qquad (87)$$

where F(t) is a random fluctuating force. It results from the chaotic molecular bombardement to which the particle is subject as it wanders through the fluid. This random Langevin force is assumed to have a Gaussian probability distribution with zero mean value

$$\langle F_L(t) \rangle = 0 \qquad (88)$$

and a correlation function

$$\langle F_L(t)\, F_L(t') \rangle = 2\lambda\, \delta(t-t') \qquad (89)$$

When this random force has its origins in the thermal fluctuations of the molecules of the fluid, the coefficients of friction α_o and the parameter λ are related to each other through Einstein's relation

$$\lambda = kT \cdot \alpha_o \qquad (90)$$

where T is the temperature and k the Boltzmann constant.

The Langevin equation is of a simple Markovian type, as already mentioned. It can be generalized, and then it reads *)

$$m_o \frac{d\dot{q}}{dt} = -\int_{t_1}^{t} \alpha(t-t')\, \dot{q}(t')\, dt' + F_L(t) \qquad (91)$$

in a typical non-Markovian fashion. The generalized Einstein relation (again, in case of thermal origin of the random forces) is

$$\langle F_L(t)\, F_L(t') \rangle = kT \cdot \alpha(|t-t'|) \qquad (92)$$

This problem is indeed an ideal one for a treatment with IF methods. Feynman and his collaborators have done just that. Consider the Lagrangian

$$L_F(q,\dot{q},t) \equiv L(q,\dot{q}) + F(t)\, q(t) \qquad (93)$$

*) Generalized non-Markovian equations of type (91) are not convenient for practical applications. This is due to the random nature of the coupling $F_L(t)$. Instead of trying to compute many trajectories (solutions of eq.(91)) for various distributions $F_L(t)$, one can first rewrite eq.(91) as an equation of motion for the normalized probability distribution P (q,p,t) for finding the representative point in phase space at time t with the generalized coordinate q(t) and the generalized momentum p(t). One then tries to solve this equation with given inital conditions. One thus arrives[5] (with suitable approximations) to equations of Fokker-Planck type for P (q,p,t).

The IF corresponding to this is

$$F\{q,q'\} = e^{\frac{i}{\hbar}\int_{t_1}^{t_2} \eta(\tau) f(\tau) d\tau} \qquad (94)$$

Now suppose that the force F(t) is of a stochastic character, i.e. that it can be split up into an average part

$$\langle F(t) \rangle = f(t) \qquad (95)$$

and a random part $F_L(t)$ such that

$$\langle F_L(t) \rangle = 0 \qquad (96a)$$

$$\langle F_L(t) F_L(t') \rangle = C(t,t') \qquad (96b)$$

Then it can easily be shown that the IF can be written thus

$$F\{q,q'\} = \exp\left[\frac{i}{\hbar}\int_{t_1}^{t_2} \eta(\tau) f(\tau) d\tau - \frac{1}{2\hbar^2}\int_{t_1}^{t_2} d\tau_1 \int_{t_1}^{t_2} d\tau_2 C(\tau_1,\tau_2)\eta(\tau_1)\eta(\tau_2)\right] \qquad (97)$$

time taken for the compound nucleus from formation to complete scission into two (or more) fragments.

Let us partition this time interval into much shorter intervals

$$\Delta\tau \ll t_2 - t_1 \qquad (102)$$

though <u>larger than the correlation time</u>

$$\tau_c = \frac{\hbar}{\Delta} \qquad (103)$$

We then argue that <u>during these short intervals $\Delta\tau$</u> the IF could be computed by perturbation theory (weak coupling) to second order in $\eta(t)$, the way that we did previously. Then invoking our rule 3, the entire IF would be the product of all these partial IF's defined in each time interval $\Delta\tau$. The result would of course again be our standard Gaussian IF.

What does "weak coupling" mean in this context? The interaction V causes the states of the entire assembly (system & medium) to spread over many states of the medium, say over a range δE of these states. Weak coupling means

$$\delta E \ll \Delta \qquad (104)$$

We are then justified in using the results discussed previously under the heading "weak coupling".

That is the main argument. The rest is straightforward.

Define the function

$$\bar{C}_a(V(q),V(q'),\tau) \equiv \sum_b \langle V_{ab}(q) V_{ab}(q') \rangle \exp(i\omega_{ab}\tau) \qquad (105)$$

with

$$\omega_{ab} = (E_a - E_b)/\hbar$$

The average force f(t) and the correlation function $C(\tau_1,\tau_2)$, respectively (66a) and (66b) can be obtained from (105) by differentiating with respect to Q, then Q', putting Q = Q' and finally taking the real and imaginary parts. which is precisely our standard form for the IF. Def.(96b) thus justifies the name "correlation function" for $C(\tau_1,\tau_2)$.

This is the IF interpretation of Langevin equation. Let us now turn to the Weidenmüller model.[3,5] This model can be used to describe the physics of "warm" nuclei, formed during a deep inelastic collision, or during fission processes following a compound nucleus formation. In all cases, we shall assume that the energy pumped into the nucleus is high enough that the patterns of excited states (the medium states) is so complex that random features result. We shall try to represent this with the following assumptions.

We split the Hamiltonian in the same way we have hitherto been doing in this chapter:

$$H = H_1(q) + H_2(\xi) + V(\xi,q) \qquad (98)$$

The intrinsic states (medium states) are eigenstates of H_2:

$$H_2(\xi)|n\rangle = E_n|n\rangle \qquad (99)$$

with energies E_n. The coupling V is defined through its matrix elements

$$\langle m|V(q,\xi)|n\rangle = V_{mn}(q) \qquad (100)$$

We shall assume that these matrix elements are Gaussian random variables, satisfying the following conditions:

a) $$\langle V_{mn}(q)\rangle = 0 \qquad (101a)$$

b) $$\langle V_{am}(q)\, V_{bn}(q')\rangle = (\delta_{ab}\delta_{mn} + \delta_{an}\delta_{mb}) \cdot \frac{w\left(\frac{q+q'}{2}\right)}{\sqrt{\rho(\epsilon_m)\rho(\epsilon_n)}} e^{-\frac{\eta^2}{2\sigma^2}} e^{-\frac{(\epsilon_m-\epsilon_n)^2}{2\Delta^2}} \qquad (101b)$$

with Q and η having the usual meaning (cf.eq.22). $\rho(\epsilon)$ is the level density at energy ϵ. The function W(Q) is an interaction strength. The factor σ is a correlation length (≈ 2.5 fm) and Δ (≈ 8 MeV) a correlation energy.

With these assumptions, and account taken of our previous discussions, it is relatively straightforward to write down the IF of this problem.

A point is that our previous discussion was based on expansions around $\eta = 0$, keeping only the leading terms. This was justified in the weak coupling approximation and also in the adiabatic approximation, where the coupling need not be weak. But with the problem at hand, one has to be more careful, as there is no a priori reason to suppose that η is particularly small. However, we could argue as follows. Consider the time interval that we are interested in, viz. $t_2 - t_1$ - in the case of deep inelastic scattering, that would naturally be the reaction time; in the case of fission, that could for example be the

Using the assumptions a) and b) above, the function $\bar{C}$ can be calculated, with the result

$$\bar{C}_a(V(q),V(q'),\tau) = \sqrt{2\pi}\, W\left(\frac{q+q'}{2}\right) e^{-\frac{1}{2}\left(\frac{q-q'}{\sigma}\right)^2} \cdot \exp\left(-\frac{1}{2}\frac{\Delta^2}{\hbar^2}\left(\tau + \frac{1}{2}i\beta\right)^2\right) \qquad (106)$$

In order to get this convenient result, one has made the "nuclear temperature" approximation, i.e. assume

$$\frac{\rho(\epsilon_b)}{\rho(\epsilon_a)} \approx e^{\beta(\epsilon_b-\epsilon_a)} \qquad \beta = \frac{1}{kT} \qquad (107)$$

The "memory" time in weak coupling

$$\tau_m = \frac{\hbar}{\Delta} \approx 10^{-22}\ \text{sec} \qquad (108)$$

is very short, and therefore the Markovian approximation probably is good enough. From the result (106) one can then conclude that

$$\lambda = \frac{1}{2}\int_{-\infty}^{\infty} \langle F_L(t)\, F_L(t')\rangle\, dt' = \pi W(Q)\frac{\hbar}{\sigma^2} \qquad (109)$$

One further approximation was necessary to get this simple result: that the speed $\dot{Q}$ is small (ie. $\dot{Q} < \frac{\sigma\Delta}{\hbar}$). This allows one also to obtain the coefficeint α_0:

$$\alpha_0 = \beta\lambda \qquad (110)$$

in agreement with Einstein's formula. If $\dot{Q}$ is not small (in the above sense) then this last result would not hold. Note that for $\dot{Q}$ small we could try the adiabatic approximation instead of the weak coupling approximation - we would then no longer need to assume that V is small in the above-mentioned sense.

REFERENCES TO CHAPTER II

1) R.P.Feynman and H.R.Hibbs, Quantum Mechanics and Path Integrals, McGraw-Hill, New York (1965)
2) R.P.Feynman and F.L.Vernon, Ann.Phys.24 (1963) 118
3) D.M.Brink, Prog.Part.Nucl.Phys.4 (1980) 323
4) K.Möhring and V.Smilansky, Nucl.Phys.A338 (1980) 227
5) H.A.Weidenmüller, Prog.Part.Nucl.Phys.3(1980) 49
6) M.C. Nemes and H.A.Weidenmüller, Phys.Rev.C24 (1981) 944

III. COLLECTIVE TRANSPORT THEORY FOR NUCLEI

This chapter of the lecture notes consists of a part of a preliminary draft of a review article[1] on "Collective transport theory for nuclei". Instead of including it here we refer the reader to ref. 1.

REFERENCES TO CHAPTER III

1) H.Hofmann, A.S.Jensen, C.Ngô and P.J.Siemens, to be published in Rev.Mod. Phys.

STATIC THEORIES OF THE FISSION BARRIER

M. BRACK
University of Regensburg, Regensburg,
Federal Republic of Germany

Contents of lectures:

1) Survey of theories of the static fission barrier

- liquid drop model
- deformed shell model
- shell-correction method
- nuclear shapes relevant to fission
- scission: exit region

2) Microscopic theory

- Hartree - Fock with effective Skyrme forces
- justification of shell-correction method
- treatment of pairing effects

3) Semiclassical theory

- extended Thomas-Fermi model (ETF)
- relation of ETF model to Strutinsky averaging
- variational energy density calculations
- justification and limitations of droplet model

All the material presented in these lectures has been previously published or is shortly being published (sect. 3). The main references are:

to 1): see previous Courses on Nuclear Theory for Applications (IAEA-ICTP)
1978: M. Brack, IAEA-SMR-43, pp. 327-352
1980: H.C. Pauli, IAEA-SMR-68/I, pp. 41-90

to 2): P. Quentin, H. Flocard, Ann. Rev. Nucl. Sci. Part 28 (1978) 523
M. Brack, P. Quentin, Nucl. Phys. A 361 (1981) 35

to 3): B.K. Jennings, R.K. Bhaduri, M. Brack, Nucl. Phys. A 253 (1975) 29
M. Brack, et al., Proc. 4th Int. Conf. on Nuclei far from stability, Helsingør 1981 (CERN 81-09) p. 65
C. Guet, H.-B. Håkansson, M. Brack, Phys. Lett. 97 B (1980) 7
C. Guet, M. Brack, Z. für Physik A 297 (1980) 247
J. Bartel, P. Quentin, M. Brack, C. Guet, H.-B. Håkansson, Nucl. Phys. A, A 386 (1982) 79
C. Guet, H.-B. Håkansson, M. Brack, to be published in Nucl. Phys. A (1983)

MASS, CHARGE AND KINETIC ENERGY DISTRIBUTION OF FISSION FRAGMENTS

H. NIFENECKER
Département Recherche fondamentale,
CEA, Centre d'études nucléaires de Grenoble,
Grenoble, France

Abstract

The material of these lectures is fully covered in the following references :

- Low Energy Nuclear Fission - H. NIFENECKER - From Nuclear Structures, Edited by K. Abrahams, K. Allart and A.E.L. Dieperink, Plenum Publishing Corporation 1981, p. 309.

- A Combinatorial Analysis of Pair Breaking in Fission - H. NIFENECKER, G. MARIOLOPOULOS, J.P. BOCQUET, R. BRISSOT, C. HAMELIN, J. CRANÇON, C. RISTORI, In Dynamics of Nuclear Fission and Related Collective Phenomena, Edited by P. David, T. Mayer-Kuckuk and A. van der Woude, p. 47, Notes in Physics 158, Springer-Verlag.

In the following we therefore only give a summary of the lectures.

The liquid drop theory of fission predicts symmetric fission fragments mass energy distributions. Experimental results for low energy fission strongly disagree with these predictions. The asymmetry of the mass distributions has been known almost since the discovery of the fission phenomenon. It has also been shown that asymmetric mass splits produce fragments with more total kinetic energy than the symmetric ones, again at variance with the liquid drop predictions. Shell effects clearly influence strongly the fragments mass and energy distributions. On the other hand pairing effects may provide an explanation for the often observed enhanced production of fragments with even charge as compared to fragments with odd charge. In order to explain the influence of shell effects upon the characteristics of fission fragments one has to resort to the general theory of shells in nuclei as it was first introduced by W. Strutinsky. The renormalization procedure introduced by W. Strutinsky is described shortly since it is, now a classic in fission physics. More time is spent on the geometrical origin of shells in deformed nuclei and its relationship to classical closed orbits.

The first consequence of the Strutinsky procedure is the prediction of a double-humped fission barrier. A short review of the experimental confirmations of this prediction is given. Models which predict asymmetric fragments mass distributions are described. These models include shell effects in very deformed nuclei. Deformed shell with N = 86 and N = 64 with an approximate 2 to 1 ratio of the length of the principal axis of the relevant fragment seem to have a decisive role in explaining the asymmetric mass distribution. The spherical shells with N = 82, Z = 50 or N = 50 play a role in determining the fission kinetic energies. Both Saddle point and Scission point models seem to be able to account semi quantitatively for the observed mass distributions. This fact suggests that mass distributions may not be a good probe of the fission dynamics. On the contrary charge distributions which show striking even-odd effects both on the charge yields and the fragments total kinetic energies may very well be a unique tool for studying large amplitude nuclear motion dynamics at low temperature. We review the experimental data and present a model relating the observed even-odd effects to pair breaking. It is shown that existing data are compatible with two pair breaking mechanisms. The first takes place at the saddle point where a statistical quasi equilibrium is realised, the second close to the scission point at the moment of the sudden separation of the fragments.

NUCLEAR DATA FOR FISSION REACTOR CORE DESIGN AND SAFETY ANALYSIS: REQUIREMENTS AND STATUS OF ACCURACY OF NUCLEAR DATA

J.L. ROWLANDS
Reactor Physics Division,
Atomic Energy Establishment,
Winfrith, Dorchester,
United Kingdom

ABSTRACT

The types of nuclear data required for fission reactor design and safety analysis, and the ways in which the data are represented and approximated for use in reactor calculations, are summarised first.

The relative importance of different items of nuclear data in the prediction of reactor parameters is described and ways of investigating the accuracy of these data by evaluating related integral measurements is discussed. The use of sensitivity analysis, together with estimates of the uncertainties in nuclear data and relevant integral measurements, in assessing the accuracy of prediction of reactor parameters is described. The inverse procedure for deciding nuclear data requirements from the target accuracies for prediction of reactor parameters follows on from this. The need for assessments of the uncertainties in nuclear data evaluations and the form of the uncertainty information is discussed.

The status of the accuracies of predictions and nuclear data requirements are then summarised. The reactor parameters considered include:

(a) Criticality conditions, conversion and burn-up effects.

(b) Energy production and deposition, decay heating, irradiation damage, dosimetry and induced radioactivity.

(c) Kinetics characteristics and control, including temperature, power and coolant density coefficients, delayed neutrons and control absorbers.

Section 1 - Neutron physics data used in fission reactor calculations

1.1 Introduction

Reactor neutron physics (or neutronics) involves the calculation of the neutron energy spectrum and spatial distribution and also relative reaction rates in this spectrum. The spectrum varies with position in the reactor. In a thermal reactor the spectrum is different in the moderator and the fuel. It also varies through the reflector and shielding. The reactor neutron energy spectrum is determined by the energy spectrum of the neutrons produced in fission and the scattering and absorption cross sections of the reactor components as a function of energy. The upper energy of interest is about 15 MeV and, for a thermal reactor, the spectrum is calculated down to an energy of about 0.001 eV.

In this section the parameters, conventions and notation of reactor neutronics calculations are introduced, neutronics characteristics of reactors are outlined and the approximations made in using nuclear data in reactor calculations summarised.

1.2 Neutron density, neutron flux and the neutron-nucleus interaction rate

Some definitions

The neutron flux is the flow of neutrons per unit area. The directional neutron flux is denoted by $N(E,x,\underline{\Omega})$ where

$N(E,x,\underline{\Omega})dEd\Omega$ = neutron flux in the solid angle $d\Omega$ about the direction $\underline{\Omega}$ having energies in the range E to E + dE (1)

The scalar neutron flux is the integral of the directional flux over all angles:

$$\phi(E,x) = \int N(E,x,\underline{\Omega})\, d\Omega \qquad (2)$$

The scalar neutron flux is often called, simply, the neutron flux. It is related to the neutron density, n(E,x), via the **speed** v, of neutrons of energy E,

$$\phi(E,x) = v.n(E,x) \qquad (3)$$

where n(E,x)dEdV is the number of neutrons in a volume element dV at x and in the energy range E to E + dE.

In the calculation of the neutron flux distribution in a reactor the angular distribution of the flux must be taken into account. In the diffusion theory approximation a simple angular dependence is assumed for the flux:

$$N(E,x,\Omega) = \frac{1}{4\pi}\left(\phi(E,x) + 3\,\underline{\Omega}.\underline{J}\,(E,x)\right) \qquad (4)$$

where $\underline{J}(E,x)$ is the net neutron current.

The reaction rate for reaction r in isotope I depends on the number density of isotope I, $N_I(x)$, in volume element dV and the cross-section for the reaction, $\sigma_r^I(E)$, at energy E.

$$R_r^I(x) = N_I(x) \int \sigma_r^I(E) \ \phi(E,x) dE \tag{5}$$

This can also be written in terms of the neutron density n(E,x) and velocity v:

$$R_r^I(x) = N_I(x) \int v \ n(E,x) \ \sigma_r^I(E) dE \tag{6}$$

The nuclear cross section $\sigma_r^I(E)$ is called the microscopic cross section to distinguish it from the macroscopic cross-section for the material, $\Sigma_r^I(E,x)$:

$$\Sigma_r^I(E,x) = N_I(x), \ \sigma_r^I(E) \tag{7}$$

When there is a neutron source density, S(E), in an infinite medium with no leakage the rate at which neutrons are removed from energy interval dE by all removal reactions must equal the source

$$\phi(E) \ \Sigma_{rem}(E) = S(E) \tag{8}$$

where S(E) is the neutron source due to fission and scattering. The flux equals

$$\phi(E) = S(E)/\Sigma_{rem}(E) \tag{9}$$

In an operating reactor the source of neutrons of energy E comprises neutrons from fission reactions, elastic and inelastic scattering and reactions such as (n,2n) and (n,3n). Charged particle reactions (for example (α,n) reactions) and photon induced reactions such as (γ,n) and (γ,f) reactions are not a significant source of neutrons in reactors at power but they can be significant in the shut-down reactor and in fuel in transport and reprocessing. Spontaneous fission is also of importance in these cases.

Neutrons are removed from an energy interval by absorption reactions such as radiative capture, (n,p) and (n,α) reactions and by leakage. Scattering reactions, which change the energy of the neutron, also remove neutrons from the energy interval. Elastic scattering in some isotopes at high energies has a component which is strongly forward peaked and, in this case, the change in energy for this component can be neglected. This is particularly the case for heavy elements at high energies. Thus instead of the removal cross-section being set equal to the total cross section it can be approximated.

The collision density is defined as:

$$C(E) = \phi(E).\Sigma_t(E) \tag{10}$$

where $\Sigma_t(E)$ is the total macroscopic cross-section. C(E) is equal to the source S(E) when leakage is absent and when all scattering is included in the source.

The slowing down density, q(E), is the number of neutrons per unit volume per second which are moderated from above energy E to lower energies:

$$q(E) = \int_E^{Eu} \int_{E_L}^{E} \Sigma_s(E' \rightarrow E'') \ \phi(E') \ dE'dE'' \tag{11}$$

where $\Sigma_s(E' \rightarrow E'')$ is the cross-section for scattering from energy E' to energy E'' and E_u and E_L are the upper and lower energy ranges of scattering about energy E.

The change in slowing down source with energy is equal to the difference between the loss of neutrons by absorption and leakage and the production of neutrons by fission:

$$\frac{dq}{dE} = \Sigma_a(E).\phi(E) + L(E) - F(E) \tag{12}$$

where L(E) is the leakage per unit energy and F(E) is the fission source per unit energy. $\Sigma_a(E)$ is the macroscopic absorption cross-section.

In the absence of absorption and leakage we have

$$q(E) = \int_E^{\infty} F(E')dE' \tag{13}$$

Instead of expressing quantities in terms of energy a related variable called the lethargy, u, is often used:

$$u = -\ln \left(\frac{E}{10MeV} \right) \tag{14}$$

and the difference in lethargy between two energies, E_1, and E_2 is:

$$\Delta u = -\ln\left(\frac{E_1}{E_2}\right) \tag{15}$$

The mean lethargy gain in elastic scattering, $\bar{\xi}$, is dependent on the mass of the nucleus and the anisotropy of scattering. For elastic scattering which is isotropic in c.m. co-ordinates $\bar{\xi}$ is independent of energy (or lethargy) and equal to

$$\bar{\xi}_o = 1 + \frac{\alpha \ln \alpha}{(1-\alpha)} \tag{16}$$

where $\alpha = \left(\frac{A-1}{A+1}\right)^2$ (17)

and A = ratio of the mass of the nucleus to the mass of the neutron.

When the slowing down density is constant in energy and the moderation cross-section is constant then the flux per unit lethargy, $\phi(u)$, is constant in lethargy. In this case the flux per unit energy is proportional to (1/E), and

$$\phi(u) = q/(\bar{\xi}\Sigma_s)$$

and $$\phi(E) = \phi(u)/E = q/(\bar{\xi}\Sigma_s E)$$

1.3 Approximate form of the neutron spectrum in thermal reactors

In a thermal reactor q varies fairly slowly over the energy range from 1eV to 100 KeV and moderator cross-sections are approximately constant. The collision density per unit lethargy can be assumed to be constant over this energy range for some purposes and so $C(E) \simeq 1/E$. It is acceptable to assume

$$\phi(E) \simeq 1/E \qquad 1eV < E < 100\ KeV \tag{19}$$

in this energy range, for the purposes of spectrum averaging some cross-sections.

In fact, the flux has a detailed energy structure through resonances but the effect of this structure averages out approximately for cross-sections in non-resonant materials, or materials present in small proportions. At higher energies the slowing down density can be approximated by the integral of the fission spectrum, $\chi(E)$ (neglecting leakage and absorption):

$$q(u) = q(E) = \int_E^\infty \chi(E')dE' \tag{20}$$

and the flux can be approximated as

$$\phi(u) \simeq q(u)$$

$$\phi(E) \simeq \frac{1}{E} \int_E^\infty \chi(E')dE' \qquad E > 100\ KeV \tag{21}$$

(assuming constant scattering cross-sections).

At thermal energies, in the absence of absorption and leakage, the flux is in thermal equilibrium with the medium and

$$\phi(E) \simeq E \exp\left(\frac{-E}{KT}\right) \qquad E < 1\ eV \tag{22}$$

where T is the absolute temperature of the medium. These three energy ranges are called the fast (> 100 KeV), intermediate (1eV - 100 KeV) and thermal (< 1eV) ranges.

1.4 Neutron producing reactions in power reactors

In an operating reactor the source S(E') of neutrons of energy E' results from the following reactions:

Fission reactions - $\sigma_{n,f}(E)$

The energy spectrum of fission neutrons is denoted by $\chi(E')$. This depends on the fissioning nucleus and, to a small extent, on the incident neutron energy.

The mean number of neutrons emitted in fission, $\nu(E)$, also depends on the fissioning nucleus and the incident neutron energy, increasing approximately linearly with energy. The angular distribution of fission neutrons is isotropic to a good approximation.

Elastic scattering - $\sigma_{n,n}(E,E',\theta)$

The cross-section is a function of the angle of scattering, θ. The cross-section can be expressed either in laboratory co-ordinates or centre-of-mass co-ordinates. A useful characteristic of the angular distribution is the mean cosine of the scattering angle, $\bar{\mu}$. The secondary energy distribution is defined by the angular distribution. For isotropic scattering in c.m. co-ordinates it is uniform in energy.

Inelastic scattering to discrete levels ℓ - $\sigma^{\ell}_{n,n'}(E,E',\theta)$

The secondary energy distribution is determined by the Q value for the level and the angular distribution. In many cases this can be taken to be isotropic in c.m. co-ordinates. Inelastic scattering occurs both when nuclear levels are excited and, at thermal neutron energies, when molecular or crystalline level transitions occur. For these thermal energy interactions the transition energy can be positive or negative. Excitation of nuclear levels occurs at KeV and MeV energies.

Inelastic scattering to the continuum $\sigma_{n,n'}(E,E',\theta)$

At energies where the individual levels are not resolved the total inelastic cross-section and the secondary energy distribution and angular distribution are determined as a function of incident neutron energy. In most practical cases the angular distribution can be taken to be isotropic.

(n,2n) reactions $\sigma_{n,2n}(E,E',\theta)$

Thresholds for (n,2n) reactions are at MeV energies. For most isotopes they are above 6 MeV, the average binding energy for neutrons in the nucleus. Consequently this reaction does not have a major effect on either the reactor neutron spectrum or the neutron balance of a reactor. The reaction is mainly of interest when it results in a radioactive reaction product which presents a handling or waste management problem. The reaction is usually treated as isotropic and the secondary energy distributions as a function of incident neutron energy are required. The total cross-section is of more interest than an accurate knowledge of the secondary energy distribution because it is the contribution to the neutron economy of the net neutron production and the reaction products which are of more interest than the small effect on the neutron spectrum. The thresholds for (n,3n) reactions are at even higher energies and they make a negligibly small contribution to the neutron economy and spectra of fission reactors.

1.5 Neutron production in shut-down reactors and irradiated fuel

Spontaneous fission neutrons and (α,n) reaction neutrons resulting from the alpha decay of transactinium isotopes and (α,n) reactions in light nuclei, such as oxygen, carbon and fluorine, are significant components of the activity of irradiated fuel. Data are required on spontaneous fission and alpha decay half-lives, spontaneous fission ν values and neutron spectra, alpha particle energies and (α,n) reaction data. For irradiated fuel the (α,n) reaction data can be represented by thick sample yields; that is, the yield of neutrons for α-particles emitted in a compound, such as uranium oxide. The yield is a function of α-particle energy, as is the energy spectrum of the emitted neutrons. For more general compositions, such as reprocessing plant solutions, the α-particle spectrum must be calculated, taking into account moderation and absorption processes and the (α,n) reaction rate in this spectrum is calculated from the (α,n) reaction cross-sections of the light isotopes present. Fluorine can be important in this case because of its high (α,n) cross-section.

Immediately after shut-down the delayed fission neutrons form the main neutron source. The longest half-life of delayed neutron precursors is 55.6 secs (Br 87). At times longer than this, neutrons from (γ,n) and (γ,f) reactions (resulting from γ rays emitted by short lived fission products) can make a contribution. This source is significant when heavy water is the moderator, from the (γ,n) reaction in deuterium. At longer times spontaneous fission and (α,n) neutrons form the main sources and this source is approximately independent of shut-down time for times of a few days.

Following shut-down of a reactor there is a time dependent change in the balance between fission and absorption reactions associated with radioactive decay of fission product isotopes and transactinium isotopes.

1.6 Neutron absorption reactions

The two dominant neutron absorption reactions in a fission reactor are fission, (n,f), and radiative capture, (n,γ). In the fissile isotopes, fission occurs at all neutron energies. The principal fissile isotopes in reactors using uranium as the primary fuel source are U235, Pu239 and Pu241. In the thorium fuel cycle U233 is the principal fissile isotope. Fission occurs in other transactinium isotopes mainly above a threshold energy (which is typically at about 1 MeV), although the smaller sub-threshold fission is not negligible in some isotopes. The threshold for fission in U238 is at about 1 MeV and sub-threshold fission is negligible, although measurable.

Most radiative capture occurs in the principal fertile isotope, which is U238 in reactors using uranium fuel and Th232 in reactors using thorium fuel.

As irradiation proceeds the composition changes. Fission reactions result in the production of neutrons and fission product nuclei. Radiative capture in some fission products is very large, Xe135 and Sm149 being two examples. The half-lives of some fission products are significant parameters because they affect the reactor absorption.

Control rods or control poisons must be introduced into reactors to compensate for the variation in fuel composition with burn-up and for reactor shut-down and safety purposes. The (n,α) reaction in B10 is one which is suitable for control purposes. This (n,α) reaction occurs at all neutron energies. In heavier substances the (n,p) and (n,α) reaction cross-sections have effective thresholds at MeV energies. These reactions do not have a large effect on the neutron economy of reactors although the (n,p) reactions are comparable with the (n,γ) reactions in some structural materials. The (n,p) and (n,α) reactions in some structural material isotopes are of significance because of the activity of the reaction products and the effect of the hydrogen and helium produced on material properties. For example helium embrittlement can occur after long irradiations because of (n,α) reactions, and swelling can occur as a result of atomic displacements caused by scattering reactions, with helium atoms acting as nucleation sites.

1.7 Neutron leakage, the effective mean free path and the diffusion coefficient

Neutron leakage depends on the effective mean free path of neutrons. For scattering which is isotropic in laboratory co-ordinates the mean free path, λ, would be inversely proportional to the total macroscopic cross-section. To allow for the anisotropy of scattering the transport cross-section can be defined:

$$\Sigma_{tr} = \Sigma_t - \bar{\mu}\,\Sigma_s \qquad (23)$$

and $\lambda = 1/\Sigma_{tr}$

where Σ_t is the total macroscopic cross-section

Σ_s is the scattering macroscopic cross-section

and μ is the mean cosine of the scattering angle.

For elastic scattering which is isotropic in c.m. co-ordinates $\mu = 2/3A$ where A is the ratio of the nuclear mass to the neutron mass.

The diffusion coefficient, D, can be defined in terms of the ratio of the net neutron current, J, to the gradient of the scalar neutron flux, grad ϕ, that is:

$$J_x = -D_x \cdot \frac{\partial \phi}{\partial x} \qquad (24)$$

for direction x. In the diffusion theory approximation:

$$D = 1/3\Sigma_{tr}$$

1.8 The structure of cross-sections

Resonance Structure

The resonance structure of the cross-sections of materials present in reactors in significant proportions must be taken into account in reactor calculations because this structure results in a reciprocal structure in the reactor neutron flux spectrum:

$$\phi(E) = S(E)/\Sigma_T(E) \qquad (26)$$

(neglecting leakage effects).

When the source of neutrons (from fission and scattering) varies slowly through the resonance the flux dips at the positions of the cross-section peaks. The flux averaged value of a cross-section is reduced relative to the infinite dilution value. This effect is called resonance shielding. Resonance shielding is significant in transactinum isotopes from thermal energies up to about 100 KeV. In structural materials such as Fe, Cr and Ni it is significant at KeV energies (1 KeV to 1 MeV). In light isotopes, like O and C, resonances occur only above about 100 KeV.

Because of resolution broadening in the measurement of cross-sections the measured shapes of resonances are broadened and, at high energies, resonances are not resolved. We speak of the resolved and unresolved resonance regions. Even in the unresolved resonance region the structure must be taken into account in reactor calculations for many substances. To derive the cross-sections in the resolved resonance region from the measurements a resonance parameter analysis is made to determine the resonance energy, E_r, the neutron orbital angular momentum, l, (s,p,d,f wave), compound nucleus spin, J, and the resonance partial widths, Γ_p, the total width being:

$$\Gamma = \Gamma_n + \Gamma_\gamma + \Gamma_f \quad \text{etc} \qquad (27)$$

that is, the sum of the neutron, radiative capture, and fission and any other reaction widths, such as inelastic scattering.

A set of parameters must be found which will reproduce the measurements of the different cross-sections taking into account the different resolution broadening in each reaction. The appropriate choice of resonance structure formula must be considered. For some applications the simple single level Breit-Wigner formula is an acceptable approximation for the shapes of cross-sections through resonances in the absence of temperature broadening. For a reaction, r, other than elastic scattering:

$$\sigma(n,r) = 4\pi\lambda^2 g \frac{\Gamma_n \Gamma_r}{\Gamma^2 + 4(E-E_r)^2} \qquad (28)$$

and for elastic scattering of s-wave neutrons (l = 0):

$$\sigma(n,n) = 4\pi\lambda^2 g \frac{\Gamma_n^2}{\Gamma^2 + 4(E-E_r)^2} + 16\pi\lambda R_g \frac{\Gamma_n (E-E_r)}{\Gamma^2 + 4(E-E_r)^2} + 4\pi R^2 \qquad (29)$$

where g is the statistical spin factor $g = (2J+1)/2(2I+1)$

I is the spin of the target nucleus

and R is the potential scattering radius.

The asymmetrical term in the expression for the s-wave elastic scattering cross-section is important because it produces a minimum in the total cross-section below the resonance. These minima are important because the neutron transmission through shielding can be high at these energies.

In general, the single level Breit-Wigner formula is not sufficiently accurate to reproduce the shapes of cross-sections and one of the more accurate formulae must be used. These include the R matrix representation and the Reich-Moore and Multi-level Breit-Wigner formulations.

Doppler broadening of cross-sections can be treated in one of the following ways:

(i) Cross-sections at temperature T can be obtained from Doppler broadened resonance functions.

(ii) Cross-sections can be obtained by numerical integration over a cross-section tabulated at a lower temperature times the appropriate broadening kernel.

(iii) Doppler broadened shielded cross-sections can be derived directly using approximate formulae.

Tests can be applied to investigate the consistency of the angular momentum and spin characterisation of resonances and to test for missing resonances (using the known statistics of level spacing distributions).

In the unresolved resonance region a statistical approach must be adopted. Average resonance parameters are derived consistently with the broad resolution cross-section measurements and the average parameters determined for the resolved resonance region.

The temperature of the material affects the shapes of resonances (in the laboratory co-ordinate system) because of the thermal motion of the nucleus. An increase in temperature broadens the resonances and reduces the resonance shielding. This is called the Doppler effect. It is mainly of importance for resonance shielding in the principal transactinium isotopes, although the small effect in iron and other structural materials is not negligible.

Crystalline binding effects can also influence the thermal motion of nuclei and hence the Doppler effect. At thermal neutron energies diffraction effects in crystalline structures can introduce a pronounced energy structure into the scattering cross-section. This is particularly marked for graphite which is used as the moderating material in some thermal reactors.

Anisotropy of elastic scattering

The angular distribution of scattered neutrons is usually represented either by an expansion in Legendre polynomials or as a point tabulation of the cross-section versus the cosine of the scattering angle. Up to 20 Legendre polynomial coefficients can be required to represent the distribution, although it is unusual to use more than 5 in reactor calculations. In fact, in most reactor core calculations just the Po and P1 components are taken into account, with more being used in shielding calculations. The anisotropy of scattering can vary through resonances, this being particularly significant for the broad oxygen resonance at 450 KeV. A variation in the anisotropy of scattering occurs through the resonances in iron. An investigation of the effect of this on neutron attenuation through iron suggests that it is not an important effect(1). At high energies elastic scattering in transactinide isotopes has a strong forward peaking and this has an effect on the mean free path of neutrons. The transport approximation can be used to allow for scattering anisotropy in this case. The scattering is treated as isotropic, but with a smaller cross-section equal to

$$\Sigma_{el,tr} = \Sigma_{el}(1 - \bar{\mu}) \qquad (30)$$

The forward scattering component is subtracted from the total scattering, the remainder being treated as isotropic. This approximation is acceptable in many cases when the anisotropy is not a strong forward peaking. However, the approximation can lead to difficulties for light isotopes and, in particular, for hydrogen for which the scattering is isotropic in c.m. co-ordinates over most of the energy range of significance in reactor calculations. The P1 scattering component is large in laboratory co-ordinates resulting in a value of $\bar{\mu} \simeq 2/3$.

Inelastic scattering

The secondary energy and angular distribution for inelastic scattering is potentially a much more complex representational problem. For inelastic scattering to discrete levels the representation is simpler, the required data being the cross-section to the level and the angular distribution as a function of incident neutron energy. For many cases the inelastic scattering can be approximated as isotropic in c.m. co-ordinates in calculating the secondary energy distribution and also as isotropic in laboratory co-ordinates when calculating the angular distribution of the emitted neutrons. There are some important exceptions, when direct interations are a major component of the scattering. An example is scattering to the first level in U238 at 45 KeV. Because the treatment of inelastic scattering to discrete levels with isotropic secondary energy distributions is comparatively simple, (with the secondary energy distribution being uniform over a range defined by the Q value of the level and the mass of the nucleus) it is advantageous to try to represent inleastic scattering to the continuum in terms of 'pseudo discrete' levels, and procedures for doing this have been proposed (2).

Fission neutrons

A small fraction of fission neutrons are not emitted during the fission process but following the decay of certain short lived fission products. These are called the delayed neutrons, while the prompt neutrons are emitted at the time of fission. Simple few parameter functions are used to characterise the energy spectrum of prompt neutrons. The Maxwellian is one commonly used form:

$$\chi_M(E) = K_1 \sqrt{E} \exp\left(-\frac{E}{T}\right) \qquad (31)$$

where T is the temperature, K_1 a normalisation constant, and the mean energy, $\bar{E} = 3T/2$. Another representation which is used is the Watt form:

$$\chi_W(E) = K_1 \exp\left(-\frac{E}{T}\right) \cdot \sinh\left(2\sqrt{U.E/T}\right) \qquad (32)$$

and the mean energy is $\bar{E} = 3T/2 + U$.

In more elaborate representations a sum of two or three of these forms has been used.

The parameters in these functional representations depend on the fissioning nucleus and can also be dependent on the energy of the incident neutron, although this dependence is usually neglected.

The delayed neutron fraction also depends on the fissioning nucleus, the fraction being 1.6% for U238 and 0.22% for Pu239. There is also a dependence on incident neutron energy although this is sometimes neglected. The variation is small and not well measured up to the energy of the (n,n'f) threshold (at about 6 MeV). There are many fission product precursors producing delayed neutrons. At present it is not customary to make summation calculations over these precursors to obtain the time dependence of the delayed neutron emission but to fit the measured total emission by the sum of six exponentials, or delayed neutron groups:

$$y(t) = \sum_i a_i \exp(-\lambda_i t) \qquad (33)$$

the values of a_i and λ_i being determined for each fissioning isotope.

Delayed neutron spectra have been measured for individual precursors and show a very complex energy structure. It is usual to simplify this structure and produce a spectrum for each of the six delayed neutron groups.

1.9 Evaluated nuclear data libraries and applications orientated data sets

Several stages are involved in obtaining the nuclear data sets used in reactor calculations:

(a) Nuclear data measurements are made.

(b) The raw measurements are analysed to correct for resolution broadening and other limitations of the experimental techniques.

(c) The measured data are compiled at one of the Four Data Centres and transmitted to the other three (Brookhaven, Obninsk, Saclay and Vienna).

(d) An evaluation is made of all the measured data for a substance to produce a single 'best' set of data. This involves examination of all the measured data for consistency and statistical averaging. Nuclear models are used to fit the measurements and extend their range.

(e) The evaluated data are compiled in a computer format such as the ENDF/B-V format and collected into a library of evaluations for different substances or reaction types. Examples of such libraries are the ENDF/B-V Standards Library. This contains neutron interaction data for substances with cross-sections which are used as standards relative to which other cross-sections are measured. Data in this library are stored (not surprisingly) in ENDF/B-V format. However, other libraries also use this format. The Japanese JENDL2 library uses the ENDF/B-IV format.

(f) Nuclear data libraries are produced for specific applications.

(i) Monte Carlo calculations can use very detailed representations but some processing of the basic evaluated nuclear data libraries is usual to reduce the amount of data to be stored and provide it in a more convenient form. However, Monte Carlo calculations of all reactor properties of interest would be too costly when run for the computer times necessary to give the required accuracy.

(ii) The standard methods employed for reactor calculations use nuclear data averaged over a few energy groups. The derivation of these group averaged cross-sections can involve a number of stages starting with either a detailed flux spectrum calculation for a simplified geometrical representation of each region of the reactor or a parametrisation derived from calculations or formulae for the spectra in simple geometries.

1.10 Energy group averaged cross sections

The energy group averaged cross-section is defined as:

$$\sigma^{I}_{r,G} = \int_{E_G^L}^{E_G^u} \phi(E')\ \sigma^{I}_{r}(E')\ dE' \Big/ \int_{E_G^L}^{E_G^u} \phi(E')\ dE' \qquad (34)$$

where E_G^L and E_G^u are the lower and upper energies of the group G. Cross-sections for scattering of neutrons from one energy group to another take the form

$$\sigma^{I}_{s,G\to G'} = \int_{E_G^L}^{E_G^u} dE' \int_{E_G^L}^{E_G^u} dE''\ \phi(E')\ \sigma^{I}_{s}(E'\to E'') \Big/ \int_{E_G^L}^{E_G^u} \phi(E')dE' \qquad (35)$$

As well as neutron flux spectrum averaging some other methods have been tried and found to have advantages in some applications. These include bilinear weighting with the neutron flux times the neutron importance spectrum, where the neutron importance

$\phi^*(E,x)$ is the probability of a neutron of energy E at position x contributing to the asymptotic fission neutron source distribution.

A neutron importance relating to other reactor properties can also be calculated and used in this way.

Overlapping energy groups have also been used in some applications.

When deriving group averaged cross-sections the aim is to produce a parameterised set suitable for calculations for a region of a particular reactor type (such as the core region of a PWR) over its whole range of operation: that is for all fuel irradiations , coolant conditions, control absorber insertion and for the full temperature range which must be considered. The group cross-sections can be tabulated (or parameterised) for a range of fuel burnup levels and fuel enrichment and a range of temperatures. These variations affect the resonance shielding in transactinium isotopes and also, to a small extent, the variation of the neutron source, S(E), or collision density $\phi(E)\ \Sigma_t(E)$, through the energy group. This has an effect, in particular, on the elastic moderation cross-sections. The cross-section of the principal moderator isotope is the most important but also, usually, the least sensitive to changes in spectrum shape. The group averaged scattering cross-sections of H and D are not significantly sensitive to the weighting spectrum. A 100 group cross-section set is found to be satisfactory for a wide range of thermal reactor applications although a different set is required for fast reactor calculations. In such a thermal reactor set about 40 of the energy groups are at energies below 1 eV and the remainder are spaced at approximately uniform lethargy intervals up to about 15 MeV.

The methods used to treat resonance shielding include tabulations of the shielding factor for each isotope and energy group as a function of the effective

removal cross-section for a typical resonance in the isotope. This effective removal cross-section makes allowance for the fraction of neutrons which are scattered within the energy width of the resonance. This fraction is a function of the scattering material and the resonant material and varies with energy group. The shielding factor is also a function of the temperature of the resonant material. When calculating the resonance shielding using this formulation allowance must be made for the geometry and size of the resonant material and the surrounding material. This is done in terms of an equivalent scattering cross-section.

Other ways of treating resonance structure include the sub-group and probability table method. In this method the distribution of cross-section values within an energy group is represented in histogram form. This is illustrated in Fig.1.1. Each element of the histogram is called a sub-group. These are different for each resonant substance and the sub-group parameters are chosen to reproduce the results of more detailed calculations. When calculating the neutron flux in each sub-group for each resonant material a constant effective removal cross-section is assumed for the other constituent materials. Overlap effects between resonances of different materials are treated only in an average way and the resonance structure must be examined to see if there are prominent resonances which are overlapping. Geometrical effects can be treated directly by calculating the flux in each sub-group for a model representing the geometry, (usually a simplified geometrical representation).

1.11 Methods used to treat the effects of the thermal motion of nuclei and chemical binding. The thermal energy region

When the absorption and leakage of neutrons is very small compared with the scattering, the energy distribution of the neutrons in the medium is a Maxwell-Boltzman distribution:

$$M(E) = \frac{2\pi}{(\pi\ KT)^{3/2}} \cdot \sqrt{E} \cdot \exp\left(-\frac{E}{KT}\right) \qquad (36)$$

(for a medium at uniform temperature, T).

The neutrons are in thermal equilibrium with the medium and their energy distribution is independent of the detailed energy structure of the scattering cross-sections.

The neutron flux spectrum has the form:

$$\phi_M(E) = v\ M(E) \qquad (37)$$

where v is the velocity of a neutron of energy E. The peak of the neutron flux per unit energy occurs at

$$E_T = KT$$

For a medium at a temperature of 293°K the peak energy is E_o = 0.025 eV and the corresponding neutron velocity is 2200 m/sec. The spectrum averaged value of a cross-section having a (1/v) energy dependence is the value for an energy of ($4\ E_o/\pi$) or

$$\sigma(1/v) = \sqrt{\frac{\pi}{4}} \cdot \sigma_o \qquad (38)$$

where σ_o is the 2200 m/sec value.

It is common to quote both 2200 m/sec cross-sections and thermal Maxwellian averaged cross-sections. Cross-sections having a (1/v) form can be related using this equation. The mean energy of the spectrum is $\bar{E} = 2KT = 2E_o = 0.05$ eV.

In a thermal reactor a neutron spectrum differs from the Maxwell-Boltzman form because absorption and leakage effects are not negligibly small compared with scattering effects. However, for approximate calculations, and for treating reactions for which a high accuracy is not required, a Maxwell-Boltzman form with an effective temperature Teff, is sometimes assumed for the thermal region. The value of Teff is derived from the thermal spectrum averaged value of a (1/v) form cross-section. Absorption cross-sections can then be obtained approximately using a formula of the form:

$$\sigma(Teff) = \sqrt{\frac{\pi}{4}} \cdot \left(\frac{T_o}{Teff}\right)^{\frac{1}{2}} \cdot g\ (Teff)\ \sigma_o \qquad (39)$$

where the factor g is a tabulated correction calculated to allow for the departure of the cross-section from (1/v) form.

To calculate reactor neutron spectra at thermal energies the detailed energy structure of absorption and scattering cross-sections must be allowed for. At energies below about 4 eV it is necessary to take into account the thermal motion of nuclei in calculating the secondary energy distributions of scattered neutrons. In the WIMS cross-section library 42 energy groups are used to describe the cross-sections below 4eV and the scattering matrices are dependent on the temperatures of the materials (3). The chemical forces binding nuclei in molecules and crystals affect the dynamics of the interactions of neutrons with nuclei. Transitions between different vibrational and rotational levels

can occur in a scattering interaction. The population of levels depends on the temperature and transitions to both higher and lower energy levels can occur with associated losses or gains in kinetic energy in this inelastic scattering reaction. Neutron diffraction effects can also modify the scattering cross-section.

It is usual to approximate the treatment of thermal scattering for all nuclei excepting the principal moderators (hydrogen, deuterium and carbon) by the monatomic gas model. The temperature dependence of capture and fission cross-sections at thermal energies ($\lesssim$ 4 eV) is usually neglected. Cross-sections which have a (1/v) form in centre of mass co-ordinates are the same in laboratory co-ordinates, being unchanged by the thermal motion of the nucleus. Cross-sections of primary interest in thermal reactors either have a form close to (1/v) or have a broad resonance in the higher energy region of the thermal spectrum, tailing off to a (1/v) form at lower energies.

The differential scattering cross-section is usually expressed in terms of the quantity $S(\alpha, \beta)$ which is called the scattering law for the material. This is stored in tabular form in nuclear data libraries, such as ENDF/B (4). Scattering matrices for different moments of scattering (Po and P1) in the required group structure are then obtained by integration of the cross-section for scattering from energy E' to energy E and through the angle θ ($\mu = \cos\theta$)

$$\sigma_s(E' \to E, \mu, T) = \frac{\sigma}{4\pi KT} \cdot \left(\frac{E}{E'}\right)^{\frac{1}{2}} \cdot \exp\left(\frac{-\beta}{2}\right) \cdot S(\alpha,\beta,T) \qquad (40)$$

where $\alpha = (E' + E - 2\sqrt{E'E}\,\mu)/KT$

and $\beta = (E'-E)/KT$

This form satisfies the required condition for detailed balance.

The form of $S(\alpha, \beta)$ for a free monatomic gas is

$$S(\alpha\ \beta) = \frac{1}{2(\pi\alpha)^{\frac{1}{2}}} \exp\left(\frac{-(\alpha^2+\beta^2)}{4\alpha}\right) \qquad (41)$$

The derivation of the scattering law usually involves simplifying approximations. It is not usually obtained directly from differential scattering measurements but by fitting a function which represents the incoherent component of the scattering or a smoothed cross section to related measurements and then by making any required adjustments for coherent scattering, or diffraction effects. The measurements fitted include partial range differential scattering measurements and specific heats. Neutron diffraction studies also provide information on the thermal motion of the nuclei.

In one procedure for generating thermal scattering cross-sections the incoherent component, or smoothed form of the scattering law, is calculated from the function $\rho(\beta)$ or $\rho(w)$ where $w = \beta KT/\hbar$. For a solid $\rho(w)$ is the phonon frequency distribution. The functional dependence of $S(\alpha,\beta)$ on α,β and $\rho(w)$ is an approximation and the validity of the functional form must be tested, along with the function $\rho(w)$. The scattering law is then defined in terms of the width function, w(t)

$$S(\alpha, \beta) = \int_{-\infty}^{\infty} \exp\left[-\alpha\, w(t) - i\beta t\right] \cdot dt \qquad (42)$$

where

$$w(t) = \int_{0}^{\infty} \frac{\rho(\beta')}{\beta' \sinh(\beta'/2)} \left[\cosh\left(\frac{\beta'}{2}\right) - \cos(\beta' t)\right] \cdot d\beta' \qquad (43)$$

For a regular lattice a two parameter phonon frequency distribution can be adopted, $\rho(w,l)$, where $l = \cos\lambda$ and λ is the angle between the incident neutron and a lattice axis.

For hydrogen in water there is no coherent scattering and for deuterium in heavy water the coherent scattering is significant only at low energies and is usually neglected in reactor calculations. For carbon in graphite a correction must be made for the coherent scattering component. This results in a detailed structure being imposed on the total scattering cross-section. The structure corresponds to neutron wave-lengths equal to dimensions of the crystal lattice, or multiples of these dimensions. The coherent scattering cross-section falls sharply at energies below these characteristic wave lengths. At energies below the longest characteristic wave length the coherent scattering cross-section is zero. This cut off (the Bragg cut-off) is represented in the total scattering cross-sections of a number of nuclei for which a full treatment of crystalline binding effects in the secondary energy distribution is not considered necessary. This is because the total scattering cross-section affects neutron diffusion while the effect on the secondary energy distribution is small.

Thermal scattering data are tested by comparing calculated total cross sections, and characteristics of calculated neutron spectra, such as diffusion coefficients and reaction rates sensitive to the spectrum shape, with measured values.

1.12 Resonance integrals

As described in Section 1.3 the neutron flux spectrum in the intermediate energy range, 1 eV to 100 KeV, can be approximated in the form $\phi(E) \propto 1/E$ for some thermal

reactor applications. The energy dependent shapes of the cross-sections can then be replaced by the resonance integrals:

$$(RI)_r^I = \int_{E_L}^{E_u} \sigma_r^I(E) \cdot \frac{dE}{E} \qquad (41)$$

where $(RI)_r^I$ denotes the resonance integral for reaction r in isotope I and E_L and E_u are the lower and upper energies of the resonance integral range.

The resonance integral of a radiative capture cross-section is (in many cases), not very sensitive to the upper energy, E_u, nor to the departure of ϕ (E) from 1/E form at higher energies (above $\sim$ 1 KeV). However, the value is sensitive to the lower energy, E_L. This is often taken as 0.5 eV because this is the effective cut-off energy for reaction rates measured in a sample shielded by cadmium. This is the lower energy cut-off used, for example, for the resonance integrals tabulated in BNL 325 Third Edition, Volume 1 (5).

Resonance integrals are usually measured in a pure moderator, such as a block of graphite, adjacent to a reactor. The intermediate flux spectrum is then very close to $\phi(E) = 1/E$. Resonance integral measurements provide a useful check on differential cross-section measurements. They can also be used together with 2200 m/sec cross-section values, suitably scaled to correct for the effective thermal Maxwellian temperature, the departure from 1/v form at thermal energies and the ratio of intermediate energy range flux to thermal energy range flux, to calculate reaction rates for substances of secondary importance. This method is used in inventory calculations for minor fission products and transactinium isotopes.

Useful data of this simple form have been obtained by measuring the compositions of irradiated fuels and pure samples of materials.

1.13 Fission spectrum averages

The reactor neutron flux spectrum above about 3 MeV is approximately proportional to the fission neutron spectrum. For reactions with an effective threshold energy above about 3 MeV the reactor spectrum averaged value of the cross-section can be related approximately to the fission spectrum averaged value by applying a scaling factor which is appropriate for the reactor region. Many (n,p), (n,α) and (n,2n) reactions have effective thresholds above about 3 MeV and so approximate values of the reaction rates can be obtained in this way. Many of these reactions are of interest because they result in radioactive products (which present handling and disposal problems) and the (n, α) reactions contribute to radiation damage effects.

Measurements of fission spectrum averaged cross-sections and cross-section ratios also provide a useful test of the differential cross-sections.

1.14 Nuclear data uncertainty information

The assessment of the uncertainties in the prediction of reactor properties is an important requirement, both for economic and safety reasons. Allowances must be made in the design and operation of reactors to cover uncertainties by introducing suitable margins. A very high level of confidence in the safety aspects of reactors must be achieved. Uncertainties in nuclear data contribute to the overall uncertainty. Consequently the uncertainties in the data and the sensitivity of calculated reactor parameters to these uncertainties must be estimated.

The estimation and representation of uncertainties in evaluated differential cross-sections is a complex problem. However, since the required information is the uncertainty in reactor neutron spectrum averaged values of cross-sections, or in ratios of such averages, the required information can take a simpler form in many cases. For example, when the cross-section does not influence the spectrum the requirement is for the uncertainty in the average value of the cross-section in a specified spectrum and its correlation with the uncertainty in other averaged cross-sections entering into the calculations. In other cases, for example, when resonance shielding effects are important, the effect of the uncertainties on the spectrum must also be taken into account. Reactor measurements can help to provide a normalisation which reduces the uncertainty in predictions and improve confidence in predictions.

1.15 Integral measurements

This is the name given to nuclear data related measurements made in reactor spectra. The information obtained is usually of the form of reactor spectrum averaged reaction rate ratio measurements or reactivity measurements. Reactor spectrum measurements have also been made. There have been extensive programs of measurements made in zero power critical facilities, and neutron source driven assemblies, which have been designed to provide a test of nuclear data .

Integral measurements have also been used to adjust differential cross-sections, taking into account the uncertainties in the two types of measurement, and to select between inconsistent differential cross-section measurements.

An example of this latter approach is in the choice between different measurements of the fission cross-section of Am241.

When integral measurements are taken into account the uncertainties in the nuclear data used in reactor calculations and, consequently, in the accuracy of predictions can be reduced.

Section 2 - Nuclear data characteristics of core neutronics parameters

2.1 Core parameter predictions for which nuclear data are required

Effective multiplication, K

When a fission reactor is operating in a steady state (in the absence of external or radioactive sources) there is a balance between the rate of production of neutrons from fission and the rate of loss by absorption and leakage. The effective multiplication of the reactor, K, is then equal to unity:

$$K = \frac{\text{Rate of production of neutrons by fission}}{\text{Rate of loss of neutrons by absorption and leakage}} \quad (42)$$

$$= 1 \text{ for a critical reactor.}$$

It is customary (in the definition of K) to include neutrons produced by reactions other than fission, such as (n,2n) and (n,3n) reactions, as negative absorption terms. The effective multiplication can also be defined in terms of the number of neutrons in successive generations of fission neutrons (when asymptotic conditions have been achieved).

$$K = \frac{\text{Number of neutrons in fission neutron generation } (g+1)}{\text{Number of neutrons in fission neutron generation } g} \quad (43)$$

(in the limit as $g \to \infty$)

The total number of neutrons has a time dependence equal to

$$n = n \exp\left\{\left(\frac{k-1}{l}t\right)\right\} \quad (44)$$

where l is the mean neutron lifetime between production in fission and absorption or leakage. When there is a neutron source present in the reactor (other than neutron induced fission and other reactions related to the neutron flux level) then, for a value of $K < 1$ a steady state condition is reached in which the fission source is equal to

$$F = S_o \phi^*/(1-K) \quad (45)$$

where ϕ^* is the importance of the source neutrons. Such a source might be spontaneous fission, (α, n) reactions or an artifical source (such as an antimony, berylium source). A reactor is never completely free from such sources and so in a reactor operating in steady state K is always slightly less than unity, although the difference is often negligibly small. The departure of the reactor from the critical state is usually expressed in terms of the reactivity, ρ, where

$$\rho = 1 - (1/K) \quad (46)$$

The reactivity of a reactor can change when the temperature of the fuel or the moderator changes or when the coolant density changes. The reactivity of the fuel changes with irradiation as the fissile material is burnt up, and fission product absorption builds up. These variations must be compensated for by moving control elements or by varying the amount of control poison in the coolant. Burnable poisons which compensate for fuel burnup effects are also used in some designs. The neutron flux and coolant temperature are monitored and the control varied to maintain the required power output. In most reactors reactivity decreases when the temperature of the fuel and moderator increases and so it is necessary to add reactivity, usually by withdrawing control absorber rods, to raise the reactor power.

Variation of Composition with fuel burnup

The number of atoms of each transactinium isotope in the fuel changes with burnup.

Absorption reactions in isotope I, reduces the number of atoms. These reactions are characterised by the absorption cross-section.

$$\sigma_a^I = \sigma_f^I + \sigma_c^I$$

(together with (n,2n) and other reactions).

Radioactive decay also reduces the number. Alpha and beta decay result in the formation of other transactinium isotopes. The number of atoms of isotope I can increase as a consequence of such decay processes and also as a result of radiative capture reactions, (n, γ), in isotope (I-1)

$$\frac{dN(I)}{dt} = (-N(I)\,\sigma_a^I + N(I-1)\,\sigma_\gamma^{I-1})\phi - \lambda_I N(I) \quad (47)$$

$$+ \text{(radioactive decay processes leading to isotope I)}$$

Variation of reactivity with burnup

Burnup is defined either in terms of the percentage of the initial fuel loading of transactinium isotopes which undergo fission (ie percentage burnup) or the heat generated in the fuel in units of Megawatt days per tonne (MWd/te).

As burnup proceeds the reactivity of the fuel varies. The loss of fissile material as a consequence of fission reactions and the build up of fission product atoms (which absorb neutrons) results in a reduction in reactivity. Burnable poisons can be introduced into thermal reactor fuel assemblies to compensate for this loss of reactivity. In other designs moveable absorbing control rods are withdrawn from the reactor to compensate for the reduction in fuel reactivity. The total burnup control requirement depends upon the maximum burnup of fuel elements and the refuelling strategy. When the whole of the core is replaced at each refuelling the maximum burnup control is required. When small fractions of the core are replaced at each refuelling then the reactivity variation overall is much smaller.

Transient effects

Allowance must be made for reactivity transients associated with the decay of short lived transactinium isotopes formed by capture reactions and with the decay of fission products. This variation of reactivity can be important following the shut-down of a reactor for refuelling or maintenance and start-up following a shut-down period. The decay of Np239 (2.35 days) results in an increase in reactivity. The fission products Xe135 (9.17 hr) and Sm149 (stable) both have very large thermal capture cross-sections and are formed both directly in fission and by the decay of fission product precursors, I135 (6.59 hr) and Pm149 (53.1 hr). These fission product transient effects are only important in thermal reactors.

Conversion and breeding

In a uranium fuelled reactor the U235 fraction in the fuel is reduced by fission and capture reactions. This loss of fissile material is partly compensated for by the production of Pu239 as a result of radiative capture in U238:

$$U238 + n = U239 \xrightarrow[(23.5\ min)]{} Np239 \xrightarrow[(2.35\ days)]{} Pu239 \qquad (48)$$

The conversion ratio is defined as

$$CR = \frac{\text{Rate of production of fissile atoms}}{\text{Rate of loss of fissile atoms}} \qquad (49)$$

Conversion is important both because it increases the fraction of uranium resources which can be converted into energy and because it reduces the rate of loss of fuel element reactivity with burnup. By recycling fissile material, reprocessed from irradiated fuel, back into reactors uranium utilisation can be further enhanced.

The conversion potential of a reactor depends on the fissile material used in the fuel and the reactor neutron spectrum. It is related to the excess neutrons produced per absorption in the fissile isotope. The number of neutrons produced per absorption is the eta value:

$$\eta = \nu/(1+\alpha) \qquad (50)$$

where $\alpha = \sigma_c/\sigma_f$

The energy dependence of η for the principal fissile isotopes is shown in Fig. 2.1. When the eta value exceeds 2 the fuel has the potential to breed more fissile material than is consumed. Some neutrons are absorbed in control absorber material, fission products, structural materials, coolant and moderator. However, fission reactions in the fertile isotopes (like U238) enhance the neutron economy. Fast reactors fuelled with Pu239 have the highest breeding potential.

Temperature and power coefficients of reactivity

To determine the control reactivity required to operate the reactor at different power levels and to shut it down for refuelling and maintenance the variation of reactivity with temperature and power is required. The total isothermal temperature coefficient can be separated into the fuel, coolant and moderator temperature coefficients. These respond differently to a change in power; the fuel temperature increases most. The temperature distributions are non-uniform and this can complicate the calculation of Doppler effects. The coolant density oefficient depends on pressure as well as temperature and this dependence is also required.

The temperature and power coefficients, and the coolant density coefficient are also required for safety studies.

Control absorbers

Control absorbers are used to compensate for the variation of fuel reactivity with burnup, to compensate for the variation of reactivity with reactor operating power, to provide a shut-down margin and for safety purposes. They are also used to alter the power distribution in the core and to compensate for local burnup effects.

In thermal reactors burnable poisons are used to partly compensate for the variation of fuel reactivity with burnup. A suitable burnable poison is one which loses reactivity more rapidly than the fuel and is converted into an isotope having negligible burnup before the end of the fuel irradiation. In a BWR gadolinium loaded fuel pins are used in the initial reactor fuel charge until

an equilibrium fuel cycle is achieved. In PWR s borosilicate glass tubes are used.

In light water reactors boric acid can be dissolved in the coolant to provide control. Such soluble poisons have the advantage that they are distributed more uniformly through the core than are control rods and consequently they do not perturb localised power distributions. They also avoid the need to have mechanisms operating in the core environment.

In the design of moveable control elements the aim is to have an absorber which will have a long lifetime. The rate of loss of absorption should be small and the element should be capable of withstanding a long irradiation without swelling and distorting. In BWRs a cruciform shaped blade which moves between fuel assemblies isused, while in a PWR a cluster of widely spaced absorber pins moves between the fuel pins of a fuel assembly. The cruciform rods use boron dispersed in stainless steel. In PWRs an Ag-In-Cd alloy is used as the absorber.

In fast reactors boron carbide (B_4C) is the most commonly used control absorber. The boron is sometimes enriched in the B10 isotope in which the predominant absorption, (n,α), occurs. For this reaction helium formation and the resultant swelling can limit the lifetime of the rod. Other absorber materials which have been used,or are being investigated,include tantalum, europium oxide and europium boride. The induced radioactivity and decay heating can present a problem with these

Power distributions

The power output of a reactor can be limited by the temperature of the hottest fuel pin. An important aim is therefore to minimise power peaking and the peak to average power distribution. This can be influenced by the reflector effectiveness, the distribution of fuel assemblies having different levels of burnup and the differential insertion of control elements. The designer and operator require to be able to predict the power distribution for different fuel loadings and control element dispositions. This depends on the ability to predict power output as a function of fuel burnup, and the flux distribution corresponding to the loading pattern of fuel assemblies and control elements.

2.2 Components of the effective multiplication in a thermal reactor

A simplified representation of the main neutronics processes in a uranium fuelled thermal reactor is illustrated in Fig. 2.2.

Fast fission factor, ϵ

Fission neutrons resulting from thermal neutron induced fission are produced in the fuel elements with a fission neutron spectrum energy distribution. That is, the neutrons have a mean energy of about 2 MeV and a spread in energy from about 10 KeV to 15 MeV. There is a probability of these neutrons causing a fission before leaving the fuel and entering the moderator. The enhanced neutron emission from the fuel (per thermal neutron induced fission neutron) is denoted by ϵ, the fast fission factor. Fission in U238 is the main source of this enhancement. The fast fission factor depends on the energy shape of the fission spectrum, the U238 fission cross-section, the probability of fission neutrons being moderated to energies below the U238 fission threshold (by inelastic scattering in U238 and elastic scattering in oxygen) and the probability of neutrons escaping from the fuel (which depends on the transport cross-section of the fuel material). This factor is generally less than 1.1,

Measurements which provide a test of these nuclear cross-sections are the U238 fission cross-section averaged over a U235 fission spectrum and the ratio of U238 to U235 fission rates measured in different reactor lattices.

Epithermal fissions in the fissile isotopes can also be included in this factor.

Fast leakage $(1-R_F)$

When the high energy neutrons leave the fuel elements the predominant nuclear interaction they undergo in scattering. The neutrons are thus moderated in energy and migrate about the reactor. A fraction of the neutrons leak from the core before reacting at thermal neutron energies. The non-leakage probability in the slowing down energy range is denoted by R_F. It depends, primarily, on the relationship of the mean free path to the moderating strength of the moderator (or the relationship of the transport cross-section, Σ_{tr}, to the moderating strength, $\Sigma_s\bar{\xi}$). A measure of the migration of neutrons is provided by the so-called 'age', τ. Neutrons which are emitted at a point with energy E_o will have migrated a mean square distance $\langle r_1^2 \rangle$ when they have been moderated to energy E_1. The age is defined as

$$\tau(E_o,E_1) = \frac{1}{6} \langle r_1^2 \rangle \qquad (51)$$

and τ can be calculated from the approximate equation:

$$\tau = \int_{E_1}^{E_o} (D(E)/\Sigma_s(E)\ \bar{\xi}(E))dE \qquad (52)$$

For fission neutrons moderated to thermal energies (taken to be 1 eV) the age is denoted by τ_{th}. The non-leakage probability R_F can be written

$$R_F = \exp\ (-B^2\ \tau_{th}) \qquad (53)$$

where B^2 is the geometrical buckling, which depends on the size of the core:

$$B^2 = \frac{\pi}{H^2} + \frac{\alpha_o}{R^2} \qquad (54)$$

where H is the extrapolated core height

R is the extrapolated core radius

and $\alpha_o = 2.405$ (first root of $J_o(r)$)

These extrapolated values are larger than the actual core dimensions by an amount which depends on the effectiveness of the reflector, called the reflector savings.

Measurements of the spatial distribution of neutrons moderated from a localised fission source to a low energy in uniform moderator material provide a valuable nuclear data check. The low energy usually taken is the age to the indium resonance at 1.457 eV. The In^{115} (n, γ) In^{116} activation reaction provides a convenient method of measuring the distribution of neutrons having energies of about 1 eV.

Resonance escape probability, p

As neutrons are moderated in energy the probability of absorption increases. This is because radiative capture cross-sections increase towards low energies whereas the elastic scattering cross-sections of the principal moderators are approximately constant from 1 eV to about 1 MeV. The predominant absorption in this energy range in a uranium fuelled thermal reactor is radiative capture in U238. Resonance shielding is very strong, the average shielding factor in the 3 lowest energy resonances being, typically, 0.05. The ability to calculate U238 resonance shielding is an important requirement. Resonance absorption in U238 is the main neutron loss mechanism in the slowing down energy range and so the probability of a neutron reaching thermal energies from the fast energy region (where loss by leakage predominates over absorption) is called the resonance escape probability.

Measurements of U238 resonance absorption have been made in reactor lattices having different dimensions and using different moderators. These measurements are used to test the differential cross-sections (both the resonance parameters and the resonance formalism). The temperature dependence of this reaction is important because it is a major component of the fuel temperature coefficient.

This reaction and its temperature dependence are also of prime importance in a fast reactor. The Doppler effect in U238 capture is the main component of the reactor power coefficient. The ratio of U238 capture to fission in either U235 or Pu239 has been measured in different compositions and spectra. Doppler effect measurements have also been made.

The thermal utilisation factor, f

This factor is the fraction of thermal neutron absorption which occurs in the fuel. Absorptions in the moderator, coolant and control absorbers are the competing reactions. The absorption cross-sections of the standard moderators and coolants are well known and so the uncertainties in predicting the relative reaction rates are associated with the energy spectrum and the spatial distribution of neutrons at thermal energies. The flux distribution in the moderator depends on the transport mean free path for thermal neutrons, λ_{th} in the moderator.

It is usual to measure reaction rate distributions and reaction rate ratios for the geometry of the reactor lattice and to test the calculation methods and nuclear data against these measurements. Not all of the reaction rates of interest can be measured in lattice experiments, however, but only those which result in detectable radioactive products or for which mass-spectrometric measurements can be made. Some information can also be deduced from the reactivity perturbation caused by introducing a sample into a critical assembly. Measurements cannot be made in all conditions of reactor operation, (for example, high temperatures and high levels of burnup), although related information can be obtained from operating reactors.

The thermal eta value for the fuel, η_F

This is the net production of fission neutrons from thermal neutron induced fission per neutron absorbed in the fuel. It depends on the η values of the fissile isotopes and the competing absorption reactions in the fertile isotopes, fission products and other diluents (such as oxygen in oxide fuel). The cross-sections do not all have a (1/v) form, resonances being present in the cross-sections of fissile isotopes at thermal energies. Consequently, the fuel eta value depends on the thermal neutron spectrum in the fuel.

Relative measurements of fission and capture reaction rates for the transactinium and fission product isotopes are used to test and complement the differential cross-sections. Reactivity perturbation and reactivity balance measurements give information on η values for fissile isotopes. Such measurements have been made in well defined thermal neutron spectra and in the spectra of

lattices representative of power reactors. The intercomparison of differential cross-sections and ν values measured at 2200 m/sec with 293°K thermal Maxwellian spectrum averaged values has been the subject of detailed study (6).

In the interpretation of lattice reaction rate measurements it is helpful to separate the reactions occurring at thermal energies and at epithermal energies. This is done by making measurements using foils both with and without a cadmium cover. Cadmium has a very high thermal cross-section and so this cover effectively eliminates reactions in the foil at thermal energies.

The ratio of epithermal to thermal fissions in the fissile isotopes is typically about 0.1. In some conventions the epithermal component of fission is included in the fast fission factor, the alternative being to include it in the thermal eta value.

Reaction rate ratios measured in thermal reactor lattice experiments include:

28_ρ = ratio of epithermal to thermal U238 capture

25_δ = ratio of epithermal to thermal U235 fission

28_δ = ratio of U238 fission to U235 fission

C^* = ratio of U238 capture to U235 fission (the modified conversion ratio)

The effective thermal cut-off energy is 0.625 eV. The value of K for the applied buckling, B^2, is also obtained.

Thermal leakage ($1-R_T$)

The fraction of thermal neutrons which leak from the reactor core is denoted here by $(1-R_T)$. The leakage fraction depends on the thermal diffusion length, L. The thermal migration area M^2_{th} is related to L and the mean square distance travelled by thermal neutrons $\langle r^2_{th} \rangle$ by;

$$M^2_{th} = L^2 = \frac{1}{6} \langle r^2_{th} \rangle \quad (55)$$

and $$L^2 = D/\Sigma_a = \lambda_{th}/3\Sigma_a \quad (56)$$

Values of L^2 for pure moderators can be obtained by fitting reaction rate distribution measurements around a neutron source.

The total migration area, M^2, is equal to

$$M^2 = \tau_{th} + L^2 = \frac{1}{6} \langle r_a^2 \rangle \quad (57)$$

where $\langle r_a^2 \rangle$ is the mean square distance travelled by a neutron between birth in fission and absorption at thermal energies.

Approximate values of λ_{th} τ_{th} L^2 and M^2 for the principal moderators are as follows:

Moderator	λ_{th} (cm)	τ_{th} (cm^2)	L^2 (cm^2)	M^2 (cm^2)
H_2O	0.63	26	8	34
D_2O	2.5	130	30,000	30,000
Graphite	2.5	365	3,500	3,865

The migration in water is much less than that in the same volume of graphite.

The migration area for reactor core material is strongly influenced by absorption in the fuel. The core leakage fraction in commercial sized thermal reactors is generally less than 5% and the core thermal leakage fraction in water moderated reactors is less than about 1%. Typical values for a PWR are τ_{th} = 53.4 cm^2, L^2 = 5.32 cm^2, B^2(fast) = 7.1 m^{-2} and B^2 (thermal) = 4.1 m^{-2}.

The infinite medium multiplication factor, K_∞

In an infinite array of lattice cells the leakage is zero. The multiplication factor in this case is the infinite medium multiplication factor:

$$K_\infty = \varepsilon.p.f.\ \eta_F \quad (58)$$

This is called the four factor formula. The effective multiplication of an actual reactor is smaller than this because of leakage:

$$K = K_\infty . R_F . R_T = \varepsilon.p.f.\ \eta_F . R_F . R_T \quad (59)$$

K_∞ is close to unity in a thermal reactor being, typically, 1.04 in a PWR.

K_∞ can also be written in the form:

$$K_\infty = \frac{\int\int \nu\Sigma_f(E,x)\ \phi(E,x)\ dE\ dx}{\int\int \Sigma_a(E,x)\ \phi(E,x)\ dE dx} \quad (60)$$

that is, the ratio of the rate of production of neutrons in fission to the rate of absorption.

The effective multiplication can be written as

$$K = K_\infty / (1 + B^2M^2) \quad (61)$$

where B^2M^2 is the leakage fraction.

The fast fission factor ε , and the leakage fractions are not significantly sensitive to temperature and burn-up effects.

The fuel temperature mainly affects the U238 component of the resonance escape probability, p. The thermal neutron spectrum in the fuel is sensitive to the coolant density in water cooled reactors. This depends on the pressure and temperature. In a graphite moderated gas cooled reactor the temperature of the moderator affects the thermal neutron spectrum in the fuel. These effects on the fuel spectrum alter the η_F value.

Burn-up mainly affects the value of η_F, although there are compensating changes in the control absorber which affect f. The change in resonance absorption must also be taken into account.

Components of neutron balance in a typical thermal reactor

Components of the neutron balance in a typical thermal reactor are shown in Table 2.1

Thermal reactor spectra

The overall shape of the spectrum in a PWR fuel element is shown in Fig. 2.3 and the shape through the U238 resonance region is shown in more detail in Fig. 2.4.

2.3 Fast reactor neutronics

In a fast reactor the mean energy for the fission reactions in fissile isotopes is about 200 KeV and for capture reactions it is about 20 KeV. Reactions below about 100 eV are generally negligibly small. The main component of the power coefficient of reactivity is the Doppler effect and this comes predominantly from the energy range 100 eV to 10 KeV. The core leakage fraction is much larger than in a thermal reactor being typically about 30%. Neutron transport cross-sections therefore have a greater effect on K.

The designs of fast reactors which are under active development are uranium-plutonium oxide fuelled, and sodium cooled and use steels for fuel pellet canning and fuel subassembly cases (or wrappers). The volume fractions of fuel, coolant and structure are roughly equal (1/3, 1/3, 1/3). The core is surrounded both axially and radially by a breeder region which contains (initially) uranium oxide pins. The axial breeder pins are usually an extension of the core pins while the radial breeder pins can be of a larger diameter because of the smaller power rating in the breeder region. Most of the neutrons which leak from the core are

	Start of Life	Equilibrium
Fission neutron production		
U235	95	56
U238	5	5
Pu239	-	35
Pu241	-	4
TOTAL	100	100
Neutron absorption		
U235	48	28
U238	32	24
Pu239	-	19
Pu240	-	3
Pu241	-	2
Pu242	-	2
Fission products	-	5
Structural materials	8	7
Moderator/coolant	6	5
Control absorbers	2	1
Leakage	4	4
TOTAL	100	100

TABLE 2.1 - Neutron balance in a typical thermal reactor

absorbed in U238 in the breeder regions and produce Pu239. Conversion of U238 to Pu239 in the core region is also significant. The net reactor breeding ratio is greater than unity but the core conversion is less than unity. Fuel reactivity falls with burn-up. The maximum percentage heavy atom burn-up achieved at the end of life in fuel subassemblies is typically 10%. Consequently, the average percentage of fission products in the fuel is higher than in a thermal reactor.

A typical maximum burnup for a PWR is 4%.

Reactor spectrum averaged cross-sections are not as high in a fast reactor as in a thermal reactor and there is less variation between fission product isotopes. Radioactive decay and burnup of fission products has only a small effect ($\sim$5%) on fission product absorption and it is usual to neglect this variation. An average called the "pseudo fission product" is used.

U238 fission makes an important contribution to the neutron economy. Consequently the data affecting the U238 fission fraction are important. These include the fission cross-section, the spectrum of neutrons from fission in Pu239 (and other fissioning isotopes) and the scattering processes which moderate neutrons to below the U238 fission threshold. These include inelastic scattering in U238, steel and sodium and elastic scattering in oxygen.

The overall reactor spectrum shape is important because the Doppler effect occurs in the low energy tail and the ratio of capture reactions to fission reactions in the fissile isotopes, α, increases towards low energies and is sensitive to the spectrum shape.

The ratio of U238 capture to Pu239 fission is an important parameter both for the calculation of K and the breeding performance.

The effect of a reduction in sodium coolant density, or loss of sodium, is to reduce the core moderation and increase the core leakage The effect of the reduced moderation predominates, the effect being to increase the proportion of U238 fissions and reduce the ratio of absorption to fission overall, thus increasing reactivity. This must be taken into account in safety studies.

A fast reactor neutron spectrum is shown in Fig. 2.5 and a fast reactor neutron balance is given in Table 2.2.

2.4 Integral measurements relating to nuclear data for reactors

Types of integral measurements can be classified as follows:

1. Reaction rate ratios (relative to a standard cross-section such as U235 fission) in a defined spectrum. This spectrum can be meqsured or shown to be calculable sufficiently accurately. Many reaction rates of interest have been measured in this way. They include power-reactor irradiation experiments.

2. The composition of a test zone having $K_\infty = 1$, and reaction rate ratios measured in this test zone (which give components of the neutron balance).

   A number of simple test zones of this form have been studied. Examples are:

   (i) Enriched uranium (e = 5.56%)

   (ii) Enriched uranium oxide (e = 7.49%)

   (iii) Enriched uranium plus graphite

   (iv) Natural uranium plus plutonium plus graphite.

   By varying the proportion of graphite the spectrum can be varied. Measurements of the ratio of U238 capture to Pu239 fission give information about the energy variation of these cross-sections. The requirement for neutron balance gives a relationship between Pu239 alpha and values of ν (which are relatively well known) to within the uncertainties in the measurements of other components of the neutron balance (the reaction rate ratio measurements of U238 fission/Pu239 fission and U238 capture/Pu239 fission).

   By introducing a diluent material, such as iron or sodium, the absorption in this diluent can be deduced.

3. Simple geometry reactors comprising a large core and reflector with a simple core composition. When combined with $K_\infty = 1$ test zones the leakage characteristics of the materials can be deduced. By measuring the reaction rate distributions over a central region (in which the spectrum is unperturbed by the reflector) the geometrical buckling, B^2, of this region can be obtained and hence the migration area, M^2, deduced from

$$K_\infty / (1 + B^2M^2) = 1 \qquad (62)$$

   with K_∞ extrapolated from the $K_\infty = 1$ test zone measurements.

4. Measurements for compositions with $K_\infty < 1$ driven by an external source. These are similar to the previous class of measurements. The geometrical buckling is measured over a region of constant spectrum. Measurements of this kind have been made for blocks of natural uranium (the Snell experiment).

5 Spectrum measurements. These give information about the relative values of moderation to absorption plus leakage and also show the detailed structure caused by resonances and cross-section minima.

6 Neutron transmission through thick samples and large blocks. The transmission is sensitive to the total cross-sections, and, in particular, minima in the cross-sections, together with the moderation by scattering. Measurements of this type have been performed on blocks of iron, sodium and mixtures. The objective is primarily to test the nuclear data used for shielding applications.

7 Temperature dependent thick sample transmission and self-indication measurements. In the self-indication measurement capture of neutrons in a foil of the material is measured in a beam of neutrons which have been transmitted through a thick sample of the material. This gives a broad resolution measurement of resonance shielding effects and the temperature dependence.

8 Small sample reactivity perturbation measurements made at the centre of a reactor. These give information about the net production or absorption of neutrons weighted by the energy dependence of the importance of the neutrons to the fission process, ϕ^* (E).

Integral measurements provide a test of nuclear data and can also be taken into account when deriving the data sets used for reactor applications. The data set is then chosen to give a best fit to both the differential cross-section measurements and the integral measurements.

Integral measurements which test the transport and moderating characteristics of moderators have been mentioned in sub-section 2.2. These include measurements of age to the indiumresonance using different neutron sources (in particular a fission source), thermal neutron spectra and the spatial distribution of neutrons at thermal energies.

Components of the neutron balance

CORE REGION			
Isotope	Neutron Production	Fission	Capture
U235	9	3	1
U238	76	28	154
Pu239	718	243	71
Pu240	43	14	20
Pu241	47	16	3
Pu242	1	0.3	0.3
Steel			32
Sodium			2
Fission products			12
Control			11
Other components			10
CORE TOTAL	894	304	316
Core Leakage	274		
AXIAL BREEDER REGION			
U235	3	1	1
U238	6	2	50
Pu239	7	2	1
Other components			20
RADIAL BREEDER REGION			
U235	6	2	1
U238	24	9	112
Pu239	60	20	9
Other components			50
REACTOR TOTAL	1000	340	560
Reactor Leakage	100		

Table 2.2 - Neutron balance in a typcial sodium cooled fast reactor

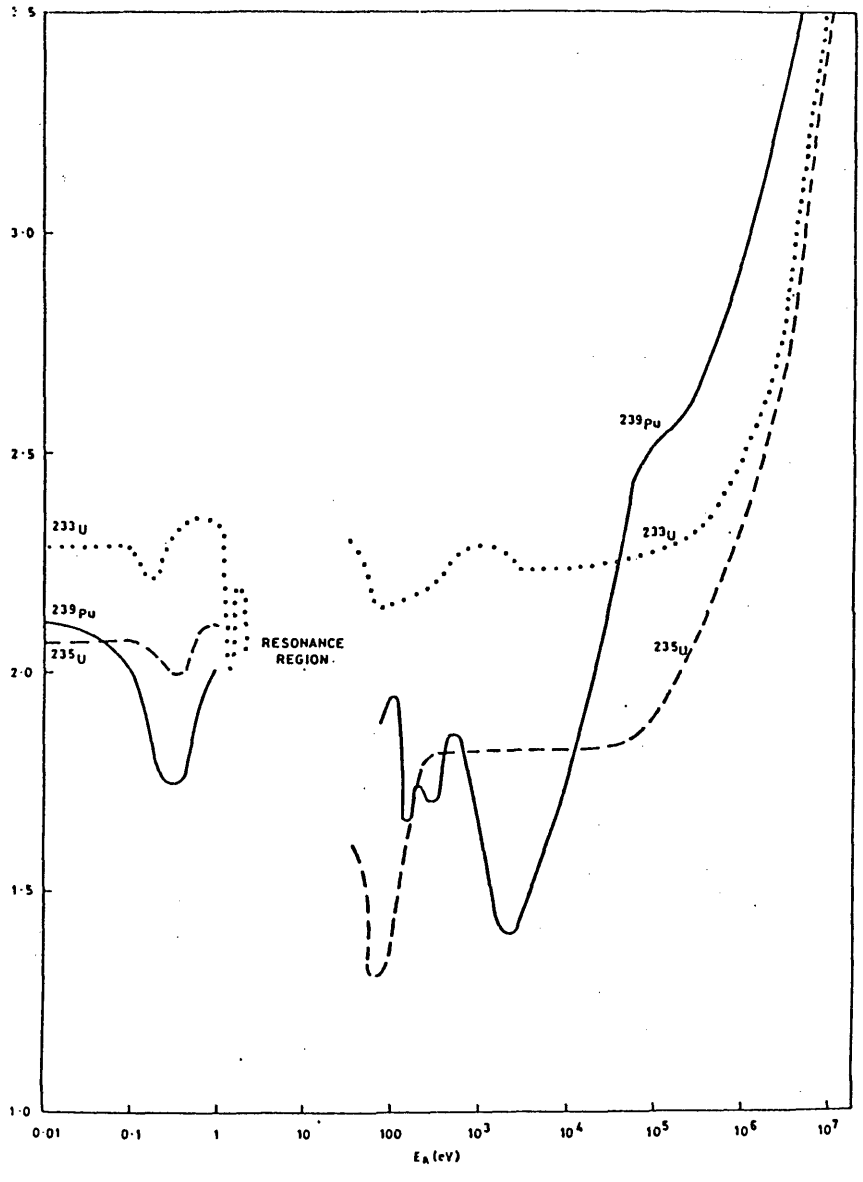

FIG. 2.1 ENERGY DEPENDENCE OF η FOR THE PRINCIPAL FISSILE NUCLIDES

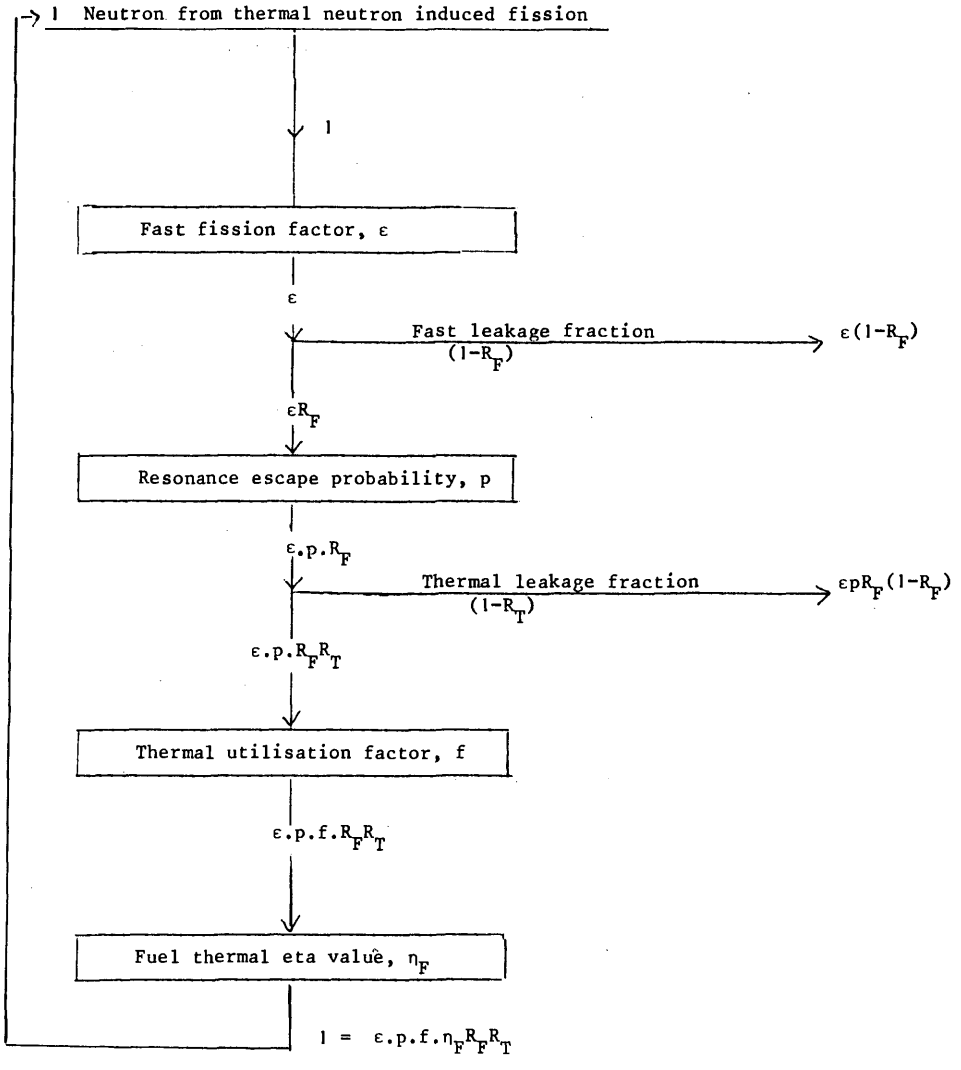

Fig. 2.2 Principal components of the neutron balance in a thermal reactor

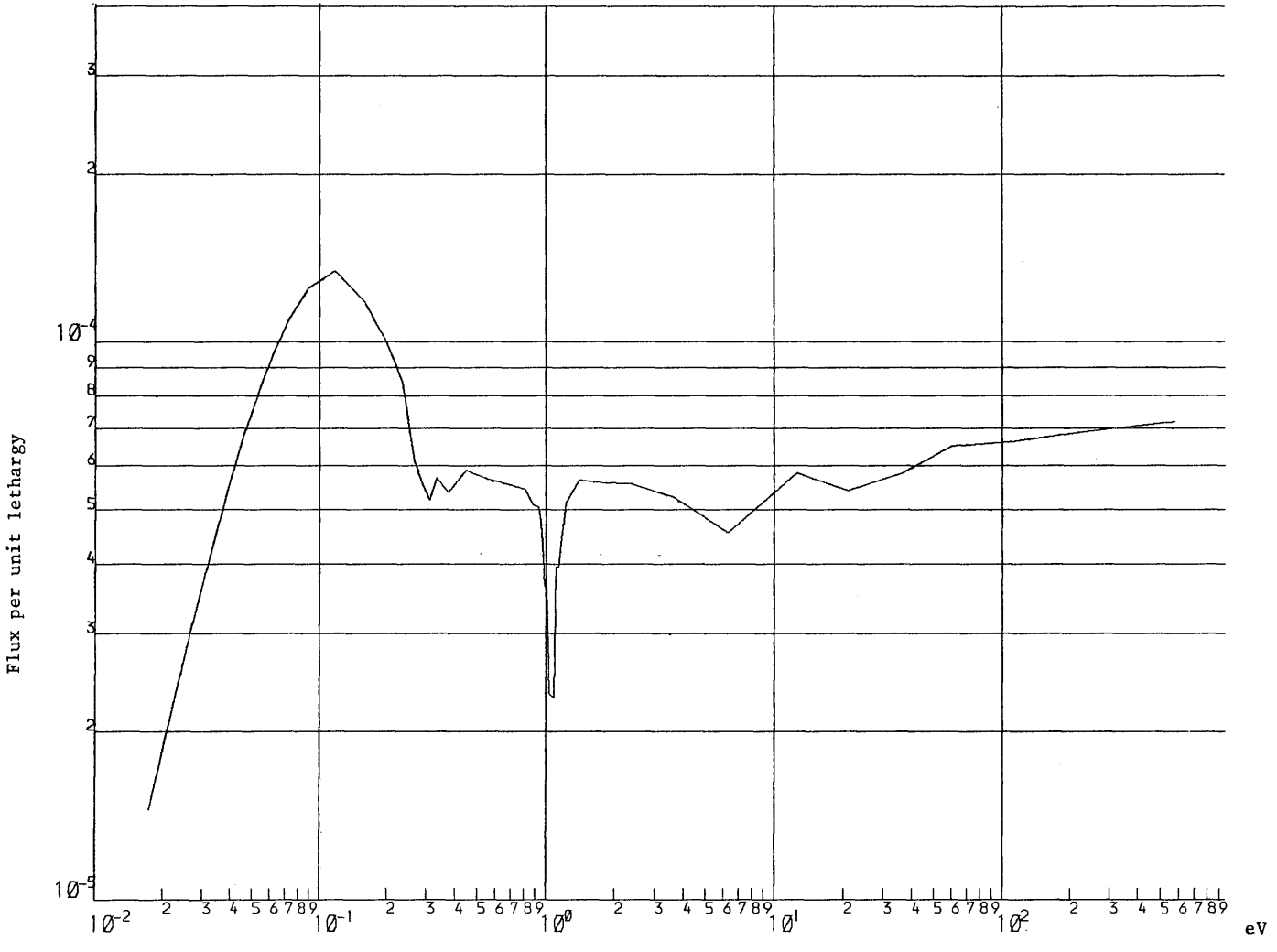

Fig. 2.3A Low energy spectrum in PWR fuel (smoothed over energy groups)

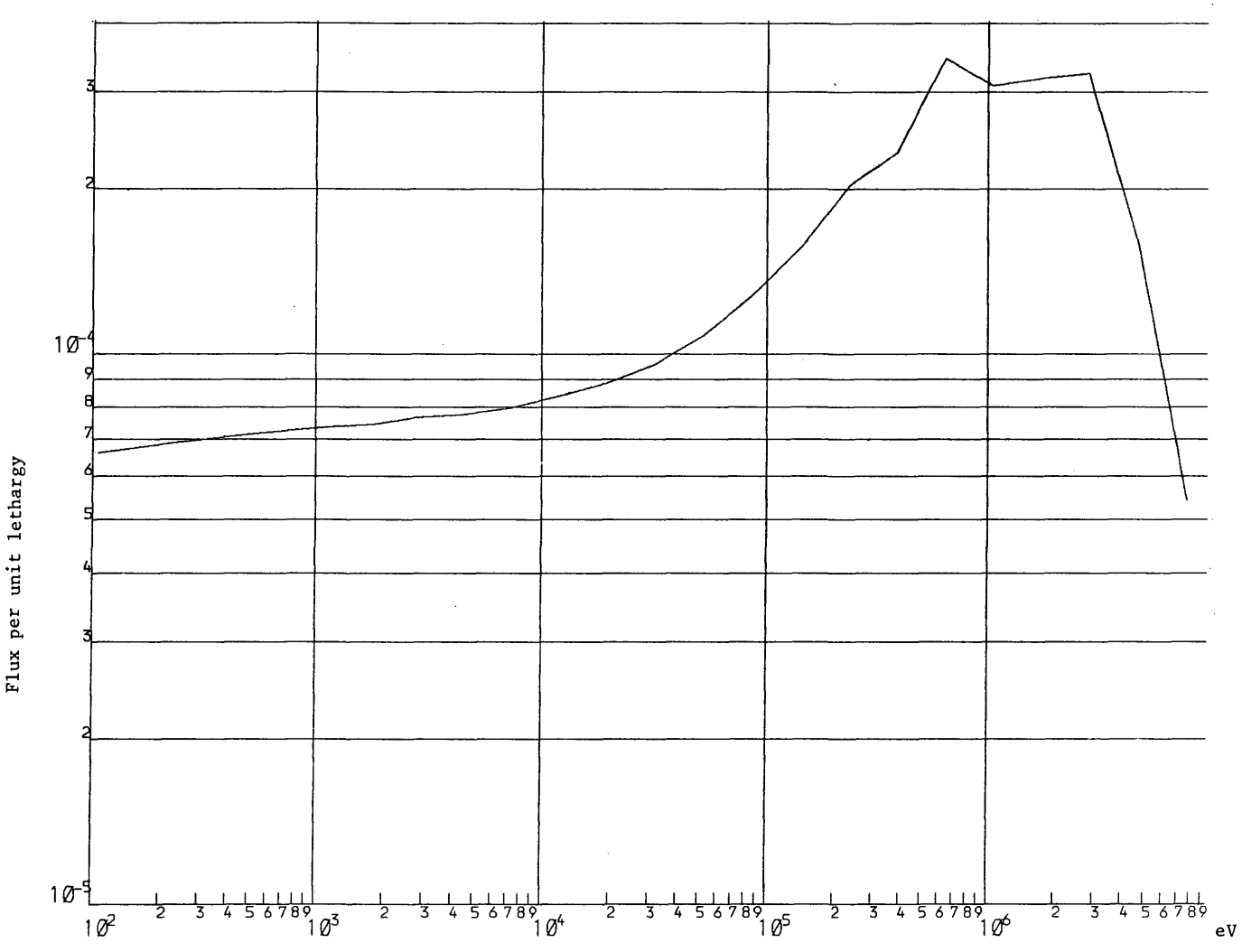

Fig. 2.3B High Energy spectrum in PWR fuel (smoothed over energy groups)

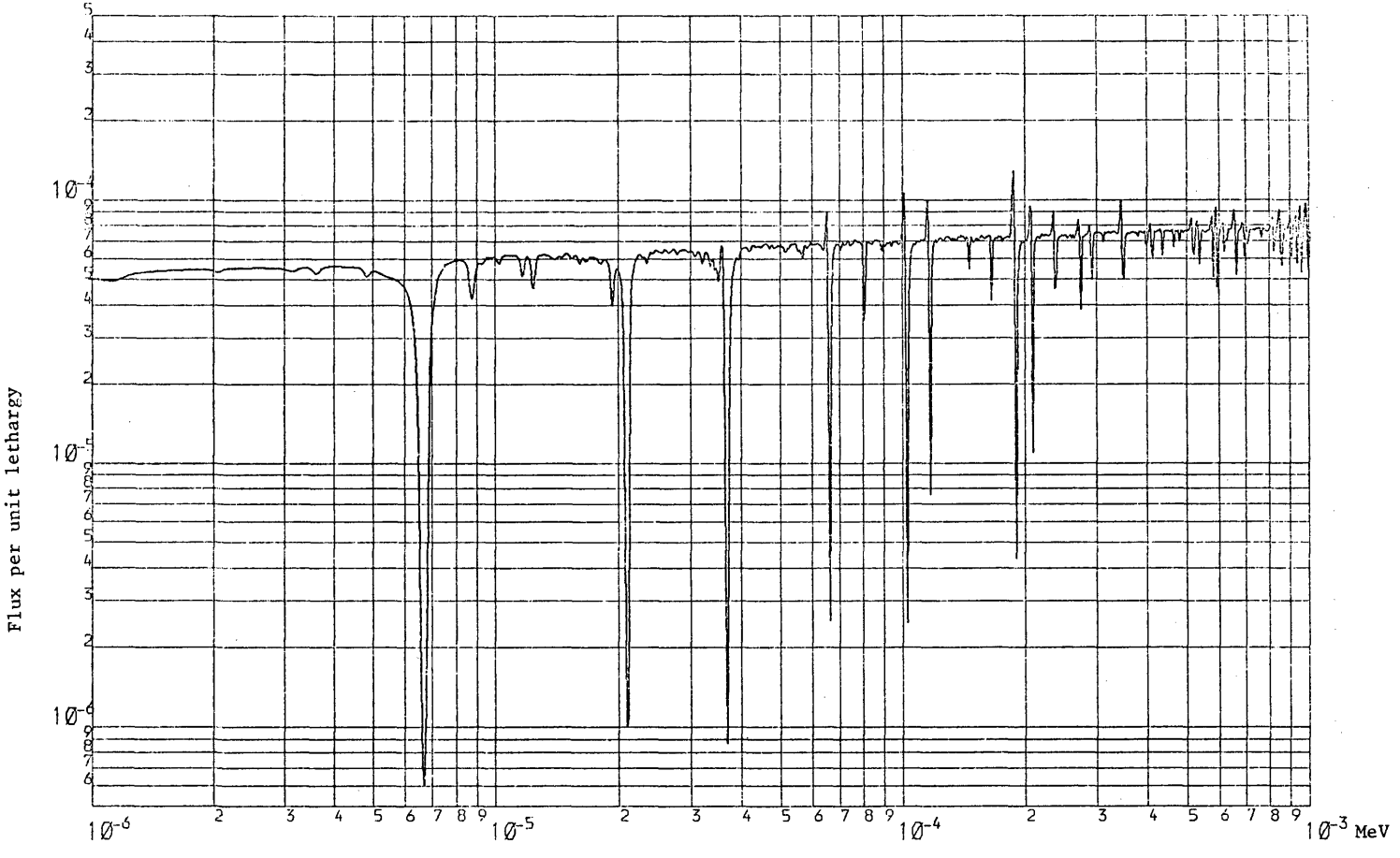

Fig. 2.4A - Resonance region spectrum in PWR fuel

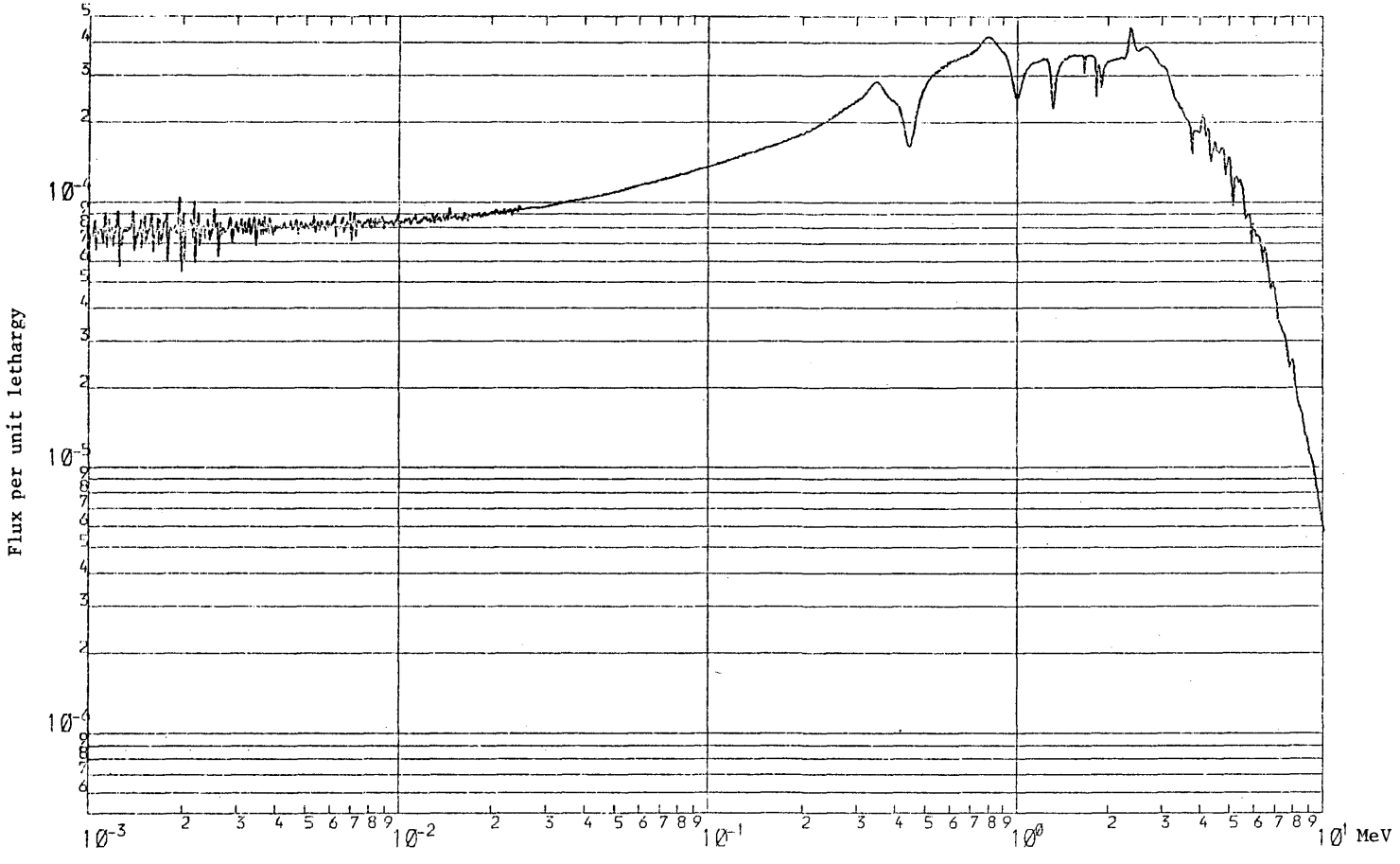

Fig.2.4B - High energy spectrum in PWR fuel

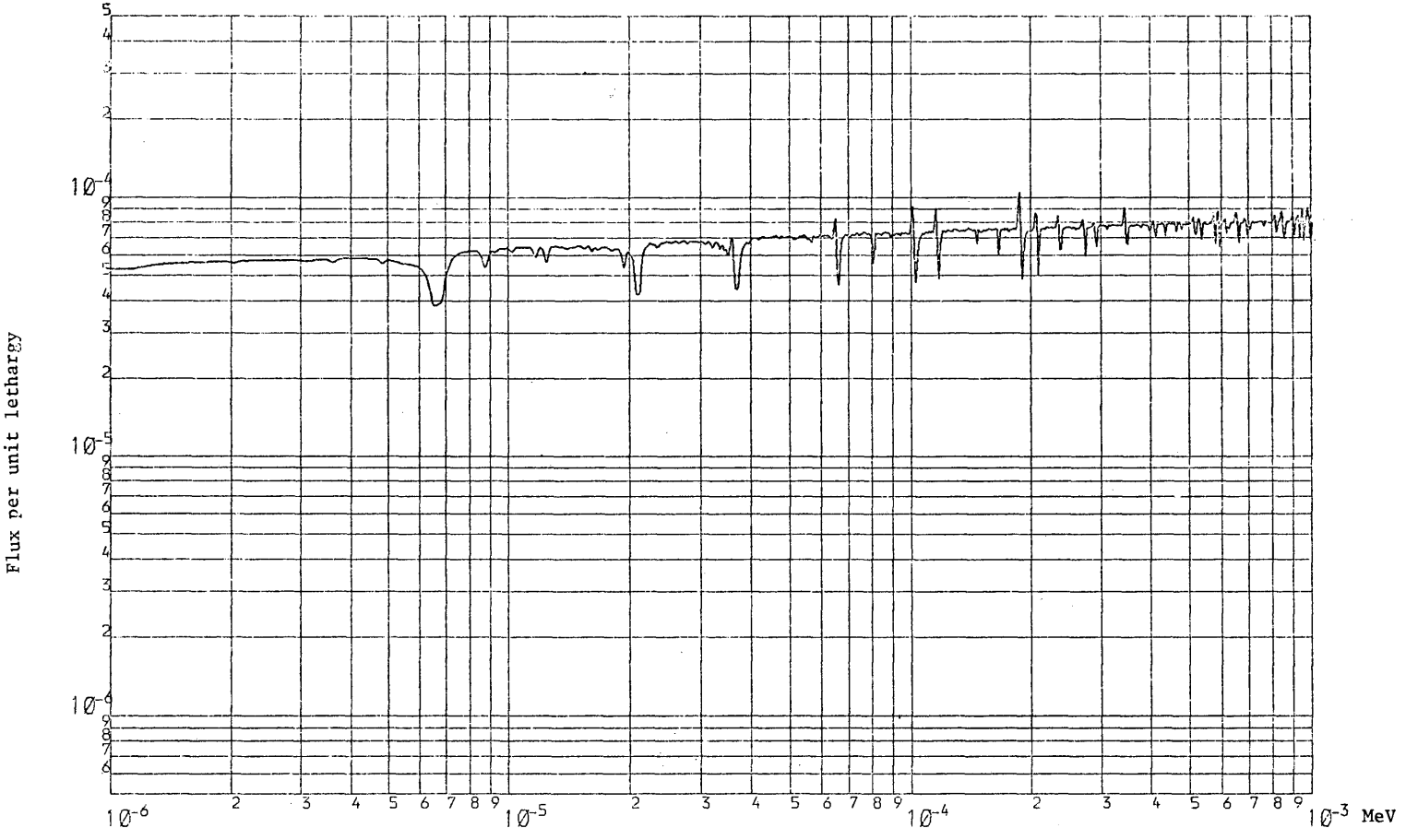

Fig.2.4C - Resonance region spectrum in PWR coolant

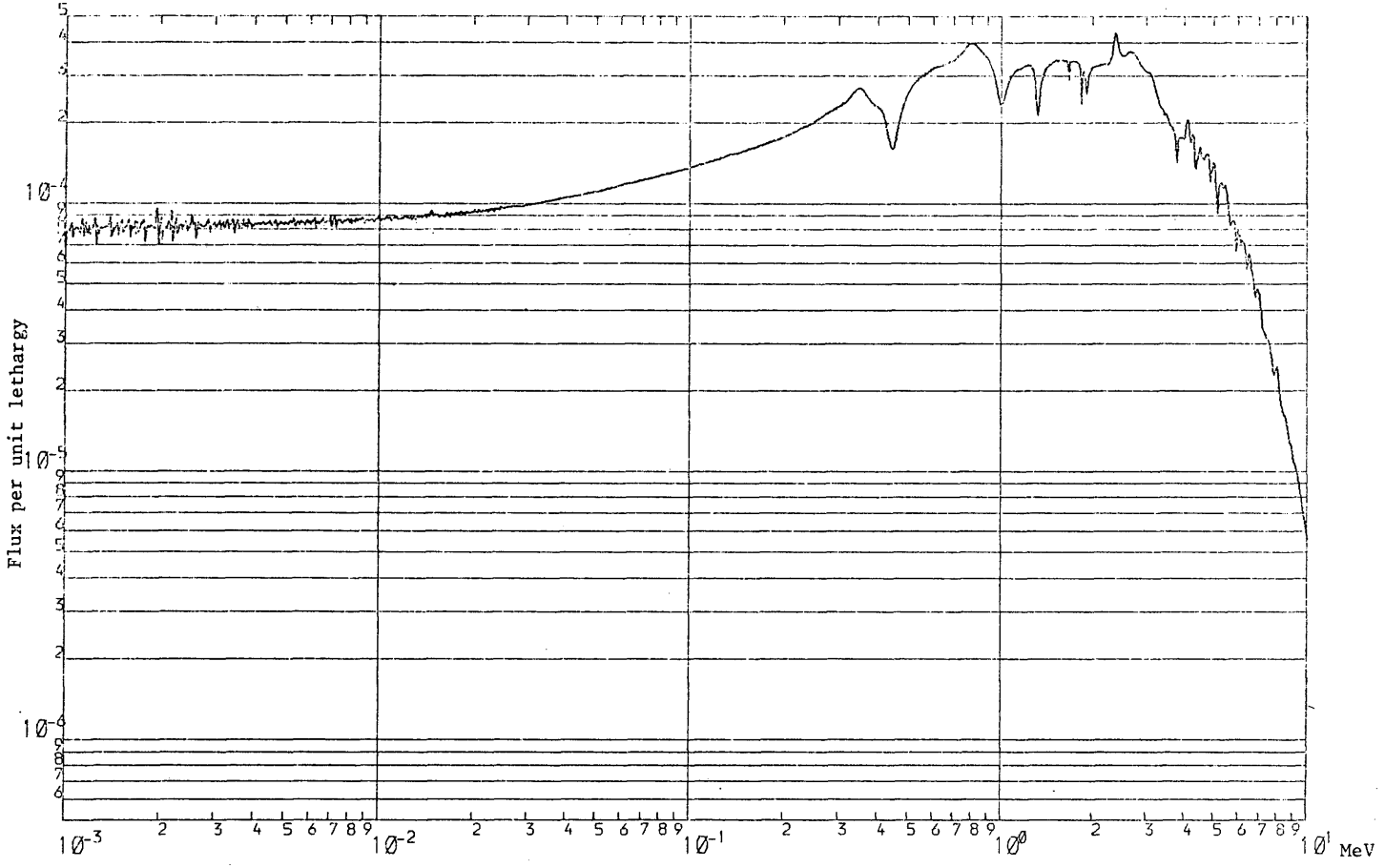

Fig. 2.4D - High energy spectrum in PWR coolant

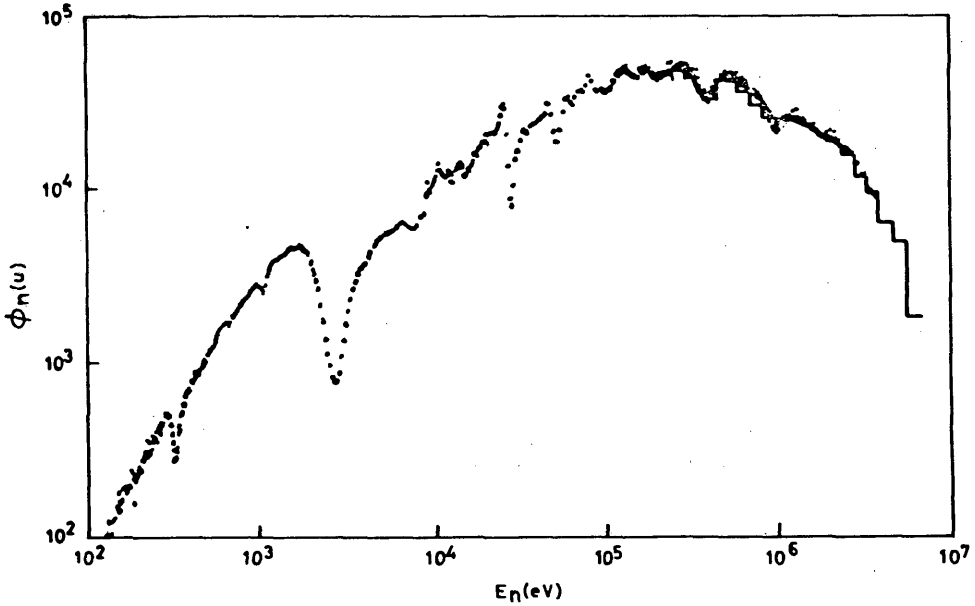

FIG 2.5 THE NEUTRON SPECTRUM MEASURED IN A SODIUM COOLED FAST REACTOR

SECTION 3 - ESTIMATION OF THE UNCERTAINTIES IN PREDICTIONS OF REACTOR PARAMETERS AND NUCLEAR DATA ACCURACY REQUIREMENTS

3.1 Introduction

Uncertainties in predictions of reactor parameters arise from nuclear data uncertainties, deficiencies in calculation methods, uncertainties in reactor operating strategies and tolerances in component dimensions and compositions. For predictions of many reactor parameters uncertainties in the nuclear data used predominate over other sources of uncertainty at the present time.

Sensitivity studies and uncertainty estimation

To estimate this component of the uncertainty the sensitivities of reactor parameters to changes in nuclear data together with the uncertainties in the nuclear data entering into the calculations are required. If we represent the nuclear data as a set of discrete parameters, σ_i, (instead of a continuous energy variable) then the sensitivities for reactor parameter, P_m, are defined as:

$$S^P_{m,i} = \left(\frac{\partial P_m}{\partial \sigma_i}\right) \frac{\sigma_i}{P_m} \quad . \tag{63}$$

These discrete nuclear data parameters could be energy group cross-sections or resonance parameters, or any convenient parametrisation of the data. Using nuclear model parameters can simplify the uncertainty representation.

The required cross-section uncertainty information is the fractional variance in σ_i, V^{σ}_{ii}, and the fractional covariance between the uncertainties in σ_i and σ_j,

$$V^{\sigma}_{ij} = \langle e_i \cdot e_j \rangle \tag{64}$$

the expectation values of the fractional deviations in the nuclear data parameters.

When integral measurements, I_K, are taken into account in the prediction of reactor properties then the sensitivity of these to nuclear data variations, together with the fractional covariances in the integral measurements, V^I_{K1}, are required. The sensitivities are

$$S^I_{K,i} = \left(\frac{\partial I_K}{\partial \sigma_i}\right) \frac{\sigma_i}{I_K} \tag{65}$$

and $$V^I_{K1} = \langle t_K \cdot t_1 \rangle \tag{66}$$

the expectation values in the fractional deviations in the integral measurements.

The diagonal components of the covariance matrix, V^I_{KK}, are the fractional variances in the integral measurements I_K.

The expression for the resulting uncertainty in reactor parameters P_m is derived in sub-section 3.3

When integral measurements are not taken into account the components of the fractional variances in the predicted values of the reactor parameters arising

from nuclear data uncertainties are

$$V^P_{m,m} = \sum_i \sum_j (S^P_{m,i} \cdot S^P_{m,j} \cdot V_{ij}) \qquad (67)$$

the fractional uncertainty f_m is given by

$$f^2_m = V^P_{mm} \qquad (68)$$

The sensitivities, $S^P_{n,i}$ and $S^I_{K,i}$, can be derived by repeating calculations of the properties and changing each item of nuclear data in turn. However, perturbation theory methods can reduce the amount of calculation involved. Such methods are described, for example, in reference (7). Nevertheless, the amount of calculation involved is considerable and simplifications, for example by restricting the sensitivities to the most important items of nuclear data and using approximate calculation models, are acceptable. This is because estimation of uncertainties and confidence levels can only be approximate.

An example of a sensitivity study is the work by Becker and Harris (8). They calculated the sensitivity of fuel cycle costs to uncertainties in nuclear data for BWR's, PWRs and CANDU type reactors. The nuclear data were changed in 3 broad energy ranges; thermal, epithermal and fast. The economic implications of current uncertainties in thermal cross-section values are also estimated.

Estimation of uncertainties in nuclear data and integral measurements is a necessary but difficult task. Improved estimates of the uncertainties can be more important than improved measurements. Reliable estimates of the margins in design and operation required to meet safety conditions have a higher priority than a repeat measurement (or an evaluation) which is not accompanied by an assessment of uncertainties (unless it leads to the resolution of a discrepancy).

Fortunately, in many important cases the uncertainties in the predictions of the reactor parameters are closely related to the uncertainties in corresponding integral measurements. When this is the case it is only necessary to estimate the uncertainties in these integral measurements reliably. However, it is preferable for both the integral and differential cross-section measurements to provide the required accuracy in prediction and provide an independent confirmation of predictions.

The closeness to which current nuclear data libraries predict some important reactor properties is summarised in sub-section 3.4

Mathematical methods for determining nuclear data requirements

The problem of deciding nuclear data measurement (and evaluation) requirements is a complex one in general. For a few specific items the requirement is clear. This is when the reactor parameter of interest depends on a single item of nuclear data. The requirement can then be simply formulated. This can be the case for induced radioactivity when the measurements of the cross-section leading to the activity are incomplete or inaccurate and nuclear model calculations cannot provide the required data.

When the required reactor parameters are sensitive to a number of items of nuclear data the accuracy required in cross-section measurements can, in principle, be defined by a cost minimisation. The cost implications of different levels of uncertainty in the reactor parameters and the cost of measuring different items of nuclear data to different accuracies must be assessed and the optimum reactor parameter uncertainty and programme of nuclear data measurements calculated. Usachev and Bokkov (9) have proposed an approach to the solution of this problem. Firstly, the target fractional accuracies for reactor parameters, t_m, are decided upon and then the nuclear data accuracy requirements are derived by assuming that the cost, or difficulty, of making a measurement to a fractional accuracy e_i is equal to λ_i/e_i^2. The required nuclear data accuracies are obtained from the condition that:

$$\left.\begin{aligned} &\sum_i (S^P_{m,i} e_i)^2 \leqslant (t_m)^2 \quad \text{for each } m \\ \text{and} \quad &M = \sum_i (\lambda_i / e_i^2) \text{ is a minimum} \end{aligned}\right\} \qquad (69)$$

The relative values of λ_i can be based on the accuracies already achieved in this type of measurement. If a measurement of one item of nuclear data is made to an accuracy higher than the value required by these conditions then the accuracies required for other items can be relaxed. The above expressions neglect the effects of correlations in the uncertainties in nuclear data measurements, caused, for example by using the same standards or techniques for measuring different items. This formulation only applies to a set of nuclear data parameters for which the uncertainties are uncorrelated.

The formulation has been extended by Bobkov, Pyatnitskaya and Usachev to include integral measurements (10). This extension is discussed in subsection 3.4.

Formulation of national nuclear data requirements

Nuclear data requirements and status have been considered in detail at a number of Advisory Group , Consultants and Specialists Meetings and Conferences. Some of these meetings and conferences are listed in Table 3.1.

The IAEA International Nuclear Data Committee (INDC) and the Nuclear Energy Agency Nuclear Data Committee (NEANDC) collaborate on reviewing the status of nuclear data for standards and for important reactions which are discrepant. These committees produce status reports on Standards (11) and Discrepancies (12).

National Nuclear Data Committees formulate nuclear data measurement requirements and produce their national request lists. These take account of the conclusions of specialist meetings and status reports. They are collected by the Four Data Centres and are combined into the World Request List for Nuclear Data, WRENDA. This is published by the IAEA, the latest version being WRENDA 81/82,edited by N Day Day (13). Requests are assigned a Priority, either 1, 2 or 3. The list provides a basis for international collaboration to try to meet the nuclear data requirements. There are arrangements for providing samples to laboratories wishing to make a measurement to meet a request in WRENDA. The IAEA Nuclear Data Section are sponsoring Co-ordinated Research Programmes to review and progress the measurement and evaluation of selected important items of nuclear data.

3.2 Target accuracy requirements for reactor parameters

Instead of finding the nuclear data requirements by minimising the sum of the consequences of reactor parameter uncertainties caused by nuclear data uncertainties and the costs of making the associated nuclear data measurements it is more usual to decide upon a set of target accuracies for reactor parameters. The targets are based on assessments of the economic consequences of uncertainties and the possibilities of achieving the targets. Having decided upon the targets the nuclear data sensitivities are used to select the nuclear data requirements. Assumptions must be made about likely correlations in measurement uncertainties and a method for partitioning the total variance between the component nuclear data parameters decided upon.

Uncertainties in the prediction of reactor properties result in:

(i) The provision of design margins to ensure a guaranteed power output,

(ii) Design margins to provide adequate control of the reactor,

(iii) Provision of funds to cover the cost of possible corrective actions,

(iv) Higher "guaranteed generation costs" which cover the uncertainties.

To ensure a guaranteed power output it might be necessary to build a larger reactor core (and associated shielding and containment). Provision of control margins to cover uncertainties in the variation of reactivity with power and burn-up might require extra control elements and, in consequence, a larger core and associated structure. Uncertainties in the required feed fuel enrichment to ensure criticality at the end of the burnup cycle, with control absorbers removed from the core might be catered for by accepting a possible lower burn-up of the fuel or insertion of extra control absorbers in the first few fuel cycles, and then adjusting the enrichment to the value found to be necessary. This results in higher fuel costs for the first few cycles.

A 1000 MW(e)* nuclear power station costs about a billion US dollars and the electrical output is worth about 100 million dollars per year. A saving of 1% in the cost of one station or an increase in output by 1% for a few years is very valuable. However, there are many other sources of uncertainty than nuclear data, and other reasons for building in margins and allowing for contingencies. Flexibility in fast-reactor design is required to allow for use of plutonium from different sources (thermal and fast reactor) having differing isotopic compositions. There are uncertainties in the composition and dimensions of materials and uncertainties in calculation methods. These set lower limits to the useful target accuracies in the prediction of reactor properties.

During the past twenty years a broad consensus on required target accuracies has been arrived at based on judgements about the accuracies which would be worthwhile and seem achievable. They should be regarded as a guide to the relative importance of different parameters. Reactors operate successfully without these targets having been reached. There is also, now, a large amount of data from operating reactors. Consequently, the emphasis on requirements (or relative priorities) has tended to change from those for design to those for efficient operation and for the management of irradiated fuel elements and other components. Efficient operation requires the monitoring of irradiation effects and, for this purpose, dosimetry (the measurement of flux doses on components) is important. The radioactivity induced in fuel and other materials, and also in the coolant, is also important. Measures aimed at reducing the irradiation exposure dose to reactor operators, maintenance staff and those involved in the handling, reprocessing and disposal of irradiated components are given a high priority.

* MW (e) denotes Mega-watts of electrical power output

What we might regard as the traditional target accuracies are summarised below:

The fissile enrichment of fuel elements

The fissile enrichments of fuel elements to be loaded into a core are chosen so that the reactor is critical at the end of an irradiation period, before refuelling, with the operational control at a minimum level. However, there must be margins in the control at this stage to allow for differences in the reactor conditions at the end of different irradiation periods, to allow, for example, for the build-up of plutonium in breeder elements in a fast reactor, for different groups of fuel elements reaching the target burn-up and for the burn-up of control absorber material.

An uncertainty in the prediction of the required fuel enrichment must be allowed for by providing extra control, by interchanging fuel of different enrichments in a core with two enrichment zones or by changing the size of the core (interchanging core and breeder elements in a fast reactor). Alternatively, the fuel can be removed at a lower burn-up, when fuel reactivity has reached the limiting value, if the feed enrichment is too low, or when the operating control is above the minimum, if too high. These different alternatives result either in a loss of power or an increase in fuel costs (more fuel elements used for a given power output), or both,at least during the first few irradiation periods until the correct feed enirchment can be manufactured and supplied. Additional control absorber mechanisms,introduced to cover uncertainties, would remain.

Typically, an accuracy of $\pm$ 0.5% in the K of fresh fuel and 0.5% to 1.0% for irradiated fuel has been judged to be the appropriate target. This leads to high accuracy requirements for the principal fissile and fertile isotopes. The cost of the extra enrichment of the fuel of an LWR required to allow for a 1% uncertainty in K is about $2M.

The variation of reactivity with burnup during an irradiation period

This is required for determining the operational control requirements and also the fuel feed enrichment. A typical target accuracy is $\pm$ 10%. It implies a corresponding accuracy in the prediction of internal breeding or conversion ratio and the reactivity effect of fission product build up.

Power coefficients of reactivity

The changes in reactivity on going from the shutdown condition to operating power, caused by changes in temperature and the associated thermal expansion, bowing, relative movements of components (for example, of core and control elements) and Doppler effects are factors which determine the shutdown control requirements. Shutdown control margins are also required to provide a level of reactivity shutdown covering all possible misloadings (including removal of one or more control elements) and changes in core configuration.

The accuracy needed for the estimation of the shutdown control reactivity depends on the way the control element functions are defined. For example, if the shutdown control is separate from the operational control,rather than interchangeable, there is a separate requirement of $\pm$ 5% in the prediction of shutdown control reactivity.

Breeding or conversion ratio

A knowledge of the total breeding ratio, conversion ratio or breeding gain is required for predicting fuel cycle costs and ore requirements, and for planning reactor programmes. A target of $\pm$ 2% in fast reactor breeding ratio or $\pm$ 0.03 in breeding gain is commonly adopted. The breeding gain is the net production of equivalent fissile material. That is, the net loss and gain of transactinum isotopes are weighted by their relative reactivity worths.

Control requirements

In a fast reactor, a typical ratio of control elements to fuel elements is 1 to 10. An uncertainty of $\pm$ 5% in control rod reactivity worth could require a contingency of $\pm$ 10% (or 2 standard deviations) and possibly a change in the pattern of rods from 1 in 10 to 1 in 9 lattice positions. This would result in an increase in core size, to maintain power output, as well as the increase in the number of control elements. An alternative is to change the control absorber material. For example, the reactor could be designed to use natural boron rods but initially could use enriched boron to provide a margin to cover uncertainties. The composition of later rods would then be changed to meet the measured requirements. However, enriched boron might still be required and this is expensive. A target accuracy of $\pm$ 5% in control rod worth has been proposed.

Reactivity scales

Temperature and power coefficients can be measured on critical assemblies and power reactors, as can control rod reactivity worths and the reactivity effects of fissile materials and fission product isotopes. It requires care to make all the different types of reactivity measurement on a consistent reactivity scale. The effective delayed neutron fraction provides a measurement of reactivity.

However this varies with reactor design and composition (depending on the relative contributions of fission in different isotopes). Different types of kinetics or reactivity balance measurement depend in different ways on the time dependence of delayed-neutron emission. In a large fast reactor, the U238 delayed-neutron source is the largest component, whereas, in smaller fast reactors, Pu239 predominates. Accurate delayed-neutron data (the total yield, the time dependence of the emission and the energy dependence of the delayed neutron spectra) are required to enable the reactor period - reactivity relationship to be determined to ± 3%. (The reactor period is the time constant in the exponential time dependence of the flux in a non-critical reactor).

Power distribution

The maximum power output is limited in some reactor designs by the temperature of the hottest element. Design and operation aims to minimise the peak to average power so as to maximise the power output, or minimise the number of elements operating at high temperatures. Accurate predictions of power distributions are required and these depend on the ability to calculate the relative reactivities of elements having different fissile material feed enrichments and different irradiation histories. A typical target accuracy for the peak to average power distribution is ± 1%.

The temperature of coolant leaving individual elements must be as nearly uniform as possible so as to provide maximum efficiency. Thermal gradients can cause bowing of elements and these effects must be predicted.

Gamma-rays migrating from fissile fuel elements make a significant contribution to the heating of control elements and reflector or breeder elements and this leads to requirements for data on gamma energy yields, gamma spectra and gamma interaction cross sections.

Radiation damage effects

There is a need to predict radiation damage doses and dose gradients for the estimation of swelling, bowing and distortion of elements. Atomic displacement rates, helium-formation rates and material temperatures must be predicted. When graphite is used as moderator its irradiation stability must be ensured. There is also a requirement to monitor the flux and flux spectrum so that the observed changes in material properties can be correlated with the irradiation and temperature history. This leads to the dosimetry requirements. Typical requirements are for the prediction of fluence and radiation damage dose to ± 5% and dose and temperature gradients to ± 10%. There is also the requirement to determine fuel burnup to ± 1%.

Heat generation and activity of irradiated materials

Estimation of the decay heat of fuel elements is needed for the design of shutdown and emergency-cooling systems and of fuel-transfer systems. Target accuracies in the range 2% to 5% have been proposed for decay times longer than about 10 seconds.

Various aspects of the activity of irradiated fuel and structural materials are important. The buildup of curium isotopes and the variation with irradiation of the neutron source due to spontaneous fission and (α,n) reactions is important for monitoring the shutdown reactivity of a reactor during refuelling. This leads to requirements for data on cross-sections leading to the formation and loss (by capture and fission) of the curium isotopes and for (α,n) cross-section data for light isotopes, such as carbon, oxygen and fluorine (a possible trace contaminant). Similar data are also required for the design of shielding for transport flasks and reprocessing plants. The activity of structural materials must be estimated for the design of handling, storage and disposal systems. Trace quantities of elements from various components in the coolant circuit can be dissolved into the coolant, carried around the circuit, activated in the core and then deposited elsewhere in the circuit. Both the activity of the coolant and the activity plated out on components can present operational difficulties. A typical target accuracy for activity predictions is ± 10%.

Temperature, density and power coefficients

Reactors must be designed to have safety margins which cover a wide range of modes of operation and fuel compositions. Consequently, these target accuracy requirements are not so stringent, being typically ± 10% to ± 15%.

3.3 Methods for taking into account integral measurements and more general reactor measurements

We can distinguish between two categories of measurements which depend on nuclear data averaged over a broad energy spectrum. In the first category the uncertainties in the calculated values of these parameters arise predominantly from uncertainties in nuclear data and are not significantly affected by approximations in calculation methods or other sources of uncertainty. We call these integral measurements. In the second category the measurements are closely related to

reactor parameters of interest and the predicted values can be significantly affected by approximations in calculation methods. The second category includes measurements made in operating reactors and in mock-up assemblies of reactors. We call these "reactor parameter reference measurements" (RPRM). Some types of measurement can be considered to be in both categories; in particular, reaction rate ratio measurements made in a well characterised reactor spectrum. The two categories are distinguished in the way that they are used. The integral measurements can be used to adjust nuclear data. The RPRM can be used to apply bias factors to calculated values of reactor parameters or to adjust the methods used to calculate the parameters.

Adjustment of cross-sections to fit integral measurements

To illustrate the procedure for adjusting cross-sections to fit integral measurements we consider the idealised case when a set of discrete nuclear data parameters, σ_i, which have uncorrelated fractional variances, V^{σ}_{ii}, can be used to represent the basic evaluations of differential nuclear data measurements and associated nuclear model calculations (that is, we assume that the energy dependent cross-sections can be represented by a set of discrete parameters, we neglect the covariances, V_{ij}, and also the covariances between different integral measurements, V^{I}_{K1}, in this outline procedure)

The fractional discrepancy between the measured value, E_K, and calculated value C_K of integral property K is denoted by D_K, where

$$D_K = (E_K - C_K)/C_K \tag{70}$$

The fractional discrepancy which will remain using the adjusted cross-sections is denoted by d_K, where

$$d_K = (E_K - C^{1}_{K})/C_K \tag{71}$$

The assumption is made that the difference between C^{1}_{K}, the value calculated using adjusted cross-sections, and C_K can be approximated as linearly dependent on the fractional adjustments to the nuclear data parameters, X_i

$$C^{1}_{K} = C_K\left(1 + \sum_i S^{I}_{K,i}\ X_i\right) \tag{72}$$

and hence

$$d_K = D_K - \sum_i S^{I}_{K,i}\ X_i \tag{73}$$

The values of X_i are found by a least squares fit to the integral and differential measurements (or by a condition of maximum likelihood):

$$M = \left[\sum_K\left(\frac{d_K^2}{V^{I}_{KK}}\right) + \sum_i\left(\frac{X_i^2}{V^{\sigma}_{ii}}\right)\right] \quad \text{is a minimum} \tag{74}$$

The condition for M to be a minimum is obtained by expressing d_K in terms of D_K and X_i, differentiating with respect to X_i and setting the derivative equal to zero:

$$\left[\sum_K\left\{\frac{S^{I}_{K,i}}{V^{I}_{K,K}}\left(D_K - \sum_j S^{I}_{K,j}\ X_j\right)\right\} - \frac{X_i}{V^{\sigma}_{i,i}}\right] = 0 \tag{75}$$

This equation has the form

$$\sum_j W_{i,j}\ X_j = \sum_K\left(\frac{S^{I}_{K,i}\cdot D_K}{V^{I}_{KK}}\right) \tag{76}$$

where

$$W_{i,j} = \frac{\delta_{i,j}}{V^{\sigma}_{i,i}} + \sum_K\left(\frac{S^{I}_{K,i}\cdot S^{I}_{K,j}}{V^{I}_{KK}}\right) \tag{77}$$

By inverting the matrix $W_{i,j}$ the values of X_j can be calculated from

$$X_j = \sum_i W^{-1}_{i,j} \sum_K\left(\frac{S^{I}_{K,i}\cdot D_K}{V^{I}_{KK}}\right) \tag{78}$$

The inverted matrix $W^{-1}_{i,j}$ has another importance. It is the covariance matrix of the adjusted cross-sections

$$V^{A}_{i,j} = W^{-1}_{i,j} \tag{79}$$

Consequently the fractional accuracy of reactor parameters calculated using adjusted cross-sections is given by eqn. (67) but with $V^{\sigma}_{i,j}$ replaced by $V^{A}_{i,j}$:

$$f^2_n = \sum_i\sum_j (S^{P}_{n,i}\cdot S^{P}_{n,j}\cdot V^{A}_{i,j}) \tag{80}$$

The value of the sum of squares of relative deviations, M, which corresponds to the minimum of eqn. (74), should be equal to the number of degrees of freedom, which, in this case, is the number of integral measurements included in the fit, N_I. The deviation of M/N_I from unity gives an indication of the consistency of the deviations between the measured and calculated values of the integral measurements with the assumed uncertainties in the nuclear data parameters and integral measurements. That is it provides a χ^2 test.

The adjustment study also tests the consistency of the different integral measurements. Values of d_K^2 and X_j^2 which are much larger than the assumed variances imply discrepancies which should be studied. Efforts should be made to resolve them if they are significant in relation to reactor predictions.

In a more general formulation the effects of correlations must be taken into account. Such a formulation is given in reference (14). The quantity minimised is

$$M = \left[\sum_K \sum_l d_K d_l (V^I)^{-1}_{Kl} + \sum_i \sum_j X_i X_j (V^\sigma)^{-1}_{ij} \right] \qquad (81)$$

Improvements in the accuracy of prediction obtained by taking account of integral measurements

A typical procedure for adjusting cross-sections is to calculate the sensitivities for changes of cross-sections in 10 energy groups and the covariance matrices for this group structure. Adjustment factors for these 10 energy groups are then calculated but the adjustments are applied to the differential cross-sections by calculating a smooth fit to the ten group factors (such as a cubic spline fit). Having derived adjusted differential cross-sections the usual procedures for calculating integral properties are followed, including derivation of multigroup cross-sections. The accuracies of the calculations of integral properties are re-examined to test the assumptions. These are that adjustments can be made in 10 energy groups and the assumptions of a linear dependence on cross-section changes . We look for any bias or residual discrepancies significantly larger than those in the predicted integral parameters obtained using the adjustment factors, X_i, and the linearised equations. It might be necessary to repeat the adjustment exercise to allow for non-linearities, starting with the adjusted cross-sections but now taking into account the biases which have been introduced into these by the first cycle of adjustments.

An alternative to making adjustments in a few energy groups is to adjust the parameters of nuclear models used to fit the differential cross-section measurements and extrapolate the range of them. This approach is used for fission product capture cross-sections and cross-sections of higher transactinium isotopes (14), (15).

Examples of the improvements in accuracies of fast reactor predictions obtained by taking account of integral measurements have been given by Rowlands et al (16) and Marable (17). The results are similar in the two studies.

Accuracy of predictions of fast reactor parameters

Parameter	Unadjusted Nuclear Data	Adjusted Nuclear Data
K	± 3%	± 0.5%
Breeding ratio	± .04	± .02

These accuracies relate to a core using fresh fuel and at 300°K. The uncertainties associated with temperature and burnup effects, and also those introduced by calculation methods approximations, must be combined with these.

It can be seen that integral measurements make an important contribution to improving the accuracy of prediction of reactor properties. However, accurate differential nuclear data are required to provide the necessary understanding of the nuclear physics underlying reactor neutronics processes, to provide an independent confirmation of predictions of key parameters and to enable extrapolations to be made from the reference integral measurements to the conditions applying in reactors at various stages in their operation.

Use of integral measurements to choose between different sets of differential cross-section measurements

Instead of carrying out an adjustment of cross sections to obtain a simultaneous best fit to both the integral and differential cross-sections, the integral measurements can be used to guide the choice of differential cross-section measurements to be included in an evaluation. The approach is valuable when there are sets of discrepant measurements and it is evident that one or another set contains an error larger than the estimated uncertainties. This approach has been adopted , for example, in evaluations for Am241 and Am243 to choose between different measurements of the fission cross-sections.

Benchmark testing has also been applied in the development of the Evaluated Nuclear Data Files in the ENDF/B series.

Adjustment of calculational packages to compensate for biases in predictions

One approach to improving the predictions of a calculational package is to make semi-empirical adjustments to the package as a whole, rather than attempting to modify separately the nuclear data and calculational methods for separate sources of error. Uotinen et al (18) describe the success of this approach in predicting properties of light water reactors. The largest discrepancy in the prediction of K for initial PWR core loadings is 0.3%. The decrease in reactivity with burnup is about 10% in the first cycle and this variation is well predicted (to within about 2% of the measured decrease). The discrepancies in the predictions of the reactivity worths of different groups of control rods increase with increasing temperature, being about $\pm$ 1% at 250°F and 400°F but up to 8% at 532°F. This reflects the fact that the control rod model used is based on zero power critical experiments made at a low temperature (70°F). Relative assembly powers are predicted to within 5%. Nuclear data requirements emphasised in the paper by Uotinen et al are those relating to burnup effects and the fuel cycle; that is, data for secondary transactinium isotopes (Pu241, Pu242, Np237, Am241, Am243, Cm242 and Cm244) and fission products (cross-sections, yields and decay data). The importance of an accurate knowledge of the shapes of cross-sections of the principal fuel isotopes at thermal energies is also emphasised.

3.4 Required information on cross-section uncertainties

Information about the fine structure of cross-sections is only required when this affects neutron spectra, which, in fast reactor spectra, is for materials present in significant proportions, such as C, O, Na, Cr, Fe, Ni, U238, Pu239 and Pu240. For other substances, such as individual fission products, higher actinides and many activation reactions, the uncertainties in broad spectrum averaged values, and in the energy gradients of the cross-sections over broad energy intervals, are sufficient for fast reactor applications. In thermal reactor spectra shielding in individual low energy resonances can be significant for substances present in small proportions.

Uncertainties in the average energy gradients over broad energy ranges (perhaps a decade in energy) are required to estimate uncertainties in the differences between reaction rates in different spectra, and to permit adjustments to be made to fit measurements made in different spectra. Effects such as coolant density reactivity coefficients depend on the differences between relative reaction rates averaged in the normal and perturbed reactor spectra. It is also necessary to specify uncertainties in cross-section shapes to ensure that adjustments to fit integral measurements are consistent with nuclear theory and the differential cross-section measurements. For reactions with a threshold we need to know the uncertainties in the threshold energy and in the average gradient up to the plateau.

Neutron transmission through shields is sensitive to cross-section values in minima and so uncertainty information is required for these. The uncertainty in the transmission depends on uncertainties in the average values of quantities like $(1/\sigma^2)$.

We can separate the types of cross-section structure for which there are uncertainty requirements into the following categories:

(a) Individual resonances and cross-section minima. These can be characterised by the uncertainties in the resonance parameters and the correlations (both between the parameters of each resonance and between resonances). Alternatively, the uncertainty in the infinite dilute and shielded cross-sections for a reference background cross-section can be used.

(b) Average resonance structure in an interval. This might be characterised by uncertainties in average resonance parameters and their distributions. Alternatively the uncertainties in some other parameters representing the distribution of cross-section values might be sufficient (parameters in shielding factors being one possibility). A simple parameterisation should be sufficient to represent uncertainties.

(c) Intermediate structure. This could be represented by components of the uncertainties in the average resonance properties, or average cross-sections, which are uncorrelated between the energy intervals in which the resonance parameters are averaged.

(d) Threshold regions. The uncertainties in the effective threshold energy, the average energy gradient up to the plateau and values on the plateau are required. For reactions with thresholds above about 3 MeV the uncertainties in the fission spectrum averaged values might be sufficient.

(e) Smooth cross-sections and the shapes of cross-sections averaged over the resonance structure and intermediate structure. The requirements are for the uncertainties in the average values and the average energy gradients over broad energy ranges. Possible averages for which the

uncertainties could be given are:

(i) Thermal Maxwellian averaged cross-sections, or ratios.

(ii) Variation of the thermal Maxwellian average with temperature (the factor g in eqn. (39)).

(iii) Resonance integral.

(iv) Resonance integrals for lattices (resonance structure), including temperature dependence.

(v) Energy averages over intervals of about ½ lethargy, E to 2E or decade intervals, depending on the importance of the cross-section. Correlations between the uncertainties in the averages in different intervals are also required.

(vi) Average energy gradients over intervals and the correlations between intervals.

(vii) Fission spectrum averaged cross-sections, or ratios.

(viii) Defined fast reactor spectrum (for less important reactions).

Several of these requirements could be met by representing the uncertainties by a energy dependent factor to be applied to the cross-section. For example, the factor could be a polynomial function of energy, (1 + a +bE), or higher order, and the uncertainties in 'a' and 'b' would be specified. This polynomial can be simpler than the polynomial required to represent the shape of the cross-section. This would be a possible form for the cross-sections of hydrogen, B10 (below 1 MeV), carbon (below 1 MeV, with resonance parameters above), Cr, Fe, Ni (below about 100 eV with resonance parameters above, and average parameters above about 100 KeV). For cross-section curves which are averages over the resonance structure a similar parametrisation over selected energy ranges might be a suitable way to represent uncertainties.

Representing the uncertainties in terms of a few parameters (such as the thermal value and the energy gradient, or the values at a few energy points, with the shapes between these points being derived from a defined polynomial fit to the point values) enables the covariances between cross-section values at different energies to be calculated as continuously varying functions of energy. However, such a representation could require new processing codes to generate energy group covariances, or to transfrom the sensitivities to relate to these parameters.

In summary, the requirements are for the uncertainties in cross-section values averaged over broad energy intervals and in the fluctuations about the averages (including resonances and minima) and the energy gradients over broad energy intervals, to be calculated from the covariance data.

3.5 Some studies of the current status of nuclear data

Data for fissile isotopes at thermal energies

Evaluations of the cross-sections and ν values measured at 2200 m/sec and in 20°C Maxwellian neutron spectra were reviewed at the 1975 Washington Conference by Lemmel (19) and Leonard (20). The methodology of the least squares fitting procedure, and the importance of the evaluation of correlations in the measurement uncertainties, is described more fully in the earlier study reported in 1969 (21). Both absolute and ratio measurements have been made for some items of data and so it is possible to test the internal consistency of the 2200 m/sec measurements and also of the thermal Maxwellian measurements. The consistency between the 2200 m/sec and the thermal Maxwellian values can also be examined. The measured values depend on other items of data. For example, the assumed half-lives. The Pu239 half-life has been revised in the past few years and this affects the Pu239 thermal cross-section values because foil masses are determined by α-decay assaying. The shape of the Cf252 spontaneous fission spectrum also has an influence because ν values are measured relative to Cf 252 and the fission spectrum shape affects the detection efficiency.

The fits to the 2200 m/sec and thermal Maxwellian measurements reported in Lemmel's paper are given in Table 3.2

	Fit to 2200 m/sec measurements	Fit to thermal Maxwellian data	Difference
σ_f			
U233	532.6 ± 3.0	528.6 ± 3.6	4.0
U235	587.7 ± 1.9	578.7 ± 4.0	9.0
U233/U235	0.906 ± 0.005	0.913 ± 0.003	0.007
Pu239/U235	1.269 ± 0.007	1.288 ± 0.006	0.019
$1 + \alpha$			
U233	1.080 ± 0.006	1.090 ± 0.001	0.010
U235	1.157 ± 0.006	1.172 ± 0.001	0.015
ν			
U233	2.469 ± 0.008	2.503 ± 0.021	0.034
U235	2.403 ± 0.006	2.451 ± 0.019	0.048

Table 3.2 Fits to 2200 m/sec and thermal Maxwellian measurements

The 2200 m/sec and thermal Maxwellian data are separately consistent but there are some significant differences between them, particularly for the uranium isotopes. These differences could be due to errors in the shapes of cross-sections at thermal energies or in the shapes of the thermal spectra.

There are other indications of possible discrepancies in the shapes of cross-sections at thermal energies. Changes in reactivity resulting from changes in the thermal spectrum, caused by changes in moderator temperature (or coolant density) are not well predicted. In order to improve predictions the shapes of cross-sections have been changed. Tellier (22) has reported that an adjustment to the shape of the U238 capture cross-section at thermal energies results in improved predictions. An alternative approach is to change the shape of the eta curve for U235.

High accuracy measurements ($\sim$ 0.3%) of the shapes of the U238 capture cross-section and eta values for fissile isotopes through the thermal energy range are considered to be important requirements.

U238 resonance integrals in reactor lattices

There has been a long-standing discrepancy in the prediction of U238 resonance integrals in reactor lattices, with calculation giving higher values than are measured. In recent years the values of the measured capture widths of the lowest energy resonances have been significantly lower than earlier measured values. Tellier (23) has made calculations using a recent evaluation of the resonance parameters together with the Reich-Moore resonance formalism. He concludes that the data are now in satisfactory agreement with the lattice measurements. He also shows that use of the single-level Breit-Wigner resonance formalism is not sufficiently accurate.

U238 capture in fast reactor critical experiments

Analyses of fast reactor critical experiments using ENDF/B-V show an over-estimate of U238 capture/U235 fission rate measurements of about 8% and so this long-standing discrepancy remains.

Prediction of some thermal reactor lattice parameters

A comparison of ENDF/B-IV and ENDF/B-V predictions of parameters measured in the TRX 1 and 2 thermal reactor lattices is reported in ref (24). These benchmarks are H_2O moderated, 1.3% enriched uranium fuelled lattices, with water/fuel volume ratios of 2.35 and 4.02 respectively. The measured and calculated values are compared in Table 3.3 It will be seen that the values of K, U238/U235 fission ratio and conversion ratio C are accurately predicted. However the ratio of epithermal to thermal U238 capture is not well predicted.

3.6 Nuclear Data Requirements

Procedure for determining differential nuclear data requirements taking into account integral measurements

Bobkov, Pyatnitskaya and Usachev (10) have proposed a procedure for determining cross-section accuracy requirements to meet a set of reactor parameter target accuracy requirements when the accuracies achieved,or achievable,in a set of relevant integral measurements is known.

It is assumed that a set of discrete nuclear data parameters, for which the measurement uncertainties are uncorrelated, can be identified and that the relative measurement costs equal λ_i/e_i^2 (and the factors, λ_i, can be estimated). The accuracy requirements must be derived from the conditions:

$$\left.\begin{aligned} &M = \sum_i (\lambda_i/e_i^2) \quad \text{is a minimum} \\ &\text{subject to the conditions} \\ &\sum_i \sum_j S^P_{m,i} \cdot S^P_{m,j} \cdot V^A_{i,j} \ll (t_m)^2 \\ &\text{and} \\ &0 < e_i^2 \leq e_{io}^2 \end{aligned}\right\} \quad (82)$$

where e_{io} is the currently achieved uncertainty.

The variance $V^A_{i,j}$, is a complex function of the values of e_i and the integral measurement sensitivities and uncertainties. A procedure is described for solving this problem which involves the penalty function method. Bobkov et al also give examples of the resulting cross-section accuracy requirements for predicting K and the breeding ratio of a fast reactor.

At present the task of calculating sensitivities for all the reactor parameters of interest and then carrying out the above procedure is such an enormous undertaking that it is probably not justified. It is probably sufficient to take the results obtained by Bobkov et al as giving an indication of the changes in requirements consequent upon using integral data and use some simpler

considerations to decide on the differential nuclear data requirements. We must also consider whether it is satisfactory for the integral and differential measurements to be complementary or whether we require the extra confidence that is obtained if they both are sufficiently accurate to predict the reactor properties to the required accuracy. A high level of confidence is required for the prediction of key safety parameters.

Choice of accuracy requirements

How, then, should the accuracy requirements be decided? Sensitivity studies are a necessary preliminary. These show the important parameters and the order of accuracies which are useful. Discussions between reactor physicists and nuclear data measurers about potential worthwhile improvements in the accuracies of prediction (and gaps in knowledge) and the possibilities of achieving them provide one way of deciding requirements. This is the way requirements are chosen at Consultants and Specialists Meetings. New measurements can be required to resolve inmportant discrepancies between different measurements (both integral and differential). These different assessments of the requirements are considered by National Nuclear Data Committees who then decide on the measurement programmes to be supported.

IAEA Advisory Group Meetings

1st Fission Product Nuclear Data. Bologna 1973 IAEA-169

2nd Fission Product Nuclear Data. Petten 1977 IAEA-213

1st Transactinium Isotope Nuclear Data Karlsruhe (1975) IAEA-186

2nd Transactinium Isotope Nuclear Data Cadarache (1979) IAEA-TEC DOC-232

IAEA Consultants Meetings

Prompt Fission Neutron Spectra (1971)

Integral Cross-Section Measurements in Standard Neutron Fields for Reactor Dosimetry (1976)

Delayed Neutron Properties (1979)

U/Pu Resonance Parameters (1981)

Brookhaven National Laboratory Specialists Meetings

Seminar on U238 Resonance Capture (1975) BNL-NCS-50451.

Nuclear Data for Plutonium and Americium Isotopes for Reactor Applications (1978) BNL-50991

NEA Specialists Meetings

Neutron Capture in the KeV Energy Range in Structural Materials for Fast Reactors Karlsruhe (1973) NEANDC-U-98

Fast Neutron Fission Cross-sections - Argonne (1976) ANL-76-90

Neutron Cross Sections of Fission Product Nuclei - Bologna (1979) NEANDC(E)-209L

Nuclear Data and Benchmarks for Reactor Shielding - Paris (1980)

Conferences

Europe. Neutron Physics and Nuclear Data - Harwell (1978)
USA Knoxville Conference (1979) USSR 5th Kiev Conference (1980)

Table 3.1 - Examples of Recent Specialist Meetings and Conferences on Nuclear Data for Fission Reactor Applications

TABLE 3.3
MEASURED AND CALCULATED
TRX LATTICE PARAMETERS

TRX 1	Measured	ENDF/B-IV	ENDF/BV	TRX 2	Measured	ENDF/B-IV	ENDF/BV
k_∞	-	1.1612	1.1726		-	1.15062	1.1608
k_{eff}	1.0000	0.9888	0.9972		1.0000	0.9909	0.9981
M^2	-	30.58	30.84		-	29.46	29.79
$B^2(m^{-2})$	57.00	-	-		54.69	-	-
ρ^{28}	1.32 ± 0.021	1.415	1.400		0.837 ± 0.016	0.881	0.870
δ^{25}	0.0987 ± 0.0010	0.1018	0.1013		0.0614 ± 0.0008	0.0623	0.0621
δ^{28}	0.0946 ± 0.0041	0.0952	0.0984		0.0693 ± 0.0035	0.0681	0.0707
CR	0.797 ± 0.008	0.815	0.812		0.647 ± 0.006	0.653	0.651

Measured lattice parameters are defined as follows:
The cut-off between epithermal and thermal region is 0.625 eV.
ρ^{28}: the ratio of epithermal-to-thermal U-238 captures
δ^{25}: the ratio of epithermal-to-thermal U-235 fissions
δ^{28}: the ratio of U-238 fission to U-235 fissions
CR: conversion ratio, the ratio of U-238 captures to U-235 fissions.

Section 4 - Energy production, radiation emission, induced radioactivity and irradiation damage

4.1 Introduction

Important products of neutron-nuclear interactions are the energy release, the radiation emissions, the reaction products (some of which are radioactive) and the irradiation damage of materials. The major sources of energy are fission reactions but the contributions from other reactions are also significant. The majority of the energy released in fission is in the form of fission product recoil energy and this is deposited close to the point of fission (within about 10 microns). The kinetic energy of the fission neutrons and the energy of the γ -rays can be deposited over a wide region (1 m). Not all of the fission energy is emitted promptly; a significant proportion is emitted as β and γ energy resulting from the radioactive decay of fission products (predominantly by β decay). This is called fission product decay heating. This component of heating is important in connection with emergency core cooling, heat removal in the shut-down reactor and the design of fuel transfer and transport flasks. A knowledge of the energy transferred to materials by neutron scattering and γ ray interactions is required in the design of cooling for moderators, control elements, reflector regions, fast reactor breeder regions and experimental rigs in reactors. Shielding must be provided for biological protection from neutrons and γ-rays and also to protect components from irradiation damage. Damage mechanisms include atomic displacements resulting from nuclear recoils in scattering reactions and in γ-emission, and helium production in (n,α) reactions. Shielding is also required when handling radioactive materials.

Dosimetry is the measurement of the time (and energy spectrum) integrated flux, or neutron dose. The dose is sometimes considered in terms of the damage flux or flux above 100 KeV. Dosimetry monitoring reactions are those which result in a suitable radioactive product, the suitability depending on the half-life, detectability and the energy spectrum to which they are senistive. Threshold reactions and reactions with prominant resonances have the advantage that they give a measure of the integral flux above the threshold energy or the flux at the resonance energy. By using a set of dosimetry reactions both the total flux and the energy spectrum can be derived, and hence the damage effects predicted. Dosimetry is used to monitor the doses that irradiated components have experienced. This is required both when correlating the measured material damage with the dose and also when checking the dose to which structures have been exposed.

The radioactive decay of transactinium isotopes makes a contribution to the decay heat following reactor shut-down and in fuel transport. Spontaneous fission and (α,n) reactions provide a source in a shut-down reactor which can be used when monitoring the reactivity of the core. If the source is known and the flux is measured then the reactivity can be derived and the approach to critical monitored. The radioactive decay must also be allowed for in the design of transport flasks and reprocessing plant studies. The decay of the curium isotopes, Cm242 and Cm244, are important in fuel which has undergone a long irradiation. The routes leading to the product of these curium isotopes are shown in Figure 4.1.

4.2 Heating

Values for the components of the energy released in fission (based on the data of Sher (25)) are given in Table 4.1. The prompt components comprise the fission fragment kinetic energy, the prompt neutron kinetic energy and the prompt gamma energy. The delayed components are the beta particle energy and the delayed gamma energy resulting from fission product decay. (The small delayed neutron component has been neglected.)

Table 4.1 - Energy released in fission (in MeV)

	U235	Pu239	U238
Fragment kinetic energy	169.1±0.5	175.8±0.1	166.6±0.5
Prompt gamma	7.0±0.5	7.8±0.2	6.5±0.5
Neutron kinetic energy	4.8±0.1	5.9±0.1	5.5±0.1
Delayed gammas	6.33±0.05	5.17±0.06	8.02±0.07
Beta	6.50±0.05	5.31±0.06	8.25±0.08
TOTAL (minus antineutrinos)	193.7±0.7	199.9±0.4	194.8±0.8

The accuracy of the total energy released in fission is higher than ±0.5% and the accuracy of the gamma component is higher than ±10%. Although the accuracies assessed for the delayed gamma and beta components are high ($\sim$ 1%) the time dependence of the decay heating is not so accurately known, this accuracy being, typically, ±5%.

In addition to the total gamma energies the gamma spectra are required. This is because the gamma energies determine the migration distances and also the probabilities for (γ,n) and (γ,f) reactions. Gamma spectra are stored in nuclear data libraries and converted into group form for reactor calculations. Coupled neutron-gamma cross-section sets are produced and used in coupled neutron-gamma flux and energy deposition calculations.

Fission product decay heating

Heat generated by fission product decay is calculated by summing the contributions from individual fission products. Summation codes, such as ORIGEN (26), FISPIN (27) and FISP (28) are used for these calculations. The data libraries they require contain fission product yields, and decay data (the half-lives, beta and gamma total energy yields and gamma energy spectra). Examples of such data libraries are given in references (29) and (30). Fission product capture reactions can have a significant effect on decay heating in some reactors and the above codes are capable of treating these effects in a simple way, using few group cross-sections and fluxes. These reactions tend to increase the total decay heat by a few percent. For applications where fission product capture effects can be neglected the decay heating can be represented by a sum of exponentials. About 20 exponentials are required to give an accuracy of 1% over the time range of interest in reactor operations.

The decay power at a time t sec following a single fission is denoted by m(t) and the decay power per fission at time t sec following an infinitely long irradiation is denoted by M(t). The decay power t seconds after an irradiation of 1 fission per second lasting for I seconds is

$$M(I,t) = \int_{t}^{I+t} m(t')dt' = M(I) - M(I+t) \qquad (83)$$

The accuracy of fission product decay heating data has been assessed in two ways. The sensitivity of the summation calculations to changes in yield and decay data have been calculated and combined with estimates of the uncertainties in these (31). The uncertainties estimated for M(t), the decay heat following a long irradiation, are about ±3% for U235 and Pu239. The uncertainties in m(t), the decay heat following a single fission, are larger, particularly at short times following the fission. They are then in the range ±5% to ±10% for times less than 100 secs. There are larger uncertainties for these short decay times because of the uncertainties in the beta and gamma energy yields of short lived fission products. Nuclear theory is used to provide some of these data, an example being the work of Yoshida (31). The accuracies of the data are also assessed by comparing with measurements of total heating as a function of time and also of the separate beta and gamma heating components. The techniques used are calorimetry, and β and γ ray detection. The agreement between these measurements

and the calculations is not as good as the summation calculation sensitivity studies suggest . The summation calculations tend to be about 5% to 10% lower than the total heat measurements for Pu239, but there are also discrepancies between the different total heat measurements. Work is in progress in several countries to try to resolve these discrepancies.

The difference between fission product decay heat for fission in thermal snd fast reactors is calculated to be small (< 2%). The differences in fission product yields between thermal and fast reactor spectra are small but not well known. However, this source of uncertainty is not considered to be important and it is not unusual to use thermal neutron fission yields in fast reactor decay heating calculations.

At times of the order of 10^7 secs (116 days), when fast reactor fuel might be transported for reprocessing, just a few fission products contribute to the total decay heat. The percentage contributions are given in Table 4.2.

Table 4.2 - Fission products contributing to decay heating at 10^7 secs

Fission product chain	Percentage of total fission product decay power
Rh106 + Ru106	30
Zr95 + Nb95	30
Ce144 + Pr144	24
Ru103	5
Y91	4
Sr89	1
Remainder	6

Table 4.3 - Decay heat in a PWR as a percentage of full power output

Time after shutdown (secs)	Low burn up fuel		High burn up fuel	
	Fission Products	Actinides	Fission Products	Actinides
0	6.1	0.22	5.6	0.34
10	4.3	0.22	4.1	0.34
100	2.7	0.22	2.7	0.33
1000	1.5	0.17	1.6	0.27
10000	0.6	0.09	0.8	0.16

Actinide decay heating

At short times the actinide decay heating following the shut-down of a power reactor arises predominantly from the decay of U239 (1,410 secs) and Np239 (2×10^5 secs). This component varies with fuel burn-up because of the variation of the number of U238 captures per fission. Relative values of actinide decay heat and fission product decay heat at short times following shut-down in a PWR are illustrated in Table 4.3.

Components of the decay heating in fast reactor fuel are shown in Fig. 4.4 Alpha decay of Cm242 (1.41×10^7 secs) makes a significant contribution at longer decay times. This arises from neutron capture in Am241 produced by the decay of Pu241 (14.6 year). The fraction of Am241 in the fuel depends on the length of time for which it was stored between the abstraction of plutonium from irradiated fuel and the loading of the plutonium in the reactor. The sensitivity of actinide decay heating in fast reactor fuel to nuclear data uncertainties has been studied by Patrick and Sowerby (32). They conclude that improved data are required for the Am241 (n,γ) cross-section (an accuracy of $\pm 8\%$).

Structural material decay heating

Heat is generated in the steels of the fuel pin cladding and the subassembly wrapper of a fast reactor fuel subassembly by the decay of radioactive products. This component of the decay heating does not exceed 10% of the total decay heating at any time. Integral measurements have been made of the activity induced in structural materials and these enable this component to be predicted to an accuracy of about $\pm 10\%$.

TABLE 4.4

Spectrum Averaged Energy Yield Cross Sections

(MeV x barns)

Substance	Point Energy Deposition					Gamma Energy Yield			
	Elastic Scattering	Inelastic Scattering	Capture	Fission	TOTAL	Inelastic Scattering	Capture	Fission	TOTAL
B10	0.163	0.002	6.059	-	6.224	0.007	1.063	-	1.070
B11	0.182	0.002	-	-	0.184	0.007	-	-	0.007
C	0.166	0.001	-	-	0.167	0.006	-	-	0.006
O	0.137	-	-0.002	-	0.135	0.002	-	-	0.002
Na	0.156	0.012	-	-	0.168	0.078	0.013	-	0.091
Fe	0.030	0.007	-	-	0.037	0.163	0.085	-	0.248
Eu	0.020	0.009	-	-	0.029	0.440	15.034	-	15.474
Ta	0.013	0.010	-	-	0.023	0.622	5.594	-	6.216
U238	0.013	0.006	-	9.657	9.657	0.554	1.590	0.870	3.014
Pu239	0.011	0.004	-	320.04	320.05	0026	2.928	24.57	27.759

4.3 Energy yields and energy deposition

Energy yield cross-sections averaged over a fast reactor core spectrum are given in Table 4.4 The point energy deposition is the kinetic energy of fission product nuclei, nuclear recoil following neutron scattering and the energies of α and β emissions. The gamma energy yield arises from inelastic scattering, (n, γ) reactions, other capture reactions (in association with other emissions such as α -particles) and from fission. The main sources of energy are fission and capture in the fuel isotopes. The energy produced by capture in the fissile isotopes is about 1% of the energy produced in fission and the energy produced by capture in the principal fertile isotope (U238) is about 2% of the total energy. Thus capture reactions contribute only about 6 MeV in a total of about 200 MeV per fission. A high accuracy is therefore not required for this capture component when calculating the total heating.

The gamma energy is of more importance in calculations of energy deposition distributions;for example, for calculating the temperatures of samples in an experimental rig in a reactor. Such a rig might contain samples of structural materials which are undergoing irradiation endurance testing. Irradiation effects are dependent on material temperatures. The main source of heating in many cases is the prompt and delayed γ-rays from fission (the two components being of about equal importance). To calculate this heating the gamma spectra must be known because this determines both the gamma migration distance and the energy deposition. The data in cross-section libraries cannot always be relied upon to represent the gamma energy yields and spectra accurately and they should be examined before being applied.

Table 4.5 gives values for the gamma energy deposition in the different materials of a fast reactor.

Table 4.5 - Gamma energy deposition rates in a fast reactor flux of $10^{15}/cm^2sec$

Material	Watts/gm	Watts/ml
Sodium	4.6	3.9
Steel	4.8	38.4
Pu-UO_2 Fuel	11.5	127.1
B_4C	4.5	11.3

The relative energy deposition rates in the materials of a fast reactor core subassembly are given in Table 4.6

Table 4.6 - Energy deposition in the materials of a fast reactor subassembly

(watts per ml of subassembly volume)

	Point Energy	Gamma Energy	Total	(Gamma Yield)
Sodium	2	3	5	(1)
Steel	1	16	17	(7)
Pu-UO_2	689	64	753	(75)
TOTAL	692	83	775	(83)

Only about 3% of the energy is deposited outside the fuel and about a half of this is deposited in the fuel cladding.

4.4 The radioactivity of irradiated fuel

Kusters (33) has reviewed the status and requirements for nuclear data relating to the radioactivity of irradiated fuel. He focuses attention on routes for the production of Pu238, Cm242 and Cm244 because of their strong γ activity and neutron sources from spontaneous fission and (α, n) reactions. In a thermal reactor production of Pu238 is mainly by the route U236 (n,γ) Np237 (n,γ) Pu238. In the fast reactors studied by Kusters α-decay of Cm242 and the route U238 (n,2n) Np237 (n,γ) Pu238 are more important sources of Pu238. For the production of Cm242 the capture cross-sections of Am241 leading to the ground and isomeric states of Am242 are required and the Pu242 (n,γ) and Am243 (n,γ) cross-sections are required for the calculation of the production of Cm244. The (n,2n) cross-sections of both U238 and Pu239 are required for fast reactor inventory calculations.

Measurements of the compositions of irradiated fuel elements provide a check on the nuclear data and can also be analysed to provide spectrum averaged data suitable for fuel inventory calculations. By adjusting cross-sections the discrepancies in predictions for an LWR have been reduced to a few percent in a French study (34) . However Kusters concludes that more analyses are needed to assess the uncertainty margins in predictions and there is a need to improve some current nuclear data libraries. Spent fuel analysis is also of high importance in nuclear safeguards investigations. A method called the isotopic correlation technique, which correlates measured isotopic ratios with fuel burn-up and plutonium content is being evaluated as a potential way of monitoring plutonium production.

Neutron output from irradiated fuel

In their assessment of the accuracy requirements for higher actinide nuclear data to predict the heating and neutron output of irradiated fast reactor fuel Patrick and Sowerby (32) point out that although any study is dependent on a number of factors (such as the reactor type, the fuel cycle strategy and the ground rules leading to the required accuracies in the fuel parameters), the results provide a useful starting point for discussions on other aspects of requirements. Their study relates to a particular fuel composition, storage time before loading into the reactor and required accuracies as a function of cooling time. One requirement is to predict the neutron source in the shut-down reactor so that flux measurements can be used to monitor reactivity. The other requirement is for design of shielding for spent fuel transport and reprocessing. The main neutron sources are Cm242 decay at shorter times and Cm244 decay at longer times. The nuclear data parameters leading to the production and loss of these isotopes are the ones in need of improvement.

To improve predictions at shorter times more accurate data are needed for Am241 (n,γ) Am242g, Cm242 (n,f) and the spontaneous fission branching ratio. Since the fission cross section of Cm242 cannot be measured (because of the high background activity) improved nuclear theory methods are required. To improve the accuracy of predictions at longer times more accurate values of the Pu242 (n,γ) and Am243 (n,γ) cross-sections are needed.

4.4 Simple methods for calculating reaction rates in thermal reactors

When a high accuracy is not required in the estimation of reaction rates in a thermal reactor a simple few parameter representation of the neutron spectrum

is acceptable. This can be used, for example, for calculating the arisings of higher transactinium isotopes, reactions in fission product isotopes and the activation of coolant and structural materials. The spectrum is represented by three components, the thermal flux, ϕ th, the epithermal flux, ϕ_e, and the fast flux, ϕ_f. The effective temperature of the thermal flux, Teff, must also be specified, and in some more refined treatments, the departure of the epithermal flux from a (1/E) dE form is taken into account. The exponent of E is taken to be $-(1+\alpha)$, instead of -1.

The cross-sections are characterised differently depending upon whether they occur at thermal energies or only above a high energy threshold. For a reaction which occurs at thermal energies the 2200 m/sec cross-section, σ_0, the g factor as a function of Teff, the resonance integral, Io, and a factor which depends on the exponent α, $f(\alpha)$, are required. The calculation of g(Teff) and $f(\alpha)$ requires a knowledge of the shape of the cross-section through the thermal energy region and the resonance region. However, when these have been calculated the values of σ_0 and I_o can be adjusted by fitting to a range of integral measurements. For threshold reactions the fast flux averaged value can be related to a U235 fission spectrum averaged value of the cross-section or a standard spectrum averaged value. The ratio of the average in the standard spectrum to the average in the reactor fast spectrum is assumed constant for all threshold reactions.

4.6 Activation of structural and coolant materials

The build-up of strong gamma emitters within the coolant circuit and on reactor components causes maintenance problems. The predominant gamma activity in the coolant circuits of light water reactors arises from the decay of Co58 and Co60. These are reaction products which result from trace quantities of cobalt and nickel which are dissolved into the coolant from components in the primary coolant circuit, activated in the core and then plated out in various parts of the circuit, such as the pumps and heat exchangers.

Integral measurements of reactions which lead to such strongly radioactive products can be readily measured in low power facilities, as well as in experiments made in power reactors (or samples taken from the reactor). Integral measurements made in zero power critical facilities have an accuracy, typically, of $\pm$5% and they can be used to predict the reaction rates in power reactors to an accuracy of $\pm$10%, which is considered to be a satisfactory accuracy. However, measurements should also be made in power reactors to check on the importance of competing reactions in the isotopes and the burnup of the radioactive products. Two-stage reactions, and reactions less easily measured in zero power facilities (such as (n,n'p) which only occurs at high neutron energies) can also be found in this way.

Some of the more important reactions in fast reactor structural materials are listed in Table 4.7, together with the cross-sections for the reactions in a fast reactor core spectrum.

Table 4.7 - Structural material activation cross-section in a fast reactor spectrum

Isotope	Percentage Abundance	Reaction	Reaction Product	Half-Life	Cross-Section (mbarns)
Cr50	4.35	(n,γ)	Cr51	27.7 days	31
Mn55	100	(n,γ)	Mn56	2.58 hrs	70
Mn55	100	(n,2n)	Mn54	312 days	0.03
Fe54	5.8	(n,p)	Mn54	312 days	10.5
Fe54	5.8	(n,α)	Cr51	27.7 days	0.08
Fe58	0.31	(n,γ)	Fe59	45.1 days	9.8
Co59	100	(n,γ)	Co60	5.27 yrs	54
Ni58	67.76	(n,p)	Co58	70.8 days	14.5
Ni60	26.42	(n,p)	Co60	5.27 yrs	0.25

The activity induced in the sodium coolant of a fast reactor is also of concern. The reactions Na23 (n, γ) Na24 (15hr) and Na23 (n,2n) Na22 (2.6 years) are important, as is the activity induced in trace contaminants in the coolant, such as K41(n,p) Ar41 (1.8 hr).

For the prediction of activation reactions in a thermal reactor a simple representation of the flux spectrum can be sufficient because a high accuracy is not required.

4.7 Irradiation damage effects and dosimetry

Atomic displacement damage in structural materials is a function of the nuclear recoil energy, Er, the temperature and the presence of nucleation sites for void formation, such as helium (resulting from (n,α) reactions). The recoil energy must exceed a threshold energy, E_T, for the atom to be displaced. For recoil energies higher than E_T the number of displacements is approximately equal to E_R/E_T but is less than this number by a factor which increases with increasing recoil energy. There are different models for calculating the number of displacements, one such model being called the NRT Model (Norgett, Robinson and Torrens (35)). This has been adopted for international reference use. Having chosen a model the displacement cross-section can be calculated. It is equal to

the sum of the cross-sections for each reaction times the number of displacements for the corresponding recoil energy. For example, the elastic scattering component of the displacement cross-section is:

$$\sigma_d^I(E) = \int \sigma_{el}^I(E \rightarrow E') \; N_d^I(E_r(E,E',A))dE' \qquad (84)$$

The recoil energy, $E_r(E,E',A)$, is a function of the incident and emergent neutron energies and the mass of the nucleus. The number of atomic displacements depends on the element, I, and also on the particular alloy. However, this dependence on the alloy is usually neglected and a displacement cross-section for iron is calculated which is used for iron in all different types of steel. The variation of E_T with alloy is not so great as to be significant compared with other sources of variability in the effects of atomic displacements.

The (n,γ) reaction contributes to the atomic displacement cross-section because of the nuclear recoil which occurs when the γ rays are emitted. Other reactions also contribute. In particular, inleastic scattering, (n,p) and (n, α) reactions. Atomic displacement cross-sections have been calculated for a number of structural material elements by Doran and Graves (36) and the data are available in a fine energy group form (the SAND II 640 group structure).

Helium embrittlement is another structural material damage mechanism. Helium is produced in (n,α) reactions. Trace quantities of boron and nitrogen in structural materials can make a major contribution to the helium production. Consideration must also be given to (n,α) reactions in isotopes which are formed as a consequence of irradiation; for example

Ni58 (n,γ) Ni59 (n,α)

Integral measurements of (n,α) reactions in structural materials have been made by irradiating samples in power reactors and measuring the helium produced. Trace quantities of elements such as boron and nitrogen can introduce uncertainties into the results. Uncertainties in the shapes of reactor neutron spectra at high energies can also result in uncertainties in derived data. It is usual to derive equivalent U235 fission spectrum averaged values from these measurements by applying a calculated factor. These are the results quoted, for example, by Gryntakis (37). For Fe the values differ by ± 30 from the mean value and this uncertainty is larger than the required accuracy of $\sim \pm 15\%$.

Irradiation has an effect on a graphite moderator. Neutron and gamma irradiation can enhance reactions between the graphite and carbon dioxide coolant resulting in a loss of structural strength of the graphite. At low temperatures energy can be stored in the graphite and an increase in temperature can result in the release of this Wigner energy which leads to a further increase in temperature. Graphite irradiation damage results in stress problems, with swelling or shrinkage depending on the conditions.

Dosimetry

Irradiation exposure can be monitored by dosimetry reactions. Foils or detectors are positioned at the point where the dose is to be measured and they are removed following the irradiation and the induced activity is measured. This induced activity depends on the cross-section for the reaction, the time history of the flux, the rate of decay of the activity and the rate of burnup of the primary isotope and the activation product. The activity must be sufficiently strong to be accurately measurable, sufficiently long lived to measure the dose over the time period of interest and the absorption cross-sections of the isotope and the activation product must be sufficiently small for burnup to be negligible or to be a correction which can be accurately made. Dosimetry reactions suitable for different applications have been subject to review and international meetings are held periodically. These include the ASTM and EWGRD (Euratom Working Group on Reactor Dosimetry) series of meetings.

The chosen dosimetry reactions are compiled in an IAEA recommended International Dosimetry File, which is an extended version of the ENDF/B-V Dosimetry File. Standardisation is important because the measured information on irradiated damage effects is often correlated with dosimetry reaction dose measurements. The derived damage cross-sections are less accurate than the correlated data because of uncertainties in the dosimetry cross-sections used to deduce the flux and flux spectrum of the irradiation. By standardising the dosimetry cross-sections and measuring doses using the same dosimetry reactions the materials damage can be deduced more accurately.

Integral measurements of the dosimetry reactions in standard neutron spectra (or benchmark fields) are used to evaluate the differential cross-sections and, if appropriate, to adjust them, and also adjust the reference benchmark fields. These benchmark fields include the Cf252 spontaneous fission neutron spectrum, the thermal neutron induced U235 fission neutron spectrum and a number of well characterised spectra (38).

The types of dosimetry reaction can be divided into fission and non-fission, threshold and non-threshold. The choice of the set of reactions to be used for a

particular application depends on the intensity of the flux, the duration of irradiation, the type of reactor spectrum (thermal reactor, fast reactor, core, shielding, vessel) and the neutron energy range of importance. In the case of fission reactions used for dosimetry in a power reactor the fraction of particular fission products present in the foil can be used to measure the number of fissions. The burn-up of fuel can also be measured in this way. Such measurements can be made either by mass spectrometry or by radiation detection. When the radioactive decay of an activation product is measured the half-life, and gamma spectrum (or gamma energy line and branching fraction) must be known accurately, as well as cross-section.

D L Smith (39) has reviewed the status of the non-fissile threshold reactions in the ENDF/B-V Dosimetry File, and the agreement between integral measurements and calculated values. For a number of these reactions the integral measurements in a Cf252 fission spectrum and the calculated values have an accuracy of better than ± 3%,and they are consistent. The decay data are also satisfactory for these reactions. For some reactions improved measurements are required. Zijp (38) has reviewed the nuclear data requirements for dosimetry on behalf of the EWGRD.

Important requirements are considered to be measurements of the cross-sections for the reactions Nb93 (n,n')m, and Np237 (n,f) and the averages in a U235 fission spectrum of the reactions Al27 (n, α), Ni58 (n,p), In115 (n,n')m and the ratio U238 (n,f)/U235 (n,f).

Measurements of the spatial distribution of gamma energy deposition are made in experimental critical assemblies using thermoluminescent dosimeters. These are also sensitive to β-particles and to the neutron flux. The assumption that β-particle energy is deposited at the point of production cannot be made in the interpretation of these measurements. The migration of β-particles is usually calculated using a Monte-Carlo tracking method. The interactions of gamma rays with matter are more accurately known than the gamma energy sources and spectra. Consequently these measurements provide a check on the gamma source data and the methods used for calculating the gamma flux from the source. Gamma interactions are strongly anisotropic and Monte-Carlo tracking calculations are made when accurate predictions are required. More approximate methods, including equivalent diffusion theory methods, which involve the derivation of effective gamma diffusion coefficients, are used in simplified design methods.

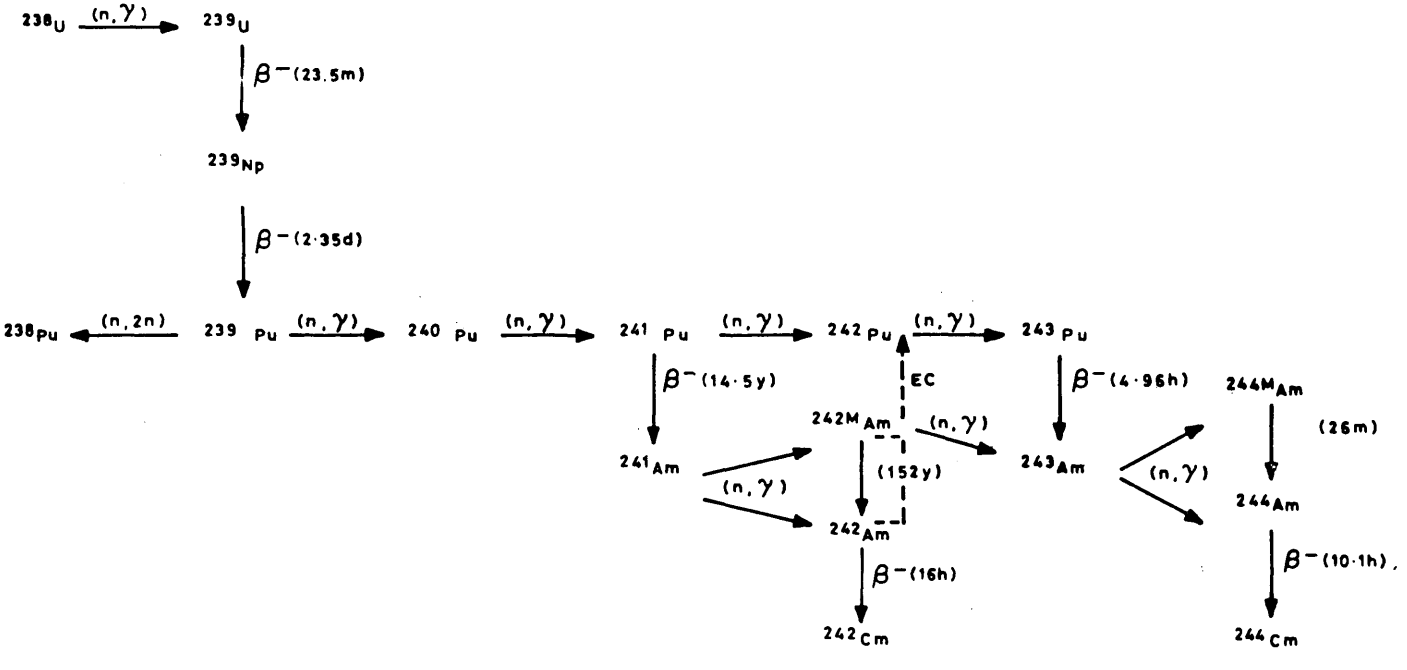

FIG 4.1

THE MAJOR ROUTES FOR THE PRODUCTION OF AMERICIUM AND CURIUM ISOTOPES

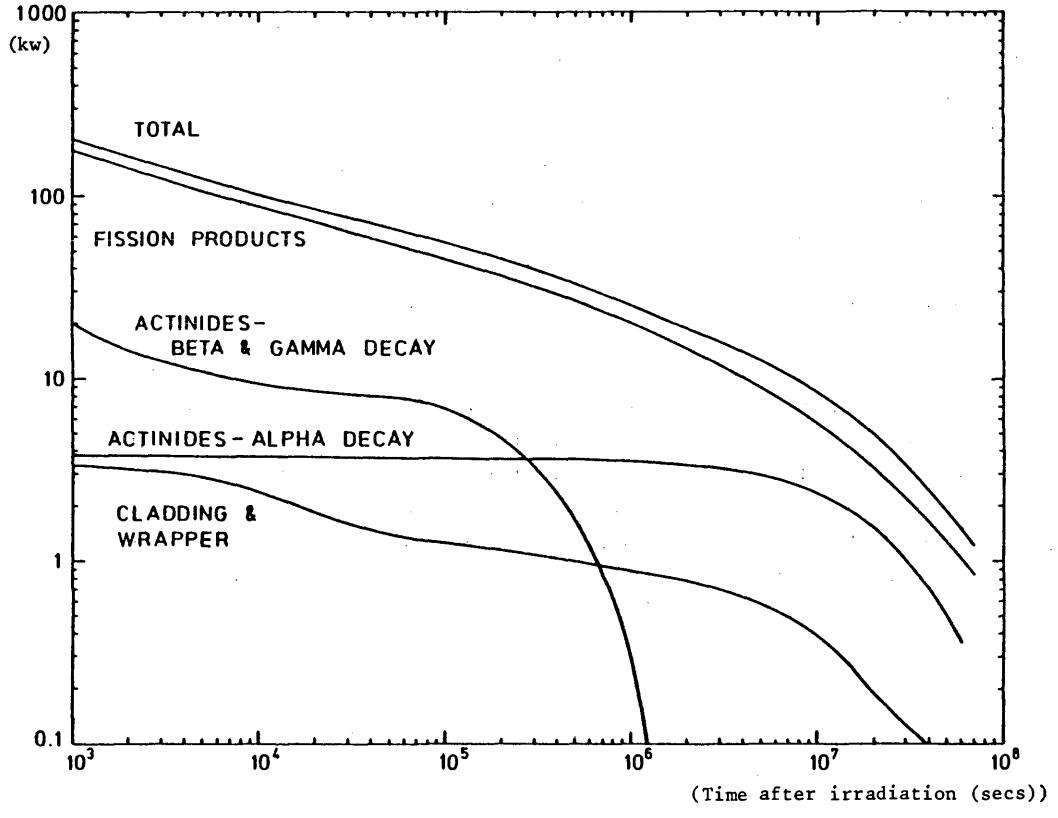

Fig. 4.2 - Decay power of a fast reactor subassembly

Section 5 - Kinetics characteristics of reactors and reactor control

5.1 Introduction

Reactor power output is proportional to the fission rate, which is approximately proportional to the total neutron flux. The shape of the neutron flux spectrum changes as the power changes (because of the associated temperature and density changes) and this affects the relationship between fission rate and total neutron flux to a certain extent. The relationship between reactor power and fission rate can also change slightly if the proportion of fissions in different isotopes changes with the change in spectrum and also if the neutron capture contribution changes.

When the power increases the temperatures of the fuel, coolant and moderator increase. These changes result in a reduction in the reactivity of the core. To raise power it is necessary to add reactivity and this is usually done by reducing the amount of control absorber in the core, either by withdrawing absorbing control elements or by reducing the amount of soluble poison in the coolant (or chemical shim). Chemical shim is usually used only to compensate for the slow changes in the reactivity of the fuel associated with burn-up. Control elements can be inserted rapidly to shut a reactor down from power.

The temperature coefficient of reactivity for component i is defined as

$$C_i^T = \frac{1}{K} \frac{\partial K}{\partial T_i} \qquad (85)$$

The coefficients for the fuel, C_f^T, the moderator, C_m^T, and the coolant, C_c^T, must be considered separately because of the differences in the rates at which the temperatures of the fuel, moderator and coolant change in response to a change in power. Also of importance is the coolant pressure coefficient and the effect of coolant voiding. The power coefficient of reactivity is the change in reactivity with power as a fraction of full power:

$$C_i^P = \left(\frac{P}{K} \frac{\partial K}{\partial P}\right)_i \qquad \text{associated with compoment i} \qquad (86)$$

The delayed neutrons influence the rate of change of power with change in reactivity. The "effective delayed neutron fraction" is defined to allow for the fact that delayed neutrons have a different probability of causing a fission than have prompt neutrons. This is because of the lower mean energy of delayed neutrons, which is below the threshold for fission in U238. They thus do not contribute to the fast fission factor (as distinct from the fast plus epithermal factor, which is, sometimes, also called the fast fission factor). The effectiveness of a neutron in continuing the fission chain reaction is expressed in terms of the neutron importance, or adjoint neutron flux, $\phi^*(E,x)$. This is the probability of a neutron contributing to the asymptotic fission source distribution. Calculation of the neutron importance involves solving equations which are a transposition of the equations for calculating the neutron flux.

Perturbation theory methods of calculating the change in reactivity resulting from a change in cross section involve the flux and the neutron importance. For

example, the change in reactivity resulting from an increase in a macroscopic absorption cross-section, $\delta\Sigma_a(E,x)$, is, to first order:

$$\delta\rho = -\frac{1}{N}\iint \delta\Sigma_a(E,x)\ \ \phi(E,x)\ \ \phi^*(E,x)\ dE\ dx \qquad (87)$$

where $N = \iiint \nu\Sigma_f(E,x)\ \chi(E',x)\ \ \phi(E,x)\ \ \phi^*(E',x)\ dE\ dE'\ dx$ (88)

The expressions for scattering cross-sections and fission cross sections, ν,Σ_f and χ, involve the change in neutron importance associated with the change in scattering, and the difference between the importance of the neutrons causing fission and those produced in fission.

For example, for moderation:

$$\delta\rho = \frac{1}{N}\iint\delta\Sigma_s(E \to E',x)\ \phi(E,x)\ (\phi^*(E',x) - \phi^*(E,x))dEdE'dx \qquad (89)$$

Changing a scattering cross-section also changes the leakage probability and this introduces an additional term.

An addition of reactivity to a critical reactor which exceeds the effective delayed neutron fraction causes the power to increase very rapidly, with an exponential time constant of milliseconds, until the fast acting power coefficients of reactivity reduce the excess reactivity to below the effective delayed neutron fraction. When the excess reactivity is greater than the effective delayed neutron fraction the reactor is prompt critical. That is, the prompt neutrons alone are sufficient to sustain a chain reaction and the rate of increase of the fission neutron population depends on the prompt neutron lifetime, l, and the superprompt critical reactivity ($\rho - \beta eff$):

$$\frac{dn}{dt} = \frac{(\rho - \beta eff)}{l}\, n \qquad (90)$$

A typical value of l for a thermal reactor is 10^{-4} secs and for a fast reactor it is 10^{-6} secs.

For reactivity additions which are less than the delayed neutron fraction (or when the power coefficients have reduced the net excess reactivity to within this range) then the time constants of the delayed neutrons influence the time response of the reactor flux, and power, to the reactivity change. The longest delayed neutron precursor half-life is 55.6 secs (Br87). In reactors containing D_2O (γ,n) reactions in deuterium produce a small fraction of delayed neutrons having a much longer half-life.

In normal operation of reactors the shut-down can be very rapid but startup and changes of power level can be sufficiently slow for the reactor to be treated as in static equilibrium, with the power level corresponding, approximately, to the control reactivity insertion and the reactivity of the steady temperature power coefficients corresponding to the instantaneous power level. For accident studies the time constants of the different components of the power coefficients must be known and the equations involving the delayed neutron responses taken into account.

In addition to the changes of reactivity with temperature and coolant pressure following a change in reactor power the changes in fuel composition must also be taken into account. The main effects are the changes in concentration of Xe135 and Sm149. An equilibrium concentration is reached in which the rate of formation by radioactive decay of the precursors is equal to the rate of burn-up, $N\sigma_o\phi_{th}$ (plus decay in the case of Xe135). When the power changes there is a reactivity transient until the concentrations reach their equilibrium values. The time constants involved are several hours and so chemical shim can be used to compensate for these transients in a water cooled reactor.

In selecting control absorbers materials and designing control elements several items of nuclear data are required.

(i) The capture cross-sections of the primary isotopes and of the reaction products. The latter influence the variation of reactivity with burn-up.

(ii) The radioactivity induced in the materials (such as tritium from the B10 (n,t 2α) reaction, and the radioactive products produced in the irradiation of tantalum and europium which are possible fast reactor control absorber materials).

(iii) The heat deposited in the elements, both from the reactions in the absorber and from γ rays migrating from neighbouring fuel elements.

5.2 Delayed neutron data

An IAEA Nuclear Data Section Consultants Meeting on Delayed Neutron Properties was held in March (1979) (41). The requirements and the status of the data were reviewed. More recently the status has been reviewed by Reeder (42).

Delayed neutron data are required for the assessment of the kinetics response of a reactor to changes and in safety analyses. In experimental reactor physics studies reactivity effects are measured in terms of the kinetic response of the reactor. Because different reactivity effects have been measured in different experimental reactors, and there is a need to extrapolate the results to commercial power reactors, accurate delayed neutron data are required. The measurements usually involve the time dependence of the flux response to a reactivity change and so the requirements are for the total delayed neutron yield of the fissioning isotope, the time dependence of the neutron emission and the time dependent energy spectra of the neutrons. The spectra are required for the calculation of the effective delayed neutron yield (by weighting with the neutron importance intergrated over the spectra).

At the Consultants Meeting Hammer proposed a target accuracy of $\pm 3\%$ for βeff. He interpreted this as a requirement for $\pm 1.5\%$ on the yields for U235, U238 and Pu239 and $\pm$ 7% for Pu240 and Pu241. The target accuracy proposed for the energy spectra is $\pm 20\%$. At present these accuracies have not been achieved. The accuracies estimated for the total yields in thermal and fast reactor spectra by Tuttle are given in Table 5.1.

Table 5.1 - Accuracies of total delayed neutron yield data (percent)

	Thermal	Fast	14 MeV
U235	3.1	2.1	3.1
U238		2.3	2.9
Pu239	6.0	2.5	3.7
Pu240		7.9	7.5
Pu241	7.3	7.3	8.4

The accuracies achieved for the total yields in a fast reactor spectrum are close to the target requirements. However, the uncertainties in the time dependence and in the reactor period-reactivity relationship could be larger.

The time dependence of delayed neutron emission is usually represented by the sum of 6 exponentials with half-lives of about:

0.23, 0.61, 2.3, 6.22, 22.7, 55.7 (secs)

These are called the 6 delayed neutron groups. However, the data for individual fission product precursor half-lives and neutron emission probabilities are now approaching an accuracy which could result in summation calculations providing data of comparable accuracy to the integral measurements. In the future this approach could provide more accurate time dependence data.

The uncertainties in the energy spectra are much larger than the target accuracy requirements. Delayed neutron precursors with half-lives in the range 0.05 to 55.6 secs have been identified. Spectral information has been obtained for almost all of the precursors contributing to the 4 longest half-life groups and about 50% of shorter half-life groups. However, spectrum measurements made in different laboratories are discrepant. There is an international collaboration attempting to resolve these discrepancies (including measurements for standard spectra).

5.3 Reactivity coefficients

Fuel temperature coefficient

The main contribution to the fuel temperature coefficient arises from the resonance shielding Doppler effect in the U238 capture cross-section (in uranium and uranium-plutonium fuelled reactors). The temperature dependence of resonance shielding is different for low energy resonances and high energy resonances. This is because of the change in the ratio of the Doppler broadening width to the resonance width with increasing energy . In a thermal reactor spectrum the effect has the form:

$$C_f^T \simeq - d/T^{\frac{1}{2}} \qquad (91)$$

while in a fast reactor spectrum

$$C_f^T \simeq - D/T \qquad (92)$$

D is called the Doppler constant.

The Doppler effect decreases more rapidly with increasing temperature in a fast reactor than in a thermal reactor.

A source of uncertainty in the extrapolation of Doppler effect measurements made in experimental facilities operating over a low temperature range to the temperature range of fuel in a power reactor (and of possible concern in accident studies) is the effect of crystalline binding on Doppler broadening. Different models have been used to represent the crystalline binding. In one method the velocity distribution of the target nucleus is taken to be that of

a free atom but at an effective temperature T* which is a function of the actual temperature T and an effective Debye temperature, θ

$$\frac{T^*}{\theta} = \frac{3}{2}\int_0^1 x^3 \coth\left(\frac{x\theta}{2T}\right) dx \qquad (93)$$

T* is larger than T by a factor which decreases with increasing values of T. When T = θ,T* is about 5% higher than T. For lower temperatures T* can be substantially higher than T.

In another model, both an effective Debye temperature and an effective nuclear mass, A*, are used to reproduce the neutron-nucleus interaction kinetics. Other studies recommended the use of a two oscillator model, rather than a Debye temperature model.

On the basis of neutron diffraction and thermal scattering studies Butland (43) and Willis (44) found crystalline binding effects for U in UO_2 to be small. Butland concluded that an effective Debye temperature of about 250°K would reproduce the velocity distribution for uranium nuclei in a UO_2 lattice at 293.6°K. For oxygen the derived effective Debye temperature is 749°K, the value for the lattice as a whole being 630°K. For a value of θ as low as 250°K the difference between T* and T is very small for values of T above 300°K.

Golinelli et al (45) have made measurements of the temperature dependence of the U238 resonance integral for a UO_2 rod in a thermal reactor lattice. They conclude that a Debye temperature of 620°K gives a best fit to the observed temperature dependence. Brugger and co-workers (46) have made broad resolution measurements for different uranium compounds at several energies in the KeV range. They derive both an effective Debye temperature and an effective mass from the observed temperature dependence. The effective Debye temperature which they obtain for U in UO_2 is typically, about 600°K and the effective mass, A*,is about 600. The measurements also indicate a possible discontinuity in the Doppler effect at the melting point of the uranium compound. Meister et al (47) have measured the differences in the shapes of the U238 resonances in different compounds at different temperatures. They observe asymmetrical effects in the changes on the two sides of a resonance. They use a two oscillator model to represent the crystalline effects and find significant effects for some compounds, including UO_2. The effects for uranium metal are very small.

The energy breakdown of the U238 Doppler effect in fast and thermal reactors is given approximately in Table 5.

Table 5.2 Energy regions contributing to the U238 Doppler effect
(in percent)

Energy range	Thermal reactor	Fast reactor
Above 1 KeV	30	50
300 eV - 1 KeV	40	40
100 eV - 300 eV	15	10
Below 100 eV	15	-

About 70% of the Doppler effect in this thermal reactor spectrum is contributed by resonances above 300 eV. The energy range 100 eV to 2 KeV contributes most of thw U238 Doppler effect in both thermal and fast reactors. The smaller contributions to the Doppler effect in a fast reactor from Pu239 and Pu240 also come from this energy range.

In a fast reactor the net Pu239 Doppler effect is only about 5% of the total effect. This is because the positive component resulting from the increase in the shielded fission cross-section (about 20% of the total) is largely cancelled by the capture component (about 15% of the total).

The small contribution to the Doppler temperature coefficient of a fast reactor arising from structural materials is mainly from the 1.15 KeV resonance in Fe.

The Doppler effect changes with burn-up because of the resulting changes in the reactor neutron spectrum. In a sodium cooled fast reactor, the Doppler effect in an accident in which the coolant is lost (for example, by vapourisation) is only about half the value in the normal core. Accurate values of the coefficients in the voided core are required for accident studies.

Apart from the requirement to predict Doppler effects accurate data on the resonance structure of the cross-sections of fuel isotopes is required for the prediction of resonance shielding factors. A high accuracy is required in the calculation of resonance shielding effects. One reason is so that differences in the shielding in experimental assemblies and power reactors can be corrected for.

Moderator and coolant temperature coefficients

In a graphite moderated reactor an increase in moderator temperature causes the mean energy of the thermal neutron spectrum to increase. The resulting change in reactivity is associated with the energy dependence of the η values of the fissile isotopes and the ratio of absorption in fissile isotopes to absorption in competing reactions, such as U238 capture. In order to reproduce the measured variations of reactivity with moderator temperature (or thermal spectrum effective temperature) the shapes of the principal cross-sections at thermal energies have been adjusted (or selected) to fit these measurements. For example, Tellier (22) describes how the shape of the U238 capture cross-section below 1 eV has been changed from a (1/v) form to reproduce temperature coefficient measurements more accurately. Relative to the value at 0.0253eV (which is fixed) the value at 0.001 eV is increased by about 50%. The approach adopted by Chawla (48), and studied by others, has been to choose a shape for the energy dependence of the thermal U235 η or α curve to reproduce the integral measurements. More accurate measurements of the energy dependence of cross-sections, or cross-section ratios, through the thermal energy range, are high priority requirements. A typical accuracy requested for the shape measurements is $\pm$ 0.3%.

In a water cooled reactor changes in coolant density affect both the resonance escape probability and the thermal spectrum. The resonance escape probability changes because the resonance shielding increases with a reduction in coolant density and the moderation through the resonance region is reduced. When the coolant contains soluble poison a reduction in coolant density also results in a reduction in absorption by this control poison.

In a sodium cooled fast reactor a reduction in coolant density results in an increase in the mean energy of the neutron spectrum, (consequent upon the reduction in moderation) and an increase in the leakage fraction. The reduced moderation results in an increase in the U238 fission rate, a reduction in the spectrum averaged value of α in the fissile isotopes and a reduction in the ratio of capture in U238 to fission in Pu239. (In a U235 fuelled fast reactor the ratio of U238 capture to U235 fission changes in the opposite direction). The net effect in a large uranium-plutonium fuelled fast reactor of a reduction in sodium density is an increase in reactivity.

Coolant voiding effects

Because the sodium voiding effect is a balance between a positive moderation effect and a negative leakage effect the net reactivity effect depends on the region of the fast reactor which is voided. When the core is voided there is a large reactivity addition, in the range 5 to 18$ (where 1$ is the effective delayed neutron fraction, βeff). Accidents which produce fuel melting could result in a rapid vapourisation of coolant and a large and rapid reactivity addition. This could result in a Core Disassembly Accident. Some fast reactor designs, (called heterogeneous cores) aim to reduce the maximum positive reactivity addition which could result from coolant voiding. Accurate data are then required to optimise the design.

The void coefficient of a water cooled thermal reactor depends on the fuel burn-up and the density of soluble poison. The coefficient is negative and increases in magnitude as the void fraction increases.

Effect of hydrocarbon additions in a fast reactor

One investigation which is made as part of the safety assessment of a fast reactor is the effect of a small quantity of hydrocarbon entering the core. This might be oil leaking from a pump, for example. Additions of hydrogeneous materials have a strongly non-linear effect. The effect depends upon the quantity and the spatial distribution. The neutron spectrum in the region of the addition is 'softened' and can include a significant number of reactions at thermal neutron energies. The net reactivity effect depends on the localised change in the neutron spectrum and the variation of $\nu\Sigma_f(E)/\Sigma_a(E)$ with energy.

5.4 Control ansorbers

To compensate for the variation of fuel reactivity with burnup, to change reactor power and to provide a shutdown and safety margin it is usual to use a substance which strongly absorbs neutrons. Other methods of control have also been used. For example, in the experimental fast reactor at Dounreay control was obtained by moving reflecting elements at the core boundary. The most widely used absorber is B10 (either in natural boron, which contains 20% B10, or boron enriched in B10). The B10 (n, α) cross section, which is responsible for almost all of the capture, is accurately known up to several hundred KeV and is, in fact, used as a measurement standard. For some other control absorbers (or potential control absorbers) such as europium, tantalum and hafnium (and their reaction products) the (n, γ) cross-sections, in which the absorption occurs, are not sufficiently accurately known. In addition, resonance shielding effects are important and so a detailed knowledge of the resonance structure is required.

For calculating the heating (and cooling requirements) energy yields and gamma spectra must be known both for the primary reactions and the decay of radioactive products. The activity of these products determines the shielding and cooling requirements for post-irradiation handling.

When the absorbers have significant resonance shielding the effectiveness can be enhanced by using mixtures of substances, because the resonance shielding of cross-sections of each component is then reduced. A disadvantage of B10 is that its reaction products are not absorbing and so,in a high flux, the burn-up can significantly reduce the effectiveness of a boron carbide element. This is not so for europium (Eu151 and Eu153) because the reaction products, Eu152 and Eu154, are also strongly absorbing. One design of control rod which is being evaluated uses europium boride, which combines the advantages of the two substances.

The endurance of a boron carbide control rod can be limited by helium formation (by the (n,α) reaction) and the resulting swelling. Swelling beyond a certain level might cause the containing cans to burst or expand and block the cooling channels.

5.5 Reactor nucleonic instrumentation

In addition to thermocouples and flow-meters the power output of a reactor is correlated with neutron flux measurements. Counters are usually placed at several points around the core so that any flux tilting across the reactor can be detected. In large thermal reactors the spatial flux distribution is sensitive to localized reactivity perturbations. This is because K_∞ is so close to unity. Spatial harmonics in the flux distribution can be induced and these must be detected and controlled. It is usual to have a second set of neutron flux detectors, which are more sensitive, for monitoring flux when the reactor is shutdown. These are only introduced following shutdown. A neutron source might also be introduced then, if the radioactive sources in the fuel are insufficient. One problem in the design of such detectors and their environment is to ensure that they can detect neutrons without being swamped by the gamma background. Fission chambers and boron counters are used to detect the neutron flux. It might be necessary to surround the chamber position by a gamma shield, such as a region of graphite or steel. Gamma activity in the coolant can be a complicating factor. Introducing a region of graphite can moderate neutrons and so increase the sensitivity of the chamber.

The detection of leaking fuel elements involves samples being taken from the coolant. Both total coolant flow and individual channels can be monitored, essentially on a continuous basis. One method is to try to detect delayed neutron precursors.

All instruments and their associated cables must be designed to withstand high temperatures and irradiation effects and must be capable of covering a wide flux range. Different techniques have been evolved for providing a wide sensitivity range.

Section 6 - Some general remarks about nuclear data for reactor core design and safety analysis

6.1 Effective cross-sections

In Section 1 some of the ways in which nuclear data are simplified for reactor calculations were described. Simplifications are made not only because of the detailed structure of cross-sections, and secondary energy and angular distributions, but also because of the complexity of the detailed geometries of core fuel assemblies and other core components. Effective cross-sections, which represent an average over these detailed structures, through which the flux can vary quite strongly, are used in whole reactor calculations. Effective cross-sections can be derived for a single material, such as fuel rod, or for a whole reactor cell comprising a cluster of fuelpins and associated moderator and coolant. This latter procedure is called cell homogenisation. Effective cross-sections are defined to reproduce average (or cell integrated) reaction rates and leakage probabilities correctly. These cell-averaged cross-sections are then used in whole reactor calculations.

Effective cross-sections for the isotopes in a fuel rod can be energy averages over the resonance structure. These are dependent on the diameter of the rod and the density of the isotope. Approximate methods have been developed for calculating the flux in the rod through the energies of the resonances, and carrying out the energy group averaging. Care must be taken over the effect of the overlapping of resonances between different isotopes. An alternative approach is the sub-group method in which the total variation of the cross-section within an energy range is approximated by a simplified representative variation.

In thermal reactor calculations it is usual to solve the neutron transport equation in a representative cell with simplified boundary conditions and then derive equivalent cell averaged cross-sections for use in a diffusion theory whole reactor calculation:

$$\nabla D_g \nabla \phi_g + \Sigma_{rem,g} \phi_g = S_g$$

where S_g is the source in energy group g resulting from fission reactions and scattering of neutrons from other energy groups.

$$S_g = \chi_g \sum_{g'} \nu\Sigma_{fg'} \phi_{g'} + \sum_{g'} \Sigma_s^{g' \to g} \phi_{g'}$$

The scattering is treated as isotropic and the angular distribution of the cell averaged fluxes, or cell boundary fluxes, are assumed to have a simple form.

Fuel management and reload planning calculations are often made in 2 energy groups using cross-sections which have been tabulated as a function of burn-up and initial fuel enrichment.

6.2 Status and requirements

We see that in many applications gross simplifications are made in the nuclear data used. There is also extensive correlation of these simplified data with integral measurements, such as thermal Maxwellian averaged lattice resonance integrals. Effective resonance integrals have been measured as a function of fuel rod diameter, moderator to fuel ratio and temperature. These measurements can be used directly in some reactor calcualtions.

However, it is necessary to extrapolate beyond the range of integral measurements, particularly in safety assessments, and so it is necessary that the simpler calculations should be related to accurate calculations using accurate nuclear data, particularly for selected key references cases.

REFERENCES

1 Progress Report of the Japanese Nuclear Data Committee. p23. NEANDC(J)-67/U, INDC(JAP)-54/U. JAERI, Japan (Sept. 1980).

2 V I Popov. Bulletin of the USSR Nuclear Data Centre (1967).

3 J R Askew, F J Fayers and J M Terry. J. Brit. Nucl. Energy Soc. 6, 161. (1967).

4 R Kinsey. ENDF-102. Section 7. (1979).

5 S F Mughabghab and D I Garber. BNL325 Third Edition. Volume 1, (June 1973).

6 See references 19, 20, 21 and more recent studies by B R Leonard for ENDF/B-V, described in the ENDF/B-V Summary Documentation (ENDF-201) and later work.

7 A Gandini. Nucl. Sci. Eng. 35, 141 (1969).

8 M. Becker and D R Harris. EPRI NP-1632 (Nov, 1980).

9 L N Usachev and Yu G Bobkov. First All-Union Conf. on Neutron Emission Metrology. Moscow (1973).

10 Yu G Bobkov, L T Pyatnitskáya and L N Usachev. Obninsk USSR (1974) INDC(CCP) 40/L.

11 INDC/NEANDC Nuclear Standards File. 1980 Version (IAEA), INDC-36 (1981) and Reports of the INDC and NEANDC Subcommittees on Standards.

12 Report of the INDC Discrepancy Sub-Committee to the 11th INDC Meeting. Appendix 6. Minutes of the 11th INDC Meeting. June (1980). (IAEA) INDC-35. (May, 1981).

13 N DayDay. WRENDA 81/82 INDC(SEC)-78 (July, 1981).

14 H Gruppelaar and J B Dragt. Proc. B.N.L. Conf. on Nuclear Data Evaluation Methods and Procedures. p133 Brookhaven (Sept. 1980).

15 G Oliva and M Salvatores. NEANDC Topical Conference on Consistency and Complementarity of Microscopic and Integral Data. Aix-en-Provence (April 1981) NEANDC-150-U.

16 J L Rowlands et al. International Symposium on Physics of Fast Reactors Vol. III p1133, Tokyo, (October, 1973).

17 J H Marable. Proc. B.N.L. Conf. on Nuclear Data Evaluation Methods and Procedures p117. Brookhaven (Sept, 1980) BNL-NCS-51363.

18 V O Uotinen et al. Proc. Conf. Nuclear Cross-sections and Technology. Vol. 1 p7. Washington (March, 1975).

19 H D Lemmel. Proc. Conf. Nuclear Cross-sections and Technology. Vol. 1 p286. Washington (March, 1975).

20 B R Leonard. Proc. Conf. Nuclear Cross-sections and Technology. Vol. 1 p281. Washington (March, 1975).

21 G C Hanna et al. At. En. Review 7 (1969) No. 4. p3.

22 H Tellier. NEANDC Topical Conference on Consistency and Complementarity of Microscopic and Integral Data. Aix-en-Provence (April, 1981). NEANDC-150-U

23 H Tellier. Nucl. Sci. Eng. 79, 4 p393. (Dec, 1981).

24 U N Singh et al. EPRI NP 2076 (1981).

25 R Sher. Proc. B.N.L. Conf. on Nuclear Data Evaluation Methods and Procedures p835. Brookhaven (Sept, 1980).

26 A G Croff et al. ORNL/TM-6051 (Sept, 1979).

27 R F Burstall et al. UKAEA Risley Report ND-M-778(R).

28 A Tobias UKCEGB Report RD/B/N4303 (May, 1978).

29 A Tobias. Prog. Nucl. Energy 5, 1 p1 (1980).

30 G K Schenter and F Schmittroth. Int. Conf. on Nuclear Cross-sections for Technology, Knoxville. (Oct, 1979).

31 C Devillers et al. Proc. Conf. Neutron Cross-sections and Technology. Vol. 1 p29. Washington. (March, 1975).

32 B H Patrick and M G Sowerby. NEANDC(UK)-174, INDC(UK)-34. (1979).

33 H Kusters. K.f.K. 2917. (April,1980).

34 Darrouzet et al. Paper to NEACRP (1978) (quoted by H Kusters in Ref. 33).

35 M J Norgett, M T Robinson and J M Torrens. IAEA Meeting on Radiation Damage Units, Seattle (1972).

36 D G Doran and N J Graves. HEDL-TME 76-70(UC-79b,d) (Dec, 1976).

37 E M Gryntakis. Jour. Radioanalytical Chem. 52, 219 (1979).

38 A Fabry et al. 2nd ASTM-Euratom Symposium on Reactor Dosimetry. Palo Alto (1977) NUREG/CP-0004 (Vol. 3).

39 D L Smith. NEANDC Topical Conference on Consistency and Complementarity of Microscopic and Integral Data. Aix-en-Provence. (April,1980). NEANDC-150-U.

40 W L Zijp. EWGRD Comments for WRENDA 1981/82. Netherlands Energy Research Foundation. ECN Petten (Dec,1980).

41 Proc. IAEA (NDS) Consultant's Meeting on Delayed Neutron Properties. Vienna (March, 1979) INDC(NDS)-107.

42 P L Reeder. Proc. Conf. Nuclear Data Evaluation Methods and Procedures. p199. Brookhaven (Sept, 1980).

43 A T D Butland. Annals of N. S + E. 1 p575 (1974).

44 B T H Willis. Proc. Roy. Soc. A 274 p134 (1963).

45 C Golinelli et al. Proc. ANS Conf. Advances in Reactor Physics and Shielding. p243. Sun Valley (Sept, 1980).

46 R M Brugger and H Aminfar. Paper 3 IAEA Consultants Meeting on U/Pu Resonance Parameters, Vienna (Sept- Oct, 1981).

47 A Meister et al. Paper 1 IAEA Consultants Meeting on U/Pu Resonance Parameters. Vienna (Sept- Oct, 1981).

48 R Chawla. AEEW-R797. (1972).

EVALUATION OF NUCLEAR DATA AND THEIR UNCERTAINTIES

J.S. STORY
Atomic Energy Establishment,
Winfrith, Dorchester,
United Kingdom

Abstract

Some topics studied within the Winfrith Nuclear Data Group in recent years, and still of current importance, are briefly reviewed. Moderator cross-sections; criteria to be met for reactor applications are listed; thermal neutron scattering theory is summarized, with the approximations used to facilitate comutation; neutron age data test stringently the accuracy of epithermal cross-sections; a modification of the CFS effective range treatment for S-wave scatter by H is presented, and new calculations with up-to-date slow neutron scattering data are advocated.

Use of multilivel resonance formalisms; the top bound resonance should be included explicitly in calculations; additive statistical terms are given to allow for "distant" negative and positive resonances, in both MLBW and R-M formalisms; formulae are presented for estimating R-M level shifts for $l > 0$ resonances.

Resonance mean spacings; the Syson-Mehta optimum estimator is utilised in a method which up-dates the staircase plot. Resonances of ^{56}Fe have been resolved to $\sim$ 800keV, over which range the level density for given $J\pi$ should increase 2-fold; this variation is allowed for in the mean spacing calculations.

Fission-product decay power; present status of integral data and summation calculations for ^{235}U and ^{239}Pu fissions is summarized, with a variety of intercomparisons including ^{239}Pu/^{235}U ratios.

Data uncertainties are considered, but the sequence of data on Γ_γ for the 27.8keV resonance of ^{56}Fe provided a cautionary example.

1 INTRODUCTION

Data evaluation is the art of putting together experimental data, theory and guesswork so as to make something more useful and attractive out of indifferent beginnings. I do not feel that I can offer you any general theory for evaluation, and to try and write down those parts of nuclear theory which are relevant to particular fields - neutron resonance cross-sections for example - would only lead to tedious repetitions of what has been done so well by others in earlier years here at Trieste - on applied neutron resonance theory, for example, you will find the review paper by Fritz Fröhner (1978) remarkably informative.

It may be more useful, it seems to me, if I try to illustrate the theme by discussion of some of the evaluation work which has interested me during the last 10 years or so.

For nuclear data, the professional evaluator should be aware of the latest evaluation of the fundamental physical constants, by Cohen and Taylor (1973). In nuclear physics the standard reference energy in the thermal region is that of a neutron whose velocity is v_0 = 2200 m/sec

$$E_0 = (1/2)\, m_n v_0^2 \{1 + (3/4)(v_0/c)^2 + \ldots\}/(1000\,F)\ \text{eV} \qquad (1.1)$$

in which the neutron mass is given in amU, c is the velocity of light, and Faraday's constant F is in C / (g mole); the factor 1000 appears because, in SI units, the kg mole is the logical entity. Using the 1973 physical constants

$$E_0 = 0.02529907\ \text{eV} \pm 2.8\ \text{ppm}; \qquad (1.2)$$

the relativistic correction term is negligible.

Another numerical factor much used in neutron cross-section theory is that for conversion between neutron energy E and its radiom wavelength λ or wavenumber k. Writing

$$\lambda^2 E = E/k^2 = q\ \text{barn eV}. \qquad (1.3)$$

The constant q is given by

$$q = 10^{28}\, \hbar^2/(2 m_n e)$$

which may be written

$$q = (10^{28}/2\pi^2)(\hbar/2m_e)(\hbar/2e)(m_p/m_n)/(m_p/m_e)$$
$$= 2.072142 \times 10^5 \pm 3.1\ \text{ppm}; \qquad (1.4)$$

the uncertainty arises almost exclusively from the two factors containing h. Special tools for nuclear data evaluation have been greatly developed during the last decade. The CINDA reference index is now fairly well-known - the Computer Index of Neutron Data; this is published by the IAEA and is maintained by the four nuclear data centres at Brookhaven, Obninsk, Saclay and Vienna,

---

Fröhner F H (July 1978) KfK-2669, presented at the 1978 Winter course on nuclear physics and reactors, part 1, nuclear theory for applications

Cohen E R and Taylor B N (1973) J Phys Chem Reference Data 2 663; see also Cohen's paper in "Atomic Masses and Fundamental Constants 6" (Plenum Press 1980)

with help from a network of voluntary readers. Most of the measured neutron cross-section data are now available too from the four data centres, on magnetic tape or in tabular listings, and there is a greater awareness among the measurers of the necessity for the availability of new measurements. There has been good coverage too, by practising evaluators, in the proceedings of the winter courses here at Trieste in 1978 and 1980, of many aspects of the nuclear theories and of computer codes needed for the prosecution of their arts*.

I was asked to discuss principally the nuclear data for thermal reactor systems. Hitherto primary interest has been given to the neutron cross-section data for the main fissile and fertile materials, because of their importance for reactor core calculations and fuel economy. However, although there still remain discrepancies amongst these data, and inconsistencies with integral experience, reactor technologists have long been accustomed to methods of adjustment for improving the accuracy and reliability of integral parameters calculated from these data; these adjustment procedures are all based in one way or another on careful comparisons of calculations with well-chosen integral "benchmark" experiments on comparable systems. Because of this long-established use of adjustment processes relating to the principal nuclear data, Rowlands (1981) has suggested to me that more attention should be given by evaluators to other classes of nuclear data, and in what follows I have concentrated predominantly on the following topics.

Moderator cross-sections, at thermal and epithermal energies.

Some problems in the resonance cross-sections of iron (relevant to the other structural materials).

Fission product decay heating.

and in this section have added a few remarks on the thermal neutron cross-section data for the principal fissile nuclides, and on the slow neutron capture cross-section of the reference standard 197Au.

1.1 Thermal Cross-Sections of the Principal Fissile Nuclides

A few comments on the status of the thermal cross-sections of the main fissile nuclides may be of interest. Conclusions from the latest least squares evaluation commissioned by the IAEA were reported by Lemmel (1975), and the subsequent paper by Lemmel (1977) gives an interesting commentary on the residual systematic discrepancies encountered in that evaluation. Already in 1973 Lemmel had set out significant evidence that the value of 24380 ± 50 yr then in use for the 239Pu half-life was probably too high; subsequent measurements lead to a preferred value of about 24100 ± (24) yr. In all direct measurements of the 239Pu fission cross-section the 239Pu fission foils were assayed by alpha counting, and consequently the 239Pu fission cross-sections derived from these measurements are inversely proportional to the half-life.

---

174 Rowlands J L (1981) Private Communication

The value of nu-bar, neutron yield per fission, for spontaneous fission of 252Cf has long been the primary reference standard for the nu-bar data for the principal fissile materials. At the time of the previous IAEA review, by Hanna et al (1969), the experimental data on nu-bar for 252Cf formed two distinct groups differing by about 2.5%, and consequently had very little weight in the fitting procedure in comparison with the more precise data on eta and alpha for 233U, 235U and 239Pu. By 1975 however, in consequence of revisions and new measurements, the discrepancies between the nu-bar data for 252Cf had been much reduced, and yielded a relatively low weighted mean value of about 3.737 ± 0.008 which was in conflict with the eta and alpha measurements mentioned. Thus the outcome of the 1975 review was very unsatisfactory; while one important discrepancy had apparently been resolved, the resolution raised new doubts about a number of other classes of data.

A more recent review of the data on nu-bar for 252Cf has been carried out by Smith (1979); after correction of a number of small errors in earlier work, the revised value of $\bar{\nu}_t$ = 3.753 ± 0.008 is obtained, or 3.766 ± 0.007 if a preliminary new measurement by Spencer (1977) is taken into account. A least-squares fit to the thermal neutron parameters of the fissile nuclides, by Holden and Stehn, is presented by Leonard (1979) in the same report.

Leonard et al (1975, 1976) have reported the conclusions of extensive work on the simultaneous multi-level resonance analysis of neutron data for 235U in the thermal region (below 1.0 eV). This is a very interesting study, but it is based on four resonances only, from -0.916 eV to 1.135 eV. Since the mean resonance spacing of 235U is only 0.41 ± 0.04 eV we should expect as many as 6 resonances over this interval, probably 3 of each of the two s-wave spin states. This consideration warns us, for 235U at the least, to treat with reserve the use of multi-level parameterisations as a means of analysing the shape and consistency of the various slow neutron cross-section data.

Lemmel H D (1975) Washington Conf on Nuclear Cross-Sections and Technology; NBS special Publ 425, Vol 1, 286.

Lemmel H D (1977) NBS special Publ 493, 170.

Hanna G C, Westcott C H, Lemmel H D, Leonard B R, Story J S and Attree P M (1969) Atomic Energy Review 7, No 4.

Smith J R (1979) EPRI NP-1098, Section 5.

Spencer R R (1977) private communication to the 252Cf nu-bar workshop

Leonard B R (1979) EPRI NP-1098, Section 1

Leonard B R, Kottwitz D A, Jenquin U P, Stewart K B and Heeb C M (1975) EPRI-221.

Leonard B R, Kottwitz D A and Thompson J K (1976) EPRI-NP167.

1.2 197Au; The Parameters of the 4.9 eV Resonance, and the Thermal Neutron Capture Cross-Section

197Au provides the principal activation cross-section reference standard both for thermal neutron cross-section measurements and for resonance integrals. Both the thermal capture cross-section and resonance integral of 197Au arise predominantly from the 4.9 eV resonance, and there are only two significant sets of experimental data on the parameters of this resonance, those reported by Wood (1956) and those of Tellier and Michel (1969), which are listed in Table 1.1 below, in which

$$\sigma_\gamma = 4\pi\lambda^2 (1 + m/M)^2 \, g\Gamma_n/\Gamma \qquad (1.5)$$

using the usual well-established notation.

TABLE 1.1

Resonance parameters of 197Au, as reported

	Wood (1956)	Tellier and Michel (1969)
E_r	4.906±0.010 eV	4.900±0.005eV
$\sigma_\gamma \Gamma^2$	725±15 b eV^2	
$\sigma_\gamma \Gamma$	5180±130 b eV	
σ_γ	37000±500 b	36200±600 b
Γ	150±3 meV*	137.5±2.0 meV
g	5/8	
σ_{pot}	11.1±0.8 b	
Γ_n	15.6±0.4 meV*	15.00±0.20 meV
Γ_γ	124±3 meV*	122.5±2.5 meV*

*Derived values

It is easily confirmed that, in both data sets, the reported values of Γ_n are inconsistent with those of $\sigma_\gamma \Gamma$ except if we suppose that the factor $(1+m/M)^2 = 1.0102682$ was ignored (taken as unity). If this interpretation is correct, the effect would have been, most nearly, that the reported values for Γ_n should be taken as representing $\Gamma_n (1 + m/M)^2$. Revised parameter values would then be as given in Table 1.2 below: the uncertainties quoted by Wood for Γ, Γ_n and Γ_γ appear to be too large[≠]; I retain them however because perhaps they contain systematic components of uncertainty.

TABLE 1.2

Revised values for the resonance parameters of 197Au

	Wood (1956)	Tellier & Michel (1969)	Preferred Value
Er eV	4.906±0.010	4.900±0.005	4.9012±0.0045
J	2+		2+
σ_{pot} b	11.1±0.8		11.1±0.8
Γ meV	140.0±3	137.5±2.0	138.26±1.66
Γ_n meV	15.45±0.4	14.85±0.198	14.967±0.177
Γ_γ meV	124.5±3	122.65±2.01	123.29±1.67

The most accurate and reliable determinations of the slow neutron capture cross section of 197Au are those derived from transmission measurements at energies below the Bragg limit at 3.7 meV, where the scattering contributions are relatively very small; from these measurements the capture cross-section is derived absolutely. The most recent and most precise measurements, by this method, are those of Dilg et al (1973), who also summarise the majority of the earlier measurements; for a more complete summary see Holden (1981).

In considering extrapolation to 2200m/s of the low energy capture cross-section it has usually been overlooked that only about 91.79% of the measured capture cross-section stems from the 4.9 eV resonance, and it is only this part which increases slowly above the 1/v form with increase of neutron energy in the thermal region; the remaining 8.91% stems from more distant resonances at negative and positive resonance energies (mostly from the former) and therefore follows the 1/v - law more closely or falls slightly below it. Consequently the capture cross-section measured by Dilg et al just below the Bragg cut-off, in the wavelength range 4.8 to 7.5A, has to be increased by only 0.841 barns above the 1/v-form, and their measurement at long wavelengths by 0.923 barns. As weighted mean from these two measurements I obtain

$$\sigma_\gamma [^{197}\text{Au}] = 98.614 \pm 0.105 \text{ barns}$$

at 0.02529907 eV.

Wood R E (1956) Phys Rev 104 1425; Wood R E, Landon H H and Sailor V L (1955) Phys Rev 98 639

Tellier H and Michel A (1969) CEA-N-1230

Dilg W, Mannhart W, Steichele E and Arnold P (1973) Zeits Phys 264, 427

[≠] From $\sqrt{[\sigma_\gamma \Gamma^2 / \sigma_\gamma]}$ and $\sqrt{[\sigma_\gamma \Gamma^2 . \sigma_\gamma]}$ we should obtain

Γ = 139.98 ± 1.73 meV, Γ_n = 15.454 ± 0.194 meV and Γ_γ = 124.53 ± 1.66 meV

(from page 4)

Holden N E (1981) BNL-NCS-51388, Section 2

2 NEUTRON SCATTERING BY MODERATORS

To be of use for thermal reactor calculations neutron scattering data for moderators must satisfy the following conditions.

(i) They must give realistic values for the thermal neutron diffusion coefficient D(T), or for the related diffusion constant $D_0(T)$ and diffusion length L(T), for a range of moderator temperatures up to the highest likely to be required for examination of accident conditions.

(ii) There should be an adequate representation of slow neutron inelastic scattering, so that the variation of neutron spectra in the neighbourhood of boundaries and temperature discontinuity can be calculated with reasonable accuracy.

(iii) The slow neutron inelastic scattering must satisfy the condition of detailed balance, so that the scattering terms do not act as neutron sources or sinks in a reactor calculation.

(iv) The cross-section data for epithermal and fast neutrons must give realistic values for the slowing down age of the neutrons evolved in fission.

2.1 The Thermal Neutron Diffusion Parameters

No exact relationship between the diffusion coefficient, or the diffusion length, and the differential cross-sections has been rigorously established, but the following formulae are thought to be reasonably accurate.

$$D(T) = 1/[3\overline{\Sigma}_{tr}(T)] \qquad \text{(diffusion coefficient)} \qquad (2.1)$$

$$D_0(T) = 2D(T)v(T)/\sqrt{\pi} \qquad \text{(diffusion constant)} \qquad (2.2)$$

$$L(T) = \sqrt{[D(T)/\overline{\Sigma}_A(T)} \qquad \text{(diffusion length)} \qquad (2.3)$$

in which

$\Sigma_A(E)$, $\Sigma_s(E)$ denote the macroscopic absorption and scattering cross-sections for neutrons of energy E.

$$\overline{\Sigma}_A(T) = \int_0^\infty M(T, E)\,\Sigma_A(E)\,dE \qquad (2.4)$$

is the average of $\Sigma_A(E)$ over the Maxwellian neutron flux distribution at temperature T,

$$M(T, E)\,dE = (k_B T)^{-2} E \exp(-E/k_B T)\,dE \qquad (2.5)$$

which is normalised so that

$$\int_0^\infty M(T, E)\,dE = 1. \qquad (2.6)$$

The spectrum averaged transport cross-section in (2.1) may be defined, following Askew et al (1966),

$$\overline{\Sigma}_{tr}(T) = \overline{\Sigma}_A(T) + 1/\int_0^\infty M(T, E)[\Sigma_s(E)\{1-\overline{\mu}(E)\}]^{-1}\,dE \qquad (2.7)$$

in which the mean scattering cosine, $\overline{\mu}(E)$, is

$$\overline{\mu}(E) = \int_0^\infty \int_{-1}^{1} \sigma(E \rightarrow E'; \mu)\,\mu\,d\mu\,dE' / \sigma_s(E). \qquad (2.8)$$

Note that $\sigma_s(E)$ and $\sigma(E \rightarrow E'; \mu)$ may each have some temperature dependence.

Finally $v(T)$ is the most probable neutron velocity in the Maxwellian spectrum,

$$v(T) = \sqrt{(2k_B T/m_n)} = 128.3977\sqrt{T}\ \text{m/s} \pm (16\ \text{ppm}) \qquad (2.9)$$

in which k_B is Boltzmann's constant and m_n is the neutron mass.

Experimental data on the diffusion constants for H_2O and D_2O have been compiled by Butland and Chudley (1974), and for graphite by Butland (1973). The measurements extend only to 295°C for H_2O to 250°C for D_2O, and to 600°C for graphite. For the two liquid moderators it is convenient to remove the density dependence of the data, by considering the functions

$$\rho(T).D(T), \quad \rho(T).D_0(T), \quad \rho(T).L(T)$$

as these allow more reliable extrapolation of the measured data to higher temperatures. The densities $\rho(T)$ of H_2O and D_2O have been tabulated in the paper of Butland and Chudley referred to above. Reactor grade graphites may contain impurities which contribute appreciably to the absorption cross-section. They are usually very porous, with densities $\sim$1.6 g/cm^3 as compared with the theoretical maximum of 2.25 g/cm^3; supposing that the pores are filled with air at ambient temperature and pressure, the nitrogen content adds appreciably to the absorption especially at low temperature. Neutron diffusion measurements in graphite may also be affected by the presence of water. These various impurity effects must be eliminated, so far as is practicable, when comparing measured and calculated values of the neutron diffusion parameters of graphite.

Askew J R, Fayers F J and Kemshell P B (1966) J British Nuclear Energy Society 5,4.

Butland A T D and Chudley C T (1974) J British Nuclear Energy Society 13 (1) 99.

Butland A T D (1973) AEEW R 882

2.2 Slow-Neutron Scattering Cross-Sections

For an adequate treatment of slow neutron scattering by moderators we must turn to the complex and troublesome theory of the thermal neutron "Scattering Law"*. In simplest form

$$d^2\sigma/d\Omega\, d\omega = \sigma(\underline{k} \rightarrow \underline{k}') = (\sigma_b/4\pi)(k'/k)\, S(\underline{Q}, \omega) \qquad (2.10)$$

in which σ_b is the bound atom scattering cross-section,

$$\sigma_b = (1 + m_n/M)^2\, \sigma_{free} \qquad (2.11)$$

where M is the atomic mass of the scattering atom and σ_{free} is the slow neutron scattering cross-section of a stationary free-atom. It is very commonly assumed, in discussions of slow neutron scattering that σ_b and σ_{free} are constants at low neutron energies ($\lesssim 4$ eV); this is certainly a valid approximation for the common moderators and coolants, but it is not true in general because of the effects of nearby resonances and is not a very good approximation for 235_{UO_2} for example.

In (2.10) $\underline{k}$ is the wave-vector of the incident neutron and $\underline{k}'$ is that of the scattered neutron, with $k = |\underline{k}|$ etc;

$\underline{Q} = \underline{k} - \underline{k}'$ is the scattering vector (2.12)

$\omega = \hbar (k^2 - k'^2)/2m_n$ (2.13)

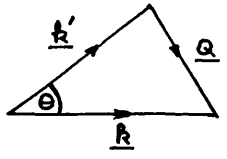

so that $\hbar\underline{Q}$ is the momentum, and

$\hbar\omega$ is the energy, transferred from the neutron to the scattering medium.

So far as the discussion of slow neutron scattering is concerned, all the usual moderators can be considered as isotropic, in the sense that whatever their orientation with respect to the incident neutron beam the scattering probabilities are unchanged. In reality reactor grade graphite often shows a small orientation effect related to the direction of extrusion (see for example Egelstaff, 1957), but the effect on the inelastic neutron scattering is quite small.

Because of the isotropy we are interested only in the average of (2.10) over all directions of $\underline{k}$, the shape and dimensions of the wave-vector triangle depicted above being conserved. It is easily seen from (2.10) that this is equivalent to averaging $S(\underline{Q},\omega)$ over all directions of $\underline{Q}$, so that instead of (2.10) may be written

$$d^2\sigma/(d\mu\, d\omega) = (\sigma_b/2)(k'/k)\, S(Q, \omega) \qquad (2.14)$$

in which μ is the cosine of the angle of scattering,

$$S(Q, \omega) = (1/4\pi) \int S(\underline{Q}, \omega)\, d\underline{\Omega} \qquad (2.15)$$

where

$$\underline{Q} = Q\,\underline{\Omega}' \qquad (2.16)$$

The detailed balance condition may be expressed by

$$M(T, E)\, \sigma(E \rightarrow E', \mu) = M(T, E')\, \sigma(E' \rightarrow E, \mu) \qquad (2.17)$$

in which M(T,E) is the Maxwellian neutron flux distribution function (2.5). Provided that σ_b is sensibly independent of the neutron energy in the energy range of interest ($E \lesssim 4$ eV), this implies that

$$S(Q, \omega) = \exp(\hbar\omega/k_B T)\, S(-Q, -\omega) \qquad (2.18)$$

Introducing the modified scattering function $\tilde{S}(Q,\omega)$ by

$$S(Q, \omega) = \exp(\hbar\omega/2k_B T)\, \tilde{S}(Q, \omega), \qquad (2.19)$$

(2.14) is rewritten as

$$d^2\sigma/(d\mu\, d\omega) = (\sigma_b/2)(k'/k) \exp(\hbar\omega/2k_B T)\, \tilde{S}(Q, \omega) \qquad (2.20)$$

From (2.18)

$$\tilde{S}(Q, \omega) = \tilde{S}(-Q, -\omega). \qquad (2.21)$$

$\tilde{S}(Q,\omega)$ is an even function of its arguments, and under this constraint (2.20) satisfies the detailed balance condition automatically.

In practical applications it has been found convenient to introduce the dimensionless variables

$$\alpha = (E' + E - 2\mu\sqrt{E'E})/A k_B T, \quad \beta = (E - E')/k_B T \qquad (2.22)$$

With

$$\tilde{S}(\alpha, \beta) = (k_B T/\hbar)\, \tilde{S}(Q, \omega) \qquad (2.23)$$

equation (2.20) may be expressed as

$$d^2\sigma/(d\mu\, dE') = (\sigma_b/2k_B T)\sqrt{(E'/E)} \exp(\beta/2)\, \tilde{S}(\alpha, \beta) \qquad (2.24)$$

The scattering law $\tilde{S}(\alpha, \beta)$ expresses the laws of conservation of momentum and energy in the context of the kinetics of the scattering system, be it monatomic gas, molecular gas, liquid, polycrystalline or amorphous solid. It has other functions, which

*See for instance Marshall W and Livesey S W "Theory of Thermal Neutron Scattering (OUP, 1971); Egelstaff P A and Poole M J "Experimental Neutron Thermalisation" (Pergamon, 1969); Williams M M R "The Slowing-Down and Thermalisation of Neutrons" (North-Holland; 1966); Parkes D E, Nelkin M S, Beyster J R and Wikner N F "Slow Neutron Scattering and Thermalisation" (Benjamin, 1970).

Egelstaff P A (1957) J Nucl Energy 5, 203.

account for the complexity of its construction: for a polycrystalline scatterer, for example, the effective mass of the scatterer for very slow neutrons is that of a typical crystallite (effectively infinite), and the mean scattering cosine $\bar{\mu}$ in the laboratory frame is zero. For neutrons of $\gtrsim 1$ eV however the scattering atoms are effectively free, so that the mass ratio is A and $\bar{\mu} = 2/(3A)$. It is the function of the scattering law to describe this transition with energy.

The scattering law for a monatomic perfect gas is simply

$$\tilde{S}(\alpha, \beta) = (1/2\sqrt{\pi\alpha}) \exp\{-(\alpha^2+\beta^2)/4\alpha\} \qquad (2.25)$$

The notation is self-explanatory in the main; $\bar{b}_\nu$ is the bound atom coherent scattering amplitude for the atoms indexed by ν. The mass ratios $A_{\nu\nu'}$ to be used in defining $\alpha_{\nu\nu'}$ for interference terms arising between atoms of different mass may be set at 1 or may be assigned differently as the user prefers. The chief difficulty in using this general form (2.35) is that of providing the various scattering laws which are needed, unless simplifying approximations can be made. For H_2O for example various alternative models are available for $\tilde{S}_s(\alpha, \beta)$ for the self-scattering by the hydrogen atoms, a monatomic gas model is customarily used for $\tilde{S}_s(\alpha, \beta)$ for the oxygen atoms (whose contribution to the scattering cross-section is small), and interference effects (which are weak) are neglected altogether.

Even for materials such as D_2O and graphite, for which the coherent scattering cross-section is not small, the incoherent approximation obtained by ignoring the interference terms has proven adequate, or nearly adequate for reactor physics calculations, so that the various models used for calculation of the incoherent scattering laws must claim principal interest. The interference terms are most important for small values of α and of β; they fluctuate about zero and fall in amplitude as α and β increase, becoming zero for large values of these arguments. The interference effect is seen at its most striking in the Bragg structure of the elastic scattering by polycrystalline materials such as graphite. Butland (1973) used the incoherent approximation for generating sets of multigroup thermal neutron cross-sections for graphite: however the elastic terms obtained in this way were revised using detailed coherent elastic cross-sections calculated from the known crystal structure of graphite; notice that this alteration does not upset the detailed-balance test (2.17), but that it reproduces the total scattering cross-section and mean scattering cosine rather accurately so that some confidence could be placed on the derived values for the diffusion coefficient.

Similar calculations for D_2O were reported by Butland and Oliver (1974) using the incoherent approximation exclusively; this reproduces the total cross-section reasonably well down to 0.005 eV, and adequately down to 0.0018 eV. A more complete treatment for D_2O, including interference effects, was developed by Butler (1962, 1963) but only very restricted calculations have been reported.

Butland A T D and Oliver S M (1974) AEEW R 950.

Butler D (1962) Eng Elec Co W/AT 849; (1963) Proc Phys Soc 81, 267,294.

Before going on to a brief discussion of models used for the "self" or incoherent scattering law $\tilde{S}_s(\alpha, \beta)$ it is worth while to set down Placzek's (1952) energy moment theorems with first the moment of zero order:

$$\int_{-\infty}^{\infty} S_s(\alpha, \beta)\, d\beta = 2\int_0^{\infty} \tilde{S}_s(\alpha, \beta) \cosh(\beta/2)\, d\beta = 1 \qquad (2.36)$$

$$\int_{-\infty}^{\infty} S_d(\alpha, \beta)\, d\beta = 2\int_0^{\infty} \tilde{S}_d(\alpha, \beta) \cosh(\beta/2)\, d\beta = S(\alpha) - 1 \qquad (2.37)$$

$$\bar{\beta} \equiv \int_{-\infty}^{\infty} S_s(\alpha, \beta)\, \beta\, d\beta = 2\int_0^{\infty} \tilde{S}_s(\alpha, \beta)\, \beta \sinh(\beta/2)\, d\beta = \alpha \qquad (2.38)$$

$$\int_{-\infty}^{\infty} S_d(\alpha, \beta)\, \beta\, d\beta = 2\int_0^{\infty} \tilde{S}_d(\alpha, \beta)\, \beta \sinh(\beta/2)\, d\beta = 0 \qquad (2.39)$$

$$\beta^2 \equiv \int_{-\infty}^{\infty} S_s(\alpha, \beta)\beta^2\, d\beta = 2\int_0^{\infty} \tilde{S}_s(\alpha, \beta)\, \beta^2 \cosh(\beta/2)\, d\beta = \alpha^2 + 4/3\, \bar{K}\alpha \qquad (2.40)$$

No equivalent formula is available for $\int_{-\infty}^{\infty} S_d(\alpha, \beta)\, \beta^2\, d\beta$. Notice from (2.38) and (2.39) that the mean energy transfer depends only on the momentum transfer and the mass of the scattering atom, but not at all on the chemical bonding of the scattering system. In (2.40) $\bar{K}$ is the mean kinetic energy of the scattering atoms in k_BT units. Wick (1954) gave the following expression for the total scattering cross-section, valid for large incident energies (above the energy of the highest bound state of the scattering system)

$$\sigma(E) = \sigma_{free}\,(1 + K\, k_BT/3AE + \ldots) \qquad (2.41)$$

This formula describes how the scattering cross section approaches the free-atom value; it is not rigorously valid for scattering by hydrogenous media.

2.3 The Gaussian Approximation for $\tilde{S}_s(\alpha, \beta)$

The major contribution to the incoherent or "self" scattering law $\tilde{S}_s(\alpha, \beta)$ is given by the so-called "Gaussian component" for which

$$\tilde{S}_s(\alpha, \beta) = (1/2\pi)\int_{-\infty}^{\infty} \exp[-\alpha\, w(t) - i\beta t]\, dt. \qquad (2.42)$$

The integrand is Gaussian in the momentum transfer, since $\alpha \propto Q^2$, and depends only on the "width function" w(t). In (2.42) t is a dimensionless variable, being the time in units of $\hbar/k_BT$; w(t) is an even function of t, because $\tilde{S}_s(\alpha, \beta)$ is even in β,

$$w(i/2) = 0 \qquad (2.43)$$

on account of (2.36) and

$$\dot{w}(i/2) = i \qquad (2.44)$$

on account of (2.38), where $\dot{w}(t) = \partial\, w(t)/\partial\, t$.

Placzek G (1952) Phys Rev 86 377.

Wick G C (1954) Phys Rev 94, 1228

For a monatomic perfect gas, from (2.25)*

$$w(t) = t^2 + 1/4 . \qquad (2.45)$$

To represent the diffusive motion of molecules in a liquid another very simple model has been proposed by Egelstaff and Schofield (1962), entitled the "effective width model", with only a single adjustable parameter q,

$$w(t) = (2/q^2)\left[\sqrt{\{q^2(t^2 + 1/4) + 1\}} - 1\right]. \qquad (2.46)$$

It is readily confirmed that this form satisfies the conditions (2.43) and (2.44); moreover the scattering law derived from (2.46) can be represented analytically

$$\tilde{S}_s(\alpha, \beta) = \frac{\exp(c\alpha/2)}{2\pi}\sqrt{\frac{c(c+1)}{\beta^2 + c\alpha^2}}\, K_1\left(\sqrt{\{(c+1)(\beta^2 + c\alpha^2)\}}/2\right), \qquad (2.47)$$

in which $c = 4/q^2$, and $K_1(x)$ is the modified Bessel function of second kind.

More generally w(t) may be expressed in the form

$$w(t) = \int_0^\infty \rho(\beta)\{\cosh(\beta/2) - \cos(\beta t)\}/\{\beta \sinh(\beta/2)\}\, d\beta \qquad (2.48)$$

in which, on account of (2.44)

$$\int_0^\infty \rho(\beta)\, d\beta = 1. \qquad (2.49)$$

For a harmonic crystal $\rho(\omega)$ may be identified with the frequency distribution of normal modes, and in the context of thermal neutron scattering is rather more generally referred to as "the phonon frequency function". Frequency distributions derived from differential cross-section measurements for a number of moderators and for UO_2 have been presented in tabular and graphical forms by Page and Haywood (1968).

*This is easily established with the help of the definite integral

$$\int_{-\infty}^{\infty} \exp(-ax^2 + bx)\, dx = \sqrt{(\pi/a)}\, \exp(b^2/4a).$$

Egelstaff P A and Schofield (1962) Nucl Science and Eng 12, 260

Page D I and Haywood B C (1968) AERE - R 5772

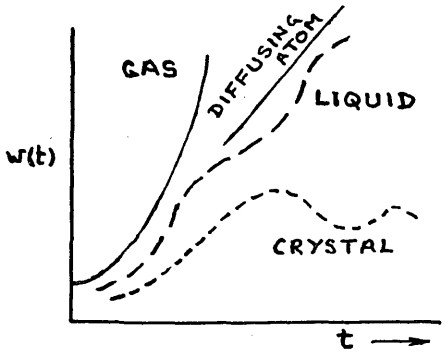

Figure 2.1 Form of the Width Function w(t)

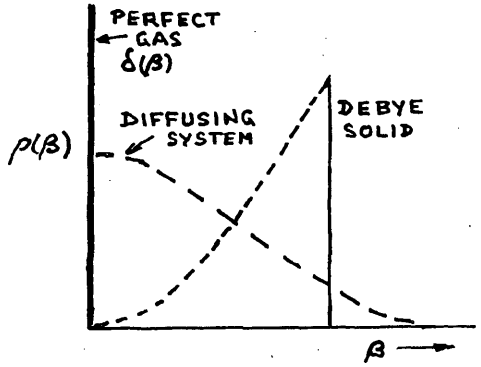

Figure 2.2 Forms of the Frequency Function $\rho(\beta)$

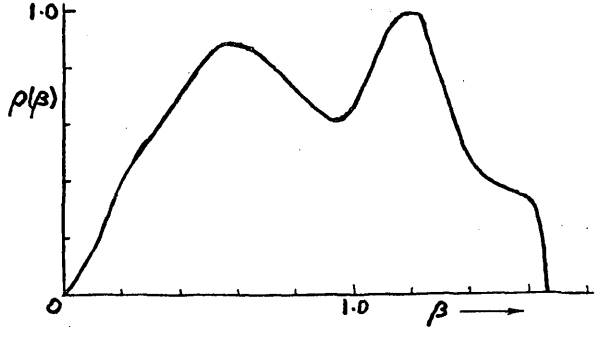

FIGURE 2.3

Frequency distribution of Graphite at 1800K (Page & Haywood, 1968)

The form of the width function w(t) is illustrated schematically in Figure 2.1 for various simple models, and in Figure 2.2 are depicted representative forms for the frequency function $\rho(\beta)$. For a crystal the distinguishing features are that w(t) remains bounded at t increases, and $\rho(0)$ is zero.

For polycrystalline materials the relationship between the specific heat and the phonon frequency function is given by

$$C_v/3R = \int_0^\infty \rho(\beta)\,\beta^2/\{\sinh(\beta/2)\}^2\,d\beta, \qquad (2.50)$$

in which R is the gas constant

R = 8.31441 J/g-mole ^oK ± 31 ppm

Butland (1973) made use of the relationship (2.50) in developing, from the single frequency function given for graphite (at 1800°K) by Page and Haywood, a whole set of frequency functions spanning smoothly the temperature range from 293K to 3273K; the specific heat data for graphite were taken from the review by Butland and Maddison (1972), who present a smooth functional representation.

As has been mentioned already, in these scattering models for graphite were included the interference effects arising in the coherent elastic cross-section. For these calculations the Debye-Waller coefficient $\lambda(T)$ was required at each temperature; this too was calculated from the corresponding phonon frequency function using

$$\lambda(T) = \int_0^\infty \rho(\beta)\,\beta^{-1}\coth(\beta/2)\,d\beta. \qquad (2.51)$$

For completeness may be remarked that the mean kinetic energy of the scattering atoms, $\bar{K}$ in k_BT units, can be obtained from (2.41) but is calculated more directly from

$$\bar{K} = (3/4)\int_0^\infty \rho(\beta)\,\beta\coth(\beta/2)\,d\beta. \qquad (2.52)$$

For a proper representation of scattering by molecular fluids it may prove convenient to decompose the width function w(t) into a component representing diffusive motion and a component which is bounded for large t

$$w(t) = w_d(t) + w_b(t). \qquad (2.53)$$

Then

$$\tilde{S}_s(\alpha,\beta) = \int_{-\infty}^{\infty} \tilde{S}_d(\alpha,\beta')\,\tilde{S}_b(\alpha,\beta-\beta')\,d\beta' \qquad (2.54)$$

on using the convolution theorem for Fourier transforms.

Butland A T D and Maddison R J (1972) AEEW R 815

Butland A T D (1969) AEEW M 954; (1972) AEEW M 1136; (1973) AEEW M 1200 and AEEW M 1201

In practical applications it has usually been necessary to set limits on the complexity of the treatment because of computational constraints, and on the nature and number of tests applied to a set of multigroup thermal scattering cross-sections once they have been computed. Butland (1969, 1972, 1973) has described some of the computer codes available for thermal neutron scattering calculations, and some comparative tests between different codes; it appears from his remarks that the code SLAB, evolved by Hutchinson and Schofield (1967) for computing $\tilde{S}_i(\alpha,\beta)$ from photon frequency functions, could be developed both in speed and precision by the introduction of Fast Fourier Transform techniques; it might then have clear advantages over alternative codes such as LEAP. The mesh of (α,β)-values at which the scattering law is to be calculated must be carefully chosen and the number of mesh points is necessarily restricted. When it comes to the calculation of multigroup cross-sections from a tabulation of $S(\alpha,\beta)$ values, computational accuracy might be improved by careful consideration of the formulae to be used in interpolating $S(\alpha,\beta)$ between mesh points.

The effective width model described at (46) and (47) above is one useful and very simple model that has been used for calculating thermal scattering cross-sections for H_2O and D_2O, the values of the single parameter q being chosen so that the derived cross-sections are consistent with measured values for the neutron diffusion coefficient. Nelkin (1960) devised another very simplified description of the frequency function $\rho(\varepsilon)$ for H in H_2O, using 4 delta functions as shown in Figure 2.4.

Butland and Chudley (1972) present comparisons of measured and calculated values for a number of representative integral parameters for four H_2O moderated reactor cores; several different thermal neutron scattering models were used in the calculations. With the exception of the simple free gas model, the calculations using the other models appear to be in surprisingly good agreement with one another and with the experimental values. It is interesting to consider what other and perhaps more stringent tests might usefully have been applied.

Figure 2.4

Nelkin's model for H in H_2O

	function	eV	Weight
A	translational	0.0	1/18
B	notational	0.06	1/2-32
C	bending modes	0.205	1/5.84
D	stretching "	0.481	1/2.92

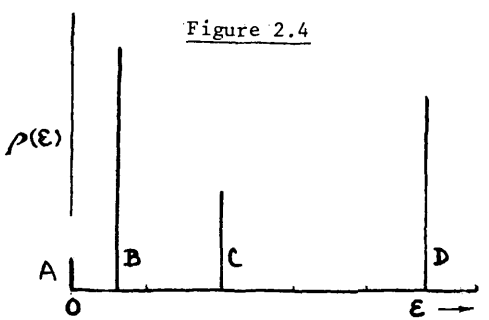

Hutchinson P and Schofield P (1967) AERE R 5536

Nelkin M S (1960) Phys ev 119, 741

Butland A T D and Chudley C T (1972) AEEW

2.4 Moderator Cross-Sections for Epithermal and Fast Neutrons

As was noted at the beginning of Section 2, the differential cross-sections for epithermal and fast neutron interactions with a moderator must give realistic values for the slowing-down age of the neutrons evolved in fission.

Neutron Age Goldstein et al (1961) say that neutron age is a measure of the spatial dispersion of slowing-down neutrons about their source, and that it is best defined in terms of some functional F of the neutron angular flux density $\phi(r,\underline{\Omega},E)$. Examples given are the neutron flux density

$$F(\phi, r, E) = \phi(r, E) = \int \phi(r, \underline{\Omega}, E)\, d\underline{\Omega} \qquad (2.55)$$

or the slowing-down density, or the current: the functional F must at least be a function of position. Given F and the material the age is a function of the energy spectrum of the neutron source, symbolised by S, and of the final energy parameter E. The age is then defined in terms of the neutron distribution about an isotropic point source in an infinite medium by

$$\tau(F, S, E) = \frac{1}{6} \frac{\int_0^\infty F(\phi, S, E, r)\, r^2\, dr}{\int_0^\infty F(\phi, S, E, r)\, dr} \qquad (2.56)$$

To reduce this to more practical terms, the neutron age is usually measured by using In activation detectors, shielded with Cd to eliminate virtually all the neutrons of $\lesssim$ 0.5 eV. Natural In contains 95.72% 115In, and radiative capture of slowing-down neutrons, predominantly in the strong resonance at 1.457 eV, produces the metastable state activity of 116In with a convenient 54 minute half-life.

In practice therefore the functional F should be represented by

$$F(S, r) = \int_{0.5\,eV} \phi(r, E)\, \sigma(E)\, dE, \qquad (2.57)$$

where $\sigma(E)$ is the neutron cross-section of In for production of 54 min. In 116m, or one might elaborate this to represent also the effect of the Cd shielding of the In foils. In principle the integral should extend far enough to include the source neutron energies, and in practice it should certainly embrace the whole of the 1.46 eV resonance.

Formally, age theory is based on the concept of replacing the life histories of individual neutrons by an average history in which the neutrons are assumed to lose energy continuously in such a manner that to any given neutron age there corresponds a definite value of the energy.

Goldstein H, Sullivan J G, Coveyou R R, Kinney W E and Bate R R (1961) ORNL 2639

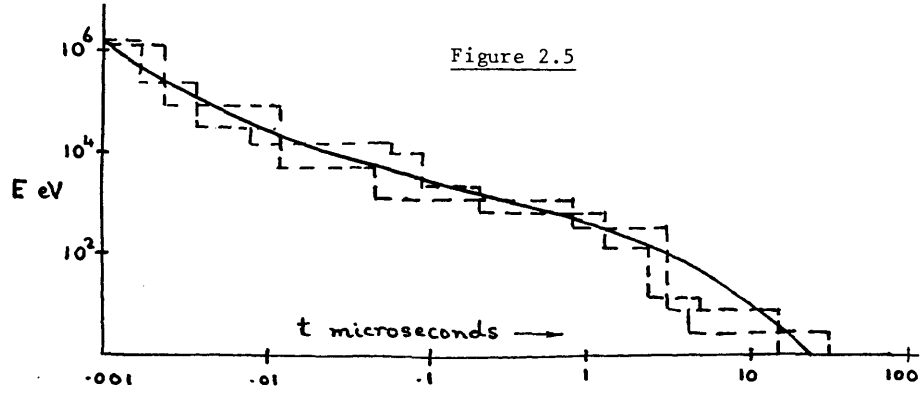

Figure 2.5

A consequence of this model is the additivity property

$$\tau(E_0, E_2) = \tau(E_0, E_1) + \tau(E_1, E_2). \qquad (2.58)$$

Without going into the derivation, which belongs to the theory of reactor physics, see Wigner and Weinberg (1958), the neutron age may be estimated from the neutron cross-sections by means of

$$\tau(E_0, E_1) = \frac{1}{3} \int_{E_1}^{E_0} \frac{\ell_s^2(E)\, dE}{\xi(E)\,[1 - \bar{\mu}(E)]\, E} \qquad (2.59)$$

in which

$\ell_s(E)$ is the scattering mean-free-path

$$= 10^{24}\, M/[N_A \rho\, \sigma_n(E)]\ \text{cm}, \qquad (2.60)$$

$\xi(E)$ is the average logarithmic energy loss in a scattering collision

$$= 1 - \frac{(M-m)^2}{2Mm} \ln \frac{M+m}{M-m}, \qquad (2.61)$$

constant, if the scattering is isotropic in the centre-of-mass frame of reference,*

$\bar{\mu}(E)$ is the average cosine of the scattering angle in the laboratory frame,

$= 2m/3M$

if the scattering is isotropic in the centre-of-mass frame.

Weinberg A M and Wigner E P "The Physical Theory of Neutron Chain Reactions" (U Chicago Press, 1958)

These expressions for ξ and $\bar{\mu}$ relate to a monoisotopic medium*.

One should not expect exact agreement between the formal age based on dfferential cross-sections, which can be calculated from (2.59), and the practical age based on the spatial distribution of In-resonance neutrons, which can be calculated from (2.56) using a multigroup or Monte Carlo neutron transport calculation. Nevertheless (2.59) should serve very well for estimating the change in the practical age which would result from small changes in the scattering cross-section $\sigma_n(E)$.

A variety of neutron sources have been used for experimental measurements of the neutron age, including 14MeV neuts from the TD reaction and 252 Cf spontaneous fission neutrons, but for fission reactor applications the measurements made with 235U neutron induced fission neutrons are of most interest, and the values listed in the upper part of Table 2.1 are believed to be the most reliable.

TABLE 2.1
AGE OF 235U FISSION NEUTRONS TO IN RESONANCE AT 1.46 eV

Moderator Density g/cm^3		H_2O 0.9972	D_2O 1.1046	Graphite 1.600
Experimental Values				
Paschall (1964-6)		26.61±0.32		
Spencer & Williamson (1967)		26.24±0.33		
Olcott (1956)	Extrapolated		112±2	
Wade (1958)	to 100%		110±3	
Graves (1962)	Purity		112±2	
Campbell & Paschall (1964)				307.8±2.0
Calculated Values	Data File			
Spanton (1973)	DFN-67×	26.08±0.08		
Spanton (1973)	DFN-68D			302.5
Kemshell (1969)	DFN-218†		108.8	
Kemshell (1969)	DFN-256		115.9	
Dunford & Alter	MAT-1001≠	26.22±0.13		
Dunford & Alter (1970)	MAT-1003≠		117.9	
Dunford & Alter (1970)	MAT-1011			295.7±0.5

×DFN-33 for oxygen †DFN-37 for oxygen ≠ MAT-1013 for oxygen

*More generally, for a mixture

$$\tau(E_0, E_1) = \frac{1}{3}\int_{E_1}^{E_0} \left[\sum_i \Sigma_n^i(E)\,\xi_i(E)\right]^{-1} \left[\sum_i \Sigma_n^i(E)\{1-\bar{\mu}_i(E)\}\right]^{-1} d\ln E$$

in which $\Sigma_n^i(E)$ is the macroscopic scattering cross-section of the medium for the i-th nuclide;

$$\xi_i(E) = \int_{-1}^{1} f_i(E,\mu)\,\ln[2/\{1+\alpha_i+(1-\alpha_i)\mu\}]\,d\mu$$

where $f_i(E,\mu)\,d\mu$ is the elastic angular distribution of the i-th nuclide, and

$$\alpha_i = (M_i - m)^2/(M_i + m)^2.$$

All the calculated age values in the lower part of the table have been revised to agree with the material densities quoted at the head of the table, and to a fission spectrum with a mean energy of 1.98 MeV. The uncertainty of Olcott's result has been increased to allow for variations of the D_2O purity during the course of the experiments.

The measured values of the neutron ages appear to be good to 1 or 2 per cent, and it is easily seen from (2.59) above that ± 1/2 per cent accuracy is needed overall in the moderator scattering cross-section to give ± 1 per cent in the calculated age. The calculated ages listed in the table were derived using rather elderly data files, and it would be valuable to have revised calculations for the most up-to-date data files and 235U fission spectrum (Adams and Johansson 1979). The required revisions could be calculated quite easily by difference, using (2.59) and the tables of $\tau(E)$ given by Goldstein et al (1961).

In order to match the accuracy of slowing-down age measurements the moderator scattering cross-sections need about ± 1/2 per cent accuracy over a good part of the energy range from 1 eV to about 2 or 3 MeV. For graphite, several sets of good quality measurements of the total cross-section have been reported during the last 10 or 20 years and, apart from the narrow d-wave resonance at about 2.08 MeV, the cross-section can be well represented from a few eV to nearly 3 MeV by means of a simple polynomial in the neutron energy, or by a more elaborate resonance formulation.

The radiative capture cross-sections of the moderators are small at thermal energies and decrease like $1/\sqrt{E}$ with increasing neutron energy, so that the epithermal scattering cross-sections are almost identical with the total cross-sections, and these have been measured with fairly good accuracy. However the slow neutron scattering parameters have been determined with particular care, by measurements at thermal energies and in the eV region. In consequence, for H and D particularly, the energy dependence of the scattering cross-sections can be identified somewhat more precisely with the help of the "effective range" theory.

Paschall R K (1966) Nucl Sci Eng 26 73; ibid (1964) 20, 436.

Spencer J D & Williamson T G (1967) Nucl Sci Eng 27, 568.

Olcott R N (1956) Nucl Sci Eng 1, 327.

Wade J W (1958) Nucl Sci Eng 4, 12.

Graves W E (1962), Nucl Sci Eng 12, 439.

Campbell R W, Paschall R K and Swanson V A (1964) Nucl Sci Eng 20, 445.

Spanton J H (1973) AEEW 1172.

Kemshell P B (1969) Private Communication.

Dunford C L and Alter H (1970) AI-AEC-Memo-12915

Adams J M and Johansson P (1979) AERER8728. The mean energy of the 235U fission neutron spectrum is given as 2.016 ± 0.044 MeV

Scattering by ^1H is predominantly isotropic, in the centre-of-mass frame of reference, to quite high energies; even at 20 MeV for example the higher partial waves contribute only about 7 mb to a total scattering cross-section of about 500 mb. This partial cross-section for $\ell > 0$ can be inferred, with sufficient accuracy, from one or another of the extensive phase-shift analyses which have been carried out on the many and various nH and pH interaction data at energies up to about 500 MeV, see Figure 2.6, and can be subtracted from the neutron total scattering cross-section data so that the s-wave component is well determined from the data.

The representation of the s-wave scattering data by means of effective range expansions

$$K_i \equiv k \cot \delta_i = -(1/a_i) + (r_i/2) k^2 - P_i r_i^3 k^4 + \ldots , \qquad (2.62)$$

for i = 1, 3 denoting the singlet and triplet states, was reviewed critically by Noyes (1963), who showed that the standard form of this expansion has to be modified to take account of, and to exploit, the predictions of the One Pion Exchange theory of the long range nucleon-nucleon interaction, and that for this purpose the approximation due to Cini et al (1959) should be reasonably adequate for neutron energies up to about 10 MeV. The s-wave phase shifts δ_i derived from this theory do not change sign, as they should, at about 310 MeV; but this fault can be rectified by a simple modification (due to Pope and Story, (1972) to the expansion proposed by Cini et al, and thereby the range and reliability of the method are enhanced, up to 20 MeV at least.

According to the theory of Cini et al, the s-wave effective range formula

$$\sqrt{\omega} \cot \delta_i = Q_i(\omega) \qquad i = 1, 3, \qquad (2.63)$$

in which

$$\omega = (k r_0)^2 \approx 0.0243865\, E, \quad \text{with } E \text{ in MeV} \qquad (2.64)$$

$$r_0 = \hbar/(m_\pi c) \approx 1.42270 \text{ fm} \qquad (2.65)$$

k is the neutron wave number in the centre of mass frame

E is the energy of the incident neutron in the laboratory frame

m_π is the average pion mass,

has to satisfy the conditions

$$Q_i(-\omega_0) = -\sqrt{\omega_0} \qquad (2.66)$$

$$Q_i'(-\omega_0) = 2\beta + 1/(2\sqrt{\omega_0}) \qquad (2.67)$$

Noyes H P (1963) Phys Rev 130, 2025; see also Noyes (1972) Annual Rev Nucl Sci 22, 465.

Cini M, Fubini S and Stanghellini A (1959) Phys Rev 114, 1633.
Pope A L and Story J S (1972) Unpublished.

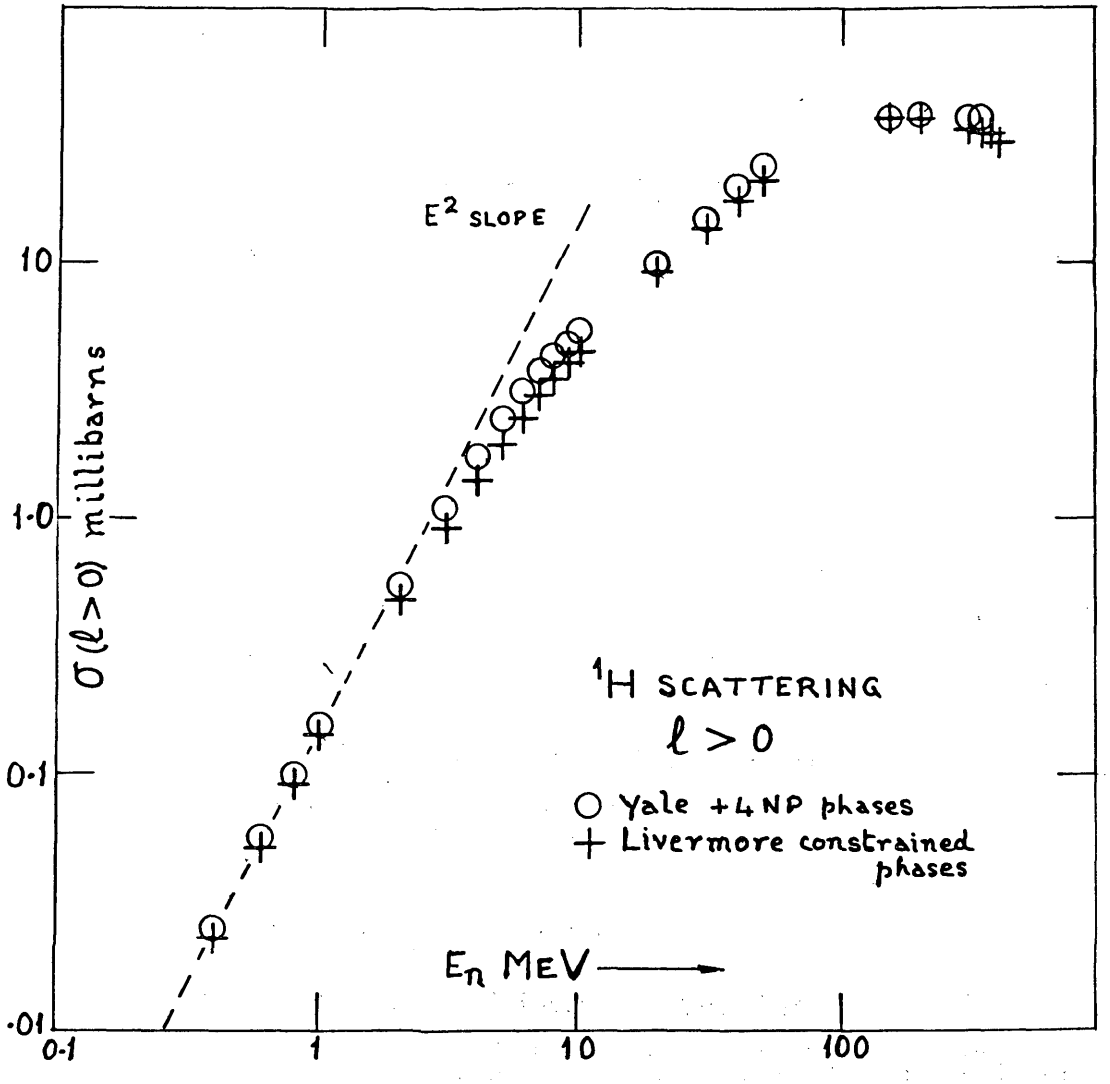

FIG. 2·6 Non s-wave contribution to n H scattering cross-section

when

$$\omega = -\omega_0 = -1/2 \tag{2.68}$$

with

$$\beta = 4\overline{M}/g_\pi{}^2 \tag{2.69}$$

in which $g_\pi{}^2$ is the pion-nucleon compling constant and $\overline{M}$ is the ratio of the average nucleon to the average pion mass;

$$g_\pi{}^2 = 14{\cdot}28 \pm 0{\cdot}18 \tag{2.70}$$

according to Bugg et al (1980),

$$M = 6.76948\,. \tag{2.71}$$

From the binding energy of the deuteron,

$$E_B \approx 2.224564 \pm 0.000017 \text{ MeV} \tag{2.72}$$

according to Greenwood and Chrien (1980), may be derived, in the triplet state

$$Q_3(-\omega_3) = -\sqrt{\omega_3} \tag{2.73}$$

when $k = -i\alpha$, that is to say when

$$\omega = -\omega_3 = -(\alpha r_0)^2 \approx -0{\cdot}108603, \tag{2.74}$$

with

$$\alpha^2 = \{2M_nM_p/(M_n+M_p)\}E_B/\hbar^2 \approx 0{\cdot}0536409 \text{ fm}^{-2} \tag{2.75}$$

Because the singlet and triplet s-wave phase shifts change sign at about 280 and 340 MeV respectively, we require further that

$$Q_i(\omega) \longrightarrow \infty \tag{2.76}$$

as E approaches this energy region from below. The modified form of the Cini et al effective range representation is now written as

$$Q_i(\omega) = A_i + \omega(B_i + C_i\omega)/[(1+D_i\omega)(1-H_i\omega)] \tag{2.77}$$

The H_i were zero in the original formulation of Cini et al, but are chosen so that (2.76) is satisfied, which requires

$$H_1 \approx 0.1464, \qquad H_3 \approx 0.1205 \tag{2.78}$$

From (2.66) and (2.67) it may now be shown that

$$D_i = 2 - [A_i'(2+H_i) - B_i]/[\beta'(1+H_i/2) - A_i'] \tag{2.79}$$

and

$$C_i = A_i'(4+D_iH_i) - \beta'(2-D_i)(2+H_i)\,, \tag{2.80}$$

in which

$$A_i' = A_i + \sqrt{(1/2)} \tag{2.81}$$

$$\beta' = \beta + \sqrt{(1/8)} = 2{\cdot}2503\,. \tag{2.82}$$

For the triplet state from (2.73)

$$B_3 = C_3\omega_3 + (A_3 + \sqrt{\omega_3})(1-D_3\omega_3)(1+H_3\omega_3)/\omega_3 \tag{2.83}$$

Comparison of (2.77) with the standard form of effective range expansion, (2.62), gives

$$a_i = -r_0/Q_i(0) = -r_0/A_i \tag{2.84}$$

relating A_i to the zero energy scattering lengths a_i,

$$r_i = 2r_0\,Q_i'(0) = 2r_0B_i \tag{2.85}$$

expressing the low energy effective ranges r_i in terms of B_i, and

$$P_i = [B_i(D_i - H_i) - C_i](r_0/r_i)^3 \tag{2.86}$$

for the low energy shape parameters P_i.

The A_i are determined at once, by (2.84), from the zero energy scattering lengths a_i, which may be derived from the measured values of the bound coherent scattering amplitude

$$b_{coh} = 3{\cdot}7409 \pm 0{\cdot}0011 \text{ fm} \tag{2.87}$$

(Koester and Nistler, 1975), and from the low energy free-atom scattering cross-section

$$\sigma_{free} = 20{\cdot}473 \pm 0{\cdot}034 \text{ barns} \tag{2.88}$$

which is the weighted mean of measurements by Neill et al (1968), Houk (1971) and Dilg (1975), noting that

$$a_{coh} = (a_1 + 3a_3)/4 \tag{2.89}$$

$$\sigma_{free} = \pi(a_1^2 + 3a_3^2) \tag{2.90}$$

with

$$a_{coh} = b_{coh}/(1 + M_n/M_H) = 0{\cdot}499791752\,b_{coh}. \tag{2.91}$$

Bugg D V, Edington J A, Gibson W R and others Phys Rev C21, 1004

Greenwood R C and Chrien R E (1980) Phys Rev C21, 498

Koester L and Nistler W (1975) Zeits Phys A272, 189

Neill J M, Russell J L and Brown J R (1968) Nucl Sci Eng 33, 265

Houk T L (1971) Phys Rev C3, 1886

Dilg W (1975) Phys Rev C11, 103

Finally, it should be noted that at low energies, for neutron energies from about 0.5 eV to 1 KeV, the scattering cross-section for H in H_2O has the form

$$\sigma_S(E) = \sigma_{free}\left[1 + \bar{K}/(3AE) - bE\right], \qquad (2.92)$$

in which A is the ratio of the mass of the hydrogen atom to that of the neutron (A = 0.99916735), and $\bar{K}$ may be considered as representing the mean kinetic energy of the hydrogen atoms in H_2O; by analysing their measured data above 0.6 eV on the total cross-section of H_2O, Neill et al (1968) obtained the value

$$\bar{K} = (0.1859 \pm 0.0117)\ eV \qquad (2.93)$$

for water at about 20°C. For the final term in (2.92), from the effective range formalism

$$b = \left[\{a_1^3(a_1 - r_1) + 3a_3^3(a_3 - r_3)\}/(a_1^2 + 3a_3^2)\right]\hbar^2 10^{-6} \qquad (2.94)$$
$$\approx 0.00000655\ eV^{-1}$$

An analysis using the modified effective range formalism (2.77) was carried out by Pope and Story (1972) for the epithermal scattering in the current file (DFN-923) for H in H_2O in the UK Nuclear Data Library. With r_1 = 2.640 fm to fit to the s-wave scattering cross-section data, particularly in the range 0.4 to 50 MeV there was found to be also excellent agreement with the s-wave phase shifts. Revision would now be worth while using the most up-to-date phase shift data and other nuclear data as listed above.

In this application to nH scattering the effective range formalism has played a dual role

(i) as a smooth fitting function

(ii) conforming to the known physical and theoretical constraints.

Similar roles are served in applying a suitably modified effective range theory to the epithermal cross-section data for deuterium; it was by this means that the shape of the total cross-section below about 500 KeV was first identified, and the discrepancy with the integral measurements of neutron age in D_2O was eliminated. The analysis has not been revised however since the total cross-section data of Stoler et al (1972) became available, spanning the energy range from 2 keV to 1 MeV.

For s-wave neutron interactions with deuterium, an effective range expansion of standard form (2.62) appears adequate for the dominant quartet state (J = 3/2), but for the doublet state an anomalous form such as

$$K_2 \equiv k\cot\delta_2 = (-1/a_2) + (r_2/2)k^2 - Pk^4/(1 + Dk^2) + \ldots \qquad (2.95)$$

Pope A L and Story J S (1972) unpublished work; but see Figure 2.7.

Stoler P, Kaushal N N, Green F, Harms E and Laroze L (1972) Phys Rev Letters 29, 1745.

is required. The underlying theory of this particular 3-body state seems not yet very clearly established, but fortunately the doublet contribution to the scattering cross-section is small.

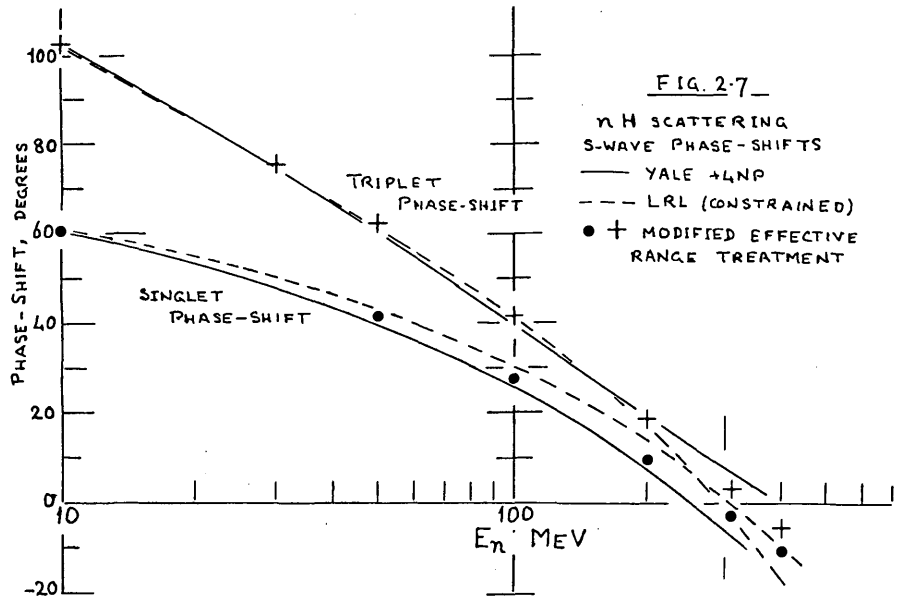

FIG. 2·7
n H SCATTERING
S-WAVE PHASE-SHIFTS
—— YALE +4NP
– – – LRL (CONSTRAINED)
● + MODIFIED EFFECTIVE RANGE TREATMENT

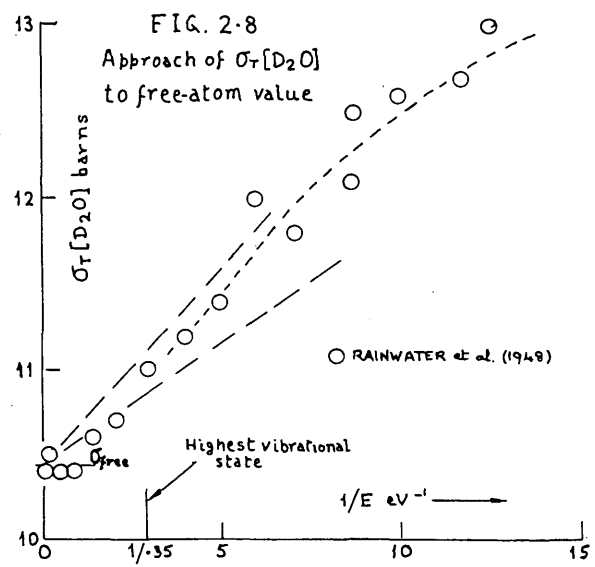

FIG. 2·8

For deuterium the higher partial waves ($\ell > 0$) contribute much more strongly to the cross-sections below 20 MeV than for ^1H, and in consequence the analysis of the deuterium cross-sections depends quite strongly on the phase-shift information available. Above the (n,2n) break-up threshold at 3.34 MeV the phase-shifts are complex, which leads to some complication of the formulae.

At low energies, above the energy of the lowest vibrational state of the D_2O molecule at about 0.35 eV, the cross-section for D in D_2O should have the form (2.92). The total cross-section data for D_2O are sparse near this energy, however a value of $\bar{K} = 0.168 \pm 0.039$ eV is indicated for D in D_2O, from Figure 2.8. Although this estimate is not very reliable, it is not inconsistent with values of 0.114 eV and 0.230 eV derived by Butland (1973) using respectively the phonon frequency functions of Page and Haywood (1973) and of Honeck (1962).

3 ON EVALUATING THE RESONANCE CROSS-SECTIONS OF THE STRUCTURAL MATERIALS

3.1 Level Spacing Studies for Resonances of Iron

Can the observed resonances of the iron isotopes be rationally assigned as to spin and parity, so as to command some degree of credence? The narrow p- and d- wave resonances of iron make a contribution to the Doppler temperature coefficient in a fast reactor so we are concerned with something more than simple average cross-sections.

For many of the fission-products the differential neutron cross-section data are restricted to the low energy range, or are non-existent, and recourse must be made to statistical theories and to systematics. This has been one of the motivations for the considerable efforts which have been given recently to development of codes for estimating resonance statistical parameters from sets of experimental resonance parameter data. Fröhner, for example, in his remarkable paper to the course held here at Trieste in Jan/Feb 1978, has described a quite sophisticated code for estimation of strength functions and average level spacings. The main emphasis behind this, and behind similar codes evolved elsewhere, has been on the importance of examining the distribution of the observed values of the reduced neutron widths $\Gamma_n^{(\ell)}$ in order to assess the numbers of missed resonances. It is reasonably well established that the family of reduced neutron widths of a set of resonances of particular spin and parity JΠ will have the Porter-Thomas distribution

$$p(\alpha, \rho; x) = [\alpha^\rho / \Gamma(\rho)]\, x^{\rho-1} \exp(-\alpha x)\, dx \qquad (3.1)$$

Rainwater L J, Havens W W, Dunning J R and Wu C S (1948) Phys Rev 73, 733

Butland A T D (1973) Private Communication

Page D I and Haywood B C (1968) AERE - R 5778

Honeck H C (1962) Trans American Nucl Soc 5 (1) 47

Fröhner F H (1978) IAEA-SMR-43; 59; KFK-2669

in which $\Gamma(\rho)$ is the gamma function, and x has been used to denote the reduced neutron width $\Gamma_n^{(\ell)}$;

$$\alpha = \langle x \rangle / \rho \,, \qquad (3.2)$$

and $\nu = 2\rho$ is the number of channel spin states involved (= 1 or 2).

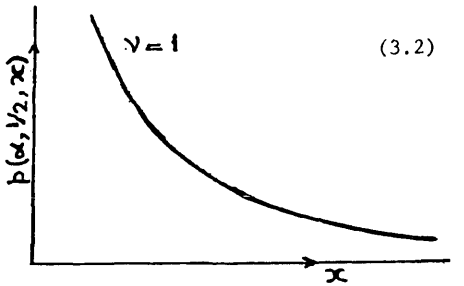

This is a very skew distribution, especially if $\nu = 1$ as is certainly true for s-wave resonances. It tells us that the resonances with smallest values for the reduced neutron widths, those which are most likely to be missed, are the most probable. By assuming that all resonances below some bias level x_0 have been missed, the distribution of observed widths greater than x_0 can be fitted with a truncated Porter-Thomas distribution and the number and mean reduced width of the missed resonances can be assessed.

Benchmark testing has shown that, used with care, these codes can be fairly reliable, especially if the resonance sample is fairly numerous However I believe that the older method, based on careful examination on the "staircase plot" of the number of resonances N(E) up to energy E, still has a role to play.

Fröhner has illustrated his theme by analysing the s-wave resonances of some of the iron isotopes, and his values for the mean spacings indicate that several resonances have been missed in each. However the neutron widths of the s-wave resonances of iron are quite broad, typically of the order of 1 keV, and should, in the main, be easily detectable with modern neutron spectrometers. In measurements of the total cross-section the s-wave resonances are easily distinguished by the characteristic interference dip a little below the energy of the resonance peak. If the resonance is relatively narrow, so too is the interference dip, and occasionally a narrow s-wave resonance may have been wrongly assigned to the non s-wave set because its interference dip is obscured, by the presence of a p-wave resonance for example; however it seems doubtful that chance coincidences of this kind can be often invoked to account for many missed resonances.

There is another factor affecting the mean spacing of resonances of the isotopes in this mass region. Resonances of 56Fe have been observed and analysed up to about 800 keV, and over such a wide energy interval the ordinary theory of level density predicts that the mean spacing should fall by a factor of about 2. The level spacing statistics of Dyson and Mehta (1963) are based on the assumption that the mean spacing D does not vary with the neutron energy. In order to use their theory for analysing the resonance spacings of materials such as 56Fe we set up a (1,1) correspondence between the resonance energies E_r and a set of energies Y_r in a modified energy scale, with the requirements

Dyson F J and Mehta M L (1963) J Mathematical Phys 4, 701

(i) The mean spacing of the Y_r does not vary with Y and has the value D_o

(ii) The mean spacing of the E_r varies with E in accordance with a suitable Fermi-gas model of level densities, $\rho(U)$, in the same compound nucleus

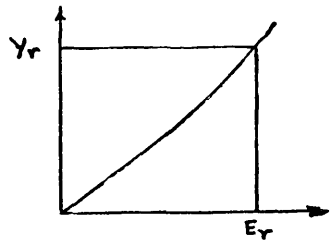

$$D(E) = D_o\, \rho(U_o)/\rho(U) \qquad (3.3)$$

so that $D_o = D(E_o)$, the mean spacing corresponding to some specified energy E_o. In this formula U, U_o are the excitation energies of the compound nucleus for incident neutron energies E, E_o, with appropriate modifications for pairing energy etc according to the prescriptions of the level density formalism adopted, e.g.

$$U = S_n + \Delta + E/(1 + m/M), \qquad (3.4)$$

in which S_n is the neutron separation energy from the compound nucleus, and Δ = back shift - pairing energy for example. In practice it proves convenient to set $E_o = 0$, so that $1/D_o$ is the mean level density of the compound nucleus at the separation energy; $\rho(U_o)$ in contrast is merely an approximate estimate of this level density.

TABLE 3.1 Gd-152; MEAN RESONANCE SPACINGS (eV UNITS)

Res No	ERES	DBAR	+-ERROR	E SPACE
1	(-1.2)			
2	3.31	4.4627	1.745	4.51
3	8	4.5587	1.240	4.69
4	12.35	4.4880	0.937	4.35
5	21.2	5.5576	0.940	8.85
6	36.86	7.7034	1.112	15.66
7	39.3	7.1145	0.917	2.44
8	42.7	6.6922	0.767	3.4
9	74.3	9.5627	0.937	31.6
10	85.1	9.9508	0.899	10.8
11	92.4	9.8907	0.827	7.3
12	100	9.7977	0.759	7.6
13	124	10.800	0.754	24
14	140	11.297	0.737	16
15	185.2	13.726	0.830	45.2
16	202	14.219	0.821	16.8
17	223	14.822	0.812	21
18	231	14.710	0.775	8
19	238	14.515	0.735	7
20	252	14.508	0.696	14
21	293	15.526	0.690	41

(iii) The expected number of resonances in the interval (Y_o, Y), with $Y_o = E_o$, is equal to the expected number in the corresponding interval (E_o, E), namely

$$(Y - Y_o)/D_o = \int_{E_o}^{E} [1/D(E')]\, dE' \qquad (3.5)$$

so that, using (3)

$$Y = E_o + [1/\rho(U_o)] \int_{U_o}^{U} \rho(U')\, dU'. \qquad (3.6)$$

The requirements (i) to (iii) and formulae (3.3) to (3.6) are intended to apply to the resonances of a single or multiple family; to all the resonances of definite spin and parity $J\pi$, for example, or to all p-wave resonances (if these can be identified). With this understanding the Dyson-Mehta theories can be applied to the set of energies Y_r. However the theories are valid only if the set is complete within an interval; there should be no missed resonances and no intruders from a different family or from an isotopic contaminant.

TABLE 3.2

Fe-58; MEAN SPACINGS OF S-WAVE RESONANCES (keV UNITS)

Res No	ERES	D_0	±	E Space
1	-10			
2	10.339	19.858	7.721	20.339
3	43.55	27.077	7.402	32.211
4	67.18	26.465	5.581	23.63
5	93.9	26.904	4.593	26.72
6	121.67	27.518	3.947	27.77
7	179.5	33.449	4.113	57.83
8	241.2	39.417	4.310	61.7
9	266	39.189	3.905	24.8
10	309.9	40.916	3.673	43.9
11	321	39.312	3.295	11.1
12	348.105	38.817	2.974	27.105

First 3 values of D are based on inadequate statistical sample; next 4 values of D are all consistent with $D \approx 6.5$ or 6.6. For $k \geq 9$ the D values increase fairly steadily because resonances have been missed experimentally. If D really is $\sim$ 7 eV the energy interval of 31.6 eV between the 8th and 9th resonances is improbably large.

The D_0 values show a jump increase between 6th and 7th resonances, suggesting that one has been missed at about 150 or 210 keV

In this table E-Space denotes the spacing between corresponding values of Y_r (see text)

The Dyson-Mehta optimum statistic is used for estimating the mean spacing $D_0 \pm \Delta D_0$ from the energies of the first k resonances of the set; with k = 2,3,4... N in turn; this represents a modernisation of the tradiational "staircase plot" of the number of resonances N(E) up to energy E. The formulae for calculating D_0 are set out in Appendix A.

For small values of k it is to be expected that statistical fluctuations between successive values of D_0 will be quite large, and their estimated uncertainties are unreliable because in principle the theory is valid only for large k, terms O(1/k) having been ignored; with k $\sim$ 10 the fluctuations should be much smaller and mostly within the calculated uncertainties. At the higher energies, if resonances have been missed for example because of loss of resolution, successive values of D_0 may show a fairly steady increase with increase of k. Table 3.1 of DBAR values for the resonances of 152Gd illustrates these trends; Table 3.2 for 58Fe is another example. From this kind of tabulation a tentative assessment of the completeness of the set of resonances (up to what value K of k is the set complete?) and of the best value of D_0 may be made. Sometimes the inclusion of 1 or 2 more resonances artificially into the set, where adjacent resonances are rather far apart, will considerably extend the range up to which the set appears to be complete and may allow an improved assessment of D_0.

Table 3.3 of DBAR=D_0 values for the s-wave resonances of 56Fe (which span the range from -3.5 to 785 keV) shows exceptional uniformity in the different estimates of D_0, and good consistency therefore with the hypothesis that D(E) has the energy dependence specified by (3.3).

Dyson and Mehta have emphasised the long-range order, "the essentially crystalline character" of a single level series. In effect this means that, for a single level series (for a set of resonances of the same $J\pi$), there should be a (1,1) correspondence between the energies of the set and the energies of a ladder of evenly spaced energy rungs

$$L_r = y_0 + rD_0 \qquad r = 1, 2, \ldots K \qquad (3.7)$$

supposing that D_0 has been well-chosen and that the set of resonances is complete and contains no impurities. By choosing

$$y_0 = \sum_1^K Y_r - (K+1)D_0/2 \qquad (3.8)$$

the mean square of the fractional deviations $(Y_r - L_r)/D_0$ of the $\{Y_r\}$ from their corresponding $\{L_r\}$ is minimised. Tabulating the two sets of energies alongside each other, along with the fractional deviations, provides a further opportunity of looking at the completeness and purity of the set of resonances. The comparison gives some indication of the approximate location in energy of vacancies due to missed resonances, or of possible intruders from other $J\pi$ states or from isotropic contaminants.

L_r	Y_r
–	—
–	—
–	—
–	—
–	—
–	—
–	—
–	—

TABLE 3.3

Fe-56; MEAN SPACING OF S-WAVE RESONANCES (KeV UNITS)

Res No	ERES	DBAR	+-ERROR	ESPACE
1	-3.4756			
2	27.66	31.363	12.324	31.136
3	73.98	39.483	10.787	46.32
4	83.65	31.052	6.710	9.67
5	129.8	34.286	5.790	46.15
6	140.4	30.769	4.492	10.6
7	169.2	30.316	3.748	28.8
8	187.6	29.097	3.180	18.4
9	220.5	29.526	2.829	32.9
10	245	29.410	2.549	24.5
11	276.6	29.921	2.349	31.6
12	317	31.262	2.238	40.4
13	331.2	30.705	2.072	14.2
14	356.9	30.727	1.928	25.7
15	362	29.792	1.790	5.1
16	380.9	29.268	1.643	18.9
17	403.5	28.995	1.521	22.6
18	437	29.304	1.428	33.5
19	469.2	29.766	1.366	32.2
20	500.2	30.255	1.316	31
21	535.67	30.989	1.280	35.47
22	560.82	31.306	1.241	25.15
23	575.87	31.192	1.197	15.05
24	603.16	31.435	1.154	27.29
25	609.77	31.067	1.114	6.61
26	613.67	30.618	1.075	3.9
27	665.72	31.239	1.019	52.05
28	693.18	31.558	0.992	27.46
29	716.8	31.764	0.966	23.62
30	742	32.006	0.941	25.2
31	752.97	31.859	0.917	10.97
32	769.7	31.790	0.890	16.73
33	785	31.683	0.863	15.3

This comparison must be used with caution however, because the picture may change if a different value of K or of D_0 is adopted for input to the ladder calculations. This warning is all the more necessary because the comparisons are very persuasive as may be seen from

Table 3.4 for 152Gd and Table 3.5 for 56Fe. It should be remarked that the resonances of 152Gd extend only to 293 eV, and over so narrow an energy range no allowance is needed, nor was any made, for energy dependence of the DBAR values; for this set of data therefore Y_r must be replaced by E_r in (3.8). For 56Fe with resonances spanning several hundred keV, the ladder calculations were carried out as specified in (3.7) and (3.8) above, but conversion was made from the Y-scale back into the E-scale (see (3.6)), for the user's convenience, before printing.

TABLE 3.4

Gd-152; RESONANCE ENERGIES COMPARED WITH THE RUNGS OF THE ENERGY LADDER (eV UNITS)

E-Ladder	ERES		(ER-EL)/D	E-Ladder	ERES	(ER-EL/D)
-15.98	-15.86			69.82	100	4.573
- 9.38	- 9.12			76.42	124	7.210
- 2.78	- 1.2		0.240	83.02	140	8.634
3.82	3.31		-0.0766	89.62	185.2	14.48
10.42	8.0		-0.366	96.22	202	16.03
17.02	12.35	*	-0.707	102.82	223	18.21
23.62	21.2		-0.366	109.42	231	18.42
30.22	36.86	**	1.007	116.02	238	18.48
36.82	39.3		0.376	122.62	252	19.60
43.42	42.7		-0.108	129.22	293	24.82
50.02	74.3	*	3.679	135.82		
56.62	85.1		4.316	142.42		
63.22	92.4		4.422	149.02		

*has been introduced whenever the absolute value of the fractional difference exceeds 0.5.

The comparison suggests that, if the value of D (6.6 eV) used in setting up the ladder was correct, about 4 resonances have been missed above 43 eV and many more at the higher energies.

TABLE 3.5

Fe-56; RESONANCE ENERGIES COMPARED WITH THE RUNGS OF THE ENERGY LADDER (KeV UNITS)

E-Ladder	ERES		(ER-EL)/D	E-Ladder	ERES	(ER-EL)/D
- 65.52	(- 63.30)			445.24	437.6	-0.355
- 34.33	(- 32.40)			468.24	469.2	0.0423
- 3.723	- 3.4756		0.00815	490.92	500.2	0.413
26.33	27.66		0.0447	513.30	535.67**	1.013
55.85	73.98	*	0.624	535.39	560.82**	1.167
84.84	83.65		-0.0415	557.20	575.87*	0.867
113.34	129.8	*	0.585	578.72	603.16**	1.151
141.36	140.4		-0.0345	599.97	609.77	0.465
168.91	169.2		0.0106	620.96	613.67	-0.349
196.01	187.6		-0.312	641.69		
222.68	220.5		-0.0823	662.17	665.72	0.174
248.93	245.0		-0.151	682.41	693.18*	0.537
274.77	276.6		0.0716	702.40	716.8*	0.727
400.21	317.0	*	0.668	722.16	742.0 **	1.015
325.27	331.2		0.239	741.70	752.97*	0.582
349.96	356.9		0.284	761.01	769.7	0.455
374.30	362.0	*	-0.507	780.10	785.0	0.258
398.28	380.9	*	-0.726	798.99		
421.93	403.5	*	-0.780	817.66		

*has been introduced whenever the absolute value of the fractional difference (ER-EL)/D exceeds 0.5.

Note that the resonance energies ER $\geq$ 665.72 have all been shifted one rung downwards, to give a better fit to the ladder. In fact the ladder comparison suggests that a resonance may have been missed at about 518 or 640 keV, and perhaps another at about 679 keV.

Ideally we should expect that

$$D_0 \rho(U_0) = 1.0 \qquad (3.9)$$

in (3.3), and the adopted value of D_0 can be used for revision of the parameter values in the level-density formula so that (3.9) is satisfied; the revised values can be used in the input for any subsequent re-run. The level-density parameter values currently available, from the tables of Gilbert and Cameron (1965) for example, were mostly obtained in just this way from earlier consideration of mean spacings of resonances, or from systematic comparisons with data for neighbouring nuclides; consequently the proposed revision is fully justifiable.

The level density formula can also be used to estimate, from the D_0-value adopted for the s-wave resonances, the mean spacings for other spin/parity states $J\pi$ of the same compound nucleus.

For several of the isotopes of materials such as iron, numbers of non s-wave resonances have been reported. Some of these can be assigned as p-wave resonances because they are too strong for d-wave assignments ($\ell = 2$). With the help of the estimated mean spacings it has been found possible to make plausible $J\pi$ assignments for all the non s-wave resonances of the even isotopes of iron. The measured capture areas $g\Gamma_n\Gamma_\gamma/\Gamma$ are also useful in this partitioning process; a large value may indicate that the spin statistical factor g is large, suggesting an $\ell=2$, $J=5/2$ assignment, for example.

Admittedly much guesswork has been involved in these examples of "evaluator's art', what benefits are gained?

(i) The resonance structure has been reasonably interpreted within the framework of current theoretical models.

(ii) Though later experimental work may well show that some of the $J\pi$ assignments are wrong, at least a basis for argument has been provided.

(iii) The partitioning has helped in estimating mean Γ_γ values and in reducing their dispersion, and this has helped in the attribution of partial widths Γ_n and Γ_γ for the non s-wave resonances. These narrow resonances of iron contribute to the Doppler temperature coefficient in fast reactors.

Gilbert A and Cameron A G W (1965) Canadian J Phys 43, 1446

If the mean spacing of resonances varies with energy as has been proposed, if the neutron strength functions

$$S_\ell = \langle \Gamma_n^{(\ell)} \rangle / D(J\pi, E) \qquad (3.10)$$

do not, as is usually supposed, the mean reduced neutron width must itself vary with energy because of (3.10). Then it should be expected that the neutron strengths of the individual resonances, defined by

$$\Theta_r = \Gamma_{nr}^{(\ell)} / D(J\pi, E_r) \qquad (3.11)$$

should have a Porter-Thomas distribution, rather than the reduced neutron widths.

It is interesting to compare the two different assessments made of the mean spacings of s-wave ($\ell = 0$) resonances of iron isotopes by Fröhner (1978-79) using the STARA code, and by Smith and Story (1981) using DEEBAR: it will be recalled that STARA estimates the number of missed resonances from the distribution of the reduced neutron widths. The comparisons are presented in Table 3.6 following:

TABLE 3.6

Fe ISOTOPES: ESTIMATES OF THE MEAN RESONANCE SPACINGS

Isotope	Frohner (1978-9) STARA Code	Smith and Story (1981) DEEBAR Code
Fe54	20.4 ± 2.7	23.9 ± 0.8
Fe-56	21.4 ± 1.9	27.0 ± 1.2
Fe-57	6.5 ± 0.8	(9.15± 0.5)
Fe-58	21.6 ± 5.6	29.1 ± 2.0

STARA makes no allowance for energy dependence of the mean spacings. For comparison therefore the values quoted from the DEEBAR code have been adjusted to relate to the mid-points of the energy ranges studied with STARA.

The STARA calculations suggest that about 20% of the s-wave resonances have been missed experimentally, even in the energy range below 400 keV. We are skeptical about this, for reasons given earlier; however it must be stated that the DEEBAR calculations cannot disprove the hypothesis, because it is always possible to put the observed resonance energies into (1,1) correspondence with a subset of the rungs of an energy ladder constructed with a smaller value of D_o.

Fröhner F H (1979) NEANDC Topical Discussion (revised values)

Smith R W and Story J S (1981) DIDWG(81)P256

TABLE 3.7

Fe-56; COMPARISON OF MEASURED Γ_γ VALUES FOR SOME S-WAVE RESONANCES

$E_r$keV	Pandey et al (1975)	Allen et al (1976)	Fröhner (1977)
27.8	1500	1.43 ± 0.07	1.25 ± 0.2
73.95		0.73 *	0.65 ± 0.15
83.6	1300	1.28 *	0.58 ± 0.22
129.8	600	0.79 *	1.30 ± 0.40
140.3	2800	2.19 *	1.48 ± 0.31

*statistical uncertainties 10%

Fe-54; COMPARISON OF MEASURED Γ_γ VALUES FOR SOME S-WAVE RESONANCES

$E_r$keV	Pandey et al (1975)	Allen et al (1977)	Beer and Spencer (1975)
52.62	1950	2.4	1.8
71.75	1540	1.32	0.8
98.61	550	1.65	3.2
130.1	3340	3.22	3.0
147.8	3380	2.31	3.0
174.0	3680	3.5	2.4

Allen B J, Musgrove A R de L, Boldeman J W, Kenny M J and Macklin R L (1976) Nucl Phys A269, 408.

Allen B J, Musgrove A R de L 1977 NEANDC/NEACRP Geel Specialists' meeting on neutron data of structural materials for fast reactors, 447 (Pergamon, 1979).

Allen B J, Musgrove A R de L, Taylor R and Macklin R L, ibid 476.

Allen B J, Musgrove A R de L, Boldeman J W and Macklin R L (1977) AAEC-E403.

Allen B J, Cohen D D and Company F Z (1980) J Phys G (Nucl Phys) 6 1173.

Beer H and Spencer R R (1975) Nucl Phys A240, 29.

Beer H et al (1979) NEANDC(E) 202, 5.

Bilpuch E G, Seth K K, Bowman C D, Tabony R H, Smith R C and Newson H W (1961) Annals Phys 14, 387.

Brusegan A, Corvi F, Rohr G, Shelly R and van der Veen T 1979 Knoxville Conf on nuclear Cross Sections and Technology, 163 (NBS special Publ. 594).

Ernst A, Fröhner F H and Kompe D 1970 IAEA Helsinki Conf on Nuclear Data for Reactors 1, 633.

Fröhner F H 1977 NEANDC/NEACRP Geel Specialists' Meeting on Neutron Data of Structural Materials for Fast Reactors, 138 (Pergamon, 1979).

Garg J B, Rainwater J and Havens W W (1971) Phys Rev C3, 2447, and Errata in Phys Rev C9, 1673 (1974).

Hockenbury R W, Bartolome Z M, Tatarczuk J R, Moyer W R and Block R C (1969) Phys Rev 178 (4), 1746.

TABLE 3.8

Fe-56; EXPERIMENTAL VALUES FOR Γ_n AND Γ_γ FOR THE 27.8 KeV RESONANCE

Reference	Γ_n eV	Γ_γ eV
Bilpuch et al (1961)	1670 ± 200	
Macklin et al (1964)	1600 ± 100	1.5 ± 0.3
Moxon (1965)	-	≤ 1.3
Hockenbury et al (1969)		1.44 ± 0.14
Ernst et al (1970)	(1600± 100)	1.4 ± 0.3
Garg et al (1971)	1520 ± 40	
Pandey et al (1975)	1500 ± 50	
Allen et al (1977) re-evaluation of 1.43 ± 0.07 eV reported by Allen (1976)		1.6 ± 0.3
Fröhner (1977)	1400 ± 200	1.25 ± 0.2
Brusegan (1979) (provisional only)		0.80 ± 0.20
Allen et al (1980)	1520	0.82 ± 0.11
Wisshak & Käppeller (1981)		1.011 ±1.3% stat ± ~5% syst
Moxon (1979,1981)	1450 ± 50	0.85 ± 0.09

TABLE 3.9

Fe-56; PARAMETER VALUES FOR THE 1.15 keV AND 27.8 KeV RESONANCES, FROM VARIOUS EVALUATIONS

	1.15 KeV Resonance			27.8 KeV Resonance		
	E_r keV	Γ_n eV	Γ_γ eV	E_r keV	Γ_n eV	Γ_γ eV
ENDF/B4	1.15	0.086	0.600	27.9	1670	1.44
ENDF/B5	1.149	0.06	0.600	27.67	1520	1.4
UKNDL	1.154	0.0592	0.581	27.7	1400	1.39
KEDAK 3	1.148	0.068	0.600	27.81	1430	1.00
JENDL1	1.15	0.068	0.600	27.66	1600	1.45
Recent estimate by Moxon	1.1519	0.0575 ±0.001	0.598 ±0.011	27.821	1450 ±50	0.9 ±0.1

Accuracy of the Capture Data What of the accuracy of available capture data for iron isotopes? Some idea of the difficulties of accuracy assessment is given by the three tables that follow, Tables 3.7, 3.8 and 3.9. The first of these, Table 3.7, compares, for a few of the s-wave resonances of 56Fe and of 54Fe, the radiation widths Γ_γ reported by Allen et al (1976, 1977), from measurements at the Oak Ridge electron linear accelerator (ORELA), and by Frohner (1977) at Geel, and by Beer and Spencer (1975) at Karlsruhe. At some resonances the two measurements differ by a factor 2, and even the comparatively good agreement between the two measurements at the 27.8 keV resonance of ^{56}Fe is seen to be illusory when we turn to Table 3.8, which shows that the most recent measurements have resulted in smaller values for both the neutron and radiation widths of this resonance. These recent changes in the parameters of the most prominent resonance of ^{56}Fe make it difficult to have much confidence in any sort of average of the measured values of the radiation widths at any other s-wave resonance: how would you assess the uncertainties?

It should be added in conclusion that the variations of Γ_γ from one s-wave resonance to another has been explained in terms of the so-called valence model; see for example Allen (1976, 1977) and Beer et al (1979). However Moxon has emphasised that at these resonances Γ_n is very much larger than Γ_γ and that, in consequence, a positive correlation between the measured values of Γ_n and Γ_γ may occur, at least in part, because of inadequate suppression of the response of the capture gamma detector to the much larger flux of scattered neutrons.

3.2 Some Remarks Relating to the Use of Multi-Level Resonance Formalisms

3.2.1 Negative Energy Resonances

It is my personal opinion that, as a general principle, an evaluation of resonance parameters in the resolved range should always include an assessment of the parameters of the top s-wave negative energy resonance, or of the two top negative energy resonances, one for each spin state, if the target nucleus has odd mass number. Terms should also be included to allow for the effects of more distant resonances, both at negative and positive energies, as will be discussed in the next section.

For some nuclides the large value and energy dependence of the low energy scattering cross-section may determine the resonance energy and reduced neutron width of the principal negative energy resonance. This is exemplified by the low energy scattering data for ^{56}Fe (see for example Moore et al 1963), and likewise for ^{58}Ni. For many nuclides however, perhaps even for the majority, the significance of the top negative energy resonance is less obvious; for a start therefore one might suppose the resonance energy is about 1 mean spacing D below the first positive energy s-wave resonance (or below the first positive s-wave resonance of the same spin), subject to the condition that E_r is to be negative, and that the reduced neutron width Γ_n^0 and radiation width Γ_γ have their expectation values, (and the fission width Γ_f also, if the material is fissile).

$$\Gamma_n^0 = S_n^0 . D, \quad \Gamma_\gamma = \langle \Gamma_\gamma \rangle \qquad (3.12)$$

in which S_n^0 is the s-wave neutron strength function.

Next should be considered whether these values for the parameters result in too small or too large a contribution to the thermal neutron capture cross-section, when the contributions of all the known positive energy resonances have been taken into account.

Macklin R L, Pasma P J and Gibbons J H (1964) Phys Rev B136, 695.

Moxon M C (1965) EANDC Antwerp Conf on Study of Nuclear Structure with Neutrons 88.

Moxon M C (1979) Private Communication cited by Wisshak and Käppeler F (1981), below; see also Moxon M C (1981) NEANDC(E) 222 Vol 8, 24.

Pandey M S, Garg J B, Harvey J A and Good W M 1975 Washington Conf on Nuclear Cross-Sections and Technology 2, 748.

Wisshak K and Käppeler F (1981) Nucl Sci Eng 77, 58.

Moore J A, Palevsky H and Chrien R E (1963) Phys Rev 132, 801

The contribution of this negative energy resonance is

$$\Delta\sigma_\gamma(E_0) = (\alpha/\sqrt{E_0})\, g\Gamma_n^0\Gamma_\gamma/[(E_r - E_0)^2 + (\Gamma_n^0\sqrt{E_0} + \Gamma_\gamma)^2/4] \qquad (3.13)$$

in which $\alpha = 2.603939 \times 10^6 \ (1 + m_n/M)^2$ barns eV. Usually (3.13) may be approximated by

$$\Delta\sigma_\gamma(E_0) \approx (\alpha/\sqrt{E_0})\, g\Gamma_n^0\Gamma_\gamma/(E_r)^2, \qquad (3.14)$$

showing that a small change in E_r has the same effect on $\Delta\sigma_\gamma(E_0)$ as a larger fractional change in Γ_n^0.

Usually the required contribution $\Delta\sigma_\gamma(E_0)$ to the thermal neutron capture cross-section, be it large or small, can be obtained without the need for extreme values for the parameters; as a rough guide, it would be a matter for comment and for further investigation if the resonance energy has to be shifted by more than D/2 from its expected value (the expected value is not necessarily very easy to identify, since the first positive s-wave resonance may be below or above its 'expected' energy), or if the reduced neutron width lies outside the range $(0.3\langle\Gamma_n^0\rangle, 1.5\langle\Gamma_n^0\rangle)$. If extreme values are needed for the parameters of the top negative energy resonance the partial widths of one or two of the low energy positive energy resonances may need reconsideration.

The low energy coherent scattering amplitude (or amplitudes) should also be considered, if experimental data are available, when trying to assess the parameters of the top negative energy resonances; see for example James and Story (1966).

3.2.2 Distant Resonances

The more distant s-wave negative energy resonances also contribute to the thermal neutron capture cross-section, and they have a larger effect on the slow neutron scattering cross-section. The scattering effect may be understood in a qualitative sense by considering the asymmetric shape of a typical s-wave resonance. The Breit-Wigner single level formula for the total cross-section in the neighbourhood of one of these resonances may be written

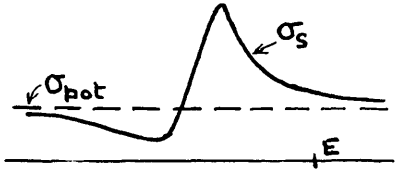

$$\sigma_T(E) = \pi\lambda^2 g\frac{\Gamma_n\Gamma}{BWD_r} + 4\pi\lambda R g\frac{\Gamma_n(E - E_r)}{BWD_r} + \sigma_{pot} \qquad (3.15)$$

in which the Breit-Wigner denominator BWD is

James M J and Story J S (1966) IAEA Paris Conf on Nucl Data for Reactors 2

$$BWD_r = (E - E_r)^2 + \Gamma^2/4 \qquad (3.16)$$

and

$$\sigma_{pot} = 4\pi R^2 \qquad (3.17)$$

is the potential scattering cross-section. The second term on the right in (3.15) arises from the interference between the resonance and potential scattering components and is the cause of the asymmetric shape of the s-wave resonance. Away from the resonance peak the Breit-Wigner denominator may be approximated by BWD = $(E-E_r)^2$, showing that the asymmetric term approaches the potential scattering background only like

$1/(E-E_r)$,

much more slowly than the $1/(E-E_r)^2$ of the resonant term alone. Consequently the effect of the asymmetric interference component extends over a much greater energy range than the symmetric resonance peak.

All the s-wave resonances to the left of a specified energy E tend to raise the background cross-section at E, and all those to the right of E tend to depress the background cross-section at E.

So far as the scattering cross-section is concerned, the effects of the unresolved negative energy resonances, and of the distant positive energy resonances beyond the resolved range are to modify the potential scattering as shown in the picture.

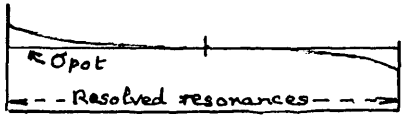

The formulae for the multi-level Breit-Wigner approximation are set out in Appendix B. The neutron partial cross-sections are expressed at (B15) and (B16) with (B18) in terms of the factors $A_x(E)$, B(E) and C(E) defined by (B19) to (B21), which sum over all resonances of the same (l,J); only single summations are involved, but they run in principle over all resonances, resolved and 'distant' of the specified (l,J). We may write

$$A_x = A_x' + A_x'', \quad \text{and likewise for B and C,} \qquad (3.18)$$

where A_x' sums over all the resolved resonances which are represented explicitly in the calculations, and A_x'' sums over all the 'distant' resonances at negative and positive energies. Because they are distant we can use the simplification

$$BWD_r \approx (E_r' - E)^2. \qquad (3.19)$$

Then for example

$$C''(E) = (1/2) \sum_r \Gamma_{nr}\,\Gamma_r / BWD_r \qquad (3.20)$$

summing over all "distant" resonances. The expectation value is

$$\langle C''(E)\rangle \approx (1/2)\langle \Gamma_{nr}(E).\,\Gamma_r(E)\rangle \int_{-\infty}^{\infty} F(X)\,(E-X)^{-2}\,dX. \qquad (3.21)$$

According to James and Story (1966) the frequency function F(X) may be represented sufficiently accurately by

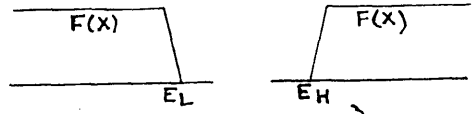

F(X) = 0 in the interval (E_L, E_H) occupied by the "known" resonances

$\approx (E_L-X)/D^2C, (X-E_H)/D^2C$ on the two sloping segments with $0 \le E_L - X \le Dc$ and $0 \le X - E_H \le Dc$ (3.22)

$= 1/D$ if $X \le E_L - Dc$ or if $X \ge E_H + Dc$

with

$C = 0.7268.$ (3.23)

In general D = D(J,X) is a slowly varying function of X but may be replaced with sufficient accuracy by

$$D_L = D(J, E_L) \text{ and } D_H = D(J, E_H). \qquad (3.24)$$

In (3.21)

$$\langle \Gamma_n(E).\,\Gamma(E)\rangle = \langle \Gamma_n\,(\Gamma_n + \Gamma_\gamma + \Gamma_F)\rangle \qquad (3.25)$$

$$= \langle \Gamma_n^2\rangle + \langle \Gamma_n\rangle(\langle \Gamma_\gamma\rangle + \langle \Gamma_F\rangle)$$

supposing Γ_γ is not correlated with Γ_n (no valence contribution); and

$$\langle \Gamma_n(E)\rangle = \langle \Gamma_n^{(l)}\rangle\, P_l(E)/k_0 R \qquad (3.26)$$

in which $\langle \Gamma_n^{(l)}\rangle$ is the mean reduced neutron width and

$$k_0 = \hbar/\sqrt{E} = 2.196795\times10^{-4}/(1+m_n/M)^2 \ fm^{-1}\ eV^{-1/2} \qquad (3.27)$$

The mean reduced neutron width is determined as usual from the neutron strength function

$$\langle \Gamma_n^{(l)}\rangle = S_n^{(l)}\, D(J\pi, E). \qquad (3.28)$$

Averaging over the Porter-Thomas distribution of neutron widths gives

$$\langle \Gamma_n^2\rangle = \langle \Gamma_n\rangle^2\,(1 + 2/\nu) \qquad (3.29)$$

in which ν is the number of effective neutron channels

$\nu = 1$ if $I = 0$, for every ℓ
$\ell = 0$, for any I
$J = \ell + I + 1/2$
$I > 0$, $\ell > 0$, $I \neq \ell$, and $J = |I - \ell| - 1/2|$
$= 2$ otherwise. (3.30)

After some algebra one finds that

$$A_x''(E) = \sum_{i=L,H} W(\ell J; E_i; E) \langle S_x(J\pi, E_i) \rangle \alpha(|E_i - E|/D_i) \quad (3.31)$$

$$B''(E) = W(\ell J; E_H; E)\, \beta((E_H - E)/D_H) - W_L(\ell J; E_L; E)\, \beta((E - E_L)/D_L) \quad (3.32)$$

$$C''(E) = (1/2) \sum_{i=L,H} W(\ell J; E_i; E) [W(\ell J; E_i; E)(1 + 2/\nu) + \langle S_\gamma(J\pi; E_i) \rangle + \langle S_F(J\pi, E_i) \rangle] \alpha(|E_i - E|/D_i), \quad (3.33)$$

in which

$$W(\ell J; E_i; E) = S_n^{(\ell)}(J\pi, E_i)\, P_\ell(E)/k_0 R \quad (3.34)$$

$$\langle S_\gamma(J\pi, E_i) \rangle = \langle \Gamma_\gamma(J\pi, E_i) \rangle / D_i \quad (3.35)$$

with a similar expression for $\langle S_F(J\pi, E_i) \rangle$.

The energy dependent factors α , β are given by

$$\alpha(|u|) = c^{-1} \ln(1 + c/|u|) \quad (3.36)$$

$$\beta(|u|) = c^{-1}\{(c + |u|) \ln(c + |u|) - |u| \ln|u|\} \quad (3.37)$$

Replacing the sums over distant levels by an integral in (3.21) is only valid if

$$E - E_L \gtrsim D(E_L)$$
$$E_H - E \gtrsim D(E_H) \quad (3.38)$$

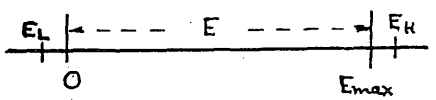

otherwise the uncertainty in the estimate diverges. So there must be at least one negative energy resonance represented explicitly amongst the resolved resonances, and at least one resonance represented explicitly (with the specified (ℓ,J)) above the top of the energy range in which the cross-sections are to be calculated.

It should be mentioned that in the derivation of (3.32) the cancellation of two infinities is incurred. These occur as a consequence of the excessive simplicity of the model used for the distribution of the neutron strength.

The formulae developed above can also be used with the multi-level Reich-Moore formalism for elastic scattering and radiative capture only; only the distant level terms

A_γ'' and B''

are required.

3.2.3 Use of the Reich-Moore Multi-Level Formalism for Elastic Scattering and Radiative Capture Only. A Problem Arising from the Level-Shift when $\ell > 0$

The multi-level Breit-Wigner (MLBW) formalism for neutron resonance cross-sections is less accurate than the Reich-Moore formalism, because the unitary condition on the collision matrix is violated. Fröhner (1980, Figure 1a,b,c,d) has illustrated some cross-section errors incurred by using the MLBW formulae with medium mass and fissile nuclides. It is natural that the Reich-Moore formalism has long been used for shape analysis of s-wave resonances observed experimentally in materials such as iron and nickel, and it must be anticipated that it will begin to be applied, using resonance analysis codes such as FANAC and REFIT, to the analysis of the non s-wave resonances also.

With both the MLBW and Reich-Moore formalisms the resonance energies or eigenvalues of the theory are shifted, if $\ell > 0$, from the observed resonance energies. In MLBW the level shift stems only from terms belonging to the particular resonance under consideration; the exact amount of this shift is easily calculated, and indeed in the formulation presented in Appendix B the shift has been formulated as zero at the observable resonance energy.

With the Reich-Moore formalism, even in the relatively simple form taking account of elastic scattering and radiative capture only, there are contributions to the level shift from all the other resonances; moreover these contributions do not appear explicitly in the formulae, but only implicitly.

If one sets out to generate tabular cross-sections from the resonance parameters, it is essential to know the amount of the level shift fairly accurately so that an adequate energy mesh can be set-up at which the cross-sections are to be calculated and tabulated, a fine mesh to define the narrowest of the p- and d-wave resonances and a broader mesh in between, so as to avoid an excessive amount of calculation and tabulation.

Fröhner F H (1980) BNL Conf on Nuclear Data Evaluation Methods and Procedures, INDC (USA) 85, Vol I, 398-399.

One method of dealing with this problem, which has been used in computing the cross-sections of ^{58}Fe, is to use the Reich-Moore formalism for calculating the contributions of the s-wave resonances, and to switch into the multi-level Breit-Wigner formalism for the $\ell>0$ contributions. However James (1982) has recently been exploring the problem of estimating fairly accurately the total level shift of $\ell > 0$ resonances in the Reich-Moore formalism; the method appears interesting, but has not yet been fully tested and would possibly break down for two very close resonances of the same (ℓ ,J).

Using the formalism given in the final section of Appendix B, put

$$U_{nn} = W \exp(-2i\phi_\ell) \tag{3.39}$$

so that

$$W = 1+2iQ/[1-iQ(1-i\delta)] = 1+2iQ/[1-(i+\delta)Q] \tag{3.40}$$

Now decompose Q

$$Q = Q_1 + q \tag{3.41}$$

in which

$$Q_1 = (1/2)\,\Gamma_{n1}/[\tilde{E}_1 - E - (i/2)\Gamma_{\gamma 1}] \tag{3.42}$$

is the contribution from the specific resonance of interest, and

$$q = (1/2)\sum_{r\neq 1} \Gamma_{nr}/[\tilde{E}_r - E - (i/2)\Gamma_{\gamma r}] \tag{3.43}$$

is the contribution from all other resonances

After some manipulation

$$W = 1 + \frac{i\Gamma_{n1}/[1-(i+\delta)q]}{\mathcal{E} - (1/2)\Gamma_{n1}[(1+\delta)/\{1-(i+\delta)q\}]} \tag{3.44}$$

in which

$$\mathcal{E} = \tilde{E}_1 - E - (i/2)\Gamma_{\gamma 1}\,, \tag{3.45}$$

the denominator appearing in (3.42).

James M F (1982) Unpublished work- I am indebted to Mr James for permission to present this preliminary account

Now look at the denominator of the fractional part of W in (3.44): This is:

$$\mathcal{E} - \frac{\Gamma_{n1}(1+\delta)}{2[1-(1+\delta)q]} = \mathcal{E} - \Gamma_{n1}\frac{(1+\delta)[1-\delta q + iq]}{2(1-\delta q)^2 + q^2} \tag{3.46}$$

in the approximation which treats the small term q as real, which can be written

$$= E_1' - E - (i/2)(\Gamma_{\gamma 1} + \Gamma_{n1}') \tag{3.47}$$

with

$$E_1' = [\tilde{E}_1 - (1/2)\Gamma_{n1}(\delta - \delta^2 q - q)/[(1-\delta q)^2 + q^2] \tag{3.48}$$

as the observable resonance energy, and

$$\Gamma_{n1}' = \Gamma_{n1}/[(1-\delta q)^2 + q^2] \tag{3.49}$$

The amount of the level shift in (3.48) depends first on

$$\delta = (S_\ell - B_\ell)/P_\ell \tag{3.50}$$

With the conventional boundary condition $B_\ell = 0$

$$S_\ell \approx -\ell + \rho^2/(2\ell-1) + O(\rho^4) \tag{3.51}$$

in which $\rho = kR$, and

$$P_\ell \approx \rho^{2\ell+1}/[(2\ell-1)!!]^2 + O(\rho^{2\ell+3}). \tag{3.52}$$

By choosing $B_\ell = -\ell$

the shift factor S_ℓ is much reduced, and so too is the factor δ appearing in (3.48) as a multiplier of the small term q. This change appears sufficient to allow the amount of the level shift in (3.48) to be calculated with reasonable accuracy. The numerator of W-1 in (3.44) still needs further exploration, and further testing is needed.

Some conclusions may be drawn however. In particular an experimenter or evaluator fitting non s-wave resonances with the Reich-Moore formalism should:-

(1) Quote the boundary conditions used

(2) Give the complete set of parameters for all resonances used in the fit

4 FISSION-PRODUCT DECAY HEAT

When a reactor is shut-down, for whatever reason, the evolution of heat will continue in consequence of the beta decay of the accummulated fission-products, with some addition from the decay of shorter-lived actinides such as ^{239}U, ^{239}Np and, on a somewhat longer timescale, ^{241}Am. Immediately after shut-down the fission-product decay heat output is about 6.3% of the preceeding operating power; for a power-station reactor operating at 3000 MW thermal, the fission-product power at shut down is therefore about 190 MW, and for reasons of safety the standby cooling provisions must be capable of removing this heat. Design engineers, conscious of the cost of the standby cooling plant, which they hope will never be needed for emergency, are naturally very much concerned with the accuracy of decay heat estimates.

In reality of course for a limited period, up to perhaps 100 secs after shut-down, there are other heat sources which contribute importantly to the uncertainty in the shut-down power; for example shut-down is in itself not an instantaneous event, and after it has been effected there will continue to be some fission heating induced by residual delayed neutrons; in consequence the accuracy requirement on the fission-product decay power is most stringent for cooling times greater than about 50 secs after shutdown. An approximate indication of the reduction in fission-product decay power as a function of cooling time t after a long-continued period (assumed infinite) of steady operation of a reactor fuelled with ^{235}U is given in Table 4.1, taken from a review made in 1965. Even after 3 hours cooling the evolution of decay heat in a power reactor is still very large.

TABLE 4.1

Cooling Time Seconds	Beta and Gamma Power, as % of Operating Power
1	6.35
10	4.77
100	3.09
1000	1.82
10^4(2.78h)	0.96

Fission-product decay heat can be calculated by summing the contributions of every fission-product, using tabulations of the average yield per fission of each one, and of the average beta and gamma energy evolved in its decay. The anti-neutrinoes which accompany the beta particle emissions, and which carry off about 40% of the total decay energy, may be supposed to escape into the void without interaction. In tables of radio-activity decay data, such as the "Tables of Isotopes" (1978) it is customary to give the end-point energy of each beta branch, which is the total kinetic energy of electron and anti-neutrinoes together. In setting up tables of decay heat data it is therefore necessary to calculate from the end-point energies the average electron energy for each beta branch of the decay scheme (the transitions represented by the sloping lines in this schematic diagram).

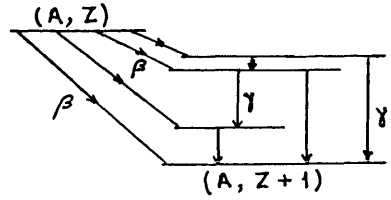

The average length of beta decay chains in fission-product can be estimated quite easily, and the values shown in Table 4.2 are from the reports of James (1969).

TABLE 4.2

Fissile Nuclide	Average No of β's
U233 thermal fission	2.61 ± 0.035
U235 thermal fission	3.02 ± 0.025
U238 fast fission	3.57
Pu239 thermal fission	2.74
Pu241 thermal fission	3.16

However, in order to cover completely all the fission-products which are produced in appreciable yields in the fission of ^{235}U, decay heat data must be provided for about 6 radioactive nuclides in each mass chain, at least for those whose masses lie near the peaks of the fission yield curve. Taking into account the fission products from other fissile nuclides of importance increases the number of nuclides for which decay data are required.

The earliest elements (of lowest atomic No. Z) in each decay chain have the greatest energy release and consequently the shortest half-lives, but because of the short half-lives detailed and accurate decay data are hard to measure, though a great deal of information has been obtained during the last decade through the use of on-line electromagnetic separators, such as LOHENGRIN at the high flux reactor in Grenoble, and OSIRIS at Uppsala, and is continuing to come forward.

To illustrate the magnitude of the task, the following statistics on the contents of the fission-product decay data file UKFPDD-2 have been drawn from the report by Tobias and Davies (1980). Comparable fission-product decay libraries have been produced in France and America, all in the ENDF/B4 or ENDF/B5 formats, and there has been a good level of co-operation in these developments.

"Tables of Isotopes, 7th edition" edited by Lederer C M and Shirley V S (Wiley 1978)

James M F (1969) J Nucl Energy 23, 517; 25, 513

Tobias A and Davies B S L (1980) RD/B/N4942

Total number of nuclides	855	
Stable nuclides	119	855
Radioactive nuclides	736	
Ground state	596	736
First isomeric state	133	
Second isomeric state	7	
Nuclides with beta/gamma spectra	390	736
Nuclides with estimated decay energies	346	
Nuclides with estimated half-lives	197	

Yoshida and Nakasima (1981) give these statistics on a preliminary version of a new fission-product decay data library being produced for the Japanese Nuclear Data Committee

Total number of nuclides		1100
Nuclides with $>$ 5 MeV decay energy:		
I	Half-life and decay scheme both known	88
II	Half-life known, but not decay scheme	98
III	Neither half-life nor decay scheme known	298

Concerning the nuclides with large decay energies, they report further that those in category III make only a minor contribution to the total decay heat, even at very short cooling times; those in category II contribute nearly 15% of the total decay heat at 10 seconds cooling time after an instantaneous burst of U235 fissions. However their further studies point to the contributions from the nuclides in category I as predominant in the cooling time interval up to several hundred seconds, and strongly indicate the need for further work on the decay schemes of these nuclides.

For a radioactive nuclide with a high energy release, the decay scheme is likely to be very complex, and unless it can be studied in great detail, with $\beta\gamma-$ and $\gamma\gamma-$ coincidence spectrometry for example, the true structure may not be properly identified. For example, the relative intensities of the various gamma rays evolved in the decay may have been measured, and if these can be assembled into a decay scheme the relative intensities of the beta branches to the excited states of the daughter nucleus can be determined, but the absolute beta intensity to the ground state of the daughter may be unknown.

The decay data alone are not sufficient for summation calculations of fission product decay power; fission-yield data are required also, and not only the chain-yield data which are relatively well-established for the principal fissile nuclides, but the independent yield for each separate fission-product, and for each fissile nuclide of interest. Crouch (1977) gives a succinct account of compilation of experimental data on fission product yields from thermal, fast and 14 MeV neutron induced fission for a considerable range of fissile nuclei, and of his evaluation of these data.

Yoshida T and Nakasima R (1981) J Nucl Sci and Technology 18, 393

Crouch E A C (1977) Atomic Data and Nuclear Data Tables 19, No 5

For the principal fissile materials reasonably good data are available for the majority of the cumulative chain yields, but the information available on the independent yields of the short-lived fission-products is much more limited, though more has become available since the Crouch review was written, and has been compiled in his computer file of fission yield data. For the majority of fission products and fissile nuclides, except perhaps for thermal neutron induced fission of ^{235}U, the independent yields must be estimated using systematic arguments; the basis and origins of these methods are conveniently summarised in Crouch's review.

A properly evaluated set of fission yields, relating to a particular class of neutron induced fissions of the fissile nuclide (A_F, Z_F) must satisfy (through the use of adjustment procedures if need be) the following physical constraints

$$\sum_{A,Z} y(A,Z) = \sum_{A} Y_A = 2 ; \qquad (4.1)$$

$$\sum_{A,Z} A.y(A,Z) = \sum_{A} A.Y_A = A_F + 1 - \bar{\nu}_p \qquad (4.2)$$

for conservation in the mean of the number of nucleons, after emission of the prompt neutrons;

$$\sum_{A} y(A,Z) = \sum_{A} y(A, Z_F - Z), \qquad (4.3)$$

the requirement that the yields of complementary elements be equal, for conservation of the number of protons; with (4.1) this is equivalent to

$$\sum_{A,Z} Z.y(A,Z) = Z_F . \qquad (4.4)$$

In these formulae y(A,Z) is the independent yield for production in fission of the nuclide (A,Z) and Y_A is the chain yield in the chain of mass number A; $\bar{\nu}_p$ is the average yield on prompt neutrons.

These constraints are extremely important and go far to balance out the effects of errors in the estimation of independent yields; they ensure for example that if the average length of the chain of mass A is made rather too long, the complementary chain (or chains) will be shortened to correspond.

From what has been stated above it will be clear that summation calculations of decay heat involve very large numbers of input data, and that particular uncertainties attach to the short-lived fission-products, those which contribute most to the decay power shortly after shut-down. How can we assess reliability of calculations based on these data?

Firstly a number of sensitivity studies have been made of the uncertainties in the summation method. These studies have been summarised conveniently in Section 5 of the review paper by Tobias (1980), and he gives a comparative table of the estimated uncertainties in decay heat from the fission-products arising from long-continued (12 to 120 day) steady thermal neutron irradiation of ^{235}U; results are given for decay times from 1 to 10^8 secs (120 days), and a selection from Tobias' table is given in Table 4.3 below. It is not clear

Tobias A (1980) "Decay Heat", Progress in Nuclear Energy 5, No 1, 1

TABLE 4.3

ESTIMATED UNCERTAINTIES OF FISSION-PRODUCT DECAY HEAT FROM SUMMATION CALCULATIONS

(from Tobias (1980) Prog Nucl Energy 5(1) 1, review paper)

Irradiation Time (10^7 secs)		1.28	1.0	8	3	1-10
Decay Secs	Source of Uncertainty	Uncertainties, Per Cent (a)	(b)	(c)	(d)	(e)
	Yields	1.22	0.9	0.61	0.92	0.95
1.0	Half-lives	-	0.2	0.31	0.46	0.2
	Decay energies	7.12	6.5	1.68	2.19	7.12
	TOTAL	7.30	6.9	1.81	2.42	7.19
	Yields	0.89	0.8	0.51	0.89	0.77
10	Half-lives	-	0.3	0.23	0.43	0.3
	Decay energies	5.26	4.3	1.55	2.20	5.26
	TOTAL	5.34	4.8	1.65	2.41	5.32
	Yields	0.36	0.6	0.32	0.98	0.51
100	Half-lives	-	0.4	0.36	0.34	0.4
	Decay energies	2.17	1.4	1.18	1.76	1.79
	TOTAL	2.20	2.5	1.27	2.05	2.26
	Yields	0.17	0.3	0.29	2.47	0.34
10^4	Half-lives	-	0.8	0.18	1.01	0.8
(2.8h)	Decay energies	1.61	1.1	0.72	0.47	1.15
	TOTAL	1.61	2.0	0.79	2.71	1.44
	Yields	-	0.3	0.37	7.84	0.44
10^6	Half-lives	-	0.7	0.14	0.41	0.7
(1-2d)	Decay energies	-	0.6	1.42	0.22	1.01
	TOTAL	-	1.1	1.48	7.85	1.39
	Yields	-	0.4	0.45	5.62	0.63
10^8	Half-lives	-	1.0	0.44	0.40	1.0
(120d)	Decay energies	-	1.6	2.72	0.34	2.16
	TOTAL	-	2.0	2.89	5.64	2.48

(a) Trapp et al (1977) OSU-NE-7701

(b) Schmittroth & Schenter (1977) Nucl Sci Eng 63, 276

(c) Devillers (1977) IAEA-213, review paper No 4

(d) Yamamoto & Sugiyama (1978) Ann Nucl Energy 5, 621

(e) Tobias, estimated for UK decay data files

why Yamamoto and Sugiyama attributed such large values to the uncertainties induced by the fission yield data at the longer decay times; on the other hand they seem to have been more optimistic than others about the accuracy at the longer decay times of the half-life data and decay energy data.

Sensitivity studies cannot take into account the possible consequences of gross experimental errors, such as the wrong assignment in Z or A of some short-lived activity, nor can they readily make allowance for unknown systematic faults in evaluations of the energetic short-lived fission-products. Since questions of reactor safety are involved it is essential to test the accuracy and reliability of the very complex summation calculations with integral measurements of decay heat.

The integral measurement methods fall into two classes:

(i) Measurements of beta and gamma spectra, with subsequent numerical integration, or measurements of the beta or gamma power with counters which integrate over the whole spectrum.

(ii) Calorimetric measurements.

The difficulty in applying the calorimetric method to the gamma heat output is that the calorimeter has to be massive enough to absorb the whole gamma ray energy, although the gamma spectra extend to 5 MeV at least. But a massive calorimeter has a slow response-time in general, so the method has not been very useful for measurements down to $\sim$ 100 secs decay time. This problem was resolved recently by Yarnell and Bendt (1977) at LANL with their "cryogenic boil-off claorimeter". Essentially a massive copper calorimeter, 52kg, was used, but by operating at liquid helium temperature the specific heat is reduced very greatly and the calorimeter has a time constant of only 0.85 secs.

Decay heat comparisons between summation calculations and integral measurements were carried out by James (1981) and were reported to the NEA Committee on Reactor Physics during its meeting at Winfrith in September 1981; this work was subsequently up-dated by James (1982) for presentation to the UK Nuclear Data Forum, and he has generously made his notes and tables and graphs available to me. Most of what follows is from his work.

A brief summary of recent integral measurements of fission-product decay heating may be useful and is given in Table 4.4: a summary of earlier work may be found in Section 2 of the review by Tobias (1980), and some comparisons between summation calculations and those integral experiments may be found in the same review.

Yarnell J L and Bendt P J (1971) LA-NUREG-6713; see also (1978) LA-7452-MS, NUREG/CR-0349.

James M F (1981) NEACRP-A463; (1982) unpublished work.

TABLE 4.4

RECENT INTEGRAL MEASUREMENTS

CALORIMETRIC	BETA AND GAMMA SPECTROMETRY METHODS	
	BETA + GAMMA	BETA
Lott + (1973) U235) Fiche + (1976) Pu239) CEA	Dickens + (1977/8) U235, Pu239 & Pu241 ORNL	Dickens + (1977/8)
Yarnell & Bendt (1977/8) U235 & Pu239 LANL	Friesenhahn + (1976/7) U235 & Pu239 IRT	Friesenhahn + (1976/7) Alain & Scobie (1974) U235 Scot URRC
Schrock + (1978) U235 UCB		Murphy + (1979) U235 & Pu239 AEEW
Gunst + (1974-7) Th232, U233, U235, Pu239 (cooling time 14 hr) BAPL		Taylor & Murphy (1980) U235 & Pu239 (AEEW)
		GAMMA
		Dickens + (1977/8)
		Taylor & Murphy (1981) U235 & Pu239 AEEW

Each measurement can be compared directly with a summation calculation effected for the corresponding irradiation time I and decay time t, and the values of the ratio of calculation/experiment can be compared by graphical representation on a convenient scale.

Several comparisons of this kind were given in James' paper, Figures 4.1 and 4.2 probably deserve most study. They show calculation/experiment ratios for both ^{235}U and ^{239}Pu total decay heat, using the measurements of Dickens et al (1977, 1978) at ORNL and of Yarnell and Bendt (1977/8) at LANL. In each graph the curves for the two fissile nuclides are similar in shape, but the ratio calculation/experiment is about 7% smaller for ^{239}Pu than for ^{235}U.

Comparisons of calculation/experiment were made also using the measurements of Friesenhahn & Lurie (1976, 1977) following a 20,000 sec (5.56 hr) irradiation of ^{235}U, and it was noted that their data are systematically about 2% lower than those of Yarnell & Bendt, who used the same irradiation period, for decay times from 20 to 1300 sec; at longer decay times the agreement is better, but the scatter in both sets of data inplies an increase in the random error to about $\pm$ 1%.

Comparisons of calculation/experiment were made using the measurements of Friesenhahn & Lurie (1976, 1977) following 1000 sec irradiations of ^{235}U and of ^{239}Pu. For ^{235}U there is good agreement with the measurements of Lott et al (1973) for the same length of irradiation, except below about 300 sec decay time where systematic errors in the calorimetric measurements by Lott et al may be appreciable. From 1 to 1300 secs decay time the calculation/experiment ratios for ^{239}Pu are about 2 to 3% below those for ^{235}U.

On the other hand comparing the total decay heat measurements of Friesenhahn et al (1976, 1977) following 1 day irradiations of ^{235}U and ^{239}Pu, in contrast to the information from other measurements, the calculation/experiment ratios for ^{239}Pu are about 2 to 3% above those for ^{235}U. Consideration of the beta decay heat alone shows, in Figure 4.3, rather good agreement between calculation and experiment for ^{235}U. With the measurements of Murphy et al (1979) following a 10^5 sec (1.16 day) irradiation of ^{235}U, the calculation/experiment ratios lie in the range 0.98 to 1.02 up to 1900 secs decay time; using the data of Friesenhahn et al (1976, 1977) following a 1 day irradiation of ^{235}U, the calculation/experiment ratios are about 3 to 6% lower.

Because of the different irradiation times that have been employed it is a more difficult task to compare the different sets of data, and to check the consistency of measurements made after different irradiation periods. With this problem in mind we introduce two decay functions.

m(t) the average decay power per fission at t secs after an instantaneous burst of fissions

M(I,t) the average decay power t secs after steady irradiation of the fissile material for I secs at 1 fission/sec.

From their definitions it is easy to see that

$$M(I,t) = \int_t^{t+t} m(t')\,dt' = \int_{\ln t}^{\ln(I+t)} t'\,m(t')\,d(\ln t') \qquad (4.5)$$

$$= M(\infty, t) - M(\infty, I+t). \qquad (4.6)$$

If (I+t) is large a summation calculation value may be used for the small correction term on the right, so that the infinite irradiation function M(∞,t) may be derived from M(I,t).

Lott M, Lhiaubet G, Dufreche F & de Tourrail R (1973) J Nucl Energy 27, 597

Fiche C, Dufreche F & Monnier A M (1976) CEA - Internal Report

Schrock V E, Grossman L M, Prussin S G, Sockalingen K C, Nuh F, Fan C-K, Cho NZ & Oh S J (1978) EPRI-NP-616 Vol 1; see also Schrock V E (1979) Prog Nucl Energy 3, 125

Gunst S B, Connor J C & Conway D E (1974) WAPD-TM-1182, -1183; (1975) Nucl Sci Eng 56, 241; (1977) Nucl Sci Eng 64, 904

Dickens J K, Emery J F, Love T A, McConnell J W, Northcutt K J, Peelle R W R Weaver H (1977) ORNL/NUREG-14; (1978) ORNL/NUREG-34; NUREG/CR-0171; ORNL/NUREG-47

Friesenhahn S J, Lurie N A, Rogers V C & Vagelatos N (1976) EPRI-NP-180;

Friesenhahn S J & Lurie N A (1977) IRT 0304-004

Alam B & Scobie J (1974) Ann Nucl Sci Eng 1, 573

Murphy M F, Taylor W H, Sweet D W and March M R (1979) AEEW - R 1212

Taylor W H & Murphy M F (1980, 1981) Unpublished

The functions m(t), M(I,t) may be applied to discussion of the beta decay power, to the gamma decay power, or to their sum. In principle there is a dependence on the neutron flux level used in the irradiation, because of the effects of neutron capture, but these effects are very small except at long decay times. To understand this it is helpful to consider the effect of neutron capture on the concentration of a particular fission product. The rate of change of the concentration during irradiation is

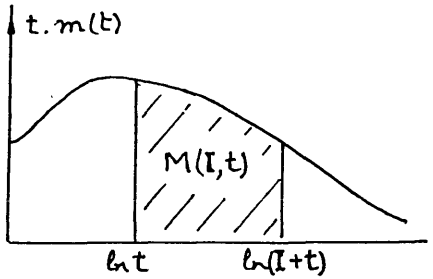

$$dC/dt = -C(\lambda+\phi\sigma_\gamma) + \phi\sigma_F N_F Y. \qquad (4.7)$$

The first term on the right denotes the rate of loss through decay, and the second term is the rate of loss through neutron capture; the final term is the source term, denoting new production by fission. Thus the effect of the capture term is to replace λ by $\lambda+\phi\sigma_\gamma$. How do λ and $\phi\sigma_\gamma$ compare?

$$\phi\sigma_\gamma/\lambda = \phi\sigma_\gamma . 10^{-24} . T_{1/2}(hr) . 3600/(\ln 2) \qquad (4.8)$$

with ϕ in neutrons/cm^2 sec, σ_γ in barns, and $T_{\frac{1}{2}}$ in hours.

Taking ^{135}Xe by way of example, with the largest measured capture cross-section, we may set

and let us assume that $\phi = 10^{12}$ neutrons/cm^{2}sec. Then

$$\phi\sigma_\gamma/\lambda = 0.14 \qquad (4.9)$$

If σ_γ is only 3000 barns, which is still a very large neutron cross-section, the half-life must be $\sim$ 1 year for the same level of competition between capture and decay. For the great majority of nuclides the capture cross-section is much smaller than this, which explains why the effects of capture may be ignored in decay heat calculations, except at very long decay times when only a few long-lived activities remain. Such neutron capture as does occur generates, in general, other active nuclides, a little more neutron rich, which must be expected to evolve as much decay heat, or slightly more, than the activities destroyed.

Some generalisations of (4.5) and (4.6) may be written down:

$$M(nI, t) = \sum_{k=0}^{n-1} M(I, kI+t) \qquad (4.10)$$

which enables data for the longer irradiation nI to be built-up, by summing data from measurements made with the shorter irradiation I, provided that the measured values extend to sufficiently long decay times. Another

such formula is

$$M(t_2-t_1, t_1) = M(t_2-t_1, nI+t_1) + \sum_{k=0}^{n-1} \{M(I, kI+t_1) - M(I, kI+t_2)\} \qquad (4.11)$$

which may be useful if $t_2 - t_1 \gtrsim I$.

If $I \ll t$, the approximation

$$M(I, t) \approx I . m(t + I/2) \qquad (4.12)$$

may allow the more sensitive "burst-function" m(t) to be generated from short irradiation measurements.

A variety of different methods have been employed for comparing measurements taken after differing periods of irradiation. One convenient method is to fit the measurements, alternatively, with

(a) cubic spline functions
(b) a sum of exponential functions

and then to derive the burst function m(t) or the infinite irradiation function M(∞, t) analytically. Burst functions m(t) for the total decay power from ^{235}U and from ^{239}Pu fission products have been derived in this way and are illustrated in Figures 4.4 and 4.5; the corresponding summation calculations made with the 1981 UK Fission Product Decay Data library are included for comparison; the fission-product yields used in the calculations are from a revised set compiled by Crouch, and include yields for production of isomeric states (this is the set C3I).

An important new development in these studies is that of comparing calculated and measured values of the ratio

$$R(I, t) = [M(I, t) \text{ for Pu-239}]/[M(I, t) \text{ for U-235}] \qquad (4.13)$$

That this is useful for the summation calculations was pointed out by Trapp and Spinrad (1978). Although the fission yield data are somewhat different for the two fissile materials, the fission product decay data (half-lives, energies and branching ratios) are the same for both; however the data for the chains of masses A = 100 to 110 are more important for ^{239}Pu, because of their larger yields.

So far as measurements are concerned, one expects that some of the systematic errors of a particular experimental method may cancel on taking the ratio; for example detector efficiencies, and in methods of determining the numbers of fissions.

Trapp T J and Spinrad B I (1978) OSU-NE-7801

By using equation (4.10) the fission-product decay data of Dickens et al (1977, 1978), following relatively short irradiations of ^{235}U and ^{239}Pu, were combined to provide data corresponding to 20,000 sec irradiations, the irradiation period used by Yarnell and Bendt (1977, 1978). The ratios R(I,t) of (Pu239 total decay heat)/(U235 total decay heat) were found to be in reasonably good agreement between the two sets of measurements, as shown in Figure 4.6, at least in the time range t = (20, 3000) secs. The corresponding ratios obtained from summation calculations show a similar variation with decay time, to the experimental data, but are 7 to 9% lower.

Busrst functions derived from the ^{235}U and ^{239}Pu fission-product decay data measurements of Lott et al (1973) and Fiche et al (1976) at the CEA, of Dickens et al (1977, 1978) at ORNL, and of Yarnell and Bendt (1977, 1978) at LANL, have also been compared. There is excellent agreement between the two sets of calorimetric measurements from the CEA and LANL over the time interval t = (60, 10^5) secs, and with the ORNL measurements over the narrower interval t = (200, 6000) secs; outside this interval the ORNL data fall considerably below the calorimetric ratio data. The corresponding ratios derived from summation calculations have a broadly similar time dependence, especially in comparison with the calorimetric data, but are 8 to 10% lower. It is interesting to speculate whether the resolution of this discrepancy in the burst function ratio

$$r(t) = [m(t) \text{ for } Pu\text{-}239]/[m(t) \text{ for } U\text{-}235] \qquad (4.14)$$

would also resolve the discrepancy in the ratio R(20000 sec,t) values which was mentioned in the preceding paragraph, but at present further work will be needed before the discrepancies between different sets of measurements and the faults in the summation data have been positively identified and sufficiently reduced.

In conclusion:

(1) There are systematic differences between the decay heat measurements at different laboratories. Some may arise from errors in estimating the numbers of fissions, but as the discrepancies show some variation with cooling time, presumably part must be caused by errors in estimating detector efficiencies (possibly because of variations of beta or gamma spectra).

(2) For some of the sets of measurements, the discrepancies are appreciably reduced if the ratio of Pu239/U235 decay heat is considered, implying that some of the systematic errors are independent of the fissile nuclide, (or if dependent on fissile nuclide are the same at each laboratory).

(3) Calculated values for ^{235}U decay heat fall roughly between the different sets of measured values, but for ^{239}Pu calculation generally underestimates the decay heat. However, when the ratio of ^{239}Pu to ^{235}U decay heat is considered the calculated values have roughly the same variation with cooling time as the measured data, which indicates significant faults among the decay data affecting the summation calculations for both fissile nuclides.

(4) Until the discrepancies have been definitively resolved, the following uncertainties are proposed for decay heat calculations with the UK Fission-Product Decay Data Library:

(a) For ^{235}U, the uncertainty in the total decay heat following an infinite irradiation should be:

$\pm$ 7% for cooling times less than 200 seconds
$\pm$ 5% for longer cooling times,

both for 1 standard deviation.

(b) For ^{239}Pu, the uncertainty in the total decay heat following an infinite irradiation should be $\pm$ 10%, for 1 standard deviation.

A basis for these uncertainty recommendations may be found in the following table.

FISSION PROD DECAY HEAT, CALCULATION/EXPERIMENT COMPARISONS

Experiment	Calc/Expt	U235	Calc/Expt	Pu239
ORNL I=1, 10, 100 secs	1.00 to 1.06	Av≈1.03	0.91 to 0.99	Av≈0.93
LANL I=20,000 secs	0.96 to 1.02	Av≈0.99	0.88 to 0.95	Av≈0.92
IRT I=20,000 secs	0.94 to 1.00	Av≈0.97		

For ^{239}Pu decay heat calculations the proposed uncertainty of $\pm$ 10% certainly does not appear excessive, if one looks at the largest discrepancies. However it should be borne in mind that in practice the decay heat may be allowed slightly to exceed the estimate for a short time, provided that thereafter it falls below the estimate.

Further work, based on the measurements of Dickens et al (1977, 1978), suggests that at short cooling times, up to about 300 seconds, the beta power is being overestimated in the summation calculations, both for ^{235}U fission-product decay heat and for ^{239}Pu, whereas the gamma power is being underestimated. The implication is that too much of the total decay energy is being assigned to the anti-neutrinoes. Much the same conclusions emerge from the calculations of Yoshida and Nakasima (1981) - reference on page 47 above. They tried the effect of replacing the beta and gamma decay energies, which had been inferred from experimental measurements of 87 of their category I fission-product nuclides, with values calculated using the gross theory of beta decay. This had the effect of reducing the beta power and increasing the gamma power in their summation calculations, and it was found that for ^{235}U, ^{239}Pu and ^{241}Pu the summation calculations were brought into reasonably good agreement with burst functions derived from the integral measurements of Dickens et al (1977, 1978).

ACKNOWLEDGEMENTS

I am glad to have this opportunity to give my sincere thanks to Mr M F James of the Nuclear Data Group at AEE Winfrith for permission to present here some of his work relating to the resonance cross-section theory, and on fission-product decay heating, and to Mr R W Smith of the same Group for some conclusions from his unpublished work on the evaluation of the resolved neutron resonances of the iron isotopes; also to Dr A T D Butland, formerly of the same Group, for much help in clarification of work on the thermal scattering law.

APPENDIX A

THE DYSON-MEHTA OPTIMUM ESTIMATOR FOR MEAN LEVEL SPACING

The authors set up an energy interval of length 2L, and examine the energies of a family of resonances in this interval: the family is assumed to consist of one or more level sequences and is assumed to be complete and uncontaminated within the interval. For convenience in derivation the zero of energies is shifted to the mid-point of the interval. Then the optimum linear statistical estimator for the mean level spacing gives

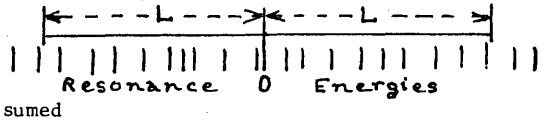

$$D = \pi L / \{2 \sum_{r} \sqrt{1-(E_r/L)^2}\} \; (1 \pm \sqrt{2m}\, D/\pi L) \qquad \text{(A1)}$$

supposing the family of resonances contains m independent sequences (e.g. the s-wave resonances of an odd-mass isotope, with 2 spin states).

Note that approximately $2L/D \approx n$, the number of resonances in the interval, so the

Fractional Uncertainty $\approx (2\sqrt{2}/\pi)\, m/n \approx 0.9\, m/n$.

This is quite good already if n = 10 for m = 1
n = 20 for m = 2

In practical application the energy zero is linked to the set of E_r, not to the arbitrary interval 2L. With E = 0 for zero kinetic energy of the incident neutron

$$2L = E_n - E_1 + (\lambda_1 + \lambda_2) D \qquad \text{(A2)}$$

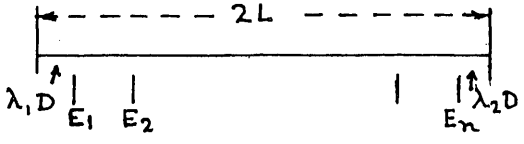

The formula (A1) now becomes

$$D = (\pi L^2/2Q)(1 \pm \sqrt{2m}\, D/\pi L) \qquad \text{(A3)}$$

in which

$$Q = \sum_{1}^{n} \sqrt{[(E_r - E_1 + \lambda_1 D)(E_n - E_r + \lambda_2 D)]} \qquad \text{(A4)}$$

Since Q contains D in a fairly complicated way, (A3) is solved approximately by inputting an initial guess $D = D_1$, to which corresponds $Q = Q_1$. Then to first order

$$Q = Q_1 + (D - D_1)\, Q_1' \qquad \text{(A5)}$$

with $Q_1' = [dQ/dD]_{D=D_1}$ (A6)

With a little algebra, and using (A2) to (A6)

$$D = [B + \sqrt{(B^2 + AC)}]/A \qquad \text{(A7)}$$

with

$$A = 8Q_1' - \pi(\lambda_1 + \lambda_2)^2 \qquad \text{(A8)}$$

$$B = 4(Q_1' D_1 - Q_1) + \pi(\lambda_1 + \lambda_2)^2 \qquad \text{(A9)}$$

$$C = \pi(E_n - E_1)^2 \qquad \text{(A10)}$$

Choice of λ_1 and λ_2 is arbitrary, subject to

$$\lambda_1 \geq 0, \quad \lambda_2 > 0 \qquad \text{(A11)}$$

and

$$\lambda_1 + \lambda_2 \leq 1, \qquad \text{(A12)}$$

since the 2L interval must not be expanded enough to include any additional reasonance. As has been stated before, the Dyson-Mehta formulae are valid only for large n; however we now choose λ_1, λ_2 so that the formula for D is self-consistent when n = 2, that is to say we require the result

$D = E_2 - E_1$

With $\lambda_1 = \lambda_2 = \lambda$ for simplicity, the requirement is

$$(\lambda + 1/2)^2 = (4/\pi)\sqrt{\lambda(1+\lambda)} \qquad \text{(A13)}$$

whence

$$\lambda = 0.64556 \qquad \text{(A14)}$$

 Dyson F J & Mehta M L (1963) J Math Phys 4, 701

This value for λ may perhaps enable the formulae to give "sensible" values for D even when n is small. For large n the results should be insensitive to the exact values chosen for λ_1 and λ_2.

As for the initial guess input for D_1, an improved value may be input each time the code is re-run on the same problem.

APPENDIX B

NEUTRON RESONANCE CROSS-SECTIONS

B.I Preliminary Remarks

The target nucleus is characterised by its mass M, spin quantum number I, parity π_0 and neutron interaction radius R. The resonant state of the compound nucleus is characterised by its total angular momentum (or spin) quantum number J and parity π, and can be excited by partial waves with any orbital angular momentum quantum number ℓ satisfying both

$$(-1)^{\ell} = \pi_0 \pi \tag{B1}$$

$$L_1 \leq \ell \leq L_2 \tag{B2}$$

with

$$L_1 = \mathrm{Min}(|J-|I-1/2||,\ |J-I-1/2|) \tag{B3}$$

$$L_2 = J+I+1/2. \tag{B4}$$

In practice it is nearly always sufficient to attribute the whole interaction to the smallest ℓ which satisfies (B1 and B2), and this approximation has been followed universally in what follows. With this approximation it becomes possible to write

$$\sigma_i(E) = \sum_{\ell=0} \sigma_i^{\ell}(E) \qquad i = nn,\ ny,\ nF,\ nT \tag{B5}$$

and further

$$\sigma_i^{\ell}(E) = \sum_J g_J \sigma_i^{\ell J}(E) \tag{B6}$$

in which the sum over J runs through the resonance J-values which have the specified ℓ

$$J = (|\ell-|I-1/2||,\ \ell+I+1/2). \tag{B7}$$

B.II The Multi-Level Breit-Wigner Formalism

For a particular target isotope and (ℓ, J) value the elastic, capture and fission cross-sections may be calculated by the formulae given below, and the total cross-section is then derived from their sum,

$$\sigma_{nT}(E) = \sigma_{nn}(E) + \sigma_{ny}(E) + \sigma_{nF}(E); \tag{B8}$$

however it should be remarked that the multi-level Breit-Wigner formalism involves approximations which destroy the unitarity of the collision matrix.

It is convenient to start by writing for the Breit-Wigner resonance denominator

$$BWD_r = (E_r' - E) + \Gamma_r^2/4; \tag{B9}$$

$$E_r' = \tilde{E}_r - \Gamma_{nr}(|E_r|)\, S_{\ell}(E)/2.P_{\ell}(|E_r|) \tag{B10}$$

E_r denotes the observed resonance energy, and $\tilde{E}_r$ is the shifted resonance energy, or eigenvalue, of the formal theory. Setting

$$\tilde{E}_r = E_r + \Gamma_{nr}(|E_r|)\, S_{\ell}(|E_r|)/2P_{\ell}(|E_r|) \tag{B11}$$

has the consequence that

$$E_r' = E_r \text{ if } E = |E_r| \tag{B12}$$

but note, from (B10), that E_r' shifts away from E_r when E does so, except if $\ell = 0$. For $\ell = 0$ the shift factor $S_{\ell}(E) = 0$ and then $E_r' = E_r = E_r$.

In (B9) the total width

$$\Gamma_r \equiv \Gamma_r(E) = \Gamma_{nr}(E) + \Gamma_{\gamma r} + \Gamma_{Fr}, \tag{B13}$$

and

$$\Gamma_{nr} \equiv \Gamma_{nr}(E) = \Gamma_{nr}(|E_r|)\, P_{\ell}(E)/P_{\ell}(|E_r|) \tag{B14}$$

in which, of course, $P_{\ell}(E)$ is the penetration factor.

The capture and fission cross-sections in the state (ℓ, J) may be written

$$\sigma_x(E) = \pi \lambda\!\!\!^{-2}\, A_x(E) \qquad x = n\gamma \text{ or } nF, \tag{B15}$$

and the scattering cross-section

$$\sigma_n(E) = 4\pi |a|^2 \tag{B16}$$

in which a denotes the complex forward scattering amplitude

$$a \equiv a(E) = -(i\lambda\!\!\!^{-}/2)\left[1 - \exp(-2i\phi_\ell)\left\{1 + i\sum_r \Gamma_{nr}/(E_r' - E - i\Gamma_r/2)\right\}\right] \quad \text{(B17)}$$

In this formula the phase factor has been chosen to conform with measurers' practice. Decomposition into real and imaginary parts gives

$$a(E) = (\lambda\!\!\!^{-}/2)\left[(1-C)\sin 2\phi_\ell - B\cos 2\phi_\ell + i\{B\sin 2\phi_\ell - C\cos 2\phi_\ell - 2\sin^2\phi_\ell\}\right]. \quad \text{(B18)}$$

In this presentation of the multi-level Breit-Wigner formulae all summations are contained in the factors A(E), B(E) and C(E), with

$$A_x(E) = \sum_r \Gamma_{nr}\,\Gamma_{xr}/BWD_r \quad \text{(B19)}$$

$$B(E) = \sum_r \Gamma_{nr}.(E_r' - E)/BWD_r \quad \text{(B20)}$$

$$C(E) = \sum_r \Gamma_{nr}\,\Gamma_r/BWD_r. \quad \text{(B21)}$$

Only single summations are involved.

The formulae for the penetration factors, shift factors and phase-shifts are set out below for ℓ = 0 to 3, with $\rho \equiv kR$.

Penetration Factors

$$P_0 = \rho \qquad P_1 = \rho^3/(1+\rho^2) \qquad P_2 = \rho^5/(9+3\rho^2+\rho^4)$$

$$P_3 = \rho^7/(225+45\rho^2+6\rho^4+\rho^6).$$

Shift Factors

$$S_0 = 0 \qquad S_1 = -1/(1+\rho^2) \qquad S_2 = -(18+3\rho^2)/(9+3\rho^2+\rho^4)$$

$$S_3 = -(675+90\rho^2+6\rho^4)/(225+45\rho^2+6\rho^4+\rho^6).$$

Phase Shifts

$$\phi_0 = 0 \qquad \phi_1 = \rho - \arctan\rho \qquad \phi_2 = \rho - \arctan[3\rho/(3-\rho^2)]$$

$$\phi_3 = \rho - \arctan[\rho(15-\rho^2)/(15-6\rho^2)].$$

B.III The Reich-Moore Multi-Level Formalism, for Elastic Scattering and Radiative Capture Only

With only a single particle channel the neutron elastic element of the collision matrix is, for specified (ℓ, J),

$$U_{nn} = \exp(-2i\phi_\ell)\left[1 + 2i(1 - i\mathcal{S})HQ\right] \quad \text{(B22)}$$

with

$$\mathcal{S} = S_\ell(E)/P_\ell(E) \quad \text{(B23)}$$

or more generally, if the boundary constant B_ℓ is non-zero,

$$\mathcal{S} = [S_\ell(E) - B_\ell]/P_\ell(E), \quad \text{(B24)}$$

$$Q = P_\ell(E).R = (1/2)\sum_r \Gamma_{nr}(E)/[\tilde{E}_r - E - i\Gamma_{\gamma r}/2] \quad \text{(B25)}$$

in which $\tilde{E}_r$ is the eigenvalue,

and

$$(1 - i\mathcal{S})H = 1/[1 - iQ(1 - i\mathcal{S})]. \quad \text{(B26)}$$

Then the cross-sections are

$$\sigma_n(E) = 4\pi|a|^2 \quad \text{(B27)}$$

as before, where a is the complex forward scattering amplitude

$$a \equiv a(E) = -(i/2)\,\lambda\!\!\!^{-}.(1 - U_{nn}). \quad \text{(B28)}$$

$$\sigma_T(E) = 2\pi\lambda\!\!\!^{-2}(1 - Rl\,U_{nn}) \quad \text{(B29)}$$

$$\sigma_\gamma(E) = \sigma_T - \sigma_n = 4\pi\lambda\!\!\!^{-2}\,Im(Q)|(1 - i\mathcal{S})H|^2; \quad \text{(B30)}$$

The latter is preferable for calculation of the capture cross-section, in order to avoid rounding errors caused by the subtraction of two nearly equal numbers.

FIGURE 4.1 TOTAL DECAY POWER

Comparison of UKFPDD-1/C2 calculations with ORNL measurements by Dickens et al (1977, 1979)

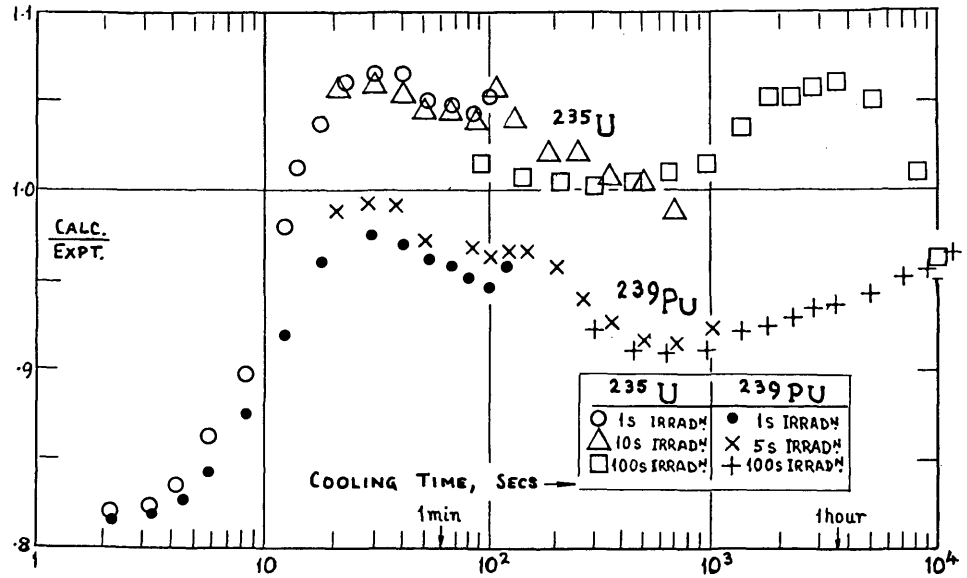

FIGURE 4.2 TOTAL DECAY POWER

Comparison of UKFPDD-1/C3I calculations with LASL measurements by Yarnell & Bendt (1977, 78)

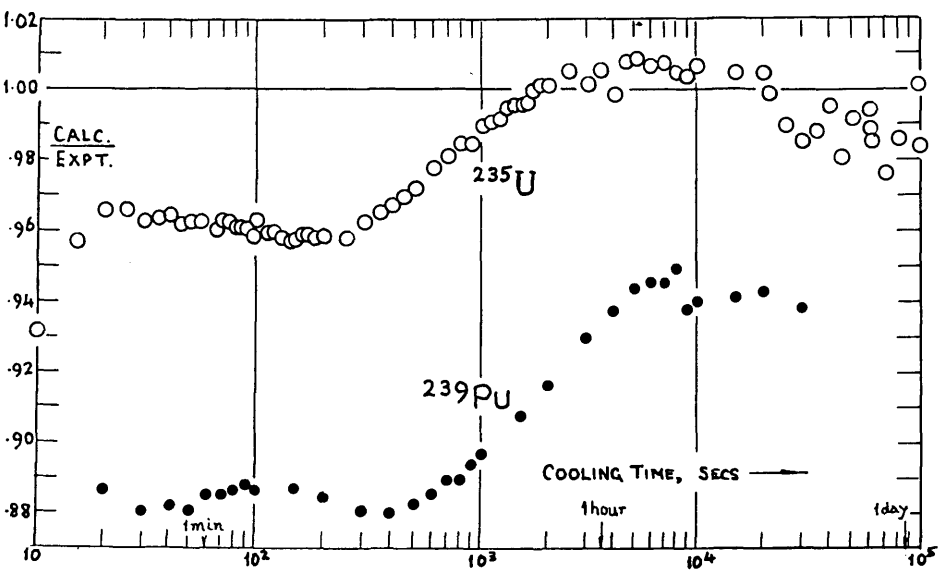

FIGURE 4.3 BETA HEATING (^{235}U FISS PRODS.)

Comparison of UKFPDD-1/C3I calculations with measurements

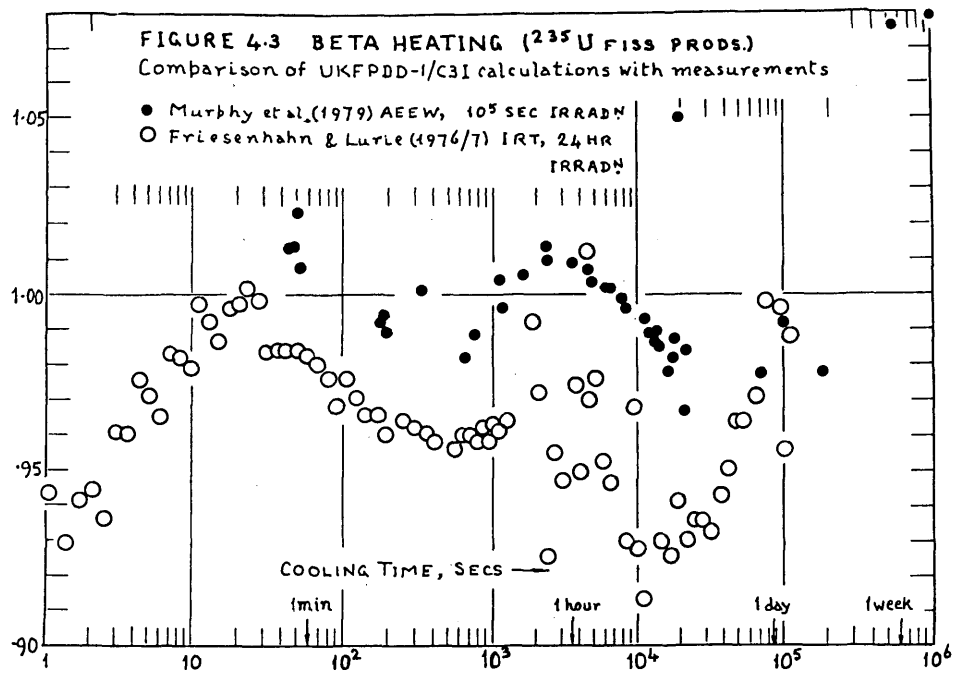

FIGURE 4.4 ^{235}U BURST FUNCTION; TOTAL DECAY POWER

($\beta+\gamma$ decay) power after instantaneous burst of thermal neutron fissions of ^{235}U)

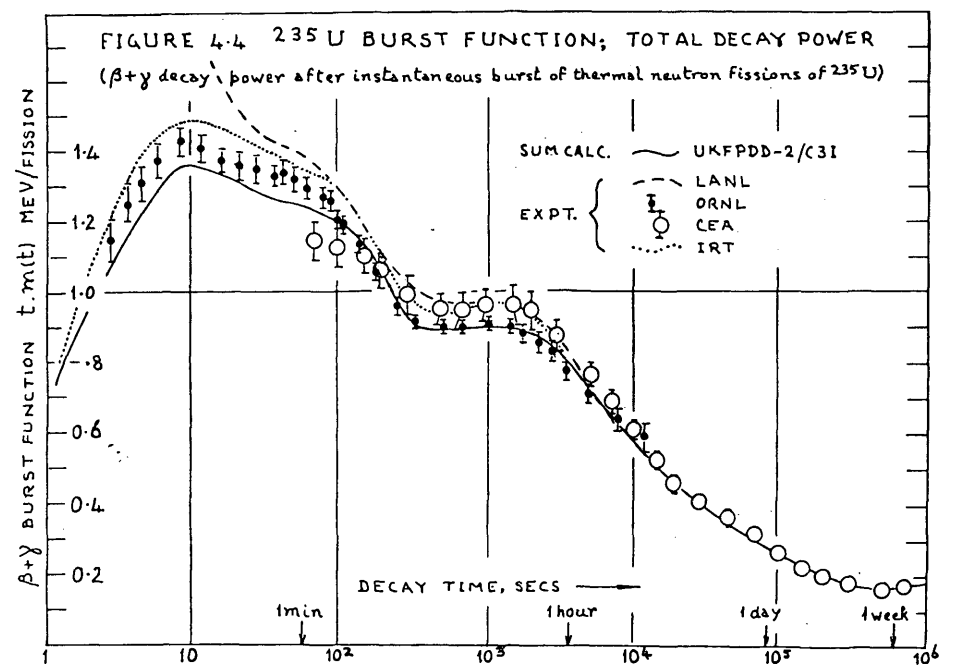

FIGURE 4·5 ^{239}PU BURST FUNCTION; TOTAL DECAY POWER

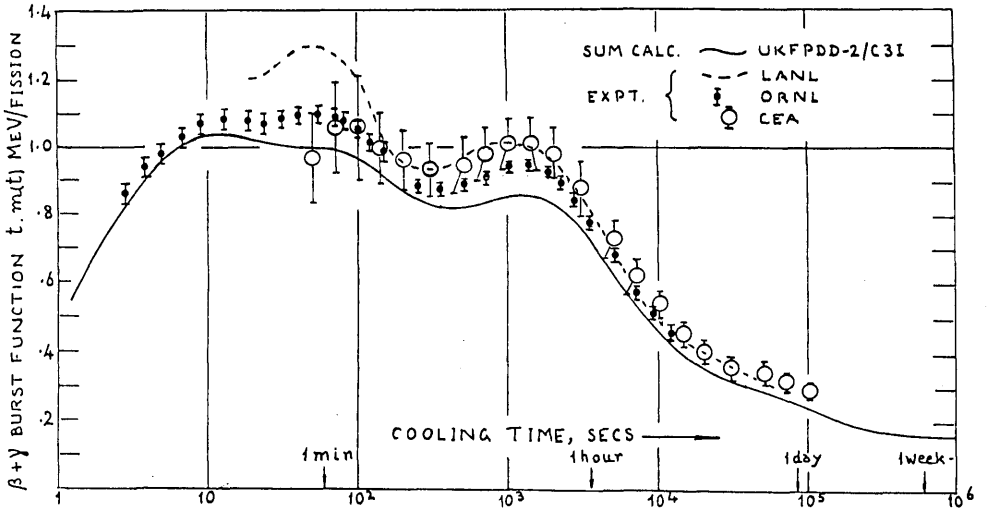

FIGURE 4·6 PU-239/U-235 TOTAL DECAY HEAT RATIO AFTER 20000 SEC IRRADN

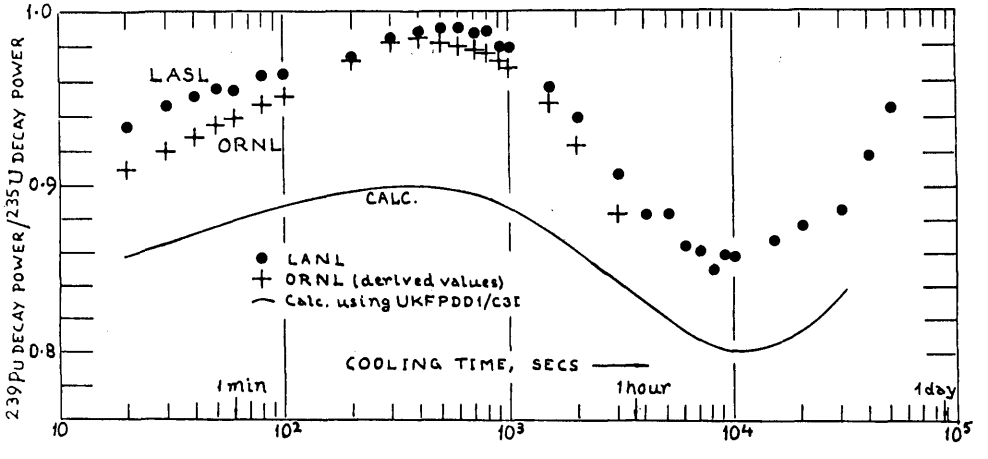

FIGURE 4·7 PU-239/U-235 TOTAL DECAY HEAT RATIO AFTER A BURST OF FISSIONS

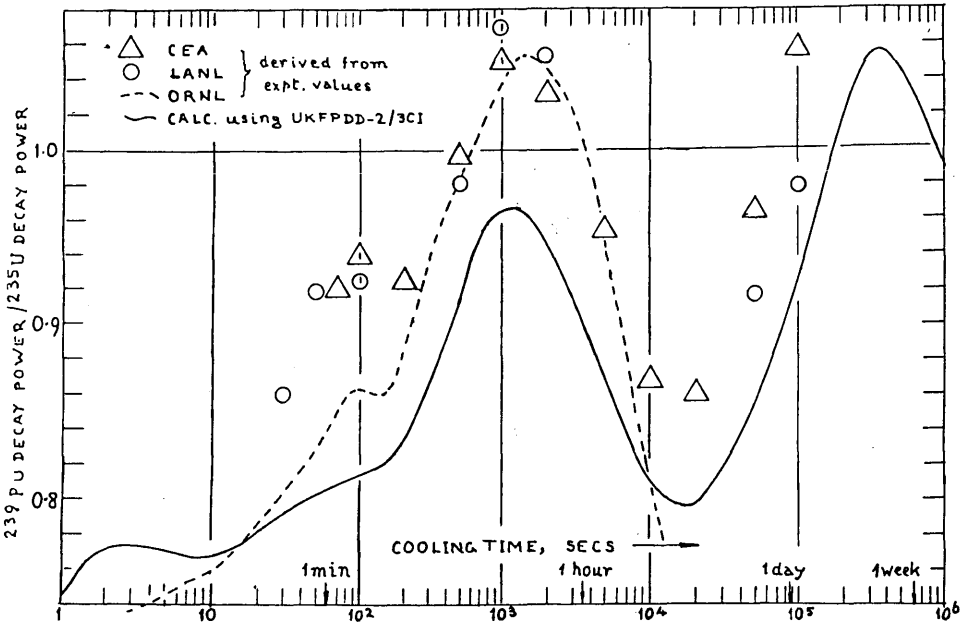

TEMPERATURE DEPENDENCE OF NEUTRON CROSS-SECTIONS AND RESONANCE INTEGRALS, AND SAFETY PROBLEMS

W. ROTHENSTEIN
Technion,
Haifa, Israel

ABSTRACT

The material covered in the lectures consists of the following topics:

I) A description is given of the basic nuclear data needed for resonance absorption calculations with particular reference to commonly used resonance formalisms and the resonance parameter files in the basic data libraries. Doppler Broadening techniques are discussed together with the construction of detailed temperature dependent resonance cross section tabulations for use in accurate resonance absorption calculations.

II) The resonance shielding problem is treated for homogeneous mixtures of a resonance absorber in infinite moderating media with hydrogen moderation only, moderation by a heavier nuclide, and moderation by mixtures of nuclides.

The narrow resonance approximation (NR), the infinite mass approximation (IM), and the λ parameter of the intermediate resonance approximation (IR) are defined.

The construction of group effective resonance integral or shielded cross section tabulations is described for individual resonance nuclides mixed homogeneously with moderating materials characterized by a single background cross section.

Lattice heterogeneity is treated with special reference to the simplifications needed to replace a unit cell by a homogeneous mixture with an equivalent effective background cross section involving the Dancoff factor. The limitations of using the Bell factor to preserve the one term equivalence relations between homogeneous mixtures and isolated fuel lumps are discussed, as well as the empirical dependence of the Bell factor on the Dancoff factor.

III) Multigroup spectrum calculations at epithermal energies are discussed mainly with reference to the MUFT and GAM procedures for homogeneous mixtures.

The direct application of the Nordheim Integral Transport calculation of effective resonance integrals in the MUFT code is described, together with its artificial separation of the shielding calculation near the resonance peaks and the unshielded wing corrections, and the use of smoothly varying corrections to the simple Breit Wigner resonance shapes. A method is described for the modification of the approximate resonance integrals to correlate the resulting epithermal to thermal absorption rates for reactor lattice unit cells with experiment.

The use of resonance shielding factors in the GAM and WIMS multigroup epithermal spectrum calculations is discussed. In the former the shielding factors refer to the group cross sections and group dependent lattice disadvantage factors must be applied. The WIMS code uses effective resonance integrals which must be translated into group cross sections with due regard to average flux depressions in each resonance group. The approximations encountered in defining the effective fuel disadvantage factors and flux depressions are emphasised.

The method used in the LATREP code for handling fuel clusters is treated briefly.

IV) Detailed resonance reaction rate calculations in lattice unit cells using Doppler broadened resonance cross section tabulations are discussed with full allowance for all resonance interference phenomena.

The one dimensional OZMA code which treats this problem by integral transport or S_n transport theory on an ultrafine energy mesh is described with special reference to the rapid calculation of the elastic slowing down sources, as well as P_1 scattering in the S_n option.

The methods of studying the effects of such detailed transport calculations in the resolved resonance region on standard multigroup reactor analysis are described.

V) Results of lattice analysis studies with accurately calculated resonance reaction rates are given for a number of problems.

- Temperature variation of effective resonance integrals for isolated fuel rods.
- Doppler reactivity coefficients of typical BWR and PWR unit cells and their variation with fuel depletion.
- Analysis of some thermal reactor lattice benchmarks
- Analysis of some D_2O moderated fuel clusters.
- Comparison of multigroup cross sections, cell fluxes and disadvantage factors calculated for a UO_2/H_2O lattice benchmark in the resolved resonance region by detailed transport calculations and by standard very rapid multigroup methods for identical group reaction rates.

A final discussion follows to indicate how accurate resonance reaction rate calculations may be used to validate or correct simple resonance shielding algorithms.

Lecture 1

Introduction

Direct utilisation of basic nuclear data libraries for reactor analysis is restricted to simple systems or special problems. Among these, Monte Carlo calculations for Benchmark Analysis, and the validation of nuclear data and reactor design codes[1], may be mentioned. Such calculations cannot be applied to the study of the behaviour of large reactor cores containing fuel assemblies of different types, undergoing burn-up at different rates, and containing also a variety of structural and control materials. Here core analysis must be broken up into several subprograms which lead in the final instance to the calculation of the detailed flux and power distributions in the entire reactor throughout the complete fuel cycle.

The final determination of the flux and power distribution is in itself a problem of considerable complexity requiring two- or three-dimensional calculations, usually of the diffusion type. Little emphasis can be placed on the neutron energy variable in such analyses; the nuclear characteristics which vary from location to location throughout the core must be represented by parameters covering very wide energy bands. Multi-dimensional few group diffusion and transport codes usually handle about two to four energy groups.

One is therefore faced with the problem of collapsing the vast amount of information contained in basic nuclear data libraries into very few groups without losing its essential content. Computer codes which perform this task must be applied on a routine basis and very rapidly, since they have to supply the local parameters representing the different parts of the reactor core. They must be updated periodically as the fuel gets depleted.

Local few group data in the reactor core are averages over regions covered by the mesh cells used in the determination of the flux and power maps for the entire reactor. They must, in general, eliminate the internal heterogeneity of the fuel assemblies, in addition to being few group averages of the basic nuclear data. Thus, the preparation of the broad group data is in itself a

procedure requiring space and energy dependent solutions of the neutron transport equation.

Even at this level, i.e., for a local solution of the transport equation in a relatively small region, usually with simple geometry, direct utilisation of the basic neutron cross section libraries is impracticable. The purpose of the calculation is to obtain a space energy dependent solution for the neutron flux which can be used for homogenisation of a fuel assembly, or part of it, and for collapse of the energy dependence into very few groups. The numerous few group parameters which must be supplied for the different fuel assemblies in the entire reactor core make it essential to use a multigroup, rather than point cross section, procedure to solve the transport equation in each assembly and subregion within it. The solutions of the transport equation are usually obtained in about one hundred to two hundred fine energy groups. The heterogeneity of the fuel assemblies may be simple or more complicated. The basic geometry is the unit cell consisting of fuel, clad and associated coolant or moderator in an infinite regular array of similar cells, the fuel being in the form of rods or plates. The arrays may also be more complicated, for example, in fuel assemblies containing some burnable poison or control rods in addition to the fuel rods themselves. In heavy water moderated reactors, the basic cell is a cluster of fuel rods in the coolant, together with the external moderator associated with it. These types of systems, shown in Fig. 1, have a double heterogeneity, in the first case for the poison rods interspersed between the fuel, in the second for the rods within the cluster, and for the array of complete clusters separated by the moderator.

Heterogeneous analysis of fuel assemblies by multigroup methods for the preparation of homogenised few group parameters refers in the first instance to regular arrays of fuel rods or plates in an infinite lattice since unit cells of these geometries can be handled quite simply. In the present course such arrays will be the principal ones discussed, although some attention will also be paid to systems with double heterogeneity. In the unit cell codes used, in practice, several tens of fine energy groups cover the thermal energy region from about 10^{-5} to about 1 eV, and a similar number of fine groups span the epithermal energy region, in which there is neutron down-scattering only, from about 1 eV to about 10 MeV.

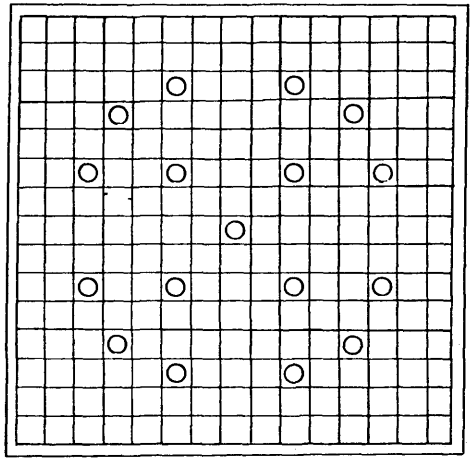

Fuel assembly of a PWR with 15x15 fuel rod unit cells except the locations indicated by circles which contain poison rods or instrumentation.

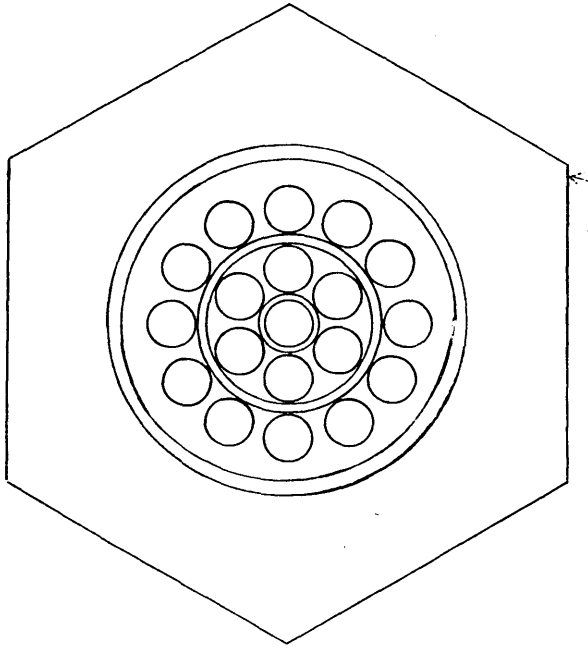

Moderator outer boundary for one fuel cluster.

Fuel rod cluster in D_2O moderator.

Fig. 1 Assemblies with more than one type of heterogeneity

The preparation of few group parameters representing the nuclear characteristics of limited regions in the reactor core consists therefore of two steps: the preparation of a library of fine group cross sections for the different nuclides in the core from the basic nuclear data library, and the solution of the transport equation in the unit cell or fuel assembly in this multigroup scheme for the purpose of obtaining the advantage or disadvantage factors for the different zones within it (such as fuel, cladding, moderator or control materials), homogenisation and group collapse to a few broad groups. The preparation of the fine group library is reactor independent, the subsequent transport calculation depends on the fuel assembly under consideration and the leakage of neutrons out of it (or the streaming into it) to (or from) neighbouring parts of the core. The leakage is usually represented by a positive or negative buckling parameter which may be fine group dependent.

The procedure followed in the two steps is the same: Neutron reaction rates must be conserved in the definition of the fine or broad group cross section. This may be illustrated by the following two equations:

$$\sigma^{x}_{g,i} = \frac{\int_{g} \sigma^{x}_{i}(E)\,\varphi(E)\,dE}{\int_{g} \varphi(E)\,dE} \qquad (1)$$

$$\Sigma^{x}_{G,i,z} = \frac{\sum_{g \in G} \sigma^{x}_{g,i}\, N_{i,z} \int_{z} \phi_{g}(\bar{r})\,d\bar{r}\,\Delta u_{g}}{\sum_{g \in G} \int_{z} \phi_{g}(\bar{r})\,d\bar{r}\,\Delta u_{g}} \qquad (2)$$

The first equation refers to the fine group (g) library preparation of microscopic cross section of type x for isotope i, the second to the definition of its macroscopic broad group average in a zone z of the assembly for which the multigroup transport equation has been solved to give the space dependent flux $\phi_{g}(\bar{r})$ in group g. For smoothly varying cross sections and narrow energy groups there is no problem in defining the weighting flux $\varphi(E)$ needed to prepare the fine group library: a reasonable guess such as the fission spectrum at high energies, a 1/E flux in the slowing down region, and a Maxwellian distribution at thermal energies (or even a unit weighting flux), is quite adequate. The smoother the variation of $\sigma^{x}_{i}(E)$ in a group g, and the finer the group, the less pronounced will be the dependence of $\sigma^{x}_{g,i}$ on the weighting flux $\varphi(E)$.

Resonance cross sections on the other hand do not fit into this general procedure. Even in groups with widths of a quarter lethargy unit only, there may be numerous resonances, or in the lower energy groups a single resonance causing the cross section to vary over several decades within the group. In addition, there is the heterogeneity problem. Consequently, resonance reaction rates cannot be treated by the two steps referred to above. The flux is depressed considerably at the resonance peaks and the depression is space dependent in a heterogeneous assembly. Figures (2) and (3) illustrate the very marked cross section changes and resulting flux depressions in the groups containing the first two resonance peaks of ^{238}U in a simple 1.33% enriched UO_2 lattice with 0.4864 cm radius fuel pins in Aluminium cladding of 0.5753 cm outer radius, for a lattice pitch of 1.5578 cm and hexagonal array geometry. Space dependence of the resonance shielding and some interference effects between the resonances of the two isotopes are noticeable.

In handling the resonance shielding problem there is no step equivalent to that of Eq. (1), since $\varphi(E)$ must contain the flux depressions which depend on the system under consideration, including its heterogeneity. In principle, the transport equation should be solved for the space dependent flux spectrum $\varphi(\bar{r},E)$ throughout the resonance region with good accuracy. In terms of this flux the group cross sections of the resonance nuclides are

$$\sigma^{x}_{g,i,z} = \frac{\int_{g} dE \int_{z} d\bar{r}\; \sigma^{x}_{i}(E)\,\varphi(\bar{r},E)}{\int_{g} dE \int_{z} d\bar{r}\; \varphi(\bar{r},E)} \qquad (3)$$

where z may be an average over a zone, such as the fuel, or the entire unit cell c. In the latter case the z is replaced by c in the denominator, but not in the numerator if the resonance nuclide is present in a single zone, such as the fuel, only.

On the other hand, the multigroup analysis must be completed in order to apply Eq. (2) to determine all broad group cross sections. It consists of solving the multigroup transport equation for $\phi_g(\bar{r})$, or its cell average $\bar{\phi}_{g,c}$ in a homogeneous multigroup code. In order to determine these fine group fluxes the resonance cross sections of Eq. (3), or their equivalent, must be used.

In practice, the resonance treatment represented by Eq. (3) is greatly simplified. In some codes effective or shielded resonance integrals, which are related to the numerator of Eq. (3), are calculated by approximate methods for the system under consideration, including its heterogeneity, if any. In other treatments accurate group values of the effective resonance integrals or cross sections are calculated for homogeneous mixtures with hydrogen moderation only and different ratios of the atom densities of the resonance nuclide and the moderator. The results are tabulated and utilised, by interpolation, for other moderators using approximate methods, and for heterogeneous assemblies through equivalence theorems, which in turn involve other approximations. These procedures will be reviewed in detail during the present course, and the nature of the inevitable simplifications will be discussed.

It will be seen that there is a clear incentive to treat the resonance problem for heterogeneous assemblies with as few approximations as possible, i.e., the derive the space-energy dependent flux $\varphi(\bar{r},E)$ needed in Eq. (3) with high precision. The way in which this is done in the OZMA code[2] will also be described quite extensively. Such calculations can serve as benchmarks against which simpler resonance treatments can be tested for the purpose of defining appropriate correction factors.

Even if a sophisticated code is used to calculate $\varphi(\bar{r},E)$ in detail in order to define the group cross sections by Eq. (3), there is no certainty that the fine group reaction rates will be conserved for all resonance nuclides after the $\phi_g(\bar{r})$ or $\bar{\phi}_{g,c}$ have been calculated by the multigroup code. This will be the case only if

$$\int_g dE \int_z d\bar{r}\, \varphi(\bar{r},E) = \Delta E_g \int_z d\bar{r}\, \phi_g(\bar{r}) \quad , \quad \phi_g(\bar{r}) \text{ per unit energy} \tag{4}$$

or if

$$\int_g dE \int_{z,c} d\bar{r}\, \varphi(\bar{r},E) = \Delta E_g \cdot V_c\, \bar{\phi}_{g,c} \quad , \quad \bar{\phi}_{g,c} \text{ per unit energy} \tag{4'}$$

for the same normalisations on both sides of the equations. There is no apriori reason why this should be so. $\varphi(\bar{r},E)$ is the result of the solution of the fine energy mesh transport equation for an adequate spatial subdivision of the heterogeneous assembly under consideration. It depends on region to region transport kernels which are non linear functions of the strongly varying cross sections in the resonance region. On the other hand, $\phi_g(\bar{r})$ is the result of a single transport equation in each group and depends on transport kernels calculated for group average cross sections. In the case of $\bar{\phi}_{g,c}$ cell average cross sections are used in a multigroup slowing down code without any direct reference to spatial effects. In view of these considerations, the use of accurately calculated resonance events in multigroup codes should rigorously conserve the resonance reaction rates by an iterative procedure. This may lead to differences between the fine group cross sections and group fluxes in the two cases (the sophisticated code, and the multigroup code), and the necessity, even under these circumstances, for applying correction factors to the resonance cross sections obtained by Eq. (3). Results of analyses made by such methods will be discussed in a later lecture.

In summary, the justification for very detailed transport calculations in the resonance region is twofold:

1) Verification of simple resonance treatments and specifications of appropriate correction factors.

2) Study of inherent problems in multigroup calculations involving resonance events, when only some tens of energy groups are used in the resonance region.

If correction factors to simple resonance treatments are evaluated by suitable benchmark calculations which compare the results of such treatments with values obtained from solutions of the transport equation on a fine energy mesh, they will overcome any problems which might arise from the use of group average cross sections in the multigroup transport or the multigroup slowing down code. In some of the multigroup codes currently in use the corrections may be quite small in most groups. Benchmarking at different temperatures to determine the temperature dependence of the correction factors will lead to information about the accuracy with which Doppler changes of resonance reaction rates can be obtained by multigroup lattice analysis codes.

Basic Data Libraries and Resonance Parameters

Basic data libraries provide microscopic cross sections for the different reaction types of individual nuclides as tabulated functions of energy. Together with specified interpolation procedures they give the values of all neutron cross sections needed for reactor analysis at any energy. The Evaluated Nuclear Data Files, ENDF[3], issued by the National Nuclear Data Center at Brookhaven National Laboratory, are in very general use and will form the basis for the material presented here. ENDF/A contains either complete or partial data sets, and may also contain several different evaluations of the cross sections of a particular nuclide. The most commonly used ENDF/B library, on the other hand, consists of only one complete recommended evaluation of the cross sections for each material in the library, and each material contains cross sections for all significant reactions.

In the ENDF/B library the energy range from 10^{-5} eV to 20 MeV for a particular nuclide may be subdivided into several parts. The smooth cross section range contains cross sections as a function of the neutron energy in File 3 of the data. Resonance data are specified in the form of resolved or unresolved resonance parameters in File 2, which covers stated energy ranges. The library also specifies the resonance formalism to be used, and the cross sections as functions of energy at 0°K in the resolved or unresolved resonance range of energy are the results of evaluating the relevant resonance formulae for the given resonance parameters, augmented by the cross section corrections (if any) contained in File 3 of the data with appropriate interpolation laws. They correct the cross sections for inadequacies in fitting the experimental data with the recommended resonance formalism. Thus, in the resonance region the cross sections require the use of two files of the data libraries.

The resonance formalisms are of varying degrees of sophistication. They are given in the Formats Manual[3]. For resonance absorption calculations in reactor cores the simplest formalisms, the Breit-Wigner formulae, are the most important. Together with the smoothly varying corrections referred to above they lead to resonance cross sections in good agreement with the measured microscopic data, and they can be readily Doppler broadened. In some cases more general formalisms are recommended in the ENDF/B data; they can be implemented precisely in some cross section preparation codes[5].

The Breit-Wigner Single Level Formulism

The Breit-Wigner Single Level Resonance formalism in the resolved resonance region may be derived by the methods given in reference (4). The resulting formulae involve the phase factors δ_ℓ for hard sphere scattering, the shift factors S_ℓ and penetration factors P_ℓ for spherical waves of order ℓ, into which the neutron plane wave incident on the nucleus, with which it interacts, may be subdivided, and the characteristics of the resonance interaction as expressed by the logarithmic derivative f_ℓ of the wave function near the nuclear surface at energies close to one of the energy levels E_λ of the compound nucleus. In the final form of the Breit-Wigner Single Level formulae[3] the energy independent absorption width Γ_a (usually composed of the fission and gamma widths $\Gamma_f + \Gamma_\gamma$ only) replaces the imaginary part of f_ℓ, while its real part is expressed linearly in terms of $E_\lambda - E$ and the shift factor

$S_\ell(E)$; the penetration factor $P_\ell(E)$ is replaced by the neutron width $\Gamma_n(E)$; and finally the spin factor g_J accounts for the multiplicities involved in combining ℓ with the neutron and target spins s and I to give the spin of the compound nucleus J .

A modified and simpler form of the Breit-Wigner Single Level formulae for s-wave resonances is frequently used for resonance absorption calculations, and accounts for this absorption in thermal reactors to a good degree of accuracy. Its form is:

$$\sigma_a(E) = \sigma_0 \frac{\Gamma_a}{\Gamma}\sqrt{\frac{E_0}{E}}\ \frac{1}{1+x^2}$$

$$\sigma_p = 4\pi\hat{a}^2, \quad \sigma_s(E) = \sigma_0 \frac{\Gamma_n}{1+x^2}, \quad \sigma_{int}(E) = 2\sqrt{g_J \sigma_0 \frac{\Gamma_n}{\Gamma}\sigma_p}\ \frac{x}{1+x^2}$$

$$\sigma_0 = 4\pi\lambda_0^2 g_J \frac{\Gamma_n}{\Gamma}, \quad x = \frac{2}{\Gamma}(E-E_0), \quad \lambda_0^2 = \frac{\hbar^2}{2mE_0}, \quad g_J = \frac{2J+1}{2(2I+1)} \qquad (5)$$

where $\Gamma_n = \Gamma_n(E_0)$ is the neutron width near the resonance peak at E_0 .

In a similar expression for p-wave resolved resonances interference scattering is negligible, and the $\Gamma_n(E)$, apart from its dependence on $\sqrt{E}$, is also proportional (on account of the penetration factor $P_1(E)$) to $E/(E+E_1)$, where $E_1 \approx 0.28$ MeV for heavy nuclides. The p-wave resonances are therefore much weaker in the resolved resonance region than the resonances for $\ell = 0$.

The $\sqrt{E_0/E}$ term in $\sigma_a(E)$ accounts for the thermal 1/v absorption by a superposition of the tails of all possible J states and different ℓ 's, and in each of many resonances. Departures from this energy dependence are caused by resonances with E_0 close to the thermal energy region.

When s and p wave resolved resonance parameters are given in the basic data libraries, they can be used as distinct sequences, since these sequences correspond to different parities even if the same compound nucleus spin may be reached from both. For d wave parameters this is no longer here, but the cross sections are still treated as distinct sequences on account of the great difference between the penetration factors for s and d wave resonances.

The Breit-Wigner Multilevel Formulae

An immediate criticism of the single level formalism is that the total cross section at each energy for absorption or scattering is the sum of individual contributions of the type of Eq. (5) due to all resolved resonances. This implies not only that the resonance peaks are well spaced (spacing greatly in excess of the total width, or more precisely, the practical width for which the resonance and background cross sections are equal), but that there is no overlap between the interference scattering terms coming from neighbouring resonances. Such overlap did occur at several energies for ENDF/B resonance parameters of fertile isotopes, in particular ^{238}U, for versions of the basic data before ENDF/B-V. Not only were the resonance dips below the peak energies (negative values of x in the $\sigma_{int}(E)$ cross section of Eq. (5)) too pronounced as compared with experimental data, but they led even to negative overall scattering cross sections below some pairs of strong resonances. These physically impossible situations should have been corrected by means of File 3 corrections for σ_s , but only in ENDF/B-V was this done in a fully consistent manner for all isotopes with pronounced interference between the potential and resonance scattering. (The interference is greatest for even-even targets with spin I = 0, since this leads to $g_J = 1$).

From the point of view of the resonance formalism the single level procedure is clearly incorrect if cross section contributions due to individual levels are added as described above. Instead, the summation over levels should be carried out before the quantities $1 - |\eta_\ell|^2$ and $|1-\eta_\ell|^2$ are evaluated for the absorption and scattering cross sections in Eq. (5). Here η_ℓ is the phase factor which perturbs the outgoing spherical wave of order ℓ in the interaction of the neutron and the target. This leads to a resonance-resonance interference term which is included in the equation for elastic scattering of

ℓ-wave neutrons. The complete cross section then involves a double summation over levels belonging to one sequence of resonances characterised by a particular ℓ and J (really J and parity), as well as a summation over all ℓ and J.

The Unresolved Resonance Region

In the energy range above the resolved resonances, in which the resonance structure of the cross sections is still significant for reactor calculations, but in which the resonance parameters have to be inferred from the resolved resonance region, average resonance parameters are provided in the ENDF/B libraries for different possible ℓ and J states. The parameters are for the single-level Breit Wigner formalism and are average parameters at specified energy points. The average refers to a number of resonances near these energies. Each width is assumed to be distributed according to a chi squared distribution with a specified number of degrees of freedom, m. Appropriate values for m are generally about 1 for Γ_n^i, 2 or 3 for Γ^i, and $m \to \infty$ for Γ_γ.

The information provided in the basic data libraries provides a means of calculating average cross secitons at the energies where the data are given. Integrating over all values of x defined in Eq. (5), replacing $\sqrt{E_\ell / E}$ by unity, and dividing by the average resonance spacing $\bar{D}_{\ell,J}$ the cross sections for a complete sequence of ℓ-wave resonances will be

$$\sigma_{s,\ell}(E) = 4\pi\lambda^2(2\ell+1)\sin^2\delta_\ell + 2\pi^2\lambda^2 \sum_J^i \frac{g_J}{\bar{D}_{\ell,J}} \left[\left\langle \frac{\Gamma_n \Gamma_n}{\Gamma} \right\rangle_{\ell,J} - 2\left(\bar{\Gamma}_n\right)_{\ell,J} \sin^2\delta_\ell \right]$$

$$\sigma_{x,\ell}(E) = 2\pi\lambda^2 \sum_J^i \frac{g_J}{\bar{D}_{\ell,J}} \left\langle \frac{\Gamma_n \Gamma_x}{\Gamma} \right\rangle_{\ell,J} \qquad (6)$$

where the summations over J cover the compound nucleus spin values which correspond to ℓ-wave neutrons, and the correct dependence of the non-resonance scattering, and the interference scattering cross sections on δ_ℓ has been kept. The subscript x in the reaction cross section refers to capture, fission or other competitive processes such as inelastic scattering. The averages, implied in the $\langle\ \rangle$, are over the statistical distributions of the widths, and Eq. (6) gives the unshielded cross sections.

The unresolved resonance parameters and their statistical distributions also enable the user to construct resonance ladders in the vicinity of the energy points to which the parameters apply. An alternative is to treat the cross sections in the unresolved resonance region by probability tables[6]. Resonance shielding problems can also be handled in terms of the average parameters, a background cross section, and the statistical distributions. One such procedure will be discussed in some detail. The way in which the parameters are derived from the available experimental information is not necessarily unique in the sense that different parameter sets can be defined which lead to the same partial cross sections in the unresolved resonance region[7]. They might lead to somewhat different values of resonance shielding factors and their termperature dependence.

Multilevel Resonance Formalisms

Apart from the multilevel formalism given previously, which is really the more rigorous way of handling the logarithmic derivative of the wave function at the nuclear surface for a particular level, there are other multilevel formalisms due to Adler-Adler, and Reich-Moore which are derived from R-matrix theory. Adler-Adler parameters can be specified in the ENDF/B libraries, and processed in strict accordance[5] with the formulae given in the library Formats Manual[3]

Doppler Broadening

The thermal motion of the resonance nuclides is usually accounted for by assuming a Maxwell distribution of nuclear velocities at the temperature of the

medium (or a slightly higher) temperature. This assumption is valid if the temperature of the medium exceeds the Debye temperature $h\nu_{max}/k$ where ν_{max} is the maximum vibration frequency of the atoms of the solid. In the Breit Wigner resonance formulae the energy is strictly the energy E' of the neutron and the target in the center of mass coordinate system, but this may be taken to be the same as the energy of the neutrons relative to the target at rest, since the reduced mass and the neutron mass are practically equal.

For velocities $\bar{v}$ and $\bar{V}$ of neutron and target, with V_z as the component of the latter on the direction of the former and distributed according to the Maxwell Boltzmann distribution

$$E' = \frac{1}{2} m |\bar{v} - \bar{V}|^2 \approx E - \sqrt{2mE}\, V_z \quad , \quad f_1(V_z) = \left(\frac{M}{2\pi kT}\right)^{1/2} e^{-\frac{MV_z^2}{2kT}} \tag{7}$$

where m and M are the neutron and target masses respectively. Consequently, for symmetric resonance cross sections of the type of Eq. (5) with peak σ_{0x}

$$\sigma_x(E) = \sigma_{0x} \int_{-\infty}^{\infty} \frac{1}{1 + \frac{4}{\Gamma^2}(E' - E_0)^2} f_1(V_z)\, dV_z = \frac{\sigma_{0x}}{\Delta\sqrt{\pi}} \int_{-\infty}^{\infty} \frac{e^{-\left(\frac{E - E'}{\Delta}\right)^2}}{1 + \frac{4}{\Gamma^2}(E' - E_0)^2} dE' \tag{8}$$

where $\Delta = (4EkT\, m/M)^{1/2} = (4E\,kT/A)^{1/2}$. This expression may be regarded as the convolution of a natural resonance shape of Eq. (5) of width Γ, centered at E_0, and a Gaussian shape of width Δ, the Doppler width, centered at the energy E of the neutron.

At low temperatures, or at any temperature T when $|E - E_0| \gg \Delta$, the Gaussian shape behaves like a δ function, and the original natural shape of the resonance, Eq.(5), is obtained. For narrow resonances, high temperatures, and neutron energies not too remote from the resonance peak, the natural line shape of Eq. (5) behaves like a δ function and $x = s, c, \ldots f$

$$\sigma_x(E) = \sigma_{0x} \frac{\Gamma\sqrt{\pi}}{2\Delta} e^{-\left(\frac{E - E_0}{\Delta}\right)^2} \tag{9}$$

In general, however,

$$\sigma_x(E) = \sigma_{0x}\, \psi(x,\theta), \quad \psi(x,\theta) = \frac{1}{\sqrt{4\pi\theta}} \int_{-\infty}^{\infty} \frac{e^{-\frac{(x-y)^2}{4\theta}}}{1+y^2} dy, \quad \theta = \left(\frac{\Delta}{\Gamma}\right)^2, \quad x = \frac{2}{\Gamma}(E - E_0) \tag{10}$$

for a symmetric natural resonance line shape, and similarly

$$\sigma_{inc}(E) = 2\sqrt{\frac{g_s}{g_n}\frac{\Gamma_n}{\Gamma}\sigma_p}\; \chi(x,\theta) \quad , \quad \chi(x,\theta) = \frac{1}{\sqrt{4\pi\theta}} \int_{-\infty}^{\infty} \frac{y\, e^{-\frac{(x-y)^2}{4\theta}}}{1+y^2} dy \tag{11}$$

for the asymmetric part of the scattering cross section of Eq. (5). Computer subroutines are available for the rapid calculation of the Doppler broadened line shape functions ψ and χ, in particular one which is based on the use of continued fractions for certain ranges of the arguments, and asymptotic expansions when the arguments make the results of such expansions accurate[8].

Resonance Cross Section Profile Tabulations

The development of complete evaluated nuclear data files for all nuclides of importance in fission reactors and for the entire energy range from about 10^{-5} eV to 20 MeV, together with the availability of fast computers with large storage memories, have led to the possibility of handling resonance absorption calculations with much greater precision than previously. The direct use of the

tabulated resonance parameters in such calculations inevitably leads to approximations, because strict adherence to the procedures recommended by the cross section evaluators, and rigorous Doppler broadening, are time consuming processes which have to be repeated at many energy points. The cross section formulae given by Eqs. (5), (10) and (11') treat the resonances separately, and use line shape Doppler broadening functions. They are therefore not in complete accord with the recommended resonance formalisms, even if the evaluators specify that the single level Breit-Wigner formulae should be used. As stated previously, corrections have to be applied, for example, to the interference cross section between resonance and potential scattering. Such corrections are given in data sections separate from the resonance parameters and, when used, will not be Doppler broadened by the line shape functions. Also when other resonance formalisms, such as the multi-level Breit Wigner formulae, are recommended, corrections may be needed at certain energies to improve the agreement of 0°K cross sections calculated from the specified resonance parameters with experimental information both in the vicinity of the resonance peaks and at the minima between them.

Since resonance parameters for recommended resonance formalisms together with appropriate corrections are merely a means for the representation of the resonance cross sections, it is clearly desirable to eliminate these type of data from the basic nuclear data libraries and replace them by 0°K cross sections which describe the resonance shapes in full detail. The tabulations will clearly be lengthy, but if handled properly, possibly by making use of extended fast core storage, this presents no insurmountable problem. For ENDF/B data a resonance cross section processing code exists[9] which uses the recommended resonance formalisms without any approximations and applies the specified corrections to produce at 0°K a modified ENDF/B data tape which has no resonance parameters but instead only very detailed resonance profile tabulations which can be linearly interpolated. The procedure for producing these tabulations is to calculate the unbroadened cross sections from the stated formalism and given parameters without any simplifications, and including corrections (if any), at a set of nodes which are the energies of the lower and upper limits of the resolved resonance region and of all cross section peaks in this energy range. Between any two successive nodes the cross sections are similarly calculated at the mid point energy and the results are compared with those obtained by linear interpolation. Discrepancy in excess of a specified accuracy criterion makes the mid point energy itself a node, enabling the process to be continued by successivley halving the interval between two nodes until linear interpolation of the cross sections is accurate within the chosen criterion. The final tabulations have a very fine energy mesh near the regions of large curvature of the cross section curves, and the mesh interval is large when the cross section varies smoothly. Typically the number of mesh points in the resolved resonance region of fuel and fission product resonance nuclides is of the order of several thousand to a few tens of thousand for a linear interpolation accuracy of 0.5 percent. Some examples of resonance profile tabulations will be given subsequently.

Accurate Doppler Broadening

When cross sections at 0°K are represented by tabulations which can be interpolated by linear-linear interpolation, an exact procedure for Doppler broadening can be developed. It was discussed by Hinman, et. al.[10] and by Cullen and Weisbin[11]; the code SIGMA1 for Doppler broadening was written by Cullen[12]. Since linear interpolation is a necessary prerequisite, a further code[13] ensures that energy regions outside the one relating to the resolved resonance profile tabulations are also extended so that the same interpolation procedure holds.

For neutron and target velocities $\bar{v}$ and $\bar{V}$ the exact form of Eq. (8) becomes

$$v\,\sigma(v,T) = \int v_r\,\sigma(v_r,0)\,P(\bar{V})\,d\bar{V}\,, \quad P(\bar{V}) = \left(\frac{m\beta}{2\pi}\right)^{3/2} e^{-\frac{m\beta V^2}{2}}\,, \quad \beta = \frac{A}{kT} \tag{12}$$

where $\bar{v}_r = \bar{v} - \bar{V}$ is the relative velocity. After integration over all angles between $\bar{v}_r$ and $\bar{v}$

$$v^2\sigma(v,T) = \sqrt{\frac{mA}{2\pi}} \int_0^\infty v_1^2 \sigma(v_1,0)\left[e^{-\frac{1}{2}mA(v-v_1)^2} - e^{-\frac{1}{2}mA(v+v_1)^2}\right] dv_1$$

or

$$\sqrt{E}\,\sigma(E,T) = \frac{1}{2}\sqrt{\frac{A}{\pi E}} \int_0^\infty \sqrt{E_1}\,\sigma(E_1,0)\left[e^{-\beta(\sqrt{E}-\sqrt{E_1})^2} - e^{-\beta(\sqrt{E}+\sqrt{E_1})^2}\right] dE_1 \qquad (13)$$

The exact Doppler broadening represented by Eq. (13), and applied in practice to cross section tabulations which can be linearly interpolated, ensures that a $1/v$ cross section is unaffected by temperature changes. For other dependence of the cross section on the neutron speed the shapes become smoother as the temperature increases. Consequently the tabulations can be thinned at the higher temperatures, i.e., some of the tabulated values can be omitted without changing the linear interpolation accuracy. The code referred to above[12] performs such thinning of the tables, and some saving of computer storage requirements results.

The cross section curves for the first two resonances of ^{238}U, and the ^{235}U absorption cross section in their vicinity, obtained from ENDF/B-IV room temperature tabulations are the ones shown in Figs. (2) and (3). Table (1) shows the number of energy mesh points in the tables for these nuclides at three different temperatures for the same linear interpolation accuracy criterion, 0.5 percent. At the higher temperatures the variation of σ with E is less pronounced as can be seen from the smaller number of mesh points required. The fact that ^{235}U requires a somewhat finer mesh than ^{238}U is connected with the closer spacing of its resonances.

Table 1

Number of Energy mesh points required for cross section tabulations, with 0.5% linear interpolation accuracy, in a lethargy interval of 0.25 near the first two resonance peaks of ^{238}U

Energy Interval	Temp. °K	Mesh Points ^{238}U	Mesh Points ^{235}U	Energy Interval	Temp. °K	Mesh Points ^{238}U	Mesh Points ^{235}U
	300	79	84		300	101	195
6.5-8.3	600	70	78	17.6-22.6	600	91	163
	1200	61	71		1200	80	136

As example for the reduction of peak cross section values with increasing temperature and the increase of their values in the wings some of the σ_c values of ^{238}U near 20.9 eV are shown in Table II.

Table II

^{238}U Capture Cross section values in Resonance Profile Library near the 20.9 eV s-wave peak.

E(eV)	300°K	600°K	1200°K
22.64	2.49	2.50	2.53
21.22	85.6	129.	344.
20.96	4780.	4060.	3210.
20.91	6360.	4700.	3460.
20.85	5150.	4220.	3280.
20.69	315.	717.	1240.
20.07	11.3	11.5	12.1

In Table III a complete set of entries in the tabulations very close to the weak 10.2 eV p-wave resonance peak of ^{238}U is shown. It demonstrates clearly that even weak resonances are well represented in the tables with reduction of the peaks at the higher temperatures and reduced number of entries. The energies of the tabulated mesh points also do not coincide exactly at the different temperatures because of the thinning process.

Table III

^{238}U Capture Cross Section entries in Resonance Profile Library in close vicinity of the 10.2 eV p-wave peak

E(eV)	300°K	E(eV)	600°K	E(eV)	1200°K
				10.2426	2.7387
10.2392	4.5343				
		10.2347	3.6032		
10.2290	4.7682				
				10.2222	2.8065
		10.2191	3.6775		
10.2182	4.8379				
10.2079	4.7253				
		10.2044	3.6071		
				10.2018	2.7742
10.1974	4.4451				
		10.1888	3.3939		

In addition to its application to tabulated resonance cross section values at epithermal energies, exact Doppler broadening is also applicable in the thermal energy region. Absorption cross sections at some energy peaks near the thermal resonance peaks of ^{235}U, ^{239}Pu, and ^{135}Xe are shown in Table IV. These resonances give the thermal σ_a a non $1/v$ character which is slightly temperature dependent.

Table IV

Thermal temperature dependent absorption cross sections near resonance peaks.

	^{235}U			^{239}Pu			$^{135}Xe(10^6$b.)	
E(eV)	300°K	1200°K	E(eV)	300°K	1200°K	E(eV)	300°K	1200°K
0.212	219.85	220.98	0.179	1140.9	1170.7	0.0253	2.669	2.719
0.255	233.89	233.33	0.212	1784.0	1852.5	0.0306	2.652	2.700
0.308	224.45	221.88	0.255	3567.4	3589.6	0.0428	2.720	2.757
0.376	155.42	155.81	0.308	4549.6	4381.2	0.0569	2.842	2.850
0.462	105.57	105.89	0.376	1682.1	1728.1	0.0652	2.882	2.855
			0.462	464.4	478.7	0.0748	2.837	2.781
						0.0992	2.263	2.206
						0.152	0.816	0.828

These slight thermal temperature effects are additional to the temperature dependence of the thermal scattering kernels and cross sections which may be obtained from the basic temperature dependent scattering law data by suitable processing codes[14]. The variation of σ_s with temperature for Hydrogen at a few energy points is shown in Table V. More detailed information is given in Ref. (15).

Table V

Some thermal energy values of σ_s for H in H_2O.

E	σ_s		E	σ_s	
	300°K	600°K		300°K	600°K
.00025	215.2	361.5	.114	32.6	33.3
.00633	75.2	92.5	.255	26.6	26.9
.0253	53.6	57.1	.703	21.7	21.9

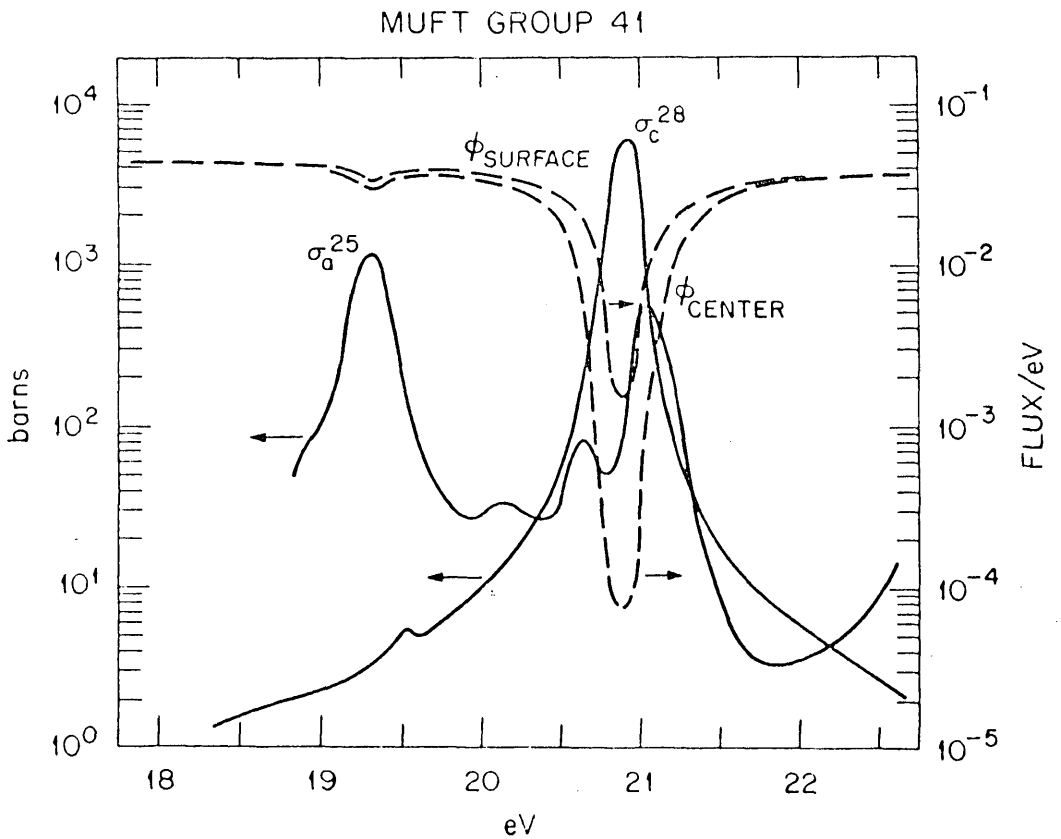

Fig. 2 Effect of ^{238}U and ^{235}U Resonances on Flux Depression in MUFT Group 41 at the Center and near the Surface of a Fuel Rod in Benchmark NB-1.

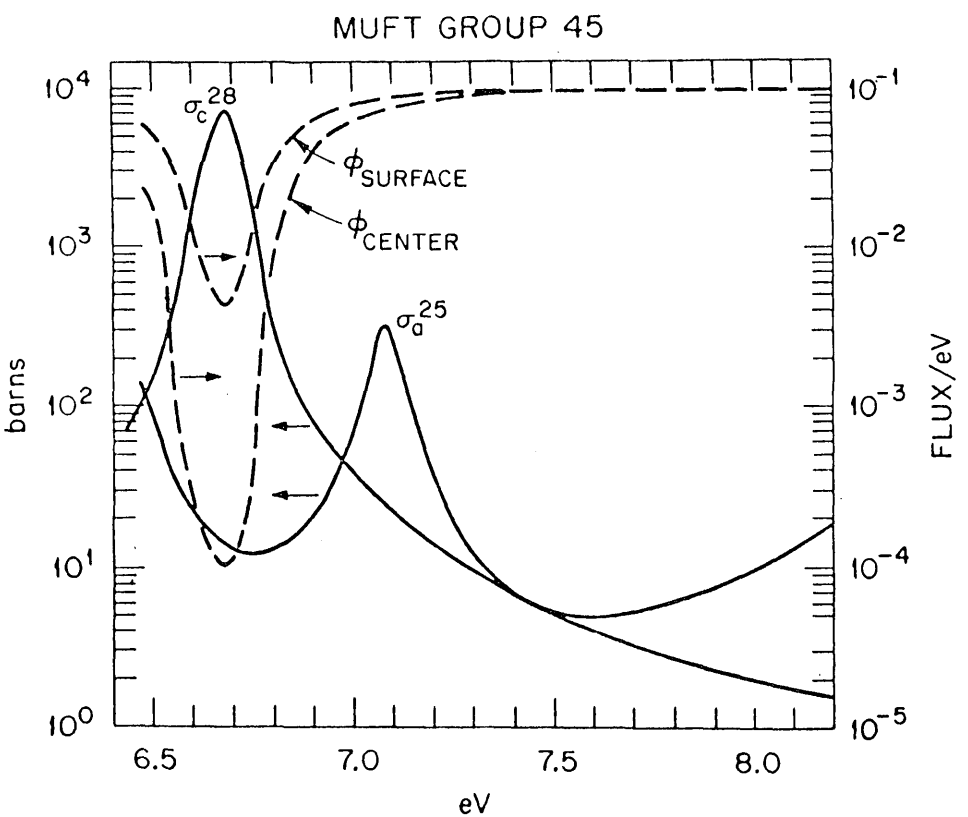

Fig. 3 Effect of ^{238}U and ^{235}U Resonances on Flux Depression in MUFT Group 45 at the Center and near the Surface of a Fuel Rod in Benchmark NB-1.

Lecture II

Shielded Resonance Integrals in Homogeneous Mixtures in Infinite Media. Hydrogen Moderation Only.

The space independent neutron balance equations in homogeneous mixtures can be solved rigorously at epithermal energies (down-scattering only) for any energy dependence of the absorption cross section and neutron source, when Hydrogen is the only moderator. This exact solution serves as a starting point for resonance absorption calculations under more general conditions for homogeneous mixtures and heterogeneous assemblies, for which approximations cannot be avoided except in the case of Monte Carlo studies. The latter, however, have their difficulties because of the lengthy computer runs which have to be made, and the inevitable statistical inaccuracies which may become large when results relating to relatively narrow energy bands or their variation with temperature are required.

The solution of the infinite homogeneous medium problem with Hydrogen moderation only contains all the elements needed for practical resonance absorption calculations. Shielded or effective resonance integrals appear in a form which suggests how corresponding quantitites should be defined in other systems, even if the treatment is then approximate. The analytical expression for the flux, when Hydrogen is the only moderator, may be interpreted in such a manner that resonance shielding and flux decay due to resonance absorption are separable. This separability becomes an assumption for the general resonance absorption problem, although it is usually well justified.

For these reasons the Hydrogen moderated homogeneous system is of such central importance in resonance absorption calculations. The results are frequently tabulated in the form of temperature dependent shielded group resonance integrals which are used in codes handling the epithermal energy region. Alternatively, temperature dependent fine group shielded resonance cross sections for Hydrogen moderation may be tabulated in the group structure of the multigroup code. The tabulations with their accurate temperature dependence are then used for moderation by other nuclides, or mixtures of nuclides, and for heterogeneous assemblies on the basis of approximate treatments. As already discussed earlier, one must be aware of errors which may arise on account of these approximations rather than any inaccuracies in the tabulated fine group parameters (effective resonance integrals or shielded cross sections). Studies of temperature coefficients of absorption rates and reactivity in particular should be benchmarked against sophisticated calculations which do not depend on the results for the Hydrogen moderated case as an intermediate step.

The neutron balance equation at epithermal energies for moderation by Hydrogen only and in the absence of space dependence is

$$\Sigma(E)\varphi(E) = \int_E^\infty \Sigma_s(E')\varphi(E')\frac{dE'}{E'} + S(E) \qquad (14)$$

Its solution[16] is

$$\Sigma(E)\varphi(E) = S(E) + \frac{1}{E}\int_E^\infty dE' S(E')\frac{\Sigma_s(E')}{\Sigma(E')}\, e^{-\int_E^{E'}\frac{\Sigma_s(E'')}{\Sigma(E'')}\frac{dE''}{E''}} \qquad (15)$$

Multiplying the solution by the scattering probability $\Sigma_s(E)/\Sigma(E)$ at energy E the scattering rate is seen to be given by a contribution due to the source at this energy E multiplied by the scattering probability at the same energy, and the sources at higher energies E' multiplied by the scattering probability at E', the probability $1/E'$ per unit energy interval of reaching final energy E (normalised to the fraction of neutrons E/E' scattered below E), i.e., $\frac{1/E'}{E/E'}$, and the non absorption probability between E' and E.

If the source and absorption energies are well separated the integral in the exponent has to be evaluated only from E to E_c, the maximum energy at which absorption occurs. The source $S = \int_{E_1}^{\infty} S(E')dE'$ is then the total source above this energy and Eq. (15) becomes

$$E\Sigma(E)\varphi(E) = F(u) = Q(u) = S\, e^{-\int_{u_0}^{u}\frac{\Sigma_a(u')}{\Sigma(u')}du'} \qquad (16)$$

since the slowing down density $Q(u)$ is the collision density per unit lethargy for Hydrogen moderation.

In Eq. (16) the exponential decrease of the slowing down density, or the flux per unit lethargy, due to absorption is evident while the resonance shielding appears separately in $-\tau_{eff}(u)/\sigma_m$:

$$\bar{I}_{eff}(u) = \int_{u_0}^{u} \frac{\sigma_a(u')}{1 + \frac{\sigma_a(u')}{\sigma_m}} \, , \quad \sigma_m = \frac{\Sigma_s}{N_a} \tag{17}$$

where Σ_s is the (constant) scattering cross section of Hydrogen and N_a the atom density of the resonance absorber.

One may interpret $\bar{I}_{eff}(u)$ as the absorption between u_0 and u per single absorbing atom and for unit (asymptotic) flux, per unit lethargy, which is unaffected by the absorption itself. The latter manifests itself as the exponential decay of the flux or slowing down density in Eq. (16).

Shielded Resonance Integrals in Homogeneous Mixtures in Infinite Media Moderation by Nuclides other than Hydrogen, and Mixtures of Nuclides.

The above treatment for Hydrogen moderation, Eqs. (16) and (17) may be modified somewhat by writing it in the form

$$dQ(u) = -\frac{\sigma_s(u)}{\Sigma_s} N_a \sigma_a(u) f(u) \, du \, , \quad f(u) = \frac{1}{1 + \frac{\sigma_s(u)}{\sigma_m}} \, , \quad \sigma_m = \frac{\Sigma_s}{N_a} \tag{18}$$

Defining $Q(u)/\Sigma_s$ as a flux decay function $\Phi(u)$, the change in the slowing down density is identical with

$$dQ(u) = -N_a \sigma_a(u) \varphi(u) \, du \tag{19}$$

if the flux per unit lethargy $\varphi(u)$ is given by

$$\varphi(u) = \Phi(u) f(u) \tag{20}$$

Thus the flux per unit lethargy is the product of the flux decay function $\Phi(u)$, which is proportional to the slowing down density, and the shielding function $f(u)$. The former satisfies

$$\Phi(u) = \frac{\Phi_0}{Q_0} Q(u) \tag{21}$$

in terms of the asymptotic flux (before it decays) Φ_0, at energies for which $\sigma_a(u) = 0$ and where the slowing down density is $Q_0 = S$, while $f(u)$ is the weighting function with which the effective absorption integral is calculated.

also replacing $\frac{1}{\Sigma_s}$ by Φ_0 / Q_0 in Eq. (18) using Eq. (21) one obtains from Eq. (17)

$$Q(u) = Q_0 \exp\left[- N_a \bar{I}_{eff}(u) \frac{\Phi_0}{Q_0} \right] \tag{22}$$

The separation of the flux into two functions of lethargy, the one $\Phi(u)$ varying slowly with lethargy, the other $f(u)$ accounting for the resonance shielding, is assumed to hold for moderation by nuclides other than Hydrogen, and for mixtures, together with the other equations given above. Q_0 / Φ_0 becomes of course $\Sigma_i(\xi, \Sigma_{s,i})$ in the absence of absorption, and assuming that Placzek oscillations produced by the neutron source have already died out before absorption becomes appreciable. Similarly $\bar{I}_{eff}(u)$ is replaced by the sum of the effective absorption integrals of all nuclides.

Consequently, if the resonance absorption problem for scattering by mixtures of nuclides, or a single nuclide other than Hydrogen, is to be solved by means of shielded resonance integrals the following assumptions are made:

1) The resonances are located at energies well below the fission spectrum.
2) The flux is the product of a slowly varying function which decreases with increasing lethargy due to neutron absorption, and a shielding function which is depressed in the vicinity of the resonances, but is unaffected by neutron absorption.

The second assumption is omitted if effective resonance integrals are not used as an intermediate step.

In any event, the collision density per unit energy on the left side of Eq. (14) is written as a function of the lethargy variable, $\psi(u)$. For mixtures of nuclides the homogeneous part of Eq. (14) takes the form

$$\psi(u) = \sum_i T_i \psi \tag{23}$$

where T_i is an operator, which operates on $\psi(u')$, and is defined by

$$T_i = \frac{1}{1 - \alpha_i} \int_{u - \frac{1}{\alpha_i}}^{u} du' \frac{\Sigma_{s,i}(u')}{\Sigma_t(u')} \, , \quad \alpha_i = \left(\frac{A_i - 1}{A_i + 1} \right)^2 \tag{24}$$

Eq. (23) is to be solved so that above the energy region where the absorption takes place

$$\psi(u) \longrightarrow \psi_{as}(u) = \frac{\Sigma_B}{E_c\, e^{-u}} \tag{25}$$

If applied to the calculation of the shielding function, the energy range in the resonance region is split up into narrow intervals, e.g. intervals containing a single or a few resonances. For such an interval Eq. (23) is solved subject to the asymptotic condition of Eq. (25) and

$$f(u) = E_c\, e^{-u}\, \psi(u) / \Sigma_t(u) \tag{26}$$

since the absorption fraction in each interval is negligibly small. Σ_B is the background cross section of all nuclides in the mixture, including the constant potential scattering cross section of the resonance absorbers, or part thereof according to the approximation employed.

If, on the other hand, the resonance absorption rates are to be calculated directly throughout the entire resonance region, Eq. (23) is solved subject to Eq. (25) which is applied only once above the entire region, and not separately above every subinterval of the resonance region. In this case

$$q(u) = E_c\, e^{-u}\, \psi(u) / \Sigma_t(u) \tag{27}$$

since the gradual decrease of the flux due to absorption is taken into account in the calculation of $\psi(u)$ which is the collision density per unit energy corresponding to lethargy u.

The Narrow Resonance, Infinite Mass, and Intermediate Resonance Approximations.

The calculation of the resonance shielding function for small energy intervals, in accordance with the above considerations, is usually applied to individual resonances which are treated as though all other resonances are absent, or do not interfere at all with the resonance under consideration. The function $\psi(u) = \Sigma_t(u) f(u)\, e^{u}/E_c$ to be evaluated by Eq. (23) is then asymptotic to $\Sigma_B\, e^{u}/E_c$ above the resonance, where $\Sigma_B = \Sigma_{Pc} + \Sigma_s'$ includes the potential scattering cross section of the resonance absorber c and the scattering cross section of all other nuclides Σ_s'.

In the Narrow Resonance (NR) approximation the resonance is assumed to be so narrow that it covers a negligible part of the scattering interval in Eq. (24) for the resonance absorber i. In this range $\Sigma_{sc}(u')/\Sigma_t(u')$ is less than the asymptotic value Σ_{Pc}/Σ_B, and the same holds for the other nuclides. However, since this range is assumed to be neglibible compared with $\ell_n(1/\alpha_c)$, a negligible error will be introduced if the asymptotic values are used for the scattering probability of the resonance absorber in Eq. (24) and also of all other nuclides (generally of smaller mass), throughout their scattering intervals. This leads to the N.R. value $\Sigma_B\, e^{u}/E_c$ for $\psi(u)$ at all lethargies so that

$$f_c(u) = \Sigma_B / \Sigma_t(u) \qquad \text{(NR)} \tag{28}$$

On the other hand, if the resonance of nuclide i is wide compared with the scattering interval $\ell_n(1/\alpha_i)$, the alternative extreme assumption can be made that this interval tends to zero, or the mass ratio A_i to the neutron mass tends to ∞. For the other nuclides, the NR approximation is still assumed to hold. Carrying out the appropriate limits in Eq. (23) one obtains

$$\psi(u) = \frac{\Sigma_s'\, e^{u}/E_c}{1 - \Sigma_{sc}(u)/\Sigma_t(u)}, \quad \therefore f_c(u) = \frac{\Sigma_s'}{\Sigma_t(u) - \Sigma_{sc}(u)} = \frac{\Sigma_s'}{\Sigma_s' + \Sigma_{Pc}} \text{(IM)} \tag{29}$$

In the intermediate resonance approximation the resonance absorber is treated according to the NR and IM approximations with fractions λ_c and $(1-\lambda_c)$ respectively. The resonance shielding function then becomes

$$f_c(u) = \frac{\Sigma_B - (1-\lambda_c)\Sigma_{Pc}}{\Sigma_t(u) - (1-\lambda_c)\Sigma_{sc}(u)} = \frac{\Sigma_s' + \lambda_c \Sigma_{Pc}}{\Sigma_s' + \Sigma_{sc}(u) + \lambda_c \Sigma_{sc}(u)} \qquad \text{(IR)} \tag{30}$$

In these expressions $\Sigma_{sc}(u)$ includes the potential scattering cross section Σ_{Pc}. The effective resonance integral for these approximations is simply given by

$$I_{eff,x,c} = \int \sigma_{x,c}(u)\, f_c(u)\, du \tag{31}$$

in accordance with Eq. (18) where the integral extends over the entire resonance, and x represents the reaction type. In Eq. (22) $I_{eff}(u)$ includes the contributions for $x = a$, absorption, for all resonance nuclides i and all resonances below lethargy u.

Application to Unresolved Resonances

The above formulae are immediately applicable to unresolved resonances. If for a particular resonance sequence the average parameters and their statistical distributions are given at a specified energy, the shielded resonance integral for the resonances of this sequence in the vicinity of this energy have the expectation value

$$\langle I_{eff,x,i} \rangle = \langle \int \sigma_{x,i}(u) \phi_i(u) du \rangle$$

where all cross sections are derived according to the given formalism from the average resonance parameters multiplied by the appropriate frequency function for the statistical distribution.

Tabulated Effective Resonance Integrals or Shielded Cross Sections for Narrow Energy Groups

If resonance absorption calculations are to be performed rapidly in multigroup lattice analysis codes, tabulated effective group resonance integrals or shielded group cross sections provide the most effective means for handling this problem which is, in general, very complicated and time consuming. To prepare the tabulations, resonance absorption calculations are made with the aid of accurate codes for homogeneous mixtures of a heavy resonance absorber and Hydrogen as a moderator, for different atom densities of the heavy absorber and Hydrogen, and at different temperatures. Such accurate calculations should use resonance cross sections prepared in strict accordance with the recommended resonance formalism and the specified resonance parameters, and with precise Doppler broadening.

If the mass of the absorbing nuclide was infinite, Eq. (22) would be rigorous and give the absorption integral exactly for any fine energy group. In general there is a very slight approximation in applying Eq. (22) to such mixtures as explained above. In addition, there is also a very small approximation in accounting for the Hydrogen absorption (unshielded) by

$$I_{eff,g} = - \frac{Q_i}{N_a \Phi_i} \ln\left(\frac{Q_{i,gr}}{Q_{i,g}}\right) - \frac{1}{N_a} \int_g \Sigma_H'(u) du \qquad (32)$$

where $\Sigma_H'(u)$ is the small absorption cross section of Hydrogen. Alternatively, Eq. (1) would give the group cross section.

Eq. (30) suggests that the result should be tabulated as a function of Σ_s' which is, in this case, the scattering cross section of Hydrogen. The effect of the scattering, including resonance scattering, of the resonance absorber is implicitly taken into account by the way the accurate resonance absorption code for the mixture of a heavy resonance absorber and Hydrogen solves the slowing down problem for the case in which the absorber has finite mass. One can then repeat similar calculations for other moderators instead of Hydrogen, and from comparison of the calculated results ($I_{eff,g}$ or σ_g) with values obtained by interpolation in the tables prepared for Hydrogen moderation, one can assign λ values to the other moderators with which the resonance absorber is mixed. These λ values (generally a single number for each nuclide for all fine groups in the resonance energy region) can then be assumed to be valid also for the calculation of the background cross section Σ_s' required to determine $I_{eff,g}$ (or σ_g) by interpolation between tabulated values for Hydrogen moderation, when Σ_s' refers in fact to several nuclides i' with which the resonance absorber i is mixed ($\Sigma_s' = \sum_{i' \neq i} \lambda_{i'} \Sigma_{si'}$).

In a similar manner, mixtures of resonance absorbers can be treated by utilising the tabulations separately for each of them. The argument Σ_s' used for each resonance absorber includes the $\lambda \Sigma_s$ values of all the other resonance absorbers. The resulting effective group resonance integrals, or shielded group cross sections, do not make any allowance for the effect of interference between neighbouring resonances of different resonance absorbers on the shielding function. Attempts which are sometimes made to take such interference effects into account very approximately, within the framework of the type of tabulations referred to above, will be discussed later.

In utilising the $I_{eff,g}$, or σ_g , values of the different resonance absorbers, the question arises, in the case of the former, what Φ_i / Q_i value should be used in Eq. (22) if the non absorption fraction of neutrons is to be derived. Should it be the asymptotic value above the resonance region or the value above each group which may be slightly different due to changes of $\xi \Sigma_s$ of the mixture from group to group? Alternaltively, if $I_{eff,g}$ is obtained from

the tabulations, what group flux integral should be used to convert it into a group cross section σ_g ? Finally, if σ_g is obtained from shielded resonance absorption group cross section tabulations for Hydrogen moderation, may the values thus obtained for mixtures be assumed to be based on the same group flux integral as the one used to prepare the tabulations? These questions are likely to be more serious for heterogeneous assemblies, as discussed in connection with Eqs. (4) and (4').

Lattice Heterogeneity Equivalence Relations

If fuel and moderator are separated from one another in a heterogeneous assembly, the simplest way of taking this heterogeneity into account is to assume that the lattice may be replaced by a homogeneous assembly with appropriate Σ_s'. This value uniquely determines $I_{eff,g}$, or σ_g, by interpolation in the table which refers to Hydrogen moderation in a homogeneous mixture for the appropriate fuel temperature.

The simplest equivalence principle is based on the definition of a geometrical cross section Σ_σ which replaces the effect of the finite size of the fuel lump and the effect of its proximity with neighbouring fuel lumps. Then

$$\Sigma_s' = \sum_{i \neq j}' \left(\lambda_{ij} \Sigma_{sij} \right)_{\bar{r}} + \Sigma_\sigma \qquad (33)$$

The form of Σ_σ will be discussed in the next section. In the WIMS code[17], two different Σ_σ's are used to deal with different aspects of the heterogeneity problem, each leading to an $I_{eff,g}$ value by interpolation in the tabulations relating to a homogeneous mixture of the resonance absorber and Hydrogen as moderator; these are then combined with appropriate weights.

Equivalence principles do not account for the spatial distributions of the shielded flux at the energies within the resonance peaks in detail, since they rely on one (or perhaps two) parameters only to describe the heterogeneity completely. Consequently, the problems referred to in the case of homogeneous mixtures of moderating nuclides and different resonance absorbers are now more serious.

We summarise the assumptions and approximations in using tabulations of group effective resonance integrals, or shielded cross sections, together with those given previously as follows:

1) The resonance are located at energies well below the fission spectrum.
2) The flux is the product of a slowly varying function which allows for the loss of neutrons by absorptions and a shielding function which accounts for the flux depressions in the vicinity of the resonance peaks.
3) Group effective resonance integrals or cross sections may be derived from tabulations of such quantities which relate to homogeneous mixtures of a single resonance absorber and Hydrogen as moderator, since these quantities can be defined unambiguously when the absorber has infinite mass.
4) If moderators other than Hydrogen are mixed with the heavy resonance absorber, this mass (differing from unity) may be allowed for by means of an intermediate resonance parameter λ (possibly group dependent) irrespective of the fuel composition, or its lump size and lattice pitch in a heterogeneous assembly.
5) Interference effects between resonances of different absorbers are negligible. (To correct for them, if they are appreciable, more sophisticated methods must be used in principle than those which can be formulated on the basis of the tabulations mentioned in (3) above, by very rough approximations).
6) The size of the fuel lumps and the lattice pitch in heterogeneous assemblies are accounted for by a geometrical cross section which replaces the non-fuel regions.
7) It is assumed that the energy dependence of the flux used to prepare the tabulations in (3) above is the same as the average energy dependence of the fuel flux for the heterogeneous assembly with the same background cross section.
   Similarly, it is assumed that an approximate group average fuel disadvantage factor needed to change fuel average to cell average cross sections does not introduce additional errors.

An Early Rigorous Treatment of the Effect of Lattice Heterogeneity on Resonance Absorption.

A low order solution of the neutron transport equation in the resonance energy region, but capable in principle of generalisation to any order, was developed

by Corngold[18] in 1957 for regular two region slab lattices.

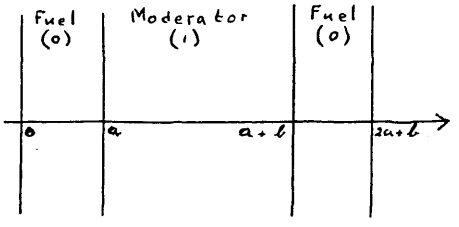

Fig. 4 Regular Lattice of Infinite Slabs

He used an integral transport treatment for the direction dependent flux and applied interface continuity and periodicity conditions. The fluxes and slowing down sources in the different regions were then expanded in the double Legendre series (for space and angle). The lowest order solutions are given by:

$$\Sigma_0 f_{00}(E) = a\,\Sigma_0(E)\varphi_0(E) = \left[1 - \frac{\mathcal{G}(E)}{2a\,\Sigma_0(E)}\right] S_{00}(E) + \frac{\mathcal{G}(E)}{2\ell\,\Sigma_1(E)}\, t_{00}(E)$$

$$\Sigma_1 g_{00}(E) = \ell\,\Sigma_1(E)\varphi_1(E) = \frac{\mathcal{G}(E)}{2a\,\Sigma_0(E)} S_{00}(E) + \left[1 - \frac{\mathcal{G}(E)}{2\ell\,\Sigma_1(E)}\right] t_{00}(E)$$

$$\mathcal{G}(E) = 2\int_0^1 \frac{\left(1 - e^{-\frac{a\,\Sigma_0(E)}{\mu}}\right)\left(1 - e^{-\frac{\ell\,\Sigma_1(E)}{\mu}}\right)}{\left(1 - e^{-\left\{\frac{a\,\Sigma_0(E) + \ell\,\Sigma_1(E)}{\mu}\right\}}\right)}\,\mu\,d\mu \qquad (34)$$

In the forms of Eq. (34) the quantities multiplying the scattering sources in fuel and moderator can readily be understood physically to represent the fuel single flight collision probability for a uniform isotropic source in the fuel, and the corresponding escape probability from the moderator, in the first line, and the reverse probabilities in the second.

Although applicable mainly in its basic form the above treatment relates the collision and escape probability approach directly to the solution of the transport equation. The generalisation to higher orders is available and has been used by Corngold to show that for a few isolated resonances corrections to the basic solution are small.

General Expression for Collision and Escape Probabilities in Regular Two Region Lattices.

The quantities $\frac{a}{\mu}$ and $\frac{\ell}{\mu}$ in the expression for $\mathcal{G}(E)$ in Eq. (34) are in fact chord lengths in the two regions (fuel and moderator) for neutron paths inclined at an angle $\cos^{-1}\mu$ with the normal to the slabs. Such chord lengths and integrations over μ occur in fact quite generally in expressions for collision and escape probabilities[19]. For a periodic lattice with fuel lumps of any shape there is an additional integration over the surface of the lumps leading to general formulae for the escape probabilities $(1 - P_0)$ from the fuel and $(1 - P_1)$ from the moderator for uniform isotropic sources in the regions from which the neutrons orginate:

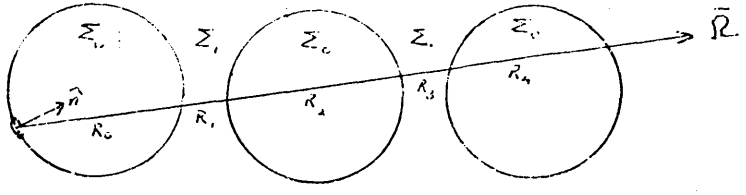

Fig. 5 Random Chords in a periodic lattice

$$1 - P_0(E) = \frac{\mathcal{G}(E)}{\ell_0\,\Sigma_0(E)}, \quad 1 - P_1(E) = \frac{\mathcal{G}(E)}{\ell_1\,\Sigma_1(E)}, \quad \ell_0 = \langle R_0 \rangle, \quad \ell_1 = \langle R_1 \rangle$$

$$\mathcal{G}(E) = \left\langle 1 - \left\{\Gamma_0 - \Gamma_0\Gamma_1 + \Gamma_0\Gamma_1\Gamma_2 - \cdots\right\} - \left\{\Gamma_1 - \Gamma_1\Gamma_2 + \Gamma_1\Gamma_2\Gamma_3 - \cdots\right\} \right\rangle$$

$$\Gamma_0 = e^{-R_0\Sigma_0(E)}, \quad \Gamma_1 = e^{-R_1\Sigma_1(E)}, \quad \Gamma_2 = e^{-R_2\Sigma_0(E)}, \ldots$$

where all averages are calculated by integrating over the fuel lump surface S and all chord directions $\bar{\Omega}$ with weight $(\hat{n}\cdot\bar{\Omega})$ .Chords distributed in this way correspond to uniform isotropic sources [19]. The mean chord lengths ℓ_0 and ℓ_1 are $4V_0/S$ and $4V_1/S$ where V_0 and V_1 are the fuel volume and moderator volume associated with a single fuel lump.

For a slab lattice the form of Eq.(35)is simplified since all moderator chords in Γ_{2n+1} are equal, and $2n$ are all fuel chords in Γ_{2n}. In addition ℓ_0 and ℓ_1 are $2a$ and 2ℓ respectively. Thus Eq. (35) leads to Eq. (34).

In the resonance shielding problem one is interested in the black limit of the fuel escape probability (when $\Sigma_o(E) \to \infty$). From Eq. (35) it is seen immediately that

$$1 - P_i(E) \longrightarrow \begin{cases} \dfrac{1-\bar{\tau}_i}{\ell_i \Sigma_o(E)} & \left[\Sigma_o(E) \to \infty\,,\ \bar{\tau}_i = \langle \tau_i \rangle\right] \\ 1 & \left[\Sigma_o(E) \to 0\right] \end{cases} \qquad (36)$$

Here $\bar{\tau}_i$ is the moderator transmission probability, also called the Dancoff factor [21]. The white limit of Eq. (35) is also readily seen to be unity.

The Geometrical Cross Section.

A simple rational expression which has the same limits as Eq. (36) is the Wigner rational approximation

$$1 - P_o(E) = \frac{\Sigma_G}{\Sigma_G + \Sigma_o(E)}\,, \qquad \Sigma_G = \frac{1-\bar{\tau}_i}{\ell_i} \qquad (37)$$

Here Σ_G is in fact the geometrical cross section which was introduced in Eq. (33) to establish the equivalence between heterogeneous and homogeneous assemblies for which the resonance reaction rates are to be calculated.

The expression for Σ_G is approximate. It has been adjusted to give better agreement between effective resonances integrals based on the equivalance theorems and those calculated by sophisticated methods, by the introduction of a Bell factor [22].

$$\Sigma_G = \frac{a(1-\bar{\tau}_i)}{\ell_o}\,, \qquad a = \frac{\left[2.366 + \sqrt{1-\bar{\tau}_i}\right]^2}{\left[2.366 + \sqrt{1-\bar{\tau}_i}\right]^2 - 1.866(1-\bar{\tau}_i)} \qquad (38)$$

The dependence of the Bell factor a on the lattice pitch, i.e. on the Dancoff factor, is due to Leslie et al [23]. The value of a is usually about 1.2.

Finally Sauer [24] has suggested a simple approximation for the Dancoff factor in rod lattices. It is based on assuming an exponential distribution for the difference between moderator chord lengths and the closest distance between the rods t, and forcing this distribution to yield the proper moderator mean chord length. Sauer applied this to rod lattices in water in square and hexagonal geometry and empirically adjusted the results to agree with more precise calculations. His approximation is given by:

$$\bar{\tau}_i = \frac{e^{-t\Sigma_i \ell_i}}{1 + (1-c)\Sigma_i \ell_i}\,, \qquad t = \frac{\left(\frac{\pi}{4\alpha}\right)^{1/2}\left(1 + \frac{\nu_i}{1+\nu_c}\right)^{1/2} - 1}{\nu_i^{1/2}\left(\frac{\nu_i}{1+\nu_c}\right)^{1/2}} + t_o\left[1 + \frac{1}{2}\left(\frac{\nu_c}{1+\nu_c}\right)^{1/2}\right]$$

$$\nu_i = \frac{V_i}{V_o}\,, \quad \nu_c = \frac{V_c'}{V_c}\,, \quad \ell_i = \ell_o \nu_i\,, \quad \alpha = \begin{cases} 1 \\ \frac{\sqrt{3}}{2} \end{cases}\,, \quad t_o = \begin{cases} -0.08 & \text{(square lattice)} \\ -0.12 & \text{(hexag lattice)} \end{cases} \qquad (39)$$

Multiregion Transfer Probabilities

The reciprocity relation $\Sigma_o \ell_o (1-P_o) = \Sigma_i \ell_i (1-P_i)$ which results from Eq. (51) at any energy for a two region system, is of more general validity when a lattice unit cell is subdivided into a number of subregions. The corresponding relation is then

$$\Sigma_\ell V_\ell P_{n\leftarrow\ell} = \Sigma_n V_n P_{\ell\leftarrow n} \qquad (40)$$

for uniform isotropic sources in the regions where the neutrons originate. These relations, which are a direct consequence of the integral transport equation for the scalar flux, are used in codes which treat the unit cell in reactor lattices as multi-region assemblies with subregions of volume V_n.

The transfer probabilities from one subregion to another in cylindrical geometry can be obtained from the escape and collision probabilities relating to a fuel rod [19] by adapting the treatment to annular regions [17,44], and by making use of certain approximations, such as the cosine current approximation [31]. Alternatively a more precise technique due to Carlvik may also be used [55].

Lecture III

Calculation of Resonance Reaction Rates in Lattice Analysis Codes

The principles discussed previously for the evaluation of effective resonance integrals or shielded cross sections are applied in lattice analysis codes in different ways because of the alternatives that exist in formulating the inevitable approximations, and in accordance with the degree of complexity permitted for the resonance reaction rate calculations in the development of the code, and the computation time set aside for this purpose. The analysis codes in the resonance region can be essentially homogeneous codes, such as MUFT[26] and GAM[27], or they may allow for lattice heterogeneity at these energies, as is the case in WIMS[28] and LATREP[29]. In order to provide insight into the direct use of effective resonance integrals in multigroup calculations on the one hand, and shielded cross sections on the other, an account will be given of the slowing down treatment in codes which analyse the neutron spectrum in the homogenised lattice unit cell at epithermal energies. The multigroup slowing down calculations are the final part of the treatment; the calculation of the resonance shielding with varying degrees of sophistication precedes it. If the multigroup slowing down treatment refers to the heterogeneous lattice, spatial effects in the unit cell may be handled better than in the case when it is simply homogenised by volume weighting the atom densities of the constituent nuclides, but the heterogeneous analysis including the resonance treatment remains necessarily approximate.

Effective resonance integrals are directly related to the slowing down density, as shown in Eq. (22) ; and applied to an energy group, they give the difference in the slowing down density at its energy boundaries and therefore the fractional absorption in the group. The MUFT code[26] utilizes these fractions in its resonance absorption treatment. In addition, it handles the effect of leakage from the unit cell by a Fourier Transform method since it deals with the homogenised assembly; a P-1 or B-1 approximation is used. Similarly, shielded resonance cross sections can be used directly in multigroup codes to calculate the resonance reaction rates. The homogeneous consistent P-1 or B-1 multigroup fast spectrum code GAM[27], which utilises groups of lethargy widths 0.25 throughout the entire epithermal energy region, is based on this procedure. It does not refer to the slowing down densities for elastic scattering like MUFT but treats the elastic scattering by cross sections for transfer from group to group of moments zero and one. In both MUFT and GAM inelastic transfers are handled by means of a transfer matrix of order zero.

In the fast spectrum calculations referred to, the basic equation is the Fourier transform of the transport equation for the direction dependent flux density f and for transform variable (buckling) B is:

$$(iB\mu + \Sigma_t)\tilde{f} = \tilde{S}\,, \quad \tilde{f} = \tilde{f}(B,u,\mu)\,, \quad \tilde{S} = \tilde{S}(B,u,\mu) \tag{41}$$

The transformed flux $\tilde{f}$ and source $\tilde{S}$ are expanded in Legendre polynomial series

$$\tilde{f} = \sum_{l=0}^{N} \frac{2l+1}{2}\, i^{-l}\, \tilde{f}_l\, P_l(\mu)\,, \quad \tilde{S} = \sum_{l=0}^{N} \frac{2l+1}{2}\, i^{-l}\, \tilde{S}_l\, P_l(\mu) \tag{42}$$

which are then substituted back in Eq. (41). In the P-L approximation Legendre moments of the resulting equation are taken, leading to a set of coupled equations from the moments $\tilde{f}_l$. In the B-L approximation the moments are taken after dividing the equation by $(iB\mu + \Sigma)$. They give the moments $\tilde{f}_l$ of the transformed direction dependent flux directly, the only approximation being that the moments of the scattering cross section from one lethargy to another can be neglected after order L. When L=1 the lowest two moments of $\tilde{f}$ may be identified with the flux φ and the current j, and the lowest moments of $\tilde{S}$ with the sources s_0 and s_1, calculated with φ and j at an initial lethargy u', multiplied respectively by the zero-th and first moments of the scattering cross section from u' to u and integrated over u'. The resulting P-1 and B-1 equations then take the form:

$$\Sigma_t \varphi + \varepsilon B j = S_0 \quad , \quad -\frac{1}{3} B \varphi + \gamma \Sigma_t j = S_1$$

$$B = (|B^2|)^{1/2} \quad , \quad a = \frac{B}{\Sigma_t} \qquad \varepsilon = \begin{cases} 1 & (B^2 > 0) \\ -1 & (B^2 < 0) \end{cases}$$

$$\gamma = 1 \quad (P\text{-}1 \text{ approx.}) \; ; \quad \gamma = \begin{cases} \frac{a^2}{3}\left(\frac{\tan^{-1} a}{a - \tan^{-1} a}\right), & (B^2 > 0) \\ \frac{a^2}{3}\left(\frac{\ln \frac{1+a}{1-a}}{\ln \frac{1+a}{1-a} - 2a}\right), & (B^2 < 0) \end{cases} \quad (B\text{-}1 \text{ approx.}) \tag{43}$$

Here the ε results from the fact that for $B^2 < 0$ the first order moments $\hat{f}_1$ and $\hat{S}_1$ are $-j$ and $-S_1$, respectively, in terms of the real current j and first order source S_1. In the B-1 approximation $\gamma = 1 + \frac{2}{15}\frac{B^2}{\Sigma_t^2}$ both for positive and negative B^2.

Since the steady state transport equation forms the basis of the above treatment, B^2 is the eigenvalue which ensures that a non trivial solution is obtained for the entire energy spectrum and a fission source. Alternatively, B^2 may be an input quantity, and the eigenvalue k_{eff}, which leads to a non trivial solution when the number of neutrons per fission ν is replaced by ν / k_{eff}.

The moment of order zero S_0 includes the source due to elastic scattering, inelastic scattering, the n→2n reaction and fission. The first order moment consists mainly of the elastic scattering component, the other phenomena being assumed to be practically isotropic.

The MUFT code does not use a group to group matrix for elastic scattering. Instead it expresses this process in terms of the slowing down density and handles it separately for scattering by hydrogen (slowing down density η), which can be treated exactly, and other nuclides (slowing down density q). For hydrogen the scattering source per unit lethargy of moment zero and the slowing down density are both given by

$$\int_{-\infty}^{u} du' \, e^{-(u-u')} \Sigma_s^H \varphi(u')$$

and the source of moment one is

$$\int_{-\infty}^{u} du' \, e^{-\frac{3}{2}(u-u')} \Sigma_s^H j(u')$$

These expressions lead to the following differential equations for the lowest two moments η and ρ of the slowing down density by hydrogen:

$$\eta + \frac{d\eta}{du} = \Sigma_s^H \varphi \quad , \quad \rho + \frac{2}{3}\frac{d\rho}{du} = \frac{2}{3}\Sigma_s^H j = \bar{\mu}_0^H \Sigma_s^H j \tag{44}$$

For heavier isotopes the scattering source of moment zero and the slowing down density are calcualted by

$$\int_{u - \ln \frac{1}{\alpha}}^{u} du' \, \frac{e^{-(u-u')}}{1-\alpha} \Sigma_s'(u') \varphi(u') \quad , \quad \alpha = \left(\frac{A-1}{A+1}\right)^2$$

and

$$\int_{u - \ln \frac{1}{\alpha}}^{u} du' \, \frac{e^{-(u-u')} - \alpha}{1-\alpha} \Sigma_s'(u') \varphi(u')$$

while the source of moment one is

$$\int_{u - \ln \frac{1}{\alpha}}^{u} du' \, \frac{e^{-(u-u')}}{1-\alpha} \left[\frac{A+1}{2} e^{-\frac{(u-u')}{2}} - \frac{A-1}{2} e^{\frac{(u-u')}{2}} \right] \Sigma_s'(u') j(u')$$

These expressions involve the scattering cross section $\Sigma_s'(u') = \Sigma_s(u') - \Sigma_s^H$. A three term Taylor expansion of $\Sigma_s'(u')\varphi(u')$ in the scattering source of order zero and a two term expansion in the slowing down density q lead to the Groeling-Goertzel approximation for q.

$$q + \lambda \frac{dq}{du} = \xi \Sigma_s' \varphi \, , \quad \xi = \langle u - u' \rangle = 1 - \frac{\alpha}{1-\alpha} \ln \frac{1}{\alpha} \, , \quad \xi\lambda = \left\langle \frac{(u-u')^2}{2} \right\rangle = \xi - \frac{\alpha}{2(1-\alpha)^2} \left(\ln \frac{1}{\alpha}\right)^2 \tag{45}$$

while the basic approximation $\Sigma_s'(u')\,\phi(u') \simeq \Sigma_s'(u)\,\phi(u)$ in the integral for the first moment of the source expresses it in the form $\bar{\mu}_c \Sigma_s' \phi$, where $\bar{\mu}_c = \frac{2}{3A}$. The quantities $\bar{\mu}_c$, ξ and λ are in fact scattering cross section weighted averages over all nuclides except hydrogen.

In summary, the MUFT code writes S_0 and S_1 in Eq. (43) in the form

$$S_0 = \Sigma_s \phi - \frac{d\eta}{du} - \frac{dq}{du} + \omega + \chi \quad , \quad S_1 = \bar{\mu}_c \Sigma_s \phi - \frac{2}{3}\frac{d\rho}{du} \tag{46}$$

with the auxilliary equations Eq. (44) and (45) for η, q and ρ. For the inelastic scattering source ω a group to group matrix is used, as in the GAM code, (see below). It includes the n→2n reaction with a weight factor 2, the inelastic scattering (with unit weight) being subracted from the absorption cross section to preserve neutron balance. The quantity χ in Eq. (46) is the fission spectrum.

Integration of the first two equations of Eq. (43) over a fine energy group of width Δ in the multigroup structure leads to the possibility of representing the resonance absorption rate in terms of the neutron slowing down density by elastic scattering at the high energy group boundary $\eta_0 + q_0$, for hydrogen and the other nuclides in the homogenised mixture, multiplied by the resonance absorption fraction α_r

$$\varepsilon B J \Delta + (\Sigma_a + \Sigma_{in})\phi\Delta + (\eta_0 + q_0)\alpha_r = \eta_0 - \eta + q_0 - q + \omega\Delta + \chi\Delta \quad , \quad -\frac{1}{3} B \phi\Delta + (\gamma\Sigma_t - \bar{\mu}_0\Sigma_s)\bar{J}\Delta = \frac{2}{3}(\rho_0 - \rho) \tag{47}$$

Here ϕ and $\bar{J}$, as well as the cross sections, are group averages, and η, q, ρ refer to the low energy group boundary. The group equations are completed by integrating the three auxilliary differential equations, Eqs. (44) and (45), also over the group width Δ. Together with Eq. (47) the five group equations may then be solved very readily in any group to yield ϕ, J, η, q, ρ given η_0, q_0, ρ_0 at the top of the group. In the highest energy group, in which the calculation starts, η_0, q_0, ρ_0 are clearly zero. Also $\omega\Delta$, the inelastic scattering source into any group, is clearly dependent only on the inelastic scattering cross section group to group matrix and the group fluxes in the groups at higher energies, which have been calculated previously; in the highest energy group $\omega\Delta = 0$.

A further approximation should be noted in the MUFT treatment for the number of neutrons absorbed by resonance absorption $\alpha_r(\eta_0 + q_0)$. The quantity α_r is calculated in the absence of leakage. Its use together with the elastic scattering source into the group neglects the effect of leakage on the group resonance absorption rate. In addition, this rate usually refers to simplified resonance cross sections such as those given in Eq. (5), or even expressions neglecting the $\sqrt{E_0/E}$ term in $\sigma_a(E)$ in the vicinity of the resonance peak. Part of the resonance cross section must then be included in Σ_a in Eq. (47) and this part is an unbroadened group cross section. The artificial separation of the cross section into a resonance and a smooth contribution is clearly undesirable and may lead to small errors.

On the other hand, the MUFT procedure lends itself to the use of calculated effective resonance integrals which are related to the group absorption fraction α_r through Eq. (22) $\alpha_r = -\Delta Q / a_{cg}$ where a_{cg} neutrons enter group g. Two direct methods for the calculation of $I_{eff,g}$ of the resonance nuclides in the lattice unit cell will be discussed below together with their approximations.

The GAM code[27] does not make use of slowing down densities. It solves the first two moments of the transport equation, Eq. (43) in group form for a set of 68 epithermal energy groups of equal width, 0.25, on the lethargy scale. These equations are

$$\varepsilon B J + \Sigma_t \phi = \chi + \sum_{g' \le g} (\Sigma_{in} + \Sigma_s + 2\Sigma_{n,2n})_{g' \to g}\phi \quad , \quad \Sigma_t = \Sigma_a + \Sigma_{in} + \Sigma_s + \Sigma_{n,2n}$$
$$-\frac{1}{3} B \phi + \gamma \Sigma_t J = \sum_{g' \le g} (\Sigma_{s,1})_{g' \to g} J \tag{48}$$

where all quantities without subscripts belong to group g. Here group to group matrices are used for inelastic, and elastic scattering (zero and first moment), as well as the n, 2n reaction, so that this procedure is a consistent P-1 or B-1 method to determine the epithermal neutron spectrum. The solution of Eqs. (48) proceeds along similar lines as in the MUFT code.

The GAM method includes the shielded resonance cross sections in Σ_a, and is therefore well suited for the use of shielded cross section tabulations and

equivalence relations as discussed earlier. Disadvantage factors have to be used for the fuel in order to homogenise the unit cell.

Even in the MUFT code there is some need for a calculation of disadvantage factors, not withstanding the fact that the group absorption fraction α_r is calculated for the entire unit cell. The flux ratios are used to homogenise the group cross sections in the various regions of the unit cell.

Two alternatives for handling the spatial flux dependence in the resonance energy region can be applied. The first is a two region treatment of the unit cell[30], in which $V_c = V_c' + V_f'$ and the volume V_0 refers to the fuel. The two region equations for the flux at energy E, Eq. (50), are

$$V_0 \Sigma_0(E)\,\phi_0(E) = P_0(E)\,V_0\,S_0(E) + [1 - P_0(E)]\,V_1\,S_1(E)$$
$$V_1 \Sigma_1(E)\,\phi_1(E) = [1 - P_0(E)]\,V_0\,S_0(E) + P_1(E)\,V_1\,S_1(E)$$
[$S_0(E)$, $S_1(E)$ are here zero moment sources in regions 0, 1] (49)

where $P_0(E)$ and $P_1(E)$ are the collision probabilities in the fuel and non fuel regions, and $S_0(E)$ and $S_1(E)$ the slowing down sources by elastic scattering per unit volume ($S_{s0}(E)$ of Eq. (34)) is $V_0 S_0(E)$, and similarly in the region outside the fuel). Using the reciprocity relation of Eq. (35) and the intermediate resonance approximation Eqs. (30) and (33) the disadvantage factor at energy E in the resonance becomes

$$D(E) = \frac{\phi_0(E)\,(V_0 + V_1)}{V_0\,\phi_0(E) + V_1\,\phi_1(E)} = \frac{1}{1 + \frac{V_1}{V_1 + V_0}\left(1 - \frac{\Sigma_c}{\Sigma_1}\right)\frac{\Sigma_a(E)}{\Sigma_B}}\,, \quad \Sigma_B = \Sigma_c + \sum_i' \lambda_i \Sigma_{si} \tag{50}$$

where Σ_c is given by Eq. (38), Σ_1 is the scattering cross section outside the fuel region, the summation in Σ_{i3} includes all nuclides in the fuel (potential scattering only), and resonance scattering is ignored. An approximate group disadvantage factor D is given by Eq. (50) with $\Sigma_a(E)$ replaced by the group average $\bar{\Sigma}_a$, and may be applied in the GAM code[30].

In the version of the MUFT code contained in the HAMMER multigroup analysis[31] at epithermal energies, an integral transport treatment is applied to homogenise the unit cell. It is given by

$$(\Sigma_{tr}\phi)_n = \sum_{n'}' T_{nn'}\,(P\phi + S)_{n'}\,, \quad \Sigma_{tr} = \Sigma_t - \bar{\mu}_c \Sigma_s \tag{51}$$

where ϕ_n is the group flux in subregion n of the unit cell, $P_{n'}$ the in-group scattering source and $S_{n'}$ the source into the group from higher energy groups. $T_{nn'}$ is the transfer matrix element from region n' to n, which will be discussed further in connection with the resonance treatment in the HAMMER[31] and ZUMA[2] codes. Approximate forms of $P_{n'}$ and $S_{n'}$ may be derived in a manner consistent with the MUFT slowing down procedure for the homogenised unit cell. The group integrated forms of Eqs. (44) and (45)

$$\eta = \eta_0\,\frac{1 - \frac{\Delta}{2}}{1 + \frac{\Delta}{2}} + \frac{\Sigma_s''\,\phi\,\Delta}{1 + \frac{\Delta}{2}}\,, \quad q = q_0\,\frac{\lambda - \frac{\Delta}{2}}{\lambda + \frac{\Delta}{2}} + \frac{\xi\Sigma_s'\,\phi\,\Delta}{\lambda + \frac{\Delta}{2}} \tag{52}$$

for group width Δ, and with η_0, q_0 referring to the upper group boundary and η, q to the boundary at the low energy of the group, may be combined with a simplified version of Eq. (47) in the resonance region (below the fission spectrum and the inelastic scattering region, and without leakage).

$$\Sigma_a\,\phi\,\Delta + (\eta_0 + q_0)\,\alpha_r = \eta_0 - \eta + q_0 - q \tag{53}$$

where α_r is the group resonance absorption fraction. The combined form of Eqs. (52) and (53) is

$$\Sigma_{tr}\,\phi = P\phi + S\,, \quad P = (1 - \bar{\mu}_c)\Sigma_s - \frac{\Sigma_s''}{1 + \frac{\Delta}{2}} - \frac{\xi\Sigma_s'}{\lambda + \frac{\Delta}{2}}\,, \quad S = \frac{\eta_0}{1 + \frac{\Delta}{2}} + \frac{q_0}{\lambda + \frac{\Delta}{2}} - \frac{(\eta_0 + q_0)\alpha_r}{\Delta} \tag{54}$$

Thus in analogy with the homogneised cell values, $P_{n'}$ and $S_{n'}$ may be defined by the quantities given in Eq. (54) applied to subregion n' of the unit cell. This approximate treatment requires two iterations if resonance absorption fractions are to be determined from simple calculations of effective resonance integrals. In

the first, α_r is determined from Eq. (22) with $G_u = \sum_n' (\eta_o + q_-)_n V_n$ referring to the entire unit cell at the upper group boundary and $\Phi_u = \sum_n' \phi_n V_n$ summed over the fuel region only for subregion fluxes ϕ_n determined in the absence of resonance scattering. The resulting resonance absorption fraction α_r is then introduced into Eq. (54) in the second iteration to determine the ϕ_n in the presence of resonance absorption by solving Eq. (51) (In Eq. (54) the resonance absorption should be limited to the fuel subregions only by using an increased $\alpha_r' = \alpha_r V_c/V_o$ in them with V_c the cell volume and V_o the fuel volume. Outside the fuel region $\alpha_r' = 0$).

Apart from the problems enocuntered in calculating effective resonance integrals approximately, or using shielded cross section tabulations together with equivalence theorems, Bell and Dancoff factors and intermediate resonance parameters, it is seen that there are further approximations in the spatial treatment which must be made before a consistent P-1 or B-1 epithermal spectrum analysis can be made for the homogenised unit cell.

The (m,r,α) Method for the Calculation of Effective Resonance Integrals

A very simple approximate method for calculating effective resonance integrals is based on storing for each resolved resonance three parameters which are needed to obtain the result very rapidly. These parameters are:

$$m = \sigma_o \Gamma_u / E_o \quad , \quad r = \sigma_c \Gamma_u / \Gamma \quad , \quad \alpha = \Gamma_f / \Gamma \qquad (55)$$

where $\sigma_c = 4\pi \lambda_o^2 g_J \Gamma_n / \Gamma$, $\lambda_o^2 = \hbar^2/(2mE_o)$, see Eq. (5) These parameters can be used to define a shielding factor $\beta = \Sigma_s'/(N_i r)$ for the resonance absorber of atom density N_i , where Σ_s' is given by Eq. (33) for a heterogeneous system, and $N_i r$ is the peak absorption cross section. Applying the infinite mass approximation, Eq. (29) and the Breit Wigner single level formula $\sigma_u(E) = r/(1+x^2)$ near the resonance peak (with $\sqrt{E_o/E} \approx 1$)

$$I_{eff} = \int \sigma_u(u) \frac{\Sigma_s'}{\Sigma_s' + N_i \sigma_u(u)} du \simeq \frac{\sigma_c \Gamma_u}{\Gamma} \int_{-\infty}^{\infty} \frac{1}{(1+x^2) + \frac{1}{\beta}} \cdot \frac{\Gamma}{2E_o} dx = \frac{m\pi}{2\sqrt{1+\frac{1}{\beta}}} \qquad (56)$$

for the particular resonance of nuclide i at zero temperature.

The I_{eff} values for all resonances whose peaks lie in the group under consideration are calculated by Eq. (56) ignoring Doppler broadening and combined as in Eq. (22) to derive the group resonance absorption fraction α_r , when this simple resonance treatment is applied in the MUFT code. Corrections to the Breit Wigner formula, the effects of resonances not treated explicitly, and the tail of the thermal abosrption cross section, which accounts for the $\sqrt{E_o/E}$ dependence of $\sigma_u(E)$, have to be treated as part of the group smooth Σ_{a} value in Eq. (47) and may lead to errors in addition to those which are due to the neglect of Doppler broadening and resonance scattering.

L-Factors for Correlation of Calculated Effective Resonance Integrals with Experimental Data

The numerous approximations in the above procedure for the calculation of I_{eff} for individual resonances have been corrected in certain versions of the MUFT program, for example, the one contained in the LEOPARD code[32], by correlations with Hellstrand's integral experiments. These experiments determined the ratio of epithermal to thermal absorptions in fertile materials for rods of different sizes. Strawbridge and Barry[33] expressed the I_{eff}^{total} values for ^{238}U in UO_2 rods obtained from the Hellstrand experiments in the form

$$I_{eff}^{total} = \alpha + \beta x + (\gamma + \delta x)\sqrt{T} \quad , \quad x = \left[\frac{\Sigma_s}{N}(1-P_o) + \frac{1-C}{N_o \ell_o} \right]^{1/2} \qquad (57)$$

where I_{eff}^{total} refers to the entire epithermal energy range, Σ_s/N is the cross section of the fuel rod per atom of ^{238}U in the absence of resonances, and $(1-P_o)$ the single flight escape probability from the rod of cross section Σ_s , while the last term in the expression for x is Σ_e/N of Eq. (37) and expresses the lattice effect. The Dancoff factor C , is given by Eq. (39). Applying this quantity in Eq. (22) the overall epithermal non-capture probability is

$$P = \exp\left[- \frac{N I_{eff}^{total} V_o}{\xi \Sigma_s V_c} \right] \qquad (58)$$

and $\omega = (1-P)/P$ is the ratio of epithermal to thermal captures.

On the other hand, the MUFT treatment given previously can be used to calculate the epithermal captures in ^{238}U and the number of neutrons slowing down to thermal energies, when absorptions by all nuclides other than ^{238}U as well as leakage are ignored (the latter in accordance with the expression for I_{eff}^{total}, Eq. (57) which refers to zero buckling). Comparison of the calculated value by the MUFT code and the ω obtained in accordance with the Hellstrand experiments, makes it possible to determine iteratively an L correction factor by which all calculated resonance integrals for the individual ^{238}U resonances must be multiplied to obtain agreement between the two.

In this way the very simple formulation for calculating shielded resonance integrals for individual resonances may be correlated with integral experiments. The L factor regards those integral experiments as the most reliable source of information, rather than the basic nuclear data libraries. It can only be used for the few (fertile) nuclides for which such experimental data are availabe. The current trend is to attempt to obtain the best evaluated basic nuclear data files which can be influenced only partly by the results of integral experiments.

The Nordheim Integral Transport Treatment for Resolved Resonances

A more satisfactory procedure for calculating I_{eff} values for individual resonances is the Nordheim Integral Transport (NIT) treatment which is incorporated in the HAMMER[31] version of the MUFT code.

Basically the NIT treatment calculates the shielding function $f(u) = E\psi(u)/\Sigma_c(u)$ of Eq. (26) for a two region system consisting of a fuel region, denoted by subscript c, and an outer non fuel region which may be subdivided into a number of subregions n'. The shielding function is calculated for the central part of a resolved resonance of a fuel isotope as though this resonance is completely isolated. Neutrons collide in the fuel at energies near the resonance peak after elastic scattering by fuel nuclides, provided they have not escaped from the fuel, and after elastic scattering by nuclides outside the fuel region, provided they are transferred in a single flight to the fuel region. The extension of Eq. (49) to this subdivision of the lattice unit cell may be written in the form

$$V_c \psi(u) = V_c P_c(u) \sum_i T_i \psi + \sum_{n'} \frac{\Sigma_{n'} V_{n'}}{E} P_{cn'}(u) d_{n'} \qquad (59)$$

where the collision density per unit energy $\psi(u)$ has been expressed as a function of lethargy, so that the integral operators T_i are again given by Eq. (24) The $P_{cn'}(u)$ are single flight transfer probabilities of neutrons which have reached lethargy u by elastic scattering in subregion n' to the fuel region c where they make their next collision. In all the non fuel regions n' the Narrow Resonance approximation leads to the slowing down source $\Sigma_{n'}/E$ per unit volume (per unit asymptotic flux). The advantage factors $d_{n'}$ are the ratios of the asymptotic fluxes in regions n' to that in the fuel region.

In the NIT treatment exact expressions are used for the fuel collision probability $P_c(u)$, i.e., the rational approximation is avoided. No approximation is made in relating $P_{cn'}(u)$ to $P_{n'c}(u)$. In accordance with Eq. (40)

$$\Sigma_{n'} V_{n'} P_{cn'}(u) = \Sigma_c(u) V_c P_{n'c}(u) \qquad (60)$$

which after substitution into Eq. (59) leads to the following integral equation for $\psi(u)$, and consequently to the central contribution to the resonance integral $I_{eff,c}$ calculated over the lethargy region c near the resonance peak for which the integral equation is solved:

$$\psi(u) = P_c(u) \sum_i T_i \psi + [1 - P_c'(u)] \frac{\Sigma_c(u)}{E}, \quad 1 - P_c'(u) = \sum_{n'} P_{n'c} d_{n'}$$

$$I_{eff,c} = \int_c \sigma_a(u) f(u) du, \quad f(u) = E\psi(u)/\Sigma_c(u) \qquad (61)$$

In the asymptotic region, at lethargies below those in region c, all cross sections have their background values; in lethargy region c only the particular resonance of the nuclide, for which the effective resonance integral is to be calculated, is taken into consideration. When the asymptotic flux is flat $[1 - P_c'(u)]$ becomes $[1 - P_0(u)]$, i.e., the usual fuel escape probability.

The solution of the integral equation and the calculation of $I_{eff,c}$ in Eq. (61) proceeds on the following lines:

a) Tables of values are prepared for P_0 and $1 - P_0'$ as functions of $\Sigma_s R_0$ which is the fuel rod radius in mean free paths; the tables refer to arguments from 0 to 20.0 in 1000 equal steps. The actual probabilities $P_0(u)$ and $1 - P_0'(u)$ can then be obtained by interpolation (a four point difference technique is used), or by extrapolation for large arguments, when $\Sigma_s(u) R_0$ has been calculated. Further details of the preparation of the probability tables will be given in connection with the OZMA code. Clearly when the asymptotic flux is flat only the P_0 table needs to be prepared. It is calculated from the formulae for the isolated lump escape probabilites, and the Dancoff factor C, Eq. (39), by

$$1 - P_0 = \frac{[1 - \beta_0]\,(1 - C)}{1 - C\,[1 - \Sigma_0 \ell_0 (1 - \beta_0)]}, \qquad \ell_0 = \frac{4V}{S} = 2R_0 \tag{62}$$

This is the relation between the fuel escape probability in the lattice and the value for the isolated lump, when the rational approximation holds, Eq. (37). However in Eq. (62) this approximation is only used to obtain the connection of $(1 - P_0)$ for the lattice, and $(1 - \beta_0)$ for the isolated lump. For the latter the correct value,[19] is used in the construction of the probability tables.

b) The central portion of the resonance is determined for the resonance absorber in terms of the practical width of the resonance on the lethargy scale $\Gamma(\bar{\sigma}_0/\bar{\sigma}_p)^{1/4}/\xi_0$ or the Doppler width Δ/ξ_0 of Eq. (8). In fact, the larger of five times the former or twenty times the latter is chosen, the resonance peak lethargy being in the center. This lethargy range is divided into intervals of width $\varepsilon \approx \frac{2\Delta}{7\xi_0}$ where $\xi = \sqrt{\frac{\Delta}{4A}}$ for application in Eq. (61), ensuring an adequate number of mesh points for the Doppler broadened resonance shape. By slight adjustment of the ratio of the mass of the resonance absorber to the neutron mass A, the lethargy integration interval in Eq. (24) is made to contain an even number of mesh intervals ε. The same is attained for the nuclides mixed with the resonance absorber in the fuel by a slight adjustment of their mass.

Initial values (back values) of Σ_{sc}/ξ are stored for each fuel nuclide at the lethargy mesh points below the central region c of the resonance under consideration, Σ_{sc} including potential scattering only. This makes a Simpson integration for $\bar{\gamma}_i \psi$ possible for the first mesh point in c for all nuclides i, so that $\psi(u)$ is immediately obtained from Eq. (61) for this lethargy. $\Sigma_{sc}(u)\psi(u)/\Sigma_0(u)$ is then added to the back value table for each nuclide i in the fuel, so that the procedure can be repeated for the next and succeeding lethargy mesh points in c. These Simpson integrations can be carried out very efficiently, since in c the lethargy mesh has constant intervals.

The calculation of $I_{eff,c}$ by Eq. (61) is accomplished readily by numerical (trapezium) integration using the same integration mesh. In the Nordheim procedure the cross sections for the isolated resonance under consideration are obtained from Eq. (5) with the Doppler broadened line shape functions of Eqs. (10) and (11) and including the $\sqrt{\xi_0/\xi}$ term of Eq. (5) in the absorption cross section.

c) Wing corrections are added to $I_{eff,c}$ of the isolated resonance to account for the following three contributions:

i) The high energy region beyond the upper limit of the central part c of the resonance.

ii) The low energy region outside c and down to the thermal cut off ξ_{th}.

iii) A negative term to remove the $1/v$ tail which this resonance contributes to the 2200 m/sec cross section. To this end the absorption cross section at ξ_{th} is calculated from Eq. (5)

for the resonance under consideration, and assuming a $1/\sqrt{E}$ energy dependence, the epithermal (negative) contribution to I_{eff} is determined.

All three wing corrections are determined for unbroadened Breit Wigner single level cross sections, Eq. (5) in a $1/E$ flux. The neglect of Doppler broadening is justified by the width of the central region c of the resonance, which ensures asymptotic unbroadened cross sections outside it with good accuracy. The third correction is needed since the tail of the $1/v$ thermal absorption cross section is included in the smooth epithermal group cross section library. The three corrections together are given by

$$\left(\frac{1-3\chi_1}{\chi_1 y_1} - \frac{3}{2}\ln\frac{y_1+1}{y_1-1}\right)\frac{\sigma_c\Gamma\Gamma_a}{4E_c^2} + \left(\frac{1-3\chi_2}{\chi_2 y_2} - \frac{1-3\chi_c}{\chi_c y_c} + \frac{3}{2}\ln\left\{\frac{1+y_2}{1-y_2}\frac{1-y_c}{1+y_c}\right\}\right)\frac{\sigma_c\Gamma\Gamma_a}{4E_c^2}$$

$$- 2\left(\frac{E_c}{E_c}\right)^{3/2}\frac{\sigma_c\Gamma\Gamma_a}{4(E_c-E_{th})^2}$$

$$\chi_1 = \frac{E_c'-E_c}{E_c}, \quad \chi_2 = \frac{E_c-E_c''}{E_c}, \quad \text{central part of resonance in } (E_c'', E_c')$$

$$y_1 = \sqrt{1+\chi_1}, \quad y_2 = \sqrt{1-\chi_2}, \quad \chi_c = \frac{E_c-E_c}{E_c}, \quad y_c = \sqrt{1-\chi_c}, \quad E_c = \text{thermal cut-off energy} \tag{63}$$

They are added to $I_{eff,c}$.

It is clear that the NIT method avoids many of the approximations in the (m,t,α) individual resonance treatment, and in particular the use of equivalence principles between heterogeneous and homogeneous systems, and the use of the rational approximation for fuel escape probabilities. Doppler broadening of the cross sections is taken into account. On the other hand, isolated resonance treatments assume full flux recovery to the asymptotic shapes between the resonances, and all interference effects between resonances belonging to different fuel nuclides are ignored.

The Nordheim Method in the Unresolved Resonance Region

In the unresolved resonance region the Narrow Resonance approximation is generally valid since the widths of the resonances are small compared with the maximum slowing down interval in a single elastic collision, $\ln(1/\alpha)$, even for the heaviest nuclides. Using Eq. (28) for the shielding function, with $\Sigma_0 = \Sigma_s + \Sigma_c$ where Σ_s is the fuel scattering cross section, without resonances, and Σ_c the geometric cross section of Eq. (37) the effective resonance integral for one of the multigroups may be expressed in the form

$$I_{eff} = \int I(E)\frac{dE}{E}, \quad I(E) = \frac{\Sigma_0\Gamma_a}{N_0 D E}\left\langle\int_0^\infty \frac{\psi}{\beta+\psi}dx\right\rangle, \quad \beta = \frac{\Sigma_0}{N_0\xi}, \quad \sigma_0 = 4\pi\lambda^2\frac{\Gamma_a}{\Gamma}g_J \tag{64}$$

where interference between resonance and potential scattering has been ignored; N_0 is the atom density of the resonance absorber. The quantity dc/D which occurs in $T(c)dc$ is the expected number of resonances in interval dc for mean spacing D of the resonances; the expectation value refers to the Porter Thomas distribution of neutron widths. The integration over all values of x implies that the complete resonance integral of each individual resonance is included. In fact, Eq. (64) is analogous to Eq. (56) for resolved resonances, but is based on the NR instead of the IM approximation, and includes all resonances in a group.

There are special techniques for calculating

$$J(\xi,\beta) = \int_0^\infty \frac{\psi(\xi,x)}{\beta+\psi(\xi,x)}dx, \quad \xi = \frac{\Gamma}{\Delta} = \left(\frac{A\Gamma^2}{4\Gamma kT}\right)^{1/2} \tag{65}$$

and these can be utilised for the numerical integration of

$$\left\langle\int_0^\infty \frac{\psi}{\beta+\psi}dx\right\rangle = \int_0^\infty \frac{e^{-\frac{w^2}{4}}}{\sqrt{2\pi w}}J(\xi,\beta)dw, \quad \xi = \frac{\Gamma_a+\bar{\Gamma}_n(E)w}{\Delta} \tag{66}$$

where Γ_a, $\bar{\Gamma}_n$, D are the average resonance parameters specified in the basic data library at energy E. In the HAMMER code[31] shielded resonance integrals are calculated by the above expressions for the unresolved resonance sequences of the fertile nuclides. Special care is needed in the group integration in Eq. (64) for unresolved p-wave resonance sequences, since the energy dependence of the average neutron width is that of the penetration factor ratio P_1/P_0, i.e., $E/(E+E_1)$ where E_1 is approximately 2.5 x 10^5 keV; in the keV region

this energy dependence is roughly like E itself. The additional energy dependence of $\Gamma_n(E)$ on $\sqrt{E}$ for both s-wave and p-wave neutrons (the reduced neutron width being approximately independent of energy) is compensated for by the $\sqrt{E}$ dependence of Δ in Eq. (66)

In general, the unresolved resonance integrals have shielding factors I_{eff}/I_{∞} between about 0.9 and 1.0 for thermal reactor lattices so that the rather approximate nature of the above shielding treatment produces only minor errors.

The Use of Tabulated Effective Resonance Integrals. The WIMS Method.

The WIMS code[28] makes use of tabulated effective resonance integrals for individual resonance isotopes homogeneously mixed with pure hydrogen as moderator. The tabulations were obtained with the SDR code[34] which solves the moderation problem for such homogeneous mixtures on a very fine energy mesh in the 13 energy groups between 9.118 keV and 4.0 eV, the latter being the cut off of the 42 thermal groups. The thermal groups are fine enough to deal adequately with the low lying resonances of the ^{235}U and the Plutonium isotopes.

For the calculation of resonance absorption in mixtures intermediate resonance λ factors are used, which are group independent quantities ranging from 1.0 for light nuclides, 0.94 for Oxygen to 0.2 for heavy nuclides. A constant Bell factor $\alpha = 1.16$ is employed for the Bell modification[54] of the Wigner rational approximation.

The equivalence principles relating heterogeneous to homogeneous systems are formulated rather differently than in the treatment given previously. In particular, the Dancoff factor, representing the lattice effect, is not used directly, although it can be identified in terms of quantities used in the WIMS procedure.

Instead of using a Dancoff factor, the WIMS code relates the fuel collision probability in a lattice P_0, in which collisions in neighbouring fuel lumps are also allowed for, to the collision probability in an isolated lump, p_0, through:

$$P_0 = p_0 + \frac{p_{sc}\, p_{0s}}{1 - p_{ss}} \qquad (67)$$

which is applied below to a cylindrical unit cell. (It can also be applied in the case of slab geometry). Here p_{s0} is the fuel to boundary escape probability and p_{0s} the probability that a neutron entering the outer boundary of the unit cell of area S_c (from a uniform distribution outside it) will make its next collision in the fuel, while p_{ss} is the probability that the neutron entering the unit cell in this way will reach the outer surface again without collision. Clearly $1 - p_{0s} = p_{1s} + p_{0s}$ which are the probabilities of collision in outer region (1) and inner region (o) in a two region unit cell. The latter probabilities satisfy surface reciprocity theorems of the type:

$$\frac{S_c}{4}\, p_{0s} = \Sigma_0 V_0\, p_{s0} \qquad (68)$$

which is the analogy of Eq. (40) and refers to collision rates in unit flux $\Sigma_0 V_0$ on the right side of the equation, and the transfer rate across the outer cell surface of area S_c, i.e. $\frac{S_c}{4}$, on the left side. Thus,

$$1 - p_{ss} = p_{1s} + p_{0s} = \frac{4\Sigma_1 V_1}{S_c} p_{s1} + \frac{4\Sigma_0 V_0}{S_c} p_{sc} = \frac{4\Sigma_1 V_1}{S_c}(1 - p_1 - p_{01}) + \frac{4\Sigma_0 V_0}{S_c}(1 - p_{00} - p_{10}) \qquad (69)$$

where p_{0i} is the probability that a neutron born in the outer region makes its next collision in the inner region and vice versa. The probabilities p_{s0}, p_{10} and p_{01} appearing in Eqs. (68) and (69) may be expressed in terms of G_1 which is the probability that a neutron entering the outer region from within will collide there:

$$p_{s0} = (1 - p_0)(1 - G_1), \quad p_{10} = (1 - p_0) G_1, \quad p_{01} = \frac{\Sigma_0 V_0}{\Sigma_1 V_1} p_{10} \qquad (70)$$

Finally, the collision probability p_1 in the outer region may be expressed in the form

$$p_1 = p_1' - p_{01} G_1 \qquad (71)$$

where p_1' is the collision probability in the outer region if the inner region is void. From this, the number of neutrons p_{01} is subracted in Eq. (71) and

since these neutrons would have reentered the outer region if the inner region were void, p_o must be multiplied by G_1 in order to collide in the outer region. Combining Eqs. (68) through (71)

$$P_o = p_o + \frac{V_o\Sigma_c(1-p_o)^2 C_1}{V_o\Sigma_c(1-p_o)C_1 + B_1} \quad , \quad C_1 = (1-G_1)^2 \quad , \quad B_1 = 1-p_1 \tag{72}$$

The quantities G_1 and p_1 which relate to the non fuel region can be obtained with good accuracy by methods developed by Bonalumi[36] and Jonsson[37], and account for the lattice effect as may be seen by writing Eq. (72) in the form

$$1-P_o = \frac{1-p_o}{1+V_o\Sigma_c(1-p_o)\frac{C_1}{B_1}} = \frac{1-p_o}{1+V_o\Sigma_c\left(\frac{a}{a+\Sigma_o\ell_o}\right)\frac{C_1}{B_1}} \tag{73}$$

Here in the correction term in the denominator $(1-p_o)$ has been replaced by the Bell modification of the rational approximation $\Sigma_o/(\Sigma_o+\Sigma_e)$ where $\Sigma_e = a/\ell_o$ for an isolated fuel lump. In terms of the Dancoff factor τ_1 the lattice effect is given by $\Sigma_e = a(1-\tau_1)/\ell_o$, Eq. (38) so that:

$$1-P_o = \frac{1}{1+\frac{\Sigma_o\ell_o}{a(1-\tau_1)}} \quad , \quad 1-p_o = \frac{1}{1+\frac{\Sigma_o\ell_o}{a}} \quad , \quad 1-P_o = \frac{1-p_o}{1+\frac{4}{S}\frac{\Sigma_oV_o}{(a+\Sigma_o\ell_o)}\frac{\tau_1}{(1-\tau_1)}} \tag{74}$$

Comparison with Eq. (73) yields

$$1-\tau_1 = \frac{4B_1}{aSC_1+4B_1} \tag{75}$$

Since in the preparation of the group I_{eff} tables pure Hydrogen was used as the moderator, the background cross section of the resonance absorber multiplied by its λ value should be included in the background cross section used to determine the effective resonance integral from the tabulation. Thus

$$I_{eff} = I_{eff}(\sigma_{ro}+\sigma_e) = \frac{1}{N_i}\sum_j \lambda_j N_j \sigma_{pj} \quad , \quad \sigma_e = \frac{a(1-\tau_1)}{N_i\ell_o} = \frac{\frac{4aB_1}{aSC_1+4B_1}}{N_i\ell_o}$$

$$\ell_o = \frac{4V_o}{S} \tag{76}$$

where S is the surface area of the fuel lump, N_i the atom density of the resonance absorber and $(1-\tau_1)$ is given by Eq. (75)

The above treatment has been extended to a subdivision of the non fuel region into more than one subregion which results in a superposition of two of the tabulated I_{eff} values for different arguments and with different weights[28]. It has also been extended to clusters of rods with approximate differences in the results for the inner and outer rings of rods, and bundles of plates by Leslie and Jonsson[38].

The LATREP Method

In the LATREP code[29] the use of tabulated effective resonance integrals is specially adapted to clusters of fuel rods, as in the case of CANDU reactors. A good fit to the measured effective resonance integrals is obtained by

$$I_{eff} = A + B\sqrt{\frac{S}{M}} \tag{77}$$

where M is the mass of the fuel lumps and S their effective surface area. The constants A and B have been obtained from single rod experiments and calculations.

The square root makes it difficult to calculate I_{eff} values in each ring of rods in the cluster separately. However a linear relation

$$\bar{I}_{eff} = A'\frac{\bar{\Phi}}{\phi_a} + B'\frac{S}{M} \tag{78}$$

is better suited for this purpose. $\bar{\phi}$ and ϕ_a are the average flux in the rod and the flux at its surface. Eq. (78) may be regarded as a cluster average of

$$I_{eff,i} = A'\frac{\phi_i}{\phi_a} + B'\frac{S_i}{M_i} = A'\frac{\bar{\phi}}{\phi_a} + B'\frac{S_i}{M_i} \tag{79}$$

for the i th ring of fuel rods, where S_i and M_i refer to all rods in the ring (together), and ϕ_i / ϕ_{i1} is assumed to be constant throughout the cluster. The average $\overline{I}_{eff} = (\sum_i M_i I_{eff,i})/M$, and $S = \sum_i M_i$. Equating $\overline{I}_{eff}$, Eq. (78), with I_{eff}, Eq. (77) the value of $I_{eff,i}$ of Eq. (79) becomes

$$I_{eff,i} = A + B\sqrt{\frac{S}{M}} - B'\frac{S}{M} + B'\frac{S_i}{M_i} \qquad (80)$$

To determine the effective surface areas of the rods in the clusters for use in Eq. (80), the total surface area S_t of all N rods is divided into an outer rubber band surface area S_R, stretched around the N_n rods in outer ring n, and an inner surface area $S_{inner} = S_t - S_R$. With d_n as the distance between centers of neighbouring rods in outer ring

$$S_R = N_n d_n + 2\pi r \qquad (81)$$

The basic approximation[39] is to regard S_R as being unaffected by interaction effects between neighbouring rods (the different clusters being very far apart), and that S_{inner} is diminished by an internal Dancoff correction calculated effectively for slab geometry

$$\gamma = \left[1 - 2E_3(\alpha d \Sigma_c)\right] \qquad (82)$$

Here Σ_c is the coolant cross section, α is a factor similar to the intermediate resonance parameter λ, and d the effective slab thickness or half the mean chord length $4V_c/S_f$; V_c is the volume of coolant in a polygon formed by joining the centers of the rods in the outer fuel ring and S_f is the surface area of the fuel within this polygon. This leads to

$$S = S_R + \gamma S_{inner} \qquad (83)$$

In order to differentiate between the fuel rods in the different rings, the second term in Eq. (83) is multiplied by a factor β for the rods in the outermost ring, given by

$$\beta = \left(\frac{N_n}{2} - 1\right) \Big/ \left[N - \left(\frac{N_n}{2} - 1\right)\right] \qquad (84)$$

since S_{inner} refers to all N rods, and the inward facing surface of the rods in the outer ring contribute only an area $\left(\frac{N_n}{2} - 1\right)2\pi r$ to S_{inner}.

Such Dancoff factor corrections have been developed further[29] for rings of fuel rods in the cluster inside the outermost by dividing their rod surface areas into outer parts and inner parts with respect to polygons of the centers of the rods in each ring. Similarly the coolant volume between the different rings refers to the coolant between these polygons. With these volumes and surface areas, slab type Dancoff factors can be formulated as above for the outer and inner parts of the fuel rod surfaces in the inner rings. To the inner part the β factor of Eq. (84) is also applied.

Finally streaming corrections are applied to account for the fact that the rubber band S_R should be diminished for the neutron fraction which streams inwards between the rods. The correction factor is calculated for a cosine distribution of neutrons incident on the surface of the cluster, and also allows approximately for the scattering properties of the coolant. Similar streaming corrections are applied to the inner rings of rods, decreasing the outer parts of their surface areas (outside the polygon of the rod centers) somewhat and increasing the inner parts.

The LATREP code calculates absorption fractions from an expression similar to Eq. (22) in which the exponent for a single resonance absorber of atom density N_i and total fuel volume V_i is given by

$$I_{eff,i} = \frac{N_i V_i \phi_i'}{\overline{\Sigma_s}\, V_{cell}\, \phi_{cell}} \qquad (85)$$

where ϕ_i' / ϕ_{cell} is the ratio of the flux in the absence of resonances in the region in which the rods are located to the average cell flux under these conditions.

Derivation of Fine Group Cross Sections from Shielded Resonance Integrals

If multigroup codes are used which require group cross sections instead of shielded resonance integrals, and the latter are obtained from tabulations by interpolation procedures and equivalence theorem techniques, a method must be developed to relate the two. This was discussed previously in connection with the preparation of group effective resonance integral tabulations for resonance absorbers mixed with Hydrogen as moderator, and in connection with the WIMS code.

In the description of this code[28] an approximate treatment for the overall flux depression in resonance groups is given for resonances which are distributed fairly uniformly throughout the group. The resulting expression is

$$\sigma_a = \frac{I_{eff}}{\Delta - \dfrac{I_{eff}}{\sigma_{po} + \sigma_G}} \qquad (86)$$

where Δ is the group width and the other quantities are defined in Eq. (76).

Again benchmark tests are needed to examine the general validity of this relation under different circumstances.

Lecture IV

Detailed Reaction Rate Calculations with Full Allowance for all Resonance Interference Effects

The previous discussion of practical methods of handling the resonance absorption problem in thermal reactor lattices, including temperature effects, has demonstrated the need for benchmarking such calculations with more accurate calculations.

At present, preprocessing procedures are available to transform basic point cross section nuclear data libraries with resonance parameters into accurately Doppler broadened files of cross section data which follow the resolved resonances in detail, contain no resonance parameters, and can be used easily with linear interpolation to provide the desired resonance cross sections at any energy to a specified interpolation accuracy criterion. They have been described in connection with the basic data libraries.

The detailed point data libraries can be used in Monte Carlo codes which are useful for certain types of problems. They have also been used in a transport code, OZMA[2], specially written for calculating resonance reaction rates. This code treats the one dimensional unit cell problem with a spatial subdivision specified by the user on a very fine energy mesh by integral transport or discrete ordinate methods.

The Monte Carlo Method and its Limitations

Monte Carlo calculations in the resolved resonance region can be performed when an exact neutron tracking routine is available for the assembly under consideration. Regular reactor lattice unit cells can readily be dealt with, since the tracks of neutrons leaving the unit cell can be continued in the same unit cell by re-entering it, by a shift of the origin of the coordinate system, at a point which corresponds to the point of entry into the neighbouring cell. Such a code is the REPC program[40] which deals with regular hexagonal or square lattices of cylindrical rods, each subdivided into a number of annular regions. The geometry routine has recently been extended so that clusters of fuel rods placed in the coolant contained in a pressure tube can also be handled, the complete unit cell being a square or hexagonal array of such clusters in a moderator.

The cross sections of the REPC code in the resolved resonance region are the pre-processed detailed Doppler broadened resonance profile tabulations which were discussed earlier. Since these tables can be used with linear-linear interpolation, cross sections are readily available at any energy point reached by the neutron during its history.

The REPC program is an updated version of the former REPETITIOUS code[41]. Neutrons are followed between prespecified energies E_{max} and E_{min} in which all collisions are taken to be elastic and isotropic in the center of mass coordinate system. These conditions apply in the resolved resonance region, and also approximately in the unresolved energy region. The isotropic neutron injection routine introduces each neutron into the lattice unit cell with unit weight at the first energy with which it emerges below E_{max} after an elastic collision above this energy, assuming that the cell flux is proportional to $1/E$ for $E > E_{max}$. This collision occurs with a nuclide randomly chosen from the mixture of nuclides contained in the lattice region where the neutron commences its history. The choice is made in accordance with the Σ_s values of the different nuclides in the mixture, while the choice of initial location is uniform within each of the lattice regions and proportional to the overall Σ_s of the regions. In tracking the neutron histories the neutron weight is degraded by the scattering probability Σ_s/Σ_t at each collision, these values referring to the mixture contained in the region in which the collision occurs. Reaction rates for reaction type x are stored by regions and prespecified energy groups from appropriate accumulations of $w\Sigma_x/\Sigma_t$. If E_{max} refers to an energy in the unresolved resonance region, and if the resonance cross section tabulations referred to above are used, resonance reaction rates above the energies where the resonances are resolved are not properly shielded since, as previously discussed, the cross sections in the tabulations are then infinitely dilute averages for the mean resonance parameters specified in basic data libraries and their statistical distributions. However, the procedure can be improved by the use of randomly constructed resonance ladders at these energies, or by the use of probability tables[6].

While Monte Carlo codes of the above type can produce quite accurate overall results for quantities like the resonance escape probabilities between E_{max} and E_{min}, or E_t and E_{min} with E_t as the top of the resolved resonance region, fine group results have much greater statistical errors. Temperature differences of reaction rates are similarly subject to considerable fluctuations. For benchmarking purposes Monte Carlo calculations are therefore of limited value in the resonance energy region, except in as much as broad energy group parameters are required.

The Transport Code OZMA

The OZMA code[2] solves the point energy neutron transport equation by using two alternative approaches. In the first the anisotropic angular flux in the multiregion unit cell is obtained by solving the integro-differential transport equation. A discrete ordinates treatment is applied, which features a new and efficient formulation for the scattering integral, as required to handle resonance profiles. Alternatively, the isotropic flux in the multiregion unit cell is computed by solving the integral transport equation for the collision density using collision probability methods. In both alternatives the flux is the flux per unit energy, but it is expressed as a function of lethargy in order to facilitate the calculation of the slowing down sources. The rationale for this particular formulation is that for elastic scattering from E' to E the cross section is proportional to $1/E'$ when the scattering is isotropic in the center of mass system, which is generally the case in the resolved resonance region. Multiplication by the flux in the interval dE' leads immediately to the lethargy increment du'.

In accordance with these considerations the two basic forms of the neutron transport equation which are solved by the OZMA code are:

a) The Integral Transport mode

$$\phi(\bar{r},u) = \int_V d\bar{r}' \frac{e^{-(\Sigma s)_u}}{4\pi|\bar{r}-\bar{r}'|^2} S(\bar{r}',u) \quad , \quad (\Sigma s)_u = \int_0^{|\bar{r}-\bar{r}'|} ds' \, \Sigma\{\bar{r}'+s'(\bar{r}-\bar{r}'),u\} \tag{87}$$

For a lattice unit cell subdivided into a number of subregions n, in each of which the cross sections and flux are independent of $\bar{r}$, this equation becomes

$$V_n \Sigma_n \phi_n(u) = \sum_{n'} V_{n'} P_{nn'}(u) S_{n'}(u) \tag{88}$$

b) The Integro-Differential mode

$$\bar{\Omega}\cdot\nabla\phi(\bar{r},u,\bar{\Omega}) + \Sigma(\bar{r},u)\phi(\bar{r},u,\bar{\Omega}) = S(\bar{r},u,\bar{\Omega})$$

$$\phi(\bar{r},u) = \int d\bar{\Omega}\,\phi(\bar{r},u,\bar{\Omega}) \quad ; \quad \bar{J}(\bar{r},u) = \int d\bar{\Omega}\,\bar{\Omega}\,\phi(\bar{r},u,\bar{\Omega}) \tag{89}$$

For discrete ordinates $\bar{n}$, $\bar{m}$ in space and direction, which are at the centers of mesh cells with spatial and directional boundaries denoted by n, $n+1$ and m, $m+1$ respectively, this euqation becomes

$$\mu_{\bar{m}}\left[A_{n+1}\phi_{n+1,\bar{m}}(u) - A_n\phi_{n,\bar{m}}(u)\right] +$$

$$\frac{1}{W_{\bar{m}}}\left[\beta_{\bar{n},m+1}\phi_{\bar{n},m+1}(u) - \beta_{\bar{n},m}\phi_{\bar{n},m}(u)\right] + V_{\bar{n}}\Sigma_{\bar{n}}\phi_{\bar{n},\bar{m}}(u) = V_{\bar{n}}S_{\bar{n},\bar{m}}(u)$$

$$\phi_{\bar{n}}(u) = \sum_{\bar{m}}' W_{\bar{m}}\phi_{\bar{n},\bar{m}}(u) \quad , \quad J_{\bar{n}}(u) = \sum_{\bar{m}}' \mu_{\bar{m}} W_{\bar{m}}\phi_{\bar{n},\bar{m}}(u) \tag{90}$$

The spatial subdivision is again made so that the total cross section $\Sigma_{\bar{n}}(u)$ is regionally constant. The A_n's are the surface areas of the "space-direction" mesh cells normal to the spatial boundary coordinates r_n, and the $\beta_{\bar{n},m}$'s are the angular redistributions of the "space-direction" mesh cells at the directional boundaries denoted by the subscript m. The quadrature weights $W_{\bar{m}}$ and the direction cosines $\mu_{\bar{m}}$ refer to the characteristic directions $\bar{m}$.

As stated above the fluxes and sources per unit energy in both modes are expressed as functions of lethargy u. The fluxes must be multiplied by the energy E to convert them to fluxes per unit lethargy which can then be multiplied by any desired cross section and integrated over lethargy to obtain group reaction rates per unit volume.

The sources per unit energy $S_{\bar{n},\bar{m}}(u)$, expressed as functions of lethargy, will be given for the integro differential mode in which scattering anisotropy in the laboratory coordinate system can be taken into account. For the integral transport mode only the isotropic component in the laboratory system in needed, and, as indicated above in Eq. (88), the subregion is denoted merely by n and not by $\bar{n}$.

The zeroth and first moments of the slowing down cross section in the laboratory system from energy E' to unit energy interval near E in a scattering collision with isotope j in subregion $\bar{n}$ are given by

$$\frac{\Sigma^s_{\bar{n},j}(E')}{1-\alpha_j} \text{ and } \frac{\Sigma^s_{\bar{n},j}(E')}{1-\alpha_j}\cdot\frac{1}{2}\left[(A_j+1)\left(\frac{E}{E'}\right)^{1/4} - (A_j-1)\left(\frac{E'}{E}\right)^{1/4}\right]; \quad \alpha_j = \left(\frac{A_j-1}{A_j+1}\right)^2 \tag{91}$$

respectively for elastic scattering, isotropic in the center of mass system. These are multiplied by the flux and current per unit energy at E' in subregion $\bar{n}$, integrated and summed over all nuclides j in subregion $\bar{n}$ to obtain the source $S_{\bar{n},\bar{m}}(u)$ per unit energy at E which corresponds to u:

$$S_{\bar{n},\bar{m}}(u) = S^0_{\bar{n}}(u) + \frac{3}{2}\mu_{\bar{m}}\left[S^+_{\bar{n}}(u) - S^-_{\bar{n}}(u)\right] \tag{92}$$

where

$$S^0_{\bar{n}}(u) = \sum_{j\subset\bar{n}} \frac{I^0_{\bar{n},j}(u)}{1-\alpha_j} \quad , \quad I^0_{\bar{n},j}(u) = \int du'\,\Sigma^s_{\bar{n},j}(u')\,\phi_{\bar{n}}(u')$$

$$S^{\pm}_{\bar{n}}(u) = \sum_{j\subset\bar{n}} \frac{I^{\pm}_{\bar{n},j}(u)}{1-\alpha_j}\,E^{\pm\frac{1}{2}}(A_j\pm 1)$$

$$I^{\pm}_{\bar{n},j}(u) = \int du'\,\Sigma^s_{\bar{n},j}(u')\,J_{\bar{n}}(u')\,(E')^{\mp\frac{1}{2}} \tag{93}$$

and the integrations in Eq. (93) are from $u - \ell_n(1/\alpha_j)$ to u in every case.

The calculation of the sources which appear in the transport equation, Eq. (88) and Eq. (90), therefore reduces to the evaluation of the integrals in Eq. (93). In the resolved resonance region great emphasis must be placed on the lethargy variable; the fluxes are required in sufficient detail to ensure that resonance shielding as a function of lethargy is handled accurately. In addition, the spatial variations of resonance absorption and the effect of P-1 scattering in the laboratory system may be of some importance. The OZMA code enables the user to stress any of the coordinates (lethargy, space, direction) as desired, subject to overall computer memory storage limitations.

A constant interval lethargy mesh (interval ε) is used in the solution of the transport equation, and the equation is solved successively at all mesh points starting at the top of the resolved resonance region. The integrals in Eq. (93) cover a lethargy range which may contain a large number of mesh points. The integrands are stored in memory as "back-values"[42] at lethargies smaller than the current value u. These "back-value" vectors refer separately to all subregions $\bar{n}$ and isotopes j contained in them, and optionally to the anisotropic source components $I^{\ell}_{\bar{n},j}(u)$ as well as the isotropic component $I^{0}_{\bar{n},j}(u)$. It is clear that the maximum number of back-values which are to be stored must be limited in accordance with the available storage memory. This may be problematic specially in the case of light nuclides. In the OZMA formalism this problem is handled in the following manner: For each lattice nuclide j two integers N_j and M_j are defined so that $N_j M_j \varepsilon = \ln(1/\alpha_j)$. Here M_j is the lowest positive integer which ensures that $(N_j + 1)$ is an odd integer not in excess of the largest (input) number of back-values which may be stored for each of the integrals in Eq. (93). Note that hydrogen is excluded from these considerations. It is treated separately by an analytic algorithm. Exact equality of $N_j M_j \varepsilon$ as selected in the input, and the slowing down interval $\ln(1/\alpha_j)$, may require a slight adjustment of α_j which is made automatically in the code. It amounts effectively to a slight adjustment of the mass ratio A_j of the nuclide to the neutron mass.

When N_j and M_j are known for the j^{th} lattice nuclide the back-values for any integral in Eq. (93), referring to nuclide j in any subregion $\bar{n}$ in which it is present, are stored at every M_j^{th} lethargy mesh point only. The back-value integrations are performed by Simpson integrations over the range of lethargies covered by the stored back-values, with end corrections based on trapezium integrations. Suppose an integral $I_j(u)$ is required for isotope j of the type of the integrals in Eq. (93) and that the integrand is denoted by g (the subscript $\bar{n}$ and superscripts 0, $+$ or $-$ are dropped for convenience). Let u denote a lethargy mesh point such that the nearest stored back-value refers to lethargy $u - \ell_j \varepsilon$ where $\ell_j = 0, 1, \ldots, M_j - 1$. Then

$$
\begin{aligned}
I_j(u) = {} & \frac{M_j \varepsilon}{3}\Big[g(u-\ell_j\varepsilon) + 2\sum_{i=1}^{2}{}'(3-i)\sum_{\ell=1}^{\frac{N_j-i+1}{2}} g\{u-\ell_j\varepsilon-(2\ell+i-2)M_j\varepsilon\} + g(u-\ell_j\varepsilon-N_jM_j\varepsilon)\Big] \\
& + \frac{\varepsilon}{2}\Big[g(u) + 2\sum_{\ell=1}^{\ell_j-1} g(u-\ell\varepsilon) + g(u-\ell_j\varepsilon)\Big]_{\ell_j>0} \\
& - \frac{\varepsilon}{2}\Big[2g(u-\ell_j\varepsilon-N_jM_j\varepsilon) + \frac{2\ell_j-1}{M_j}\{g(u-\ell_j\varepsilon-N_jM_j\varepsilon+M_j\varepsilon)-g(u-\ell_j\varepsilon-N_jM_j\varepsilon)\}\Big]_{\ell_j>0}
\end{aligned}
\qquad (94)
$$

For the end-contribution, which has to be subracted from the Simpson integral, linear interpolation has been used between the last two stored back-values which are at lethargies $u - \ell_j\varepsilon - N_jM_j\varepsilon$ and $u - \ell_j\varepsilon - (N_j-1)M_j\varepsilon$. An alternative expression, based on lin-log interpolation, is also availabe for this term for the anisotropic scattering source components. It changes the negative contribution in Eq. (94) to

$$
-\frac{\varepsilon}{2}\Big[g(u-\ell_j\varepsilon-N_jM_j\varepsilon)\sum_{k=1}^{\ell_j} P^{\ell-1}(1+P)\Big]_{\ell_j>0}
$$

$$
P = \Big[g(u-\ell_j\varepsilon-N_jM_j\varepsilon+M_j\varepsilon)\,/\,g(u-\ell_j\varepsilon-N_jM_j\varepsilon)\Big]^{\frac{1}{M_j}}
\qquad (95)
$$

and is automatically replaced by the "linear-linear" correction in Eq. (94) if either the numerator or the denominator of P is negative. The positive end-contribution to the Simpson integral, as given in the second line of Eq. (94), is obtained cumulatively as ℓ_j proceeds from $1, 2, \ldots$ to $(M_j - 1)$.

All the terms which occur in Eq. (94) involve stored "back-values", except for the sum calculated cumulatively in the second line, and $g(u)$ which appears on the second line if $k_j > 0$, and on the first line if $k_j = 0$. Referring to Eq. (93) $g(u)$ involves the unknown $\phi_{\bar{n}}(u)$ or $J_{\bar{n}}(u)$. Consequently, if these quantities are guessed, for example, by taking the values at the previous lethargy mesh point, the sources in Eq. (93) are completely determined and the transport equation in the form of Eq. (88) or Eq. (90) can be solved by standard methods, leading to the next guess of $\phi_{\bar{n}}(u)$ and $J_{\bar{n}}(u)$. These are used to correct the sources in an iterative procedure, until convergence is attained. Clearly this convergence is extremely rapid (generally one or two, and hardly ever as many as about five iterations) since the "unknown" values of $\phi_{\bar{n}}(u)$ and $J_{\bar{n}}(u)$ contribute only very little to the sources.

Proceeding to the next lethargy mesh point merely changes k_j to $k_j + 1$ in Eq. (94) until M_j is reached, when k_j is reset to 0. If the new k_j is less than M_j the first line of Eq. (94) is unchanged and appropriate additions are made to the stored values of the second and third lines. If the new k_j is equal to M_j, it is reset to zero. In this case the second and third lines of Eq. (94) are absent and the value of the first line is updated. Its first term becomes the "unknown" $g(u)$ and the subsequent terms are all shifted on the lethargy scale by $M_j \varepsilon$ with interchanged weights 4 and 2. The quantity which is now $g(u - M_j \varepsilon)$ enters the summations with new weight 4, and the last term of the new summation with weight 2 becomes the last term of the Simpson sum with weight 1. The updating of the first line of Eq. (93) when k_j is therefore very rapid, consisting only of an addition and a substraction to existing sums and the interchange of integration weights.

At the beginning of the calculation N_j initial back-values must be stored for each lattice nuclide j in the subregions $\bar{n}$ in which it is located, together with appropriate back-values in further arrays which deal with the anisotropic source components when they are taken into account. Such back-values refer to mesh points separated by $M_j \varepsilon$ at lethargies below that corresponding to the first point in the resolved resonance region (energy E_c). They are based on a flat isotropic flux of magnitude $1/E$ per unit energy, so that these back-values are $\Sigma^s_{\bar{n},j}/E$ for the isotropic (and zero for the anisotropic) source components, with $E = E_c \exp(k M_j \varepsilon)$, $k = 1, 2, \ldots, N_j$. Here $\Sigma^s_{\bar{n},j}$ is the constant scattering cross section above the resolved resonance region.

For hydrogen there is no need to store back-values since the source integrations extend to the top of the fission spectrum. The value M_j for hydrogen is taken to be unity, so that the correction terms in Eq. (94) lines (2 and 3) are absent. In the Simpson integral [cf Eq. (94)] the last term in the first line is also effectively zero. The two summations which precede it, with weights 4 and 2, are stored as sums and updated in a similar (but even simpler) manner as above, in proceeding from one lethargy mesh point to the next. The inital values of these sums are merely the sums of geometric series assuming $\Sigma^s_{\bar{n},u}$ to be constant over a sufficient portion of the energy range above the top of the resolved resonance region.

The OZMA code can make use of an arbitrary group structure, e.g. the MUFT structure; in each energy group constant cross sections are read into the computer memory for all lattice nuclides. For the nuclides with resonance profile tabulations in any of these energy groups the constant cross sections are overwritten at every lethargy mesh point by appropriate values obtained from these tabulations by linear interpolation. The solution of the transport equation then leads to a reliable flux spectrum $\phi_{\bar{n}}(u)$ in all subregions $\bar{n}$ of the lattice unit cell.

The output of the OZMA code consists of group reaction rates per unit volume in region $\bar{n}$

$$(R^x)^g_{\bar{n},j} = \int_g \Sigma^x_{\bar{n},j}(u)\, E\, \phi_{\bar{n}}(u)\, du = \int_g \frac{\Sigma^x_{\bar{n},j}(u)}{\Sigma_{\bar{n}}(u)} \left\{ \Sigma_{\bar{n}}(u)\, E\, \phi_{\bar{n}}(u) \right\} du \qquad (96)$$

since the flux per unit lethargy is $E\phi_{\bar{n}}(u)$. The integral is calculated by trapezium integration by further subdivision of the lethargy interval ε. The new mesh can be made about as fine as the densest parts of the resonance profile tabulations. In Eq. (96) the collision density given in the brackets $\{\ \}$

is linearly interpolated in the subintervals of ξ, rather than the flux. The principal normalization of $(R^x)^g_{\bar{n},j}$ is for a flat $1/\xi$ flux throughout the lattice unit cell at all energies above the resolved resonance region. This corresponds to [cf. Eq. (21)] C_c/Φ_c where $\Phi_c = 1$ throughout the enire unit cell above the resolved resonance region of the fertile nuclides. The value of C_c is then $\xi \Sigma_s$ integrated over the cell volume above this energy. An option is available to utilize a spatial weighting factor for each of the cell subregions in the asymptotic energy region. This weighting factor is then also used in the summation over subregions of the $\xi \Sigma_s$ multiplied by the subregion volumes.

The group reaction rates, Eq. (96), are the quantities directly needed in lattice analysis codes; they obviate any reference to effective resonance integrals. However, as other computational techniques frequently calculate effective resonance integrals, OZMA evaluates and lists them according to the following expression

$$\left(\frac{I^x}{\xi}_{eff}\right)^g_{\bar{n},j} = \frac{(\xi \Sigma_s V)_{cell}}{N_{\bar{n},j} V_{\bar{n}}} \ln\left(1 - \frac{V_{\bar{n}} (R^x)^g_{\bar{n},j}}{C_c^g}\right) \tag{97}$$

where $(\xi \Sigma_s V)_{cell}$ is the total number of neutrons entering the unit cell at the top of the resolved resonance region (assuming constant scattering cross sections for all nuclides above this region), and C_c^g is this source diminished by all neutron absorptions in the unit cell before group g is reached. Eq. (97) expresses the effective resonance integral in a form in which it accounts for the shielding in the resonances, but is not influenced, except for second order effects, by the absorption caused by the resonances themselves in group g, see Eq. (22).

In addition to the down scattering source which is calculated according to the methods described in connection with Eqs. (93) and (94) an upscattering correction by hydrogen at low epithermal energies is available[43]. It is based on the free proton gas kernel in which the upscattering part is approximated by a delta function, while the total scattering cross section for hydrogen is the appropriate integral of this kernel in an approximate form which applies at energies greatly in excess of the effective kT*.

The Region to Region Transfer Probabilities in the Integral Transport Option of the OZMA Code.

The principal quantities needed to solve the integral transport equation, Eq. (88), apart from the slowing down sources $S_{n'}(u)$, are the probabilities for transfer of neutrons from subregion $n \leftarrow n'$ in a single flight $P_{nn'}(u)$.

These probabilities can be calculated accurately in cylindrical geometry by a method developed by Carlvik[55] for unit cells with cylindricised outer boundaries, from which the neutrons can effectively be scattered back in such a manner that $P_{nn'}(u)$ allows for transfer from subregion n' in one unit cell to subregion n in another. The probabilities clearly depend on the cross sections of all subregions through which the neutrons might pass, and since the calculation is lengthy, it is not practicable to perform it at thousands of lethargy points in the resonance region, and for a multiregion subdivision of the unit cell. It is also generally prohibitive to store the matrix $P_{nn'}$ as a function of the optical thichnesses of the various subregions in order to derive all required $P_{nn'}(u)$ by interpolation in such tabulations.

A practical way to store probabilities related to $P_{nn'}$ is to concentrate on each subregion in isolation from the others. The method is related to the procedure used in the Nordheim Integral transport calculation of resolved resonance integrals[42], in which two probabilities are stored for the fuel region, cf. the discussion following Eq. (61). In the generalisation, for any annular subregion two probabilities are stored which depend only on the cross section and thickness of the region itself, so that they can be tabulated conveniently. They are the probabilities of escape through the inner and outer surfaces of radii a and b respectively, for a uniform isotropic source in the annulus,

$$P^i = \frac{b}{\Sigma V} \int_0^{\sin^{-1} k} 2a\psi \cos\psi \int_0^{\pi/2} d\theta \sin^2\theta \left[1 - e^{-\frac{\Sigma(b\cos\psi - a\cos\psi')}{\sin\theta}}\right] = \frac{k}{k+1} G(k,x)$$

$$G(k,x) = \frac{1}{2kx} \int_0^k \left[1 - \frac{4}{\pi} K_{i3}\left\{\frac{x}{1-k}\left(\sqrt{1-t^2} - \sqrt{k^2-t^2}\right)\right\}\right] dt$$

$$P^0 = P^i + \frac{k}{k+1} \frac{1}{2kx} \int_k^1 \left[1 - \frac{4}{\pi} K_{i3}\left(\frac{2x\sqrt{1-t^2}}{1-k}\right)\right] dt, \quad S(k,x) = P^i + P^0 \tag{98}$$

where $\ell = a/b$, $x = \Sigma(b-a)$ is the optical thickness of the annulus of volume V and θ, ψ and θ, ψ' are the polar and azimuth angles which a neutron trajectory makes at the outer and inner faces of the annulus (with respect to the rod axis and the normal to the surfaces). The Bickley function is defined at the end of Eq. (98). The additional term in P^0 accounts for the source neutrons which move in a direction which does not intersect the inner surface. These two probabilities are functions of the variables x and ℓ . The dependence on the latter is only slight. Extreme values at $\ell = 0$ and $\ell = 1$ are

$$G(0,x) = \frac{1}{2x}\left[1 - \frac{4}{\pi} k_{i3}(x)\right] \quad , \quad S(0,x) = \frac{1}{2x}\int_0^1 d\ell \left[1 - \frac{4}{\pi} k_{i3}(2x\sqrt{1-\ell^2})\right]$$

$$S(1,x) = G(1,x) = 2P^0(1,x) = \frac{1}{2x}\left[1 - 2E_3(x)\right] \tag{99}$$

where $S(0,x)$ and $S(1,x)$ are the escape probabilities from a solid cylinder and an infinite slab. Kennedy[44] has suggested that the weak dependence on ℓ can be utilised to determine $G(\ell, x)$ and $S(\ell, x)$ by interpolation between the extreme values given in Eq. (99) , so that P^0 and P^i follow immediately from Eq. (98) . The latter can then be tabulated as functions of the optical thickness x of the annulus. Three transmission probabilities through the annulus T^{ii} , T^{oi}, T^{oo} are related to the basic P^0 and P^i and refer to neutrons incident on the inner and outer faces of the annulus with distributions proportional to the cosine of the angle of incidence. For neutrons entering through the outer face there is of course a probability of transmission without collision to the inner face and to the outer face.

Although the two basic probabilities P^a and P^i for cylindrical annuli can be tabulated as a function of $x = \Sigma(b-a)$, and conveniently interpolated when the cross section Σ is known for any energy in the resolved resonance region, an approximation is needed to derive the region to region transfer probabilities from them. It is the cosine current approximation. As may be seen in connection with Eqs. (98) and (99) uniform isotropic sources in an annulus give rise to escape probabilities which are connected with transmission probabilities for cosine distributions of neutrons entering the annulus. When a cylindrical unit cell is subdivided into a number of annular subregions such cosine distributions at the interfaces are not assured when the flux, although constant in each subregion, is allowed to vary as a step function at the interfaces. Consequently cosine currents at these interfaces become an assumption under these conditions. They affect the accuracy of the balance equations, given below, in which the probabilities discussed above appear:

$$J_1^+ = S_1 P_1^0 + J_1^- T_1^{oo} \quad , \quad J_N^+ = J_N^-$$

$$J_{n-1}^- = S_n P_n^i + J_n^- T_n^{ii} \quad , \quad J_n^+ = S_n P_n^0 + J_{n-1}^+ T_n^{oo} + J_n^- T_n^{io} \quad , \quad 2 \le n \le N$$

$$T_n^{oo} = 1 - \frac{2}{\pi}\frac{\Sigma_n V_n P_n^i}{a_n} \quad , \quad T_n^{oi} = \frac{a_n}{b_n} T_n^{ii} \quad , \quad T_n^{io} = 1 - \frac{a_n}{b_n}\left[1 + \frac{2}{\pi}\frac{\Sigma_n V_n}{a_n}(P_n^0 - P_n^i)\right] \tag{100}$$

For given source strengths these equations make it possible to calculate the inward and outward directed currents at all interfaces of the subregions numbered from $n=1$ for the innermost cylindrical region to $n=N$, the annulus near the cell boundary. In particular, a unit source in subregion n' only will give a flux in region n which is the transfer kernel $T_{nn'}$ from region n' to region n of Eq. (51)

$$\Sigma_n T_{nn'} V_n = V_{n'} S_{nn'} + J_n^- + J_{n-1}^+ - J_n^+ - J_{n-1}^- \tag{101}$$

This kernel is related to the region to region transfer probability by

$$P_{nn'} = \frac{\Sigma_n T_{nn'} V_n}{V_{n'}} \tag{102}$$

The above procedure for calculating the transfer probabilities $P_{n'0}$ is also used in the Nordheim integral transport method for calculating effective resonance integrals, see Eq. (61).

The Discrete Ordinate Option in the OZMA Code

The discrete ordinate option in the OZMA code is solved by standard procedures for handling the S_N equations[45],[46], for vacuum, reflective, periodic, or white boundary conditions at the inner and outer boundaries of the lattice unit cell.

In the S_N approximation, as used in the OZMA code, there are (N + 1) characteristic directions in slab and spherical geometry with μ values of increasing magnitude in the range (-1,1). The first direction has zero weight; for every other negative μ there is a positive μ of the same magnitude and weight W. Also $\sum W = 1.0$. In cylindrical geometry there are 3,5,...,(N+1) characteristic directions on N/2 equatorial planes. These directions are numbered 1,2,...,N(N+4)/4. On each plane the extreme negative μ value has zero weight, the other characteristic directions forming pairs as in the other geometries. The total weight for all N(N+4)/4 directions is unity.

The angular redistribution coefficients in Eq. (90) are defined by

$$\beta_{\bar{n},m} = 0 \quad (\text{if } W'_{\bar{m}} = 0) \; ; \; \beta_{\bar{n},m} = \beta_{\bar{n},m+1} - \mu_{\bar{m}} W'_{\bar{m}} (A_{m+1} - A_m) \quad (\text{if } W'_{\bar{m}} \neq 0) \tag{103}$$

so that $\beta_{\bar{n},m}/W'_{\bar{m}}$ and $\beta_{\bar{n},m+1}/W'_{\bar{m}}$ are required for the solution of Eq. (90) for the "space,direction" mesh point $\bar{n},\bar{m}$ with spatial boundaries of areas A_m and A_{m+1}, and direction boundaries corresponding to the subscripts m and $m+1$. Eq. (103) ensures that the redistribution coefficients are defined separately on each equatorial plane in cylindrical geometry.

The solution of Eq. (90) proceeds through all space points $\bar{n}$ for the first direction $\bar{m}$, then similarly for the next $\bar{m}$, etc. When $f_{\bar{n},\bar{m}}$ is calculated at the center of a particular "space direction" cell, the mid boundary flux values are known at two adjacent faces of this cell. If $f_{\bar{n},\bar{m}}$ is assumed to be the average of the mid boundary flux values both for the space and direction coordinates, the method of solution is the diamond scheme; if $f_{\bar{n},\bar{m}}$ is assumed to be the same as the mid boundary values at the two adjacent faces of the "space direction" cell, where these values are not yet known, the method of solution is the step function scheme. In accordance with the specified boundary conditions at the spatial boundaries of the unit cell, and zero angular flux density at the direction of zero weight, the solution proceeds from the outer spatial boundary of the cell inwards when $\mu_{\bar{m}}$ is negative, and from the inner spatial boundary of the cell outwards when $\mu_{\bar{m}}$ is positive. For the vacuum boundary condition the inward directed angular flux density is zero (for negative $\mu_{\bar{m}}$ at the outer cell boundary, and for positive $\mu_{\bar{m}}$ at the inner cell boundary); for the reflective boundary condition it is the same for any given direction and its reflection (equal $|\mu_{\bar{m}}|$ but of opposite sign, except for the direction of zero weight which is reflected into the direction of largest $\mu_{\bar{m}}$); for the periodic boundary condition, the angular flux densities for a given $\mu_{\bar{m}}$ are the same at the inner and outer cell boundaries; for the white boundary condition, the inward directed flux density at the cell boundary is the outward directed current (positive $\mu_{\bar{m}}$'s at the outer, negative $\mu_{\bar{m}}$'s at the inner cell boundary) multiplied by the appropriate albedo. The sweep through the "space direction" cells passes in this way from cell to cell, in which always two adjacent boundary fluxes are known at the start of the calculation for a particualr cell, the central flux and the fluxes at the remaining two adjacent boundaries being calculated.

The S_N option has several advantages compared with the integral transport mode of the OZMA code. Among these the most important is that P-1 scattering can be taken into account. It also requires less storage since only the quantities referred to in connection with Eq. (90) have to be stored, and not the tabulations needed to evaluate the $P_{nn'}$ matrix of Eq. (102) at each energy point. On the other hand, the S_N option requires rather more computer time, typically up to as much as the integral transport mode.

Consistent Use of Accurately Calculated Resonance Reaction Rates in Multigroup Lattice Analysis Codes

When accurately calculated reaction rates in the resolved resonance region are available, such as those calculated by means of the OZMA code according to Eq. (96) for energy groups which correspond to those of a multigroup lattice analysis code, they can be used in such a code in an indirect manner.

In the MUFT procedure, for example, one would eliminate the resonance absorption term $\alpha_r(\eta_r+1)$ from Eq. (47) and use cell averaged absorption cross sections for all resonance absorbers in the lattice unit cell as part of Σ_a. This would be done at zero buckling and in the absence of Σ_{ex}, ω, and χ in the resolved resonance region, consistent with the method used in the OZMA code. The absorption cross sections of the resonance absorbers in Σ_a would be estimated values initially, but they would be modified iteratively until, for all resonance absorbers, the absorption and fission rates in all groups in the resolved resonance region agree with the values predicted by the OZMA code for the same normalisation at the top of this region. When convergence has been reached, a further

calculation could be made at a finite input buckling, and in the presence of any (small) Σ_{in}, ω, and χ values which had been ignored in the resonance groups during the iterations. This procedure also eliminates the problem which had been mentioned earlier, that the resonance absorption rate $\omega_r(\eta + \varrho_r)$ does not allow for any interaction between resonance absorption and leakage. As part of the overall Σ_r the group resonance absorption cross sections of the resonance nuclides are treated together with the leakage in Eq. (47) in a consistent manner.

This procedure has been implemented in the HAMMER code[31] and most of the results of lattice analysis calculations which will be described subsequently have been obtained in this way by a combination of OZMA[2] and HAMMER[31]. It is also possible to treat resonance absorption in a space dependent manner, for example, for the different annuli containing fuel rods in cluster geometry, provided such annuli are represented by homogeneous mixtures of fuel and coolant. The same resonance isotope in different fuel bearing annuli is treated effectively as a different material in each of these annuli, so that the OZMA/HAMMER analysis can proceed normally, reaction rates being preserved for the resonance nuclides in the interface between the two codes separately for all the annuli containing fuel. Hyperfine heterogeneity corrections within the annuli have to be handled by appropriate correction factors.

Similar procedures can be used in the GAM[27] code. If implemented, they can serve as a means of testing the adequacy of the use of tabulated group resonance cross sections for the different resonance absorbers together with equivalence theorems to relate heterogeneous to homogeneous assemblies.

Temperature Dependence of Neutron Cross Sections and Resonance Integrals, and Safety Problems

Lecture V

Results of Thermal Reactor Lattice Analysis Studies with Accurately Calculated Resonance Reaction Rates

Thermal reactor lattice calculations with accurate temperature dependent resonance absorption treatments have a direct bearing on safety problems. Since such calculations are time consuming they can be applied only to a limited range of problems. However they can also be used as a means of testing and correcting the algorithms for rapid calculations of resonance reaction rates in multigroup lattice analysis codes, so that these can be employed with greater confidence for problems of practical importance, and in particular in cases where the temperature dependence of reactor parameters are required.

Detailed resonance absorption treatments are also of great value in data and methods testing programs. Differences between calculated and experimental values of integral parameters can, in general, be attributed to a mixture of experimental errors, inadequacy of the basic data, and approximations in the calculational procedures. The availability of modern computing facilities provide an incentive to reduce errors due to calculational models as far as possible. Approximations in the solution of the Boltzmann equation are inevitable even for problems of simple geometry, except in the case when point energy Monte Carlo methods are used for the complete assembly under investigation and the entire range of neutron energies. However detailed results in limited spatial region and small energy ranges require numerical procedures free from statistical fluctuations. In the resolved resonance region, and subject to appropriate generalisation also in the unresolved and thermal energy regions, the detailed methods described previously, enable to user to estimate the accuracy of his calculational models. This is of great value for the analysis of differences between results of calculations and integral experiments.

In the following sections a number of problems will be discussed by referring to results of calculations published in recent years. They deal with effective resonance integrals of isolated rods and their temperature variations; Doppler reactivity coefficient in BWR and PWR unit cells and their variation with fuel depletion; the analysis of some thermal reactor lattice benchmarks; resonance absorption calculations in D_2O moderated fuel clusters; and the detailed analysis of a light water moderated UO_2 lattice which throws light on the differences between group cross sections, cell fluxes, and fuel disadvantage factors in detailed calculations within a resonance group and in standard multigroup calculations. In the conclusion, a procedure is proposed for the specification of temperature and composition dependent correction factors to simple and rapid resonance treatments in multigroup lattice analysis codes.

Temperature Dependence of Effective Resonance Integrals: Interference Between Resonance Absorption due to Different Nuclides.

As discussed previously, the OZMA code provides an accurate means for calculating the temperature dependence of resonance absorption in reactor lattices, since the point cross sections used are evaluated with rigorous Doppler broadening. In addition, all resonance interference effects are implicit in the treatment; the cross sections of mixtures of nuclides are obtained at all discrete energy points by summing the partial cross sections of the constituents, before the transport and resonance shielding calculations are made.

In Tables VI and VII resonance integrals of ^{235}U and ^{238}U are given for 3% enriched UO_2 rods of widely differing radii[47]. The OZMA calculations were made with the integral transport mode for practically isolated rods, by placing them in water in an array with large water to fuel volume ratio. The flux was initialised only once to its asymptotic value, above the ^{238}U resolved resonance region. In both tables the values are compared with those resulting from the Nordheim Integral Transport treatment[42] for individual resonances in the ZUT code. The ^{235}U results in Table VI cover its resolved resonance region. In the case of ^{238}U in Table VII the effective resonance integrals are extended by adding $\sum_g (\sigma_a)_g \Delta u_g$ to cover the entire energy region from 10 MeV to 0.625 eV for group cross sections obtained from the ENDF/B-IV data with a fission spectrum weighting flux above 67 keV, and a constant weighting flux per unit lethargy below this energy, without resonance shielding in the groups belonging to the unresolved resonance region; a contribution was also added for the epithermal group below the resolved resonance region. Table VII also shows the temperature coefficients of the effective resonance integral when $[I_{eff}(T) - \delta]$ is assumed to depend linearly on $(\sqrt{T} - \sqrt{T_r})$, or for a quadratic dependence. These coefficients, which refer to the OZMA calculations, are in reasonable agreement with the values resulting from the Nordheim treatment, and values given by Todosow and Carew[48]. The quantity δ is the 1/v capture integral, based on $\sigma_c(2200) = 2.71$ barns, in a $1/v$ flux above 0.55 eV.

TABLE VI

^{235}U Absorption Integral for 3 Percent Enriched UO_2 Rods (0.834-101.3 eV).

		R(cm) ($\sqrt{S/M}$ cm/gr$^{1/2}$)				
T°K	Code	0.125 (1.227)	0.250 (0.886)	0.500 (0.632)	1.00 (0.447)	2.00 (0.316)
293	OZMA1	273.0	262.6	244.3	216.5	179.3
	ZUT	286.8	280.7	270.3	254.4	235.3
450	OZMA1	273.0	262.8	245.0	217.4	180.2
	ZUT	287.5	281.7	271.8	256.5	237.5
600	OZMA1	273.0	263.0	245.5	218.2	180.8
	ZUT	287.9	282.4	272.9	257.9	239.1
800	OZMA1	272.8	263.0	245.9	218.8	181.4
	ZUT	288.3	283.1	273.9	259.3	240.7
1200	OZMA1	272.2	262.7	246.0	219.4	182.2
	ZUT	288.8	284.0	275.4	261.4	243.1

TABLE VII

^{238}U Total Capture Integral for 3 Percent Enriched UO_2 Rods (0.625 eV-10MeV).

T°K	Code	0.125 (1.227)	0.250 (0.886)	0.500 (0.632)	1.00 (0.447)	2.00 (0.316)
		R(cm) ($\sqrt{S/M}$ cm/gr$^{1/2}$)				
293	OZMA1	39.75	29.73	22.34	16.94	12.93
	ZUT	39.87	30.39	23.40	18.43	15.04
450	OZMA1	41.42	30.71	22.94	17.34	13.20
	ZUT	41.46	31.33	23.98	18.83	15.34
600	OZMA1	42.85	31.54	23.44	17.65	13.41
	ZUT	42.88	32.17	24.49	19.17	15.59
800	OZMA1	44.59	32.54	24.02	18.01	13.65
	ZUT	44.61	33.18	25.10	19.57	15.87
1200	OZMA1	47.61	34.29	25.04	18.63	14.04
	ZUT	47.64	34.98	26.16	20.24	16.34

$$[I_{eff}(T) - S] = [I_{eff}(T_0) - S][1 + \beta(\sqrt{T} - \sqrt{T_0}) + \gamma(T - T_0)^2]$$ [illegible]

^{238}U Doppler Coefficients for 3 Percent Enriched UO_2 Rods

Linear Fig		Quadratic Fit	
R(cm)	$10^2\beta$	$10^2\beta$	$10^5\gamma$
0.125	1.17	1.06	6.5
0.250	0.91	0.82	5.1
0.500	0.73	0.68	2.6
1.00	0.61	0.60	0.5
2.00	0.54	0.56	-1.2

The effect of the detailed space-energy calculations of the flux in the OZMA code is apparent when the results in Tables VI and VII are compared with the values obtained from the ZUT code individual resonance treatment which uses a flat flux in the fuel. As heterogeneity becomes more pronounced the differences in the effective absorption integrals increase.

In addition, there is a marked effect due to nuclide interference in Table VI which refers to the ^{235}U resolved resonance region. The difference between the I_{eff} values with and without interaction between the resonances of the two nuclides increases more considerably with increasing rod radius for ^{235}U than for ^{238}U. In order to show this effect more clearly a breakdown of the room temperature OZMA results for the separate MUFT groups is given in Table VIII and IX.

There is strong correlation between the decrease in I^{25}_{eff} and I^{25}_{eff} with increasing rod size in groups 39, 41 and 45 which contain the large ^{238}U resonance peaks at 36.8, 20.9, and 6.67 eV. The flux depressions due to these ^{238}U resonance effect I^{25}_{eff} more strongly than the flux depressions caused by the ^{235}U resonances themselves. In other groups such as 47 and 48, in which there are significant contributions to I^{25}_{eff}, the decrease of the group I_{eff} with increasing rod size is much less marked and close to the behaviour of the overall I^{25}_{eff} for all groups as given in Table VI.

TABLE VIII

I_{eff} of ^{235}U for Absorption for 3% Enriched, Isolated UO_2 Rods at Room Temperature, Calculated by the OZMA Code

MUFT Group	Rod Radius (cm.) 0.125	0.25	0.50	1.0	2.0
35	7.76	7.68	7.51	7.14	7.46
36	8.02	7.87	7.61	7.14	6.35
37	19.76	19.41	18.68	17.34	15.10
38	12.80	12.54	12.04	11.15	9.72
39	21.65	20.71	18.97	16.18	12.47
40	16.36	16.06	15.44	14.26	12.29
41	21.74	19.75	16.94	13.38	9.56
42	12.61	12.41	11.95	11.05	9.47
43	28.17	26.90	24.63	21.23	17.01
44	33.73	32.13	29.24	24.91	19.62
45	6.36	5.76	4.91	3.87	2.80
46	15.05	13.24	10.62	7.65	4.97
47	6.06	5.92	5.62	5.04	4.10
48	11.54	11.36	10.96	10.17	8.88
49	4.18	4.14	4.04	3.83	3.45
50	6.69	6.62	6.45	6.09	5.49
51	4.55	4.52	4.42	4.21	3.84
52	13.19	13.02	12.60	11.75	10.37
53	22.83	22.51	21.73	20.10	17.33
Total	273.04	262.55	244.35	216.46	179.27

TABLE IX

I_{eff} of ^{238}U for 3% Enriched Isolated UO_2 Rods at Room Temperature, Calculated by the OZMA Code

MUFT Group	Rod Radius (cm.) 0.125	0.25	0.50	1.0	2.0
35	0.873	0.697	0.534	0.413	0.322
36	1.760	1.256	0.918	0.685	0.513
37	0.035	0.034	0.033	0.031	0.028
38	0.691	0.625	0.538	0.441	0.343
39	3.935	2.750	1.912	1.320	0.892
40	0.173	0.170	0.164	0.153	0.132
41	6.298	4.355	2.995	2.040	1.357
42	0.113	0.111	0.107	0.100	0.086
43	0.074	0.072	0.070	0.065	0.057
44	0.218	0.213	0.203	0.185	0.158
45	11.110	7.088	4.437	2.762	1.709
46	2.568	2.276	1.856	1.373	0.915
47	0.277	0.273	0.264	0.244	0.208
48	0.162	0.160	0.155	0.145	0.128
49	0.129	0.128	0.125	0.119	0.107
50	0.118	0.117	0.114	0.108	0.098
51	0.117	0.116	0.114	0.108	0.098
52	0.115	0.114	0.111	0.104	0.094
53	0.147	0.145	0.140	0.130	0.112
Total (27-53)	37.28	27.33	20.00	14.68	10.71

The WIMS code estimates the interference effect by the expression

$$\tilde{I}^{25}_{eff,g} = \left(\frac{\Sigma_p + \Sigma_c}{\Sigma_p + \Sigma_c + \bar{\Sigma}^{25}_{res,g}}\right) I^{25}_{eff} \left(\frac{\Sigma_p + \Sigma_c + \bar{\Sigma}^{25}_{res,g}}{N^{25}}\right) \qquad (104)$$

where Σ_p is the potential scattering cross section of the fuel, $\Sigma_c = 1/\ell_c$ with ℓ_c the mean chord length for isolated rods, and $\bar{\Sigma}^{25}_{res,g}$ the average resonance cross section of ^{238}U in group g. Eq. (104) produces an interference effect which tends to reduce $\tilde{I}^{25}_{eff,g}$ compared with the value without interference, i.e. with $\bar{\Sigma}^{25}_{res,g} = 0$. The reason is that the presence of the ^{238}U average cross section in Eq. (104) reduces the multiplying factor much more strongly than the increase caused by the larger background cross section, at which I^{25}_{eff} is evaluated. On the other hand the magnitude of the interference effect is predicted poorly in the groups with the large ^{238}U peaks, specially when the change of this effect for widely differing rod diameters is considered. As the rod diameter increases Σ_c becomes smaller, but so does $\bar{\Sigma}^{25}_{res,g}$ in the groups with the large resonances. Consequently, the change of the interference effect, as given by Eq. (104), in groups 39, 41, 45, and even still in group 46, with increase in rod diameter is much smaller than that obtained by the OZMA code, see Table VIII. Even allowing Σ_p and $\bar{\Sigma}^{25}_{res,g}$ to be replaced by effective values in Eq. (104), for example close to those which apply in the case of a resonance absorber of infinite mass, cannot reproduce the variation of ^{235}U resonance integral with rod size in the principal ^{238}U resonance groups, obtained from the detailed resonance absorption calculations with an implicit interference treatment. It must be concluded that reliance on Eq. (104) can only give a rough estimate of the interference effect. For more accurate estimates detailed calculations are needed, or fits to such calculations by means of empirical formulae. An alternative is the use of sub-group theory[49], which can give better estimates of the flux depressions caused by the principal absorber, and their effects on the less abundant resonance absorbers.

Temperature Dependence of Resonance Absorption in LWR Lattices during Fuel Depletion. Spatial Shielding and Mutual Shielding by Different Nuclides.

A study was made recently[15] of the temperature dependences of the resonance absorption and of the multiplication factor in LWR lattices when changes in the fuel composition due to depletion are taken into account. The OZMA[2] and HAMMER[31] codes were used for the multigroup lattice analysis. Changes in the fuel composition during burn-up were obtained by CINDER[50] calculations.

Apart from the calculations performed at epithermal energies, which were described in connection with the resonance calculations, the HAMMER code determines the space dependent thermal spectrum in a 30 group structure below 0.625 eV[31]. Some information about the thermal library was given in connection with the preparation of temperature dependent resonance cross section profile shapes. The CINDER code[50] depletes the fuel for a specified power density, generating fission product nuclides in a number of fission product chains, and actinides in depletion chains.

Differences in I_∞ and other parameters due mainly to Doppler broadening of the resonances were initially calculated for two fuel temperatures and fuel compositions in a BWR lattice unit cell. The composition is given in Table X; the end of life composition was approximate, no attempt being made in this initial study to account for the depletion in detail. Two fission products with pronounced resonances, as well as the Uranium and Plutonium isotopes listed, were included in the detailed resonance treatment.

Table X

BWR Unit Cell Specifications for Initial Study

Fuel Atom Densities per Barn-Cm			Moderator Atom Densities per Barn-Cm	
Nuclide	BOL	EOL	Nuclide	BOL and EOL
^{235}U	6.203(-4)	1.970(-4)	^{1}H	3.42(-2)
^{238}U	2.167(-2)	2.108(-2)	^{16}O	1.71(-2)
^{239}Pu		7.65 (-5)		
^{240}Pu		4.70 (-5)		
^{241}Pu		3.40 (-5)		
^{242}Pu		1.72 (-5)		
^{145}Nd		2.46 (-5)		
^{147}Pm		4.89 (-5)		
^{26}O	4.2 (-2)	4.2 (-2)		

Fuel Outer Diameter	1.041 cm	Fuel Temperatures	800°K and 1200°K
Unit Cell Outer Diameter	1.615 cm	Moderator Temperature	1200°K

In Table XI microscopic ^{238}U capture rates are shown for four subregions n into which the fuel rod was subdivided in the OZMA calculations, in the groups containg the first three principal resonances. The subregion $n=4$ is a thin layer near the surface of the rod. The capture rates refer to an intialisation of $\Phi_n(u)$ to unity above the ^{238}U resolved resonance region for all subregions into which the fuel unit cell is divided. Their average (av) over the four fuel subregions is shown, as well as the average (av^*) which renormalises it to allow for neutron absorption in the groups prior to g, i.e. which ensures that the same number of neutrons slow down into region g, as into the first group in the resolved resonance region. This latter quantity may be compared with I_{eff} in the group g which, as discussed in connection with Eq. (22) does not take the absorption in group g into account, and which is therefore slightly in excess of the capture integral.

TABLE XI

^{238}U Microscopic Absorption Rates and I_{eff} Values for BWR Unit Cell: and

MUFT Group	Subregion n	BOL 800°K	BOL 1200°K	EOL 800°K	EOL 1200°K	Principal Resonance peaks and group boundaries (eV)
	1	0.720	0.690	0.772	0.741	
	2	0.758	0.726	0.811	0.778	
	3	0.864	0.831	0.919	0.887	
39	4	1.734	1.795	1.826	1.892	36.80
	av	1.189	1.195	1.259	1.266	(29.0 - 37.3)
	av*	1.476	1.499	1.525	1.551	
	I_{eff}	1.500	1.524	1.550	1.576	
	I_∞	42.15	41.91	42.15	41.91	
	1	1.045	1.011	1.115	1.081	
	2	1.100	1.065	1.173	1.138	
	3	1.247	1.218	1.327	1.299	
41	4	2.568	2.699	2.722	2.863	20.90
	av	1.745	1.780	1.853	1.892	(17.6 - 22.6)
	av*	2.291	2.363	2.350	2.426	
	I_{eff}	2.349	2.425	2.410	2.491	
	I_∞	62.34	62.33	62.34	62.33	
	1	1.016	0.978	1.090	1.049	
	2	1.081	1.033	1.159	1.109	
	3	1.270	1.204	1.362	1.293	
45	4	3.504	3.604	3.754	3.867	6.67
	av	2.129	2.137	2.282	2.294	(6.48 - 8.32)
	av*	3.114	3.167	3.176	3.232	
	I_{eff}	3.224	3.281	3.287	3.348	
	I_∞	127.39	126.56	127.39	126.56	
	av	13.279	13.740	13.842	14.325	
Total	av*	16.788	17.467	17.037	17.731	
	I_{eff}	17.059	17.755	17.312	18.024	
	I_∞	275.01	275.00	275.01	275.00	

The increased shielding in the rod interior is clearly seen at both temperatures and for both fuel compositions. In addition, the Doppler effect changes sign in these groups: the microscopic absorption rate increases with increasing temperature near the rod surface, but the increased absorption at the higher temperature shields the rod interior to some extent causing a decrease in the absorption rate near its axis. The average fuel absorption rate, as well as I_{eff}, rises when the temperature is increased. For the EOL composition there is slightly less shielding (a slightly increased I_{eff} and ΔI_{eff}) due to the changed ^{238}U atom density and the presence of the new resonance nuclides. The apparent changes in the group I_∞ values with temperature are due to the location of the group boundaries with respect to the resonance peaks; they disappear in the total I_∞.

Table XII gives I_{eff} and δI_{eff} values (between 800°K and 1200°K) at BOL and EOL in some of the important groups in the resonance region for the Uranium isotopes, and at EOL for some of the other isotopes for which the explicit resonance absorption treatment was used in the mixture of fuel nuclides.

The ^{235}U resonance shielding is clearly much less pronounced than that of ^{238}U due to its small atom density. Its $\delta I_{eff}/I_{eff}$ amounts to about 0.3 percent in magnitude compared to 4 percent for ^{238}U. It is also very noticeable how nuclide interference changes the sign of δI_{eff} of ^{235}U in group 53, and even in group 41, due to ^{240}Pu build-up. The large ^{240}Pu resonance is located in group 53. Negative values of δI_{eff} are obtained in groups 45 and 46 which contain the 6.67 eV ^{238}U peak and low energy tail respectively. As regards the fission products similar effects may be noted. In particular the principal ^{147}Pm resonance at 5.36 eV has positive δI_{eff} values in groups 46 and 47, but the two smaller resonances at 6.57 and 6.92 eV in group 45 are so heavily shielded by the principal ^{238}U peak, that their δI_{eff} is negative.

TABLE XII

I_{eff} and δI_{eff} Values at BOL and EOL for BWR Unit Cell

	^{238}U				^{235}U			
	BOL		EOL		BOL		EOL	
MUFT Group	$I^{abs.}_{eff}$	$\delta I^{abs.}_{eff}$	$I^{abs.}_{eff}$	$\delta I^{abs.}_{eff}$	$I^{abs.}_{eff}$	$\delta I^{abs.}_{eff}$	$I^{abs.}_{eff}$	$\delta I^{abs.}_{eff}$
38	0.48	+0.022	0.48	+0.022	11.68	+0.055	11.86	+0.029
39	1.50	+0.025	1.55	+0.026	16.95	+0.128	18.55	+0.032
41	2.35	+0.076	2.41	+0.080	14.16	+0.128	16.39	-0.021
45	3.22	+0.057	3.29	+0.061	4.04	-0.120	4.12	-0.132
46	1.57	+0.053	1.60	+0.051	7.99	-0.400	8.25	-0.466
47	0.26	+0.000	0.26	+0.000	5.45	+0.018	5.56	-0.005
53	0.14	0.000	0.08	-0.002	21.39	+0.026	10.71	-0.282
54								
Total (27-54)	17.06	+0.697	17.31	+0.712	230.29	+0.804	231.30	-0.648

I_{eff} and δI_{eff} Values of EOL

	^{239}Pu		^{240}Pu		^{145}Nd		^{147}Pm	
	EOL		EOL		EOL		EOL	
MUFT Group	$I^{abs.}_{eff}$	$\delta I^{abs.}_{eff}$	$I^{abs.}_{eff}$	$\delta I^{abs.}_{eff}$	$I^{abs.}_{eff}$	$\delta I^{abs.}_{eff}$	$I^{abs.}_{eff}$	$\delta I^{abs.}_{eff}$
38	18.07	-0.034	41.50	+0.156	40.40	+0.375	51.43	+0.234
39	1.47	+0.003	0.11	-0.003	0.53	-0.006	3.70	-0.145
41	21.22	-0.370	8.12	-1.242	0.28	-0.005	15.89	-0.059
45	34.24	+0.107	0.09	-0.002	0.40	-0.006	62.23	-5.98
46	1.54	-0.019	0.21	-0.002	1.01	-0.004	1164.54	+4.97
47	2.03	+0.000	0.52	-0.000	106.97	+0.657	78.24	+3.214
53	8.29	-0.187	1858.1	+56.0	1.04	-0.025	3.89	-0.094
54			132.74	+1.061	1.95	-0.002	7.28	-0.007
Total (27-54)	328.42	-0.654	2508.53	+91.94	186.84	+0.666	1454.89	+1.77

*Note: The column $I^{abs.}_{eff}$ refers to $(I_{eff})_{800°K}$

The column $\delta I^{abs.}_{eff}$ refers to $(I_{eff})_{1200°K} - (I_{eff})_{800°K}$

In Table XIII ℓ_∞ and $\delta\ell_\infty$ values are shown for this BWR unit cell. The breakdown is by group (with boundaries at 10 MeV, 0.82 MeV, 5.53 keV, 0.625 eV, 10^{-5} eV) and nuclide, in accordance with

$$\ell_G = \left[\chi_G + \sum_{G'=1}^{G-1} \chi_{G'} \left(\prod_{G''=G'}^{G-1} P_{G''}\right)\right] M_G \quad , \quad \ell_{eff} = \sum_G \ell_G$$

$$P_G = \left[\Sigma_R/(\Sigma_a + \Sigma_R + DB^2)\right]_G \quad , \quad M_G = \left[\nu\Sigma_f/(\Sigma_a + \Sigma_R + DB^2)\right]_G \qquad (105)$$

and its first differences.

TABLE XIII

Breakdown of k_∞ for BWR Unit Cell

MAT	BOL δk_3	BOL δk_4	BOL δk_∞	EOL δk_3	EOL δk_4	EOL δk_∞
^{238}U	-0.00271	-0.01090	-0.01361	-0.00172	-0.00956	-0.01128
^{235}U	+0.00016	-0.00018	-0.00002	-0.00016	+0.00007	-0.00009
^{239}Pu				-0.00011	+0.00009	-0.00002
^{240}Pu				-0.00025	-0.00144	-0.00170
^{241}Pu				-0.00017	+0.00007	-0.00010
^{242}Pu				-0.00003	-0.00013	-0.00016
^{145}Nd				0	0	0
^{147}Pm				0	+0.00001	+0.00001
Removal	+0.00073	-0.00234	-0.00161	+0.00069	-0.00344	-0.00275
Overall			-0.0152			-0.0161

Most of the contributions to $\delta\ell_\infty$ are in group 4, the thermal group, and are due to $\delta(\Sigma_a)_3$ in δP_3, and the breakdown of $\delta(\Sigma_a)_3$ by nuclide. ^{238}U is the main contributor to the negative $\delta\ell_\infty$, but at EOL its effect is somewhat reduced with compensation by ^{240}Pu. Individual fission products with pronounced resonances contribute negligibly to $\delta\ell_\infty$ on account of their low concentrations. It is unlikely that the neglect of most fission products, some of which may also have quite strong resonances, will greatly alter this conclusion.

Although $\delta\ell_{\infty,}$, the change in the eigenvalue between fuel temperatures of 800°K and 1200°K, in Table XIII is somewhat greater in magnitude at EOL than at BOL, this trend is reversed when the BOL composition is depleted in steps in detailed burn-up calculations made with the CINDER code. The atom densities at a number of depletion stages are shown in Table XIV for the nuclides taken into account explicitly in the resonance absorption treatment. For the CINDER runs the four broad group libraries were modified at each of these stages to take the changed resonance shielding factors and broad group flux ratios into account. The fission product absorption by nuclides not explicitly taken into account in the detailed resonance treatment was allowed for by a lumped fission product method recommended in the CINDER code for use with the library containing eleven fission product chains.

Table XIV

BWR Unit Cell Atom Densities in Fuel (Power Density 213 Watts/cc)

Isotope	Integrated Power MWd/MTU BOL	80	7000	14000	28000
^{235}U	6.203(-4)	6.181(-4)	4.662(-4)	3.558(-4)	2.116(-4)
^{238}U	2.167(-2)	2.167(-2)	2.153(-2)	2.138(-2)	2.105(-2)
^{239}Pu		1.452(-6)	7.772(-5)	1.258(-4)	1.750(-4)
^{240}Pu		3.291(-9)	1.083(-5)	2.461(-5)	4.846(-5)
^{241}Pu		1.753(-11)	4.757(-6)	1.688(-5)	4.286(-5)
^{242}Pu		1.100(-14)	2.768(-7)	1.922(-6)	9.164(-6)
^{135}Xe		6.860(-9)	7.649(-9)	8.949(-9)	9.642(-9)
^{149}Sm		7.342(-9)	8.288(-8)	1.135(-7)	1.388(-7)
^{145}Nd		7.538(-8)	6.193(-6)	1.173(-5)	2.136(-5)
^{147}Pm		4.330(-9)	2.746(-6)	4.240(-6)	5.330(-6)
^{16}O	4.460(-2)	4.460(-2)	4.460(-2)	4.460(-2)	4.460(-2)

The change in $\delta\ell_{\infty,}$ (and also $\delta\ell_{\infty,}/\ell_{\infty}$) with burn up is shown in Table XV. It will be noted that $\delta\ell_{\infty,}$ is now slightly smaller at the end of life than it is

at BOL. This is due to the fact that fission product absorption was properly accounted for by nuclides treated explicitly in the resonance treatment and by lumped fission product absorbers. The latter had been ignored in the initial calculations, Tables X - XIII. The ratio $\delta\ell_\infty/\ell_\infty$ increases somewhat in magnitude as the fuel depletes. As regards the breakdown by nuclides, the principal Doppler change, affecting $\delta\ell_\infty$, is due to ^{238}U. Its effect is slightly reduced in magnitude by Plutonium build up, but this is compensated for by the Doppler effect in ^{240}Pu which becomes quite pronounced (about fifteen percent of that due to ^{238}U) at end of life.

Table XV

k_∞ and δk_∞ Values for BWR Unit Cell

INT. POWER MWd/MTU	k_∞ 800°K	k_∞ 1200°K	δk_∞	$\delta k_\infty/k_\infty$
0	1.2084	1.1932	-0.0152	-0.0126
80	1.1692	1.1546	-0.0146	-0.0125
7000	1.0629	1.0489	-0.0140	-0.0132
14000	0.9956	0.9816	-0.0140	-0.0141
28000	0.9134	0.9002	-0.0132	-0.0144

Similar conclusions were reached[15] for a typical PWR unit cell during its burn-up in a power reactor. In the detailed study of the temperature dependence of the multiplication factor of both LWR lattices during fuel depletion, both ^{149}Sm and ^{135}Xe were included in the explicit resonance treatment. The Doppler changes of their absorption cross sections near the principal epithermal and thermal resonance peaks, respectively, were therefore accounted for. Their effect of $\delta\ell_\infty$ was found to be almost negligible (about two percent at the end of life). In addition, the explicit treatment of ^{236}U as a resonance absorber reduced the $\delta\ell_\infty$ for the PWR unit cell by about 7 percent in magnitude at EOL.

Resonance Absorption and Lattice Analysis for D_2O Moderated Fuel Clusters

The OZMA code can be applied directly to clusters of fuel rods in a moderator, if the hyperfine structure or heterogeneity within the annuli in which the rods are located is ignored (see Fig. 1), i.e. if all materials in such annuli are mixed homogeneously. The code will then take all resonance interference effects and their spatial dependence into account by the use of detailed resonance cross section profiles, as it does in the case of simple lattices. The spatial treatment produces additional shielding in the inner annuli because of the neutron absorption in the fuel contained in the outer annuli. It is possible to estimate hyperfine structure effects within the fuel bearing annuli by Monte Carlo methods and to apply appropriate corrections to the results of the OZMA calculations before the multigroup analysis for the entire neutron spectrum is completed by the HAMMER code.

The above procedure was applied to the analysis of a CANDU fuel cluster containing 19 natural UO_2 rods in a D_2O moderator, with varying pitch between the axes of the clusters and with D_2O as coolant[51]. The large dimensions of the unit cell result in a spatial flux distribution which is not flat above the resolved resonance region. This distribution was applied to the calculation of the initial slowing down sources into the resolved resonance region in all the subregions into which the unit cell is subdivided: the asymptotic flux per unit lethargy above the resolved resonances was assumed to be constant in each subregion with unit volume average for the entire unit cell. In practice the spatial distribution was taken to be the one calculated by the HAMMER code for the MUFT group immediately above the resolved resonance region of ^{238}U.

The HAMMER code treated the Uranium isotopes in all annuli containing fuel as separate nuclides, preserving for each the region dependent group resonance reaction rates resulting from the OZMA calculations. The output of the HAMMER code was modified so that the reaction rate ratios of nuclides, for which the explicit resonance treatment was used, could be obtained separately for each annulus.

The hyperfine structure effects within the annuli containing fuel rods were estimated by Monte Carlo REPC[40] calculations into which an additional subroutine was introduced to handle the lattice unit cells with fuel clusters. This geometry routine is somewhat more time consuming than the one dealing with simple lattices or lattices with homogenised fuel annuli. However the most time consuming part of the calculation arises from the numerous collisions a neutron makes with the D_2O moderator compared with fuel collisions. In the resolved resonance region it is difficult to modify the neutron history in such a way

that the discrete neutron energies in the random walks are concentrated in energy intervals near the numerous resonance peaks. Biasing techniques are therefore not very fruitful, but even by using the simple weight reduction methods discussed previously in connection with the REPC code, reasonable overall estimates of resonance absorption in the fuel clusters can be obtained.

The UO_2 fuel rods in the cluster studied had UO_2 density of 10.45 gm/cc and weight fractions ^{235}U (0.00627267), ^{238}U (0.875230) and ^{16}O (0.118497). The Zirconium clad density was 6.55 gr/cc. The fuel, gap and clad outer radii were 0.7105, 0.7155 and 0.7609 cm respectively. Coolant and moderator atom densities were for D_2O of 99.67% purity and density 1.1053 gr/cc. The Aluminium pressure tube (inner radius 4.1275 cm, outer radius 4.3945 cm), and the Aluminium calandria tube (inner radius 5.08 cm, outer radius 5.222 cm), with density 2.699 gm/cc were homogenised with the gap between them into a single region. Apart from the central fuel rod, six further rods were located with their axes on a cylinder of 1.57915 cm radius, and twelve rods on a cylinder of 2.1533 cm radius. In the calculations the clusters were arranged in infinite arrays with five different pitches of 18, 21, 24, 28, 36 cm.

In the OZMA runs, in which the fuel bearing annuli and central fuel region were represented by a homogeneous mixture of fuel clad and coolant, results for the ^{238}U and ^{235}U resonance integrals were listed in the output between 3355 eV and 0.625 eV (MUFT groups 27-54). They are given in Tables XVI and XVII for subdivision of each fuel bearing region into two subregions, and for the integral transport mode. In the table, region 1 refers to the central rod and region 3 to the outer fuel annulus. Three subregions were used in the outer moderator for the tighter lattices ranging to ten for the largest pitch.

Table XVI

^{238}U Resonance Integrals for 19 UO_2 Rod Cluster in D_2O with D_2O Coolant for MUFT Groups 27 - 54 (3355 - 0.625 eV).

		Pitch				
		18	21	24	28	36
Region 1	OZMA	8.37	8.74	8.69	8.86	10.59
	REPC(Hom)	9.1±0.6		8.4±0.4		8.5±0.5
	REPC(Het)	9.4±0.6		8.8±0.5		9.3±0.5
Region 2	OZMA	9.64	9.46	9.43	9.59	11.40
	REPC(Hom)	9.9±0.2		9.8±0.2		8.7±0.3
	REPC(Het)	8.5±0.2		8.1±0.2		8.2±0.3
Region 3	OZMA	13.66	13.44	13.31	13.36	15.59
	REPC(Hom)	13.9±0.3		13.7±0.2		12.8±0.2
	REPC(Het)	11.7±0.3		11.3±0.2		11.1±0.2

Table XVII

^{235}U Resonance Integrals for 19 UO_2 Rod Cluster in D_2O with D_2O Coolant for MUFT Groups 27 - 54 (3355 - 0.625 eV).

		Pitch				
		18	21	24	28	36
Region 1	OZMA	266	261	248	248	297
	REPC(Hom)	267±20		262±14		253±16
	REPC(Het)	287±24		248±14		244±17
Region 2	OZMA	276	271	268	268	308
	REPC(Hom)	277±12		267±7		266±10
	REPC(Het)	230±6		230±9		228±11
Region 3	OZMA	304	298	295	293	334
	REPC(Hom)	308±7		302±6		283±7
	REPC(Het)	267±9		255±6		256±7

The table also shows corresponding REPC results for homogenised fuel bearing regions and for the case in which the hyperfine heterogeneity effect of rods in each annulus is taken into account.

In the OZMA results tabulated for I_{eff} the fuel disadvantage factor was taken into account by specifying a spatial flux distribution above the resolved resonance region. The REPC calculaitons were made before a procedure for specifying the spatial flux distribution above EMAX, the upper energy of the runs, had been introduced into the code. The OZMA results clearly show the effect of this distribution on the source into the resolved resonance region, since at the largest pitch the effective resonance integrals tend to increase. Such an increase is absent in the Monte Carlo results which based the source into the resolved resonance region on a flat asymptotic flux. As regards the accuracy of the Monte Carlo results it should be noted that for overall results such as the resonance escape probability good precision was attained (For the tightest lattice run with homogenised fuel annuli resulted in p = 0.7517 ± .0032, while the run with hyperfine structure led to p = 0.7835 ± .0028; with increasing pitch the corresponding results were 0.8692 ± 0.0019 and 0.9469 ± 0.0010 for the homogenised fuel annuli, and 0.8882 ± 0.0013, and 0.9526 ± 0.0007 for the cases with heterogeneity in the fuel annuli). On the other hand the accuracies of the I_{eff} values in different spatial regions and a narrower energy interval were poorer. Nevertheless they show the effect of hyperfine heterogeneity within the fuel bearing annuli, and an average ratio of the REPC (Het) to the REPC (Hom) results may be regarded as a reasonable correction to be applied to the OZMA reaction fractions to account for the additional shielding within the individual rods.

The results of applying these corrections to the HAMMER analysis with OZMA resonance reaction rates are shown in Table XVIII which also shows the uncorrected results. The values are compared with calculational results from the LATREP code[29] and with experiment. The reaction rate ratios are cluster averages. The calculated results for the different annuli containing fuel show about the same spatial variation as the experimental values.

The results for the effective multiplication factor, obtained with the experimental buckling show that there is a definite trend for k_{eff} to increase with increasing pitch when the fuel bearing annuli are treated as homogeneous mixtures. At low values of the pitch the k_{eff}'s are low and the ICR values high. This trend is eliminated when the hyperfine heterogeneity correction, obtained from the Monte Carlo estimates, is applied. These estimates have rather large probable errors and may exaggerate the corrections to some extent as evidenced by the low ICR and high k_{eff} values (compared with experiment). However, it appears reasonable to estimate hyperfine heterogeneity correction by Monte Carlo methods, provided the statistical fluctuations in the spatially dependent output can be reduced. The underestimate of the ν_{25} values is a consequence of the high energy basic data in the ENDF/B lbiraries and has also been noticed in other D_2O lattice calculations.

Table XVIII

Reaction Rates and k_{eff} for 19 Rod Natural UO_2 Clusters in D_2O

Pitch cm.	Item	OZMA/HAMMER uncorrected	OZMA/HAMMER corrected	LATREP	Experiment
18	ICR	1.0072	0.9485	0.9752	0.9669
	δ_{28}	0.0518	0.0503	0.0582	0.0564
	k_{eff}	0.9788	1.0064		1.0000
21	ICR	0.8768	0.8386	0.8610	0.8576
	δ_{28}	0.0479	0.0470	0.0547	0.0543
	k_{eff}	0.9898	1.0081		1.0000
24	ICR	0.8039	0.7764	0.7967	0.8054
	δ_{28}	0.0461	0.0455	0.0531	0.0528
	k_{eff}	0.9973	1.0105		1.0000
28	ICR	0.7518	0.7320	0.7476	0.7483
	δ_{28}	0.0451	0.0447	0.0522	0.0481
	k_{eff}	0.9990	1.0085		1.0000
36	ICR	0.7094	0.6955	0.7061	0.7082
	$\delta 28$	0.0446	0.0443	0.0517	0.0475
	k_{eff}	1.0021	1.0086		1.0000

Note: ICR = capture in ^{238}U/absorption in ^{235}U
δ_{28} = fission in ^{238}U/ fission in ^{235}U
corrected/uncorrected: allowing for/not allowing for hyperfine structure in fuel bearing annuli.

Finally it should be pointed out that the MUFT slowing down treatment for Deuterium is less precise than for Hydrogen since it is based, as previously discussed, on the Greuling Goertzel approximation. The application of the multigroup analysis methods with accurate resonance absorption treatements based on detailed resonance profile tabulations should therefore be regarded as rather preliminary. As far as these resonance absorption calculations are concerned there is a clear incentive to develop them further for lattices containing fuel clusters, without the necessity for Monte Carlo estimates of hyperfine heterogeneity effects.

Benchmark Analysis for Regular Lattices

Thermal reactor benchmark lattices specified in ENDF-202[52] were analysed a few years ago[53] with the OZMA/HAMMER and REPC/HAMMER code systems. In both the resonance reaction rates calculated by the first code were preserved during the multigroup lattice analysis made with the HAMMER code by the iterative procedure discussed previously.

The TRX-1 and TRX-2 lattices are H_2O moderated 1.3% enriched Uranium metal benchmarks with rods of 0.4915 cm outer radius in hexagonal arrays. The outer radii of the void and the Al clad are 0.5042 and 0.5753 cm, the pitch being 1.806 and 2.174 cm for the two lattices respectively. Atom densities are ^{235}U (6.253×10^{-4}), ^{238}U (4.7205×10^{-2}), Al (6.025×10^{-2}), H (0.06676×10^{-2}) and ^{16}O (0.03338). Experimental bucklings were 0.0057 cm^{-2} for TRX-1 and 0.005469 for TRX-2.

Table XIX shows the results obtained for k_{eff}, and the principal reaction rate ratios ρ_{28} (epithermal to thermal capture by ^{238}U), δ_{25} (epithermal to thermal fission of ^{235}U), δ_{28} (fissions of ^{238}U to fissions of ^{235}U), CR (captures by ^{238}U/fissions of ^{235}U). The TRX-1 results show the relatively small influence of P-1 scattering in the OZMA - S_6P_1 run, as may be seen by comparing δ_{28} with the value obtained for S_6P_0. On the other hand the integral transport OZMA-IT results predict a higher ρ_{28} which is still below the one resulting from the Nordheim integral treatment (NIT) of I_{eff} of the individual resonances.

Thus the accurate treatment of resonance absorption including resonance interference effects tends to reduce the ρ_{28} values. The fact that for all cases δ_{28} is in excess of the experimental value was interpreted as an indication that the basic ENDF/B-IV resonance data for ^{238}U tend to overestimate resonance absorption. The TRX-2 results show a similar trend. The calculated k_{eff} values were consistently below unit for the same reason. The experimental results were those obtained from a re-analysis of the original experiments by Sher and Fiarman[54].

Table XIX

TRX-1 Benchmark Lattice

	k_{eff}	ρ_{28}	ρ_{25}	δ_{28}	CR
Experiment	1.0000	1.320 ±0.021	0.0987 ±0.0010	0.0946 ±0.0041	0.797 ±0.008
NIT/HAMMER	0.9832	1.408	0.1052	0.0950	0.809
OZMA-IT/HAMMER	0.9854	1.384	0.0997	0.0948	0.805
OZMA-S6P0/HAMMER	0.9896	1.350	0.0984	0.0943	0.795
OZMA-S6P1/HAMMER	0.9906	1.343	0.0987	0.0942	0.792
REPC/HAMMER	0.9880	1.367	0.0994	0.0944	0.799

TRX-2 Benchmark Lattice

	k_{eff}	ρ_{28}	ρ_{25}	δ_{28}	CR
Experiment	1.0000	0.837 ±0.016	0.0614 ±0.0008	0.0693 ±0.0035	0.647 ±0.006
NIT/HAMMER	0.9885	0.873	0.642	0.669	0.648
OZMA-IT/HAMMER	0.9930	0.837	0.601	0.666	0.638
REPC/HAMMER	0.9921	0.846	0.612	0.666	0.640

The MIT-1, MIT-2, MIT-3 lattices are D_2O moderated natural Uranium arrays. In these the rods had 1.283 cm outer radius while the clad radius was 1.354 cm. The hexagonal lattice had pitches of 11.43, 12.70 and 14.605 cm respectively, the experimental bucklings being 8.48×10^{-4}, 8.65×10^{-4} and 8.15×10^{-4} cm^{-2} respectively. Atom densities were ^{235}U (3.441×10^{-4}), ^{238}U(4.745×10^{-2}), Al (6.049×10^{-2}), ^{1}H (1.850×10^{-4}), ^{2}H (6.641×10^{-2}), 16^{O} (3.321×10^{-2}).

Table XX gives the comparison of calculated and experimental results. As regards resonance absorption, the trends of ρ_{28} are similar to those obtained for the TRX lattices. The ^{238}U fast fission effect, δ_{28}, is somewhat underestimated in the calculations, a trend which is similar as that found in the case of the D_2O moderated fuel clusters.

Table XX

MIT - 1, 2, 3 Benchmark Lattices

		k_{eff}	ρ_{28}	δ_{25}	δ_{28}	Cr
MIT-1	Experiment	1.0000	0.502 ±0.010	0.0469 ±0.0019	0.0588 ±0.0030	1.017 ±0.023
	NIT/HAMMER	0.9826	0.530	0.0490	0.0573	0.982
	OZMA-IT/HAMMER	0.9924	0.487	0.0455	0.0566	0.958
	REPC/HAMMER	0.9905	0.500	0.0462	0.0579	0.965
MIT-2	Experiment	1.0000	0.400 ±0.004	0.0335 ±0.0030	0.0587 ±0.0030	0.948 ±0.020
	NIT/HAMMER	0.9833	0.434	0.0400	0.0556	0.926
	OZMA-IT/HAMMER	0.9909	0.402	0.0374	0.0551	0.908
	REPC/HAMMER	0.9897	0.411	0.0376	0.0562	0.913
MIT-3	Experiment	1.0000	0.313 ±0.005	0.0265 ±0.0011	0.0575 ±0.0030	0.859 ±0.016
	NIT/HAMMER	0.9862	0.338	0.0304	0.0540	0.869
	OZMA-IT/HAMMER	0.9918	0.314	0.0291	0.0536	0.855
	REPC/HAMMER	0.9921	0.316	0.0294	0.0546	0.856

Comparison of Group Fluxes and Resonance Cross Sections from Multigroup and Dense Energy Mesh Calculations for Identical Group Resonance Reaction Rates

The discussions presented here have emphasised the basic difference between multigroup calculations for smoothly varying cross sections, and the detailed evaluation of resonance reaction rates on a very fine energy mesh allowing for the spatial variation of resonance shielding and all resonance interference effects between resonances belonging to the same and to different nuclides. OZMA calculations are an example of the latter, HAMMER calculations of the former, in particular in the groups above the resolved resonance region. Even in the resonance region the HAMMER multigroup integral transport calculations at epithermal energies can be iterated to reproduce the OZMA group resonance reaction rates (absorption and fission) by changing the appropriate group cross sections.

It has been pointed out that when a lattice is analysed as above, there is no a priori reason that group fluxes, group cross sections and group disadvantage factors will be identical in the fine energy mesh and the multigroup calculations in the resonance region. In fact, the opposite is to be expected since the order of calculating averages is reversed in the two cases. In the fine energy mesh calculations the resonance cross sections at the energy mesh points are used to obtain slowing down sources and region to region transfer probabilities (which depend non linearly on the cross sections), if integral transport methods are used, or to solve the S_N equations, if the transport equation is solved by discrete ordinate methods. The resulting fluxes and cross sections are then group averaged. In multigroup lattice analysis codes group average cross sections are obtained first, usually by approximate methods in the resonance region, and for these the group fluxes are found; multiplication by the group average resonance cross sections gives the resonance reaction rates. But even if one forces the reaction rates to be identical in the two cases by iteratively changing the group resonance cross sections, the problem remains. One compares group fluxes obtained from average cross section instead of calculating the group average of fluxes obtained at discrete energy points from the point cross sections.

In Table XXI a comparison of this type is made. It refers to a simple BAPL 1.33 percent enriched UO_2 lattice with 0.4864 cm radius fuel pins in Aluminium cladding of radius 0.5753 cm, lattice pitch of 1.5578, and with the fuel arranged in a hexagonal array. The atom densities in the respective regions are: ^{235}U (0.0003112), ^{238}U (0.023127), ^{16}O (0.046946); ^{27}Al (0.04899); ^{1}H (0.06676), ^{16}O (0.03338). The results given in Table XXI refer to ENDF/B-V data, unlike the results in the previous tables which were all obtained with ENDF/B-IV as the basic data library.

For identical group reaction rates the OZMA (fine energy mesh integral transport) and HAMMER (multigroup integral transport) average cell fluxes are shown in the resonance energy groups together with fuel disadvantage factors

and the ^{238}U microscopic group cross sections which reproduce the OZMA reaction rates. There is good overall agreement, but in the principal resonance groups such as 45, 41 and 39 containing the 6.7 eV, 20.9 eV, and 36.7 eV resonance peaks of ^{238}U differences of a few percent are apparent.

Although in these comparisons the HAMMER code was not used with an approximate resonance treatment such as the Nordheim integral transport method for individual resonances, it is clear that comparisons of the above type can be utilised to correct such approximate treatments in addition to allowing for intrinsic differences between fine energy mesh and multigroup calculations.

Table XXI

HAMMER and OZMA Average Cell Fluxes, Disadvantage Factors, and Group Values of $^{28}_{a}$ in NB-1, for ENDF/B-V Data. (Allows for Fuel Disadvantage Factor in the Resolved Resonance Groups.)

NUFT Group	ϕ^C_H	ϕ^C_{OZ}	$(\phi^f/\phi^C)_H$	$(\phi^F/\phi^C)_{OZ}$	$(\sigma_a)_H$	$(\sigma_a)_{OZ}$
26	1.3319	1.3295	0.9953	0.9941	0.8668	0.8694
27	1.3071	1.3025	0.9945	0.9907	0.9816	0.9889
28	1.2900	1.2840	0.9943	0.9886	0.9594	0.9694
29	1.2703	1.2654	0.9927	0.9869	1.2244	1.2364
30	1.2535	1.2482	0.9919	0.9868	1.3194	1.3319
31	1.2438	1.2381	0.9927	0.9886	1.1338	1.1437
32	1.2177	1.2109	0.9874	0.9795	1.6870	1.7100
33	1.2146	1.2077	0.9912	0.9881	1.2297	1.2407
34	1.1615	1.1450	0.9693	0.9566	3.8525	3.9601
35	1.1759	1.1869	0.9862	0.9864	2.0725	2.0528
36	1.1450	1.1410	0.9757	0.9681	3.6239	3.6649
37	1.1793	1.1707	0.9927	0.9903	0.1392	0.1406
38	1.1577	1.1367	0.9873	0.9777	1.7791	1.8298
39	1.0297	1.0347	0.9083	0.9322	8.5819	8.3218
40	1.1273	1.1281	0.9880	0.9889	0.6807	0.6798
41	0.9489	0.9382	0.8972	0.8979	14.0611	14.2106
42	1.0899	1.0869	0.9896	0.9886	0.4496	0.4513
43	1.0905	1.0904	0.9905	0.9872	0.3396	0.3407
44	1.0740	1.0767	0.9868	0.9825	0.8542	0.8557
45	0.8566	0.87015	0.8924	0.8569	21.1801	21.7170
46	0.9348	0.9101	0.9566	0.9338	7.6610	8.0615
47	1.0142	1.0250	0.9920	0.9840	1.1281	1.1232
48	1.0236	1.0402	0.9932	0.9859	0.6174	0.6120
49	1.0328	1.0557	0.9959	0.9869	0.5050	0.4986
50	1.0351	1.0671	0.9955	0.9843	0.4739	0.4649
51	1.0416	1.0862	0.9960	0.9819	0.4787	0.4656
52	1.0407	1.1011	0.9934	0.9754	0.5031	0.4848
53	1.0437	1.1239	0.9912	0.9675	0.5452	0.5191
54	1.0614	1.1821	0.9920	0.9609	0.6169	0.5723
					21.980	22.239

The availability of fine energy mesh resonance absorption calculations for thermal reactor lattices is therefore of great value in assessing the adequacy of rapid resonance shielding algorithms in the resonance groups, and correcting them by means of group dependent correction factors. They will be to some extent nuclide and temperature dependent, and will be appropriate to a particular resonance shielding algorithm used in the multigroup code.

Conclusion

Multigroup analysis of reactor lattices requires separate procedures to handle the problem dependent resonance shielding within the individual energy groups. Codes in common use employ approximate methods for the evaluation of effective group cross sections, or resonance integrals, in the resonance reigon. A number of methods of this type have been reviewed and the approximations on which they are based have been emphasised.

Temperature effects do not depend only on the effectiveness of the resonance shielding calculations, but in particular also on the accuracy with which the temperature changes can be determined. The approximations inherent in the shielding algorithms may affect the temperature changes in a different way than the shielding factors themselves. For safety problems it is improtant that these questions be examined by sophisticated calculations in the resonance region.

Codes now exist which can evaluate the resonance reaction rates in thermal reactor lattices with considerable precision, completely in accordance with the recommended resonance formalisms and basic nuclear data, and with accurate Doppler broadening. These codes have been used for a number of types of benchmark problems, the results of which have been presented.

As regards using these detailed resonance absorption calculations as a means of testing the validity of commonly used rapid algorithms for the calculation of resonance shielding factors at different temperatures, and formulating appropriate correctiong factors, the following procedure could be used. It refers particularly to codes employing tabulated shielding factors as functions of a background cross section and temperature for each resonance nuclide.

a) The tabulations refer in general to homogeneous mixtures of the resonance absorber and different amounts of pure hydrogen as moderator.

b) The tabulations are used within the framework of a particular multigroup lattice analysis code, and a particular form of the equivalence relations between homogeneous and heterogeneous assemblies.

c) The parameters used in the equivalence relations should be identified and the methods to be used for this evaluation should be fixed. This applies for example to the Bell factor, the Dancoff factor and the intermediate resonance λ factor.

d) Appropriate benchmark lattice analyses should be made by the procedures outlined above, and repeated with the same multigroup lattice analysis, but with resonance reaction rates obtained from codes which calculate these quantities as accurately as possible by transport calculations using very dense energy grids. The multigroup calculations, which are to reproduce the accurately calculated resonance reaction rates, require an iterative procedure in the multigroup analysis code.

e) The group cross sections for the resonance nuclides for the two methods referred to in (c), above, will differ in general. Correction factors to the background cross sections and/or other factors referred to in (c), above, should be formulated so that the resonance shielding formalism used in the multigroup code will produce directly those group cross sections which will lead to resonance reaction rates in agreement with the ones obtained by sophisticated calculations.

f) The above correction factors will account for inaccuracies in the approximate resonance shielding factor calculations, and for intrinsic problems in the use of multigroup calculations in the resonance region. The correction factors for the individual energy groups may be problem dependent to a certain extent, and should be expressed in a suitable parametric form.

References

1. Beer, M., and Rose, P., (1981), "Implementation of the SAM-CE Monte Carlo Benchmark Analysis Capability for Validating Nuclear Data and Reactor Design Codes", EPRI NP-1791, Electric Power Research Institute, Ca.

2. Barhen, J., and Rothenstein, W., (1981), "OZMA - A Code to Calculate Resonance Reaction Rates in Reactor Lattices using Resonance Profile Tabulations", EPRI NP-926, Electric Power Research Institute, Ca.

3. ENDF-102, (1979), "Data Formats and Procedures for the Evaluated Nuclear Data File", ENDF, BNL-NCS-50496, National Nuclear Data Center, Brookhaven National Laboratory, N.Y.

4. Blatt, J.M., and Weisskopf, V.F., (1952), Theoretical Nuclear Physics, Chapter VIII, John Wiley & Sons, N.Y.

5. Cullen, D.E., (1979), "Program RECENT (Version 79-1): Reconstruction of Energy Dependent Neutron Cross Sections from Resonance Parameters in the ENDF/B Format", UCRL-50400, Vol. 17, Part C, Lawrence Livermore Laboratory.

6. Pearlstein, S., (1978), "The probability table method and correlated data", Nucl. Sci. Eng., 68, 10.

7. Ganesan, S., (1981), Private Communication, Reactor Research Centre, Kalpakkem, India.

8. O'Shea, D.M., and Thatcher, H., (1963), "Computation of resonance line shape functions", Trans. ANS, 6, 1, 36.

9. Ozer, O., (1973), "RESEND. A program to process ENDF/B materials with resonance files in point-wise form", BNL-17134, Brookhaven National Lab. See also ref. (5).

10. Hinman, G.W., Kuncir, G.F., Sampson, J.B., and West G.B., (1963), "Accurate doppler broadened absorption", Nucl. Sci. Eng., 16, 202.

11. Cullen, D.E., and Weisbin, C.R., (1976),"Exact Doppler broadening of tabulated cross sections", Nucl. Sci. Eng., 60, 199.

12. Cullen, D.E., (1977), "Program SIGMA1 (version 77-1): Doppler broaden evaluated cross-sections in the evaluated nuclear data file/version B (ENDF/B) format", UCRL-50400, Vol. 17, Part B, Lawrence Livermore Lab.

13. Cullen, D.E., (1977), "Program LINEAR (Version 77-1): Linearize data in the evaluated nuclear data file/ version B (ENDF/B) format", UCRL-50400, Vol. 17, Part A, Lawrence Livermore Laboratory.

14. Honeck, H.C., and Finch, D.R., (1971), "FLANGE-II, A Code to Process Thermal Neutron Data from an ENDF/B Tape", DP-1278, ENDF-152, Savanna River Laboratory.

15. Rothenstein, W., and Taviv, E., (1981), "Temperature Dependence of the Multiplication Factor in LWR Lattices", EPRI NP-1694, Electric Power Research Institute, Ca.

16. Weinber, A.M., and Wigner, E.P., (1958), The Physical Theory of Neutron Chain Reactors, Chapter X, University of Chicago Press.

17. Askew, J.R., Frayers, F.J., and Kemshell, P.B., (1966), "A general description of the lattice code WIMS", J. Br. nucl. Energy Soc. 5, 564.

18. Corngold, N., (1956), "Resonance escape probability in slab lattices", J. nucl. Energy I, 4, 293.

19. Case, K.M., de Hoffman, F., and Placzek, G., (1953), Introduction to the Theory of Neutron Diffusion, U.S. Government Printing Office.

20. Rothenstein, W., (1960), "Collision probabilities and resonance integrals for lattices", Nucl. Sci. Eng. 7, 162.

21. Dancoff, S.M., and Ginsberg, M., (1944), "Surface resonance absorption in a close-packed lattice", Manhattan Project Report CP-2157.

22. Levine, M.M., (1963), "Resonance Integral Calculations for U-238 Lattices", Nucl. Sci. Engng. 16, 271.

23. Leslie, D.C., Hill, J.G., and Jonsson, A., (1965), "Improvements to the Theory of Resonance Escape in Heterogeneous Fuel", Nucl. Sci. Eng. 22, 78.

24. Sauer, A., (1963) "Approximate escape probabilities", Nucl. Sci. Eng. 16, 329.

25. Watson, G.N., (1922), A Treatise on the Theory of Bessel Functions, Chapter 13, Cambridge University Press.

26. Bohr, H., Gillbard, E.M., and Ryan G.H., (1956), "MUFT-4, A Fast Neutron Spectrum Code", Report WAPD-TM-22. See also Ref. (31).

27. Joanou, G.D., and Dudek, J.S., (1961), "A Consisten P-1 Multigroup Code for the Calculaiton of the Fast Neutron Spectrum and Multigroup Constants", Report GA-1850.

28. Askew, J.R., (1966), "The Calculation of Resonance Captures in a Few Group Approximation", Report AEEW-R489. See also Ref. (17).

29. Phillys, G.J., Griffiths, J., (1976), "LATREP Users Manual", Report AECL-3857.

30. Ozer, O., (1981), Private Communication, Electric Power Research Institue, Ca.

31. Barhen, J., Rothenstein, W., and Taviv, E., (1978), "The HAMMER Code System", EPRI NP-565, Electric Power Research Institute, Ca.

32. Barry, R.F., (1963), "LEOPARD - A Spectrum Dependent Non-Spatial Depletion Code for the IBM-7094, Report WCAP-3269-26.

33. Strawbridge, L.E., and Barry, R.F., (1965), "Criticality Calculations for Uniform Water-Moderated Lattices", Nucl. Sci. Eng. 23, 58.

34. Brissenden, R.J., and Durston, C., (1965), "The Calculation of Neutron Spectra in the Doppler Region", Conference on the Application of Computing Methods to Reactor Problems, ANL 7050, p. 51.

35. Bell, G.J., (1959), "Theory of Effective Cross Sections", Report LA-2322.

36. Bonalumi, R., (1961), "Neutron First Collision Probabilities in Reactor Physics", Energia Nucl., Milano, 8, 326.

37. Jonsson, A. (1963), "THESEUS - A One Group Collision Probability Routine for Annular Systems", Report AEEW-R253.

38. Leslie, D.C., and Jonsson, A., (1964), "The Calculation of Collision Probabilities and Resonance Integrals in Cluster Type Fuel Elements", AEEW-R 384.

39. Halsall, M.J., (1967), "The Effective Surface Area of Fuel Clusters for Resonance Integral Calculations", AECL 2775.

40. Rothenstein, W., (1975), "Monte Carlo Code (REPC) to Calculate Resonance Reaction Rates in Thermal Reactor Lattice Benchmarks", BNL-20400, Brookhaven National Laboratory.

41. Davison, P., (1964), "The REPETITIOUS Code", Report WCAP-1434.

42. Nordheim, L.W., (1961), "The Theory of Resonance Absorption, Nuclear Reactor Theyory", Proc. Symposia in Applied Mathematics IX, 58; Kuncir, G.F., (1961), "A Program for the calculaiton of resonance integrals", GA 2525, General Atomic.

43. Buslik, A.J., (1974), Proton Chemical Binding in Water and its Effect on Neutron Absorption in the 1 eV Resonance of ^{240}Pu", Brookhaven National Laboratory, BNL-19411/RP-1035.

44. Kennedy, J.M., (1963), "Probability of escape from an annular region", Memorandum to A.G. Fowler, C.R.N.L. Atomic Energy of Canada.

45. Carlson, B.G., and Lathrop, K.D., (1968), Transport Theory - The Method of Discrete Ordinates, Computing Methods in Reactor Physics, p. 171, Gordon and Breach Science Publications, N.Y.

46. Engle, W.W., (1967), A Users Manual for ANISN, A One Dimension Discrete Ordinates Transport Code with Anisotropic Scattering, Union Carbide Corporation Nuclear Division, Mathematics and Computers, Report K1693.

47. Taviv, E. and Rothenstein, W., (1978), "Temperature Dependent Resonance Integrals using Resonance Profiles", Symposium on Nuclear Data Problems for Thermal Reactor Applications, paper 19, BNL-NCS-25047 (ENDF-270), Brookhaven National Laboratory.

48. Todosow, M.J., and Carew, J.F., (1977), "Evaluation of Temperature Dependent Resonance Integrals uning the HAMMER code", Trans. Am. Nucl. Soc. 27, 915.

49. Roth, M.J., (1974), "Resonance Absorption in Complicated Geometries", AEEW-R-921.

50. England, T.R., Wilson, W.B., and Stamatelatos, M.G., (1976), "Fission Product Data for Thermal Reactors, Parts 1 and 2", EPRI NP-356, Electric Power Research Institute, Ca.

51. Griffiths, J., (1971), "The Effectiveness of Latrep Calculations: A Survey and Detailed Comparison with Experiment", ORNL-407 (AECL-3739).

52. Cross-Section Evaluation Working Group; Benchmark Specifications, Thermal Benchmarks (1974), BNL 19302 (ENDF-202), National Neutron Cross-Section Center, Brookhaven National Laboratory.

53. Barhen, J., and Rothenstein, W., (1979), "Thermal Reactor Benchmark Calculations using Resonance Profiles", Symposium Proceedings: Nuclear Data Problems for Thermal Reactor Applications, p. 20-1, EPRI NP-1098, Electric Power Research Institute, Ca.

54. Sher, R., and Fiarman, S., (1976), "Studies of Thermal Reactor Benchmark Data Interpretation: Experimental Corrections", EPRI NP-209, Electric Power Research Institute, Ca.

55. Carlvik, I., (1967), "Integral Transport Theory in One Dimensional Geometries", Nukleonik, 10, 3, 104.

56. Rothenstein. W., Barhen, J., Taviv, E., Aminpour, M., (1982), "Resonance Shielding in Thermal Reactor Lattices", Annals of Nuclear Energy, 9, 141-168, (Pergamon Press).

INTRODUCTION TO THE CONTENT OF THE MAJOR AVAILABLE EVALUATED NUCLEAR DATA LIBRARIES

M. SALVATORES
Centre d'études nucléaires de Cadarache,
Saint-Paul-les-Durance, France

Abstract

The following notes were intended as complement to the main topic of the lectures presented at the Winter collge of Nuclear Physics and Reactors. Actually, the topic was covered according to the outline given in Appendix and the presentation was based as far as possible on the practical features of the basic data files, in particular the ENDF/B files. The present notes are subdivided in two parts; part I is a general introduction to the problem of the evaluated data files and gives the main references on the topic. Part II presents a few specific examples of the use of the evaluated data files in the wide application fields of neutron heating a photon production.

PART I

GENERAL REMARKS ON EVALUATED DATA FILES

- M. SALVATORES -

1 - INTRODUCTION

Many nuclear data evaluations has been published, which cover different process and field of application such as decay schemes, atomic masses and abundances fission product yields and neutron cross sections.

Neutron data related evaluation has rapidly developed due to the their relevance to nuclear power technology.

It is worthwhile to give a general definition of an evaluation of nuclear data. J. J. Schmidt has given /1/ the following ; "Evaluation denotes the comparison and critical assessment of the compiled experimental data and the selection by some appropriate averaging procedure of a complete and self-consistent set of preferred values. Much more than that, the requirement of completeness, particular for reactor physics purposes, involves the necessity of using appropriately parametrized Nuclear theories and considerations of nuclear systematics to fill in gaps and to help remove inconsistencies in the available experimental information".

As S. Perlstein has pointed out /2/, evaluations represent an attempt to estimate the true or most probable value of a nuclear parameter estimates are necessary since the number and quality of experiments have seldom been sufficient to converge toward results of high accuracy.

Historically, the nuclear data evaluation compilation in their present form (and in particular the neutron data compilations) have evolved from early collection of nuclear data, such as the General Electric Chart of Nuclides, first produced about 1947 and modeled after Seaborg tables of isotopes (originally published in the Revue of Modern Physics in 1940). The Nuclear Data Tables, published originally by the National Bureau of Standard in the USA in 1950, provides, with its more recent updating, another example of Nuclear Data compilation. However, for what concerns neutron data, the "Neutron Cross Section publication of the Brookhaven National Laboratory (BNL-325), originally published in 1955 by D.M Hughes and J. A. Harvey and successively updated /3/ ; is the actual ancestor of the present computerized compilations.

It presents in tabular and graphic form experimental neutron cross section data and an eye guide which represents the probable trend of the data.

It was early recognized that coordinated and cooperative efforts were a key point in the development of large and consistent data base for nuclear power application purposes.

Nuclear data centers developed ; the National Neutron Cross Section Center at Brockhaven, wich collects data in the USA and in Canada ; the NEA Data Bank located in Saclay Laboratory near Paris collects data for the countries partecipating to the Nuclear Energy Agency ; the Nuclear Data Section of the International Atomic Energy Agency ; the Nuclear Data Section at the Institute of Power and Engineering of Obnisk (USSR).

From these and other centers, data files were developed in particular for reactor core and shield design, and for nuclear fuel cycle evaluation.

The advancement of computer technology, coupled to the increasing availability of detailed evaluations, made possible the processing of evaluated nuclear data into computerized data files. Specific formats were developed, flexible enough to handle many types of data and mathematical models, but sufficiently compact so as to remain efficient for computer manipulation.

An important role was also played by the development of sophisticated ways of data and format documentation, necessary for the linking of evaluated data files to processing codes for the preparation and performance of nuclear calculation.

At least four major data files have developed during the last fifteen years :

- The United Kingdom Nuclear Data Library (UKNDL)

- The Karlsruhe evaluated nuclear data file (KEDAK)

- The Evaluated Nuclear Data File in the USA (ENDF)

- The USSR Evaluated Nuclear Data Library and the associated SOKRATOR format /7/

It is worth mentioning that very recently a joint effort has been imitated by many of the OECD countries to establish a Japanese-Europeen File, in the framework of the NEA Data Bank (JEF).

2 - THE EVALUATED NUCLEAR DATA FILE CONTENT

For what concerns the representation of data, in general it can be said, according to /2/, that the specification of data must be complete ; a single-valued function over the entire range of the independent variable must result . Data may be presented in either parametric or tabulated form. If tabulated values are given, an interpolation scheme must be provided to determine values between tabulated point. In some cases a variety of interpolation schemes are allowed. For common data types, a constant, linear, or logarithmic interpolation can be used.

Some flexibility in formats is needed for specifying data. As a typical example, angular distributions can be described by Legendre polynomials (light nuclei) or in a tabular form (heavy nuclei), to avoid the use of Legendre or polynomials of large order.

In general, if we speak of neutron data files, the following informations should be found in a data file useful for many purposes:

- Cross section tables for smooth cross-sections, or the smooth part of the cross section behaviour in energy ; charged particle or gas production cross-section (like (n,p), (n,d), (n,t), (n,α) etc)

- Resonance parameters for the resolved and unresolved resonance regions

- Angular distributions

- Secondary neutron energy distributions

- Scattering law data

- Fission parameters (neutron multiplicity, fission, fragment yields)

- Radioactive decaydata (Types of decay, half-lives, decay constants, branching ratios, line intensities)

- Photon production by neutron reactions (photon production cross sections, photon angular distributions, photon energy spectra, photon energy-angle distributions)

- Data uncertainties, necessary to construct variance-covariance matrices.

These informations should be provided by isotope and for an energy range from approximately 20 MeV to thermal neutron energy. In particular, the very high energy data are particularly needed for future fusion reactor applications.

3 - EXEMPLES OF EVALUATED NUCLEAR DATA FILES

The present notes will not present explicitely the basic data formats and procedures, even if they are essential to the course.

The existing literature, already indicated in the previous paragraph, is largely accessible and complete. In particular the Report ENDF-102, Revision 1979 is the necessary basis for discussions related to the widely used ENDF/B Format. A summary of the main features of the different data files can be found in the paper by G. C. PANINI "Some notes about the nuclear data libraries" distributed at the present Winter College on Nuclear Physics and Reactors.

REFERENCES

/1/ J. J. Schmidt, CODATA - Newsletter No.3 (1969)

/2/ S. Pearlstein, in Adwances in Nucl. Sci. and Techniology, Academic Press (1975)

/3/ D. J. Hughes and J. A. Harvey "Neutron Cross Sections" BNL - 325 (1955 and foll.)

/4/ K. Parker, AWRE - O - 70/63

/5/ J. J. Schmidt KFK - 120 (1962) and B. Krieg KFK - 2387 (1977)

/6/ M. K. Drake ed. , BNL - 50274

/7/ V. E. Kolesov and M. N. Nikolaev INDC (CCP) - 13/1 (1970)

PART II

THE RELATION BETWEEN DATA FILES AND PHYSICS PROBLEMS - SELECTED EXEMPLES

EXEMPLES OF USE OF THE DATA INCLUDED IN AN EVALUATED DATA FILE

Nuclear heating

A major part of the neutronics and photonics analyses of a nuclear system involves estimating a set of nuclear response rates such as nuclear heating, gas production and atomic displacement rates. The response rates provide an important input to the engineering design and analysis of the system.

These type of responses are calculated from a variety of nuclear data, which appropriately illustrate the use of an evaluated data file.

Let us consider the nuclear heating, commonly known as KERMA (Kinetic energy released to material) factor. The nuclear heating $H_t(\bar{r})$ at a spatial point $\bar{r}$, is the sum of the neutron heating $H_n(\bar{r})$, and the gamma heating, $H_\gamma(\bar{r})$ where :

$$H_n(\bar{r}) = \sum_j N_j(\bar{r}) \int \phi_n(\bar{r}, E_n)\, K_{nj}(E_n)\, dE_n \quad (1)$$

$$H_\gamma(\bar{r}) = \sum_j N_j(\bar{r}) \int \phi_\gamma(\bar{r}, E_\gamma)\, K_{\gamma j}(E_\gamma)\, dE_\gamma \quad (2)$$

and where $N_j(r)$ is the number density of nuclide j at $\bar{r}$, $K_{nj}(E_n)$ is the response function for nuclear heating known as the neutron Kerma factor for nuclide j at energy E_n ; $K_{\gamma j}$ is the gamma ray Kerma factor for nuclide j at photon energy E_γ; $\phi_n(E_n)$ is neutron flux for neutron at energy E_n; $\phi_\gamma(E_\gamma)$ is obtained by solving the transport equation for the photons, starting from a photon production source :

$$S_\gamma(\bar{r}, E_\gamma) = \sum_j N_j \int \phi_n(E_n, \bar{r})\, \sigma_{pj}(E_n, E_\gamma)\, dE_j \quad (3)$$

where σ_{pj} is the photon production cross section in nuclide j for neutrons of energy E_n and photons of energy E_γ.

The neutron Kerma factor can be written as :

$$K_{nj}(E) = \sigma_{tj}(E) \cdot \Big(E + \sum_i \frac{\sigma_{ij}}{\sigma_{tj}} Q_{ij} + \sum_{i'} \frac{\sigma_{i'j}}{\sigma_{tj}} E_{di'j} - \sum_m \frac{\sigma_{mj}}{\sigma_{tj}} E_{n',mj} - \frac{1}{\sigma_{tj}} S^*_{E\gamma,j}\Big) \quad (4)$$

where σ_t is the total cross section, Q_{ij} is the Q value of the reaction i with isotope j, defined as the difference in mass between the total mass of the reaction products and that of the neutrons plus the target nucleus j ; E_{di}, is the average decay energy per reaction i ; $E_{n',m}$ is the average secondary neutron energy per reaction m.

Finally $S^*_{E\gamma,j}$ is given by :

$$S^*_{E\gamma j}(E_n) = \int \sigma_{pj}(E_n, E_\gamma)\, E_\gamma\, dE_\gamma \quad (5)$$

where $\sigma_{pj}(E_n, E_\gamma)$ is the previously defined photon production cross-section for neutron energy E_n and photon energy E_γ.

The expression for gamma Kerma factor can be written as :

$$K_{\gamma j}(E) = \sigma_{pe,j} \cdot E + \sigma_{ca,j} \cdot E + \sigma_{pp,j}(E - 1.02) \quad (6)$$

where σ_{pe}, σ_{ca} and σ_{pp} are the gamma-interaction cross section for photoelectric, Compton absorption, and pair production cross sections, respectively.

The ENDF/B data files necessary to the calculation are indicated in table I.

For a better understanding of the use of the date included in the file, we will develop the explicit form of the neutron Kerma for a specific reactions.As we have seen, the Kerma for a specific reaction i is give in general by :

$$K_n(E) = \Sigma K_{ni}(E) \quad (7)$$

$$K_{ni}(E) = \sigma_i(E) E_{Hi}(E) \quad (8)$$

where we have dropped the index j of isotope dependant and E_{H_i} is the sum of the Kinetic energies of the recoil nucleus and charged particles produced by the reaction.

In general :

$$E_{Hi} = E + Q_i - E_{n'i} - E_{\gamma i} + E_{Di} \quad (9)$$

where the different values have already been defined and E_γ is the total energy carried away with the gamma rays emitted.

ENDF/B files necessary for KERMA factors calculations.

TABLE I

File No (MF)	Type of Data
1	General information
2	Resonance parameter data
3	Neutron cross sections
4	Angular distribution of secondary neutrons
5	Energy distribution of secondary neutrons
12	Multiplicities for photons (from neutron reactions)
13	Cross sections for photon production (from neutron reactions)
15	Energy distribution of photons (from neutron reactions)

The reaction types that have to be treated are listed in table II.

To calculate the neutron Kerma factors one then needs the reaction cross sections, the Q-values and the energies of the secondary neutrons and photons.

TABLE II

Reaction Types

	Reaction Types	ENDF/B Reaction No., MT
(n,n)	Elastic	2
(n,n')γ	Inelastic level	51-90
(n,n')γ	Inelastic continuum	91
(n,mn')a_{c1}, a_{c2},...	(n,mn', charged particles), m = 1 or 2	22-24, 28-30, 32-36, and 51-91 with flag LR
(n)a_{c1}, a_{c2}, a_{c3}...	(n, charged particles)	103-109 (700-799), 111-114
(n,γ)	Radiative capture	102
(n,2n)	Direct or level (n,2n)	16 and (6-9, 46-49)
(n,3n)	(n,3n)	17
(n,f)	Fission	18

The pointwise cross sections are processed from file 3 in ENDF/B and, for resonance nuclides, are calculated in the resolved and unresolved resonance regions from resonance parameters in file 2. The Q - Values are processed from file 3.

The average kinetic energy of all secondary neutrons is calculated from the angular distributions in file 4 for elastic and inelastic level scattering and from the energy distribution given in file 5 of ENDF/B for other reactions.

The calculation of the energy of the secondary photons is made evaluating $S_{E\gamma}$ performing the integration previously indicated eq. (5), once the gamma production cross section have been processed from files 12, 13 ans 15.

The equation to calculate explicitely eq (8) are given in the following paragraph.

NEUTRON KERMA FACTORS CALCULATION AND THEIR RELATION WITH BASIC DATA

Elastic Scattering

For elastic scattering, all terms on the right-hand side of Eq. (9) are zero except the incident neutron energy and the kinetic energy of the neutron emitted. The latter is simply

$$\bar{E}_{n'} = E \frac{A^2 + 1 + 2A\bar{\mu}_{cm}}{(A+1)^2}, \qquad (10)$$

where A is the ratio of the nuclear mass of the nuclide to that of the neutron and $\bar{\mu}$ is the average ot the cosine of the center-of-mass scattering angle,

$$\bar{\mu}_{cm} = \overline{\cos\ \theta_{cm}}$$

and (11)

$$\bar{\mu} = f_1 ,$$

with f_1 as the first coefficient of the Legendre polynomial expansion of the differential scattering probability distribution ($f_o = 1$).

Inelastic-Level scattering

For inelastic-level scattering $(n,n')\gamma$, Q = O, and $\bar{E}_{n'}$ and $\bar{E}\gamma$ are derived as follows :

$$E_{n'}(E) = \frac{2AE}{(A+1)^2}\left[\frac{A^2+1}{2A} - \frac{A+1}{2E}\cdot E_\lambda + \left(1 - \frac{A+1}{A}\frac{E_\gamma}{\bar{E}\gamma}\right)^{1/2}\bar{\mu}_{cm}\right] \qquad (12)$$

where

E_λ = energy of the excited level

$\bar{\mu}_{cm} = \overline{\cos\ \theta_{cm}}$

The average of the cosine of the scattering angle in the center-mass is evaluated from the secondary neutron angular distribution in file 4 of ENDF/B. This angular distribution can be given in either

(1) Legendre coefficients in the center-of-mass (CM) system ;

(2) tabulated normalized probability distribution in the CM, $P_{cm}(\mu,E)$;

(3) Legendre coefficients in the laboratory (LAB) system, and

(4) tabulated normalized probability distribution in the LAB system, $P_{LAB}(\mu,E)$.

For case (1), $\bar{\mu}_{cmy}$ is equal to the first coefficient (f_1) of the Legendre polynomial expansion ($f_o = 1$). In case (2),

$$\mu_{cm}(E) = \int_{-1}^{+1} \mu P_{cm}(\mu,E)\, d\mu . \qquad (13)$$

For cases (3) and (4) a transformation from the LAB to the CM system is performed and μ_{cm} is calculated.

Another procedure is to replace Eq. (12) with the following :

$$E_{n'}(E) = E\left\{\frac{1}{A+1}\bar{\mu}_L + \left[\frac{A-1}{A+1} + \frac{1}{(A+1)^2}\bar{\mu}^2_L - \frac{A}{A+1}\frac{E_\lambda}{E}\right]\right\}^2 , \quad (14)$$

where μ_1 is the cosine of the LAB scattering angle. $\bar{\mu_1}$ can be evaluated as the first coefficient of the Legendre polynomial expansion in the LAB system or from $P_{LAB}(\mu,E)$ as in Eq. (13). $\bar{\mu^2_L}$ can be evaluated as follows :

$$\bar{\mu^2_L} = \frac{1}{3}(1 + 2f_2) , \quad (15)$$

where f_2 is the second coefficient of the Legendre polynomial expansion in the LAB system. For case (4),

$$\bar{\mu^2_L} = \int_{-1}^{+1} \mu^2 p_{LAB}(\mu,E)\, d\mu. \quad (16)$$

The gamma energy is calculated directly from the ENDF/B gamma production files for Path I. In Path II, it is given by

$$\bar{E}_\gamma = \frac{1}{1 + C_F} E_\lambda , \quad (17)$$

C_F = internal conversion factor

Inelastic Scattering, (n,n')γ to the Continuum

In this case Q = O. The average kinetic energy for the secondary neutron is calculated from the secondary neutron energy distribution in file 5 of ENDF/B.

This energy distribution, $P(E \to E')$, can be broken down into partial energy distribution, $f_k(E \to E')$, where each of the partial distributions can be described by a different analytic representation :

$$P(E \to E') = \sum_{k=1}^{NK} P_k(E) f_k(E \to E'),$$

and at a particular incident neutron energy E,

$$\sum_{k=1}^{NK} P_k(E) = 1 .$$

The ENDF format allows several analytic formulations for the partial energy distributions, $f_k(E \to E')$.

An expression for $\bar{E}_{n'}$, is evaluated as follows :

$$\bar{E}_{n'}(E) = \frac{\int_{E'_{min}}^{E'_{max}} E' P(E \to E')\, dE'}{\int_{E_{min}}^{E'_{max}} P(E \to E')\, dE'}$$

$$= \sum_{k=1}^{NK} P_k(E) \int_{E'_{min}}^{E'_{max}} E' f_k(E \to E')\, dE'$$

$$= \sum_{k=1}^{NK} P_k(E) \bar{E}_{n',k} . \quad (18)$$

The analytic form of $\bar{E}_{n',k}$ depends on the analytic formulation of f_k (E → E').

For the evaporation spectrum

$$f(E \rightarrow E') = \frac{E'}{I} \exp\left[-E'/\theta\ (E)\right] ,$$

where I is a normalization constant that depends on E'_{min}, E'_{max}, and θ. The ENDF assumes that $E'_{min} = 0$. Using this assumption, we obtain

$$\bar{E}_{n',k} = \theta \frac{2\exp(x_1) - [1 + (1 + x_1)^2]}{\exp(x_1) - (1 + x_1)} , \quad (19)$$

where

$$x_1 = \frac{E'_{max}}{\theta} .$$

For a simple fission spectrum (Maxwellian),

$$f(E \rightarrow E') = \frac{\sqrt{E'}}{I} \exp\left[-E'/\theta\ (E)\right] , \quad (20)$$

and by invoking the assumption that $E'_{min} = 0$, we obtain

$$\bar{E}_{n',k} = \theta \left\{ \frac{3}{2} - \frac{x_1^{3/2}}{\left[(\sqrt{\pi}/2)\exp(x_1)\,\mathrm{erf}(\sqrt{x_1}) - \sqrt{x_1}\right]} \right\} \quad (21)$$

A similar expression can be derived for the Watt spectrum. For the other allowable representations of $f_k(E \rightarrow E')$, $\bar{E}_n$, can be obtained by numerical integration in Eq. (18). $\bar{E}_\gamma$ can be evaluated directly from the gamma energy distribution in Path I. In Path II, applying the equations for conserving linear momentum and energy balance and assuming that neutrons are emitted isotropically in the center-of-mass system, one can derive the following expression for the average excitation energy, ε, of the residual nucleus following the emission of the neutron,

$$\bar{\varepsilon} = \frac{A^2 + 1}{A(A + 1)} E - \frac{A + 1}{A} \bar{E}_{n'} . \quad (22)$$

$\bar{E}_\gamma$ is equal to $\bar{\varepsilon}$ unless internal conversion is significant in which case

$$\bar{E}_\gamma = \frac{1}{1 + C_F} \bar{\varepsilon} \quad (23)$$

(n,2n) Reaction

The (n,2n) reaction can currently be represented in ENDF/B as direct (n,2n) (MT = 16) and/or as a time-sequential reaction (MT = 6-9; 46-49). In the time-sequential (n,2n) reaction, $A(n,n_1)\ A^*\ (n_2)\ (A - 1)^*$, the first neutron is essentially an inelastic scattering event that may leave the nucleus A* in one of several excited states. The second neutron is subsequently emitted by the decay of the recoiling nucleus A*. The kerma factor for the (n, 2n) reaction is obtained by summing the contribution from the direct and each sequence (defined by an excited level of A*) of the time-sequential reactions.

For direct- and time-sequential (n,2n), Eq . (9) is applicable with the Q-value as the binding energy B, of the last neutron in the target nucleus and $\bar{E}_n$, as the average of the sum of the kinetic energies of the two neutrons. For the direct (n,2n) (MT = 16), $\bar{E}_n$, can be evaluated from the secondary neutron energy distribution given in file 5 of ENDF/B as described under inelastic scattering to continuum. For each of the time-sequential reaction, the energy of the excited level in A* is known and the average kinetic energy of the first neutron is calculated from the angular distribution in file 4 of ENDF/B according to Eq. (12). The average kinetic energy of the second neutron is calculated from the energy distribution in file 5 of ENDF/B.

If the direct gamma-production path is not selected, the average energy of the photon emitted [E_γ in Eq. (9)] can be calculated from momentum and energy balance. The results are different for direct(n, 2n), assuming isotropic emission in the center-of-mass, the excitation energy of the residual nucleus is given by [in the direct (n,2n) the time interval between the emission of the two neutrons is so short that the intermediate nucleus A* does not deposit any of its recoil energy prior to the second neutron emission]

$$\bar{\epsilon}_{A-1} = \frac{A^2+2}{A(A+1)} E - \frac{1}{A-1}\left[\frac{A^2-2}{A}\ \bar{E}_{n'1} + A\,\bar{E}_{n'2}\right] - B \quad . \quad (24)$$

where $\bar{E}_{n'1}$ and $\bar{E}_{n'2}$ are the average energies of the first ans second neutrons. At present, ENDF/B provides only the combined spectrum of the two neutrons ; and therefore evaluating Eq. (24) requires invoking the assumption that $A^2 >> 2$.

For a sequence (e.g. MT = 6 and 46) in a time-sequential (n,2n) reaction, it is assumed that the intermediate nucleus A* comes to rest prior to emission of the second neutron. Thus, the excitation energy of the residual nucleus is given by

$$\bar{\epsilon}_{A-1} = E_\lambda - B - \frac{A}{A-1}\,\bar{E}_{n2}, \quad (25)$$

where E_λ is the energy of the excited level in A* and $\bar{E}_{n2}$ is the average energy of the second neutron.

(n,3n) Reaction

Equation (9) applies here with the Q as the Q-value of the (n,3n) reaction and $\bar{E}_n$, as the average of the sum of the kinetic energies of the three neutrons. The latter is calculated from the secondary neuton energy distribution. The energy of the photons emitted is calculated in the indirect gamma-production path from the excitation energy of the residual nucleus. This can be calculated by applying linear momentum and energy balance. For direct (n,3n) the time interval between neutron emissions can be assumed to be extremely short. Assuming isotropic neutron emission in the center-of-mass system, the excitation energy of the residual nucleus can be derived as

$$\bar{\epsilon}_{A-2} = \frac{A^2+3}{A(A+1)} E + Q_{n3n} -$$

$$-\left[\frac{A^2-3}{A(A-1)}\,\bar{E}_{n1} + \frac{A^2-2A-1}{(A-1)(A-2)}\,\bar{E}_{n2} + \frac{A-1}{A-2}\,\bar{E}_{n3}\right], \quad (26)$$

where Q_{n3n} is the Q-Value of the (n,3n) reaction (always negative) and E_{n1}, E_{n2}, and E_{n3} are the average kinetic energies of the first, second, and third neutrons. Since ENDF/B provides only the combined spectrum for the three neutrons, invoking the assumption that A >> 1 is necessary for evaluating the above expression.

Radiative Capture

In an (n,γ) reaction, conservation of linear momentum causes the kinetic energy of the residual nucleus to be very small ; in general ; only a fraction of 1% of the energy of the emitted photons. The energy E_γ of the photons emitted can be derived as

$$\bar{E}_\gamma = M_r C^2 \left\{ \sqrt{1 + \frac{2}{M_r C^2}\left[Q + E\left(1 - \frac{m_n}{M_r}\right)\right]} - 1 \right\} \quad (27)$$

The recoil energy of the nucleus, E_r, is

$$\bar{E}_r = E + Q - \bar{E}_\gamma \ , \quad (28)$$

where

Q = the reaction Q-value

$M_r C^2$ = mass of the residual nucleus in energy units

$M_r C^2 = (A + 1) m_n C^2 - Q$

$m_n C^2$ = energy equivalent of the neutron mass (939.512 MeV)

Charged Particle Reactions

The reaction discussed here is of the type

$$Z_1 X^{A_1} (n; a_{c_1} a_{c_2} \ldots a_{c_n}) Z_2 Y^{A_2} \ ,$$

where a_{c1}, a_{c2} ... are charged particles, e.g. (n,α),(n,p), (n,αT). The energy deposited, E_H per reaction as defined in Eq. (9), is the sum of the kinetic energies of the recoil nucleus and charged particles emitted, i.e.

$$E_H = E_r + E_{a_{c1}} + E_{a_{c2}} + \ldots + E_{a_{c_n}} = E + Q - \bar{E}_\gamma \quad (29)$$

where Q is the reaction Q-value (mass difference) and E_γ is the average energy emitted with the photons. The residual nucleus is frequently left in one of the excited states. If we define the cross section for the i-th excited state as σ is

$$\sigma = \sum_{i=o}^{N} \sigma_i \quad (30)$$

and the total kerma factor for the reaction is

$$k = c\left[E + Q - \bar{E}_\gamma + \bar{E}_D\right] , \quad (31)$$

where

$$\bar{E}_\gamma = \sum_{i=o}^{N} P_i \varepsilon_i \ , \quad (32)$$

$$\bar{E}_D = \sum_{i=o}^{N} P_i E_{Di} \ ; \quad (33)$$

ε_i = energy of the i-th level ($\varepsilon_o = o$)

E_{Di} = contribution to energy deposition by radioactive decay of the i-th level

P_i = probability that the i-th level will be excited given that a reaction has occurred (σ_i/σ).

If other processes compete with gamma emission (e.g. internal conversion), the ε_i's in the above expressions should be adjusted.

The reaction total cross section and Q-value for (n, charged particle) reactions are given in ENDF/B with MT = 103-107. The corresponding partial cross sections to various excited states are given in the MT = 700-799 series. For many materials, however, the 700's series data are not given. In such cases (and for MT = 108-114), there is presently no method to calculate $\bar{E}_\gamma$ in Eq. (32) for the limited information given in files 1-5. This is the basic disadvantage of the indirect gamma-production path. The newly proposed format for including the energy distribution of the charged particles can help solve this problem. In pratice, however, data on gamma-production and charged-particle energy are both either lacking or both are known.

(n,n') Charged Particles

This reaction is generally of the form

$$ {}_{Z1}X^{A1}\ (n,n')\ a_{c1},\ a_{c2}\ ,\ \ldots\ a_{c_n}\ ,\ {}_{Z2}Y^{A2} $$

The energy deposition per reaction E_H is the sum of the kinetic energies of the recoil nucleus and charged particle emitted and its calculation from Eq. (9) depends on the type of data available.

In ENDF/B, some of these (n,n') charged particle reactions are represented in the format of inelastic level scattering, (n,n'x) (MT = 51-90) with an LR flag to define the exact type of the reaction. For such type of reaction, two Q-values are given ; SQ is the Q-value for the combined (n,n'x) reaction and Q' is the energy of the excited level for the (n,n') part of the reaction. The energy of the secondary neutron can thus be evaluated from Eq. (12) with $E_\gamma = |Q'|$ and the angular distribution of the secondary neutron in file 4. Threfore, with this type of format the (n,n') charged praticle reaction can be treated as inelastic level scattering except for the following differences : (1) the Q-value for the reaction is SQ instead of zero ; and (2) the energy available to the gamma rays in inelastic level scattering are taken by the charged particles and deposited locally.

The flags LR = 39 and LR = 40 are also used in ENDF/B to indicate that the final mode of decay of the residual nucleus from an (n,n') reaction is by internal conversion (LR = 39) or by electron-positron pair formation (LR = 40). These two cases are treated similar to the (n,n') charged particle reactions except that 1.02 MeV of energy is carried away with photons in the case of the electron-positron formation mode and is not available for local energy deposition.

The (n,n') charged particle reactions can also be given in ENDF/B as direct (composite) reactions (e.g. MT = 22, 23, etc.). Also, this is always the case for the (n,2n) charged particle reactions (e.g. MT = 24). In these cases, the average energy of the secondary neutron [Eq. (9)] is calculated from the energy distribution of file 5. The information in the neutronics files (1-5), however, is not sufficient to calculate the energy carried away with the emitted gamma rays. This difficulty is similar to that discussed earlier for the (n, charged particles) reactions.

An example of ambiguity in data processing

A serious ambiguity was found in the processing of the ENDF/B data necessary to prepare photon-production cross-sections, mainly in the processing of continuous energy spectra, which are expressed, as we have seen, in ENDF/B as normalized probability distribution $g(E_\gamma \leftarrow E_i)$ at selected neutron energies E_i.

Actually, different methods for interpolating can be used to determine the photon spectra at intermediate neutron energies. The problem is illustrated in the two following figures :

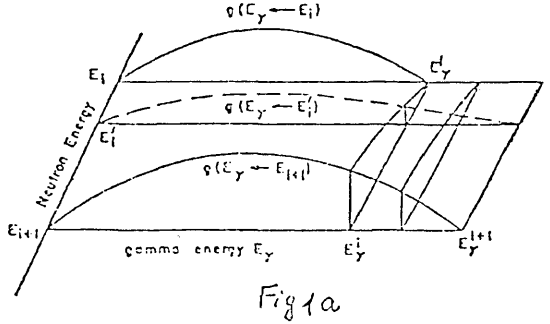

Fig 1a

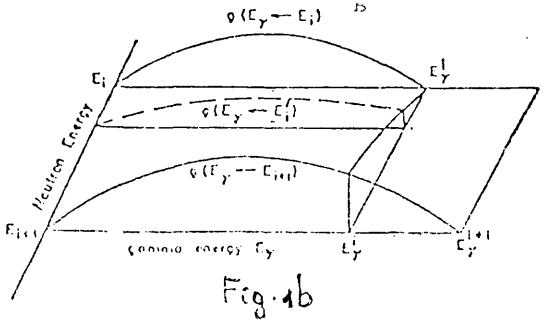

Fig 1b

At the lower energy E_i, the photon end-point energy is E_γ^i ; at the higher neutron energy E_{i+1}, the photon endpoint energy is E^{i+1}- At the intermediate neutron energy E'_i are possible interpolation (fig 1a) is such as to give photon yields (dashed line) for photon energies up to E_γ^{i+1} , whereas the second interpolation method (fig 1b) gives photon yields only up to an energy of E_γ. Because the resulting intermediate distributions are normalized, the interpolation method of fig 1a, gives more photons in high energy groups, and the method of fig 1b gives fewer photons in the same energy groups.

A further source of difficulty withe the normalized probability distributions is the use of this format to represent discrete photons. The following fig. 2 depicts the spectrum for MT = 102 in fluorine.

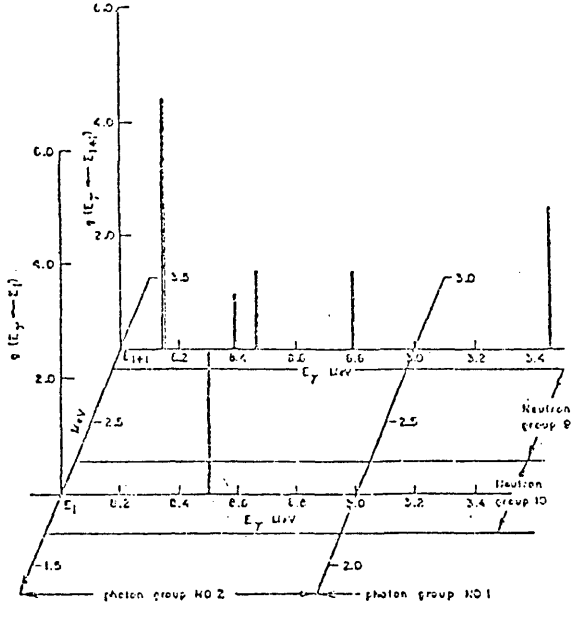

Fig2 Representative normalized probability distribution functions $g(E_\gamma \leftarrow E_i)$ for fluorine (MAT1277, MT102).

Differences in the approach to interpolation, described above, can lead to a discrepancy in a group representation of photon production cross section, of 13% in photon production from neutron group 9 to photon group 2 and 100% from neutron group 9 to photon group 1. These discrepancies demonstrate the difficulties that can result from the use of file 15 to represent discrete photons.

APPENDIX

OUTLINE OF THE LECTURES ON THE TOPIC

"INTRODUCTION INTO THE CONTENTS OF THE MAJOR AVAILABLE EVALUATED NUCLEAR DATA LIBRARIES".

-oOo-

1 - INTRODUCTORY REMARKS

. Review of the areas of application of nuclear data for reactors.

This review will be mainly devoted to fission reactors, (reactor physics problems, shielding, biological protection, etc...), and fuel cycle (decay heat, activation, etc...).

. Review of the main type of reactions, energy ranges and isotopes of interest. Graphical examples.

. The problem of extracting "evaluated data" from experimental information to feed a "data bank".

. Two alternatives : pointwise representation of data and parameters to be used in connection with models.

. Main types of data files : ENDF/B, KEDAK, UKNDL, etc... Comparison of main features.

. A major example : ENDF/B - Structure of files and formats.

. Computer related problems.

2 - TYPICAL CONTENT OF THE DATA FILES - THE "POINTWISE" DATA AND THE RESONANCE REGION DATA.

. The "pointwise" data representation. Main examples total cross-sections, charged particle reactions, etc... Interpolation schemes.

. Resonance region. The resolved resonance region :

- basic formulae for parametric representation ;
- what parameters needed ;
- conservation laws or internal consistency rules ;
- typical values (examples) ;
- how they are arranged in a file (ENDF/B format) ;
- type of problems where these data are needed.

. Resonance region. The unresolved resonance region.

The discussion will follow closely the outline for the resolved resonance region.

3 - TYPICAL CONTENT OF THE DATA FILES - ANGULAR AND SECONDARY NEUTRON DISTRIBUTIONS

. Angular distributions of secondary neutrons :

- basic formulae for elastic scattering ;
- Legendre polynomial expansion ;
- transformations, conservation laws and consistency ;
- format for description in a file (ENDF/B format);
- type of problems where these data are needed.

. Energy distribution of secondary neutrons :

- basic formulae ;
- secondary energy distribution laws ;
- format for description in a file (ENDF/B format);
- type of problems where these data are needed.

4 - THERMAL SCATTERING LAW DATA AND PHOTON PRODUCTION DATA

. Thermal scattering law data :

- thermal neutron scattering formulae ;
- parameters needed ;
- temperature dependence ;
- format for description in a file (ENDF/B format)
- problems of utilisation.

Photon production data ;

- photon production cross-sections ;
- multiplicities and transition probability arrays ;
- format for description in a file (ENDF/B format) ;
- problem of consistency ;
- an example of verification of internal consistency of data ;
- type problems where photon production data are needed.

5 - PRESENT STATE OF THE ART IN THE FIELD OF EVALUATED DATA FILES

. Quality of the evaluations and problems of uncertainties.

. Typical examples of the present state of the art for some major isotopes in different energy ranges and type of reactions.

. Cooperative efforts. Dissemination and availability of data.

. The problem of the use of the basic data files : interfaces with processing codes.

. Conclusions.

FORMATS AND PROCESSING OF EVALUATED NUCLEAR DATA INTO MULTIGROUP CROSS-SECTIONS

M. MOTTA
ENEA, Italian National Committee for Nuclear and
Alternative Energy Sources,
Bologna, Italy

Abstract

==========

PART I. THE DATA IN NUCLEAR FILES AND THEIR MANIPULATION

1 - INTRODUCTION

In the theory of nuclear reactors it has been that the neutron population is essentially treated as a population of particles and consequently the laws which govern such a population are only based on equations of balance as, for example, the diffusion or the transport equations.

The quantistic nature of the involved particles ant the interactions of the neutrons with the matter of which the reactor is built up is properly taken into account through the coefficients appearing in the balance equations. Such coefficients are in fact calculated by means of the microscopic and macroscopic cross sections which contain the full information about the nuclear reactions between the neutrons and the nuclei of the crossed material.

The corss sections for a given material are largely dependent upon the energy of the exciting neutrons and the neutron spectra are different for different type of reactors. Then, we need of a subdivion of the total energy range in a set of groups for which the balance equations can be written with the proper coefficients, averaged over prefixed intervals. Each of the balance equations, must be connected to the other, through some exchange coefficients which give the correct trasmission of neutrons from one to other groups.

The starting point for this procedure in order to arrive to the system of differential equations for a reactor calculus, is a correct knowledge of the microscopic cross sections versus energy for the different reactions of neutrons in each material.

Clearly, more fine is the subdivision in groups, a greater number of groups must be adopted with a better description of the energy dependent coefficients but with a larger number of differential equations to be solved. The choice of the number of groups is therefore determined with

an optimization criterium which takes into account the type of reactor which has been considered and the accuracy exigencies.

A number of three-four groups may be enough for a thermal reactor while for a fast reactor a number of groups of about twenty to hundred might be a good choice for calculations.

Due to the behaviour of the cross sections when we go up in the energy scale, the total energy interval is normally divided in subintervals equally spaced in lethargy. It has been seen that the maximum of energy for neutrons in a reactor is about 15 MeV. So, the contents of the Nuclear Data Files (NDF) generally covers the energy range from nearly 0 to 15 MeV.

The coefficients of the balance equations first requires to read from NDF's the microscopic cross sections and some other parameters. Then, in order to prepare a group library, we must average the mentioned data over the flux of the considered reactor. In section 6/1 is given an example of what may include a calculated group averaged library. By the formulas there given for a generation of a group library, it will be clear that we need to pick-up the cross sections from files, in a tabular form. Then, the starting point to generate the group cross sections is the reading of files of evaluated data. The file structure can be subdivided as follows:

A) RESONANCE REGION, splitted in two part:
   1- Resolved region (RR);
   2- Unresolved region (UR);

B) THE CONTINUUM REGION.

For a given isotope, the cross sections depend not only by the energy of the exciting neutrons, but also by the temperature of the crossed material, because different temperatures corresponds to different thermal agitation of nuclei and consequently different relative energies neutron-target nucleus.

In a preparation of a group cross section library typical temperatures and dilutions are considered (e.g. in the Russian library, briefly called ABBN from the Author's names, are 0, 300, 900, and 2100 Kelvin degrees, while the values considered for dilution are 0, 10, 100, 1000, 10000).

We want to look here some particular physical aspects of the cross section manipulation before discussing of the numerical averaging formulas. Some physical questions are very important to understand for a correct manipulation of the files. The description of the general theories and formalisms can be found in ref. /1-9/.

2 - THE RESOLVED RESONANCE REGION.

It has been learned that the description of cross sections in the range of resonances may be given in the files in a two different ways: through the resonance parameters or through a pointwise representation.

The representation through the resonance parameters is strongly recommended /14/, expecially when Doppler broadening and self shielding factors must be calculated . We shall see the difficulties of the pointwise reprentation in part II of the lectures.

Now, let us share the energy resonance range in two parts:the RESOLVED resonance region and the UNRESOLVED resonance region and assume that our file contains the resonance parameters. We want to examine some problems related to the generation of the tabulated cross sections in the different theoretical scheme of representation, i.e. the Single Level (SL), Multilevel (ML) Breit-Wigner formalisms, or the Multilevel Reich-Moore /7/ and Adler-Adler /8/ formalism with more than one fission open channel.

TABLE 1 gives an axample of the parameters which are needed in the resolved region for the SL Breit-Wigner representation. TABLE 2 gives the same list in the case of a ML Breit-Wigner representation. The examples refers to the structure of ENDF/B file 2. The symbols written over each row are those assumed in the file to indicate the quantities. The complete list of such symbols can be found in the report of ref. /9/. The index which defines the selected formalism is LRF(1=SL,2=ML,3=Reich-Moore,4= Adler-Adler). The last one is in practice never used in the files; more-

over it has been recently prepared some good conversion codes (in Karlsruhe by F.H.Frohner) for Reich-Moore to Kapur-Peierls parameters /5/. It must be said that the main advantage of the Adler-Adler representetion is given by the possibility to perform an analytical broadening of cross sections when the temperature changes. But now, starting from Reich-Moore parameters we can convert them in Kapur-Peierls and broad the cross section in analytical way by means of the well known funtions $\psi(\theta,x)$ and $\chi(\theta,x)$ /15/,/16/. Both the Adler-Adler and the Kapur-Peierls representation of the resonances permit an analytical Doppler broadening, nevertheless, it must be noted that the widths are complex and lightly energy dependent. The conversion must therefore be performed in more than one energy point in order to have at least a good polynomial fit of such an energy dependence of widths.

Let us recall some practical notices about the three most used representations (LRF=1,2,3).

The origin of the discovery of the Breit-Wigner representation lies in an analogy with the theory of resonance absorption and subsequent emission of optical radiation by an atomic system. Breit and Wigner adapted this time-dependent perturbation theory to the treatment of nuclear reactions giving rise to the formula that bears their name. In spite of the fact that electromagnetic interaction is "weak" while nuclear interactions are "strong", both the phenomena get out a similar formula. The reason is because both the reactions proceed through a relatively "long life" state: it is due to the weakness of the coupling in electromagnetic case; in the nuclear case the strength of the nuclear forces leads to a sharing of energy among the nucleons with a compound nucleus formation and a long life due to the small probability of the energy being concentrated in a mode that corresponds to disintegration by an "open" (i.e. energetically allowed) channel (see introduction of ref./5/).

In order to make easier the interpretation of the Breit-Wigner formula in the Single Level (SL) an Multilevel (ML) approximation let us look to the formulas as given in ref./9/ and shown in tables 3, 4. At the low energy involved in the resolved resonance region, the only possible reactions are:

- ELASTIC SCATTERING (potential + resonance)
- RADIATIVE CAPTURE
- FISSION (only for fissile nuclei)

The elastic cross section is formally the most general and includes three parts:

(1) Potential scattering (hard sphere scattering);
(2) Resonance scattering (compound nucleus elastic reaction)
(3) Interference between (1) and (2).

In order to better understand what is an interference among resonances, we may remenber the similar problem arising in a quadratic expression which can be written in a matrix form, e.g.:

$$(2x + 3y)^2 = 4x^2 + 9y^2 + 12xy = (x \quad y) \begin{vmatrix} 4 & 6 \\ 6 & 9 \end{vmatrix} \begin{vmatrix} x \\ y \end{vmatrix}$$

Here the interpretation of the central matrix is well known. It introduces a metrization of the space (is a "metric" or a fundamental tensor of the reference space) where the diagonal elements give the metric scale on the axes, while the off-diagonal elements give the interference between any couple of axis due to their "non-orthogonality". In fact, orthogonality means independence among the reference axes.

For what concerns the resonances, the interference can exist ONLY AMONG THE RESONANCES OF THE SAME SPIN AND PARITY. Then, only the resonances with the same l-quantum number and J can interfere. Now, let us consider how are taken into account the interferential contributions in the ML Breit-Wigner formalism. As in the quadratic example above, a matrix formalism can be adopted to write down the formulas of table 3 and 4.

In order to see with a better evidence the interference given by the off-diagonal terms in the BW formula for the resonance scattering, we note that by introducing the quantities:

$DE_j = E - E'_j$ (j=resonance index, ref./9/ for shifted energy E'_j)

$a_j = DE_j + i(\Gamma_j/2)$; $a_j^{\wedge} = DE_j - i(\Gamma_j/2)$ ($^{\wedge}$= complesx conjugate)
(i= imaginary unit)

$z_j = 1/a_j$; $z_j^{\wedge} = 1/a_j^{\wedge}$

$u_j = SQR(g_j) \times SQR(\Gamma_{nj}) \times SQR(\Gamma_{xj}) = SQR(g\Gamma_n\Gamma_x)j$;

$c(j,k) = u_j\, u_k$ simmetric matrix n•n (j,k=1,2,...,n resonances),

we can write the resonance part of the single or multilevel BW cross section in the very synthetic form:

cross section for x-reaction = $\pi\lambda^2 [Z^{\wedge}\ C\ Z]$

where capital Z is the column vector of Z_i, $Z^{\wedge}$ is the row vector of $Z_j^{\wedge}$ and the central (n•n)matrix C plays the role of the space metric with elements $u_j\, u_k$.

The square roots of the widths are called "REDUCED-WIDTH AMPLITUDES".

In the vector matrix vector product the contibution of the diagonal elements give a sum of pure single level Breit-Wigner formulas, while the off-diagonal elements give the interference between resonances.

The energy space is n-dimensioned with an axis for every width x_j, for the reaction x and resonance j, more or less orthogonal one to others, depending upon the amount of interference among the resonances.

The matrix formalism can be extended to the potential scattering (I) by introducing fictitiously the "dummy" widthes energy dependent for each l-quantum number.

$\Gamma_l = -2\ E \sin$ and $DE_l = E \cos$

$a_l = DE_l = i(\Gamma_l/2)$; $a_l^{\wedge} = DE_l - i(\Gamma_l/2)$

$z_l = 1/a_l$; $z_l^{\wedge} = 1/a_l^{\wedge}$

so that, for example, the elastic cross section for a single isolated resonance can be written as in TABLE 6.

The two expressions in TABLE 3,4 and in TABLE 5 are perfectly equivalent but the matrix form permits immediately to understand where the interferential terms between the potential and resonance scattering arise.

When the interferential effects among the resonances are taken into account, the ML formalism is needed, and the matrix form in this case has a central square-symmetric matrix C of dimension (n n) if n resonances are simultaneously assumed.

Clearly a coherence must exist between the adopted formalism to generate the tabulated cross section and the formalism which was adopted to fit the experimental points of that cross section. The formalisms must be the same. A flag number in the file advise us if SL or ML formalism must be used.

If we look to the multilevel term in TABLE 4, we can find the single term of summation as generated by the off-diagonal elements in the matrix representation given in TABLE 5. For a better understanding we can subdivide the complete hermitean expression in submatrices (TABLE 6) where the potential scattering (submatrix A) and the resonance scattering (submatrix C), have the matrices B and Tr (B) as interference. In the single level representation the off-diagonal elements of matrix C are normally put =∅. So making, if the terms of matrix B and Tr (B) are mantained, it happens that in some energy points the calculated ELASTIC cross section becomes negative. Such an unphysical result derives by the absence of the positive interferential terms in the hermitean form, while the negative terms of matrix B are retained. This result shows that the common SL formalism could be unadequate and is moreover wrong from a theoretical point of view, at least for elastic reaction.

In the above observations, we have implicity accepted that the products of the widths in the off-diagonal elements of matrix C, were "positive".

It is quite easy to see that positive result of the product of the reduced-width amplitudes is only true for the elastic reaction. In effect, if we consider an interferential term between two resonances of index j and k, the element in row j and column k of matrix C must be written:

$u_j = SQR(\Gamma_{nj}) \times SQR(\Gamma_{xj})$ with an uncertaint in the algebric sign.

For all the terms of the simmetric matrix, we have:

$u_k \cdot u_j = SQR(\Gamma_{nk})\ SQR(\Gamma_{xj})\ SQR(\Gamma_{nj})\ SQR(\Gamma_{xk})$ and same sign uncertainty.

In can be observed that the same random attribution of sign can be directly attached to u_j, since on half of the generated sign is positive while the other is negative, as shown in TABLE 7.

For elastic reactions, x= n and automatically a positive sign always results for the product $u_j \cdot u_k$. It is normally assumed that there is only one neutron channel, since, in the range of neutron nergy under consideration, mainly neutron with l=∅ are expected to contribute.

For the reactions, two distinct cases must be considered, on the basis of the possible open channels of the reactions. They are:

THE CASE OF RADIATIVE CAPTURE. Such a reaction gives rise to a cascade of possible jumps of nucleons to lover energy levels, with gamma ray emission. The number of possible channels is very high and consequently, on average, the positive and negative interferential effects compensate one each other, giving rise to a reaction equivalent to a Single Level mode without interference.

Then, THE CAPTURE REACTION IS ALWAYS TREATED WITHOUT INTERFERENCE.

THE CASE OF FISSION. Such a reaction evolves normally through more than one channel, at least two and even three-four channels. For the same resonance level, each channel corresponds to a mutually exclusive mode of evolution of the compound nucleus. Then, there is no interference among channels of the same level but may exist among channels of different levels (for the same reaction). To be more clear we may look to FIGURE 1 which represents the reduced-width amplitudes as axex of a multidimensional space /10/ and are orthogonal if referred to the same resonance level. The experimental determination of the channel widths is very difficoult and in the files are generally never given more than two fission widths. In TABLE 8 is possible to see the data which we can find in a file of resolved region for a fissile material, i.e. Pu-241, with a two partial channels for fission and partial widths GH1 and GF2 for each resonance.

The total fission width GF can be calculated by addition

$$GF = GF1 + GF2 \qquad \text{(two open channels)}$$

To give the two partial fission widths an alternative mode can be used as in TABLE 9 where, together with the "total" fission width GF, the angle θ is given from which the two components can be calculated with the formula of conversion from polar to rectilinear coordinates.

$$GF1 = GF \cos\theta$$

$$GF2 = GF \sin\theta$$

When the fission reaction is given for each resonance with the parameter of two fission widths, the Reich-Moore formalism is normally requested to generate the cross section. The description of such formalism will not be repeated here. It can be found in a paper by Reich and Moore /7/. We only note that the radiative capture cross section is obtained by subtrancting from the total the elastic and the fission cross sections (see TABLE 10). Thus, the accuracy of the resulting capture cross section is strictly related to that of the multichannel fission reaction. From a practical point of view, the file must contain a sequence of algebric signs which arise from the products of the reduced widths defined above. We can see in TABLE 11 an example of experimental results for U-233 obtained by a fit of experimental data using the RM multilevel approximation. The mentioned sequence of signs appear under the column head $\beta_{\lambda 1}\beta_{\lambda 2}$. In TABLE 8, the sequence of signs appears to be attached to the partial fission widths, but it must be clear that they ARE NOT algebric signs of the partial widths, even if they produce in the calculations the correct sequence of positive and negative interferential effects among the resonances. A double sequence of signs is needed when two fission channels are assumed. From the mathematical point of view the uncertainty is due to the square root extraction on the widths. From a physical point of view the sign attribution will derive from a positive or negative interferential effect among the resonances. For a fixed set of γ-signs it can be seen that the interference contribution along the energy axis changes from destructive into constructive and viceversa. An example of this typical behaviour is shown in the fission cross section curves of FIGURE 2. A two-level two-channel formula was used with a positive (curve 1) and negative (curve 2) sign of gamma products $\gamma_n\gamma_x$. Both curves are partly above and partly below the curve (3) obtained without taking into account the interferential effects (summation of pure BW).

Within the simple assumption of a two channel reaction, the two level formula produces two possible interferential cross section values, due to different choice of signs. As far as the numeber of the considered levels is increased, the number of possible sign permutations also increases. Any fit of experimental data with a multilevel formula becomes more difficult, even if all the other resonance parameters are fixed.

The total nomber of possible sequences of signs can be easily deduced. Even if a plus or minus sign has to be attached to every Γ's square root, it can be directely attached to u_j above defined because one half of the generated signs is positive while the other is negative, as shown in TABLE 7.

The random attributions of signs to the elements of the "fundamental tensor" does not modify its symmetric character. Then $c(j\ k)=c(k\ j)$ and a triangular set of elements may be determined in order to obtain the final result.

If n levels are considered, the indexes run from 1 to n and the total number of different elements to be examined is given by $n(n-1)/2$.
The number of order distinguishable sequences of size $n(n-1)/2$ with repetition of two elements (+ and -), is given by $2^{\frac{1}{2}n(n-1)}$ /2/
It corresponds to the possible sets of non-diagonal terms with different sequence of signs.
But it must be observed that, due to the fact that each element c(jk) is obtained by a product of two factors of index j and k respectively, the sign attribution is not completely free, once the signs of the factors SQR(Γ) have been assigned. More precisely, the free and bound elements are so distributed:

total	=	free	+	bound
$n(n-1)/2$	=	$(n-1)$	+	$(n-2)\,(n-1)/2$

An example of the case n=3 is shown in TABLE 12, where a maximum number of four possible distinct sequences is extractable from the total number of sign sequences for the square root of capital gammas.
Due to the special nature of the elements c(jk), only $2^{\frac{1}{2}(n-1)}$ distinguishable ordered sequences of signs can be obtained for the non diagonal elements of the matrix. In the example of TABLE 12 we can verify the prediction; the same signs are obtained from sequences no. 1 or 8, 2 or 7, 3 or 6, 4 or 5, and our prediction about the free elements is so checked.
The above considerations concerning the dependence of a multilevel cross section upon the choice of the signs of the reduced width amplitudes regards only the resonance reactions via compound nucleus and do not involve the potential scattering and the phase shift.
It is evident that the experimental data of cross sections must be fitted with the best sequence (e.g. in the least square sense) of signs for the products of the reduced width amplitudes.

Some important questions arise in connection with the mentioned freedom in the sequence of signs. The consequences in the energy by energy calculation of cross section are not negligible because they produce different interferential effects. Only when a very large number of channels are open, the interferential effects tend to elide one another. Moreover, when a large number of level must be treated, according to a Bethe's assumption /5,P.302/ the average cross section within a finite energy interval can be obtained assuming a random sign for the reduced amplitudes.

Such an assumption does not define the influence of sign distribution on the cross section values in each energy. Thus, the following problems were investigated /12/ which are particularly important:

a) The evaluation of amount of uncertainty in the cross section value, due to the random signs of the width amplitudes and its variability as a function of excitation energy.
b) The comparison between the arthmetic mean of all the cross section values at a given energy and the value obtained without interference among the resonances. The comparison must be made also with regard to a variable number of levels.
c) The search for the frequency density of cross section values in any fixed neutron energy.
d) The investigation of the sensitivity of the calculated cross section to the choice of signs. The sensitivity changes at different energies; thus, it can be useful to foresee the energy ranges of maximum sensitivity in order to pick up energy values where the sequences of γ-signs can better be determined by a fit.
e) The verification of the vanishing in the mean of the interference terms, whenever a great number of levels is considered (as it happens for sufficiently high energy /21,p.60/, /3,p.396/).

In FIGURE 3 we can see the uncertainty band of U-233 cross section for the fission reaction described with a MLBW formalism and one open channel. A reduced range of energy is plotted; the parameters of twelve resonances were used in calculations, as given in TABLE 11 shown above.
The figure shows that the amount of uncertainty of the point a) may be very large. In the next FIGURE 4 we can see the relative amplitude of uncertainty in the same energy range. The arrows show the position of the levels. The maximum spread of cross sections is at the middle between resonances.
For what concerns the point b) the calculations have shown that the value without interference is exactly the arithmetic mean of all the possible interferential values. Over a large number of resonances, such a conclusion makes valid the hypothesis of point e).
For problem of point c) the frequency function of all the possible cross section values due to different choice of the sign sequences appear to be very variable with the neutron energy. In FIGURE 5 are plotted the frequency hysto

grams of cross section values at energies of resonances (upper) and at intermediate values between the same two resonances (lower). The calculations were made by a set of 15 resonances not corresponding to a real case. A theoretical study of such distributions could contribute to solve the problem of point d) for a practical use in the determination of the multilevel cross section parameters.

Let us now summarize the main problems to take mind when we generate a cross section from a Nuclear Data File in the resolved region, starting from the resonance parameters:

1) The elastic cross section may become negative in some energy points on the left of the resonances when a SL formalism is used and the interference between the resonance and potential scattering is added in calculations. Negative values quite easily appear at very low energies, i.e. near the thermal value.
2) The non elastic cross sections, at the energies on the left of each level, increase as 1/v. This is due to the fact that the neutron wavelenght is proportional to 1/SQR(E) and the neutron width is proportional to SQR(E), as it is evident for the s-waves where $\Gamma_n = \Gamma^\circ \times SQR(E)$. The squared wavelenghts has a factor 1/E which is compensated in elastic reaction by the product of neutron widths Γ's, but is only partially compensated in non elastic where only one neutron width appear in the numerator whereas e.g. the capture width is practical constant with the energy. Then, the files start normally from an energy not lower than about 1E-5 eV for tabulated cross sections. As a related problem, it happens that, if in the experiments some resonances were lost (for example because too narrow), their 1/v contribution at thermal energy cannot appear in the calculated cross section. Consequently, we shall find some discrepancies between the experimental and calculated thermal cross section, the last one being generally underestimated. A 1/v tail must be artificially added in order to normalize the calculated to the experimental values at the Maxwellian most probable velocity, i.e. 2200 m/sec or 0.0253 eV at room temperature.

In the files, the correction for the loss of a 1/v contribution is generally obtained with the artificial introduction of a bound level at a negative energy. The creation of such a resonance has many degrees of freedom because energy and widths can be freely chosen. The evaluator generally assumes a distance from the first level of about one average spacing <D> and the average capture width. Then, the neutron and fission widths are usually determined. An algebric equation of second degree must be solved; in TABLE 13 is described the procedure which may be adopted.

The list of code RINEG for such calculation is given in APPENDIX. It is written in Basic language for a desk calculator (Olivetti P/6066).

It must be remembered that the 1/v tail also gives a contribution to the resonance integral. This calculation will be considered in the next section.

3 - THE UNRESOLVED RESONANCE REGION

Going up in the energy scale the resolution power of the instruments for the experimental determination of cross sections becomes lower and the resonances become wider and tend to overlap one to the others.

Then, it is impossible to resolve the resonances, and to separate one from the others. The calculation of cross sections can be made on the basis of average values of widths and the knowledge of strenght functions for s-and p-waves. The "statistical model" used in the calculation will not be repeated here. We want only pay attention to some pratical aspects of the calculations.

The formulas giving the cross sections can be seen il TABLE 14 and 15, taken from ref./9/.

The calculation of the ratio of widths appearing in the formulas requires the determination of average values of widths and of the factors R which are known as fluctuation integrals for capture, fission and elastic scattering. These factors arise from the fluctuation of the resonance widths which are not costant but have a distribution depending upon the number of open channels for the reaction considered, and upon the number of degrees of freedom for the decay reaction of the compound nucleus. The distribution takes the name of PORTER-THOMAS DISTRIBUTION (FIGURE 6) and as been discussed in other lectures.

Thus, associated with each of these integrals, there is the number of degrees of freedom for each of the average widths.

In the calculation of the cross section with the statistical model, it has assumed that, in a given energy interval, there is a number of resonances with their average width and a fixed average spacing <D>. This is not actually correct, because also the spacings fluctuate with a law which takes the

name of WIGNER DISTRIBUTION (FIGURE 7). But it has been seen that, in practice, the spacing fluctuations do not influence appreciably the calculation of cross sections. Thus we can see that an unweighted average D appears in the denominator of the given formulas.

The average values of widths and of resonance spacing D are normally deduced from the resonances in the resolved region. This evaluation is quite critical and must again take into account the statistical distribution of these parameters for a correct determination of the average values. In particular, the value of <D> largely influences the calculated cross section which is inversely proportional to it. Then, some adjusted values of average D are often obtained from the experimental information about the cross sections in the unresolved region.

For what concerns the calculation of the fluctuation integrals, it is often used in calculation a table of probability over which the neutron and fission widths are to be weighted. In fact, one/two degree of freedom (=one/two channels) are assumed for fission width. The capture width on the contrary, is assumed without fluctuation, because, as observed above, a very large number of channels corresponding to the gamma-rays cascade are open, and the Porter-Thomas distribution tends to become a Dirac's delta function. We can see on FIGURE 6 the Porter-Thomas distribution for different degrees of freedom. It is of the chi-square type.

As a practical example of cross section calculation in the unresolved region we give here a list of a code written in basic language for Olivetti P/6Ø66 computer which permits to follow very well the cross section calculations. The weighting probability for one to four degrees of freedom appears in the list as an "internal file" of data (see the statements 80-130 of the <GRESO> code).

An example of the structure of a Nuclear Data File in the unresolved region can be shown in TABLE 16 where the symbols of the data are those used in the rules of ENDF/B file. It can be seen that there is the indication of the number of degrees of freedom used in the neutron width distribution (AMUN =< 2) and in the fission width distribution (AMUF=<4). The average fission width may be energy dependent and a set of values in prefixed energy points, with an interpolating law (parameter INT) must be given.

A faithfull image of the file ENDF/B in unresolved region is shown in TABLE 17.

4 - IMPORTANT DATA: AVERAGE SPACING AND RESONANCE INTEGRALS.

The statistical theory we have mentioned above, clearly shows that the exactness of cross section in the unresolved region is largely determined by the exactness of the average spacing which we have evaluated from the resolved region. The greatest difficulties for this determination are given by the following items:

1) The loss of resonances made by experimenters, due to the low resolution power of the experimental apparatus (e.g. time of flight method). Generally a threshold width exists below whiwh it is impossible to see a resonance. The p-wave resonances, which have a narrower neutron width, very often cannot be seen at low energy. But when a narrow width is measured at low energy, it may be difficult to decide if the resonance belongs to the s- or p-ware type.
   Some theorical criteria, based on the Bayes theorem of probability calculus, are used for an auxiliary indication of the more uncertain cases /23/. The "BAYES TEST" for resonances is based on the knowledge of the strength functions for L=Ø and L=1 neutron waves /17/. Systematic studies of the behaviour of the strengths functions for different isotopes, give a supplementary help to these determinations.
   Anyway, the correct determination of the lower threshold is never univocally determined. The use of statistical methods based on the controll of the Porter-Thomas' width distribution, is largely employed for this determination. The most recent methods make use of the maximum likelihood principle to obtain the average neutron width and average spacing <D> /18/.
2) The average spacing <D> must be deduced by a "pure" sequence of L=Ø resonances. It is practically very difficoult to distinguish with a high degree of probability if a resonance belongs to the set of the L=0, 1 or 2 neutron waves, expecially when the width is narrow and the j of the resonance cannot be attributed with certainty.
3) One of the most used method to evaluate the real number of s-wave resonances that there would be in resolved energy range, is the one which takes the name of "MISSING LEVEL ESTIMATOR" /19/ which is based on the standard hypothesis that all the resonances which belong to the left tail of the Porter-Thomas distribution and covering 1/4 of the total area, are lost. This idea permit to evaluate an estimated increased number of resonances in our energy range.

The application of the Missing Level Estimator test may be shown even on a desk calculator.

When all the above conditions have been checked and the best "pure sequence" of resonances was obtained, the common way to obtain the average spacing <D> is the "linear fit" of the so called "staircase" which plots the number of resonances versus their energy position. If resonances are not lost, a straigth line would fit quite well the staircase. See the FIGURES 8, 9 and 1Ø to realize the difficulties of a good interpretation of a real case.

Let us now apply to the other problem of the RESONANCE INTEGRAL calculation. In the reactor theory you will see the important role played by the resonance integrals (capture and fission). They strictly influence the resonance escape probability, i.e. one of the four factors which is responsible of the reactor criticality.

From the discussion of the cross section generation by the resonance parameters in the files, it is evident theat the calculation of a resonance integral requires a numerical procedure of integration.

The formulas which generate the cross sections from the resonance parameters, weighted over a flux 1/E, actually give rise to a not integrable expression. This limitation is avoided only if a single level Breit-Wigner formula is used. In that case an analytical solution to the resonance integral have been found /22/. In TABLE 18, the formulas (see ref. /23/) are given which solve the problem. In other cases when a ML formalism must be used, it should be needed to perform a numerical integration for a correct solution of the problem. Neverthless, in many practical computations the ML parameters can be used as they be of SL type and the analytical integration may again be performed with a negligible error. This is often true because the numerical integration may be affected by a large error, due to a bad tabulation of cross section in the presence of a large number of narrow resonances.

The problem of a correct integration of a cross section, weighted over a given flux, is very critical in the resonance region. It largely depends upon the goodness of tabulation and the number of points which can be accepted by the capability and the speedness of the used computer. The convergence criterium based on the decreasing difference between two successive calculations with ticker grid of energy points is not always correct. The evaluation of the absolute error may be impossible. We shall see later, in Part II, the difficulties of a pointwise representation of the resonances.

A contribution to the resonance integral comes both from the resonances in the resolved region and, in negligible part, from the unresolved region. An approximate evaluation of the resonance integral coming from the resonances at an energy higher than about 1 eV, has been given by Walker /2Ø/. Another approximation of the same Author has been given for the evaluation of the contribution of the unresolved part of resonances. Even if more sophisticated calculations were made, it is a good rule to check the results with those approximations. In TABLE 19 and 2Ø we give the formulas of the original report.

The lower limit of the resonance integral starts normally from Ø.5 eV wich is the Cadmium cut-off for thermal neutrons? In some exceptional case a light smaller limit (e.g. Ø.47) is taken, mainly if a resonance has the peak around that limit. When the experimental and calculated integrals do not coincide and are too much different, a revision of the resonance parameters or of the experimental conditions are needed. A wrong attribution of p-waves to the s-wave resonances may be responsible of errors. The evaluated files are generally prepared taking into account the comparison of calculated and experimental data. Nevertheless, it may happen that a correction to the calculated cross section must be applied, in order to reproduce the resonance integral, the thermal cross section or to correct a Single Level set of resonance parameters, when a more proper MultiLevel set should indeed be necessary.

The so called "background" cross section is then given in the files, for some energy ranges where a compensation is needed. The background is always given pointwise with an interpolation law (generally linear) beetween any pair of points. The background is temperature independent being essentially flat in any interval and must be added to the cross section calculated from the parameters. Il makes also positive the elastic cross section, when Single Level formalism may cause negative values for the reasons we have explained above.

5 - THE CONTINUUM REGION

It is generally around 1Ø keV that the cross sections become smooth lines without fluctuations. Consequently, the cross sections are given in a pointwise mode in Nuclear Data Files. The statistical model cannot be applied with good results to calculate the cross sections.

The OPTICAL MODEL calculation is generally adopted for theoretical prevision of the cross section values. The nucleus is seen as a transparent body crossed by the neutron, with a partitioned probability of transmission, absorption and reflection, like in the optical laws for the ligth. Thus, an exponential law with a complex potential which takes into account the absorption, will appear in the model.

It is not our aim to describe this model. What is important to note is the fact that other reaction channels begin to be open. Inelastic cross section begin to appear as soon as the excitation energy of the neutron makes possible the decay of the compound nucleus with an emission of one or more neutrons. Going up in the energy scale, say beyond the MeV, other emission processes are successively open, also with the emission of charged particles.

It has been explained in other lectures that the files must contain information on the INELASTIC CROSS SECTION for the compound nucleus levels and information about the angular distribution of the emitted secondary neutrons. We shall only repeat here that the angular distribution may be given in two forms: a) trough a pointwise tabulation of the angular probability emission or through the coefficients of the Legendre polynomials which fit such a distribution.

To have a more concrete idea of the behaviour of cross sections in the total interval of interest for reactors, we may look to the following FIGURES 11 to 14 which reproduce the elastic, capture, total and inelastic cross section for the fission product Pd-105.

The evaluation has been performed in the Nuclear Data Laboratory in the Bologna Center of ENEA, the Italian Committee for Nuclear Energy.

Clearly appear the three regions with a 1/v part for capture (and total), the resonance region and the continuum. The inelastic cross section starts at a threshold energy and is possible to distinguish the opening of the successive inelastic channels for higher energies of excitation.

REFERENCES

Part I, sec. 1-5

1 - A.M. WEINBERG and E.P. WIGNER. The Physical Theory of Neutron Chain Reactors, The University o Chicago Press, Chicago, Ill., 1968.

2 - G. BIRKHOFF AND E.P. WIGNER (Editors). Nuclear Reactor Theory, Proc. Symp. Applied Math., Vol. IX, 1959.

3 - J.E. LYNN. The theory of Neutron Resonance Reactions, Clarendon press, Oxford, 1968.

4 - E. VOGT. Theory of Low Energy Nuclear Reactions, Review of Modern Physics, vol. 34, number 4, Oct. 1962.

5 - A.M. LANE and R.G. THOMAS. R-Matrix Theory of Nuclear Reactions, Review of Modern Physics, vol. 30, number 2, Part I, Apr. 1968.

6 - M.F. JAMES. Recommended Formulae and Formats for a Resonance Parameter Library, AEEW 621, 1968.

7 - M.S. MOORE and C.W. REICH. Multilevel Analysis of the Slow Neutron Cross Section of U-233, Physical Rev., 118, vol. 3, may 1, 1960.

8 - D.B. ADLER and F.T. ADLER. Multilevel Analysis of the U-235 Total and Fission Cross Sections in the Energy Region below 37 eV, TID-23396, 1966.

9 - ENDF-102 Data Formats and Procedures for the Evaluted Nuclear Data File. ENDF revised by R. KINSEY, Oct. 1979, BNL-NCS-50486.

10 - C.A. PRESKITT. MUFFLE - A code for the Multilevel Analysis of Neutron Cross Sections, ORNL-TM-1180 (1965).

11 - T. MARTINELLI and M. MOTTA. The PIUME code for the Multilevel Two channel Cross Section Calculations, CNEN, RT/FI (72)50, 1972.

12 - M. MOTTA. The effect of the Reduced Width Amplitude Sign in the Multilevel Calculation of Neutron Cross Sections, CNEN, RT/FI (72)37, 1872.

13 - E. MENAPACE, M. MOTTA and G.C. PANINI. A 26-Group Library with Self-Shielding Factors for Fast Reactor Calculations from the UK Nuclear Data File, CNEN, RT/FI (73)15, 1973.

14 - The Evaluation of Neutron Nuclear Data, Proc. of Panel on Neutron Nuclear Data Data Evaluation, IAEA-153, Vienna 1971.

15 - V.J. BELL, P.A.C. BUCKLER and I.C. PULL. The Calculation of Genaralized Doppler Functions, AEEW-R 266.

16 - P.A.C. BUCKLER and I.C. PULL. Doppler Broadening of Cross Sections, AEEW-R 226, 1967.

17 - L.M. BOLLINGER and G.E. THOMAS. Physical Review 171, (1968) 1293.

18 - M. STEFANON. Nuclear Instr. and Methods, k74 (1980) 243.

19 - G.A. KEYWORTH, M.S. MOORE and J.D. MOSES - NEANDC(US)-199/L, P. 353, (1976).

20 - W.H. WALKER. CRRP-913/AECL 1054, Mar. 1960.

21 - R.J. BRISSENDEN and C. DURSTON. The calculation of Neutron Spectra in the Doppler Region, ANL 7050, 1965.
22 - J.S. STORY. AERE T/M 77.
23 - M. MOTTA. Nuclear Theory for Application, p. 250, IAEA, Vienna, 1980.

6 - GROUP AVERAGING FORMULAS AND SELF-SHIELDING FACTORS

The process which carries out to the preparation of a group cross section library, puts in evidence that we always need to average the cross sections and other parameters over the proper reactor flux (see figs. 15-18).

Thus, we shall now look to the formulas for a standard averaging over a small number of energy groups, say the ones of the 26-group Russian library by Abagyan et al. (briefly ABBN), whose upper limits are: 10.5, 6.5 4.5, 2.5, 1.4, 0.8, 0.4, 0.2 MeV, 100, 46.5, 21.5, 10, 4.65, 2.15, 1 keV, 465, 215, 100, 46.5, 21.5, 10, 4.65, 2.15, 1, 0.465 eV, thermal.

1. THE LIBRARY QUANTITIES

The calculated group constant list includes generally:

a) the microscopic cross sections
- σ_t , total
- σ_e , elastic
- σ_r , elastic removal
- σ_{in} , inelastic
- σ_f , fission
- σ_c , capture

b) the parameters
- ν , the average number of neutrons per fission
- μ_e , the average cosine of the elastic scattering in the lab System
- ξ , the average lethargy increment in elastic scattering
- $\mu_{d(e)}$, the average cosine of the elastic scattering at which a transfer into the next lower group occurs

c) the self-shielding factors, temperature and dilution dependent:
- f_t , for the total cross section
- f_e , for the elastic cross section
- f_f , for the fission cross section
- f_c , for the capture cross section

The source of microscopic data for the calculations of the averaged values may be a file which gives the cross section in a tabular form, e.g. the UK Nuclear Data File (UKNDL). For the self-shielding factors in the unresolved region, the resonance average parameters are required for the reasons which will be later explained. Then, ENDF/B file can be used in such a case.

2. GROUP AVERAGING FORMULAS

a) The averaging procedure of microscopic cross sections implies the choice of weighting functions. For the groups 1 to 25, the same choice as in the ABBN library was adopted. More precisely, the weighting fission spectrum utilized in the first three groups is the following:

$$X(E) = 0.4527 \exp(-E/0.965) \sinh \sqrt{2.29E}$$

In the groups 4 to 25, the 1/E weighting flux was assumed. It is well known that the 1/E flux refers to an infinite dilution of the considered isotopes or natural elements in the reactor mixture.

The basic temperature of the microscopic data in the UK file is 300 °K for the isotopes and elements listed above, with the exception of B-11, Na-23, Ni, Pu-239 which are given at zero Kelvin degrees.

The problem of the temperature and dilution dependence will be discussed in the next section.

The average cross section for the x-reaction in the group g is calculated by the formula

$$\sigma_x^g = \frac{\int_g \sigma_x(E)\phi(E)dE}{\int_o \phi(E)dE} \qquad (1)$$

where $\phi(E)$ is the weighting function and x stands for total, elastic, inelastic, fission and capture reaction.

The removal cross section refers to the elastic process only and is calculated summing up the elements of the elastic scattering matrix for the transfer to the lower energy groups.

The inelastic cross section includes the (n,2n) reaction. Then, we have for the mean values in each group g and for the $g \to g'$ transfer

$$\sigma_{in}^{g} = \sigma_{n,n'}^{g} + \sigma_{n,2n}^{g}$$

$$\sigma_{in}^{g \to g'} = \sigma_{n,n'}^{g \to g'} + \sigma_{n,2n}^{g \to g'}$$

Due to the double particle emission in the (n,2n) reaction, it will be observed that

$$\Sigma_{g'} \sigma_{n,2n}^{g \to g'} = 2\sigma_{n,2n}^{g}$$

The group cross sections as well as the elements of all the scattering matrices were calculated with the GALAXY code /2/.

Finally, the cross sections here given in the 26th group correspond to the values read in the file for the most probable velocity 2200 m/sec, 0.0253 eV, of the thermal Maxwellian spectrum, at room temperature.

b) The group average values of ν were also weighted over the $\phi(E)$ function. Then, the expression for the group value of ν is:

$$\nu^{g} = \frac{\int_{g} \nu(E)\phi(E)dE}{\int_{g} \phi(E)dE}$$

The quantities μ_e and ξ will be obtained weighting both over $\phi(E)$ and the angular distributions for elastic scattering. The last ones are given in the center of mass system (CM) in the UKNDF.

The integrals over the angular distributions are calculated first, and the following energy dependent quantities are obtained:

$$\bar{\mu}_L(E) = \frac{2\pi}{\sigma_e(E)} \int_{-1}^{1} \frac{1+A\mu_c}{\sqrt{2A\mu_c+A^2+1}} \frac{d\sigma_e(E,\mu_c)}{d\Omega} d\mu_c$$

$$\xi(E) = \frac{2\pi}{\sigma_e(E)} \int_{-1}^{1} \ln\left[\frac{2}{(1+\alpha)+(1-\alpha)\mu_c}\right] \frac{d\sigma_e(E,\mu_c)}{d\Omega} d\mu_c$$

where,

A = mass number of the target nucleus

α = $(A-1)^2/(A+1)^2$ maximum energy loss fraction

μ_c = cosine of elastic scattering in CM system

$\sigma_e(E)$ = total elastic scattering cross section at energy E

$\frac{d\sigma_e(E,\mu_c)}{d\Omega}$ = differential elastic scattering cross section at energy E and cosine μ_c.

The fraction $(1+A\mu_c)/(2A\mu_c+A^2+1)^{\frac{1}{2}}$ is the cosine scattering angle μ_L in the LS system.

Finally, the above defined quantities are averaged in the groups. Then, we have the formulas:

$$\mu_e^g = \frac{\int_g \bar{\mu}_L(E)\phi(E)dE}{\int_g \phi(E)dE}$$

$$\xi^g = \frac{\int_g \xi(E)\phi(E)dE}{\int_g \phi(E)dE}$$

The calculations were carried out through the code MUXIL /3/ that is based on the formulas given in the CHAD report /4/.

For what concerns the quantity $\mu_{d(e)}$, which refers to the slowing down (index d) in the next lowest group, the isotopes of Boron, Carbon and Oxygen were the only ones considered from the given list.

Some modifications are required in the above formulas for the μ_e calculations.

The condition that only transfer from group g to group g+1 is to be considered, may cause a reduction of the (-1,+1) integration interval for the μ variable. In other words, the energy dependent cosine for the slowing down to the nearest group $\bar{\mu}_{Ld}$ is given by

$$\bar{\mu}_{Ld}(E) = \frac{\int_{\alpha(E)}^{\beta(E)} \mu_L \frac{d\sigma(E,\mu_c)}{d\Omega} d\mu_c}{\int_{\alpha(E)}^{\beta(E)} \frac{d\sigma(E,\mu_c)}{d\Omega} d\mu_c} = \frac{R(E)}{Q(E)}$$

where α and β are the cosine limit values in the CM system at which a transfer to the nearest group is possible.

For the group division and the target nuclei here involved, the $\alpha(E)$ values resulted to be always equal -1, while the energy dependence of $\beta(E)$ is given by

$$\beta(E) = \frac{1}{2A}\left[\frac{E_{low}}{E}(A+1)^2 - (A^2+1)\right]$$

with

E_{low} = the lowest energy boundary of the group g.

The group averaging procedure must now take into account the fact that the weighting function $\phi(E)$ is reduced by a fraction

$$P_g(E) = \frac{\int_{\alpha(E)}^{\beta(E)} \frac{d\sigma(E,\mu_c)}{d\Omega} d\mu_c}{\int_{-1}^{1} \frac{d\sigma(E,\mu_c)}{d\Omega} d\mu_c} = \frac{Q(E)}{S(E)}$$

which represents the probability that a neutron of energy E in the group g will be scattered to the group g+1.

Then, the final expression for $\mu_{d(e)}$ is

$$\mu_{d(e)} = \frac{\int_g \bar{\mu}_{Ld}(E)\,\frac{Q(E)}{S(E)}\,\phi(E)dE}{\int_g \frac{Q(E)}{S(E)}\,\phi(E)dE} =$$

$$= \frac{\int_g \frac{R(E)}{S(E)}\,\phi(E)dE}{\int_g \frac{Q(E)}{S(E)}\,\phi(E)dE}$$

The MUDE code /5/ was prepared for the calculation of $\mu_{d(e)}$, starting from the differential and total elastic cross sections of the UKNDF.

3. SELF-SHIELDING FACTORS

a) General definitions

It is well known that in the neighborhood of a cross section resonance line the flux is very quickly diminished.

In other words, each resonance of any nucleus shields the resonances of identical nuclei, depending upon two quantities:

i) the dilution of the considered nuclei in the reactor mixture, here assumed to be homogeneous;

ii) the temperature in the mixture and the consequent Doppler broadening of the resonances.

In the "narrow resonance approximation"(NRA), such a reduction is taken into account assuming as weighting flux in the resonance region

$$\phi(E) \propto \frac{1}{\Sigma_t E}$$

where Σ_t is the total macroscopic cross section of the mixture.

If we define:

N = the number density of the resonant nuclei

σ_t = the total cross section of the resonant isotope

Σ_m = the sum of the total macroscopic cross section of the other isotopes in the mixture

$\sigma_o = \frac{\Sigma_m}{N}$ the dilution parameter,

we have,

$$\phi(E) \propto \frac{1}{\Sigma_t E} = \frac{1}{N(\sigma_t+\sigma_o)E}$$

Then, the effective cross section σ_x in a group g as a function of the dilution parameter σ_o and temperature T is given by

$$\sigma_x^g(\sigma_o,T) = \frac{\int_g \frac{\sigma_x(E,T)}{\left[\sigma_t(E,T)+\sigma_o\right]E}\,dE}{\int_g \frac{dE}{\left[\sigma_t(E,T)+\sigma_o\right]E}}$$

Thus, it can easily be recognized that

$$\lim_{\sigma_o \to \infty} \sigma_x^g(\sigma_o,T) = \frac{1}{\Delta U}\int_g \sigma_x(E,T)\,\frac{dE}{E}$$

being Δu the lethargy interval of the group.

Since the resonance widths are much smaller than the group interval and their number within the group is sufficiently large in practical cases, the above "infinite dilution" cross section is temperature independent and is equal to the group cross section defined in Section 2.

Finally, the self-shielding factors for the elastic (f_e), capture (f_c) and fission (f_f) reactions are the following:

$$f_e(\sigma_o,T) = \frac{\sigma_e^g(\sigma_o,T)}{\sigma_e^g}$$

$$f_c(\sigma_o,T) = \frac{\sigma_c^g(\sigma_o,T)}{\sigma_c^g}$$

$$f_f(\sigma_o,T) = \frac{\sigma_f^g(\sigma_o,T)}{\sigma_f^g} \quad .$$

As explained in the ABBN library, the total self-shielding factor f_t is better defined by

$$f_t(\sigma_o,T) = \frac{\sigma_t^g(\sigma_o,T)}{\sigma_t^g} = \frac{1}{\sigma_t^g}\left[\frac{\int_g \frac{dE}{\left[\sigma_t(E,T)+\sigma_o\right]E}}{\int_g \frac{dE}{\left[\sigma_t(E,T)+\sigma_o\right]^2 E}} - \sigma_o\right] \quad .$$

Briefly, one can say that the reason for the above definition lies in the exigency of a correct preservation in the group of the neutron total mean free path which is the quantity to be weighted in the averaging process.

The above expression for $\sigma_t^g(\sigma_o,T)$ in the brackets may be better understood by writing

$$\sigma_t^g(\sigma_o,t) = \frac{\Sigma_t^g(\sigma_o,T)}{N} - \frac{1}{N}(\Sigma^g_{t_{mixture}} - \Sigma_m) =$$

$$= \frac{1}{N\lambda^g_{t_{mixture}}} - \sigma_o \quad ,$$

being $\Sigma^g_{t_{mixture}}$ and $\lambda^g_{t_{mixture}}$ the macroscopic cross section and total mean free path in the mixture.

b) Temperature dependence

The temperature effects are taken into account by Doppler broadening the resonance cross sections. Since the UKNDF gives a tabulated list of the cross section values at a fixed temperature, a numerical broadening procedure was adopted in the resolved resonances region by means of the TEMPO code /6/.

A different procedure must be adopted in the unresolved region where fluctuating or smoothed average values of cross sections are only given in UKNDF. The mean level spacing and widths of resonances and also information as to the statistical distribution functions of these quantities are required in this procedure. Since such information is not released in UKNDF, ENDF/B values were used in the calculations.

The resonance cross sections, which appear in formula (1) for the group cross section definition, were obtained by superposition of single-level resonance sequences of different ℓ and J quantum numbers.

Within every ℓ and J-sequence, the spacing between successive resonances and the radiation widths were assumed constant and equal to the mean values $\overline{D}_j$ and $\overline{\Gamma}_\gamma$.

The neutron and fission widths $\Gamma_n(\ell,J)$ and $\Gamma_f(\ell,J)$ were generated instead from the Porter-Thomas distribution function around the assigned mean values. As provided in ENDF/B, the degrees of freedom in the distribution function were 1 or 2 for Γ_n and 1 to 4 for Γ_f .

The interferential term between the potential and resonance elastic cross section was taken into account and the Doppler broadening was performed by means of the well known $\Psi(\xi,x)$ and $\chi(\xi,x)$ functions /7/.

On this basis, group cross sections and self-shielding factors in the unresolved region were calculated by means of the UNREC code, whose descriptive report /8/ includes details and comments on the formalism.

REFERENCES

Part I, sec.6

/1/ L.P. ABAGYAN et al. - Group constants for nuclear reactor calculations - Consultants Bureau, New York (1964)

/2/ V.J. BELL et al. - A user's guide to GALAXY 3 - AEEW-M422 (1964)

/3/ G.C. PANINI - MUXIL: A code for computing μ_L and ξ from UKNDL - CNEN Bologna, internal report (to be published)

/4/ R.F. BERLAND - CHAD: A code to handle angular data - NAA/SR/11231 (1965)

/5/ M. MOTTA - The MUDE code for the calculation of the group average cosine of elastic scattering - CNEN Bologna, internal report (to be published)

/6/ K. GREGSON, M.F. JAMES - TEMPO: A general Doppler broadening programme for neutron cross sections - AEEW - M 518 (1965)

/7/ V.J. BELL et al. - The calculation of generalized Doppler functions - AEEW - R 266 (1963)

/8/ L. LESCA, E. MENAPACE - Il codice UNREC per il calcolo di sezioni d'urto effettive e di integrali di risonanza in zona non risolta - CNEN report RT/FI 25(1972).

/9/ E.MENAPACE,M.MOTTA and G.C.PANINI. A 26-Group Library with Self-Shielding factors for Fast Reactor calculations from the UK nuclear Data File, CNEN RT/FI(73)15, 1973.

7 - ELASTIC AND INELASTIC SCATTERING. AVERAGE COSINE

The formulas which we have given as an example of what we need in a preparation of a group library, show that some double integrals are to be made for the angular dependence of the elastic cross section when the average cosine of scattering and the average lethargy increment at each energy E must be obtained.

In particular, the cosine limit value in the CM system at which a transfer to the nearest group is possible, must be determined.

In other words, we must be able, for each neutron which happens to fall in a given group, to recognize the starting upper group of provenience. This may be a very cumbersome work if we have not a simple set of scattering formulas extendend to the more general case of the inelastic reaction when the excitation energy Q_j of the inelastic reaction enters in the balance of the scattering process.

The present section will therefore be devoted to this problem, with the development of a very compact formalism for inelastic scattering, from which the forward and backward neutron energy, before and after the inelastic collision can be predicted. The elastic collision will be a particular case of the inelastic one, with the level energy $Q_j=\emptyset$.

THE KINEMATIC LAWS for collision between two particles as neutron-nucleus, may be written with reference to the Center of Mass (CM) or Lab. System (LS).

A cross section for ELASTIC SCATTERING reaction is a function of the excitation energy E_o of neutron in the lab system and the energy of the emitted neutron after collision in the same system is related to the angle or to the cosine μ of the scattering angle θ, between the two directions of the neutron velocity before and after collision. The three quantities E_o, E and μ are thus strictly related one to each other, according to the principles of energy and momentum conservation for the total system neutron + target nucleus.

In the case of INELASTIC SCATTERING a supplementary quantity must be taken into account which is indicated as Q_j in the CM system and corresponds to the j-level of the target nucleus exited after collision.

In order that the supplementary energy Q_j will enter in the balance, it is clearly needed that the neutron energy exceeds at least the energy of the first excited state of the nucleus. As an indication, in the light nuclei the energy of the first level is about 1 MeV, while for the heavy nucley is about Ø.1 MeV. We can thus regard an energy of about 1ØØ keV as the lower limit for a reaction of inelastic scattering. Below this limit the slowing down of the neutrons to the thermal energy is mainly obtained by means of elastic scattering.

In the study of the scattering on the basis of the mechanical laws of collision it is convenient to assume the Center of Mass (CM) system as a reference, better than the Lab. System (LS). The reasons are the following:

a) The center of mass is always on the line joining the center of the two particles, so that the motion is always directed toward the CM before and outward the CM after collision (i.e. change of sign).
b) The modulus of velocity does not change from before to after collision (changes the sign) and is inverse proportional to the masses.
c) The motion lies on a plane, while it should be in the tridimensional space if the Lab System is used.
d) In the CM system the elastic scattering at low energy is practically isotropic, i.e. the outgoing neutrons are observed from the CM with a constant density on any sphere around it.

The formulas for the elastic scattering are here given to point out the change needed in the case of inelastic scattering, when a quantic level is excited with a consequent emission of a gamma ray.

The energy Q_j of the excited level is normally given in the CM system and is then equal to the "threshold energy" of the excited level $(E_{th})_j$ in the Lab System multiplied the reduced mass $m_r = A/(A+1)$, where A=mass of the target nucleus and 1=neutron mass.

The conversion from LS to CM system is easily performed taking into account the above point b) and depends upon the reduced mass as follows:

$$\frac{\text{Energy in LS}}{\text{Energy in CM}} = \frac{\text{incident mass}}{\text{reduced mass}} = \frac{1}{m_r}$$

Q_j is normally given in CM system because the formulas for the scattering are given in the same system. Thus, a quite similar form is assumed by the formulas for elastic and inelastic scattering respectively.

We shall here present in parallel the mentioned formulas in a way which is particularly useful for the preparation of a group library. In fact, for the calculation of the average cosine of scattering in a group, it is needed a prediction of both the final energies after, in the case that energy before collision is known and viceversa the prediction of the starting energies (i.e. the starting group) when the final energy (i.e. the ending group) is known.

The obtained formulas have a high level of simmetry for both the cases. In the following pages we shall collect all the notations and formulas.

We start with some general news.

THE CHANGE OF REFERENCE SYSTEM FOR DIFFERENTIAL CROSS SECTIONS

Let it be:

e = subindex for "elastic"

i = subindex for "inelastic"

1 = mass of neutron

A = mass of the target nucleus (neutron mass = 1)

E_o = initial neutron energy before collision (Lab System)

E = final neutron energy after collision (Lab System)

μ_c = cos ϕ (ϕ = scattering angle in Center of Mass System)

μ_L = cos θ (θ = scattering angle in Laboratory System)

ELASTIC

$$\frac{E}{E_o} = \frac{A^2 + 2A\mu_c + 1}{(A+1)^2} \qquad (1)$$

$$K = 1 \qquad (2)$$

INELASTIC (see /1/)

$$\frac{E}{E_o} = \frac{A^2K^2 + 2AK\mu_c + 1}{(A+1)^2} \qquad (1)$$

$$K = \sqrt{1 - \frac{Q}{E_o}\,\frac{A+1}{A}} \qquad (2)$$

with $E_o > \frac{A+1}{A} Q_{CM}$

and $Q_{CM} > 0$

The following relations exsist between μ_L and μ_C

ELASTIC	INELASTIC
$\mu_L = \frac{A\mu_c + 1}{(A^2 + 2A\mu_c + 1)^{\frac{1}{2}}}$ (3)e	$\mu_L = \frac{AK\mu_c + 1}{(A^2K^2 - 2AK\mu_c + 1)^{\frac{1}{2}}}$ (3)i
$\mu_L = \sqrt{\frac{E_o}{E}} \frac{A\mu_c + 1}{A + 1}$ (3)e	$\mu_L = \sqrt{\frac{E_o}{E}} \frac{AK\mu_c + 1}{A + 1}$ (3)i

In literature is used

$$\frac{1}{AK} = \gamma = \frac{E_o}{E_o A^2 - QA(A+1)}$$

From the above relations, taking into account that it must be

$$\frac{\delta(\mu_c)\, d\mu_c}{d\bar{\Omega}_c} = \frac{\delta(\mu_L)\, d\mu_L}{d\bar{\Omega}_L}$$

we obtain (calculating $d\mu_L/d\mu_c$), in the elastic case:

$$\delta(\mu_c) = \frac{A(A^2 - 1 + \mu_L^2)^{\frac{1}{2}}}{A^2 - 1 + 2\mu_L(A^2 - 1 + \mu_L^2)^{\frac{1}{2}} + 2\mu_L^2} \delta(\mu_L)$$

$$d\mu_L / d\mu_c$$

A similar procedure for inelastic scattering
where the fraction on the right hand is the mentioned ratio obtained by derivation of formula (3)e.
A similar operation gives us the corresponding formula for the inelastic case.
For the caluclation of the average cosine of inelastic scattering from an arbitrary group to the next one, let us assume to start from UK Nuclear Data Library (UKNDL).

Then, the following data are given for inelastic ascattering:

1 - Q_j, i.e. the energy of the j-excited level in CM system.
2 - For every Q_j there is a tabulated "exitation function" or a $\sigma_j(E)$ for a set of $E_k > Q_j$.
3 - The same set of E_k is given for all the j-level in the common energy range.
4 - All the $\sigma_j(E_k)$ are ISOTROPIC IN THE CM SYSTEM for what concerns the angular dependence of scattering: i.e. we may think that inelastic collision dumps so much the exitation energy to reproduce - after collision - the condition of elastic scattering at low energy. Thus, the maximum loss of energy per collision is

ELASTIC	INELASTIC
$E > E_{min} = E_o \frac{A-1}{A+1}^2$	$E > E_{min} = E_o\left(\frac{AK-1}{A+1}\right)^2$ (4)

The cosine μ_c in CM is a function of E_o, E, i.e.

$\mu_c = \frac{\frac{E}{E_o}(A+1)^2 - (1+A)^2}{2A}$	$\mu_c = \frac{\frac{E}{E_o}(A+1)^2 - (1 + A^2K^2)}{2AK}$ (5)

The above formulas make use of $K(E_o)$,
with E_o = energy BEFORE collision.
We may also make use of another function $K''(E)$
with E = energy AFTER collision.
In formula (1) we started from the knowledge of $K''(E_o)$, to obtain E, once E_o is known.
Let now try to make the inverse process, i.e. E is known and we want to obtain E_o as a function of μ_c, the scattering cosine in CM system.
The maximum and minimum energy transfer in the collision is given for

$$\left.\begin{aligned} \mu_c &= -1 \\ \mu_c &= +1 \end{aligned}\right\} \quad \begin{aligned} &\text{for maximum loss of energy} \\ &\text{for minimum loss of energy} \end{aligned}$$

These values in formula $(1)_i$ give the maximum and minimum distance of energies $E - E_o$, or

For a fixed E after collision, in the formula

$$\frac{E}{E_o} = \frac{A^2K^2(E_o) + 2AK(E_o)\mu_c + 1}{(A+1)^2}$$ we have:

E_o max $\rightarrow \mu_c = -1$ and being $K(E_o) = \sqrt{1 - \frac{Q}{E_o}\frac{A+1}{A}}$

E_o min $\rightarrow \mu_c = \mp 1$

we have two values

$$\frac{E}{E_o \text{ max}} = \frac{A^2K^2(E_o \text{ max}) + 2AK(E_o \text{ max}) + 1}{(A+1)^2}$$

$$\frac{E}{E_o \text{ min}} = \frac{A^2K^2(E_o \text{ min}) - 2AK(E_o \text{ min}) + 1}{(A+1)^2}$$

The above two formulas may be written in a unified expression

$$\frac{AK(E_o) \pm 1}{A+1}^2 E_o = E \text{ where} \quad \begin{cases} E_o = E_o \text{ max} & \text{if } - \text{ is taken} \\ E_o = E_o \text{ min} & \text{if } + \text{ is taken} \end{cases}$$

Let now have some little algebra:

$$\frac{AK(E_o) + 1}{A+1}\sqrt{E_o} = \sqrt{E} \qquad \text{(by square root)}$$

$$A\sqrt{E_o}K(E_o) \pm \sqrt{E_o} = (A+1)\sqrt{E}$$

$$A\sqrt{E_o}\sqrt{1 - \frac{Q}{E_o}\frac{A+1}{A}} \pm \sqrt{E_o} = (A+1)\sqrt{E}$$

$$A^2E_o\left(1 - \frac{Q}{E_o}\frac{A+1}{A}\right) = \left[(A+1)\sqrt{E} \mp \sqrt{E_o}\right]^2$$

$$= (A+1)^2 E \mp 2(A+1)\sqrt{E}\sqrt{E_o} + E_o$$

$$A^2E_o\left(1 - \frac{Q}{E_o}\frac{A+1}{A}\right) \pm 2(A+1)\sqrt{E}\sqrt{E_o} - E_o - (A+1)^2E = 0$$

$$AE_o - A(A+1)Q \pm 2(A+1)\sqrt{E}\sqrt{E_o} - E_o - (A+1)^2E = 0$$

$$(A^2-1)E_o \pm 2\sqrt{E}(A+1)\sqrt{E_o} - \left[A(A+1)Q + (A+1)^2E\right] = 0$$

Putting $\sqrt{E_o} = y$, $E_o = y^2$ this is a 2nd degree eq. in y. Then:

$$y = \sqrt{E_o} = \frac{\mp 2(A+1)\sqrt{E} \pm \sqrt{4E(A+1)^2 + 4(A-1)(A+1)^2\left[AQ + E(A+1)\right]}}{2(A-1)(A+1)}$$

$$\sqrt{E_o} = \frac{\mp\left[\pm\sqrt{E}\right] \pm \sqrt{E + (A-1)\left[AQ + E(A+1)\right]}}{A-1}$$

$$\sqrt{E_o} = \frac{\pm\sqrt{E} \pm \sqrt{E + A^2Q - AQ + E(A^2-1)}}{A-1}$$

In conclusion, we have the expression

$$\sqrt{E_o} = \frac{\pm\sqrt{E} \pm \sqrt{QA(A-1) + A^2E}}{A-1} \qquad (6)$$

if Q = 0 (elastic case) we have

$$\sqrt{E}_o = \frac{\pm\sqrt{E} \pm \sqrt{E}A}{A-1}\ ; \qquad \sqrt{\frac{E_o}{E}} = \frac{\pm 1 \pm A}{A-1} = \frac{\pm(A+1)}{A-1}$$

$$\frac{E}{E_o} = \frac{(A-1)^2}{[\pm(A+1)]^2} = \left(\frac{A-1}{A+1}\right)^2 \qquad \text{(usual relation)}$$

By similarity with the relation between E and E_o written using K (E_o), let us collect A^2E under the root in expression (6) above and introduce the symmetrical variable

$$K(E) = \sqrt{1 + \frac{Q}{E}\ \frac{A-1}{A}}$$

With this definition the expression (6) may be written

$$\sqrt{E}_o = \frac{\pm\sqrt{E} \pm \sqrt{E}\ AK^{::}(E)}{A-1} \qquad \text{from which}$$

$$E_o = E\left(\frac{AK^{::}(E) \mp 1}{A-1}\right)^2 \rightarrow \begin{cases} E_{o\ max} & \text{if + is taken} \\ E_{o\ min} & \text{if - is taken} \end{cases}$$

to be compared with

$$E = E_o\left(\frac{AK(E_o) \pm 1}{A+1}\right)^2 \rightarrow \begin{cases} E_{max} & \text{if + is taken} \\ E_{min} & \text{if - is taken} \end{cases}$$

Note the symmetry of formulas with signs reversed and

$$K^{::}(E) = \sqrt{1 + \frac{Q}{E}\ \frac{A-1}{A}}$$

$$K(E_o) = \sqrt{1 - \frac{Q}{E_o}\ \frac{A+1}{A}}$$

EXERCISE: Check for Q = 1 and A = 10

Given E_o = 2 → find E (take + sign)

Given E = 0.982089 → find E_o

The two calculations must be consistent.

REFERENCES

Part I, sec. 7

1 - Journal of Research of the Nat. Bureau of Standard, A. Phys. and Chem., vol. 63 A, no. 2, sept-oct. 1959, p. 1Ø8, form. (4.4), (4.6).

2 - W. HAUSER and H. FESHBACH. The inelastic scattering of neutrons, Phys. Rev., 87,2,366, July 15, 1952.

8 - NUMERICAL INTEGRATION

We could realize, from the above sections, that one of the most important problems for a generation of a group cross section library, is the numerical integration, over the group energy interval, of the tabulated cross sections wheighted with the proper flux.

The common methods of numerical integration are well known and can be found in every publication on the numerical calculus. The methods are generally based on a polynomial fit of the discrete points $y(x_J)$ more frequently generated for a grid of evenly spaced values xi with constant interval h. The 3-points Simpson rule, the 5-points Villarceau rule and the 7-points Hardy rule are the most used /1/,/2/.

A recent powerful method which can sometimes conveniently substitute the traditional ones based on the piecewise approximation of integrand by polynomials, is the ROMBERG method. A description of the Romberg method is well presented in ref. /3/, where Archimede's process for computing π is recalled as the basis for such method. The process was lost untill Romberg applied it to numerical quadrature.

The Romberg's formula can be written in terms of the trapezoidal rule for EQUALLY SPACED ABSCISSAE with constant interval h. To compute the integral I, the trapezoidal rule is

$$I = \int_a^b y(x)ds = h\sum{}'' y(a + kh) = T(h) \qquad (1)$$

where h=(b-a)/n and Σ'' indicates that the boundary values y(a) and y(b) are to be taken with weights 1/2.

The general Romberg quadrature method is represented by a set of nested recurrence formulas. The first of them from which all the following can be generated, is given by

$$S_m(h) = \frac{4^{m-1}T(h) - T(2h)}{4^{m-1}-1}$$

beginning with the "order" m=2. Increasing the order by a unit (m=3), S may substitute T in the formula and so on. Therefore, putting the set $S_1 \equiv T(h)$; $S_2 \equiv S_1(h)$; etc., a general formula can be written (k=2,3,4,...)

$$S_k(h) = \frac{2^{2(k-1)}S_{k-1}(h) - S_{k-1}(2h)}{2^{2(k-1)}-1} \qquad (2)$$

It can be verified /4/ that S_2 is equal to the Simpson rule for equally spaced points, while S_3 is equal to the Villarceau rule, i.e. the polynomial integration with five equally spaced points. The following formulas (k=4,5,...) do not coincide with any known polynomial integration.

Since in the problems of integration for group averaging, more often unequally spaced points are needed (due to the cross section profile in resonance region), the Romberg method has been extended to unequally spaced points /4/ and over a large number of cases was tested to be a good improvement to the traditional methods.

Then, we present here without demonstration the final formulas for such a case.

MATRIX FORM FOR THE GENERAL ROMBERG QUADRATURE.

Let us indicate by T(h), T(2h), T(4h),...etc. the trapezoidal areas calculated assuming a scanning of abscissa with 1, 2, 4,...etc. intervals at one time, extending the same meaning to the case of unequal intervals ($h_1 \neq h_2 \neq h_3 \neq \ldots$).

Then all the expressions (2) for the Romberg areas of every order can be written in the following matrix form

$$\begin{vmatrix} a_{11} & 0 & 0 & \ldots \\ a_{21} & a_{22} & 0 & \ldots \\ a_{31} & a_{32} & a_{33} & \ldots \\ \ldots & \ldots & \ldots & \ldots \\ \ldots & \ldots & \ldots & \ldots \end{vmatrix} \begin{vmatrix} +T(h) \\ -T(2h) \\ +T(4h) \\ \ldots \\ \ldots \end{vmatrix} = \begin{vmatrix} D_1S_1(h) \\ D_2S_2(h) \\ D_3S_3(h) \\ \ldots \\ \ldots \end{vmatrix} \qquad (3)$$

where $S_1(h) \equiv T(h)$, $S_2(h)$, $S_3(h)$ ... etc. are the successive Romberg integrals of formula (2) and the elements a_{kj} of the constant triangular matrix are given by the recursive formula:

$$a_{kj} = 2^{2(k-1)}a_{k-1,j} + a_{k-1,j-1} \qquad \text{if} \quad k \geq j$$

$$a_{kj} = 0 \qquad \text{if} \quad k < j \,.$$

The elements with one or two indexes lower than 1 are attributed the value 0. The first element $a_{11} = 1$.

The coefficients D_K are given by the following recursive formulas:

$$D_1 = 2^0 = 1$$

$$D_2 = D_1(2^2-1)$$

$$D_3 = D_2(2^4-1)$$

$$\ldots\ldots\ldots$$

$$\ldots\ldots\ldots$$

$$D_k = D_{k-1}(2^{2(k-1)}-1)$$

The triangular matrix is therefore built up exclusively through power of two and all the elements of its principal diagonal are equal one.

A calculation of the system (3) up to order five, gives

$$\begin{vmatrix} 1 & 0 & 0 & 0 & 0 \\ 4 & 1 & 0 & 0 & 0 \\ 64 & 20 & 1 & 0 & 0 \\ 4096 & 1344 & 84 & 1 & 0 \\ 1048576 & 348160 & 22848 & 340 & 1 \end{vmatrix} \begin{vmatrix} +T(h) \\ -T(2h) \\ +T(4h) \\ -T(8h) \\ +T(16h) \end{vmatrix} = \begin{vmatrix} S_1(h) \\ 3\ S_2(h) \\ 45\ S_3(h) \\ 2835\ S_4(h) \\ 722925\ S_5(h) \end{vmatrix} \quad (4)$$

An interesting property of the numbers in this system may be immediately checked out. The summation of the elements with alternating signs of any k-row in the matrix, is equal to the corresponding coefficient of the S_K area along the right hand side vector.

Therefore, each of the Romberg areas S_K appears to provide a weighted value for successive trapezoidal areas with bases varying according to a factor two. An explanation for such weights is easily provided. Let us, for instance, attribute a weight 4096 to a trapezoidal area T(h) obtained through a subdivision of the integration interval into 8 subintervals. By duplicating the number of intervals (i.e. 16), the weight of the same trapezoidal area T(h) will increase by a square factor 16x16=256, i.e. the new weight must become 4096 x 256 = 1048576.

The same factor must be applied to the numbers in columns two, three, etc., but now the weights must be added to the starting value for the same subdivision in the row above. For example, 4096+(1344x256) = 348160 where 4096 is the starting value for a subdivision of the total interval into 8 subintervals.

The numbers in the right hand side of (4) are the sum, with alternate signs, of the corresponding row of the matrix.

In appendix the list is given of the ROMB code, which performs the quadrature by this method.

It must be observed that the finite number of digits which can be manipulated by the computer makes it impossible to have some of the numbers of the triangular matrix correctly stored in the memory.

A truncation error cannot be avoided for orders of quadrature too high. By this reason, it has been found convenient in the ROMB code to stop the order of the triangular matrix at number five.

REFERENCES

Part I. sec. 8

1 - J. LEGRAS. Precis d'analyse numerique, Dunod, Paris, 1963.

2 - H. MINEUR. Techniques de calcul numerique, Dunod, Paris, 1966.

3 - F.L. BAVER, H. RUTISHAUSER and E. STIEFEL, New Aspects in Numerical Quadrature, proc. Simp. Appl. Mathem., 15, 1963.

4 - M. MOTTA. The Romberg Quadrature Method for not equally spaced points, unpublished.

5 - P.J. DAVIS. Interpolation and approximation, Blaisdell Publ. Co., New York, 1961.

6 - P.J. DAVIS and P. RABINOWITZ. Numerical Integration, Blaisdell Publ. Co., New York, 1967.

PART. II. NUCLEAR DATA FILES HANDLING AND CONVERSION

BY G.C. PANINI (ENEA, BOLOGNA, ITALY)

presented by M. Motta

I. DEFINITIONS

A library is a collection of data evaluations stored in a computer redable format that can be used as input into cross section processing programmes. Library data are subdivided into materials.

A material is defined either an isotope or a collection of isotopes. It may be a single nuclide, a natural element containing several isotopes, a molecule containing several elements or a (standard) mixture of elements. Each evaludaded set of data for a material is assigned an identification number which is unique in that library.

Each material is subdivided into sections which contain the same type of data.

A type of data defines the data for a certain type of information. Integral data and differential data are different types of data. Also resonance parameters (if any) are a type of data. Each type is assigned an identification number: not all materials have all types of data, but the most part of them have. Each type of data is subdivided into subsections xhich are called reactions.

A reaction generally refers to a specific neutron-nucleus interaction mechanism, but occasionally it indicates that a particular type of information is given. Total cross section is a reaction, but also the mean number of neutrons per fission is referred to as a reaction. General information section (if any) is a reaction too. Each reaction is assigned an identification number; a reaction may belong to different types of data: this is the case of the inelastic process which appears as integral cross sections, as secondary neutron angular distributions and as secondary neutron energy distributions.

Within each reaction data can be given in a variety of form, depending on the data type and on the reaction itself. Integral neutron cross sections are often given in tabular form, i.e. with pairs of cross section vs. energy. Angular differential cross sections can be given both in tabular and parametric (Legendre polynomial) form. Resonance parameters can represent the cross section curves using different approaches.

It is generally agreed that all the numerical quantities are given in increasing order of magnitude. Within some subset a library is given:

a) in increasing order of the material identifier;
b) in increasing order of the data type identifier;
c) in increasing order of the reaction type identifier;
d) in increasing order of energy.

Nuclear Data Libraries are generally contained into magnetic tape support, being the size of each library so large as the use of other supports may be very expensive. Two basic format exist for the libraries:

a) card image (decimal) data representation which is suitable for the immediate understanding of the contents and for easy communication among different computers;
b) binary (machine dependent) representation which speed up the run time of processing codes.

Most part of the existing Libraries has the same Reaction Identification Number sequence, but has not identical Data Type Identification numbers: the table listed in the following (which is particular of ENDF/B) is here presented as an example.

A common peculiarity of the Nuclear Data Libraries is that all use six field records in the card image format. This is due to some FORTRAN features: all Libraries have in fact been designed keeping in mind FORTRAN processing and maintenance codes.

The following standard information are given through numbers:

DATA TYPE IDENTIFICATION NUMBERS

1. General Information
2. Resonance Parameters
3. Neutron Cross Sections
4. Angular Distributions of Secondary Neutrons
5. Energy Distributions of Secondary Neutrons
6. Energy-angular Distibutions of Secondary Neutrons
7. Thermal Neutron Scattering Law Data

DESCRIPTION OF CLASS OF REACTIONS

Range	
1-100	Reaction types in which secondary particles of the same type as the incident particles are emitted.
100-150	Reaction types in which no secondary particles of the same type as the incident particles are emitted.
201-450	Quantities derived from the basic data
451-699	Miscellaneous quantities
700-799	Excitation cross-sections for reactions that emit charged particles

REACTION IDENTIFICATION NUMBERS

I.	Total cross section (sum of all partial cross sections)
2.	Elastic scattering cross section
3.	Non-elastic cross section (##1 - ##2)
4.	Total inelastic cross section (sum of #/ 5I to #/ 9I)
I6.	(n,2n) cross section
I7.	(n,3n) cross section
I8.	Total fission cross section (sum of #/ I9, #/ 20, #/ 2I)
I9.	(n,f) cross section (first chance fission)
20.	(n,n'f) cross section (second chance fission)
2I.	(n,2nf) cross section (third chance fission)
22.	(n,n'α) cross section
23.	(n,n'3α) cross section
28.	(n,n'p) cross section
5I.	(n,n') to the first excited level
52.	(n,n') to the second excited level
..	
90.	(n,n') to the 40th excited level
9I.	(n,n') to the continuum
I0I.	Neutron disappearance
I02.	(n,γ) cross section (radiative capture)
I03.	(n,p) cross section
I04.	(n,α) cross section
I05.	(n,t) cross section
I06.	(n,He-3) cross section
I07.	(n,α) cross section
I5I.	Resonance parameters
25I.	$\overline{\mu}_L$, the average cosine of the scattering angle (laboratory system for elastic scattering
252.	ξ , the average logarithmic energy decrement for elastic scattering
253.	γ , the average of the square of the logarithmic energy decrement for elastic scattering, divided by twice the average logarithmic energy decrement for elastic scattering
45I.	Alphanumerical information (Data type #/ I only)
452	$\overline{\upsilon}$, the average number of neutrons released per fission event
457.	Radioactive decay data.
459	Fission product yield data.

Basic references for the description of the main libraries are hereni listed.

REFERENCES

UKNDL

K. Parker: The Aldermaston Nuclear Data Library as at May I963. AWRE 0-70/63 (I963)

ENDF/B

R. Kinsey, rev.: ENDF I02 - Data Format and Procedures for the Evaluted Nuclear Data File, ENDF. BNL-NCS-50496 (ENDF I02)2nd Ed. UC - 80 (TID-4500) (I979)

KEDAK

D. Woll: Card Image Format of the Karlsruhe Evaluated Nuclear Data File. KFK - 880 EANDC (E)-II2"U" EUR 4I60 e (I968)

See also:

B. Goel, B. Krieg: Status of the Nuclear Data Library KEDAK-3 October I975. KFK-2234 NEANDC (E) I7I"U" (I975)

ENDL

R.J. Howerton, R.E. Dye, S.T. Perkins: Evaluated Nuclear Data Library UCRL -50400 Vol. 4 Rev. I (I98I)

SOKRATOR

V.E. Kolesov, M.N. Nikolaev: Sokrator Manual. INDC (CCP)-97/L+Special. Translated by IAEA (I977)

2. MAINTENANCE CODES

The maintenance of a Nuclear Data Library is one of the important chapter in its history. As well as each collection of information, a Library of Nuclear Data should be:

- checked
- updated
- retrieved
- displayed

In addition, due to the nature of the contents, the possibility of a point-by-point and integral quantities calculation should be available.
The checking includes a two step process:
a) consistency check;
b) physical check.
In general the first one is referred to clerical errors which may arise from the physical nature of data (e.g. a cross section cannot be negative) or from the Fortran format (e.g. an exponent E+02 not right adjusted leads to a 10^{20} quantity). The latter is more strictly concerned with the physics of data (e.g. total cross section must be the sum of all partial reactions) or with its representation (e.g. a tabular distribution should extent from -I to +I cosine values). A checking code should in addition provide the reading of the data to be checked also in the case when the format of some records is completely altered by manipulation errors.
Updating includes the possibility of:

- inserting
- deleting
- altering

information. It should be noted that inserting and deleting can modify the numeber of items included in some set or subset; in this case the indexes and the tables of contents must be updated. Library updating occurs periodically when a sufficient numeber of modifications have been collected. A new release should be issued when completely new data from experiment or modell calculations become available.
Retrieving is a necessary step when library data are to be processed or when portions of the library are to be transmitted outside. In addition, processing codes, in general, include tape scanning while some material is searched, but when more than one material is requested and they resides on different tapes, they are to be merged together before the processing code read them. Also retrieving some few i tems of a library may be useful.
Displaying a library can be done (mainly) in two ways:

- interpreted list;
- graphical output.

Interpreted lists can give a key to the library reading and are suitable for the retrieval of some more often required information such as e.g. the resonance parameter. Its disadvantage is that, in general, they requires a large amount of paper with subsequent storage problems.
More compact is the graphical representation which can be useful in studying the shape of some reactions, in a by eye checking of clerical errors and in a fast (but approximate comparison among data from different sources.
Other codes allow the calculation of resonance integrals, 2200 m/sec cross sections, resonance peaks and other quantities which are often required.
Finally, when binary data representation is allowed, decimal to binary and viceversa conversion programmes exist.
Many maintenance codes exist which perform some or all of the above listed steps; no reference is given for some of them.

REFERENCES

O. Ozer, ed.: ENDF-IIO Description of the EDNF/B Processing Codes and Retrievol subrautines. BNL-50300 (TID-4500) (I97I) (Most recent codes not included are: FIZCON, RESEND, PSYCHE, INTER, INTEND, SUMRIZ, PLOTEF, LSTFCV)

M.R. Bhat: ENDF- I48 ENDF/B Processing Codes for the Resonance Region. BNL 50296 (TID - 4500) (I97I)

SODRATOR

V.E. Kolesov, A.S. Krivtsov, N.A. Solovev: Automation of the Procedure for checking Information contained in the Library at Evaluated Nuclear Data: POSOSHOK Programme. INDC (CCP) - 23/G. Translated by IAEA (I972)

UKNDL

Code name	Reference		Description
ADDENDUM	Unpublished		Adds arbitrary energy polynomial to any specified reaction
AMEND	AEEW internal		For amending and modifying data files in various ways
CHECK-I	AEEW-M347		Checks format and arithmetical consistency of data files
CHECK-2			See CHECK-I
EDIT	AEEW-M604 & internal		For merging files from various tapes to form a data library
AID	Unpublished		See AMEND
GROD-360			Prepares tapes for graphical representation of data data on a CRT
JOIN	Unpublished		For joining together two data files at a prescribet energy
LCHECK	AEEW (internal)		For performing elementary sequential checks
MINIGAL	Unpublished		For computing integral quantities from the Data File
PANDIT			For adjusting Data Files from calculated adjustment to group cross-sections
SICAR	AEEW internal		Calculates Doppler broadened cross sections from resonance parameters using MLBW (AEEW-M5I7) and TEMPO (AEEW-M5I8): has much improved energy point selection.

ENDF/B

Code name	Reference		Description
ADLER	ENDF-I48		Calculates resonance cross-sections using Adler-Adler formula
AVERAGE-4	ENDF-I48		Calculates infinitelt-dilute resonance cross-sections from unresolved parameters
CHECKER	ENDF-II0		Detects errors in the file
CRECT	ENDF-II0		Corrects Data Tapes
DAMMET	ENDF-II0		Deletes, alters mode and merges tapes
DICTION	ENDF-II0		Constructs dictionary for a material
EDIT	ENDF-I05		Reads, writes and plots data
INTER			For computing various integral quantities
LISTFS	ENDF-II0		Reads and writes data
OVERLAY			Overlays ENDF/B with any other data set
PLOTFB	ENDF-II0		See EDIT
PSYCHE			Physics checking code for neutron data
RAMP-I	ENDF-I48		Calculates resonance cross-sections for Reich-Moore parameters
RESEND			For producing a pointwise file from resonance parameters
RIGEL	ENDF-I48		See DAMMET
SIGMA-2	ENDF-I48		Calculates resonance cross-sections from single or multi-level Breit-Wigner
SUMUP			Performs sums of partial cross-sections to check with total

./..

ENDF/B

Code name	Reference		Description
FIZCON	ENDF-IIO		Checks data for physics consistency
INTEND	ENDF-IIO		General purpose integration Programme
SUMRIZ	ENDF-IIO		Create a summary at an ENDF/B material
STNRD	ENDF-IIO		Standardize ENDF/B data formats
PLOTEF	ENDF-IIO		Plotting code
LISTFCV	ENDF-IIO		Produces interpreted listings
EVALPLOT	UCRL-50400		Plotting code

List C

KEDAK

Code name	Reference		Description
KEDABE	KFK (internal)		Generation of consistent data in case of redundant information for input to KEMA
KEMA			Checks, updates and alter KEDAK library
LDEPAC			General retrieval routine package
NDF			See LDFPAC
REFOR	KFK (internal)		Generation of input for KEMA
RESEDI			Printing of resonance information
RETPAC			See LDEPAC
SELPLO	unpublished		Plotting of elastic angular distributions
SELDIF	KFK (internal)		Printing of partial data
SGIPAR	KFK (internal)		See SELDIF
SIGEDI			See SELDIF
SIGPLO	unpublished		Plotting of cross-sections
SIGPR	KFK (internal)		See SELDIF
TSTKED			Testing programme for KEDAK

3. THE NEED OF CONVERSION AMONG DIFFERENT FILES

The need of translating all or part of one Nuclear Data Library from one format into another may arise from different requirements.

a) When an Institute has adopted for its purpose one Nuclear Data Library, all maintenance and processing codes are, in general, devoted to that Library format. While users are gaining experience in using the various codes, their knowledge is going more and more deeply into the format. Thus when a new Library becomes available, it seems in general the case of translating it into the home format, for comparison and/or improvement purposes, rather than using the new Library with its own codes.

b) Some format is gaining a more general adoption with respect to others, so as to be used as transmission format among different Institutes. Conversion into thet format shoul then be available.

c) No data exist in a given Nuclear Data Library for some material, while a different one has.

d) Format conversion sometimes implies only the fact of translating data from parametric to pointwise representation.

Format conversion involves not only a change in the structure of a Library, but also in the logic configuration. The striking example for this assessment is the precence or absence of resonance parameters, which implies the use of different approaches to reactor physics problems. In addition, when a material has been translated into a new format, comparison between the results of the processing codes of either formats (source and object) may lead to shocking results. When this happens, is the difference due to the translating code, to the processing codes or are both steps responsible?

Another problem is the presence of some data for which no provision are made in the object format or, worst case, the absence of data in the source library which are needed in the object. A one-to-one correspondence is in this case highly desiderable.

Codes exist which perform "good" conversions of data from one source format to another, but their results should be handled with care and, in general, amended from slight inconsistencies and completed with some kind of data.

The object of the complete automation could probably be achieved provided that data are tested for consistency errors and, mainly, for physical errors. Integral quantities, such as averages based on different functions, should in addition be calculated from the original as well as the translated data for their comparison. Anyway the best approach to conversion is to combine the use of a translation code wich a certain amount of evaluation effort.

A limited number of codes exists which accepts several formats: its phylosophy is structuring the data internally in a format which exists only for the time the code is in the computer. These programmes eliminate the ambiguity of using different algorithms in processing the same data either in the original or in the translated version. They seem to be a useful tool during the data evaluation process, in checking and comparing data.

Main conversion codes are listed here: it should be noted that most of them are no longer used.

CONVERSION CODES

Programme	Translation from	Translation to	Author	Laboratory of origin
BRIGITTE	ENDF/B	KEDAK	J.C.Schepers	CEN. Mol, Belgium GFK, Karlsruhe, Germany
MISSIONARY	ENDF/B	UKNDL	J. Cameron	AWRE, Aldermaston, UK
TRAKEDAK	KEDAK	UKNDL	A. BEYELER	CEN, Saclay, France
UTOE	UKNDL	ENDF/B	G.C.Panini	CNEN, Bologna, Italy
KTOE	KEDAK	ENDF/B	G.C.Panini	CENN, Bologna, Italy
UKTOA	UKNDL	ENDF/A		JAERI, Japan Report JAERI - Memo - 3I62
LTOE	ENDL	ENDF/B		LLL, Livermore, USA
LRL-UK	ENDL	UKNDL		LLL, Livermore, USA
ENDF-LRL	ENDF/B	ENDL		LLL, Livermore, USA
UK-LRL	UKNDL	ENDL		LLL, Livermore, USA
ETOS	ENDF/B	SPENG		AE, Sweden R.Q.Wright et al.
UKE	UKNDL	ENDF/B		ORNL, Oak Ridge, USA Report ORNL-TM-2880

Other conversion codes:

a) From parametric to paintwise ENDF/B: O. OZER: RESEND. A Programme to Prepocess FNDF/B Material with Resonance Files in Pontwise form BNL-I7I34 (I976)
D.E. Cullen: RECENT. Recoustruction of Energy Dependent Cross Sections from Resonance Paramenters in ENDF/B format. UCRL-50400 Vol. I7 Part. C (I979)

b) Change the interpolation lows to linear linear in ENDF/B :
D.E. Cullen: LINEAR. Linearize Data in the Evaluated Nuclear Data File/ Version B. UCRL-50400 Vol. I7 Part. A Rev. 2 (I979)

Multigranp processing codes which accept more than one format:

a) P. Vertes: FEDGROUP. A Program System for producing Graup coustants from Evoluated Nuclear Data of Files Disserminated by IAEA.
INDC (HUN) - I3/0+Sp. (I976)

b) G.C. Panini: FOURACES. A Programme for Producing Group Averaged cross Sections from Different Files. RT/FI (73) I6 (I973)

4. PONTWISE REPRESENTATION

The format adopted in the Nuclear Data Libraries should be sufficiently flexible to allow the inclusion of manu different kinds of reaction data, both in point-by-point tabulations and in parametric forms. The first one may include not only the simplest cross-section vs. energy sample, but also threedimensional arrays as is the case of a temperature dependence.

Parametric form is comprehensive of a large variety of ways to represent data, such as resonance formulas, Legendre polunomials, analytical expressions such as Maxwell, Watt and Klein-Nishima formulas.

Although sometimes one can freely choose between the pointwise and parametric forms (as iti is the case of neutron angular distributions), in general the parametric form may have physical significance and may used to correlate the results of a number of separate experiments. Examples are:

a) the resonance parameters, which may be derived from measurements;

b) the parameters of statistical distributions of resonance widths and spacings which can be used to convey not only the average cross-sections but also their probable fluctuations.

Use of parametric forms can yield a great saving of storage space in the data library. Thus representing the cross sections in the resolved resonance region accurately, requires sometimes several thousands of tabular points for each cross section at a well defined temperature, whereas a set of some hundreds of parameters would suffice to convey all the information needed to generate the cross sections at some required temperature. On the other hand, problems may arise conflicting with the need of reducing the computer time required for the generation of Doppler broadened cross sections from resonance parameters.

A considerable saving of computer time can be achieved through the following procedure: using a Nuclear Data Library with resonance parameters, one may generate a certain number of libraries of pointwise Doppler broadened cross sections, say at 300 ^{o}K, 900 ^{o}K, I200 ^{o}K, for use in processing codes with the requested group scheme. Taking care of generating for each reaction a sufficient number of energy points so that the linear-linear interpolation law can be used, an additional computer time saving in the processing code running can be obtained.

In the case when resonance data are given, processing codes shoul in general join together the resonance region and the continuum region by adding each other.

The pointwise section may have a "background" which should be also added to the resonance parameter computed cross section. This background has in general no phusical meaning, but its aim is to obtain a correct cross section curve taking into account the following:

a) sometimes the resonance data are originated from different experiments and a "correction" should be made in order to homogenize the resulting cross section; or

b) single level Breit-Wigner formula is used in the processing codes instead of a multi level formula. This is in fact very time consuming and it is convenient to calculate once (at the time when the evaluation is generated) both the MLBW and SLBW cross section curve, to subtract the second from the first one and to assign the difference as background in the pointwise section, so that a SLBW calculation can be made by processing codes.

See LINEAR, RECENT, RESEND codes listed in the previans ponograph. See also:

D.E. CULLEN: SIGMA I. Doppler Broaden Evaluated Cross Sections in the Evaluated Nuclear Data File/version B UCRL-50400 Vol. I7, Part. B, Rev. 2 (I979).

5. FROM THE NDL TO THE POINTWISE CROSS SECTION

Processing of Nuclear Data Libraries involves the computation of the following basic quantities:

$$\int \sigma\phi dE \quad ; \quad \iint \sigma\phi dE'dE$$

where the integrals span over same energy range, σ, ϕ are function of the neutron incident energy and K is a transfer kernel function of E and of the outgoing energy E'. The second quantity is always very hard to compute in terms of numerical accuracy and of computer time.

The first one can take advantage of some simply expressions for ϕ (e.g. $\phi(E)$= constant or $\phi(E)=I/E$) in order to perform fast semianalytical computations. When σ is given in parametric form (resonance region) a full analytical computation of the resonance integral is allowed. Problems arise when σ is given in parametric form and ϕ is point-by-point or when σ is pointwise and ϕ assumes some complicated form. On the other hand the best situation occurs when any point in a reaction can be predicted from the adjacent ones by means of linear-linear interpolation; and possibly ϕ is a simply expression. This latter opportuny cannot meet everywhere, while it is always possible to transform cross-section data in such a way they can be interpolated on linear-linear basis, eventhough the source of the data are resonance parameters. It should be here remembered that the best representation of cross sections in the resolved resonance region is obtained through a log-log interpolation; nevertheless, by introducing several intermediate points, a linear-linear interpolation to a given accuracy degree can be used.

Modern processing codes work on this basis.

Care should be taken in generating the resolved resonance region energy grid to avoid:

a) the curve not be described to a required accuracy degree where the shape is awkward to follow;

b) an excessive number of points be generated where the curve is smooth.

Algorithms has been designed in order to follow the shape of the cross section with a certain degree of accuracy, i.e. by increasing the number of energy point in the regions where the cross section curves rapidly vary and decreasing it when a predetermined interpolation law can approximate them.

The algorithms generally consist of the following steps:

a) a set of initial energy "node points" is selected; node points are set at the peak of the resonances and at some optional energy;

b) the cross section is calculated at the node points: let S_I and S_2 be the computed value at any pair of consecutive node points E_I and E_2 ($E_2 > E_I$);

c) and additional cross section value S_3 is computed at the midpoint E_3,

$$E_3 = \tfrac{1}{2}(E_I + E_2) \; ;$$

d) the value of the approximate cross section S'_3 at the mid-point is obtained by a given interpolation law and compared with the exact value S_3 at the same point;

e) if the fractional difference at the mid-point is not larger than the convergence criterion, i.e. if:

$$\frac{|S_3 - S'_3|}{S_3} \leq \varepsilon \qquad (I)$$

occurs, the interval is assumed to have converged and the process is repeated between the next pair of nodes;

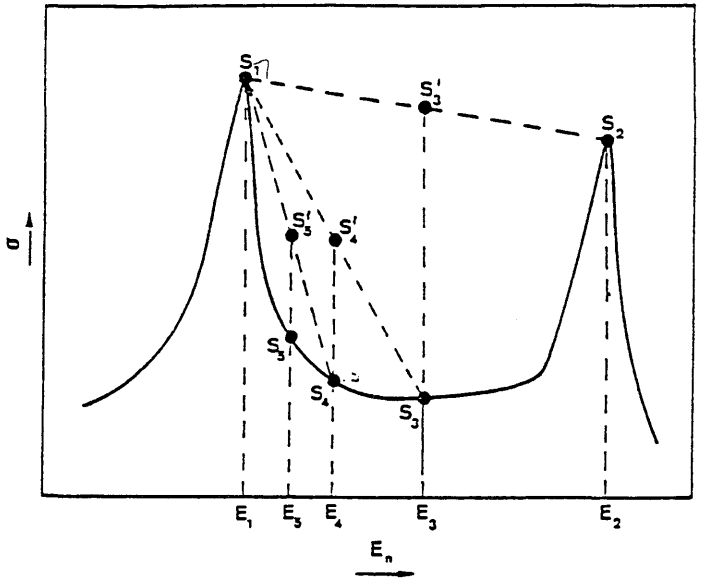

If $\frac{|S_5 - S'_5|}{S_5} \leq \varepsilon$, S_5 is accepted and the range

(E_4, E_3) is investigated.

f) if the fractional difference at the mid-point is larger than the convergence criterion, i.e. when (I) does not occur, the mid-point is defined as a new node and the process is repeated in the halved intervals.

Some veru sophisticated codes have, in addition, an algorithm which further on reduces the number of data after the generation process which normally produces more points than are required for a given interpolation.
More details con be found in the references existed below the previans paragraph.

6. THE MOST COMMONLY USED GROUP SCHEMES AND WEIGHTING SPECTRA

Groupwise representation of nuclear data is the commonly used medium to perform reactor calculations. Group data span over the entire energy range of interest and include in general 3 regions:

a) thermal (low energy) region

b) resonance region, split in B') resolved
B") unresolved

c) continuum (high energy) region.

Depending upon the type of calculation, each region may include more energy groups than others contain (e.g. a fast reactor calculation does not need an accurate description of the cross sections in the low energy range, while a thermal calculation does). All calculations are performed starting from a limited number of groups, sau a few tens. On the contrary, schemes exist with a large number of groups (e.g. 600 or 2000) but those group cross sections are used as a starting Library in order to calculate reduced group scheme libraries with a considerable time saving.
Groups are in general equally spaced in lethargy so as to have a balanced description of the phenomena in different energy regions? Care should be taken mainly in desigining new large group schemes, in order to pick up some typical energies which are of interest from the point of view both of the materials involved and the calculation to be performed. Some examples will explain this point.

a) The important p-ware resonance of Iron-56 at I.I5 keV should be included in its integrity into a unique energy group;
b) the thermal energy range around 0.0253 eV should also be covered by a unique group;
c) thresholds of important reactions such as the inelastic processes, should on the contrary coincide with some group boundary;
d) energies which are typical of some assembly should be regarded too.

When a group scheme has to be used as subsequent input to processing codes which calculate a new (reduced) group scheme or collapse it to a minor number of groups, then a large number of groups is used, say more than 50 and up to 2000;
in this case an equally lethargy spacing is adopted either in the whole range or with constant Δu in some subranges. On the contrary, working libraries use less

than 30 energy groups which are in general either equally spaced in lethargy in the entire range or with larger groups at the higher energies (continuum region).

Also a variety of functions exists over which the cross sections are weighted. Typical measured fluxes of reference assemblies are sometimes used and their shapes are not easily predictable (those weighting functions are normally given point by point to the processing codes). When a group scheme is to be used in subsequent cell calculation a "guess" is adopted for simulating the shape of the flux. One of the most used functions is so defined:

a) A maxwellian shape with the maximum near the thermal energy (0.0253 eV)
$F(E) = \exp(-E/\theta)/\theta^2$,

b) $\phi(E) \propto I/E$ in the intermediate energy range,

c) a fission spectrum at higher energies, say some hundred keV.
$F(E) = C \cdot \exp(-E/0.965) \sinh(\sqrt{2.29E})$

This describes with sufficient approximation the shape of the neutron flux. It should be noted that the I/E function mainly applies in the resolved resonance region: this fact allows to speed up the integral quantity calculations by means of semi-analytical formulas.
Basic multigroup libraries are generated at a given temperature and at infinite dilution, supposing, i.e., the material uniformly distributed in the medium.
Problem dependent libraries, also called working libraries, are then generated at the effective temperature and with the actual densities of the components by means of codes based upon different approaches, the main ones being the Bondarenko method and the Nordheim integral treatment.
A large number of codes exist xhich produce multigroup library for varians purposes. A list of selected codes fallows.

Code name	Reference	Description
UKNDL:		
GALAXY	AEEW-R379	For calculating spectrum averaged multigroup cross-sections
DICE (MOULD)	AWRE 0-27/66	Preparation of nuclear data in a form suitable for Monte Carlo calculations
KEDAK:		
MIGROS-3	KFK-2388	ABBN type microscopic group constant calculation
FIDAS		208 high energy group calculation
GRUMA	KFK (internal)	For manipulating the GRUBA microscopic library
GRUSEEK	KFK (internal)	For reading GRUBA library
GRUPRINT	KFK (internal)	For printing GRUBA library
GRUCAL	KFK (internal)	For production of macroscopic group costants from GRUBA
DASU	KFK (internal)	Prepares data for Monte Carlo calculations
ENDF/B		
AMPX	ORNL/TM-3706	A large code system which will prepare neutron, photon production, and photon interaction cross sections for use in a variety of codes.
BDASS	DPSTM-500 Vo. 5	A collection of IO modules that process neutron interaction, photon interaction, photon production, and fission product data files from ENDF to the JOSHUA system data base.
ENDRUN	GEAP-I3952	Prepares neutron cross sections and shielding factor tables for use in the TDOWN code.
ETOE-2/MC^2-2	ANL-8I44	Prepares broad group neutron cross sections

Follows List 6

Code name	Reference	Description
		for fast reactor calculations. Also used to prepare fine group neutron cross section libraries for use in the SDX code.
ETOG-5	WCAP-3845-I	Prepares neutron cross sections for use in the MUFT, GAM, ANISN, and LASER codes.
ETOT-5	WCAP-7363	Prepares pointwise or group thermal neutron cross sections from Files 2 and 3 of ENDF/B format data.
ETOX	BNWL-I002	Prepares neutron cross sections and shielding factor tables for use in the 1DX code.
FLANGE II	DP-I278	Prepares thermal neutron cross sections from ENDF/B data including S(,) data in file 7. No Adler-Adler capability.
MINX	LA-6486-MS	Prepares neutron cross section and shielding factor tables for the SPHINX code.
GROUPIE	UCRL-50400	Computes group averaged cross sections, Bondarenko factors and multiband parameters.

REFERENCES

ENDL

R.J. Doyas, R.E. Dye, R.J. Howerton, S.T. Parkins: CLYDE a code for the Production of Calculational Constant from Nuclear Data. UCRL-50400 Vol. 5, Rev, I (I975)

See also the FEDGROUP and FOURACES codes listed under paragraph 3.

APPENDIX

Some lists of codes are here reported which performs the following calculations:

BW: Calculates the cross sections in the resolved resonance region, starting from Breit-Wigner resonance parameters.

CRESO: Calculates the cross sections in the unresolved resonance region, starting from average parameters and by means of statistical model.

RINEG: Calculates the unknow parameters of a bound level starting from the input arbitrary parameters resonance energy and radiation width.

ROMB: Performs a numerical quadrature with the Romberg method extended to not equally spaced points.

All the codes are self-guided in their use, being written in the interactive BASIC language (for an Olivetti Desk computer P6066).

A translation in FORTRAN language of the codes may be easy for an expert programmer.

```
      TRIESTE WINTER COLLEGE 1982. LECTURES BY M.MOTTA                Page  1

0010 REM  *  <BW> CODE FOR CROSS SECTION CALCULATION IN RESOLVED REGION  *
0020 REM  *  SINGLE LEVEL AND MULTILEVEL FORMALISMS, ONE or TWO CHANNELS  *
0030 DCL 80(Z$)
0040 PAD Z$,95
0050 FOR I=1 TO 3 STEP 1
0060 PRINT
0070 NEXT I
0080 PRINT " * <BW> CODE FOR CROSS SECTION CALCULATION IN RESOLVED REGION *"
0090 PRINT
0100 DIM A(6),B(3,6),C(3,6),D(3,6),E(250,6),S(6),P(6),F(3),G(10,4),R$(250)
0110 DCL S(E())
0120 FILES *;FIPLO
0122 DISP "          INPUT FILENAME ";
0124 INPUT F$
0126 FILE : 1,F$
0130 DCL 7R$
0140 :'CCCCCCCCCCC'CCCCCCCCCCC'CCCCCCCCCCC'CCCCCCCCCCC'CCCCCCCCCCC'CCCCCCCCCCC
0150 :##.##########.##########.##########.##########.##########.##########
0190 DISP " RECALL DATA FROM <ENDFA> FILE"
0200 RESTORE :1
0210 LET N8=1
0220 READ :1,A(1),A(2),A(3),A(4),A(5),A(6),R$(N8)
0230 FOR J0=1 TO A(5) STEP 1
0240 LET N8=N8+1
0250 READ :1,B(J0,1),B(J0,2),B(J0,3),B(J0,4),B(J0,5),B(J0,6),R$(N8)
0260 LET E1=B(J0,1)
0270 LET E2=B(J0,2)
0280 PRINT "The resolved region is between";E1;" AND";E2;" eV"
0290 LET N8=N8+1
0300 READ :1,C(J0,1),C(J0,2),C(J0,3),C(J0,4),C(J0,5),C(J0,6),R$(N8)
0310 LET J9=1
0320 FOR J1=1 TO C(J0,5) STEP 1
0330 LET N8=N8+1
0340 READ :1,D(J1,1),D(J1,2),D(J1,3),D(J1,4),D(J1,5),D(J1,6),R$(N8)
0350 FOR J2=J9 TO J9+D(J1,6)-1 STEP 1
0360 LET N8=N8+1
0370 READ :1,E(J2,1),E(J2,2),E(J2,3),E(J2,4),E(J2,5),E(J2,6),R$(N8)
0380 NEXT J2
0390 LET J9=J9+D(J1,6)
0400 NEXT J1
0410 NEXT J0
0420 PRINT "DATA ON <ENDFA> FILE HAVE BEEN RECALLED FROM DISK"
0430 PRINT Z$
0440 DISP "     INITIAL ENERGY [eV] = ";
0450 INPUT E1
0460 DISP "      FINAL ENERGY [eV] = ";
0470 INPUT E2
0490 LET J5=E0=0
0500 FOR J0=1 TO A(5) STEP 1
0510 LET J5=J0
0530 DISP "    STEP FOR ENERGY [eV] = ";
0540 INPUT E3
0550 DISP "0,0->no plot ■ I,K -> plot G(I,K)";
0560 INPUT N1,N2
0570 IF N1*N2=0 THEN 640
0580 LET W0=2
0590 SCRATCH :2
0600 WRITE :2,INT((E2-E1)/E3+1),W0,2,0
0610 LET Y1=1E63
0620 LET Y2=-Y1
0630 PRINT TAB(26);"REQUESTED CROSS SECTION"
0640 REM          *  CROSS SECTION CALCULATION  *
0650 REM      ?? LOOP ON ENERGY  ??
0660 FOR E0=E1 TO E2 STEP E3
0670 LET J0=J5
```

```
      TRIESTE WINTER COLLEGE 1982. LECTURES BY M.MOTTA                Page  2

0680 IF (E0-B(J0,1))*(E0-B(J0,2))>0 THEN 2380
0690 FOR J=1 TO 10 STEP 1
0700 FOR J6=1 TO 4 STEP 1
0710 LET G(J,J6)=0
0720 NEXT J6
0730 NEXT J
0740 LET J9=1
0750 REM      ?? LOOP ON L-STATES  ??
0760 FOR J1=1 TO C(J0,5) STEP 1
0770 LET K1=FNA(D(J1,1),E0)
0780 LET L1=1/K1
0790 LET R0=(1.23*D(J1,1)↑(1/3)+0.8)/10
0800 LET R1=K1*R0
0810 LET S(1)=S7=0
0820 LET Q1=1+R1↑2
0830 LET S(2)=-1/Q1
0840 LET Q2=9+3*R1↑2+R1↑4
0850 LET S(3)=-(18+3*R1↑2)/Q2
0860 LET P(1)=R1
0870 LET P(2)=R1↑3/Q1
0880 LET P(3)=R1↑5/Q2
0890 LET R2=C(J0,2)*K1
0900 LET F(1)=R2
0910 LET F(2)=R2-ATN(R2)
0920 LET F(3)=R2-ATN(3*R2/(3-R2↑2))
0930 LET G(1,1)=4*PI*L1*L1*SIN(F(1))↑2
0940 LET G(1,2)=12*PI*L1*L1*SIN(F(2))↑2
0950 LET G(1,3)=20*PI*L1*L1*SIN(F(3))↑2
0960 LET G(1,4)=G(1,1)+G(1,2)+G(1,3)
0970 REM      ?? LOOP ON RESONANCE  ??
0980 FOR J2=J9 TO J9+D(J1,6)-1 STEP 1
0990 DISP "E=";E0;"   Er(";J2;")=";E(J2,1)
1000 LET L=D(J1,3)+1
1010 LET K2=FNA(D(J1,1),E(J2,1))
1020 LET L2=1/K2
1030 LET R3=K2*R0
1040 LET Q3=1+R3↑2
1050 LET Q4=9+3*R3↑2+R3↑4
1060 LET P(4)=R3
1070 LET P(5)=R3↑3/Q3
1080 LET P(6)=R3↑5/Q4
1090 LET S(4)=0
1100 LET S(5)=-1/Q3
1110 LET S(6)=-(18+3*R3↑2)/Q4
1120 IF B(J0,4)=3 THEN 1160
1130 LET E4=P(L)*E(J2,4)/P(L+3)
1140 LET E5=E4+E(J2,5)+E(J2,6)
1150 GOTO 1180
1160 LET E4=P(L)*E(J2,3)/P(L+3)
1170 LET E5=E4+E(J2,4)+ABS(E(J2,5))+ABS(E(J2,6))
1180 LET E6=E(J2,1)+E4*(S(L+3)-S(L))/(2*P(L+3))
1190 LET W1=2*SIN(F(L))*(2*(E0-E6)*COS(F(L))-E5*SIN(F(L)))
1200 LET G1=(2*E(J2,2)+1)/(4*C(J0,1)+2)
1210 LET S1=E0-E6
1220 LET S2=E5/2
1230 LET P0=FNZ(0,S1,S2,S1,-S2)
1240 LET W=G1/SQR(P*P+Q*Q)
1250 REM "W=";W;"AJ=";E(J2,2);"L1*L2";L1*L2;"E'=";E6;"Err";E4
1260 LET G(2,L)=W*E4*E4+G(2,L)
1270 ON B(J0,4) GOTO 1670,1280,1280
1280 IF D(J1,6)=1 THEN 1670
1290 REM      ?? INTERFERENTIAL PART FOR SCATTERING AND FISSION ??
1300 FOR J7=J2+1 TO J9+D(J1,6)-1 STEP 1
1310 IF E(J2,2)<>E(J7,2) THEN 1630
1315 LET S7=0
```

```
1320 LET K2=FNA(D(J1,1),E(J7,1))
1330 LET L2=1/K2
1340 LET R3=K2*R0
1350 LET Q3=1+R3↑2
1360 LET Q4=9+3*R3↑2+R3↑4
1370 LET P(4)=R3
1380 LET P(5)=R3↑3/Q3
1390 LET P(6)=R3↑5/Q4
1400 LET S(4)=0
1410 LET S(5)=-1/Q3
1420 LET S(6)=-(18+3*R3↑2)/Q4
1430 IF B(J0,4)=3 THEN 1470
1440 LET E7=P(L)*E(J7,4)/P(L+3)
1450 LET E8=E7+E(J7,5)+E(J7,6)
1460 GOTO 1490
1470 LET E7=P(L)*E(J7,3)/P(L+3)
1480 LET E8=E7+E(J7,4)+ABS(E(J7,5))+ABS(E(J7,6))
1490 LET E9=E(J7,1)+E7*(S(L+3)-S(L))/(2*P(L+3))
1500 LET S3=E0-E9
1510 LET S4=E8/2
1520 LET W2=(S1*S3+S2*S4)/(S1*S1+S2*S2)/(S3*S3+S4*S4)
1530 LET W2=W2*SQR(E4*E7)
1540 LET G(3,L)=G(3,L)+2*W2*SQR(E4*E7)
1550 IF B(J0,4)<3 THEN 1610
1560 LET S7=S7+SGN(E(J2,5))*SGN(E(J7,5))*SQR(ABS(E(J2,5)*E(J7,5)))
1570 LET S7=S7+SGN(E(J2,5))*SGN(E(J7,6))*SQR(ABS(E(J2,5)*E(J7,6)))
1580 LET S7=S7+SGN(E(J2,6))*SGN(E(J7,5))*SQR(ABS(E(J2,6)*E(J7,5)))
1590 LET S7=S7+SGN(E(J2,6))*SGN(E(J7,6))*SQR(ABS(E(J2,6)*E(J7,6)))
1600 GOTO 1620
1610 LET S7=SGN(E(J2,6))*SQR(ABS(E(J2,6)*E(J7,6)))
1620 LET G(8,L)=G(8,L)+2*W2*S7
1630 NEXT J7
1640 LET G(3,L)=G1*G(3,L)
1650 LET G(8,L)=G1*G(8,L)
1660 REM          ‹‹‹‹ THE END OF INTERFERENTIAL PART  ››››
1670 LET G(4,L)=G(4,L)+W*E4*W1
1680 IF B(J0,4)=3 THEN 1720
1690 LET G(6,L)=G(6,L)+W*E4*E(J2,5)
1700 LET G(7,L)=G(7,L)+W*E4*E(J2,6)
1710 GOTO 1790
1720 LET G(6,L)=G(6,L)+W*E4*E(J2,4)
1730 LET G(7,L)=G(7,L)+W*E4*(ABS(E(J2,5))+ABS(E(J2,6)))
1790 NEXT J2
1800 LET G(5,L)=G(1,L)+G(2,L)+G(3,L)+G(4,L)
1810 LET G(9,L)=G(7,L)+G(8,L)
1820 LET G(10,L)=G(5,L)+G(6,L)+G(9,L)
1830 REM      ‹‹  END OF LOOP ON RESONANCES  ››
1840 LET L3=L1*L1*PI
1850 LET G(2,L)=G(2,L)*L3
1860 LET G(3,L)=G(3,L)*L3
1870 LET G(4,L)=G(4,L)*L3
1880 LET G(6,L)=G(6,L)*L3
1890 LET G(7,L)=G(7,L)*L3
1900 LET G(8,L)=G(8,L)*L3
1910 LET G(5,L)=G(1,L)+G(2,L)+G(3,L)+G(4,L)
1920 LET G(9,L)=G(7,L)+G(8,L)
1930 LET J9=J9+D(J1,6)
1940 NEXT J1
1950 REM      ‹‹  END OF LOOP ON L-STATES  ››
1960 FOR J=1 TO 4 STEP 1
1970 LET G(5,J)=G(4,J)+G(3,J)+G(2,J)+G(1,J)
1980 LET G(10,J)=G(5,J)+G(6,J)+G(9,J)
1990 NEXT J
2000 FOR J=1 TO 10 STEP 1
2010 LET G(J,4)=G(J,1)+G(J,2)+G(J,3)
```



```
2020 NEXT J
2030 IF N1*N2<>0 THEN 2320
2040 PRINT
2050 DISP "  Output for  E =";E0;" eV"
2060 PRINT "ENERGY eV","wave no.","wave length","channel radius"
2070 PRINT E0,K1,L1,R0
2080 PRINT "PARAMETERS","l=0","l=1","l=2"
2090 PRINT "shift factors",S(1),S(2),S(3)
2100 PRINT "pen.factors",P(1),P(2),P(3)
2110 PRINT "phase shift",F(1),F(2),F(3)
2120 ON B(J0,4) GOTO 2130,2150,2180
2130 PRINT "CROSS SECTIONS barns";"   (single level Breit-Wigner)","  SUM"
2140 GOTO 2200
2150 PRINT "CROSS SECTIONS barns";
2160 PRINT "    (one-channel multilevel Breit-Wigner)","  SUM"
2170 GOTO 2200
2180 PRINT "CROSS SECTIONS barns";
2190 PRINT "    (two-channels multilevel Breit-Wigner)","  SUM"
2200 PRINT "pot.scattering",G(1,1),G(1,2),G(1,3),G(1,4)
2210 PRINT "res.scattering",G(2,1),G(2,2),G(2,3),G(2,4)
2220 PRINT "res*res scatt.",G(3,1),G(3,2),G(3,3),G(3,4)
2230 PRINT "res*pot scatt.",G(4,1),G(4,2),G(4,3),G(4,4)
2240 PRINT "total elastic",G(5,1),G(5,2),G(5,3),G(5,4)
2250 PRINT "rad. capture",G(6,1),G(6,2),G(6,3),G(6,4)
2260 PRINT "fission",G(7,1),G(7,2),G(7,3),G(7,4)
2270 PRINT "fiss*fiss",G(8,1),G(8,2),G(8,3),G(8,4)
2280 PRINT "total fission",G(9,1),G(9,2),G(9,3),G(9,4)
2290 PRINT "TOTAL",G(10,1),G(10,2),G(10,3),G(10,4)
2300 PRINT Z$
2310 IF N1*N2=0 THEN 2380
2320 WRITE :2,E0,G(N1,N2)
2330 IF G(N1,N2)<=Y2 THEN 2350
2340 LET Y2=G(N1,N2)
2350 IF G(N1,N2)>=Y1 THEN 2370
2360 LET Y1=G(N1,N2)
2370 PRINT E0,G(N1,N2),
2380 NEXT E0
2390 REM      ‹‹  END OF LOOP ON ENERGY  ››
2400 IF N1*N2=0 THEN 2520
2410 WRITE :2,0,0,0,0
2420 PRINT
2430 PRINT "■ CROSS SECTION G(";N1;",";N2;") STORED FOR PLOT ON FILE <FIPLO>  ■"
2440 PRINT "ABSCISSA min=";E1;" max=";E2;"■■ ORDINATE min=";Y1;" max=";Y2
2450 LET E1=E0
2460 NEXT J0
2470 IF J5>0 THEN 2520
2480 DISP "Energy out range. Chain <CRESO>"
2490 DELAY 30
2500 CHAIN "CRESO"
2510 DEF FNA(A,E0)=2.196771E-3*SQR(ABS(E0))*(A/(A+1))
2520 DISP "      THE END OF CODE <REICH>"
2530 DELAY 10
2540 GOTO 2850
2550 DEF FNZ(T,X1,Y1,X2,Y2)
2560 IF T<>0 THEN 2600
2570 LET P=X1*X2-Y1*Y2
2580 LET Q=X1*Y2+Y1*X2
2590 GOTO 2630
2600 LET P=X1*X2
2610 LET Q=Y1+Y2
2620 LET Q=FNC(Q)
2630 LET FN*=0
2640 FNEND
2650 DEF FNC(T)P2
2660 LET P2=PI*2
```

```
2670 LET T=T-INT(T/P2)*P2
2680 IF T>PI THEN 2710
2690 IF T<=-PI THEN 2710
2700 GOTO 2720
2710 LET T=T-T/T*P2
2720 LET FN*=T
2730 FNEND
2740 GOTO 2850
2750 DEF FNQ(T,X,Y)R
2760 IF T<>0 THEN 2810
2770 LET R=X*X+Y*Y
2780 LET P=X/R
2790 LET Q=-Y/R
2800 GOTO 2830
2810 LET P=1/X
2820 LET Q=-Y
2830 LET FN*=0
2840 FNEND
2850 END
```



```
0010 REM  * CRESO CODE :  CHAINED TO <ENDFB> FOR CROSS SECTION CALCULATION *
0020 FILES *;FIPLO
0022 DISP "INPUT FILENAME (EOL=STOP)";
0024 RKB F$
0026 IF F$="" THEN 2230
0028 FILE : 1,F$
0030 FKEY #15,-1:
0040 DIM Q(6),O(15,6)
0050 DIM A(6),B(3,6),C(3,6),D(3,6),E(25,6),S(6),P(6),F(3),G(10,4),W(10,4)
0060 DIM B$(3),C$(3),D$(3),E$(25)
0070 DCL 8A$,8B$(),8C$(),8D$(),8E$()
0080 DATA 0.005252,0.037171,0.103126,0.207836,0.359852,0.574283,0.879334
0090 DATA 1.33481,2.105227,4.3908,0.051755,0.163095,0.288421,0.431766
0100 DATA .59921,.80056,1.053224,1.39301,1.91623,3.301643,.112995,.265600
0110 DATA .404385,.547724,.704048,.882440,1.096835,1.374373,1.786357,2.824583
0120 DATA .169150,.340780,.480571,.617825,.762381,.922898,1.111387,1.350285
0130 DATA 1.697511,2.546602
0140 :'CCCCCCCCCCC'CCCCCCCCCCC'CCCCCCCCCCC'CCCCCCCCCCC'CCCCCCCCCCC'CCCCCCCCCCC
0150 :##.##########.##########.##########.##########.##########.##########
0160 RESTORE
0170 FOR I=1 TO 4 STEP 1
0180 LET T(I)=0
0190 FOR K=1 TO 10 STEP 1
0195 LET G(K,I)=0
0200 READ W(K,I)
0210 LET T(I)=T(I)+W(K,I)
0220 NEXT K
0230 NEXT I
0240 DISP " RECALL DATA FROM <";F$;"> FILE"
0250 RESTORE :1
0260 READ :1,A(1),A(2),A(3),A(4),A(5),A(6),A$
0270 FOR J0=1 TO A(5) STEP 1
0280 READ :1,B(J0,1),B(J0,2),B(J0,3),B(J0,4),B(J0,5),B(J0,6),B$(J0)
0290 LET E1=B(J0,1)
0300 LET E2=B(J0,2)
0310 READ :1,C(J0,1),C(J0,2),C(J0,3),C(J0,4),C(J0,5),C(J0,6),C$(J0)
0320 ON B(J0,3) GOTO 324,330
0324 DISP "NOT UNRESOLVED REGION !"
0325 BEEP
0326 GOTO 22
0330 IF A(4)=0 THEN 360
0335 FOR J3=1 TO C(J0,6) STEP 1
0340 READ :1,Q(J3)
0350 NEXT J3
0360 LET J9=1
0370 FOR J1=1 TO C(J0,5) STEP 1
0380 READ :1,D(J1,1),D(J1,2),D(J1,3),D(J1,4),D(J1,5),D(J1,6),D$(J1)
0390 FOR J2=J9 TO J9+D(J1,6)-1 STEP 1
0400 READ :1,E(J2,1),E(J2,2),E(J2,3),E(J2,4),E(J2,5),E(J2,6),E$(J2)
0410 ON B(J0,3) GOTO 324,420
0420 IF A(4)=0 THEN 450
0425 FOR J3=1 TO C(J0,6) STEP 1
0430 READ :1,O(J2,J3)
0440 NEXT J3
0450 NEXT J2
0460 LET J9=J9+D(J1,6)
0470 NEXT J1
0480 PRINT "THE UNRESOLVED REGION IS BETWEEN";E1;" AND";E2
0490 PRINT "DATA ON ";F$;" FILE HAVE BEEN RECALLED FROM DISK"
0500 DISP "Point by point [1] or tabul. [2] ";
0510 INPUT S0
0520 ON S0 GOTO 530,590
0530 DISP "  ENERGY  = ?     (FKEY#15=STOP)  ";
0540 INPUT E0
0550 LET N1=N2=0
```

```
0560 IF E0<0 THEN 1650
0570 LET E1=E2=E3=E0
0580 GOTO 800
0590 DISP " INPUT: [1]=#points; [2]=step   ";
0600 INPUT Y3
0610 ON Y3 GOTO 620,680
0620 DISP "Emin, Emax, # of points = ";
0630 INPUT E1,E2,N
0640 IF N>1 THEN 660
0650 LET N=2
0660 LET E3=(E2-E1)/(N-1)
0670 GOTO 710
0680 DISP "  Emin, Emax, step = ";
0690 INPUT E1,E2,E3
0700 LET N=(E2-E1)/E3+1
0710 DISP "0,0=no plot ■ I,K = plot G(I,K)";
0720 INPUT N1,N2
0730 IF N1*N2=0 THEN 800
0740 SCRATCH :2
0750 WRITE :2,N,0
0760 LET Y1=1E63
0770 LET Y2=-Y1
0780 REM≀≀≀≀≀≀≀≀≀≀≀≀≀≀≀≀≀≀≀≀≀≀≀≀≀≀≀≀≀≀≀≀≀≀≀≀≀≀≀≀≀≀≀≀≀≀≀≀≀≀≀≀≀≀≀≀≀≀≀≀≀≀≀≀≀≀≀
0790 REM                    LOOP ON ENERGY
0800 FOR E0=E1 TO E2 STEP E3
0810 LET J9=1
0820 REM >>>>>>>>>>>>>>>>>>>>>>>>>>>>>>>>>>>>>>>>>>>>>>>>>>>>>>>>>>>>>>>>>>
0830 REM                   LOOP ON L-STATES
0840 IF C(J0,5)<=3 THEN 860
0850 LET C(J0,5)=3
0860 FOR J1=1 TO C(J0,5) STEP 1
0870 LET L=D(J1,3)+1
0880 REM     RESET ALL THE CROSS SECTIONS RELATED TO THE L-STATE IN PROCESS
0890 FOR I=1 TO 7 STEP 1
0900 LET G(I,L)=0
0910 NEXT I
0920 LET K1=FNA(E0)
0930 LET L1=1/K1
0940 LET R1=K1*(1.23*D(J1,1)↑(1/3)+0.8)/10
0950 LET Q1=1+R1↑2
0960 LET Q2=9+3*R1↑2+R1↑4
0970 LET R2=K1*C(J0,2)
0980 LET S(1)=0
0990 LET S(2)=-1/Q1
1000 LET S(3)=-(18+3*R1↑2)/Q2
1010 LET P(1)=R1
1020 LET P(2)=R1↑3/Q1
1030 LET P(3)=R1↑5/Q2
1040 LET F(1)=R2
1050 LET F(2)=R2-ATN(R2)
1060 LET F(3)=R2-ATN(3*R2/(3-R2↑2))
1070 LET G(1,L)=G(1,L)+(2*L-1)*SIN(F(L))↑2
1080 REM⊣⊣⊣⊣⊣⊣⊣⊣⊣⊣⊣⊣⊣⊣⊣⊣⊣⊣⊣⊣⊣⊣⊣⊣⊣⊣⊣⊣⊣⊣⊣⊣⊣⊣⊣⊣⊣⊣⊣⊣⊣⊣⊣⊣⊣⊣⊣⊣⊣⊣⊣⊣⊣⊣⊣⊣⊣⊣⊣⊣⊣⊣⊣⊣⊣
1090 REM                 LOOP ON AJ-SPIN
1100 FOR J2=J9 TO J9+D(J1,6)-1 STEP 1
1110 DISP "E=";E0;" L=";D(J1,3);" AJ=";E(J2,2)
1115 IF A(4)=0 THEN 1130
1120 GOSUB 2100
1130 LET G0=(2*E(J2,2)+1)/(4*C(J0,1)+2)
1140 REM WEIGHTING GN(=W1),GF(=W2) AND GT(=W3) ON PORTER-THOMAS DISTRIBUTION
1150 LET A=A1=A2=0
1160 FOR K=1 TO 10 STEP 1
1170 LET P=W(K,E(J2,3))
1180 LET W1=E(J2,4)*SQR(E0)*FNB(R1,D(J1,3))*E(J2,3)
1190 LET W2=W3=0
```



```
1200 FOR J4=1 TO 10 STEP 1
1205 IF A(4)=0 THEN 1224
1210 LET W2=W2+W(J4,E(J2,6))/(W1*P+E(J2,5)+W(J4,E(J2,6))*F6)
1220 LET W3=W3+1/(W1*P+E(J2,5)+W(J4,E(J2,6))*F6)
1222 GOTO 1230
1224 LET W2=F6=0
1226 LET W3=W3+1/(W1*P+E(J2,5))
1230 NEXT J4
1240 LET A=A+W1*W1*P*P*W3/100
1250 LET A1=A1+W1*P*E(J2,5)*W3/100
1260 LET A2=A2+W1*P*F6*W2/100
1270 NEXT K
1280 LET G(2,L)=G(2,L)+G0/E(J2,1)*(A-2*E(J2,4)*SIN(F(L))*SIN(F(L)))
1290 LET G(5,L)=G(5,L)+G0/E(J2,1)*A1
1300 LET G(6,L)=G(6,L)+G0/E(J2,1)*A2
1310 NEXT J2
1320 REM⊣⊣⊣⊣⊣⊣⊣⊣⊣⊣⊣⊣⊣⊣⊣⊣⊣⊣⊣⊣⊣⊣⊣⊣⊣⊣⊣⊣⊣⊣⊣⊣⊣⊣⊣⊣⊣⊣⊣⊣⊣⊣⊣⊣⊣⊣⊣⊣⊣⊣⊣⊣⊣⊣⊣⊣⊣⊣⊣⊣⊣⊣⊣⊣⊣⊣
1340 LET J9=J9+D(J1,6)
1350 LET B=2*PI*PI*L1*L1
1360 LET G(1,L)=G(1,L)*4*PI/K1/K1
1370 LET G(2,L)=G(2,L)*B
1380 LET G(3,L)=0
1390 LET G(4,L)=G(1,L)+G(2,L)+G(3,L)
1400 LET G(5,L)=G(5,L)*B
1410 LET G(6,L)=G(6,L)*B
1420 LET G(7,L)=G(4,L)+G(5,L)+G(6,L)
1430 NEXT J1
1440 REM>>>>>>>>>>>>>>>>>>>>>>>>>>>>>>>>>>>>>>>>>>>>>>>>>>>>>>>>>>>>>>>>>>>>
1450 FOR I=1 TO 7 STEP 1
1460 LET G(I,4)=G(I,1)+G(I,2)+G(I,3)
1470 NEXT I
1480 IF N1*N2=0 THEN 1560
1490 WRITE :2,E0,G(N1,N2)
1500 IF G(N1,N2)<=Y2 THEN 1520
1510 LET Y2=G(N1,N2)
1520 IF G(N1,N2)>=Y1 THEN 1540
1530 LET Y1=G(N1,N2)
1540 PRINT E0,G(N1,N2),
1550 GOTO 1570
1560 GOSUB 1900
1570 NEXT E0
1580 ON S0 GOTO 530,1590
1590 REM                 END OF LOOP ON ENERGY
1600 IF N1*N2=0 THEN 1650
1610 PRINT
1620 PRINT "■ CROSS SECTION G(";N1;",";N2;") STORED FOR PLOT ON FILE <FIPLO>  ■"
1630 PRINT "ABSCISSA min=";E1;" max=";E2;"■■ ORDINATE min=";Y1;" max=";Y2
1640 NEXT J0
1650 FOR I=1 TO 10 STEP 1
1660 PRINT
1670 NEXT I
1680 GOTO 2230
1690 REM≀≀≀≀≀≀≀≀≀≀≀≀≀≀≀≀≀≀≀≀≀≀≀≀≀≀≀≀≀≀≀≀≀≀≀≀≀≀≀≀≀≀≀≀≀≀≀≀≀≀≀≀≀≀≀≀≀≀≀≀≀≀≀≀
1700 REM               WAVE NUMBER CALCULATION
1710 DEF FNA(E0)=2.19685E-3*SQR(E0)*D(J1,1)/(D(J1,1)+1)
1720 REM               PENETRATION FACTOR CALCULATION
1730 DEF FNB(R1,L)
1740 ON L+1 GOTO 1750,1770,1790
1750 LET FN*=1
1760 GOTO 1800
1770 LET FN*=R1*R1/(R1*R1+1)
1780 GOTO 1800
1790 LET FN*=R1↑4/(R1↑4+3*R1↑2+9)
1800 FNEND
1810 REM                 SQUARE SIN OF FASE SHIFT CALCULATION
```

```
1820 DEF FND(R,L,J)
1830 ON R GOTO 1840,1840,1840
1840 LET FN*=1
1850 GOTO 1890
1860 LET FN*=1
1870 GOTO 1890
1880 LET FN*=1
1890 FNEND
1900 PRINT
1910 DISP "PRINTING OUTPUT FOR ENERGY";E0
1920 PRINT "ENERGY","wave no.","wave length","channel radius"
1930 PRINT E0,K1,L1,R1
1940 PRINT "PARAMETERS","l=0","l=1","l=2"
1950 PRINT "shift factors",S(1),S(2),S(3)
1960 PRINT "pen.factors",P(1),P(2),P(3)
1970 PRINT "phase shift",F(1),F(2),F(3)
1980 PRINT "CROSS SECTIONS","(Unresolved region, Statistical model)","  SUM"
1990 PRINT "pot.scattering",G(1,1),G(1,2),G(1,3),G(1,4)
2000 PRINT "res.scattering",G(2,1),G(2,2),G(2,3),G(2,4)
2010 PRINT "res*pot scatt.",G(3,1),G(3,2),G(3,3),G(3,4)
2020 PRINT "total elastic",G(4,1),G(4,2),G(4,3),G(4,4)
2030 PRINT "capture",G(5,1),G(5,2),G(5,3),G(5,4)
2040 PRINT "fission",G(6,1),G(6,2),G(6,3),G(6,4)
2050 PRINT "total",G(7,1),G(7,2),G(7,3),G(7,4)
2060 RETURN
2100 REM SUB. FOR CALCULATION OF FISSION WIDTH AT GIVEN ENERGY AND SPIN STATE
2110 IF (E0-Q(1))*(E0-Q(C(J0,6)))<0 THEN 2180
2120 FOR J3=1 TO C(J0,6)-1 STEP 1
2130 IF (E0)=Q(J3)) AND (E0<=Q(J3+1)) THEN 2150
2140 NEXT J3
2150 LET F6=O(J2,J3)+(O(J2,J3+1)-O(J2,J3))/(Q(J3+1)-Q(J3))*(E0-Q(J3))
2160 GOTO 2220
2170 REM ENERGY OUT OF RANGE
2180 IF E0<Q(1) THEN 2210
2190 LET F6=O(J2,C(J0,6))
2200 GOTO 2220
2210 LET F6=O(J2,1)
2220 RETURN
2230 END
```



```
0010 REM        <RINEG> PROGRAM FOR Γn AND Γf CALCULATION
0020 REM                    OF THE BOUND LEVEL
0030 DCL 50F$
0040 DEF FNA(M,E9)=2.296771E-3*SQR(ABS(E9))*(M/(M+1))
0050 DEF FNB(A,B,C)=(-B+SQR(B*B-4*A*C))/2/A
0060 DEF FNC(A,B,C)=(-B-SQR(B*B-4*A*C))/2/A
0070 LET F$="'LLLLLLLLLLLLLLLLLLLLLLLLLL=#######.######"
0080 PRINT TAB(15);"<RINEG> PROGRAM FOR CALCULATION OF Γn AND Γf"
0090 PRINT TAB(30);"OF THE BOUND LEVEL"
0100 PRINT
0110 PRINT "Ev and Barns units"
0120 DISP "NUCLEUS MASS (AWRI) =";
0130 INPUT M
0140 PRINT USING F$,"Nucleus mass (=AWRI)",M
0150 DISP "THERMAL CAPTURE CROSS SECTION=";
0160 INPUT S1
0170 PRINT USING F$,"Thermal capture S1",S1
0180 DISP "THERMAL FISSION CROSS SECTION=";
0190 INPUT S2
0200 PRINT USING F$,"Thermal fission S2",S2
0210 DISP "NUCLEUS SPIN I=";
0220 INPUT I
0230 PRINT USING F$,"I",I
0240 DISP "RESONANCE SPIN J =";
0250 INPUT J
0260 PRINT USING F$,"J",J
0270 DISP "RESONANCE ENERGY =";
0280 INPUT E
0290 PRINT USING F$,"Er",E
0300 DISP "RADIATION WIDTH Γg=";
0310 INPUT G
0320 PRINT USING F$,"Γg",G
0330 LET G7=(2*J+1)/(2*(2*I+1))
0340 LET L1=1/FNA(M,0.0253)
0350 LET L2=1/FNA(M,E)
0360 LET C=PI*L1*L2*G7
0370 LET D0=0.0253-E
0380 LET F1=S2*G/S1
0390 PRINT USING F$,"Γf (=Γg*S2/S1)",F1
0400 LET A1=S1
0410 LET B1=2*S1*(G+F1)-4*C*G
0420 LET C1=S1*(4*D0*D0+(G+F1)↑2)
0430 LET D=B1*B1-4*A1*C1
0440 IF D>0 THEN 470
0450 PRINT "IMAGINARY SOLUTION FOR Γn. CHANGE THE GUESS"
0460 GOTO 560
0470 PRINT "POSSIBLE SOLUTIONS:
0480 LET G1=FNB(A1,B1,C1)
0490 PRINT "Γn =";G1,
0500 LET G2=FNC(A1,B1,C1)
0510 PRINT "Γn =";G2
0520 PRINT TAB(23);"Γ0n=";G1/SQR(ABS(E)),
0530 PRINT "Γ0n=";G2/SQR(ABS(E))
0540 LET Q1=D0*D0+(G+F1+G1)*(G+F1+G1)/4
0550 LET Q2=D0*D0+(G+F1+G2)*(G+F1+G2)/4
0560 LET S1=C*G1*G/Q1
0570 LET S2=C*G2*G/Q2
0580 LET S3=C*F1*G1/Q1
0590 LET S4=C*F1*G2/Q2
0600 PRINT "CHECK CAPTURE          S1 =";S1,"S1 =";S2
0610 IF F1=0 THEN 630
0620 PRINT "CHECK FISSION          S2 =";S3,"S2 =";S4
0630 END
```

```
0010REM        * <ROMB> CODE FOR GENERALIZED ROMBERG INTEGRATION *
0020 PRINT "                  * <ROMB> CODE FOR ROMBERG QUADRATURE *"
0030 FKEY #1,START 290:
0040 FKEY #2,START 430:
0050 FKEY #3,START 590:
0060 FKEY #4,START 740:
0070 FKEY #5,START 740:
0080 FKEY #6,START 1480:
0090 FKEY #16,START 1650:
0100 GOSUB 120
0110 GOTO 170
0120 PRINT
0130 PRINT
0140 RETURN
0150 DISP "KEY OPTIONS. KEY #1=MENU'";
0160 STOP
0170 REM        ROMBERG QUADRATURE FOR INPUT PAIRS X,Y
0180 REM
0190 DIM C(5,5),D(5)
0200 DATA 1,0,0,0,0,4,-1,0,0,0,64,-20,1,0,0,4096,-1344,84,-1,0,1048576
0210 DATA -348160,22848,-340,1,1,3,45,2835,722925
0220 LET R=0
0230 RESTORE
0240 READ C(1,1),C(1,2),C(1,3),C(1,4),C(1,5),C(2,1),C(2,2),C(2,3),C(2,4),C(2,5)
0250 READ C(3,1),C(3,2),C(3,3),C(3,4),C(3,5),C(4,1),C(4,2),C(4,3),C(4,4)
0260 READ C(4,5),C(5,1),C(5,2),C(5,3),C(5,4),C(5,5)
0270 READ D(1),D(2),D(3),D(4),D(5)
0280 GOTO 150
0290 PRINT
0300 PRINT TAB(9);"GENERALIZED ROMBERG QUADRATURE FOR INPUT PAIRS X,Y"
0310 PRINT
0320 PRINT TAB(5);"KEY OPTIONS"
0330 PRINT
0340 PRINT TAB(5);"KEY #1: Menu"
0350 PRINT TAB(5);"KEY #2: Input keyboard"
0360 PRINT TAB(5);"KEY #3: Input disk file <FIPLO>"
0370 PRINT TAB(5);"KEY #4: Integration"
0380 PRINT TAB(5);"KEY #5: Order and interval change, same input"
0390 PRINT TAB(5);"KEY #6: Print of input disk file <FIPLO>"
0400 PRINT TAB(5);"KEY #16:Stop! Program exit"
0410 GOTO 150
0420 REM
0430 REM                    *  KEYBOARD INPUT *
0440 REM
0450 LET R8=0
0460 DISP "NUMBER OF X,Y PAIRS = ";
0470 INPUT N
0480 DIM X(100),Y(100)
0490 PRINT " I","X(I)","Y(I)"
0500 FOR I=1 TO N STEP 1
0510 DISP "X(";I;") = ";
0520 INPUT X(I)
0530 DISP "Y(";I;") = ";
0540 INPUT Y(I)
0550 PRINT I,X(I),Y(I)
0560 NEXT I
0570 GOTO 150
0580 REM
0590 REM                   *  INPUT FROM DISK FILE  *
0600 REM
0610 GOSUB 120
0620 FILES FIPLO
0630 LET R8=0
0640 RESTORE :1
0650 READ :1,N,E1
```



```
0660 PRINT "NUMBER OF PAIRS FROM DISK = ";N
0670 FOR I=1 TO N STEP 1
0680 IF E1>0 THEN 710
0690 READ :1,X(I),Y(I)
0700 GOTO 720
0710 READ :1,X(I),Y(I),E
0720 NEXT I
0730 REM
0740 REM                        *  INTEGRAL CALCULATION *
0750 REM
0760 LET R=0
0770 PRINT
0780 DISP "INDEX LOWER LIMIT=";
0790 INPUT N1
0800 DISP "INDEX UPPER LIMIT=";
0810 INPUT N2
0820 DISP "INTEGRATION ORDER=";
0830 INPUT I1
0840 PRINT "INTEGRATION ORDER ";I1
0850 IF (I1>5) OR (I1<1) THEN 900
0860 GOTO 910
0870 REM
0880 REM
0890 REM
0900 LET I1=1
0910 LET I2=I1-1
0920 LET M1=2↑I2
0930 LET N3=N2-N1
0940 LET N4=N1
0950 LET I3=0
0960 LET R2=0
0970 ON I1 GOTO 1080,1060,1040,1020,980
0980 IF N3>16 THEN 1100
0990 LET I1=I1-1
1000 LET M1=2↑(I1-1)
1010 GOTO 970
1020 IF N3>=8 THEN 1100
1030 GOTO 990
1040 IF N3>=4 THEN 1100
1050 GOTO 990
1060 IF N3>=2 THEN 1100
1070 GOTO 990
1080 IF N3>=1 THEN 1100
1090 GOTO 1350
1100 LET N5=N4+M1
1110 LET N6=N4
1120 LET M3=2↑I3
1130 LET I3=I3+1
1140 LET N7=N6+M3
1150 LET R1=0
1160 IF N7>N5 THEN 1220
1170 LET T=(X(N7)-X(N6))*((Y(N6)+Y(N7))/2)
1180 LET R1=R1+T
1190 LET N6=N6+M3
1200 LET N7=N7+M3
1210 GOTO 1160
1220 LET R2=R2+R1*C(I1,I3)
1230 IF I3>=I1 THEN 1300
1240 LET I4=I3+1
1250 IF (I4>5) OR (I4<1) THEN 1280
1260 ON I4 GOTO 1080,1060,1040,1020,980
1270 GOTO 1300
1280 LET I4=1
1290 GOTO 1260
1300 LET R2=R2/D(I1)
```

```
1310 LET R=R+R2
1320 LET N4=N5
1330 LET N3=N2-N5
1340 GOTO 950
1350 LET R8=R8+R
1360 PRINT "INTEGRAL BETWEEN X(";N1;")=";X(N1);". e  ";"X(";N2;")=";X(N2);
1370 PRINT ": R=";R;" AND CUMULATIVE VALUE = ";R8
1380 DISP "INTEGRAL = ";R;
1390 STOP
1400 STOP
1410 GOSUB 120
1420 PRINT "I","X(I)","Y(I)"
1430 FOR I=1 TO N STEP 1
1440 PRINT I,X(I),Y(I)
1450 NEXT I
1460 GOTO 150
1470 REM
1480 REM                  *  INPUT PRINT FROM DISK FILE  *
1490 REM
1500 GOSUB 120
1510 RESTORE :1
1520 READ :1,N,E1
1530 PRINT TAB(8),"NUMBER OF PAIRS X,Y FROM DISK = ";N
1540 PRINT
1550 PRINT " I","  X(I)","  Y(I)","  DY(I)"
1560 FOR I=1 TO N STEP 1
1570 IF E1>0 THEN 1610
1580 READ :1,X(I),Y(I)
1590 PRINT I,X(I),Y(I)
1600 GOTO 1630
1610 READ :1,X(I),Y(I),E
1620 PRINT I,X(I),Y(I),E
1630 NEXT I
1640 GOTO 150
1650 GOSUB 120
1660 PRINT TAB(25);"*  STOP!  <ROMB> CODE EXIT *"
1670 END
```

TABLE 1. Parameters in the resolved region for SL Breit-Wigner representation

TABLE 1. SINGLE LEVEL BW PARAMETERS IN RESOLVED REGION. BARIUM 138.
FKEY# 6: PRINT OF THE RECALLED FILE <BA138>

ZAI	ABN	b	LFW	NER	b	ref.
4.81380E+04	1.00000E+00	0.00000E+00	0.00000E+00	1.00000E+00	0.00000E+00	
EL	EH	LRU	LRF	b	b	
1.00000E-05	9.00000E+04	1.00000E+00	1.00000E+00	0.00000E+00	0.00000E+00	
SPI	AP	b	b	NLS	NE	
0.00000E+00	6.23350E-01	0.00000E+00	0.00000E+00	3.00000E+00	0.00000E+00	
AWRI	AM	L	b	6*NRS	NRS	
1.36720E+02	0.00000E+00	0.00000E+00	0.00000E+00	7.20000E+01	1.20000E+01	
ER	AJ	GT	GN	GG	GF	
-2.52400E+03	5.00000E-01	8.63100E+01	8.60000E+01	3.10000E-01	0.00000E+00	1
3.09100E+04	5.00000E-01	2.25350E+02	2.25000E+02	3.50000E-01	0.00000E+00	2
3.65000E+04	5.00000E-01	2.83100E+01	2.80000E+01	3.10000E-01	0.00000E+00	3
4.02500E+04	5.00000E-01	1.50250E+02	1.50000E+02	2.50000E-01	0.00000E+00	4
5.04000E+04	5.00000E-01	2.50325E+02	2.50000E+02	3.25000E-01	0.00000E+00	5
5.91000E+04	5.00000E-01	7.03600E+01	7.00000E+01	3.60000E-01	0.00000E+00	6
6.30000E+04	5.00000E-01	1.00200E+02	1.00000E+02	2.00000E-01	0.00000E+00	7
6.90000E+04	5.00000E-01	4.00587E+02	4.00000E+02	5.87000E-01	0.00000E+00	8
7.40000E+04	5.00000E-01	1.00245E+02	1.00000E+02	2.45000E-01	0.00000E+00	9
7.98000E+04	5.00000E-01	1.50223E+02	1.50000E+02	2.23000E-01	0.00000E+00	10
8.18000E+04	5.00000E-01	2.02840E+01	2.00000E+01	2.84000E-01	0.00000E+00	11
8.94000E+04	5.00000E-01	2.02800E+01	2.00000E+01	2.80000E-01	0.00000E+00	12
AWRI	AM	L	b	6*NRS	NRS	
1.36720E+02	0.00000E+00	1.00000E+00	0.00000E+00	1.14000E+02	1.90300E+01	
ER	AJ	GT	GN	GG	GF	
4.71400E+03	5.00000E-01	8.50000E-02	3.50000E-02	5.00000E-02	0.00000E+00	13
7.87600E+03	1.50000E+00	3.04500E+00	3.00000E+00	4.50000E-02	0.00000E+00	14
1.40400E+04	1.50000E+00	3.03400E+00	3.00000E+00	3.40000E-02	0.00000E+00	15
1.97000E+04	5.00000E-01	1.04300E+00	1.00000E+00	4.30000E-02	0.00000E+00	16
1.99800E+04	1.50000E+00	7.55000E+00	7.50000E+00	5.00000E-02	0.00000E+00	17
2.34400E+04	1.50000E+00	1.00460E+01	1.00000E+01	4.60000E-02	0.00000E+00	18
2.43000E+04	5.00000E-01	5.04600E+00	5.00000E+00	4.60000E-02	0.00000E+00	19
2.29500E+04	1.50000E+00	5.05000E+00	5.00000E+00	5.00000E-02	0.00000E+00	20
3.26300E+04	5.00000E-01	1.40440E+01	1.40000E+01	4.40000E-02	0.00000E+00	21
3.54200E+04	1.50000E+00	1.00410E+01	1.00000E+01	4.10000E-02	0.00000E+00	22
4.37500E+04	1.50000E+00	5.03900E+00	5.00000E+00	3.90000E-02	0.00000E+00	23
4.98500E+04	1.50000E+00	5.07100E+00	5.00000E+00	7.10000E-02	0.00000E+00	24
5.13000E+04	5.00000E-01	1.07300E+00	1.00000E+00	7.30000E-02	0.00000E+00	25
5.34000E+04	1.50000E+00	1.07300E+01	1.00000E+01	7.30000E-02	0.00000E+00	26
5.55000E+04	1.50000E+00	2.00790E+01	2.00000E+01	7.90000E-02	0.00000E+00	27
6.16000E+04	1.50000E+00	2.00760E+01	2.00000E+01	7.60000E-02	0.00000E+00	28
6.55000E+04	1.50000E+00	5.09400E+00	5.00000E+00	9.40000E-02	0.00000E+00	29
7.29000E+04	1.50000E+00	5.08600E+00	5.00000E+00	8.60000E-02	0.00000E+00	30
8.35000E+04	1.50000E+00	5.06800E+00	5.00000E+00	6.80000E-02	0.00000E+00	31
AWRI	AM	L	b	6*NRS	NRS	
1.36720E+02	0.00000E+00	2.00000E+00	0.00000E+00	4.80000E+01	8.00000E+00	
ER	AJ	GT	GN	GG	GF	
9.95600E+03	2.00000E+00	1.12000E-01	1.20000E-02	1.00000E-01	0.00000E+00	32
2.62400E+04	2.00000E+00	1.12000E-01	1.20000E-02	1.00000E-01	0.00000E+00	33
3.13100E+04	2.00000E+00	1.24800E-01	2.48000E-02	1.00000E-01	0.00000E+00	34
3.28300E+04	2.00000E+00	1.18000E-01	1.80000E-02	1.00000E-01	0.00000E+00	35
3.33500E+04	2.00000E+00	1.20000E-01	2.00000E-02	1.00000E-91	0.00000E+00	36
6.10000E+04	2.00000E+00	1.44000E-01	4.40000E-02	1.00000E-01	0.00000E+00	37
7.33000E+04	1.50000E+00	3.40000E-01	2.40000E-01	1.00000E-01	0.00000E+00	38
7.80000E+04	1.50000E+00	1.07500E+00	1.00000E+00	7.50000E-02	0.00000E+00	39

TABLE 2. Parameters in the resolved region for ML Breit-Wigner representation

TABLE 2. MULTILEVEL BW PARAMETERS IN RESOLVED REGION. CHROMIUM 54.
FKEY# 6: PRINT OF THE RECALLED FILE <CR54>

ZAI	ABN	b	LFW	NER	b	ref.
2.40540E+04	2.36500E-02	0.00000E+00	0.00000E+00	1.00000E+00	0.00000E+00	
EL	EH	LRU	LRF	b	b	
1.00000E-05	6.42848E+05	1.00000E+00	2.00000E+00	0.00000E+00	0.00000E+00	
SPI	AP	b	b	NLS	NE	
0.00000E+00	4.80000E-01	0.00000E+00	0.00000E+00	2.00000E+00	0.00000E+00	
AWRI	AM	L	b	6*NRS	NRS	
5.34750E+01	0.00000E+00	0.00000E+00	0.00000E+00	9.00000E+01	1.50000E+01	
ER	AJ	GT	GN	GG	GF	
-1.12900E+04	5.00000E-01	4.32500E+02	4.30000E+02	2.50000E+00	0.00000E+00	1
2.29000E+04	5.00000E-01	5.90200E+02	5.90000E+02	2.00000E-01	0.00000E+00	2
1.20100E+05	5.00000E-01	3.50250E+03	3.50000E+03	2.50000E+00	0.00000E+00	3
1.79000E+05	5.00000E-01	1.90100E+03	1.90000E+03	1.00000E+00	0.00000E+00	4
2.48000E+05	5.00000E-01	1.20240E+03	1.20000E+03	2.40000E+00	0.00000E+00	5
2.76000E+05	5.00000E-01	9.00250E+03	9.00000E+03	2.50000E+00	0.00000E+00	6
2.83000E+05	5.00000E-01	3.00250E+03	3.00000E+03	2.50000E+00	0.00000E+00	7
2.88400E+05	5.00000E-01	9.50250E+03	9.50000E+03	2.50000E+00	0.00000E+00	8
2.90500E+05	5.00000E-01	6.02500E+02	6.00000E+02	2.50000E+00	0.00000E+00	9
3.00500E+05	5.00000E-01	5.02500E+02	5.00000E+02	2.50000E+00	0.00000E+00	10
3.33300E+05	5.00000E-01	1.00025E+04	1.00000E+04	2.50000E+00	0.00000E+00	11
3.51000E+05	5.00000E-01	2.02040E+02	2.00000E+02	2.04000E+00	0.00000E+00	12
3.55100E+05	5.00000E-01	3.00250E+03	3.00000E+03	2.50000E+00	0.00000E+00	13
3.60500E+05	5.00000E-01	5.02040E+02	5.00000E+02	2.04000E+00	0.00000E+00	14
3.93500E+05	5.00000E-01	4.00250E+03	4.00000E+03	2.50000E+00	0.00000E+00	15
AWRI	AM	L	b	6*NRS	NRS	
5.34750E+01	0.00000E+00	1.00000E+00	0.00000E+00	7.20000E+01	1.20000E+01	
ER	AJ	GT	GN	GG	GF	
1.03000E+04	1.50000E+00	6.75000E-01	7.50000E-02	6.00000E-01	0.00000E+00	15
1.44000E+04	5.00000E-01	9.30000E-01	3.30000E-01	6.00000E-01	0.00000E+00	16
1.91000E+04	1.50000E+00	7.30000E-01	1.30000E-01	6.00000E-01	0.00000E+00	17
5.11000E+04	5.00000E-01	1.04000E+00	4.40000E-01	6.00000E-01	0.00000E+00	18
5.49000E+04	1.50000E+00	8.00000E-01	2.00000E-01	6.00000E-01	0.00000E+00	19
6.75000E+04	1.50000E+00	1.21000E+00	6.10000E-01	6.00000E-01	0.00000E+00	20
1.69800E+05	5.00000E-01	5.00600E+02	5.00000E+02	6.00000E-01	0.00000E+00	21
1.89300E+05	5.00000E-01	2.55600E+02	2.55000E+02	6.00000E-01	0.00000E+00	22
2.85000E+05	5.00000E-01	3.00600E+02	3.00000E+02	6.00000E-01	0.00000E+00	23
3.32000E+05	5.00000E-01	8.10600E+02	8.10000E+02	6.00000E-01	0.00000E+00	24
3.58700E+05	5.00000E-01	4.00600E+02	4.00000E+02	6.00000E-01	0.00000E+00	25
3.87500E+05	5.00000E-01	1.04060E+03	1.04000E+03	6.00000E-01	0.00000E+00	26

TABLE 3. The formulas for the cross section representation with the SL Breit-Wigner approximation

Single-Level Breit-Wigner Formula: LRU=1, LRF=1

The formulae appearing in Gregson et al.,[1] which omit the resonance-resonance interference terms, are adopted. These formulae, written in the laboratory system for all ℓ-values and without Doppler broadening, are (for a particular isotope)

1. Elastic Scattering Cross Section

$$\sigma_{n,n}(E) = \sum_{\ell=0}^{NLS-1} \sigma_{n,n}^{\ell}(E),$$

where

$$\sigma_{n,n}^{\ell}(E) = (2\ell+1)\frac{4\pi}{k^2}\sin^2\phi_\ell + \frac{\pi}{k^2}\sum_J g_J \sum_{r=1}^{NR_J} \frac{\Gamma_{nr}^2 \cos 2\phi_\ell - 2\Gamma_{nr}(\Gamma_{\gamma r}+\Gamma_{fr})\sin^2\phi_\ell + 2(E-E_r')\Gamma_{nr}\sin 2\phi_\ell}{(E-E_r')^2 + 1/4\,\Gamma_r^2}.$$

2. Radiative Capture Cross Section

$$\sigma_{n,\gamma}(E) = \sum_{\ell=0}^{NLS-1} \sigma_{n,\gamma}^{\ell}(E),$$

where

$$\sigma_{n,\gamma}^{\ell}(E) = \frac{\pi}{k^2}\sum_J g_J \sum_{r=1}^{NR_J} \frac{\Gamma_{nr}\Gamma_{\gamma r}}{(E-E_r')^2 + 1/4\,\Gamma_r^2}.$$

3. Fission Cross Section

$$\sigma_{n,f}(E) = \sum_{\ell=0}^{NLS-1} \sigma_{n,f}^{\ell}(E),$$

where

$$\sigma^{\ell}_{n,f}(E) = \frac{\pi}{k^2} \sum_J g_J \sum_{r=1}^{NR_J} \frac{\Gamma_{nr}\Gamma_{fr}}{(E-E_r')^2 + 1/4\ \Gamma_r^2},$$

where

$$g_J = \frac{2J+1}{2(2I+1)}.$$

I is the spin of the target nucleus and J is the spin of the compound nucleus for the resonance state.

I = SPI, as given in File 2 data for each isotope.

TABLE 4. The Multilevel interferential part in the Breit-Wigner cross section approximation

Multilevel Breit-Wigner Formula: LRU=1, LRF=2

The equations are exactly the same as above, except that a level-level interference term is included in the equation for elastic scattering:

$$\frac{\pi}{k^2} \sum_J g_J \sum_{r=2}^{NR_J} \sum_{s=1}^{r-1} \frac{2\Gamma_{nr}\Gamma_{ns}\left[(E-E_r')(E-E_s') + 1/4\ \Gamma_r\Gamma_s\right]}{\left[(E-E_r')^2 + 1/4\ \Gamma_r^2\right]\left[(E-E_s')^2 + 1/4\ \Gamma_s^2\right]}.$$

TABLE 5. Matrix form of the elastic cross section for one resonance with Breit-Wigner formula

$$\sigma^{\ell}_{n,n} = (2\sin\phi_\ell \quad \frac{1}{e^{-i\phi_\ell}.a_j^*}) \cdot \begin{vmatrix} 2\ell+1 & \Gamma_{nj} \\ \Gamma_{nj} & \Gamma_{nj}^2 \end{vmatrix} \cdot \begin{Bmatrix} 2\sin\phi_\ell \\ \frac{1}{e^{i\phi_\ell}.a_j} \end{Bmatrix}$$

from which, by the identity

$$2\sin\phi_\ell = \frac{2E\sin\phi_\ell}{e^{-i\phi_\ell}\left[E\cos\phi_\ell - i(-E\sin\phi_\ell)\right]} = \frac{2E\sin\phi_\ell}{e^{+i\phi_\ell}\left[E\cos\phi_\ell + i(-E\sin\phi_\ell)\right]}$$

and introducing the fictitious width and the energy distance

$$\Gamma_\ell = -2E\sin\phi_\ell \qquad ; \qquad \Delta E_\ell = E\cos\phi_\ell$$

which are "energy dependent", we can write down the elastic cross section including potential, resonance and interferential res.×pot. of one isolated resonance:

$$\sigma^{\ell}_{n,n} = \pi\lambda^2 \sum_j g_j \left(\frac{1}{e^{-i\phi_\ell}.a_\ell^*} \quad \frac{1}{e^{-i\phi_\ell}.a_j^*}\right) \begin{vmatrix} (-\Gamma_\ell)^2(2\ell+1) & -\Gamma_\ell\Gamma_{nj} \\ -\Gamma_\ell\Gamma_{nj} & \Gamma_{nj}\Gamma_{nj} \end{vmatrix} \begin{Bmatrix} \frac{1}{e^{i\phi_\ell}.a_\ell} \\ \frac{1}{e^{i\phi_\ell}.a_j} \end{Bmatrix}$$

where

$$a_\ell = \Delta E_\ell + i\frac{\Gamma_\ell}{2} \qquad ; \qquad a_\ell^* = \Delta E_\ell - i\frac{\Gamma_\ell}{2}$$

TABLE 6. Matrix form of the ML Breit-Wigner elastic cross section with many resonances and one neutron channel

$$\sigma_{nn} = \pi\lambda^2 \sum g_J \begin{vmatrix} z_\ell \\ z_1 \\ z_2 \\ \cdot \\ \cdot \\ \cdot \end{vmatrix}^* \begin{vmatrix} \Gamma_\ell(2\ell+1) & \Gamma_\ell\Gamma_{n1} & \Gamma_\ell\Gamma_{n2} & \cdots \\ \Gamma_\ell\Gamma_{n1} & \Gamma_{n1}\Gamma_{n1} & \Gamma_{n1}\Gamma_{n2} & \cdots \\ \Gamma_\ell\Gamma_{n2} & \Gamma_{n1}\Gamma_{n2} & \Gamma_{n2}\Gamma_{n2} & \cdots \\ \cdot & \cdot & \cdot & \\ \cdot & \cdot & \cdot & \\ \cdot & \cdot & \cdot & \end{vmatrix} \begin{vmatrix} z \\ z_1 \\ z_2 \\ \\ \\ \\ \end{vmatrix}$$

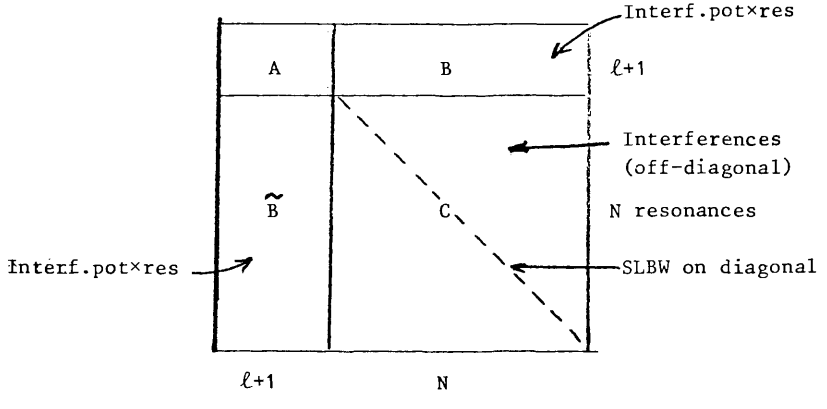

$$z_j = \frac{1}{\Delta E_j + i\Gamma_j/2}$$

Γ_j = total width of res. j

* = row vector complex conjugate

TABLE 7. The random generation of signs for u_j

$(\Gamma_n^{\frac{1}{2}})_j$	$(\Gamma_c^{\frac{1}{2}})_j$	u_j	% events
+	+	+	50
−	−	+	
+	−	−	50
−	+	−	

TABLE 8. The data in the resolved region for Reich-Moore formalism

FKEY# 6: PRINT OF THE RECALLED FILE <PU241>

ZAI	ABN	b	LFW	NER	b	ref.
9.42410E+04	1.00000E+00	0.00000E+00	1.00000E+00	1.00000E+00	0.00000E+00	
EL	EH	LRU	LRF	b	b	
1.00000E-05	1.04000E+02	1.00000E+00	3.00000E+00	0.00000E+00	0.00000E+00	
SPI	AP	b	b	NLS	NE	
2.50000E+00	9.60000E-01	0.00000E+00	0.00000E+00	1.00000E+00	0.00000E+00	
AWRI	AM	L	b	6*NRS	NRS	
2.38986E+02	0.00000E+00	0.00000E+00	0.00000E+00	5.52000E+02	9.20000E+01	
ER	AJ	GN	GG	GF1	GF2	
2.60000E-01	3.00000E+00	4.37142E-05	4.00000E-02	7.50000E-02	0.00000E+00	1
4.28000E+00	3.00000E+00	6.19714E-04	4.00000E-02	2.90000E-02	0.00000E+00	2
4.58000E+00	2.00000E+00	4.50000E-04	4.00000E-02	-2.40000E-02	1.00000E-01	3
5.93000E+00	2.00000E+00	3.35760E-03	4.00000E-02	-1.29200E+00	1.60000E-02	4
6.93000E+00	3.00000E+00	7.09714E-04	4.00000E-02	-8.90000E-02	0.00000E+00	5
8.61000E+00	3.00000E+00	8.70000E-04	4.00000E-02	4.10000E-02	0.00000E+00	6
9.62000E+00	2.00000E+00	4.70400E-04	4.00000E-02	1.02000E-01	3.10000E-02	7
9.38000E+00	2.00000E+00	2.22000E-03	4.00000E-02	3.92000E-01	6.18000E-01	8
1.27700E+01	2.00000E+00	9.36000E-04	4.00000E-02	-2.33000E-01	0.00000E+00	9
1.34200E+01	3.00000E+00	2.19771E-03	4.00000E-02	0.00000E+00	2.90000E-02	10
1.39000E+01	2.50000E+00	2.00000E-05	4.00000E-02	5.30000E-02	0.00000E+00	11
1.47500E+01	2.00000E+00	6.98880E-03	4.00000E-02	1.00000E-01	1.70000E-02	12
1.59600E+01	2.00000E+00	1.82040E-03	4.00000E-02	-4.00000E-01	5.50000E-02	13
1.66700E+01	3.00000E+00	1.16228E-03	4.00000E-02	1.84000E-01	0.00000E+00	14
1.78300E+01	3.00000E+00	3.49971E-03	1.40000E-02	0.00000E+00	0.00000E+00	15
1.82900E+01	3.00000E+00	1.60285E-04	4.00000E-02	2.70000E-02	0.00000E+00	16
2.07000E+01	3.00000E+00	3.57428E-04	4.00000E-02	5.00000E-02	3.00000E-03	17
2.18700E+01	3.00000E+00	4.88571E-05	4.00000E-02	0.00000E+00	-3.30000E-02	18
. . ↑ .	. . ↑ .	. . ↑ .	. . ↑ .	. . ↑ .	. . ↑ .	
. ⇗ . .	. ⇗ . .	. ⇗ . .	. ⇗ . .	. ⇗ . .	. ⇗ . .	
. -↓ . .	. ↓ . .	. ↓ . .	. ↓ . .	. ↓ . .	. ↓ . .	
9.54200E+01	2.00000E+00	1.11120E-03	4.00000E-02	5.90000E-02	2.80000E-01	83
9.61200E+01	2.00000E+00	4.70400E-04	4.00000E-02	-1.90000E-02	-6.90000E-02	84
9.65500E+01	2.00000E+00	6.50400E-04	4.00000E-02	3.55000E-01	5.00000E-03	85
9.75800E+01	3.00000E+00	5.29714E-04	4.00000E-02	0.00000E+00	2.71000E-01	86
9.84100E+01	3.00000E+00	6.54771E-03	4.00000E-02	1.71000E-01	-1.80000E-02	87
9.97800E+01	3.00000E+00	2.42742E-03	4.00000E-02	3.87000E-01	7.40000E-02	88
1.00700E+02	2.50000E+00	4.00000E-04	4.00000E-02	2.32000E-01	0.00000E+00	89
1.01610E+02	3.00000E+00	8.75142E-04	4.00000E-02	-4.20000E-02	-5.00000E-03	90
1.02380E+02	2.00000E+00	1.82280E-03	4.00000E-02	8.76000E-01	0.00000E+00	91
1.03660E+02	3.00000E+00	1.09971E-03	4.00000E-02	0.00000E+00	2.10000E-02	92

TABLE 9. Resonance parameters for Cm-245. Phase angles refer to the fission-width-vector orientation in a two-fission-channel, single-spin-state analysis

E_0 (eV)	$2g\Gamma_n^0$ (meV)	Γ_γ (meV)	Γ_f (meV)	θ (deg)
21.36	0.457	(40)	485	−16
24.90	0.521	(40)	226	99
25.84	0.007	(40)	549	89
26.83	0.147	(40)	131	160
27.63	0.114	(40)	165	90
29.42	0.638	(40)	328	−171
31.71	0.088	(40)	691	−69[a]
32.99	0.064	(40)	4	−61
34.59	0.039	(40)	61	113
35.31	1.276	(40)	4195	54
36.32	0.256	(40)	189	177
39.45	0.104	(40)	102	−126[a]
40.44	0.705	(40)	585	128
42.45	0.824	(40)	10	56
43.10	0.264	(40)	537	−55
44.57	0.391	(40)	694	−67
45.74	0.087	(40)	901	−9
47.51	0.516	(40)	28	28
49.20	0.718	(40)	1399	58
50.48	0.252	(40)	751	92
51.64	0.087	(40)	207	106
53.63	1.687	(40)	896	−173
54.63	0.045	(40)	1057	174
56.32	0.186	(40)	505	54
58.54	1.811	(40)	393	162
59.99	0.079	(40)	518	−39

[a]Best fits were obtained by placing those resonances marked with an a in a different spin group.

TABLE 10. The formulas for Reich-Moore representation of the ML two fission channel cross section

D.1.3. Reich-Moore Formulae

A detailed derivation of these formulae is to be found in Reich and Moore.[2] Neutron cross sections with an exit channel c are given by*

$$\sigma_{nc} = \pi \lambda_n^2 \sum_J g_J \left|\delta_{nc} - U^J_{nc}\right|^2 , \quad (1)$$

where λ_n is calculated in the center-of-mass system; and

$$\frac{1}{\lambda_n} = k_n = 2.196771 \frac{AWRI}{AWRI+1.0} \times 10^{-3} \sqrt{E(eV)} , \quad (2)$$

where AWRI is the mass of the target nucleus in units of neutron mass. The statistical factor

$$g_J = \frac{(2J+1)}{2(2I+1)} , \quad (3)$$

where J is the spin of the compound nucleus resonance and I is the target nucleus spin.

In terms of the Reich-Moore approximation one may write

$$U^J_{nc} = e^{-i(\phi_n+\phi_c)} \left\{2\left[(I-K)^{-1}\right]_{nc} - \delta_{nc}\right\} , \quad (4)$$

where $(I-K)_{cc'} = \delta_{cc'} - \frac{i}{2} \sum_\lambda \frac{\Gamma_{\lambda c}^{1/2} \Gamma_{\lambda c'}^{1/2}}{E_\lambda - E - \frac{i}{2}\Gamma_{\lambda\gamma}}$, (5)

where the summation in Eq. (5) is over the resonance levels λ; E_λ is the resonance energy; $\Gamma_{\lambda\gamma}$, the corresponding radiation widths; and $\Gamma_{\lambda c}$ and $\Gamma_{\lambda c'}$, are the widths for the λ-th level and channels c and c', respectively.

If we define

$$\rho_{nc} = \delta_{nc} - \left[(I-K)^{-1}\right]_{nc} = \delta_{nc} - \frac{m_{nc}}{\Delta} ,$$

where $\Delta = |I-K|$ is the determinant of the matrix I-K and m_{nc} is the cofactor of the element $(I-K)_{nc}$ of the matrix I-K, we obtain

$$\sigma_{nT} = \sum_J \sigma^J_{nT} = 2\pi \lambda_n^2 \sum_J g_J \mathrm{Re}\left(1-U^J_{mn}\right)$$

$$= 2\pi \lambda_n^2 \sum_J \left\{g_J(1-\cos 2\phi_n) + 2g_J \mathrm{Re}\left(e^{-2i\phi_n} \rho_{nn}\right)\right\} . \quad (6)$$

$$\sigma_{nn} = \Pi \lambda_n^2 \sum_J g_J \left|1-U^J_{nn}\right|^2 . \quad (7)$$

$$\sigma_{nAbs} = \sigma_{nT} - \sigma_{nn} = 4\Pi \lambda_n^2 \sum_J g_J \left[\mathrm{Re}\left(\rho_{nn}\right) - \left|\rho_{nn}\right|^2\right] . \quad (8)$$

$$\sigma_{nFiss} = 4\pi \lambda_n^2 \sum_J g_J \left(\sum_c \left|\rho_{nc}\right|^2\right) . \quad (9)$$

$$\sigma_{n\gamma} = \sigma_{nAbs} - \sigma_{nFiss} . \quad (10)$$

TABLE 11. The U-233 experimental parameters for resolved region evaluated with the Reich-Moore multilevel approximation

	One fission channel parameters						Two fission channel paramgters								
Level (λ)	E_λ (ev)	g_J[a]	$\Gamma_{\lambda n}$[a] (10^{-3} ev)	$\Gamma_{\lambda\gamma}$ (10^{-3} ev)	$\Gamma_{\lambda f}$ (10^{-3} ev)	Relative sign of $\beta_{\lambda 1}\beta_{\lambda 2}$	E_λ (ev)	g_J[a]	$\Gamma_{\lambda n}$[a] (10^{-3} ev)	$\Gamma_{\lambda\gamma}$ (10^{-3} ev)	$\Gamma_{\lambda f}$ (10^{-3} ev)	$2\beta_{\lambda 2}^2$ (10^{-3} ev)	$2\beta_{\lambda 3}^2$ (10^{-3} ev)	Relative signs of $\beta_{\lambda 1}\beta_{\lambda 2}$	$\beta_{\lambda 1}\beta_{\lambda 3}$
1	0.195	7/12	0.00059	44	60	+	0.150	7/12	0.00002	30	60	35	25	−	+
2	1.55	5/12	0.165	60	562	...[b]	1.56	7/12	0.104	54	420	0	420	...	−
3	1.76	7/12	0.155	36	182	−	1.755	7/12	0.162	36	186	186	0	−	...
4	2.31	7/12	0.086	34.6	48	+	2.305	7/12	0.086	34.6	48	45.6	2.4	+	−
5	3.61	7/12	0.060	62	174	+	3.65	7/12	0.057	53	149	129	20	+	+
6	4.75	5/12	0.130	80	718	...[b]	4.825	7/12	0.105	80	850	750	100	+	−
7	5.82	7/12	0.047	80	316	−	...[c]	...	...	...	...	...	...		
8	6.82	7/12	0.300	55	146	+	6.82[d]	7/12	0.300	55	146	0	146	...	−
9	7.6	7/12	0.007	48	125	−	...[c]	...	...	...	...	...	...		
10	8.7	7/12	0.010	40	300	−	...[c]	...	...	...	...	...	...		
11	9.2	7/12	0.019	50	180	−	...[c]	...	...	...	...	...	...		
12	10.47	7/12	0.411	85	270	+	10.47[d]	7/12	0.411	85	270	0	270	...	−

[a] Based on considerations presented in the text (discussion).
[b] Sign immaterial, since the contribution was calculated using a single-level formula.
[c] Not included in the two fission channel analysis.
[d] Carried over from the one fission channel analysis.

TABLE 12. The possible sequence of signs for a matrix of order 3

No.	γ_1	γ_2	γ_3	No.	a_{12}	a_{13}	a_{23}
1	+	+	+	1	+	+	+
2	+	+	−	4	+	−	−
3	+	−	+	6	−	+	−
4	+	−	−	7	−	−	+
5	−	+	+	7	−	−	+
6	−	+	−	6	−	+	−
7	−	−	+	4	+	−	−
8	−	−	−	1	+	+	+

TABLE 13. The procedure for a determination of the bound level as adopted in the code RINEG

The code calculates the neutron and fission (if fissile) widths of the negative bound level which better reproduce the thermal capture and fission cross-sections at 0.0253 eV.

The single level Breit-Wigner resonance profile is assumed with the following known input parameters

AWRI = atomic mass unit (neutron = 1) of the isotope
S1 = thermal capture cross section
S2 = thermal fission cross section (if non fissile put = 0)
I = spin target nucleus
J = resonance spin for ℓ=0 bound level
E_r = resonance energy for ℓ=0 bound level
Γ_g = radiative width

The calculation immediately provides for computing $\Gamma_f = \Gamma_g$*(S2/S1) and from the BW simplified formula for x-reaction

$$\sigma_x = \pi\lambda^2 g_j \frac{\Gamma_n \Gamma_x}{(E-E_r)^2 + \frac{\Gamma_t^2}{4}}$$

we solve with respect to Γ_n or Γ_x by the equations

$$a_1 \Gamma_n^2 + b_1 \Gamma_n + c_1 = 0$$

$a_1 = \sigma_c$

$b_1 = 2\sigma_c(\Gamma_\gamma+\Gamma_f) - 4C\Gamma_\gamma$

$c_1 = \sigma_c \{4(E-E_r)^2 + (\Gamma_\gamma+\Gamma_f)^2\}$

$C = \pi\lambda^2 g_j$

or

$$a_2 \Gamma_x^2 + b_2 \Gamma_x + c_2 = 0$$

$a_2 = \sigma_x$

$b_2 = 2\sigma_x(\Gamma_n+\Gamma_\gamma) - 4C\Gamma_n$

$c_2 = \sigma_x \{4(E-E_r)^2 + (\Gamma_n+\Gamma_\gamma)^2\}$

$C = \pi\lambda^2 g_j$

The reaction index x is generally referred to fission reaction.

TABLE 14. Cross sections in the Unresolved Region

a. Elastic Scattering Cross Section

$$\sigma_{n,n}(E) = \sum_{\ell=0}^{NLS} \sigma_{n,n}^{\ell}(E)$$

$$\sigma_{n,n}^{\ell}(E) = \frac{4\pi}{k^2} \sum_{J}^{NJS_\ell} g_J (2\ell+1) \sin^2\phi_\ell + \frac{2\pi^2}{k^2} \sum_{J}^{NJS_\ell} \frac{g_J}{\bar{D}_{\ell,J}} \left[\left\langle \frac{\Gamma_n \Gamma_n}{\Gamma} \right\rangle_{\ell,J} - 2\bar{\Gamma}_{n_{\ell,J}} \sin^2\phi_\ell \right]$$

b. Radiative Captive Cross Section

$$\sigma_{n,\gamma}(E) = \sum_{\ell=0}^{NLS} \sigma_{n,\gamma}^{\ell}(E)$$

$$\sigma_{n,\gamma}^{\ell}(E) = \frac{2\pi^2}{k^2} \sum_{J}^{NJS_\ell} \frac{g_J}{\bar{D}_{\ell,J}} \left\langle \frac{\Gamma_n \Gamma_\gamma}{\Gamma} \right\rangle_{\ell,J}$$

c. Fission Cross Section

$$\sigma_{n,f}(E) = \sum_{\ell=0}^{NLS} \sigma_{n,f}^{\ell}(E)$$

$$\sigma_{n,f}^{\ell}(E) = \frac{2\pi^2}{k^2} \sum_{J}^{NJS_\ell} \frac{g_J}{\bar{D}_{\ell,J}} \left\langle \frac{\Gamma_n \Gamma_f}{\Gamma} \right\rangle_{\ell,J}$$

TABLE 15. Cross sections in the Unresolved Region (continuation)

The summation over ℓ, in the above equations, extends up to $\ell = 2$ or to NLS (where NLS is the number of ℓ-states for which data are given). For each value of ℓ, the summation over J-states extends to NJS_ℓ (the number of J-states for a particular ℓ-state).

NLS and NJS are given in File 2.

$$\left\langle \frac{\Gamma_n \Gamma_n}{\Gamma} \right\rangle_{\ell,J} = \left(\frac{\bar{\Gamma}_{n_{\ell,J}} \bar{\Gamma}_{n_{\ell,J}}}{\bar{\Gamma}_{\ell,J}} \right) R_{n\ell,J}$$

$$\left\langle \frac{\Gamma_n \Gamma_\gamma}{\Gamma} \right\rangle_{\ell,J} = \left(\frac{\bar{\Gamma}_{n_{\ell,J}} \bar{\Gamma}_{\gamma_{\ell,J}}}{\bar{\Gamma}_{\ell,J}} \right) R_{\gamma\ell,J}$$

$$\left\langle \frac{\Gamma_n \Gamma_f}{\Gamma} \right\rangle_{\ell,J} = \left(\frac{\bar{\Gamma}_{n_{\ell,J}} \bar{\Gamma}_{f_{\ell,J}}}{\bar{\Gamma}_{\ell,J}} \right) R_{f\ell,J}$$

where $R_{\gamma\ell,J}$, $R_{f\ell,J}$, and $R_{n\ell,J}$ are fluctuation integrals for capture, fission, and elastic scattering, respectively. Associated with each of these integrals is the number of degrees of freedom for each of the average widths.

TABLE 16. Parameters for the Unresolved Region. Curium 245

```
FKEY# 6: PRINT OF THE RECALLED FILE <CM245U>
    ZAI          ABN          b            LFW          NER          b            ref.
 9.62450E+04 1.00000E+00 0.00000E+00 1.00000E+00 1.00000E+00 0.00000E+00
    EL           EH           LRU          LRF          b            b
 6.10000E+01 1.00000E+04 2.00000E+00 1.00000E+00 0.00000E+00 0.00000E+00
    SPI          AP           b            b            NLS          NE
 3.50000E+00 9.50000E-01 0.00000E+00 0.00000E+00 3.00000E+00 2.00000E+00
  ■ ES = 61   10000   ■
    AWRI         AM           L            b          6*NJS        NJS
2.42960E+02 0.00000E+00 0.00000E+00 0.00000E+00 1.20000E+01 2.00000E+00
    DJ           AJ           AMUN         <GN0>        <GG>         MUF
2.83430E+00 3.00000E+00 1.00000E+00 3.37280E-04 3.60000E-02 2.00000E+00      1
  ■ GF = .394  .419   ■
2.20444E+00 4.00000E+00 1.00000E+00 2.62329E-04 3.44000E-02 2.00000E+00      2
  ■ GF = .432  .465   ■
    AWRI         AM           L            b          6*NJS        NJS
2.42960E+02 0.00000E+00 1.00000E+00 0.00000E+00 2.40000E+01 4.00000E+00
    DJ           AJ           AMUN         <GN0>        <GG>         MUF
3.96800E+00 2.00000E+00 1.00000E+00 8.33280E-04 3.70000E-02 2.00000E+00      3
  ■ GF = .36   .378   ■
2.83430E+00 3.00000E+00 2.00000E+00 5.95203E-04 3.60000E-02 2.00000E+00      4
  ■ GF = .394  .419   ■
2.20444E+00 4.00000E+00 2.00000E+00 4.62932E-04 3.40000E-02 2.00000E+00      5
  ■ GF = .432  .465   ■
1.80364E+00 5.00000E+00 1.00000E+00 3.78764E-04 3.20000E-02 2.00000E+00      6
  ■ GF = .469  .518   ■
    AWRI         AM           L            b          6*NJS        NJS
2.42950E+02 0.00000E+00 2.00000E+00 0.00000E+00 3.60000E+01 6.00000E+00
    DJ           AJ           AMUN         <GN0>        <GG>         MUF
6.61333E+00 1.00000E+00 1.00000E+00 0.00000E+00 3.60000E-02 2.00000E+00      7
  ■ GF = .4    .4    ■
3.96800E+00 2.00000E+00 2.00000E+00 0.00000E+00 3.60000E-02 2.00000E+00      8
  ■ GF = .4    .4    ■
2.83430E+00 3.00000E+00 2.00000E+00 0.00000E+00 3.60000E-02 2.00000E+00      9
  ■ GF = .4    .4    ■
2.20444E+00 4.00000E+00 2.00000E+00 0.00000E+00 3.60000E-02 2.00000E+00     10
  ■ GF = .4    .4    ■
1.80364E+00 5.00000E+00 2.00000E+00 0.00000E+00 3.60000E-02 2.00000E+00     11
  ■ GF = .4    .4    ■
1.52616E+00 6.00000E+00 1.00000E+00 0.00000E+00 3.60000E-02 2.00000E+00     12
  ■ GF = .4    .4    ■
```

TABLE 17. Parameters for the Unresolved Region in ENDF/B format. Curium 245

```
MF2CM245.FORT
9.62450+ 4 2.42960+ 2          0          0          1          09645 215100001
9.62450+ 4 1.00000+ 0          0          1          2          09645 215100002
1.00000- 5 6.10000+ 1          1          3          0          09645 215100003
3.50000+ 0 9.50000- 1          0          0          1          09645 215100004
2.42960+ 2 0.0    + 0          0          0        240        409645 215100005
-1.00000- 1 3.50001+ 0 4.55000- 5 5.00000- 2 3.00000- 1 0.0    + 09645 215100006
 8.50000- 1 3.50002+ 0 1.02000- 4 4.00000- 2 8.00000- 1 0.0    + 09645 215100007
 1.98000+ 0 3.50003+ 0 2.40000- 4 4.00000- 2 1.75000- 1 0.0    + 09645 215100008
 2.45000+ 0 3.50004+ 0 1.10000- 4 4.00000- 2 3.00000- 1 0.0    + 09645 215100009
 4.68000+ 0 3.50006+ 0 2.10000- 3 4.00000- 2 3.25000- 1 0.0    + 09645 215100010
 5.75000+ 0 3.50007+ 0 1.10000- 4 4.00000- 2 3.00000- 1 0.0    + 09645 215100011
 7.53000+ 0 3.50008+ 0 1.91000- 3 4.00000- 2 3.00000- 1 0.0    + 09645 215100012
 8.65000+ 0 3.50009+ 0 5.30000- 4 4.00000- 2 5.00000- 1 0.0    + 09645 215100013
 9.15000+ 0 3.50010+ 0 3.90000- 4 4.00000- 2 2.00000- 1 0.0    + 09645 215100014
 1.01500+ 1 3.50012+ 0 4.00000- 4 4.00000- 2 2.00000- 1 0.0    + 09645 215100015
 1.13400+ 1 3.50013+ 0 8.80000- 4 4.00000- 2 1.50000- 1 0.0    + 09645 215100016
 1.35800+ 1 3.50014+ 0 5.90000- 5 4.00000- 2 4.50000- 2 0.0    + 09645 215100017
 1.37500+ 1 3.50015+ 0 3.40000- 4 4.00000- 2 1.70000- 1 0.0    + 09645 215100018
 1.60000+ 1 3.50016+ 0 1.20000- 3 4.00000- 2 4.00000- 1 0.0    + 09645 215100019
 2.13600+ 1 3.50000+ 0 2.11211- 3 4.00000- 2 4.48151- 1-3.68483- 29645 215100020
 2.49000+ 1 3.50000+ 0 2.59978- 3 4.00000- 2-5.53061- 3 2.20469- 19645 215100021
 2.58400+ 1 3.50000+ 0 3.55831- 5 4.00000- 2 1.67220- 4 5.48832- 19645 215100022
 2.68300+ 1 3.50000+ 0 7.61425- 4 4.00000- 2-1.15675- 1 1.53240- 29645 215100023
 2.76300+ 1 3.50000+ 0 5.99232- 4 4.00000- 2 0.0    + 0 1.65000- 19645 215100024
 2.94200+ 1 3.50000+ 0 3.46852- 3 4.00000- 2-3.19973- 1-8.02673- 39645 215100025
 3.17100+ 1 3.50000+ 0 4.95542- 4 4.00000- 2 8.87434- 2-6.02256- 19645 215100026
 3.29900+ 1 3.50000+ 0 3.67596- 4 4.00000- 2 9.40160- 4-3.05984- 39645 215100027
 3.45900+ 1 3.50000+ 0 2.29371- 4 4.00000- 2-9.31292- 3 5.16870- 29645 215100028
 3.53100+ 1 3.50000+ 0 7.58227- 3 4.00000- 2 1.44933+ 0 2.74566+ 09645 215100029
 3.63200+ 1 3.50000+ 0 1.54281- 3 4.00000- 2-1.88482- 1 5.17680- 49645 215100030
 3.94500+ 1 3.50000+ 0 6.53216- 4 4.00000- 2-3.52401- 2-6.67598- 29645 215100031
 4.04400+ 1 3.50000+ 0 4.48326- 3 4.00000- 2-2.21737- 1 3.63262- 19645 215100032
 4.24500+ 1 3.50000+ 0 5.36866- 3 4.00000- 2 3.12697- 3 6.87303- 39645 215100033
 4.31000+ 1 3.50000+ 0 1.73317- 3 4.00000- 2 1.76667- 1-3.60332- 19645 215100034
 4.45700+ 1 3.50000+ 0 2.61034- 3 4.00000- 2 1.05953- 1-5.88046- 19645 215100035
 4.57400+ 1 3.50000+ 0 5.88392- 4 4.00000- 2 8.78950- 1-2.20490- 29645 215100036
 4.75100+ 1 3.50000+ 0 3.55665- 3 4.00000- 2 2.18287- 2 6.17130- 39645 215100037
 4.92000+ 1 3.50000+ 0 5.03624- 3 4.00000- 2 3.92859- 1 1.00614+ 09645 215100038
 5.04800+ 1 3.50000+ 0 1.79044- 3 4.00000- 2-9.14700- 4 7.50085- 19645 215100039
 5.16400+ 1 3.50000+ 0 6.25190- 4 4.00000- 2-1.57270- 2 1.91272- 19645 215100040
 5.36300+ 1 3.50000+ 0 1.23543- 2 4.00000- 2-8.82692- 1-1.33075- 29645 215100041
 5.46300+ 1 3.50000+ 0 3.32604- 4 4.00000- 2-1.04545+ 0 1.15489- 29645 215100042
 5.63200+ 1 3.50000+ 0 1.39586- 3 4.00000- 2 1.74473- 1 3.30526- 19645 215100043
 5.85400+ 1 3.50000+ 0 1.38562- 2 4.00000- 2-3.55471- 1 3.75281- 29645 215100044
 5.99900+ 1 3.50000+ 0 6.11880- 4 4.00000- 2 3.12849- 1-2.05150- 19645 215100045
 6.10000+ 1 1.00000+ 4          2          1          0          09645 215100046
 3.50000+ 0 9.50000- 1          0          0          2          29645 215100047
 6.10000+ 1 1.00000+ 4                                           9645 215100048
 2.42960+ 2 0.0    + 0          0          0          2          09645 215100049
 0.0    + 0 0.0    + 0          0          2          8          09645 215100050
 2.83430+ 0 3.00000+ 0 1.00000+ 0 3.37280- 4 3.60000- 2 0.0    + 09645 215100051
 3.94000- 1 4.19000- 1                                           9645 215100052
 0.0    + 0 0.0    + 0          0          2          8          09645 215100053
 2.20444+ 0 4.00000+ 0 1.00000+ 0 2.62329- 4 3.44000- 2 0.0    + 09645 215100054
 4.32000- 1 4.65000- 1                                           9645 215100055
 2.42960+ 2 0.0    + 0          1          0          4          09645 215100056
 0.0    + 0 0.0    + 0          1          2          8          09645 215100057
 3.96800+ 0 2.00000+ 0 1.00000+ 0 8.33280- 4 3.70000- 2 0.0    + 09645 215100058
 3.60000- 1 3.78000- 1                                           9645 215100059
 0.0    + 0 0.0    + 0          1          2          8          09645 215100060
 2.83430+ 0 3.00000+ 0 2.00000+ 0 5.95203- 4 3.60000- 2 0.0    + 09645 215100061
 3.94000- 1 4.19000- 1                                           9645 215100062
 0.0    + 0 0.0    + 0          1          2          8          09645 215100063
 2.20444+ 0 4.00000+ 0 2.00000+ 0 4.62932- 4 3.40000- 2 0.0    + 09645 215100064
 4.32000- 1 4.65000- 1                                           9645 215100065
 0.0    + 0 0.0    + 0          1          2          8          09645 215100066
 1.80364+ 0 5.00000+ 0 1.00000+ 0 3.78764- 4 3.20000- 2 0.0    + 09645 215100067
 4.69000- 1 5.18000- 1                                           9645 215100068
                                                                 9645 200000069
                                                                 9645 000000070
```

TABLE 18. The analytical integration for the resonance integral with a 1/E weighting flux

RESONANCE INTEGRAL CALCULATION

The integration of a Breit-Wigner cross section, weighted over a standard flux 1/E, can be carried through explicitly. Assuming the cross section given by

$$\sigma(E) = \sigma_r \frac{E_r}{E} \cdot \frac{\Gamma^2/4}{(E-E_r)^2 + \Gamma^2/4} \qquad \text{with } \sigma_r, E_r, \Gamma \text{ constants}$$

we have, for integration between the limits E_1 and E_2 :

$$I(E_1,E_2) = \int_{E_1}^{E_2} \frac{\sigma(E)}{E}\, dE =$$

$$= \frac{\sigma_r \Gamma^2}{4\mu^2 E_r^2}\left[\frac{2}{\sqrt{X_1}} - \frac{2}{\sqrt{X_2}} + \frac{2+\mu}{\mu\sqrt{2(\mu+1)}}\left\{\tanh^{-1}\frac{\sqrt{2X_2(\mu+1)}}{\mu+X_2} - \tanh^{-1}\frac{\sqrt{2X_1(\mu+1)}}{\mu+X_1}\right\}\right.$$

$$\left. + \frac{2-\mu}{\mu\sqrt{2(\mu-1)}}\left\{\mathrm{tg}^{-1}\frac{\sqrt{2X_2(\mu-1)}}{\mu-X_2} - \mathrm{tg}^{-1}\frac{\sqrt{2X_1(\mu-1)}}{\mu-X_1}\right\}\right]$$

with the proviso that E_r is positive and when either of the inverse tangents has negative argument it lies in the quadrant $\pi/2$ to π .

In the above expression

$$\mu = \sqrt{1 + \Gamma^2/(4E_r^2)} \quad ; \quad X_1 = E_1/E_r \quad ; \quad X_2 = E_2/E_r \quad .$$

TABLE 19. Walker's approximation for the reduced resonance integral in the resolved region

For resonance above 1 ev, the contribution of the k^{th} Breit-Wigner resonance to the reduced resonance absorption integral, in barns, is given by

$$I'_k = \left\{\frac{4090\ g^*}{\Gamma}\left|\frac{\Gamma_\gamma\,\Gamma_n}{E_r^2}\right|\right\}_k$$

Here Γ_n and Γ_γ are the partial widths for neutron scattering and radiative capture, respectively, measured in milli-eV, Γ is the total width of the resonance in milli-eV, and for fission product nuclei is equal to the sum of Γ_n and Γ_γ ; E_r is the energy in eV at which the cross section is a maximum; and g* is a function of the spin states J_1 and J_2 of the target and compound nuclei respectively ($J_2 = J_1 \pm 1/2$ for l=0 neutrons) given by

$$g^* = \frac{1}{2}\left[\frac{2J_2+1}{2J_1+1}\right]$$

For all even-even nuclei ($J_1 = 0$) g*=1; for the remainder, g* is calculated where J_2 is known but otherwise is assumed to take the value 1/2.

Each resonance also contributes to the 2200 m/s cross section an amount $(\sigma_o)_k$ barns, given by

$$(\sigma_o)_k = \left\{\frac{4.09\ g^*}{\sqrt{E_r}}\left|\frac{\Gamma_\gamma\,\Gamma_n}{E_r^2}\right|\right\}_k$$

TABLE 20. Walker's approximation for the resonance integral due to the unresolved part of resonances

Using the average cross section given by Sampson and Chernick (1958) for l=0 neutrons (which does not take into account statistical fluctuations in the reduced neutron width Γ_n° (equals $\Gamma_n/\sqrt{E_r}$)) and integrating over a 1/E spectrum, the reduced resonance absorption integral for the unresolved levels, above energy E_L, say, is given by

$$I'_{unres.} = 4090 \left(\frac{2g^*\bar{\Gamma}_n^\circ}{D\bar{\Gamma}_\gamma}\right) (a - \ln(1+a))$$

where $$a = \frac{\bar{\Gamma}_\gamma}{\bar{\Gamma}_n^\circ \sqrt{E_L}}$$

$\bar{\Gamma}_n^\circ$ and $\bar{\Gamma}$ are the average reduced neutron and radiative capture widths in milli-eV, and D is the average level spacing. D and E_L are in units of electron volts. Since the approximations made concerning the orbital angular momentum of the neutrons (l = 0 only) and the statistical variation of reduced neutron widths introduce errors more or less equal in magnitude but opposite in sign, no serious error arise in using this expression for $I'_{unres.}$.

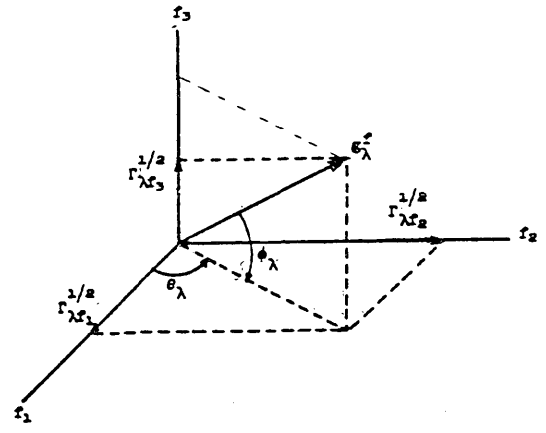

Fig. 1

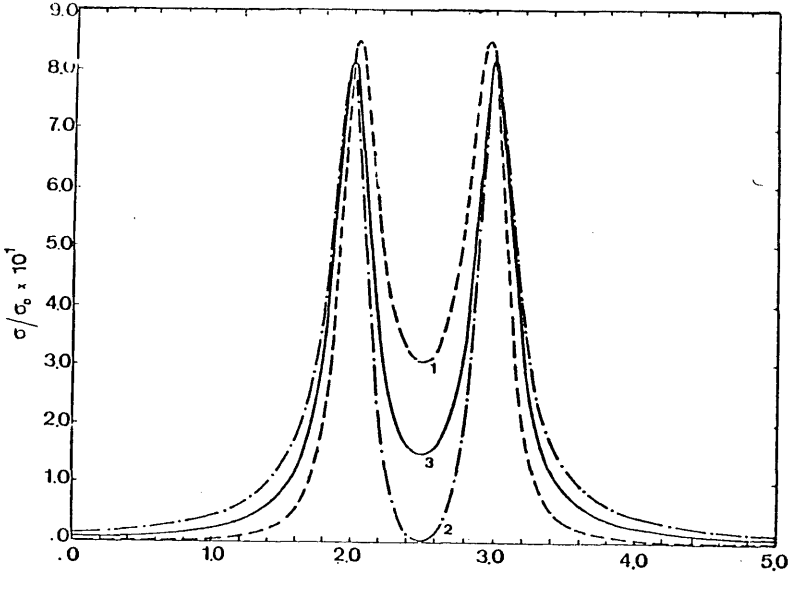

Fig. 2

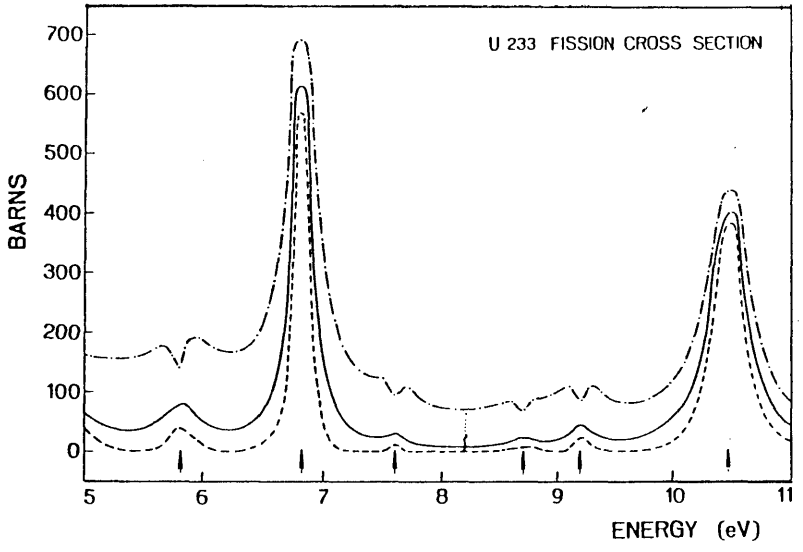

Fig. 3

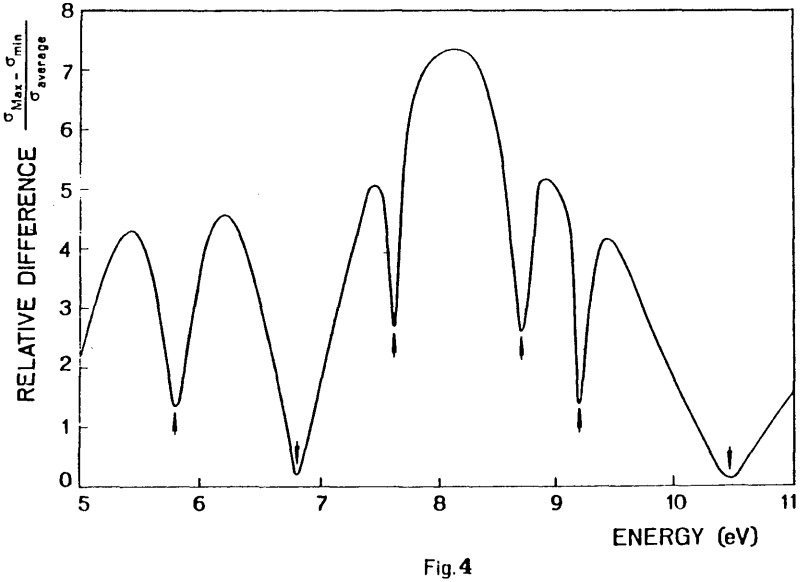

Fig. 4

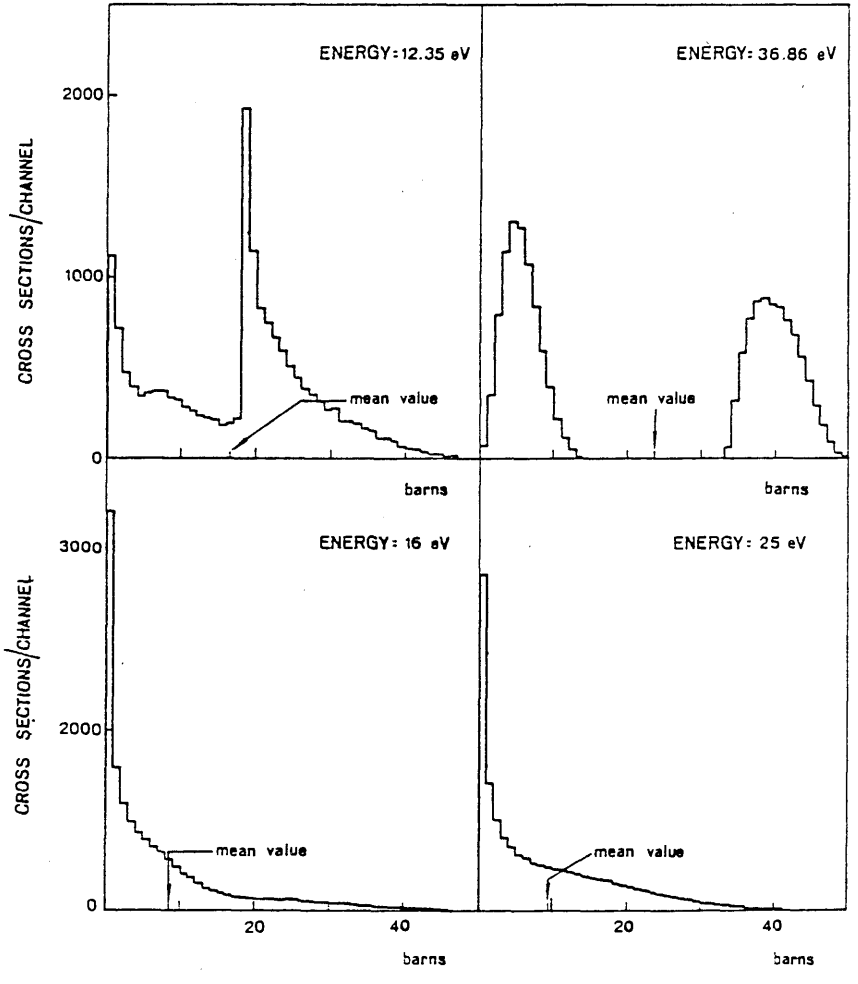

Fig. 5

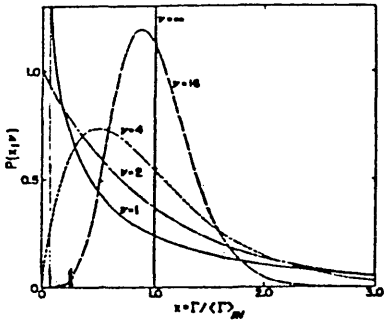

fig.6

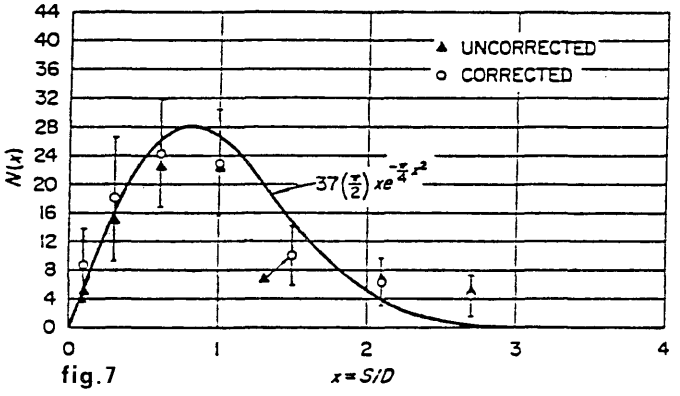

fig.7

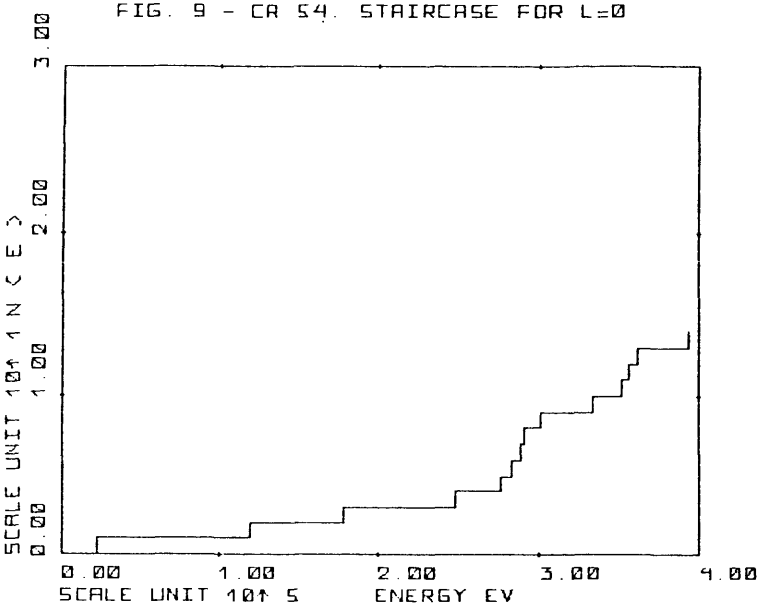

fig.9

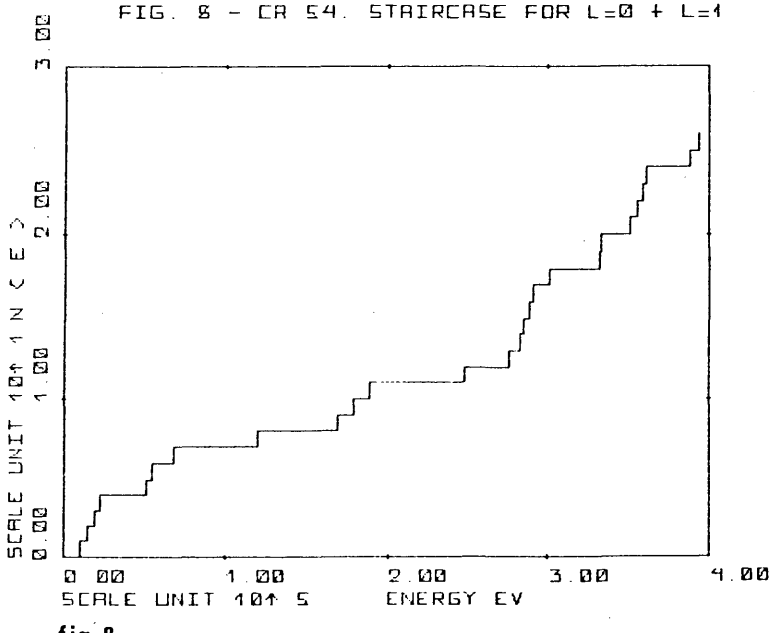

fig.8

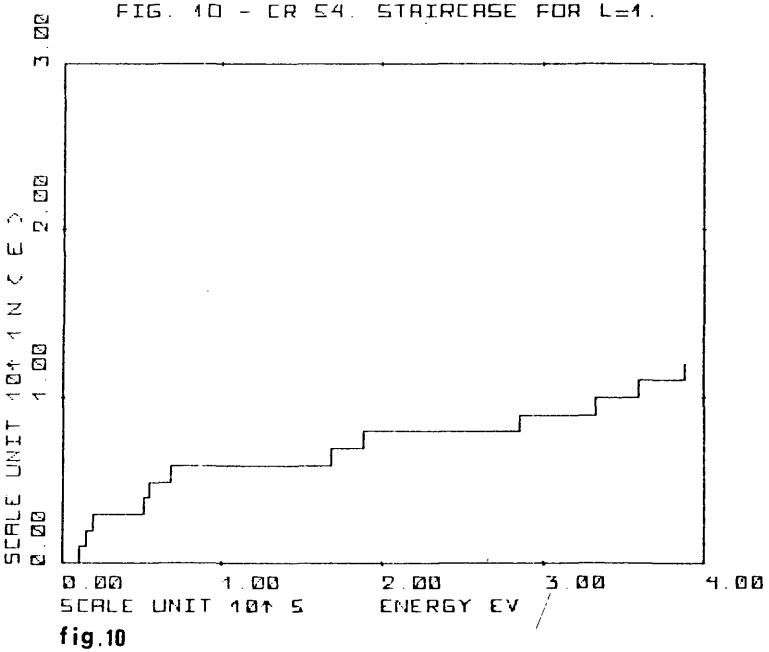

fig.10

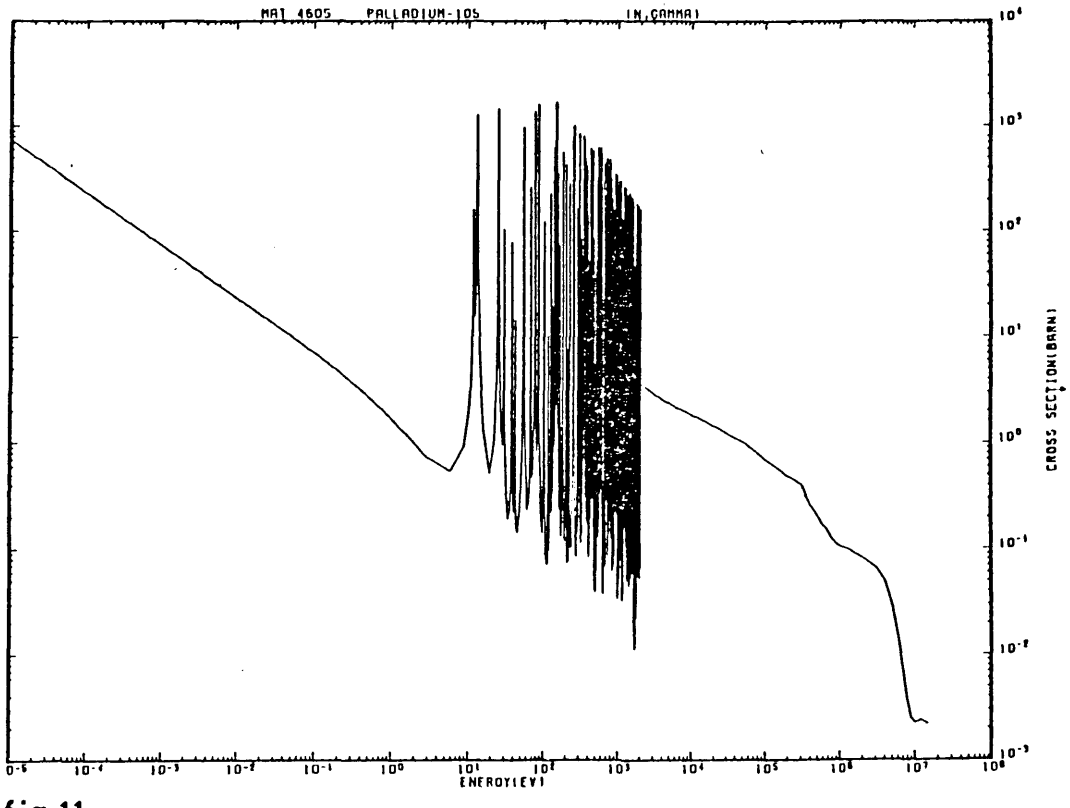
MAT 4605 PALLADIUM-105 (N,GAMMA)
CROSS SECTION(BARN)
ENERGY(EV)

fig.11

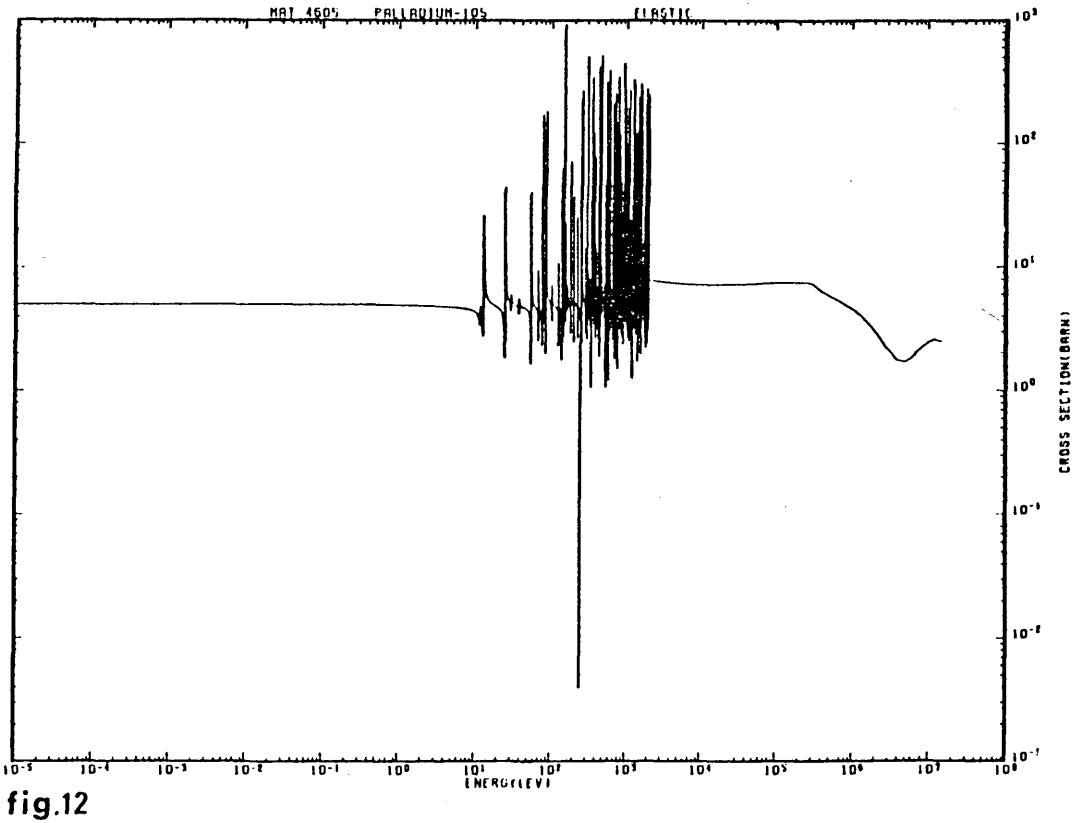
MAT 4605 PALLADIUM-105 ELASTIC
CROSS SECTION(BARN)
ENERGY(EV)

fig.12

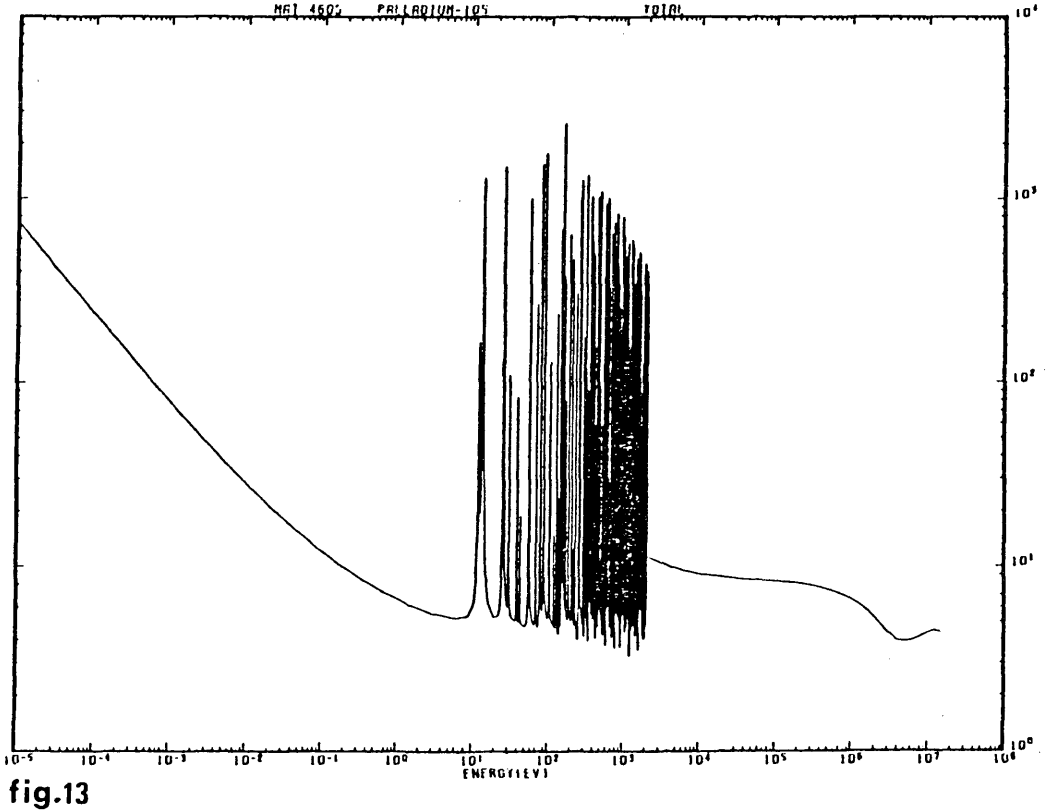
MAT 4605 PALLADIUM-105 TOTAL
CROSS SECTION(BARN)
ENERGY(EV)

fig.13

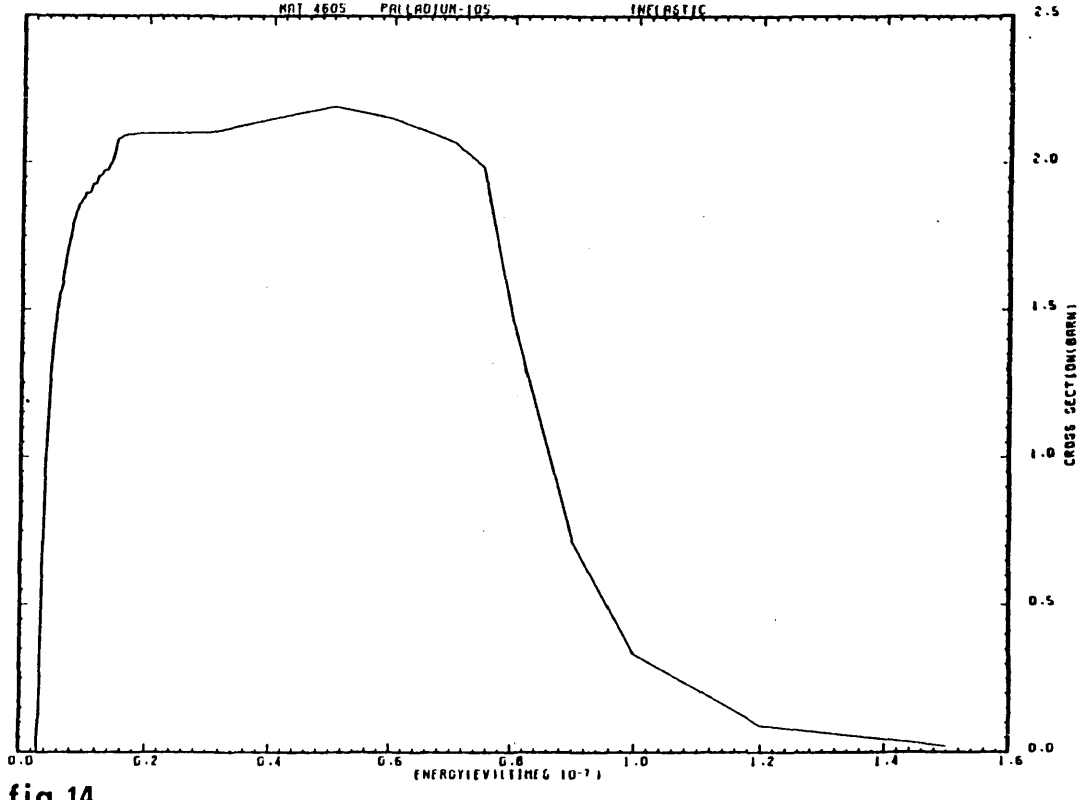
MAT 4605 PALLADIUM-105 INELASTIC
CROSS SECTION(BARN)
ENERGY(EV)(TIMES 10⁻⁶)

fig.14

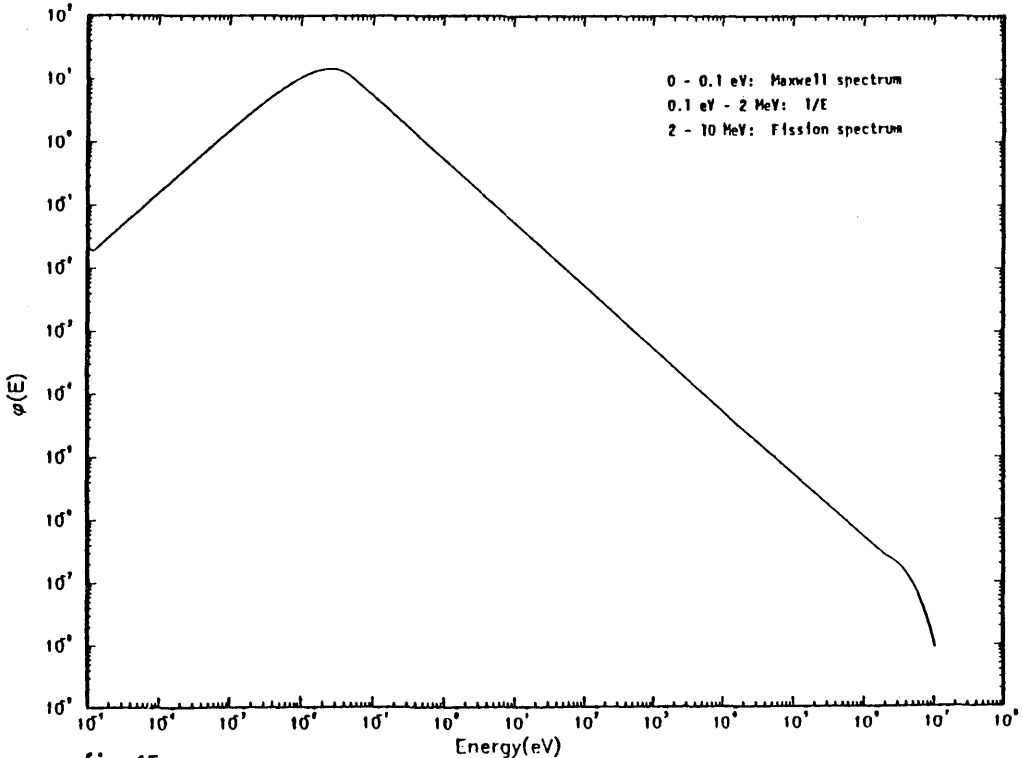
0 - 0.1 eV: Maxwell spectrum
0.1 eV - 2 MeV: 1/E
2 - 10 MeV: Fission spectrum
φ(E)
Energy(eV)

fig.15

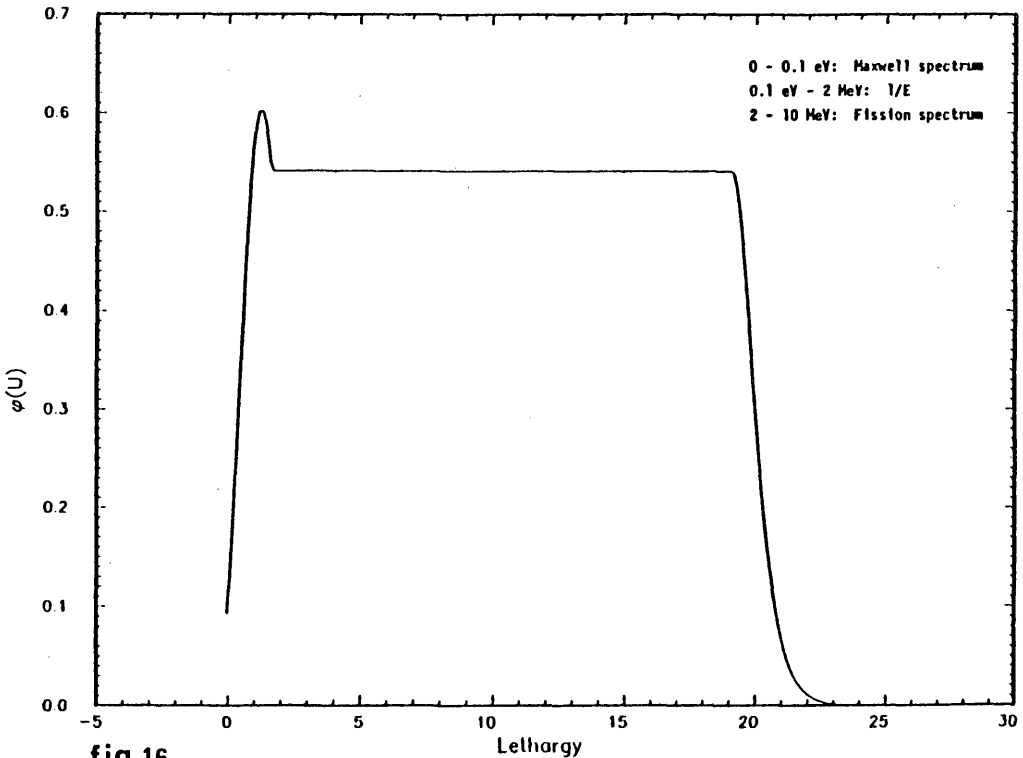
0 - 0.1 eV: Maxwell spectrum
0.1 eV - 2 MeV: 1/E
2 - 10 MeV: Fission spectrum
φ(U)
Lethargy

fig.16

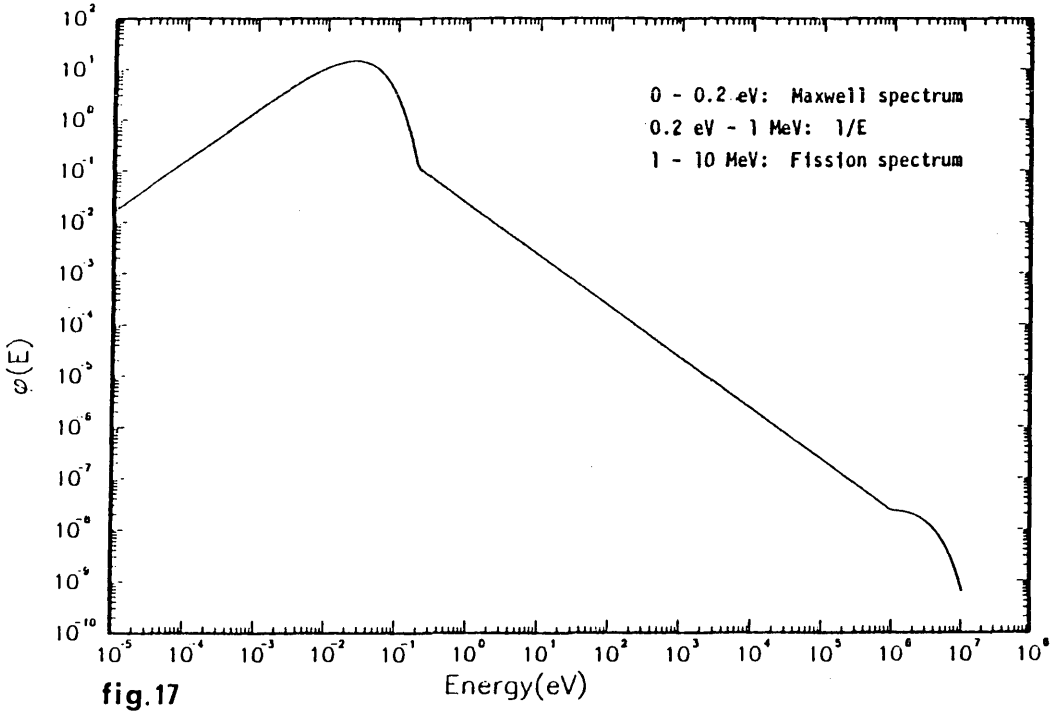
0 - 0.2 eV: Maxwell spectrum
0.2 eV - 1 MeV: 1/E
1 - 10 MeV: Fission spectrum
φ(E)
Energy(eV)

fig.17

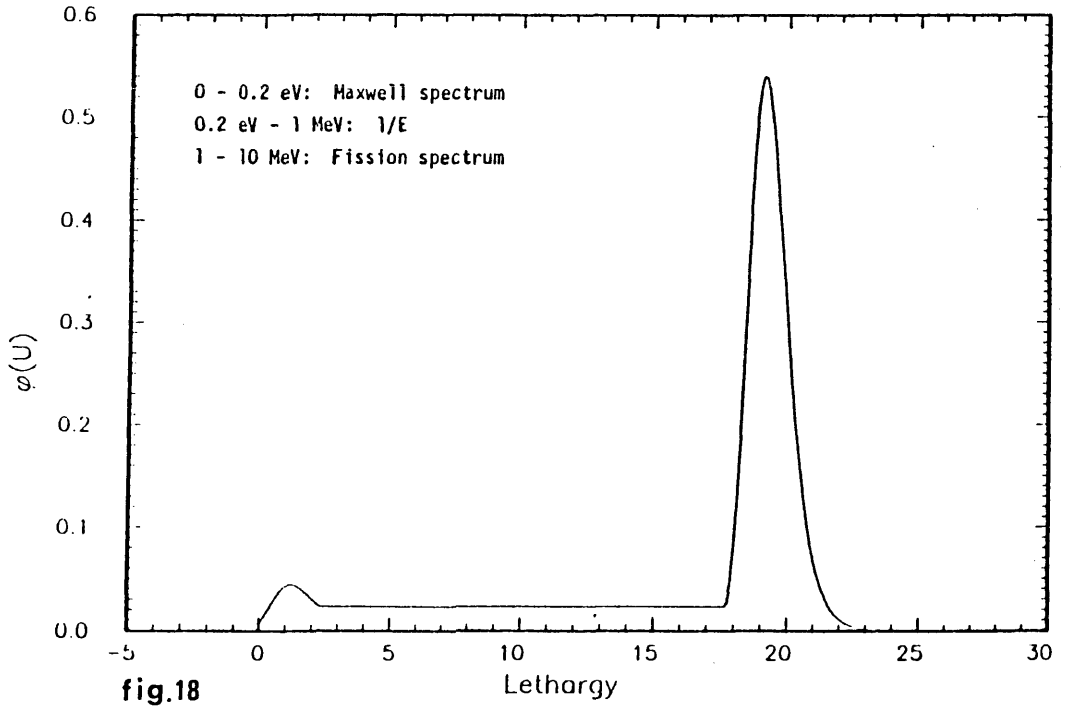
0 - 0.2 eV: Maxwell spectrum
0.2 eV - 1 MeV: 1/E
1 - 10 MeV: Fission spectrum
φ(U)
Lethargy

fig.18

FACULTY AND PARTICIPANTS

DIRECTORS

DALAFI, H.D.
I.C.T.P.
Trieste
Italy

FONDA, L.
University of Trieste/ICTP
Trieste
Italy

CULLEN, D.E.
Nuclear DAta Section
I.A.E.A.
Wagramerstrasse
P.O. Box 100
A-1400 Vienna
Austria

MEHTA, M.K.
Bhabha Atomic Research Center
Trombay, Bombay 400 085
India

PRONYAEV, V
Nuclear Data Section
I.A.E.A.
Wagramerstrasse 5
P.O. Box 100
A-1400 Vienna
Austria

SCHMIDT, J.J.
Nuclear Data Section
I.A.E.A.
Wagramerstrasse 5
P.O. Box 100
A-1400 Vienna
Austria

LECTURES

ANZALDO MENESES, A.M.
Institut f. Neutronenphysik
und Reaktortechnik
Kernforschungszentrum
Karlsruhe
Postfach 3640
D-7500 Karlsruhe
Federal Republic of Germany

BRACK, M
University Regensburg
Fachbereich Physik I
Institut f. Physik.I
Universitaetsstrasse 31
D-8400 Regensburg
Federal Republic of Germany

JAHN, H.
Institut f. Neutronenphysik
und Reaktortechnik
Kernforschungszentrum
Karlsruhe
Postfach 3640
D-7500 Karlsruhe
Federal Republic of Germany

JENSEN, A.S.
Institute of Physics
University of Aarhus
DK-8000 Aarhus
Denmark

KOONIN, S.E.
California Institute of
Technology
Pasadena, CA 91109
U. S. A.

MOTTA, M.
Centro di Calcolo del CNEN
Via Mazzini 2
40138 Bologna
Italy

NIFENECKER, H.
DRF/CPN
Centre d'Etudes Nucléaires
de Grenoble
B.P. No. 85X
F-38041 Grenoble Gare
France

ROWLANDS, J.L.
Room 220, Building B.21
Atomic Energy Establishment
Winfrith, Dorchester
Dorset DT2 8DH
U. K.

SALVATORES, M.
Centre d'Etudes Nucléaires
de Cadarache
C.E.A., BP No. 1
F-13115 Saint Paul-lez-
Durance
France

STORY, J.S.
(Private)
37 Fernside Road
Poole, Dorset BH15 2QU
U. K.

STROHMAIER, B.
Institut f. Radiumforschung
und Kernphysik
Boltzmanngasse
A-1090 Vienna
Austria

TAMURA, T.
Department of Physics
University of Texas
Austin, Texas 78712
U. S. A.

UHL, M.
Institut f. Radiumforschung
und Kernphysik
Boltzmanngasse
A-1090 Vienna
Austria

WEIGMANN, H.
CEC/EURATOM
Bureau Central de Mesures Nucléaires
Steenweg naar Retie
B-2440 Geel
Belgium

PARTICIPANTS

ABZOUZI, A.
Centre de Sciences et de la
Technologie Nucleaire
Ave. Franz Fanon
B.P. 1017, Alger-Gare
Algeria

AHMAD, G.U.
Department of Physics
Bangladesh University of Eng.
& Technology
Dacca 2
Bangladesh

ANAND,
Nuclear Physics Division
Bhabha Atomic Research Centre
Trombay, Bombay 400 085
India

ARDANI,
PPBMI-BATAN
Jl. Babarsari
P.O. Box 8, Jakarta
Indonesia

ATASOY, H.M.
Cekmece Nuclear Research &
Training Centre
P.k. 1 Havaalani, Istanbul
Turkey

ATHIMENE, H.
C.S.T.N.
B.P. 1017, Alger-Gare
Algeria

AVRIGEANU, M.
Central Institute of Physics
Institute of Physics & Nucl. Eng.
P.O. Box MG-6
Magurele-Bucharest
Romania

BHASKAR RAO, P.
Reactor Research Centre
Kalpakkam 603102
Tamilnadu
India

BIKIT, I.S.
Institute of Physics
P.O. Box 224-Ilije Duricica 4
2100 Novi Sad
Yugoslavia

BISHAY, S.T.
Department of Physics
University College for Women
Ain Shams University
Heliopolis, Cairo
Egypt

BÖDY, Z.T.
Institute of Experimental Physics
Kossuth University
H-4001 Debrecen pf. 105
Hungary

BRUSEGAN, A.
EURATOM - Bureau Central de Mesures Nucleaires
Steenweg naar Retie
B-2440 Geel
Belgium

CHALHOUB, E.S.
Centro Tecnico Aeroespacial
Inst. de Ativades Espaciais
CTA-IAE-EAV
12 200 Sao Jose dos Campos
Brazil

CHAUBEY, A.K.
Department of Physics
Aligarh Muslim University
Aligarh U.P.
India

CHIRAPATPIMOL, N.
Department of Physics
Chiengmai University
Chiengmai
Thailand

OUICHAOUI, A.
C.S.T.N.
B.P. 1017, Alger-Gare
Algeria

COBAN, A.
Department of Physics
Karadeniz Technical University
Trabzun
Turkey

DE BARROS, S.M.C.
Instituto de Fisica
Universidad Federal Rio de Janeiro
Rio de Janeiro
Brazil

FINDLAY, D.J.S.
A.E.R.E. Harwell
B. 418
Ozon OX11 ORA
U. K.

FRISANCHO PINEDA, I.
Universidad Nacional de Ingenieria
Av. Tupac Amaru s/n
Apartado 1301
Lima
Peru

GARG, S.C.
Hindu College
Delhi
India

GUNGOR, S.
C.N.A.E.M.
P.k. 1 Istanbul
Turkey

HAROON, M.R.
Centre for Nuclear Studies
Pakistan Institute of Nuclear Science & Technology
P.O. Nilore, Rawalpindi
Pakistan

HLAVAC, S.
Institute for Physics
Slovak Academy of Sciences
899 30 Bratislava
Czechoslovakia

HUSSEIN, A.Z.
Reactor and Neutron Physics Department
Nuclear Research Centre
Atomic Energy P.O. Box
Cairo
Egypt

HUSSEIN, H.M.
Department of Engineering Physics & Mathematics
Faculty of Engineering
University of Cairo
Giza
Egypt

ISRAR, M.
Reactor Operation & Maintenance Group
Pakistan Institute of Nuclear Science and Technology
P.O. Nilore, Rawalpindi
Pakistan

JORDANOV, J.D.
Institute of Nuclear Research & Nuclear Theory
Boul Lenin 72, Sofia
Bulgaria

JUJURATISBELA, U.
National Atomic Energy Agency
Research Centre for Nuclear Technology
Jalan Tamansari No. 71
Bandung, Indonesia

KHAN, A.M.
Department of Physics
University of Dacca
Dacca-2
Bangladesh

KOIUMJIEVA, N.T.
Institute of Nuclear Research & Nuclear Theory
Sofia
Bulgaria

KOO, W.-K.
School of Physics
University of Science of Malaysia
Penang
Malaysia

KRISTIAK, J.
Institute of Physics
Dubravska Cesta
899 30 Bratislava
Czechoslovakia

KUNTORO, I.
PPBMI-BATAN
Jl. Babarsari
P.O. Box 8, Jakarta
Indonesia

KUSNO, D.
Department of Physics
FIPIA, University of Indonesia
Salemba 4, Jakarta
Indonesia

LAKSHMANA DAS, N.
Department of Nuclear Physics
Andhra University
Waltair, Visakhapatnam 530003
India

LEE, J.-T.
Fast Reactor Division
Korea Advanced Energy Research Institute
P.O. Box 7, Cheong Ryang
Seoul
Republic of Korea

LEE, U.-C.
Seoul National University
Department of Nuclear Eng.
Sinrin-dong
Gwanag-gu, Seoul 151
Republic of Korea

LOLICH, J.V.
Centro Atomico Bariloche
Comision Nacional de Energia Atomica
8400 S.C. de Bariloche
Argentina

MAJUMDER, A.R.
Department of Physics
University of Dacca
Dacca-2
Bangladesh

MANNAN, M.A.
Institute of Nuclear Science & Technology
Bangladesh Atomic Energy Commission
P.O. Box 158, Dacca-2
Bangladesh

MEDJADI, D.E.
C.S.T.N.
Ave. Franz Fanon
B.P. 1017
Alger-Gare
Algeria

MOLLA, N.I.
Atomic Energy Cewntre
P.O. Box 164
Ramna, Dacca
Bangladesh

MORALES-PENA, J.R.
Facultad de Ciencias
Departamento de Fisica
Universidad de Chile
Casilla 653, Santiago
Chile

NADKARNI, D.M.
Nuclear Physics Division
Bhabha Atomic Research Centre
Trombay, Bombay 85
India

NAGUIB, K.M.
Atomic Energy Establishment
Nuclear Research Centre
Neutron and Reactor Physics Department
Cairo, Egypt

NARAIN, R.
Departamento de Energia Nuclear
Universidade Federal de Pernambuco
Cidade Universitaria
50.000 Recife, Pernambuco
Brazil

PANGGABEAN, L.
B.P.P. Teknologi
Jalan Tamrin no. 8
Jakarta
Indonesia

PARANJAPE, S.D.
Theoretical Reactor Physics Section, B.A.R.C.
5th floor, Central Complex
Trombay, Bombay 400 085
India

PEVEC, D.
Faculty of Electrical Eng.
P.O. 170
41001 Zagreb
Yugoslavia

PICON, C.
Department of Physics
Universidad Nacional de Ingeneria
Casilla 1301, Lima
Peru

RAMA RAO, J.
Department of Physics
Banaras Hindu University
Varanasi 221005
India

REGO, R.A.
CRA/IAE/EAV
Sao Jose dos Campos
SP 12200
Brazil

REHMAN, A.H.
Reactor Operation & Maintenance Group
Pakistan Institute of Nuclear Science & Technology
P.O. Nilore, Rawalpindi
Pakistan

REHMAN, M.U.
Government College
Hanzara Division
Kanpur
Pakistan

RIBANSKY, I.
Institute of Physics
EPRC Slovak Academy of Science
899 30 Bratislava
Czechoslovakia

SABEK, M.
Neutron & Reactor Physics Department
Nuclear Research Centre
Atomic Energy Establishment
Cairo, Egypt

SAHU, R.
Physical Research Laboratory
Ahmedabad 380 009
India

SAJO BOHUS, L.
Universidad Simon Bolivar
Dep. to de Fisica
P.O. Box 80659
Caracas 1080 A
Venezuela

SALLAM, O.H.
Atomic Energy Establishment
Nuclear Research Centre
Neutron & Reactor Phys. Dept.
Cairo
Egypt

SANGARIYAVANISH, A.
Department of Physics
Faculty of Science
Srinakharinwiret University
Prasarnmitr, Sukhumvit 23
Bankok 11, Thailand

SEFIDVASH, F.
Nuclear Eng. Department
UFRGS
Praca Argentina s/n
90.000 Porto Alegre RS
Brazil

SEHGAL, M.L.
Department of Physics
Aligarh Muslim University
Aligarh (UP)
India

SHUKLA, V.K.
Experimental Reactor Physics Section
Hall no. 1, B.A.R.C.
Bombay 400 085
India

STANCIC, V.
Boris Kidric Inst. of Nuclear Sciences
P.O. Box 522
11001 Beograd
Yugoslavia

SUDAR, S.
Institute of Experimental Physics
Kossuth University
H-4001 Debrecen
Hungary

TOGUN, E.A.
Department of Physics
University of Ife
Ile-Ife
Nigeria

TRKOV, A.
Institute Josef Stefan
Jamova 39
61001 Ljubljana
Yugoslavia

UPADHYAYA, G.P.
Deptartment of Physics
Government College Bareli
Dist. Raisen MP
India

WRIEKAT, A.H.
Department of Physics
University of Jordan
Amman
Jordan

YOUSSEF, M.I.
Faculty of Science
Department of Physics
Mansoura University
Mansoura
Egypt

84-01479